14 April 2006 | $10

Science

BIOCHEMISTRY

TOOLS FOR NEW FRONTIERS

AAAS

There's a new kit on the block.

Introducing StrataClone™ PCR Cloning Kits: A new, more affordable choice in Topoisomerase I technology

Our StrataClone™ PCR Cloning Kit* saves you time and money with topoisomerase-based PCR cloning priced lower than the competition. The simple, three step process, >95% efficiency guarantee, and affordable pricing make StrataClone™ PCR Cloning Kits your kit of choice for topoisomerase-based PCR cloning.

- **High-performance PCR cloning at a more affordable price**
- **Clone both long and short PCR amplicons with the same kit**
- **High efficiency results in >95% clones with insert**

Need More Information? Give Us A Call:

Stratagene USA and Canada
Order: (800) 424-5444 x3
Technical Services: (800) 894-1304 x2

Stratagene Europe
Order: 00800-7000-7000
Technical Services: 00800-7400-7400

Stratagene Japan K.K.
Order: 03-5159-2060
Technical Services: 03-5159-2070

Ask Us About These Great Products:

StrataClone™ PCR Cloning Kit	**20 reactions**	**240205**
	10 reactions	**240206**

StrataClone™ is a trademark of Stratagene in the United States.
* Patent pending.

STRATAGENE®

www.stratagene.com

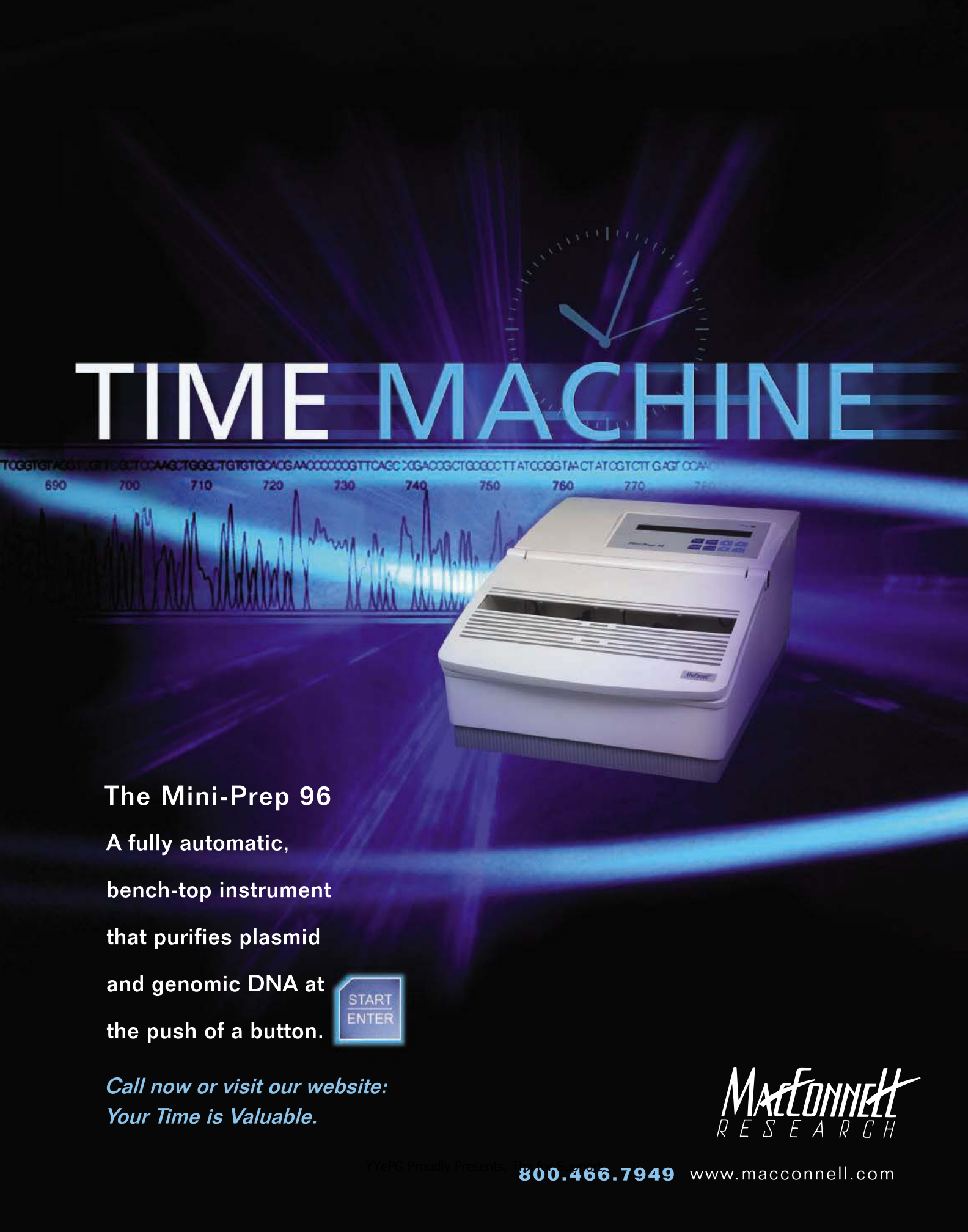

The Mini-Prep 96

A fully automatic, bench-top instrument that purifies plasmid and genomic DNA at the push of a button.

Call now or visit our website:
Your Time is Valuable.

MacConnell RESEARCH

800.466.7949 www.macconnell.com

GE Healthcare

Bringing science to life

When it comes to life sciences, GE Healthcare is setting the standard. Tens of thousands of scientists in over 100 countries around the world rely on our products every day. We have delivered more than 60 000 research protein purification systems, 1500 BioProcess™ systems and 12 000 BioProcess columns worldwide. Our Amersham family of consumables, with its 60-year heritage, is trusted to provide accurate results time and time again.

But we're never content to stand still. We constantly strive for new innovations for tomorrow's research and drug development. And the result is groundbreaking products like the ÄKTAdesign™ platform, IN Cell Analyzer, Ad-A-Gene Vectors, and MabSelect™ media. Thanks to our technological achievements and global presence, we're able to help you turn your scientific ideas into reality – bringing science to life and helping transform healthcare.

We call it Life Science Re-imagined.

Discover more at www.gehealthcare.com/life

imagination at work

GE Healthcare

Faster protein purification? It's not rocket science.

HiTrap™ columns give you pure proteins with less effort. They come prepacked with the widest choice of media, ensuring results you can depend on in a broad range of applications, and the highest level of convenience.

But we're never content to stand still. We constantly strive for new innovations for tomorrow's research and drug development. And thanks to our technological achievements and global presence, we're able to help you turn your scientific ideas into reality – bringing science to life and helping transform healthcare.

We call it Life Science Re-imagined.

Discover how HiTrap columns can help power your protein purification.
Visit www.gehealthcare.com/life

imagination at work

GE Healthcare Bio-Sciences AB, a General Electric Company.
Björkgatan 30, 751 84 Uppsala, Sweden.

GE05-06

Volume 312, Issue 5771

COVER

A variety of new and old localization methods are used to visualize components of a cultured human adenocarcinoma (HeLa) cell. The nucleus is labeled with a small-molecule dye (blue), the Golgi apparatus is immunolabeled with quantum dots (yellow), microtubules are genetically tagged with a fluorescent protein (green), and the actin cytoskeleton is labeled with a tetracysteine/biarsenical pair (red). See the special section beginning on page 211.

Image: National Center for Microscopy and Imaging Research/B. N. G. Giepmans

DEPARTMENTS

EDITORIAL

SPECIAL SECTION

Tools for Biochemistry

INTRODUCTION

REVIEWS

PERSPECTIVE

>> Perspective p. 208; Research Article p. 237; Report p. 273

For related online content, see page 153 or go to www.sciencemag.org/sciext/biochemtools/

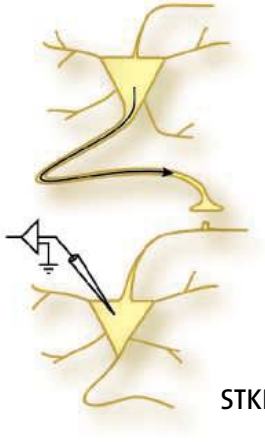

STKE

NEWS OF THE WEEK

>> Report p. 257

>> Research Article p. 233

NEWS FOCUS

CONTENTS continued >>

Systems Biology — Proteins and Proteomics

Standardized solutions for proteins

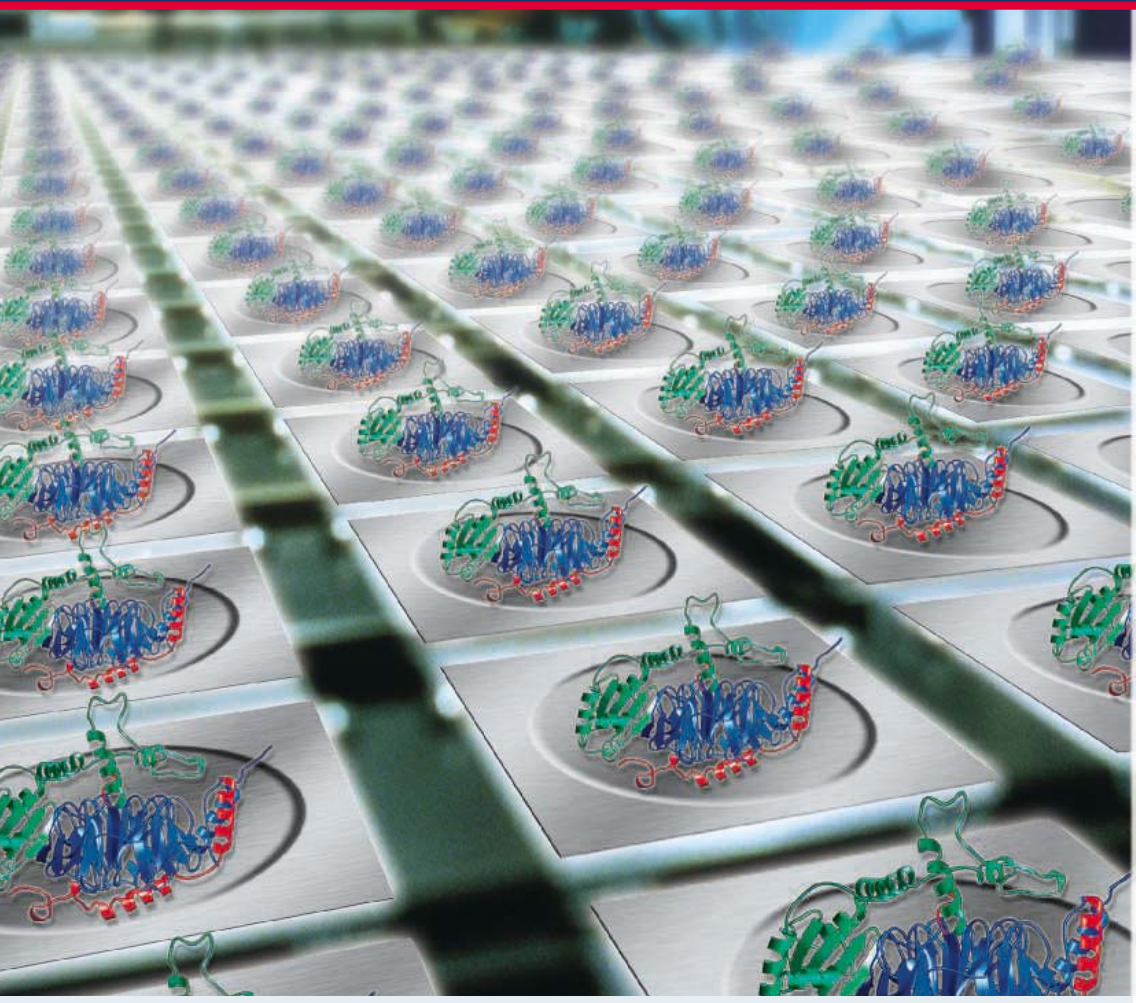

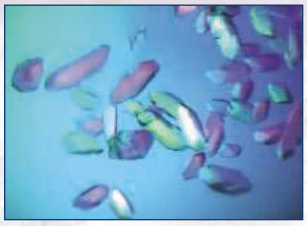

More reproducibility, streamlined crystallization*

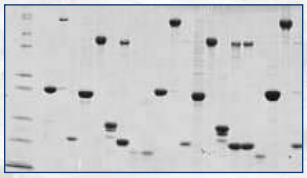

More proteins, purer, faster

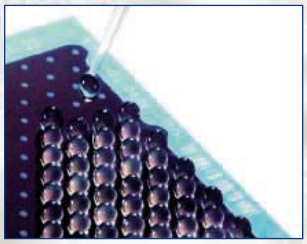

More peptide matches, more protein hits

Success with proteins — made possible by QIAGEN's expertise!

QIAGEN's comprehensive protein portfolio will help you rise to the challenge of working with proteins. QIAGEN provides easy-to-use, integrated solutions to help you succeed with:

- Expression
- Purification
- Detection
- Assay
- Crystallization
- MALDI sample prep
- Proteomics sample prep
- Automation
- Fractionation

Find a standardized solution for your protein challenge at www.qiagen.com/protein !

* Image shows *E. coli* gyrase A C-terminal domain crystals. Courtesy of Alex Ruthenburg from Prof. Verdine's laboratory, Harvard University, Boston, USA.

QIAGEN

Science

SCIENCE EXPRESS

www.sciencexpress.org

PLANT SCIENCE

An SNP Caused Loss of Seed Shattering During Rice Domestication
S. Konishi et al.
A gene that controls the retention of rice grains on the plant after ripening is from a transcription factor of a different class from that of another recently identified gene for this trait.
10.1126/science.1126410

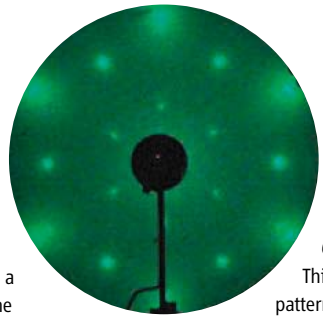

APPLIED PHYSICS

Electronic Confinement and Coherence in Patterned Epitaxial Graphene
C. Berger et al.
Thin graphene layers grown on silicon carbide can be patterned into ribbons that exhibit high electrical conductivity and quantum confinement effects at near zero kelvin.
10.1126/science.1125925

NEUROSCIENCE

Bruchpilot Promotes Active Zone Assembly, Ca^{2+}-Channel Clustering, and Vesicle Release
R. J. Kittel et al.
A protein necessary for organization of the vesicle release site in neuronal synapses also influences calcium channel localization and interaction with vesicles.
10.1126/science.1126308

CHEMISTRY

Cyclopropenylidenes: From Interstellar Space to an Isolated Derivative in the Laboratory
V. Lavallo, Y. Canac, B. Donnadieu, W. W. Schoeller, G. Bertrand
The triangular C_3H_2 molecule, which appears to be stable only in the near-vacuum of interstellar space, has been isolated by appending amino groups to the ring.
10.1126/science.1126675

LETTERS

BOOKS *ET AL.*

POLICY FORUM

PERSPECTIVES

TECHNICAL COMMENT ABSTRACTS

EVOLUTION

BREVIA

ECOLOGY

RESEARCH ARTICLES

DEVELOPMENT

BIOCHEMISTRY

CONTENTS continued **>>**

TRANSFECTION

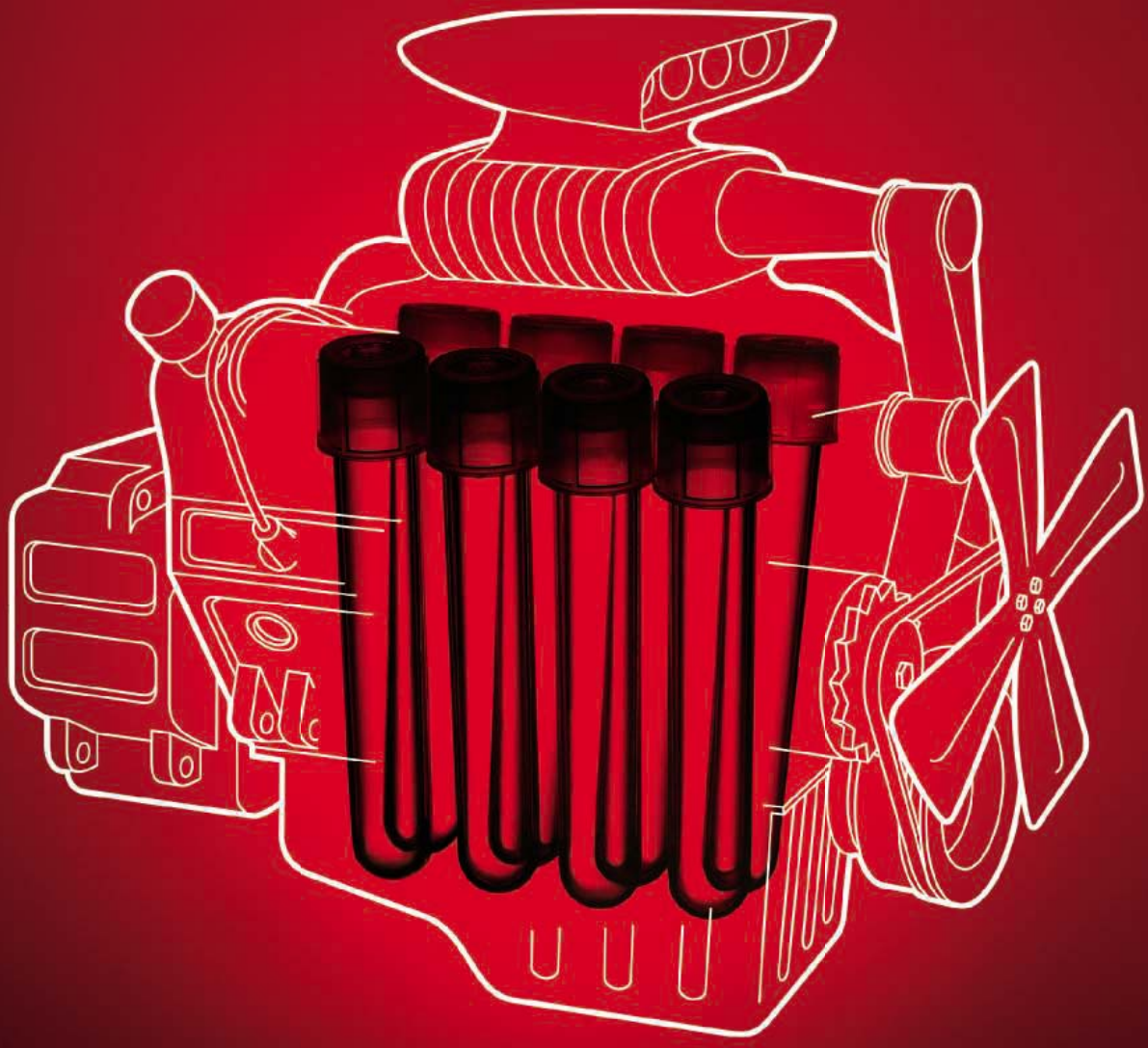

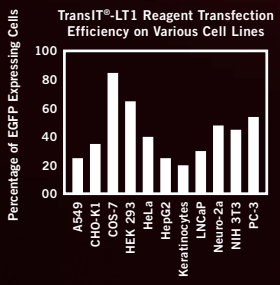

POWER YOUR RESEARCH

***Trans*IT®-LT1 Transfection Reagent from Mirus Bio. Efficiency at its peak.** Get powerful plasmid delivery and expression without sacrificing cell viability. Invented by Mirus Bio scientists to work with a broad range of cell types, our low-toxicity reagent delivers accurate results in two simple steps. Keep cells healthy and research moving forward with transfection technology from the pioneers in gene delivery. Because your research begins at the bench — it doesn't end there.

Mirus®

It All Begins at the Bench

Visit mirusbio.com to view our extensive citation database.

Science

REPORTS

AAAS
ADVANCING SCIENCE, SERVING SOCIETY

SCIENCE (ISSN 0036-8075) is published weekly on Friday, except the last week in December, by the American Association for the Advancement of Science, 1200 New York Avenue, NW, Washington, DC 20005. Periodicals Mail postage (publication No. 484460) paid at Washington, DC, and additional mailing offices. Domestic individual membership and subscription (51 issues): $139 ($74 allocated to subscription). Domestic institutional subscription (51 issues): $650; Foreign postage extra: Mexico, Caribbean (surface mail) $55; other countries (air assist delivery) $85. First class, airmail, student, and emeritus rates on request. Canadian rates with GST available upon request, GST #1254 88122. Publications Mail Agreement Number 1069624. **Printed in the U.S.A.**

Change of address: Allow 4 weeks, giving old and new addresses and 8-digit account number. **Postmaster:** Send change of address to *Science*, P.O. Box 1811, Danbury, CT 06813–1811. **Single-copy sales:** $10.00 per issue prepaid includes surface postage; bulk rates on request. *Science* is indexed in the *Reader's Guide to Periodical Literature* and in several specialized indexes.

CONTENTS continued **>>**

iQ™ Multiplex Powermix

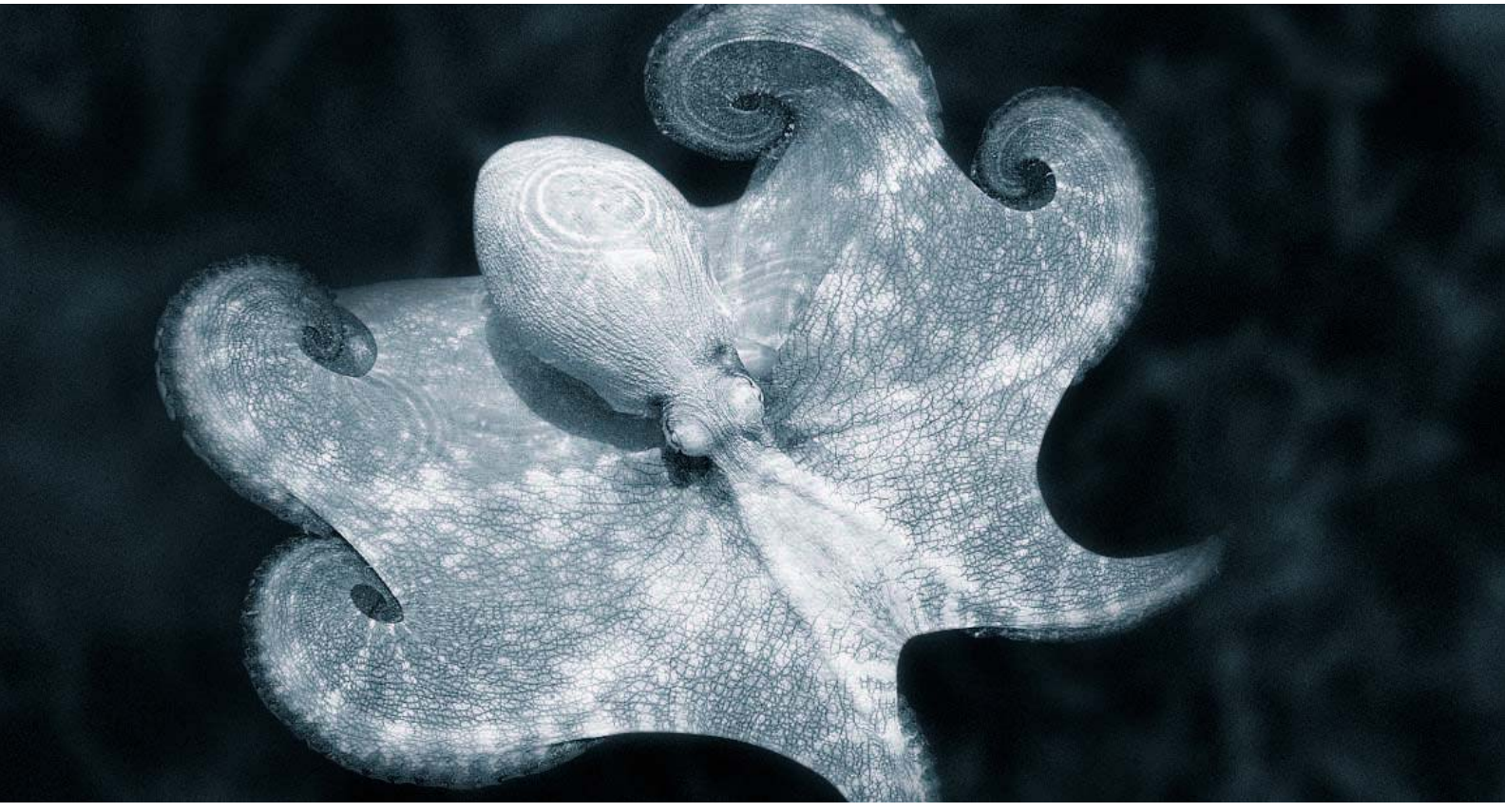

Bring the Power of Multiplex to Your qPCR

iQ multiplex powermix simplifies real-time detection of multiple targets in a single tube, routinely yielding efficiencies equivalent to corresponding singleplexes. Increase throughput, control costs, and maximize your data output with this powerful blend.

- Reliable real-time multiplex PCR detection of up to 5 targets
- Detection of up to 4 targets when one differs in expression up to 10^6-fold relative to the others
- Linearity over 6 orders of magnitude of input cDNA and 4 orders of magnitude of input genomic DNA

For more information, visit us on the Web at **www.bio-rad.com/supermixes/**

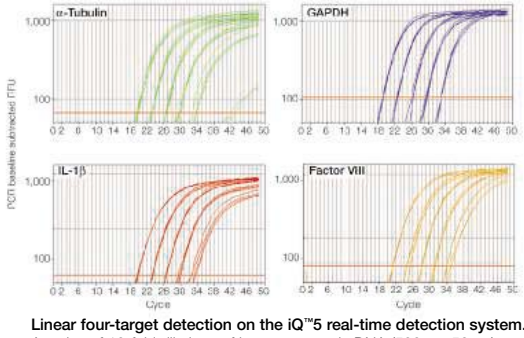

Linear four-target detection on the iQ™5 real-time detection system. A series of 10-fold dilutions of human genomic DNA (500 ng–50 pg) was amplified to assay for four target genes using the iQ multiplex powermix. Targets were α-tubulin (FAM-labeled probe, efficiency = 96%); GAPDH (HEX-labeled probe, efficiency = 95%); IL-1β (Texas Red-labeled probe, efficiency = 102%); and factor VIII (Cy5-labeled probe, efficiency = 102%). Singleplex reactions of these targets yielded statistically indistinguishable efficiencies and C_T values compared to those of the four-plex result.

Visit us on the Web at **discover.bio-rad.com**
Call toll free at 1-800-4BIORAD (1-800-424-6723);
outside the US, contact your local sales office.

BIO-RAD

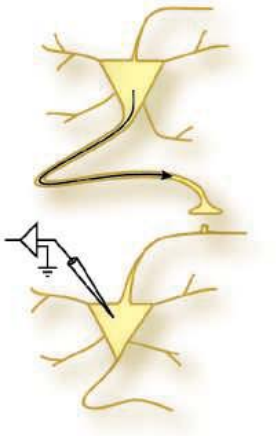

Monitoring an individual synapse.

SPECIAL ONLINE CONTENT

Tools for Biochemistry

SCIENCE'S **STKE**

www.stke.org SIGNAL TRANSDUCTION KNOWLEDGE ENVIRONMENT

EDITORIAL GUIDE: Focus Issue—Peering Into the Proteome
E. M. Adler
New approaches leverage the wealth of proteomic data to reveal insights into protein function and localization.

REVIEW: Fanciful FRET
S. S. Vogel, C. Thaler, S. V. Koushik
Accurate measurement of energy transfer efficiency enhances the usefulness of FRET analysis.

PROTOCOL: Rapid Photoinactivation of Native AMPA Receptors on Live Cells Using ANQX
P. M. England
ANQX provides a means of directly monitoring native AMPA-type glutamate receptor trafficking in real time.

SCIENCE**NOW**

www.sciencenow.org DAILY NEWS COVERAGE

Slamming the Moon
A rocket will smash into a crater on the lunar surface looking for water.

Twinkle, Twinkle, Little E.T.
New telescope will look for alien intelligences that use lasers to communicate.

A "His" or "Hers" Brain Structure?
Amygdala tied to inner feelings in women; interacting with world in men.

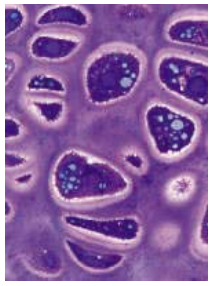

Cells in context.

SCIENCE'S **SAGE KE**

www.sageke.org SCIENCE OF AGING KNOWLEDGE ENVIRONMENT

NEWS FOCUS: Environmental Movement
M. Leslie
Molecules in cells' surroundings contribute to aging—and tweaking them might rejuvenate tissues.

GENES/INTERVENTIONS DATABASE: Plau
Overproduction of an extracellular protease in the brain is associated with life-span extension in mice.

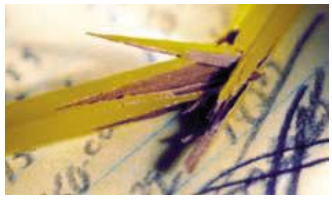

The joy of teaching statements.

SCIENCE **CAREERS**

www.sciencecareers.org CAREER RESOURCES FOR SCIENTISTS

US: Writing the Teaching Statement
R. N. Austin
Here's how to minimize the pain of writing teaching statements on faculty applications.

EUROPE: Chinese Whispers
T. Reynolds
What's it like working as a foreign scientist in China?

US: Career Reentry and Overseas Postdocs
GrantDoctor
Where do you get money to hire a postdoc who is returning from a family-related leave?

MISCINET: The Graduate School Application
C. Barrera
A graduate school dean explains how to handle each component of a typical graduate school application.

GRANTSNET: International Grants and Fellowship Index
A. Kotok
Get the latest listing of funding opportunities from Europe, Asia, and the Americas.

ISI Web of Knowledge℠

Take the next step

Where ideas turn into knowledge.

The search for new knowledge is an ongoing challenge …
but the search for the best research resources need not be.

ISI Web of Knowledge assures your access to the critical information you require. Whether the ideas you seek are across the globe, have their roots in the past, or can be found in today's newest discoveries, *ISI Web of Knowledge* delivers all the research data and tools you need to reach your goals.

Navigate freely. Explore confidently. Search successfully.

with *ISI Web of Knowledge*

THOMSON

EDITED BY STELLA HURTLEY AND PHIL SZUROMI

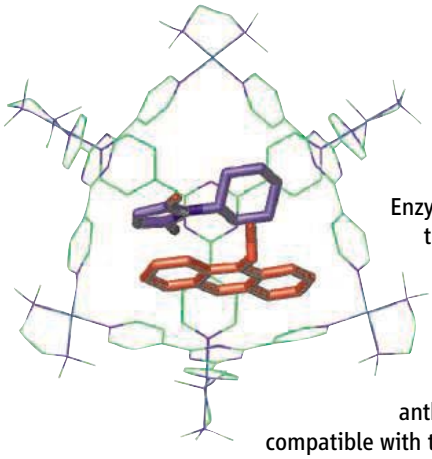

Catch, React, Release

Enzymes derive much of their remarkable selectivity by orienting substrates in ways that facilitate specific reaction paths. Recently, chemists have sought to achieve similar effects using relatively simpler hollow structures, assembled from organic and metallic building blocks in solution. However, these synthetic hosts often bind products as effectively as they do reactants so that catalysis is inhibited. **Yoshizawa *et al.*** (p. 251) find that a palladium and triazine–based host that adopts a bowl shape can catalyze the Diels-Alder reaction of anthracenes and phthalimides in water because the product geometry is no longer compatible with the host. A related host structure, shaped like a cage, can be used stoichiometrically to orient the same reagents in a different way and yields an unusual Diels-Alder adduct at a terminal, rather than central, site on the anthracene framework.

Sending Charges Their Separate Ways

Devices implanted in the body require power, which is normally delivered by batteries, but a number of approaches have been proposed to tap into the power or fuel sources the body already provides. **Wang and Song** (p. 242) have converted mechanical energy into electrical energy by deflecting anchored ZnO nanowires with a conductive atomic force microscope tip. The strain field created by bending the nanowires with the tip caused charges to separate and build up on opposite sides of this polar material. The tip and nanowire form a rectifying Schottky barrier so that built-up charge is released as electrical current when the tip crosses from one face polarity to the other.

Ductility Through Deformation

In traditional metalworking, a metal is cold-deformed in order to introduce dislocations that make it stronger, and then annealed to restore its ductility. As the number of dislocations increases, their movement and ability to multiply are hindered, which is the source of the strengthening. **X. Huang *et al.*** (p. 249) now show that an opposite cycle of processes can be used to prepare ductile nanostructured aluminum. During heat treatment, dislocation sources are removed, making it harder for new dislocations to form, and a subsequent deformation step restores these sources, thus enhancing the ductility.

Anode Alternatives

In order for solid-oxide fuel cells to run directly on natural gas, improved anode materials will be needed to avoid problems such as carbon buildup and sulfur poisoning. **Y.- H. Huang *et al.*** (p. 254) report on the use of double-perovskite materials, $Sr_2Mg_{1-x}Mn_xMoO_{6-\delta}$, as anodes at temperatures between 650° and 1000°C. The active Mo(VI)-Mo(V) couple is paired with the Mg and Mn cations that are not reduced by the fuel. The Mg cation appears to be especially resistant to sulfur poisoning and allows for stable operation (200 hours) in the presence of 50 parts per million H_2S.

An Extra Thymus in Mice

The thymus lies directly above the heart and acts as a cradle for developing T cells that will eventually protect the body from the many pathogens encountered during a lifetime. The thymus has been considered one of a kind, but **Terszowski *et al.*** (p. 284, published online 2 March; see the Perspective by **von Boehmer**) find that mice frequently possess a second, smaller thymus located in the neck. This "cervical" thymus displays all of the classical features that define the larger thoracic organ, including boundaries between distinct thymocyte compartments and markers for thymic epithelia and developing thymocytes. Moreover, T cells emerging from this smaller cousin also appear functionally competent and can populate athymic adult recipients after cervical thymus transplantation.

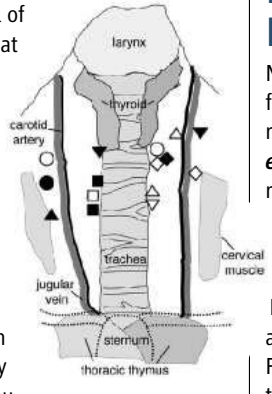

Alkane Shuffle

Olefin metathesis, which swaps molecular fragments on either side of a carbon-carbon double bond, has become an efficient and widely used chemical process. However, the few effective catalysts for the analogous transformation of saturated hydrocarbons. Such rearrangements around C–C single bonds would be useful in generating fuel from lighter alkanes (methane to hexane) derived from sources other than petroleum. **Goldman *et al.*** (p. 257; see the news story by **Service**) achieve alkane metathesis by combining two catalysts. A molecular iridium catalyst first dehydrogenates alkanes to form olefins, which can be combined and rearranged with a well-established olefin metathesis catalyst. The iridium complex then rehydrogenates the rearranged products. In this way, two equivalents of hexane can be converted to decane and ethane, as well as a small distribution of other alkanes stemming from isomerization at the olefin stage.

Bile Buildup and Liver Regeneration

Numerous secreted factors, including growth factors and cytokines, have been implicated in regulating hepatocyte proliferation. **W. Huang *et al.*** (p. 233; see the news story by **Vogel**) report that bile acids are essential stimulatory factors for liver regeneration in mice. An increase in bile acids stimulates regeneration and requires the nuclear bile acid receptor FXR. The authors propose a homeostatic mechanism for determination of liver size, in which FXR and perhaps other nuclear receptors sense the levels of endogenous metabolites to determine the liver's functional capacity. When liver function is decreased as a result of injury, the resulting accumulation of bile acids activates FXR, which stimulates signaling pathways to protect the liver from bile acid toxicity and also promotes liver growth to handle the overload.

Continued on page 157

CREDITS (TOP TO BOTTOM): YOSHIZAWA *ET AL.*; TERSZOWSKI *ET AL.*

We thank Proceedings Reviewers, Inc. for support.

What if staying up to date with the latest technology published in journals and patents were as easy as pushing a button?

It is.

With the "Keep Me Posted" alerting feature, SciFinder sends you automatic updates on areas you—and your competitors—are interested in.

You can monitor specific research topics, companies, authors, substances, or sequences, and choose how frequently you receive notifications: daily, monthly, or weekly.

The service isn't just convenient, it's incredibly current. Journal article records often appear in SciFinder before they're even in print. New references, substances, and sequences are added daily. Patents from all the major offices are added within two days of issuance.

As with all SciFinder features, Keep Me Posted is integrated with your workflow. At any point in a search (including the beginning), simply click on the Keep Me Posted button. SciFinder tracks your steps and will generate the appropriate alert—even for complex topics. When you receive a notification, you can follow each reference as you would in a search: find citing or cited articles (with links to the electronic full text), and follow referenced substances and reactions for further information.

Comprehensive, intuitive, seamless—SciFinder doesn't just alert you, it's part of the process. To find out more, call us at 800-753-4227 (North America) or 614-447-3700 (worldwide) or visit www.cas.org/SCIFINDER.

SciFinder®

Part of the process.™

Continued from page 155

Biochemical Quantum Tunneling

Whether enzymes have evolved to use quantum tunneling to facilitate proton transfer is a topic of considerable debate. **Masgrau *et al.*** (p. 237; see the Perspective by **Benkovic and Hammes-Schiffer**) present an atomic-level description of the reaction pathway for tryptamine oxidation by aromatic amine dehydrogenase. Proton transfer occurs in a reaction dominated by tunneling over a distance of 0.6 angstrom. Tunneling does not require long-range motions coupled to the reaction coordinate but is promoted by short-range motion that reduces the proton-acceptor distance.

Controlling a Plant's Water Balance

Plants lose much of their water through stomata, tiny pores on their leaves. The opening and closing of these pores, and thus a considerable part of the plant's water management, is at least partially under control of the hormone abscisic acid (ABA). **Mishra *et al.*** (p. 264) have now elucidated the signaling pathway between ABA in the opening and closing of stomatal pores. This mechanistic understanding has the potential to be used to produce plants with enhanced water-usage efficiency and drought tolerance.

Gamete Recognition and Reproductive Success

To ensure the reproductive success of a species at fertilization, egg and sperm must be compatible. In field studies with the sea urchin *Strongylocentrotus franciscanus*, **Levitan and Ferrell** (p. 267) examine the selective factors that shape highly polymorphic bindin gamete recognition proteins involved in species specificity. The reproductive success of males was greatest with common genotypes relative to rare genotypes; however, females with common genotypes had half the reproductive success of females with rare genotypes. In addition, common bindin alleles are selected with low sperm densities, but rare bindin alleles are selected with high densities. The interaction between spawning density and genotype frequency provides insight into why different species evolve at different rates.

Directing Nonribosomal Peptide Synthesis

Nonribosomal peptide synthetases (NRPSs) operate through an assembly line where peptidyl carrier proteins (PCPs) transfer peptide intermediates between acyl-adenylate–forming (A) domains and peptide-bond–forming (C) domains. **Koglin *et al.*** (p. 273) now show how PCP reorients a cofactor that holds the growing peptide chains. Both apo and holo-PCP exist in two stable conformations and have one conformation in common between them. This double two-state equilibrium facilitates directed movement of the cofactor and may modulate specific interactions with the A and C domains.

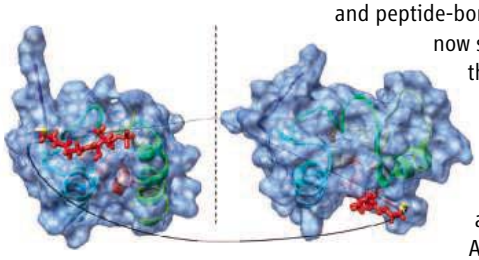

CREDIT: KOGLIN *ET AL.*

Genetic Link to Obesity?

Obesity is thought to be in part heritable, but the genes responsible are difficult to identify, probably because they are numerous and each exerts only a small effect. **Herbert *et al.*** (p. 279) scanned the genomes of a group of well-characterized patients with markers for over 86,000 genetic polymorphisms. One of the markers was associated with an index of obesity, the body mass index. In follow-up studies of five completely independent groups of people that included adults and children, the association was present in four of the groups. The polymorphism is located upstream of a gene involved in global fat metabolism and could potentially affect its function.

Particulate Impact

Aerosols influence climate mainly through cloud formation and their interactions with solar radiation. Anthropogenic aerosol emissions are fairly well documented, but much less is known about natural emissions, such as biogenic volatile organic carbon (BVOC) from boreal forests. **Tunved *et al.*** (p. 261) show that Scandanavian boreal forests provide significant natural fluxes of climate-relevant aerosols, and propose a straightforward relation between emissions of monoterpenes and gas-particle formation over regions where there are few to no local anthropogenic aerosol sources.

INTRODUCING...

THE DR. PAUL JANSSEN AWARD FOR BIOMEDICAL RESEARCH

To honor the work of an active scientist in academia, industry or a scientific institute who exhibits the standards of innovation, insight and leadership that Dr. Paul Janssen showed while moving the boundries of medical science and touching the lives of patients.

INNOVATIVE

INSPIRING

GIFTED

PASSIONATE

REVOLUTIONARY

BRILLIANT

EXCEPTIONAL

PROMINENT

SUCCESSFUL

LEADER

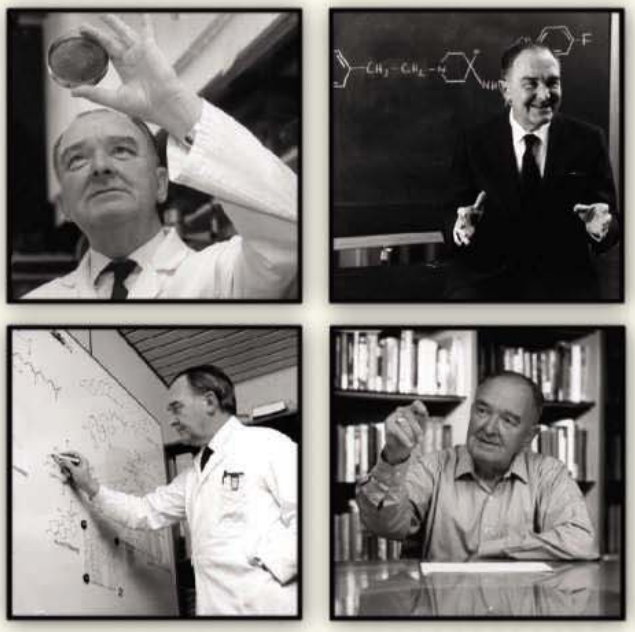

To be awarded September 2006
at The Dr. Paul Janssen Biomedical
Research Symposium in Beerse, Belgium.

Visit **www.pauljanssenaward.com** for more information.

Johnson & Johnson

Donald Kennedy is Editor-in-Chief of *Science*.

Nick Cozzarelli

IT IS A SAD MOMENT WHEN ONE NOTES THE PASSING OF A VALUED AND RESPECTED FELLOW EDITOR. Nick Cozzarelli served the U.S. National Academies for more than a decade as editor in chief of *Proceedings of the National Academy of Sciences* (*PNAS*). During that time, he turned the journal around, and no one should think it was an easy task. When Nick came aboard in 1995, members of the Academy (it wasn't pluralized yet) were fond of their ability to sponsor papers for colleagues or to get their own published, and some objected to the institution of more formal and rigorous peer review. The current multiple-track process conserves some initiative for members but puts all prospective authors on a more even footing. As a result, *PNAS* has broadened its appeal to more fields of science and increased its publication volume so much that it now accumulates in forkload lots at academic offices. *PNAS* is as lively as it is big, and it's one of the places where we at Science regularly look to find papers we admire and somehow missed.

Nick came to his editorial job during a distinguished scientific career in the Department of Molecular and Cell Biology at the University of California, Berkeley. He managed to combine those commitments in a way that was continuously productive on both fronts, a source of admiration for those of us who try these things only one at a time. He did distinguished work on a complex set of reactions involving enzymes that can unwind DNA helices, others that perform re-isomerization, and still others that are responsible for condensation. Cozzarelli more recently had been using DNA microarrays to examine the role of these enzymes in folding, replication, and transcription in bacterial chromosomes.

He had strong views about science, about publishing, and about life. He was among the passionate advocates for open access to scientific publications and engaged the support of the National Academies and his publications committee to make *PNAS* available in that way. In the course of this debate, he was a strong and occasionally astringent advocate, as he was in the discussions about changing the rules for submitting papers to *PNAS*. In both instances, the position he supported gained strength from his consistency and energy. Principled stands supported by passionate commitment can ruffle feathers, and Nick sometimes did. But his combination of candor and good humor made him so likeable and forgivable that he left little scorched earth.

For the work he did for *PNAS*, Nick deserves and will get the thanks of the scientific community. But he understood that scientific publication depends on a host of volunteer laborers who really make it work. There are those who work as editors for society journals and there are editorial boards, most of which serve without compensation. Some journals go to outside committees for quick reactions about whether a paper should receive in-depth peer review. Finally, there are the peer reviewers themselves: the referees who perform close analysis on each paper. In this remarkable system, authors put themselves willingly into the hands of peers, and the reviewers treat their responsibilities with painstaking seriousness. One might expect angry cries of "foul" or "theft" in this competitive universe, but disagreements over fairness are actually remarkable for their scarcity.

There are many activities to which smart people devote themselves generously without getting paid for it. This may be a human need that requires fulfillment by some commitment or other. (There are those persistent volunteer reviewers for the books on Amazon.com). But there is something different and special about those who make themselves available for challenging work just to sustain what is inherently a competitive activity. Not only are the reviewers unpaid; no resume listing "best peer review of 2006" is likely to be presented to a tenure committee this year. Maybe an extension of the open access idea would solve that problem. Suppose reviews were signed and made public along with the paper? Would the benefits of transparency outweigh the costs to candor? That would not only let readers into the evaluation process, but it would let the efforts of the identified reviewers be recognized and perhaps rewarded professionally. Nick might even have liked this. I wish it weren't too late to ask.

– Donald Kennedy

10.1126/science.1128103

FastStart Taq DNA Polymerase

Set Your Sights on The New Standard for Everyday PCR

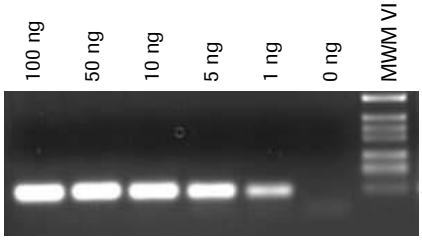

FastStart Taq DNA Polymerase†

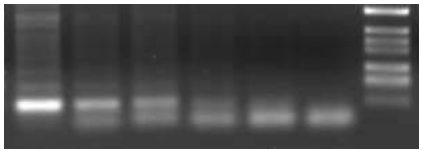

Taq DNA Polymerase†

Detect products from 100-fold less template DNA, without the primer-dimers that plague Taq DNA Polymerase.

Still using standard Taq DNA Polymerase for everyday PCR applications? It's time to upgrade to hot start PCR with FastStart Taq DNA Polymerase:

- **Achieve 100-fold higher sensitivity, and easily detect low-abundance genes.**
- **Obtain results that are easy to interpret** by minimizing nonspecific amplification products and primer-dimers.
- **Save time, effort, and money** by utilizing the same robust, economical enzyme in all your applications; use the supplied buffers and additives to optimize for virtually any template up to 3 kb.
- **Select the best product for your lab's needs:** Choose from the versatile polymerase, a convenient new master mix, or economical dNTPacks combining the enzyme, all buffers, and Roche's unmatched PCR-Grade Nucleotides.

Upgrade from basic Taq for a lot less than you would expect

Raise your standards for everyday PCR applictions. Start your upgrade today by **requesting a free sample* at *www.start-faststart-fast.com***

* Some conditions apply. Samples are limited. See website for details.

Roche Diagnostics

† Purchase of this product is accompanied by a limited license to use it in the Polymerase Chain Reaction (PCR) process for the purchaser's life science research in conjunction with a thermal cycler whose use in the automated performance of the PCR process is covered by the up-front license fee, either by payment to Applied Biosystems or as purchased, *i.e.,* an authorized thermal cycler.

FASTSTART is a trademark of Roche.

YYePG Proudly Presents, Thx for Support

Roche Diagnostics GmbH
Roche Applied Science
68298 Mannheim
Germany

Approaching a boundary.

HIGHLIGHTS OF THE RECENT LITERATURE

SPACE POLICY

A Line in the Sky

Where does airspace end and outer space begin? Space exploration has proceeded for nearly 50 years without a clear answer, but the increased use of spacecraft and satellites by many nations has spurred calls to define the boundary precisely. Harris and Harris argue that international law should establish a boundary based on the vertical distance from Earth's surface, rather than on more complicated functional criteria that could change as technology evolves. They note that airspace is heavily regulated and comes under the jurisdiction of sovereign nations, who have the authority to restrict airplane flight above their territories. In contrast, outer space is considered to be a public realm—described in the Outer Space Treaty as "the province of all mankind"—and an orbiting object is accountable to its owners and not to the countries beneath it. At the moment, orbiting satellites can be used to observe any country, whereas aircraft can be prohibited from doing so legally. Moreover, modern satellites can image the ground with meter-scale resolution, yielding pictures as sharp as those captured by a spy plane operating in airspace. A vertical boundary definition would promote discussion of the policy issues arising from technological progress. — JB

Space Policy **22**, 3 (2006).

ASTROPHYSICS

Galactic Flapping

The Milky Way's flattened disk contains vast reservoirs of hydrogen gas. Near the edges, the disk consists mostly of hydrogen, with few stars. Radio astronomical observations have revealed warping at these edges, as in a dish or saddle. Weinberg and Blitz modeled this warping phenomenon using perturbation theory calculations. Their results attribute the shape to tidal effects induced by motions of the Milky Way's small neighboring galaxies, the Large and Small Magellanic Clouds. As these satellite galaxies move in orbital loops around the Milky Way, they create trailing wakes in the Milky Way's halo of surrounding dark matter. These wakes in turn can cause the outer edges of the Milky Way's lightweight gas disk to bend and flap like a flag in the breeze. The model describes a dynamic disk, which continually changes its shape as the clouds move along their orbits. The authors further suggest that warp observations offer a useful constraint for determining dark matter distributions. — JB

Astrophys. J. **641**, L33 (2006).

CHEMISTRY

THF Up Close

Although molecules in the liquid state are in constant random motion, they appear to adopt specific average configurations that account for such properties as heat capacity and solvation. Insight into these configurations has come mainly from theoretical simulations, whose accuracy is gauged by the extent to which bulk properties are correctly predicted. The pentagonal $(CH_2)_4O$ tetrahydrofuran (THF) is a widely used solvent in organic synthesis because of its relatively high polarity in the absence of hydrogen bonding capacity.

Bowron *et al.* have taken advantage of progress in neutron scattering technology to probe the molecular structure of liquid THF at room temperature directly. Because neutrons are scattered preferentially by protons, the authors refined their analysis by comparing spectra of protiated and deuterated THF, as well as a 1:1 mixture of the isotopomers. Computer modeling of the data revealed a propensity for T-shaped interaction geometries, in which adjacent molecules were oriented edge to face. This arrangement leads to 2.5–Å diameter void spaces, which may account for the solvent's capacity to harbor free electrons. — JSY

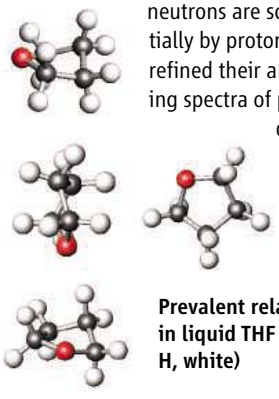

Prevalent relative orientations in liquid THF (O, red; C, black; H, white)

J. Phys. Chem. B **110**, 21023 (2006).

BIOMEDICINE

Only Skin Deep

Although smallpox was declared eradicated by the World Health Organization in 1980, the threat of bioterrorism means that future vaccination against this virus is being considered. However, for sufferers of atopic dermatitis, vaccination itself poses a problem because these individuals are prone to developing the condition eczema vaccinatum: an exacerbated skin infection that follows inoculation with the vaccinia virus used in smallpox vaccination.

In looking at why atopic dermatits patients might be more susceptible, Howell *et al.* conclude that the effective control of vaccinia virus may hinge on an antimicrobial peptide called cathelicidin LL-37, which has been shown to have direct antiviral properties in vitro. In explant studies, patient skin had reduced LL-37 expression and allowed higher levels of viral replication than skin from normal individuals. Further experiments showed that the T helper cell type 2 cytokines interleukin-4 (IL-4) and IL-13 elevated viral replication and decreased LL-37 in normal skin, with the opposite effect seen after blocking the cytokines in skin from atopic dermatitis subjects. Mice lacking a homolog of LL-37 also showed poor control of vaccinia replication. These results suggest that as well as modulating adaptive immune responses to poxviruses, the cytokine environ-

Continued on page 163

CREDITS (TOP TO BOTTOM): NASA; BOWRON *ET AL.*, *J. AM. CHEM. SOC.* **128**, 10.1021/JA058305Z (2006).

PathFinder

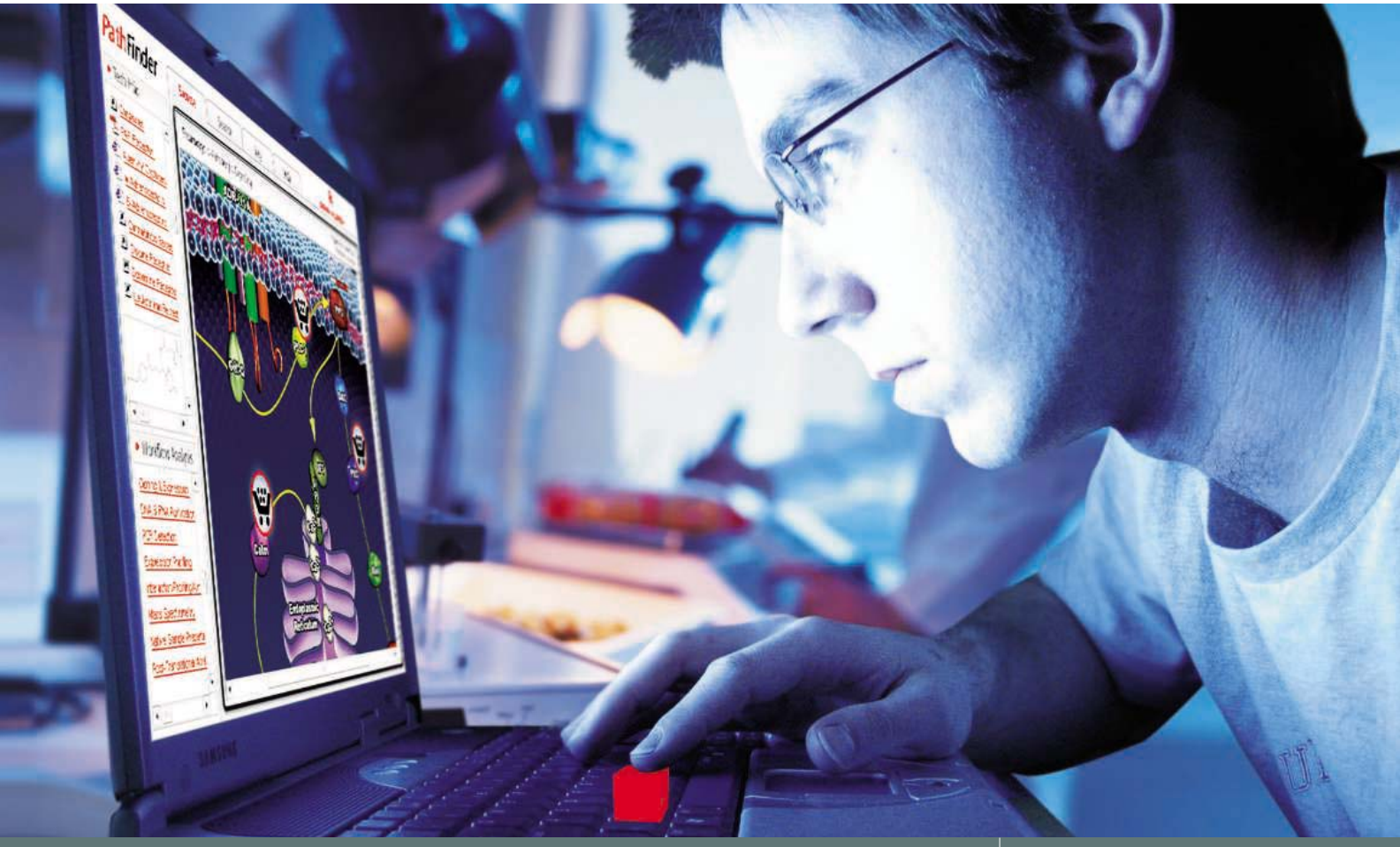

INNOVATION @ WORK

Discover Your Path to Innovation

On your path to innovation, Sigma is with you every step of the way. PathFinder is an online collection of interactive, interconnected maps showing biological signaling and metabolic pathways. For you to explore the relationships between different pathway elements, individual components are linked with related high-quality products.

You know your destination. PathFinder will get you there.

With Sigma's broad range of products, you will discover that we offer everything from antibodies and enzymes to QPCR components and RNAi tumor suppressors. A valuable resource, PathFinder provides fast and accurate information all in one place – and all linked to the important products that are key to the success of your research. In addition to products and services, you'll have immediate access to these helpful tools:

- Specific workflow analysis
- Detailed product descriptions
- In-depth technical information
- Relevant technical articles

Learn how PathFinder can help you discover your path to innovation by visiting us at:

sigma-aldrich.com/pathfinder

Accelerating Customers' success through Leadership in Life Science, High Technology and Service
SIGMA-ALDRICH CORPORATION • BOX 14508 • ST. LOUIS • MISSOURI 63178 • USA

SIGMA®

Continued from page 161

ment of the skin substantially influences early innate immune protection. — SJS

Immunity **24**, 341 (2006).

APPLIED PHYSICS

Optical Sifting

The separation and sorting of micrometer-scale particles by size, shape, optical properties, or some combination thereof is necessary in a broad range of applications, from fundamental lab-on-chip studies to the filtering of colloids for materials synthesis. The available techniques tend to rely on the precisely controlled microfluidic flow of particles through a separator.

Ricárdez-Vargas *et al.* present a simple alternative method, based on reconfigurable patterns of light, that eliminates the need for a microfluidic system. Two interfering laser beams form a periodic potential energy landscape, resembling a washboard, in the liquid layer suspending the polydisperse sample of particles. The spatial periodicity of the fringes is varied to accommodate particles of different sizes. By modulating one of the laser beams with a sawtooth signal that directs an interferometer mirror, the authors effectively vibrate the potential landscape from side to side. This jiggling motion is sufficient to separate particles that are 1 to 5 μm in diameter by size: the larger ones are driven in one direction and the smaller ones in the opposite direction. Moreover, particles of similar size but different optical refractive index (such as latex and silica) can be separated by varying the intensity of the light. — ISO

Appl. Phys. Lett. **88**, 121116 (2006).

CELL BIOLOGY

A Multistep Process of Healing

Delayed wound healing is a debilitating condition affecting millions of individuals, particularly diabetics; successful wound healing requires cell migration to cover the lesion. Skin has one layer of epidermal cells and another of dermal cells. In intact skin, cells are bathed in plasma, but after wounding, they are exposed to serum.

Bandyopadhyay *et al*. examined the effects of the switch from plasma to serum and the role of transforming growth factor–β3 (TGF-β3) on the motility of primary human skin cells. They found that human serum promotes the migration of epidermal cells and inhibits the migration of dermal cells, whereas plasma promotes dermal cell migration but not that of epidermal cells. These complementary effects are modulated by the high levels of TGF-β3 in serum and the high levels of TGF-β3 receptors on dermal cells. In contrast, plasma has only low levels of TGF-β3, and epidermal cells have low levels of TGF-β3 receptors. Depleting serum of TGF-β3 renders it plasma-like in promoting dermal cell migration. Similarly, changing the expression levels of TGF-β3 receptor switched the motile responses as predicted. Thus, the transition from plasma to serum and then back to plasma encourages the appropriate and sequential migratory responses in epidermal and dermal cell layers during healing. — SMH

J. Cell Biol. **172**, 1093 (2006).

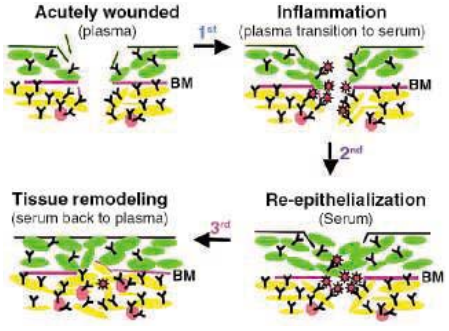

CREDIT: BANDYOPADHYAY *ET AL.*, *J. CELL BIOL.* **172**, 1093 (2006)

Skin architecture and the plasma-serum transition in wounding and healing. Epidermal cells (green), dermal cells (yellow and pink), TGF-β3 (red), TGF-β3 receptor (black).

BIOMEDICINE

A Maestro at Work

In global surveys of proteins, from those based on sequence to those based on function, mitochondria have often lost out, in part because of the small proportion (7%) of cellular proteins that localize to this organelle. Calvo *et al.* set out to remedy this gap in proteomics by integrating their analysis over eight data sets, each of which is organized along a different dimension: mitochondrial targeting sequence, protein domain, transcriptional regulatory element, yeast homology, similarity to *Rickettsia* (the nearest living relative), coexpression, mass spectrometry, and proliferation induction. These data were used to train a Bayesian classifier, the Maestro, that when challenged with the Ensembl set of 33,860 human proteins, properly predicted 71% of the known mitochondrial proteins.

On a smaller scale, Maestro was applied to a human mitochondrial disorder—hepatic mitochondrial DNA depletion, in which the loss of mitochondrial DNA leads to organ failure—that had been mapped to a region on chromosome 2 containing 150 annotated genes. Spinazzola *et al.* sequenced the highest scoring candidates and found one, *MPV17*, for which mutations segregated with affected individuals in three unrelated families. They show that the absence of this inner mitochondrial membrane protein results in deficits in mitochondrial DNA and oxidative phosphorylation in mice. — GJC

Nat. Genet. **38**, 10.1038/ng1776; 10.1038/ng1781 (2006).

www.sciencemag.org

Science

1200 New York Avenue, NW
Washington, DC 20005
Editorial: 202-326-6550, FAX 202-289-7562
News: 202-326-6500, FAX 202-371-9227

Bateman House, 82-88 Hills Road
Cambridge, UK CB2 1LQ
+44 (0) 1223 326500, FAX +44 (0) 1223 326501

Subscription Services For change of address, missing issues, new orders and renewals, and payment questions: 800-731-4939 or 202-326-6417, FAX 202-842-1065. Mailing addresses: AAAS, P.O. Box 1811, Danbury, CT 06813 or AAAS Member Services, 1200 New York Avenue, NW, Washington, DC 20005

Institutional Site Licenses please call 202-326-6755 for any questions or information

Reprints: Author Inquiries 800-635-7181
Commercial Inquiries 803-359-4578
Corrections 202-326-6501

Permissions 202-326-7074, FAX 202-682-0816

Member Benefits Bookstore: AAAS/BarnesandNoble.com bookstore www.aaas.org/bn; Car purchase discount: Subaru VIP Program 202-326-6417; Credit Card: MBNA 800-847-7378; Car Rentals: Hertz 800-654-2200 CDP#343457, Dollar 800-800-4000 #AA1115; AAAS Travels: Betchart Expeditions 800-252-4910; Life Insurance: Seabury & Smith 800-424-9883; Other Benefits: AAAS Member Services 202-326-6417 or www.aaasmember.org.

science_editors@aaas.org	(for general editorial queries)
science_letters@aaas.org	(for queries about letters)
science_reviews@aaas.org	(for returning manuscript reviews)
science_bookrevs@aaas.org	(for book review queries)

Published by the American Association for the Advancement of Science (AAAS), *Science* serves its readers as a forum for the presentation and discussion of important issues related to the advancement of science, including the presentation of minority or conflicting points of view, rather than by publishing only material on which a consensus has been reached. Accordingly, all articles published in *Science*—including editorials, news and comment, and book reviews—are signed and reflect the individual views of the authors and not official points of view adopted by the AAAS or the institutions with which the authors are affiliated.

AAAS was founded in 1848 and incorporated in 1874. Its mission is to advance science and innovation throughout the world for the benefit of all people. The goals of the association are to: foster communication among scientists, engineers and the public; enhance international cooperation in science and its applications; promote the responsible conduct and use of science and technology; foster education in science and technology for everyone; enhance the science and technology workforce and infrastructure; increase public understanding and appreciation of science and technology; and strengthen support for the science and technology enterprise.

Information for Contributors

See pages 102 and 103 of the 6 January 2006 issue or access www.sciencemag.org/feature/contribinfo/home.shtml

val´i·da´tion

It's a synonym for TaqMan® Gene Expression Assays.

Your single easiest solution
TaqMan® Gene Expression Assays deliver accurate real-time PCR results to validate your microarray discoveries. TaqMan® Assays are designed to run under universal thermal cycling conditions and are formulated into a single 20X solution—less pipetting means less chance of error.

NOW AVAILABLE
Arabidopsis and Drosophila Assays!

>600,000 assays, and all very affordable
Virtually every gene and every transcript for human, mouse, rat, Arabidopsis and Drosophila is covered—with no time, reagents or effort spent on design and optimization, you save money on every experiment.

The gold standard in quantitative gene expression analysis
TaqMan Assays provide unmatched sensitivity, specificity and reliability for true gene expression validation—you can publish your data with confidence.

To learn more about TaqMan Gene Expression Assays and how they can help you validate your research, visit **www.allgenes.com**.

Applied Biosystems

25 YEARS ADVANCING SCIENCE

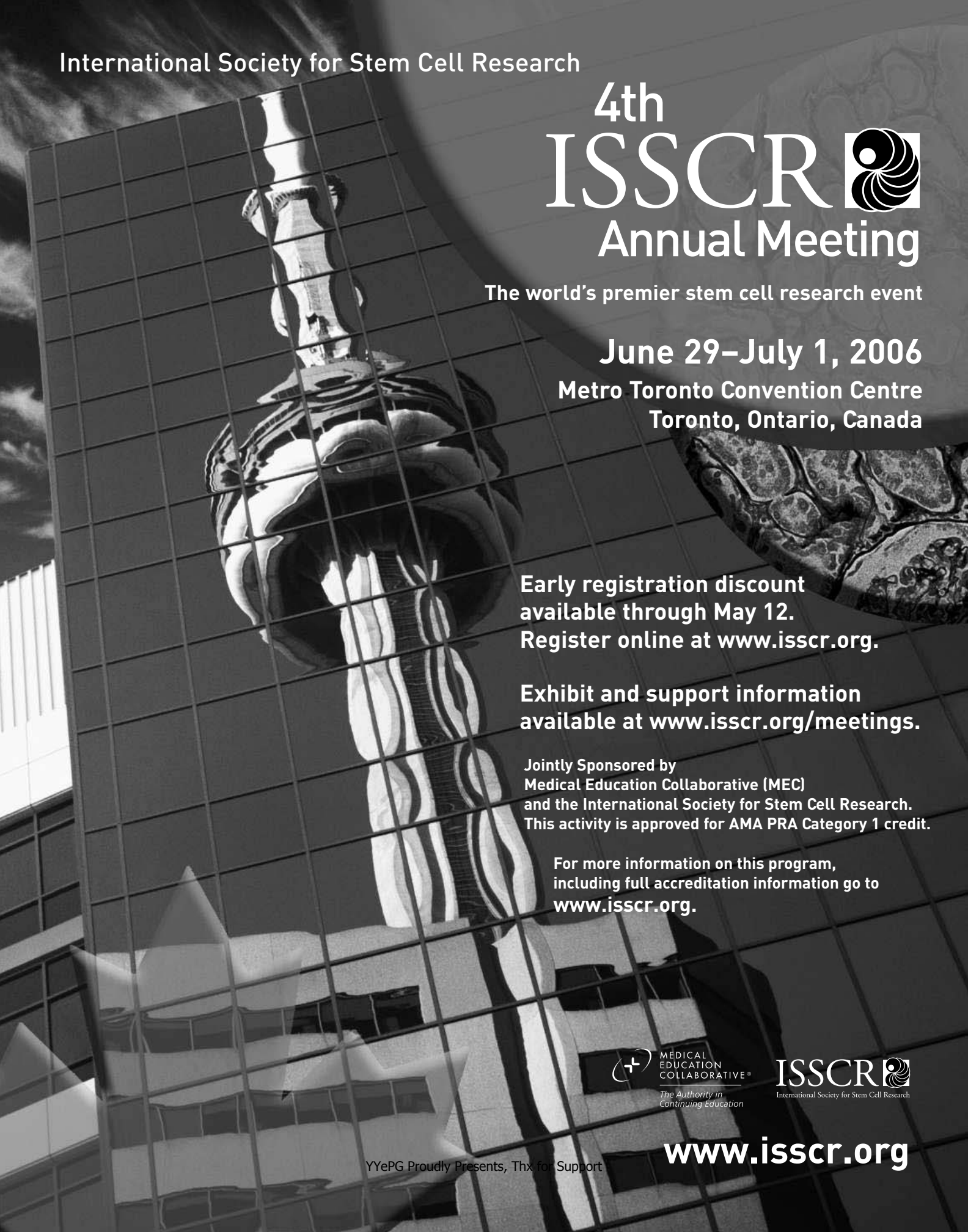
International Society for Stem Cell Research
4th
ISSCR
Annual Meeting
The world's premier stem cell research event
June 29–July 1, 2006
Metro Toronto Convention Centre
Toronto, Ontario, Canada
Early registration discount
available through May 12.
Register online at www.isscr.org.
Exhibit and support information
available at www.isscr.org/meetings.
Jointly Sponsored by
Medical Education Collaborative (MEC)
and the International Society for Stem Cell Research.
This activity is approved for AMA PRA Category 1 credit.
For more information on this program,
including full accreditation information go to
www.isscr.org.
MEDICAL
EDUCATION
COLLABORATIVE®
The Authority in
Continuing Education
ISSCR
International Society for Stem Cell Research
YYePG Proudly Presents, Thx for Support
www.isscr.org

GE & Science Prize for Young Life Scientists

Your essay may be the winner this year

GE & Science Prize for Young Life Scientists was established in 1995, and is presented by *Science*/AAAS and GE Healthcare. The prize was established to help bring science to life by recognizing outstanding PhDs from around the world and rewarding their research in the field of molecular biology.

This is your chance to gain international acclaim and recognition for yourself and your faculty, as well as to turn your scientific ideas into reality. If you were awarded your PhD in molecular biology* during 2005, describe your work in a 1,000-word essay. Then submit it for the 2006 GE & Science Prize for Young Life Scientists. Your essay will be reviewed by a panel of distinguished scientists who will select one grand prizewinner and four regional winners.

The grand prizewinner will get his or her essay published in *Science*, receive US$25,000, and be flown to the awards ceremony in Stockholm, Sweden. Entries should be received by **July 15, 2006**.

GE & Science Prize for Young Scientists: Life Science Re-imagined.

For more information on how to enter, go to www.gehealthcare.com/science

Established and presented by:

YYePG Proudly Presents, Thx for Support

* For the purpose of this prize, molecular biology is defined as "that part of biology which attempts to interpret biological events in terms of the physico-chemical properties of molecules in a cell" (McGraw-Hill Dictionary of Scientific and Technical Terms, 4th Edition).

microRNA

Labelling - Array - Bioinformatics

miRCURY™ Array

From sample to results in 24 h

- **Use less sample**
  - *Works on <1 µg total RNA*
  - *Highly sensitive LNA™ capture probes*
- **Save time**
  - *No miRNA enrichment required*
  - *1 hour labelling protocol*
- **Get instant target prediction**
  - *Free online miRNA Resource Center*

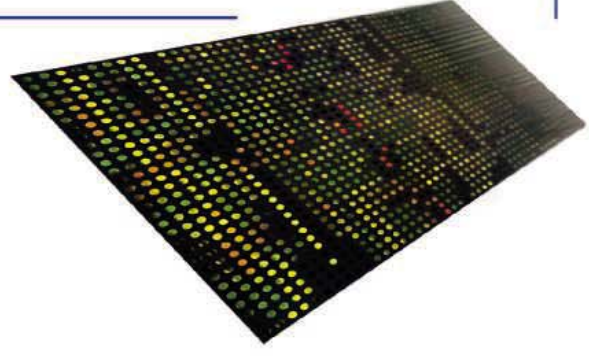

www.exiqon.com

EXIQON

THE HOME OF LNA™

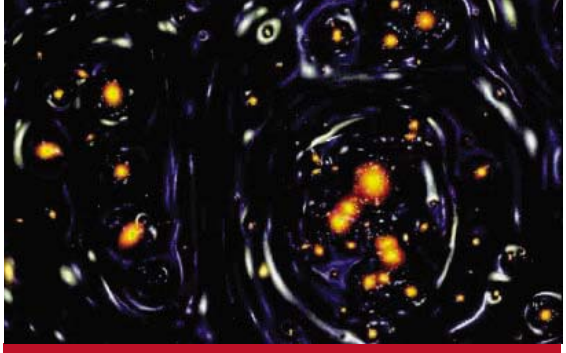

IMAGES

SPACE CINEMA

The Milky Way ensnares a neighboring galaxy, squashes it, and sucks it into orbit. A pale bubble bulges from the sun's surface and then explodes into a ragged fountain. Those are just two of the dramatic selections you can screen at the Astrophysics Visualization Archive from the American Museum of Natural History's Hayden Planetarium. Produced by researchers at various institutions, the site's 50 movies and animations show off topics in planetary science and astronomy. The ripples in this still (above), for example, illustrate how a cluster of galaxies warps passing light, a phenomenon known as gravitational lensing. >> haydenplanetarium.org/hp/vo/ava/index.html

CREDITS (TOP TO BOTTOM): TONY TYSON AND AYANA HOLLOWAY; AKHILESH PANDEY; JIM MCCARTER AND TIM SCHEDL

WEB TEXT

Elemental, My Dear Watson

Published in the 3rd century B.C.E., Euclid's *Elements* stood as the authority on geometry for more than 2000 years. In this Web edition of the classic text, math professor David Joyce of Clark University in Worcester, Massachusetts, furnishes explanatory notes and updates. The pages also feature Java applets so that readers can, say, fiddle with the dimensions of a triangle to convince themselves of Proposition 6 from Book I, which holds that if two angles in a triangle are equal, the sides opposite them are also equal. >> aleph0.clarku.edu/~djoyce/java/elements/elements.html

LINKS

Let's Get Analytical

Looking for virtual experiments to introduce students to the idea of chemical equilibrium? How about a primer on flow injection analysis? Drop by the Analytical Sciences Digital Library, edited by Cynthia Larive of the University of California, Riverside. The site houses annotated links to more than 300 sites about chemical measurements and instruments. Aimed at high school through professional levels, the offerings include class notes, tutorials, simulations, and protocols. To help teachers share ideas, the site also posts original content, such as a complete lab manual and other peer-reviewed contributions. Online forums let users discuss how to integrate the materials into class. >> www.asdlib.org

DATABASE

Blood Work

Because it ferries most of the proteins in the body, blood is a rich resource for doctors trying to diagnose disease and researchers fishing for new molecules. Tap into a comprehensive list of blood proteins at the Plasma Proteome Database from Johns Hopkins University in Baltimore, Maryland, and the Institute of Bioinformatics in Bangalore, India. Stowed here are data from the literature on the more than 7500 protein variants that enter the plasma at some time. For each version, or isoform, you'll find standard genomic information such as gene and amino acid sequences. Entries also indicate the molecule's usual cellular location, whether its gene harbors any common mutations, and whether it contributes to any diseases. You can also link to PubMed abstracts of papers that furnish gene activity measurements. >> www.plasmaproteomedatabase.org

RESOURCES

<< The Word on the Worm

High school students and cell biologists alike have consulted *WormBook* to learn about *Caenorhabditis elegans* and methods for studying it. The year-old reference serves as a companion for the genomics storehouse WormBase and provides almost 90 peer-reviewed chapters, all written by wormologists, on different aspects of nematode biology. Page through the molecular biology section to learn how the animals fix broken DNA, or visit the evolution and ecology chapters to meet some of the pathogens that make life miserable for worms. Beginners will find tips on basic procedures such as how to stain the slippery creatures to delineate cellular structures. The cool blue spots freckling this nematode (left), for example, are cell nuclei tagged with DAPI, a compound that clings to DNA. Lab veterans can bone up on more advanced techniques such as how to shut down genes. >> www.wormbook.org

Send site suggestions to >> netwatch@aaas.org
Archive: www.sciencemag.org/netwatch

VISIT US
at Analytica
Hall A3, Stand 341

IS YOUR

hot-start method giving you more questions

THAN ANSWERS?

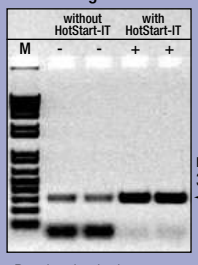

Results clearly demonstrate a shift from predominantly primer-dimers to the specific target when HotStart-IT is included in the reactions.

"Are my PCR reactions specific enough? Will my experiment be contaminated from animal-sourced antibodies? Will the DNA be damaged from extensive heat denaturation? Will my results be compromised?" If these are some of the questions you're asking yourself, try HotStart-IT.™ Developed by USB scientists, HotStart-IT is an elegant new method that doesn't use antibodies or chemically modified enzymes. Instead, HotStart-IT relies on a unique protein that binds and sequesters primers at lower temperatures which prevents mispriming and the formation of primer-dimers. When PCR is initiated, the protein is inactivated during the heat denaturation step and the primers are free to participate in the subsequent amplification cycles. The result? Higher specificity. Higher yield. And, most importantly, a higher level of confidence for you.

usb
Fueling Innovation™

For a FREE sample of new HotStart-IT, call 800.321.9322 or visit www.usbweb.com/hotstart

EDITED BY CONSTANCE HOLDEN

HWANG LOVE PERSISTS

Although the name of Woo Suk Hwang is fading fast in the public mind, die-hard supporters of the disgraced South Korean stem cell researcher are busier than ever with activities from one-person vigils to mass demonstrations. Pro-Hwang rallies involving several thousand people have taken place almost every weekend in downtown Seoul, some accompanied by performances, fundraising bazaars, and lit candles.

Now, Hwang followers have taken up a fresh cause: pressuring the Korean Broadcasting System (KBS) to screen a TV program that defends Hwang's science and accuses collaborators of having deceived him. On recent weekends, more than 1000 people—many of them members of an online community called "I Love Hwang Woo Suk"—have gathered in front of the broadcaster's offices. On 3 April, police arrested 65 who were camping out near KBS. (They were released the next day.) The station announced on 4 April that it would not run the program; the producer vowed to put it on the Internet.

Demonstrations have by no means all been peaceful. Last week, a man drove his car into the Seoul National University administration building; a month earlier, several women swore at and pulled the hair of the spokesperson of the investigative panel that accused Hwang of fraud. Others conducted mock funerals of the school's president and dove under his car. In February, a man burned himself to death, saying Hwang should be allowed to resume his research.

KBS has reported that Hwang, dismissed from his university post last month, has received job offers from two research institutes abroad.

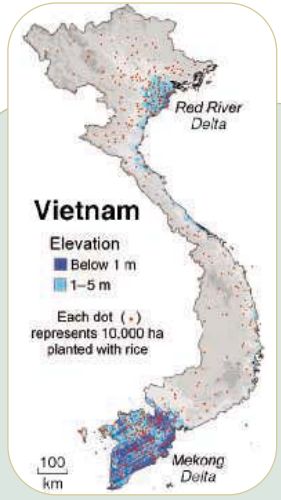

Cooked Rice

One of the more ominous results of global warming may be the inundation of rice-growing areas in Asia. Responding to this threat, the International Rice Research Institute (IRRI) in the Philippines is setting up a consortium to study the impact of global warming on the world's largest food crop.

Flooding is not the only concern. Higher temperatures threaten to harm yields and nutritional value. They will also worsen water shortages and complicate weed and pest management. A plan outlined last month calls for the establishment of three rice-growing supersites, about 20 hectares each, in the Philippines, southern China and northern India. There, scientists will experiment with crop combinations and test new cultivars for tolerance to heat, drought, ozone, and other pollutants. "When we find those tolerance genes in rice, we'll be able to make them available to other crops as well," says ecologist John Sheehy of IRRI, which is fronting $2 million toward the consortium.

DIORAMA DAYS

The habitat dioramas at the American Museum of Natural History in New York City, created during the diorama heyday of the 1920s through the 1950s, star in a new book, *Windows on Nature*. "This was an early form of virtual reality to recreate nature within walls," said author Stephen Quinn, the museum's diorama guru, at a reception last week. At right is Gunflint Lake, Minnesota, looking toward the Northern Lights at 3 a.m. on 7 December 1941—Pearl Harbor Day—as shown in the placement of Polaris and the Big Dipper. The taxidermist studied animal locomotion extensively before posing the wolves. An imaginary moon shines over the scene, picking out the tracks of the wolves and of their fleeing prey, a white-tailed deer. The diorama's lights are too diffuse to cast shadows, so the foreground artist added his own by sprinkling pigment in the mica-and–marble-dust snow.

AGING BET

A scientific competition between Jason Pontin, editor in chief of the Massachusetts Institute of Technology's (MIT's) *Technology Review*, and biogerontologist Aubrey de Grey of Cambridge University in the U.K. is heating up with the announcement last month of the panel of judges.

Pontin is challenging de Grey's prescription for extending the useful human life span by hundreds of years by treating aging as an engineering problem susceptible to damage control. Pontin calls the theory, known as SENS (Strategies for Engineered Negligible Senescence), "outrageous and unverifiable." Frustrated by scientists' reluctance to criticize it in public, he proposed a contest last July. The $20,000 prize will go to the submission that best demonstrates SENS "so wrong that it is unworthy of learned debate," says Pontin. Entries can be sent to Jason.pontin@technologyreview.com. The five-person panel includes Rodney Brooks, director of MIT's artificial intelligence lab, and genome sequencer J. Craig Venter. The winner will be announced at www.technologyreview.com on 11 July. The original prize fund of $10,000 donated by the magazine's publisher, Thus far Foundation, de Grey's organization, tossed in an additional $10,000.

CREDITS (TOP TO BOTTOM): D. YVETTE WOHN; R. J. HIJMANS/IRRI; AMNH; POPPY BERRY

Catalysts take another crack
175

Life in the slow lane
179

INTERNATIONAL EXCHANGES

Secret Pyongyang Meeting Builds Science Ties Between Two Koreas

SEOUL—In secret, some 200 researchers from South and North Korea met in the North Korean capital of Pyongyang last week to discuss ways to jumpstart scientific cooperation across the divided peninsula. The unprecedented gathering was "historic" in its scale and ambition, says attendee You-Hyun Moon, secretary general of the Korean Federation of Science and Technology Societies (KOFST) in Seoul.

Officials from the South Korean organizations that sponsored the event say they expect to catalyze joint projects in nanotechnology, information technology, environmental sciences, and biotechnology. Researchers in the south, aided by South Korea's $600,000 budget for inter-Korean science projects, must now raise money for specific goals. The long-term objective is to narrow the technological gap between North and South to make it easier to reunify Korea, says conference organizer Chan-Mo Park, president of Pohang University of Science and Technology.

Removing barriers. Chan-Mo Park (first row, second from right) and other scientists from North and South Korea met last week in hopes of healing the breach between their two countries (*inset*).

The meeting has deep symbolic value, observers say. With six-party talks over North Korea's nuclear program stalled, "the South Korean government seems interested in expanding inter-Korean civic activities to break the current deadlock," says Jekuk Chang, director of international cooperation at Dongseo University, who has worked with North Korea on sustainable development along the Tumen River. An expansion of scientific ties, adds Donald Gregg, president of the Korea Society in New York, "is a manifestation of the growing belief in South Korea that North Korea wants to become a more normal country and needs to be supported."

The Korean Conference on Science and Technology, from 3 to 8 April, came close to being called off. Scheduled for March, it was postponed after North Korea protested joint South Korea–U.S. military exercises last month. And North officials told their South counterparts that the meeting would be scuttled if word leaked to the press beforehand. (*Science* agreed to an embargo in December.) In the hours before the event, Japan, citing a recent chill in relations with North Korea, barred 10 Korean-Japanese scientists from attending, says Park. "I could not sleep, worrying that it could be canceled at the last minute," he says.

But everything went according to plan. Approximately 25 scientists from the South and an equal number of Korean scientists ▶

CLINICAL MEDICINE

Accident Prompts a Closer Look at Antibody Trials

CAMBRIDGE, U.K.—After investigating a clinical trial in London that sent six healthy volunteers into critical care last month, a U.K. agency has found no simple explanation for the accident. As a precaution, the Medicines and Healthcare Products Regulatory Agency (MHRA) announced that it will not approve any more "first-in-human" tests of antibodies like the one in this trial without first consulting "additional expert opinion."

In an interim report on 5 April, MHRA said that it could find "no deficiency" in the manufacture of the test drug, TGN1412, a proposed therapy for autoimmune diseases. Nor did it find a flaw in the way the drug was administered. The inflammation that threatened volunteers' lives, MHRA concluded, was "most likely" caused by "an unpredicted biological action," as many others had concluded (*Science*, 24 March, p. 1688).

The companies were relieved. Trial manager Parexel of Boston took comfort in the fact that the MHRA findings "support our internal review that best practices and policies and procedures were correctly followed." TeGenero, a firm in Würzburg, Germany, that developed TGN1412 and paid for the trial, felt vindicated. "We observed the highest standards in developing this drug, and … these symptoms were both unexpected and unforeseeable," the company said in a statement.

[illegible] not been released, however. MHRA and the companies have declined to give out clinical data—to protect privacy, they say. (They also refused to release the consent form.) In its report, MHRA noted that Parexel described the patients' condition as "cytokine release syndrome," which occurs when activated T cells produce a systemic inflammatory response. TGN1412 was designed to activate T cells, including a subset called regulatory T cells that help keep inflammation in check.

MHRA has asked Gordon Duff, a professor of molecular biology at Sheffield University, to head a committee that will report back in 3 months on what could be done to prevent another such accident. **–ELIOT MARSHALL**

CREDITS: CHAN-MO PARK; (INSET) KIM KYUNG-HOON/REUTERS

from China and the United States met with some 150 North Korean colleagues. After early awkwardness over language, "the ice melted once they began to talk about science," says Park. "Participants spoke freely and with an open mind," adds Moon.

Researchers zeroed in on a series of joint projects. One on software development aims to bridge the information technology gap between the two sides, says Park. North Korean scientists expressed a strong interest in alternative energy, breeding crops better suited to conditions in the North, and observing and mitigating the effects of dust storms from China. Plans are afoot to sample the flora of North Korea's uplands. In addition, South Korean scientists have proposed an ecological survey of the demilitarized zone between the nations, subject to approval by military officials from both sides.

The North Koreans emphasized that the projects must proceed on the initiative of individual scientists or nongovernmental organizations such as KOFST. Moon and others believe that ample money should be available from the South but that it will be more difficult to win approval for each project from the North Korean government. Last week's meeting included officials from a new North Korean agency, the People's Science and Technology Association, that is expected to be a major player in any North-South collaboration.

Past experience suggests that many challenges lay ahead. From 1999 to 2005, South Korea's science ministry spent $4.4 million on inter-Korean science projects, with little to show for the investment. Some projects have been delayed by export controls that limit high-tech transfers to the North. Others have languished for lack of communication. Several researchers have pointed to a common disappointment: After a connection is established, North Korean middlemen often have demanded cash up front before discussing substance. But the situation may be changing. Park says there was "hardly any money talk" in planning the meeting with his North Korean counterparts.

The most successful project by far focused on improving corn hybrids. Observers say the key to its success was the leadership of Soon-Kwon Kim of Kyungbuk University in Daegu, who has visited North Korea 27 times since 1998. "Science may be the best option to open North Korea, change North Korea, and help North Korea," says Kim.

The conference is "a meaningful starting point," says Moon, who notes that both sides will have to labor hard to get projects off the ground. A working-group meeting is planned for June in Shenyang, China, and if all goes well, a follow-up conference—"hopefully bigger than the one in Pyongyang," Park says—will be held in in 2007. The South Korean government also intends to hold bilateral talks with the North in late 2006, with the aim of launching an "Inter-Korean Science Center" in Pyongyang.

–RICHARD STONE

With reporting by Ahn Mi-Young in Seoul.

ARCHAEOLOGY

Iraq Antiquities Find Sparks Controversy

TRIESTE, ITALY—Italian researchers in Iraq claim to have stumbled on an important cache of ancient clay tablets in one of the world's oldest cities. But others dispute the claim, and Iraqi authorities say the scientists have been acting illegally.

No archaeologist has been given permission to excavate since the U.S. invasion in March 2003 toppled Saddam Hussein. But last month, Italy's National Research Council announced that it had discovered some 500 rare tablets on the surface at Eridu, a desert site in southern Iraq. The team was reconnoitering artifacts and architecture for an online virtual museum project.

According to team member Giovanni Pettinato, an Assyriologist at the University of Rome "La Sapienza," the tablets date from 2600 to 2100 B.C.E. and hold inscriptions featuring an unusually wide variety of literary, lexical, and historical content. He thinks they may have been part of a library.

But the find, which was widely publicized in recent weeks, has puzzled and outraged archaeologists in Iraq and abroad. Eridu was largely abandoned during the period in question, and Elizabeth Stone, an anthropologist at Stony Brook University in New York, says most real libraries were created much later than the dates the Italian team suggests. Stone, who was part of a U.S. team that inspected the site a month after the war began, says they did spot ancient bricks stamped with kings' names, but that such bricks are common and hardly [illegible] for support.

No tablets? Iraqis say they found only bricks such as this one at Eridu.

CREDIT: CNR

Donny George, chair of Iraq's State Board of Antiquities and Heritage, sent an irate e-mail to the Pettinato team on 6 April in search of an explanation. An Iraqi group sent recently to Eridu to investigate found no evidence of tablets, he wrote: "Why all this media propaganda ... for something that is not real?" George also scolded the Italians for unauthorized work at nearby Ur, another ancient Sumerian city, where he says they have dug out "foundation stones and door sockets" and taken them to a nearby museum. As at Eridu, he wrote, they only had permission to take photos, so their actions are "a clear violation of the Iraqi antiquities law. … This means that you may be taken to an Iraqi court."

In a statement to *Science* on 10 April, Pettinato confirmed that an inscribed foundation stone was taken to Nassiriya's museum following a judge's authorization. As for the Eridu find, he said the bricks and tablets have not been removed by the researchers.

–SUSAN BIGGIN AND ANDREW LAWLER

Competent Cells from New England Biolabs

SUPERIOR COMPETENT *E.COLI* STRAINS FOR CLONING AND PROTEIN EXPRESSION

For many years staff scientists at New England Biolabs have been using their own line of optimized chemically competent *E.coli* cells for cloning and protein expression. These strains have made all the difference to a highly demanding research and production program. Now when you are looking for a versatile cloning strain, rapid colony growth, or tight control of protein expression, you can benefit from the superior performance and high quality of these strains.

- **NEB Turbo Competent *E.coli*** **C2984H**
  Ligate, transform, plate and pick colonies in one day
- **NEB 5-alpha Competent *E.coli*** **C2991H**
  Versatile cloning strain
- **T7 Express Competent *E.coli*** **C2566H**
  High efficiency transformation and protein expression
- **T7 Express *I*^{q} Competent *E.coli*** **C2833H**
  Tight control of protein expression
- **dam^{-}/dcm^{-} Competent *E.coli*** **C2925H**
  Grow plasmids free of dam and dcm methylation

Advantages:

- Ready to transform – packaged in single-use transformation tubes (20 x 0.05 ml)
- Free of animal products
- 5 minute transformation protocols
- Supplied with outgrowth media and control DNA

	NEB Turbo	NEB 5-alpha	T7 Express	T7 Express *I*^{q}	dam^{-}/dcm^{-}
Transformation Efficiency (cfu/µg)	>10^{9}	1-3 x 10^{9}	2-6 x 10^{8}	2-6 x 10^{8}	>2 x 10^{6}
Strain	K12	K12	B	B	K12
T1 Phage Resistant	✓	✓	✓	✓	✓
Blue/White Screening	✓	✓	–	–	–
lac *I*^{q}	✓	✓	–	✓	–
Colonies Visible after 8 hours	✓	–	–	–	–
Endonuclease I Deficient	✓	✓	✓	✓	✓
Protease Deficient	–	–	✓	✓	–
Restriction Deficient	✓	✓	✓	✓	✓
M13 Phage Capable (F^{+})	✓	✓	–	✓	–
RecA Deficient	–	✓	–	–	–

Chemically Competent *E.coli* Strain Characteristics

For more information and international distribution network, please visit www.neb.com

- **New England Biolabs Inc.** 240 County Road, Ipswich, MA 01938 USA 1-800-NEB-LABS Tel. (978) 927-5054 Fax (978) 921-1350 info@neb.com
- **Canada** Tel. (800) 387-1095 info@ca.neb.com
- **Germany** Tel. 0800/246 5227 info@de.neb.com
- **UK** Tel. (0800) 318486 info@uk.neb.com
- **China** Tel. 010-82378266 beijing@neb-china.com

NEW ENGLAND BioLabs® Inc.
the leader in enzyme technology

CHEMISTRY

Catalyst Combo Offers New Route for Turning Waste Products Into Fuel

With oil prices approaching $70 a barrel and long-term oil supplies in doubt, researchers are scrambling to come up with fresh sources of transportation fuel. Now, chemists report a reaction that could squeeze fuel out of the waste from oil refineries.

When energy companies refine oil into gasoline, they break down or "crack" long-chain hydrocarbons in oil into medium-sized ones that make up an easily flowing liquid. But the process also generates many short and relatively inert hydrocarbons called alkanes that are far less useful. On page 257, researchers led by Alan Goldman, a chemist at Rutgers University in Piscataway, New Jersey, and Maurice Brookhart of the University of North Carolina (UNC), Chapel Hill, unveil a combination of two catalysts that can stitch together some of those short alkanes to make an ideal transportation fuel. Down the road, the catalysts could work the same magic on hydrocarbons from sources as diverse as renewable biomass, coal, and tar sands.

"It's a very clever idea," says Robert Bergman, a chemist at the University of California, Berkeley. Bergman notes that researchers have been developing both types of catalysts independently in recent years. But this is the first time they've been paired. The new catalysts still work too slowly for large-scale use, Bergman says, but they probably can be improved: "I don't think this will be an industrial process tomorrow. But conceptually, it is important."

Stitching short alkanes together is usually an arduous task, in part because both their carbon-atom "backbones" and the hydrogen atoms sprouting from them are attached by strong single bonds. So the Goldman and Brookhart groups began by looking for a way to convert alkanes into more-reactive compounds. The Rutgers and UNC labs had developed a class of compounds called dehydrogenation catalysts that can do that. But the compounds produced, called olefins, slow down the catalysts. The researchers hoped to solve that problem by adding a second set of catalysts that would take olefins out of the system.

The team turned to compounds that promote a reaction known as olefin metathesis. Last fall, three researchers in the United States and France won the Nobel Prize in chemistry for developing these catalysts, which are now widely used to link olefins together to make everything from plastics to pharmaceuticals. The catalysts grab on to two olefin molecules at a time and rearrange the number of carbon atoms in them. Starting with hexane, a six-carbon chain, the researchers found that they could generate a wide range of compounds, including hydrocarbons up to 18 carbons long. One catalyst combo yielded primarily 10-carbon chains, an ideal component of ultraclean diesel.

The new catalytic duo is still much too slow to compete with commercial petrochemical catalysts. Goldman suspects that part of the problem is that the olefin metathesis catalysts can break down under the 125° to 175°C temperatures in their reactor. The team is working to make them more stable at high temperatures.

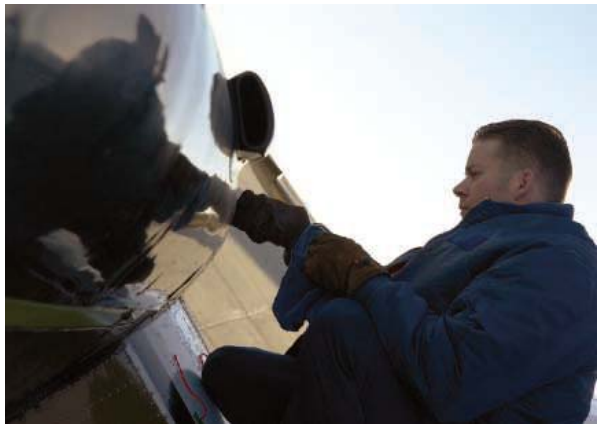

Union organizer. New catalysts that link short hydrocarbons may one day transform gasoline and diesel into renewable fuels.

CREDIT: PHOTOS.COM

Another "especially interesting" path forward could be to use the new catalysts to convert agricultural waste into liquid fuels, says James Dumesic, a chemist at the University of Wisconsin, Madison. Two years ago, Dumesic's group came up with a catalytic duo that can transform a derivative of glucose—a chief component of plant matter—into hexane. The new work shows that it's possible to convert hexane into the hydrocarbons in gasoline and diesel. If the two processes can be put together and made commercially viable, the combination could offer energy companies a way to produce gasoline from plant wastes. That could transform gasoline into a form of renewable energy and dramatically change the world's long-term energy outlook.

–ROBERT F. SERVICE

Data From Pesticide Tests OK'd

The Environmental Protection Agency (EPA) can use nine studies in which humans were intentionally dosed with pesticides in its decisions this year about reregulating the chemicals, a new advisory board has concluded. Activists have complained for years about the ethics of intentional-dosing studies (*Science*, 1 January 1999, p. 18), and in 2004, a report by a National Academies' National Research Council panel called for the review board.

Meeting last week for the first time, EPA's Human Studies Review Board was charged by the agency with examining 11 studies for scientific merit and whether there was "clear and convincing evidence that the research was intended to seriously harm participants or [purposely] failed to obtain informed consent." The 16-member group found no such flaws but rejected two studies as scientifically inadequate; it will meet again in May and June to review more studies.

Jennifer Sass of the Natural Resources Defense Council in Washington, D.C., says all 11 studies have some ethical flaws, such as possibly harming subjects, and shouldn't be used by the agency. But she's pleased that the board will use a higher standard when it vets protocols for proposed research.

–ERIK STOKSTAD

Venus Rendezvous Succeeds

European Space Agency officials breathed a sigh of relief this week after their Venus Express spacecraft entered a highly elliptical orbit around Venus. Similar although riskier maneuvers have failed at Mars, and ground controllers at the European Space Operations Centre in Darmstadt, Germany, were relieved by the 10 April milestone. The 50-minute rocket burn that put the craft into orbit around Earth's planetary neighbor was considered the most dangerous part of the mission after the launch, 5 months ago.

The $260 million spacecraft will conduct climate and atmospheric studies of the planet's surface in unprecedented detail using ultraviolet and visible light, radar, and infrared cameras. Magnetometers and spectrometers will study the effects of solar winds on the atmosphere.

Everyone is "very pleased," says Fred Taylor of the University of Oxford, U.K., one of the founders of the mission. The first set of data from Venus Express is expected in about a month.

–GOVERT SCHILLING AND LAURA BLACKBURN

NUCLEAR POWER

DOE Asked to Fill in the Blanks on Fuel Recycling Research Plan

The Bush Administration's plans for a grand research program aimed at eventually recycling nuclear waste aren't ready for prime time, legislators said at a pair of hearings last week. But they seem willing to support at least most of the $250 million price tag for next year.

Dubbed the Global Nuclear Energy Partnership (GNEP), the program was launched in February as a high-tech effort to expand nuclear power globally. At its technical core is a move to reprocess nuclear waste to extract fuel to be burned in so-called fast reactors. But although scientists are hashing out the particulars—researchers from nine Department of Energy (DOE) national laboratories met last week in Salt Lake City, Utah, to put together a research plan—the lack of detail is frustrating lawmakers.

Hurry up and waste. The Energy Department's new research program is affected by prolonged delays in the Yucca Mountain repository.

"Why doesn't Congress know more about [GNEP]?" asked Michael Simpson (R–ID) at a 5 April meeting of the House Appropriations Energy and Water subcommittee, which funds DOE's civilian research programs. (The next day, a panel of the House Science Committee held another hearing on the project.) Simpson supports GNEP, but he's unhappy that DOE Assistant Secretary for Nuclear Energy Dennis Spurgeon couldn't provide a road map for the project that includes estimates of foreign contributions and full costs. Outside scientists are as flummoxed as policymakers. "I'm not sure anybody really knows what GNEP is," says nuclear engineer and longtime DOE grantee Denis Beller of the University of Nevada, Las Vegas.

Part of the rationale for GNEP is to reduce the volume of waste that will require long-term storage. The government is responsible for disposal of some 55,000 metric tons of spent fuel rods at U.S. sites, but its designated repository—at Yucca Mountain in Nevada—isn't expected to open before 2020 and is expected to reach its legal capacity by then.

Subcommittee Chair David Hobson (R–OH) added nonbinding language to a spending bill last year instructing DOE to develop chemical reprocessing facilities that would extract fuel to be used in current U.S. reactors—a move DOE says would reduce the volume of wastes destined for Yucca by an estimated 10%. Now Hobson wants any reprocessing facilities DOE builds to offer storage for spent fuel rods. But DOE says it cannot legally hold the waste in such facilities. And DOE officials argue that burning recycled fuel in fast reactors would increase Yucca's capacity by at least sixfold.

GNEP's opponents, such as Tom Cochran of the Natural Resources Defense Council in Washington, D.C., say the dismal record of fast reactors abroad—the Monju reactor in Japan ▶

CREDIT: OCRWM/DOE

PEER REVIEW

Australia's Proposed U.K.-Style Merit Ranking Stirs Debate

MELBOURNE—Australia is considering a radical overhaul of the way it allocates funds to universities and research institutions. But some academics worry that the changes, proposed in March by an expert panel, could be costly without significantly improving basic research.

The so-called Research Quality Framework (RQF) would rate all publicly funded research institutions and award block grants based on a new formula. Critics note that the United Kingdom, which pioneered a similar system, is now debating whether to scrap it because it is seen as unduly complex (*Science*, 31 March, p. 1848). The new Australian system could go into effect as early as 2008.

There's no doubt that RQF would have "dramatic effects" on universities, says Bradley Smith, a spokesperson for the Federation of Australian Scientific and Technological Societies (FASTS), which supports the concept of the framework but worries that its methods may be flawed. "It will drive the stronger groups and destroy the weak ones," says Smith. Adds Judith Whitworth, director of the John Curtin School of Medical Research in Canberra: "We all agree that scarce resources need to be focused and that quality needs to be measured," but "the devil lies in the detail."

Some $614 million of the Australian government's current $4.4 billion investment on research comes in the form of block grants to 38 universities and research institutes. In 2004, then–Education Minister Brendan Nelson said it was time to develop a better rationale for allocating the money, which critics say is spread too thin. Physicist Gareth Roberts, president of Wolfson College at the University of Oxford and architect of the U.K.'s Research Assessment Exercise, led an advisory group that produced the RQF.

Government block grants are now awarded based on measures of productivity such as the number of publications and Ph.D. students completing degrees at an institution. The proposed RQF would use a system of peer review to assess research quality and add another parameter, namely, a count of social, environmental, and economic dividends. But some scientists worry that too much emphasis on impact could favor applied research at the expense of academic research.

There is also concern that the framework plan will impose a corporate, target-oriented culture onto the academic research sector. "We cannot set targets. We cannot say that next year we are going to produce 10 papers, and we are going to get *x* amount of funding from the outside," says Patricia Vickers-Rich of Monash University's School of Geosciences. Virginia Walsh, executive director of the Group of Eight Universities (Australia's major universities), says, "There's no way we'd do justice to all the disciplines" if the government were to adopt the panel's proposal to have a dozen peer-review committees when the U.K. system used 67.

An advisory group headed by Australia's chief scientist Jim Peacock is expected to report by June on the weighting factors and other issues.

–ELIZABETH FINKEL

Elizabeth Finkel is a writer in Melbourne.

has yet to restart after a 1995 sodium fire—should be a lesson for DOE. And IBM physicist Richard Garwin, who supports an expansion of nuclear energy, told Science Committee Energy Subcommittee Chair Judy Biggert (R–IL) that DOE's plan to do detailed systems and cost analysis in parallel with GNEP was akin to "driving without a map." Garwin also critiqued DOE's initial focus on the reprocessing of waste; he says showing that a fast reactor can be economical and safe is more important.

GNEP technical manager David Hill says an outline of the research plan hashed out at the Salt Lake City meeting should be available soon. And DOE manager Shane Johnson says the department would consider Garwin's advice to save money by scaling back recycling performance goals "if upon further investigation, that was [found to be] the correct form of action." Such flexibility is exactly what Congress hopes to see as it mulls DOE's latest project.

–ELI KINTISCH

U.S. IMMIGRATION

Congress Weighs Steps to Retain Foreign Talent

Fu Chiu spent months looking for a job as a technology transfer specialist with a U.S. biotech company after he received his Ph.D. in molecular biology from the University of Illinois, Urbana-Champaign. But the native of China couldn't hang around the United States indefinitely, because his student visa expired 1 year after his 2003 graduation. So Chiu crossed the Atlantic to work for a U.K. government–funded organization, then headed home to China to join a biotech firm in Shenzhen that specializes in gene therapy.

U.S. academic and business leaders have lobbied hard to include reforms in several pending bills that would make it easier for highly skilled foreigners like Chiu to stay. Such reforms are needed, they argue, if the country is to compete effectively in today's global economy. Last week, they lost their best chance to date to see them enacted, however, when a bipartisan immigration reform bill stalled in the U.S. Senate. But supporters haven't abandoned hope: They expect the issue to be back on the table when Congress returns later this month.

One key provision in the failed immigration bill would have granted automatic permanent residency, or "green cards," to foreign students like Chiu who find a job in their field. Other measures include increasing the cap on H-1B visas—temporary visas for skilled workers—from the existing 65,000 to 115,000 annually, with a built-in provision to add 20% if the quota was filled in the preceding year, exempting spouses and minor children of foreign workers from this cap, and increasing the annual employment-based green card cap from 140,000 to 290,000 (see table, above). (Under current rules, foreign workers need their employers to sponsor them for a green card. The entire process can take several years.)

"There's a growing realization that this issue is not about immigration but about competitiveness," says Bill Bates, vice president for government affairs at the Washington, D.C.–based Council on Competitiveness. "The prospects for some of these measures going through are definitely bright." A cluster of bills introduced in January by senators Lamar Alexander (R–TN) and Jeff Bingaman (D–NM) (*Science*, 3 February, p. 594), and an upcoming measure sponsored by Senator John Cornyn (R–TX), may provide a home for such measures.

There is sharp disagreement on what those measures would do to high-tech employment, however. Ira Mehlman of the Federation for American Immigration Reform (FAIR) in Washington, D.C., which opposes the measures, says increasing high-tech immigration would dampen interest by native-born Americans in science and engineering by increasing the competition. That, in turn, depresses wages, he believes.

But Ralph Wyndrum Jr., president of the Institute of Electronic and Electrical Engineers-USA, thinks permanent residency will free well-trained foreign students from the limitations imposed by an H-1B visa and bolster salaries. "These people will be able to go around shopping for the best jobs," Wyndrum says. "The free market shall prevail."

–YUDHIJIT BHATTACHARJEE

Scientific Welcome Mat

The stalled Senate agreement on immigration contains these provisions to attract and retain scientific talent:

- Foreign students graduating from U.S. institutions with advanced science and engineering degrees would be eligible for permanent residency and exempt from a cap on H-1B visas.
- The annual number of H-1B visas issued would rise from 65,000 to 115,000.
- The annual number of employment-based green cards issued would rise from 140,000 to 290,000.

Apes to Retire in Style

AMSTERDAM—Eighty-one chimps living at Europe's last remaining ape colony for biomedical research will retire later this year—but not under the Spanish sun, as previously planned.

Last week, the Dutch government said that 28 HIV-infected animals from the Biomedical Primate Research Centre in Rijswijk will go to a facility operated by AAP, a Dutch foundation, as planned. But the government canceled a plan to house 33 healthy chimps in a proposed AAP resort near the Spanish coast after the idea met with local opposition (*Science*, 27 August 2004, p. 1227). Instead, they will go to a "safari park" in Hilvarenbeek, the Netherlands. The remaining 20 healthy animals will go to a zoo in Amersfoort.

–MARTIN ENSERINK

Stalking Indian Ocean Illness

PARIS—Responding to a major outbreak of the crippling chikungunya virus on the island of La Réunion (*Science*, 24 February, p. 1085), the French government has announced the creation of a new research and surveillance center for emerging diseases in the Indian Ocean. France has pledged a start-up budget of $2.7 million, but details are still sketchy. "My dream is that it will be open for researchers from around the world," says Antoine Flahault, who coordinates France's chikungunya research program. With an international scope and sufficient funding, the center could fill an important need, says epidemiologist Mark Wilson of the University of Michigan, Ann Arbor.

–MARTIN ENSERINK

Pittsburgh Goes Italian

The University of Pittsburgh Medical Center (UPMC) has joined the Italian government and its National Research Council to build a $398 million Biomedical Research and Biotechnology Center in Palermo, Sicily. The center will host as many as 600 researchers focused on medical imaging, regenerative medicine, vaccine development, and computational biology. It will expand on the connections UPMC has established with Palermo through its ISMETT organ-transplant hospital, founded in 1997.

ISMETT Director General Bruno Gridelli says the center, funded by Italy and managed by UPMC, will provide opportunities that today are only available abroad. "We will have the control we need to make it work," says UPMC medical school dean Arthur Levine. The new research center will begin hiring this year, and the building is expected to be completed in 2011.

–JACOPO PASOTTI

DEVELOPMENT

Two Unexpected Players Add Twists To Liver's Comeback Story

If only other organs had the regenerative power of the liver. Surgeons can remove more than two-thirds of the organ, and within weeks, it will regrow to its previous size. Scientists so far have found at least a dozen signals that seem to play a role in such regeneration, and now two groups have identified two new and unexpected players.

On page 233, scientists reveal that the concentrations of bile acids in the liver help control both the start and end of liver regeneration. And last week, a different research team published evidence that the neurotransmitter serotonin also governs the liver's regrowth (*Science*, 7 April, p. 104).

Serotonin is best known for its role in the brain; the family of antidepressants that includes Prozac works in part by influencing the brain's serotonin levels. But serotonin can also prompt cell division. Pierre-Alain Clavien of the University Hospital of Zurich, Switzerland, and his colleagues showed that knockout mice lacking the chemical had drastically reduced ability to regenerate their livers in response to partial surgical removal. That capacity was restored when the scientists gave the animals a serotonin precursor. A compound that triggers the serotonin receptor likewise resurrected the animals' regenerative powers. Clavien and his colleagues suggest that such molecules might speed regeneration in liver transplant patients.

The unexpected discovery that bile acids influence liver regeneration may provide as much insight into how the process ends as how it starts. These acids seem to tell the body when the organ is big enough to do its job. A healthy liver removes bile acids from the blood. The acids help digest fats, but they are toxic outside the digestive system. David Moore of Baylor College of Medicine in Houston, Texas, and his colleagues found that when mice ate diets rich in the bile acid cholic acid, their livers regenerated faster than did those of control mice following surgical removal of most of the organ. Mice fed a diet that lowers bile acid levels did not regenerate their livers as quickly as controls did.

The effect seems to involve the bile acid receptor called FXR; mice lacking FXR took much longer to begin regenerating their livers. Moore and his colleagues propose that FXR keeps tabs on the level of bile acids passing through the liver. If the liver isn't keeping up, the molecular sensor triggers the proliferation of new hepatocytes until the organ can handle the bile acid load, he says.

Both finds highlight that the liver has overlapping systems that can trigger regeneration in response to a variety of problems, says George Michalopolous of the University of Pittsburgh Medical Center in Pennsylvania. "There's a tremendous amount of redudancy," he says. Liver regeneration is "like a car with 20 cylinders. You crank up the engine, all 20 cylinders fire. These are cylinders 21 and 22." **–GRETCHEN VOGEL**

PALEOANTHROPOLOGY

Fossils Clinch Identity of Lucy's Ancestor

The meter-tall australopithecine named Lucy has reigned for 30 years as the world's most famous human ancestor. But who were Lucy's ancestors? A series of fossils from a stack of sediments more than a kilometer high in northeastern Ethiopia now helps prove what many researchers had suspected: that Lucy's species, *Australopithecus afarensis*, evolved from a 4-million-year-old upright hominid called *Australopithecus anamensis*.

The discoverers of the new fossils, who present their finds in this week's issue of *Nature*, also propose that an even older hominid called *Ardipithecus*, whose bones were found closer to the base of the rock layers, was the most likely ancestor of *A. anamensis* and all later australopithecines. Thus, they claim a three-part evolutionary series of human ancestors in a single river valley.

Many researchers are now convinced that *A. anamensis* was the long-sought ancestor of *A. afarensis*, which ranged across east Africa from 3 million to 3.6 million years ago. "It's clear you can see the trend over time from *A. anamensis* to *A. afarensis*," says paleontologist Alan Walker of Pennsylvania State University in State College. But he and others aren't sure about *Ardipithecus* as direct ancestor of australopithecines. "It has been postulated but not demonstrated," says paleoanthropologist William Kimbel of Arizona State University in Tempe.

Researchers from the international Middle Awash research project, co-led by Tim White of the University of California, Berkeley, found fossils of the three species in the Middle Awash valley over the past 12 years. In one area, they found the newly dusty trees at *anamensis* fossils, including jaws, teeth, a finger, a toe, and a thighbone, directly below a younger rock layer containing *A. afarensis* fossils. The fossils confirm that *A. anamensis*'s teeth and jaws were more primitive than those of *A. afarensis*, but the thighbone, the first from this species, was more like Lucy's species, suggesting upright walking, says White.

That fits with Kimbel's independent analysis of fossils from Kenya and Tanzania, to be published this spring in the *Journal of Human Evolution*. His team found that key skull and teeth traits support *A. anamensis* as *A. afarensis*'s ancestor.

At another site, the Middle Awash team found a jawbone of *A. anamensis* just 80 meters above a 4.4-million-year-old layer with fossils of *Ardipithecus ramidus*. Changes in the teeth and skull, such as canines that get smaller, suggest that the two may have been members of a single lineage that evolved between 4.4 million and 4.2 million years ago, rather than separate lineages. However, "testing these hypotheses will require additional fossils from other sites," admits White.

Others agree. "I don't think that the published evidence shows [the link between *A. ramidus* and *A. anamensis*] very convincingly," says zoologist Meave Leakey of the National Museums of Kenya. Stay tuned: The discovery last year of another 4-million-year-old skeleton and more fossils of *Ardipithecus* under study could provide the missing data. **–ANN GIBBONS**

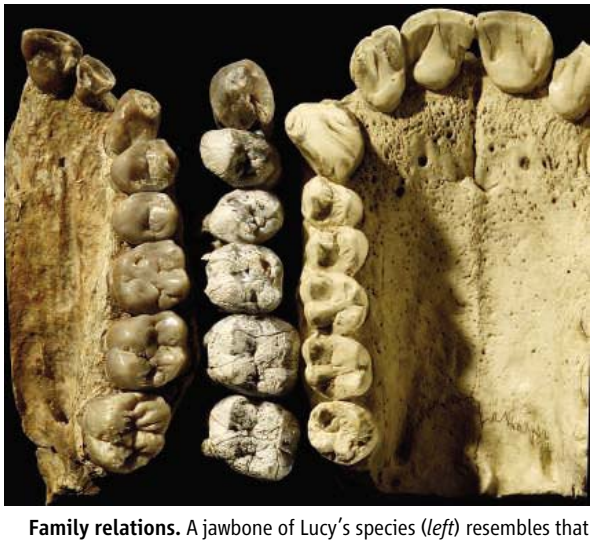

Family relations. A jawbone of Lucy's species (*left*) resembles that of its ancestor, *Australopithecus anamensis* (*center*), compared to a modern chimp (*right*).

CREDIT: 2005 DAVID L. BRILL/BRILL ATLANTA

Muddy haul. Microbes in deep-sea sediment cores lived very slowly.

Life Slow Enough to Live on Radioactivity

Life is slow at Earth's extremes—buried for millions of years beneath kilometers of cold ocean mud, say, or sweating out the heat in ancient rock 3 kilometers down in South Africa. Really, really slow. So slow, a new measurement suggests, that a substantial number of subsurface microbes might be surviving solely by consuming a product of feeble radioactive decay lingering from before Earth's formation. Even life on Mars, if any exists, could be hanging on beneath the martian surface living off such radiolysis.

At the meeting, geochemists Arthur Spivack, Guizhi Wang, and Steven D'Hondt of the University of Rhode Island (URI), Narragansett, explained how they used variations in the chemistry of 400 meters of cored sediment to gauge the pace of life beneath the sea floor of the eastern equatorial Pacific. Microbes there make a living by oxidizing organic matter—which was buried up to 12 million years ago—while chemically reducing sulfate, iron, and manganese. By tracking the changing concentrations of the carbon dioxide produced and the sulfate, iron, and manganese consumed with increasing depth beneath the sea floor, the URI group could calculate the rate of those reactions and thus the rate at which microbes could extract energy from them. Dividing by the number of cells seen in the sediment yields the rate at which a cell uses energy.

In the old and cold muds of the eastern equatorial Pacific, microbes "are utilizing very, very low levels of maintenance energy," said Spivack. The rate comes to 2.8×10^{-16} kilojoules per cell per year, or 10,000 times lower than energy consumption in a slow-living bacterial culture in the laboratory. At that rate, sediment microbes are certainly not "thriving," as the headlines often have it. They may not be doing any more than repairing the inevitable molecular decay due to radiation damage and the passage of time.

Such slow-mo microbes may point the way to creatures that live entirely "off the grid," independent of the energy the sun supplies by means of photosynthesis. One way to live sun-free would be to consume the hydrogen gas generated when rock's natural store of radioactive uranium, thorium, and potassium decays and splits water molecules (*Science*, 28 February 2003, p. 1307). The URI group calculates that marine sediment in another core has enough natural radioactivity to "feed" 10% of the microbes there. In mid-ocean sediments, which have much less organic matter, radiolysis may be the dominant energy source, they say. And a Mars soil, they calculate, could support a respectable 10,000 cells per cubic centimeter on radiolysis alone.

To astrobiologist Tori Hoehler of NASA's Ames Research Center in Mountain View, California, the vanishingly slow pace of life in deep-sea sediments is a vivid reminder that "there are energetic boundary conditions to the survival of life." It's all well and good to find signs of past water on Mars, he says, as at the Opportunity rover landing site, but NASA needs to "follow the energy" as well. As the new sediment work shows, that could be a far greater challenge.

–RICHARD A. KERR

Diversity Before Life

In the beginning, Darwin posited a "warm little pond" where life's chemical starting materials and then life itself first appeared. But lately, prebiotic chemists have favored sea-floor hot springs as the site where simple carbon compounds merged into the complex ones needed to begin life. At the meeting, prebiotic chemist George Cody warned that deep-sea hot springs couldn't have produced all of the necessary components. Instead, the final assembly of molecules leading to life must have happened somewhere between deep-sea vents, warm little ponds, and any number of other chemical stew pots.

Cody, who works at the Carnegie Institution of Washington's Geophysical Laboratory in Washington, D.C., has been a central player in the search for high-temperature and high-pressure reactions that produce the basic biochemistry of life. He's had some success producing carboxylic acids, key intermediates in sequences of biochemical reactions that extract energy from sugars. Metal sulfides commonly found in hot spring rocks make particularly good catalysts for such reactions, he found. And in other hydrothermal reactions, adding ammonia to the mix results in a variety of amino acids. But it takes unfamiliar starting components to get the metabolic intermediates, and the amino acids produced are not usually the ones life prefers. Worst of all, important sugars and nucleobases fall apart under hydrothermal conditions.

Submarine hot springs no doubt could have played a role in brewing the primordial soup that gave rise to life, Cody said, but other environments must have contributed too. "If I said it all happened in hydrothermal vents, that won't move this field ahead," he says. "Thinking more globally could open up something." Perhaps the real action came along continental margins, he said. There, prebiotic compounds from deep-sea vents rose to meet drainage from the land's warm little ponds and fallout from atmospheric reactions triggered by lightning and sunlight. "This is a very good approach, quite novel," says organic chemist Vera Kolb of the University of Wisconsin, Parkside. "People get bogged down with the particular conditions they're studying, but he wasn't pushing his own work."

Such a "global origin" scenario, however, would make it less likely that life arose elsewhere in the solar system, Cody says. The subsurface oceans on the icy moons Europa and Enceladus might not have offered the required diversity of environments. And Mars may not have had even a short-lived ocean.

–R. A. K.

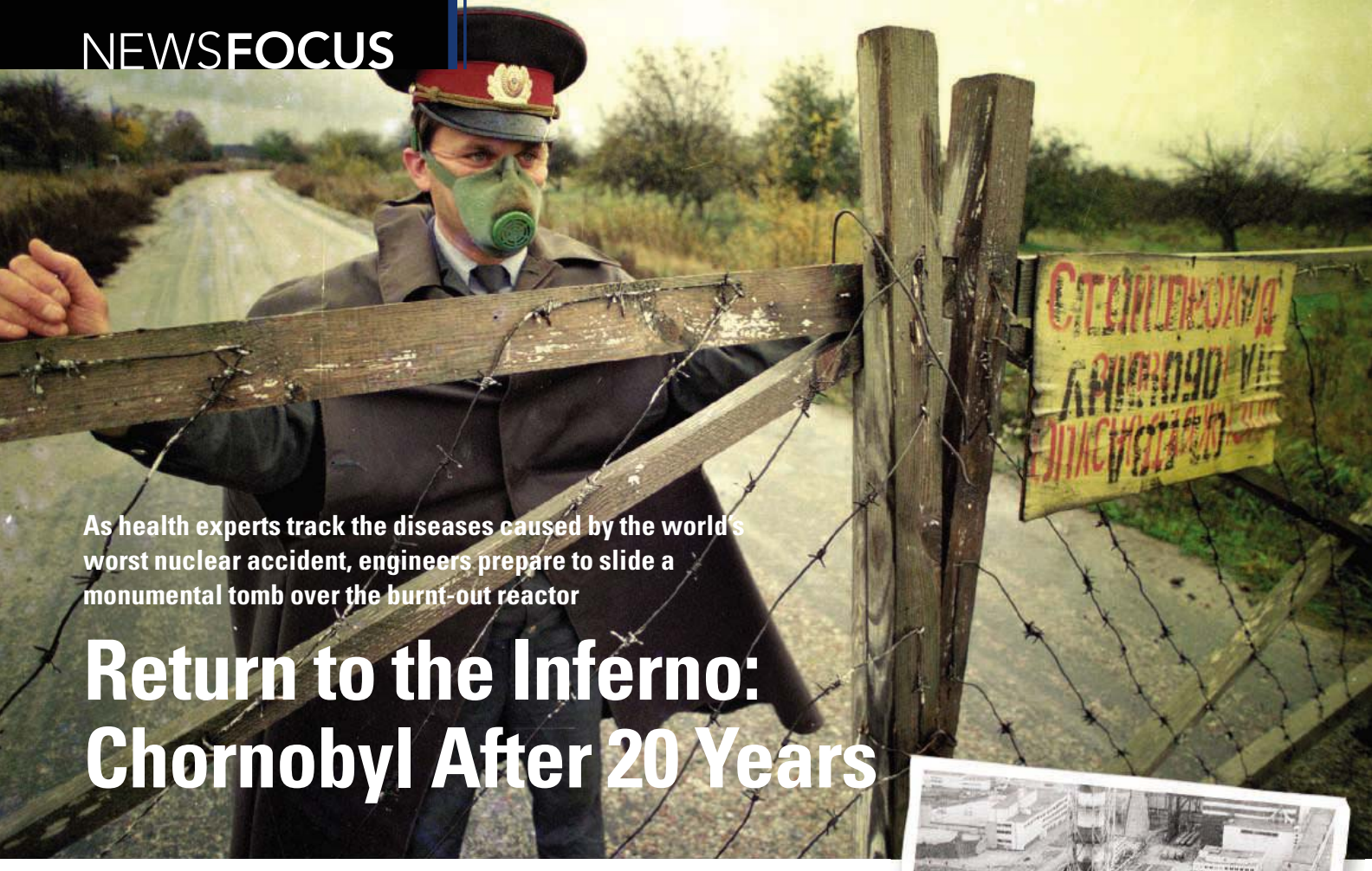

As health experts track the diseases caused by the world's worst nuclear accident, engineers prepare to slide a monumental tomb over the burnt-out reactor

Return to the Inferno: Chornobyl After 20 Years

HOMYEL, BELARUS, AND CHORNOBYL, UKRAINE—In a cavernous marketplace, radiologist Alla Oplachikova strides past stalls with slabs of beef and pork dangling from hooks, past canvas sacks brimming with grains and dried fruits, and makes a beeline for the produce section of the Central Bazaar in Homyel.* She stops at one vendor, flashes her badge, and picks a handful of mushrooms. "For analysis," she tells the seller, then whisks the samples to a room at the back of the hall.

Every morning, Oplachikova's dawn patrol swings into action. As trucks roll into the bazaar, her team scans goods with a Geiger counter. "We measure every shipment," she says. For good reason: 20 years ago this month, the Homyel region was drenched with radioactivity from an explosion at the nearby Chornobyl nuclear power plant. The aftereffects of the infamous disaster are still being felt here in southern Belarus, where levels of two radionuclides—cesium-137 and strontium-90—will remain high, in patches, for decades.

The threat of contamination keeps the Homyel rad-rangers on their toes. Oplachikova puts some mushrooms in a gray, lead-lined brick box wired to a radiometer and eyes the needle. A feeble tremor indicates that it's safe to eat. A few years earlier, she says, a fillet of wild boar drove the needle off the scale. "It's dangerous to handle that kind of sample," Oplachikova says. "But we get paid extra." Impounded food is buried, and tainted milk is diluted to acceptable levels of radioactivity and sold to consumers, she says. In recent months, her team has flagged only a few risky shipments. "The trend is getting better," she says.

As the years have passed since the world's worst nuclear accident spewed fallout across Europe, the hardest-hit regions in Belarus, Russia, and Ukraine are slowly healing. In Belarus, fields are fertilized and limed to expel or bind radionuclides before sowing crops. Elderly evacuees have reclaimed their homes. And later this year, work will begin on a massive structure to isolate Chornobyl's destroyed reactor from the environment, permitting safe dismantlement and disposal of its toxic innards.

But scars run deep among the survivors. For some, Chornobyl was a death sentence: According to a U.N. report issued last September, an estimated 4000 people are expected to succumb to fallout-induced cancers, in line with predictions from studies of the survivors of the atomic bombs dropped on Hiroshima and Nagasaki (*Science*, 9 September 2005, p. 1663). Some experts have challenged that figure, contending that the cancer toll could be much higher.

"There are many uncertainties. Nobody can say the exact number," says Shunichi Yamashita, a radiation expert at the World Health Organization (WHO) who has studied Chornobyl victims for 15 years and affirms that the effects of low-dose radiation are diabolically hard to pin down. However, Yamashita believes the ultimate figure will be closer to the U.N. figure.

For many victims, life goes on—but with complications. Studies point to an elevated incidence of cataracts; anxiety and depression, linked to brooding over an invisible threat, are rampant. Some scientists in Belarus claim to

CREDITS: IGOR KOSTIN/CORBIS; (INSET) AP PHOTO

* Post-Soviet spellings are used throughout: Homyel (formerly Gomel), Chornobyl (Chernobyl), and Kyiv (Kiev).

No-go zone. A Ukrainian officer controls access to villages near Chornobyl after an explosion ripped apart the nuclear power plant in 1986.

have detected a rise in birth defects since the accident, although the general consensus is that this is an artifact of better reporting. Still, many agree that the story of Chornobyl-inflicted diseases is still unfolding. Says oncologist Alexey Okeanov of the International Sakharov Environmental University in Minsk, "Belarus is one big laboratory."

First wave

In a grassy field, row upon ragged row of derelict vehicles used in the emergency are decaying in the Exclusion Zone, a Luxembourg-sized area around Chornobyl that's deemed uninhabitable for people of reproductive age or younger. The scene attests to the scale of the unparalleled operation 2 decades ago to stifle the burning nuclear reactor. From a 3-meter-tall viewing platform, you can see the motley assemblage of 2000 trucks, fire engines, armored bulldozers, and hulking gray military helicopters parked in front of a pine forest that's too dangerous to enter without protective gear.

The fatal events are now part of nuclear lore. In the early morning of 26 April 1986, Chornobyl's number four reactor exploded after a botched safety test, killing two technicians and exposing 28 other workers and firemen who raced to the scene that night to a lethal blast of radiation. The reactor burned for 10 days, disgorging 400 times the radioactivity released by the Hiroshima bomb.

In a secret operation, the Soviet military dispatched hundreds of thousands of "liquidators"—mainly soldiers, scientists, and engineers—to smother the fire in the reactor core, consolidate radioactive waste in several hundred dumps in the Exclusion Zone, and build a concrete-and-steel sarcophagus, now known as "the shelter," over the destroyed reactor building. Each morning, as liquidators boarded buses from camps on territory deemed clean, they received a calming (and as many Soviet scientists believed, protective) glass of red wine, says Galina Lyatusova, a physician who headed a first aid station for liquidators in 1986 and now monitors the health of plant workers and scientists in Chornobyl village.

Of the 600,000 registered liquidators, about a third were deployed in the first months after the accident, the high-risk period. "We could see the influence of radiation on their blood," Lyatusova recalls. "Their white blood cells were dropping. If the counts got too low, we wouldn't let them go to work the next day. The sickest people tried to go home. I don't know if they made it." Only in the spring of 1988 did the Soviet government declassify information on Chornobyl research and cleanup operations.

A sheltering sky. Work is about to start on a steel arch—the world's biggest movable structure—to cover the disintegrating shelter now enclosing the ruins.

To find out precisely how much radiation the liquidators absorbed, Vadim Chumak of the Scientific Center of Radiation Medicine in Kyiv and his colleagues in the mid-1990s began exploiting a reliable chronicle of dose: teeth. Their technique measures the warping of tooth enamel inflicted by radiation, detected in electron paramagnetic resonance. "Instead of throwing the teeth in the wastebasket, the dentists send them to us," Chumak says; 6000 have been collected in Ukraine so far. After accounting for background radiation, including dental x-rays, they've concluded that liquidators generally received smaller doses than Chornobyl records indicate.

Chumak and his colleagues on the Ukrainian-U.S. team have found that cataracts, a hallmark affliction of Japanese atomic bomb survivors, are more prevalent among liquidators who received higher doses. And he says they have "some indication" of a small number of cases of radiation-induced leukemia among liquidators, although the analysis is not yet complete. An earlier study in Russia, however, failed to detect a significant increase, although it did report high rates of stroke, high blood pressure, and digestive disorders. Okeanov, meanwhile, asserts that liquidators are far more likely to contract lung cancer. It may take years to sort through the conflicting claims, says Yamashita: "This high-risk group needs to be closely monitored."

Discerning health effects among the general population is even trickier. The radiation "signal" is weak, easily swamped by other factors that degrade health, such as smoking, alcoholism, and poor nutrition. "There remains a lack of evidence of any measurable effect of Chernobyl radiation exposures on solid cancers in the general population except for childhood thyroid cancer," notes the September 2005 report from the U.N.'s Chernobyl Forum.

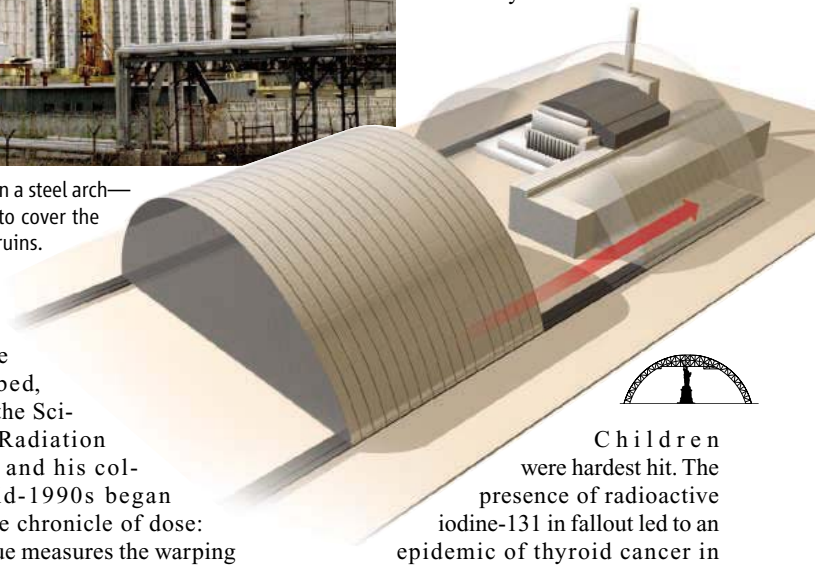

Children were hardest hit. The presence of radioactive iodine-131 in fallout led to an epidemic of thyroid cancer in children: some 4000 cases to date, including nine deaths (*Science*, 20 April 2001, p. 420). Belarus was totally unprepared. "We didn't get any notice about the Chornobyl accident," says Jacov Kenigsberg, chair of the National Commission of Radiation Protection in Minsk. Kept in the dark in the crucial first days after the accident, Belarusian officials did not begin to distribute iodine pills to children and evacuate hard-hit villages until a week after the accident—"too late," Kenigsberg says. The developing thyroid gland absorbs iodine like a sponge; taking stable iodine as a pill blocks the uptake of the hazardous radioisotope, which has a half-life of 8 days. Children exposed to the highest levels of iodine-131, mainly through milk, suffered irreparable harm to their thyroids.

Despite the fallout cloud's huge footprint, studies have not established a link between Chornobyl and noncancer illnesses. But

CREDITS (LEFT TO RIGHT): SERGEI SUPINSKY/AFP/GETTY IMAGES; (ILLUSTRATION) C. BICKEL/*SCIENCE*

anecdotal data abound. Throughout the 1990s, doctors in Homyel and other contaminated regions registered increases "in all kinds of diseases," from heart disease to endocrine and nervous system disorders—many lacking a plausible mechanistic link to radiation, says Valery Gurachevsky, a physicist who chairs Belarus's Committee for the Consequences of the Chernobyl Catastrophe. "This is a big riddle." The likeliest explanation, he argues, is that a grab bag of woes—from pollution to lingering stress—has eroded public health. "So far, almost no serious research has been done on noncancer health effects," says Okeanov. "Medical science says the danger is not that high, the situation is under control. But we need thorough studies."

Ever vigilant. In Homyel's Central Bazaar, Alla Oplachikova prepares to analyze mushrooms for radiocesium in a lead-lined sample chamber (*above*).

A monumental task

In a bunkerlike office deep inside the Chornobyl shelter, Pyotr Lyushnya, a plant engineer, points to a diagram on the wall, a blueprint of the several-story reactor complex marked with radioactivity levels. The hottest recorded spot could deliver a lethal dose in minutes. The shelter's high humidity, from leaks of rain and melting snow, rusts the debris core, a hardened mixture of building materials and melted nuclear fuel, including about 180 metric tons of uranium. Dust in the building is studded with hot particles—radioactive howitzers that can riddle internal organs with alpha or beta particles. Lyushnya admits that this preternatural environment can be nerve-wracking, especially when he's the only one working the night shift. "It's natural to feel creepy," he says, "when you have to make trips by yourself into the destroyed rooms."

All work in the shelter is now focused on one goal: keeping the frail structure intact until a massive enclosure can be slid over it. After 10 years of arduous negotiations, construction of the $800 million New Safe Confinement (NSC) is set to start later this year. Two international consortia with Ukrainian partners—one led by CH2M Hill, the other by Novarka—are bidding for the contract. A decision is imminent, officials say.

Billed as the world's largest movable structure, the NSC is conceived as a steel lid 150 meters long and 100 meters high—taller than the Statue of Liberty. Its construction presents unprecedented perils. "There are very many interesting engineering problems. Not everything has been solved yet," says Nikolai Steinberg, an official with the Ministry of Fuel and Energy of Ukraine who helped design the original shelter. After the accident, fuel elements and waste were buried haphazardly and will pose a risk during excavations for the NSC's foundations, says Serge Gronier, an engineer with Electricité de France, part of the NSC design consortium with Battelle Memorial Institute in Richland, Washington, Bechtel International Systems in San Francisco, and the Chornobyl Nuclear Power Plant.

Originally, engineers proposed building the NSC upright several hundred meters from the shelter and sliding it into place, says Eric Schmieman, a Battelle environmental engineer who was involved in the NSC's conceptual design. Health physicists knew that workers at ground level would be exposed to radiation from buried materials and to radiation emanating from the shelter. They were also concerned about "sky shine": radiation emanating from the roof that's reflected downward by atmospheric particles. "As you go up in elevation, sky shine becomes more of a problem," says Schmieman. To reduce dose (and the mundane risk of falling), the NSC will be constructed in segments on the ground and then hoisted up.

"Enemy of the forest." Near Homyel, signs warn of the danger of forest fires on contaminated land.

After completion, forecast for 2010, the NSC will be slid on rails over the shelter. The unique hazards won't end there. It will be essential to prohibit condensation on the inside of the NSC to prevent corrosion of the steel frame, for example. And air movement must be minimized to avoid stirring up and resurrecting the bane of shelter workers, radioactive dust. Calculating the fluid dynamics of this unusual milieu is no mean feat. "The modeling effort challenged the limits of computational capacity available even at the U.S. national laboratories," Schmieman says.

Perhaps the biggest challenge will be to pick apart and permanently entomb what remains within the rickety shelter. Engineers will use remotely operated cranes for the disassembly. But the fuel-containing masses will stay put for the time being. "The technology does not yet exist to safely remove it," Gronier says. With the NSC designed to last at least a century, the hope is that the fuel can eventually be moved to a deep geological repository. That will be a problem for the next generation to solve, he says.

A generation hence, most people will only vaguely recall one of the most notorious accidents of the 20th century. Already, symbols of the nightmare are disappearing. Most contaminated settlements in the Exclusion Zone have been torn down; the timber and other building materials have been buried in the sandy soil to reduce the amount of radioactivity dispersed by wildfires. The only indications of those former villages today are grassy barrows topped with yellow, triangular radiation-hazard signs.

In two generations, most of the radioactive cesium and strontium will have decayed, and most of the liquidators who put their lives on the line will be gone. But the generation that experienced the disaster is still haunted by memories. "The true story of Chornobyl," says Ronald Chesser, a radioecologist at Texas Tech University in Lubbock who carries out studies in the Exclusion Zone, "is the human tragedy."

–RICHARD STONE

CREDITS: R. STONE

ECOLOGY

Once a Terminal Case, the North Aral Sea Shows New Signs of Life

A dike supported by the World Bank and repairs along the banks of the Syr Darya River have increased the water level dramatically

ALMATY, KAZAKHSTAN—By the early 1990s, much of the area around the northern end of the Aral Sea had become a salt-encrusted wasteland, desiccated by decades of ill-conceived cotton irrigation. Some ecologists seemed ready to write it off, but the World Bank decided in 1999 to support a rescue mission. Among other measures, the project created a 13-kilometer dike designed to raise the sea's level and decrease its salinity.

Managers settled in for a long haul, assuming that it would take up to 10 years for the water to rise 3 meters and cover 800 square kilometers of dry seabed (*Science*, 18 February 2005, p. 1032). They were wrong. Just 7 months after the dike's completion, the Small Aral Sea has reached the target level, 42 meters above the level of the Baltic Sea. Spare water is already flowing through the spillway—evidence of what may become one of the biggest reversals of an environmental catastrophe in history.

"We are very pleased," says Masood Ahmad, the World Bank project coordinator. Looking back, Ahmad points to several factors that may have sped the project to an early success. All relate to the health of the Syr Darya River in the north, one of Central Asia's two great givers that flow into the Aral Sea and sustain it.

The Syr Darya itself deteriorated in the years following the collapse of the Soviet Union, as barriers along its banks fell into disrepair, lowering the amount of water it could carry safely. Another key problem, according to Ahmad and other specialists, was that Kyrgyzstan took an increasing volume of water during winter to run power turbines. To avoid flooding the eroded infrastructure downstream, this water had to be shunted off into lakes along the river, where it served no useful purpose. During summer, when the water level was naturally low, more water was withdrawn for crop irrigation. The result: Little water reached the sea.

Now, after several years of rehabilitation work on dams, sluices, and barrages along the Syr Darya in Kazakhstan, the river's capacity has been safely doubled to 700 cubic meters per second, which allows nearly all of the water released by Kyrgyzstan to reach the Aral, according to Ahmad. The increased flow may eventually bring enough water to the southern sea to slow the decline there as well, Ahmad says.

Nikolai Aladin of the St. Petersburg Academy of Sciences, a Russian biologist who has been studying the sea for nearly 3 decades, calls it "a paradise in the desert." Even though it's only 10,000 years old and has no endemic species, the sea is exceptionally rich in both biodiversity and biomass, he says. And the Syr Darya River is home to one of the world's rarest sturgeon species, a half-meter-long shovelnose. "The bigger water flow is going to considerably increase the chances for recovery of this evolutionary relic," says sturgeon specialist Phaedra Doukakis of the Pew Institute for Ocean Science. "The way and the speed with which the marine flora and fauna will expand with the water will be very instructive for future rehabilitation projects," says Aladin.

Residents of Aralsk, the Aral Sea's main northern port—built on the shore in the 19th century—also have more than passing interest in the sea life. Aralsk once boasted one of the biggest canneries in the Soviet Union. Lenin famously asked Aralsk fishers to send 17 wagons of fish to the front during the Civil War in the 1920s, an event immortalized in a huge mosaic mural in Aralsk's train station.

But starting in the 1960s, the Soviet government promoted the diversion of water from the Syr Darya and the Amu Darya in the south for cotton irrigation, making a calculated bet that cotton was more valuable than fish. By the time the Soviet Union collapsed, the sea had lost 70% of its surface and retreated 80 kilometers from Aralsk, leaving hundreds of rusting ships stranded along the way amid grazing horses and camels. The city's population dropped from 80,000 to 30,000, its airport closed, and its cannery is now an enormous, spindly steel skeleton.

But today, after the sea crept back to within 15 kilometers from Aralsk, the markets are already selling fresh fish at a fraction of the old price, says Marat Turemuratov, a hospital physician. He hopes the change will reduce chronic malnutrition and help abate a tuberculosis epidemic in Aralsk's children.

Michael Glanz, an Aral Sea specialist with the U.S. National Center for Atmospheric Research in Boulder, Colorado, calls the North Aral Sea project "a bright spot in a dismal landscape." To the south, however, the Amu Darya River continues to shrink. Civil strife once prevented Afghanistan from drawing water from this river. But now Afghans in the relatively peaceful north are starting to draw from the river for irrigation—and they're planning to draw much more, Glanz says: "Once the Afghans start withdrawing a lot of water, the delta is going to dry up, and people upstream are going to suffer."

Meanwhile, Kazakhstan has become flush with cash from high oil and metals prices. President Nursultan Nazarbayev announced a popular decision to raise the northern sea's level another 4 to 6 meters, senior Kazakh officials say. This would cover another 925 km^2 of dry seabed and bring the northern sea to about two-thirds of its size before desiccation began in the 1960s. It would also bring water back to within a few kilometers of Aralsk.

Just how that is going to be done—by digging upstream canals, raising the dike, or other means—is still being studied, but Kazakhstani officials say they are committed to the project.

–CHRISTOPHER PALA

Christopher Pala is a writer in Hawaii.

Rising tide. After a long decline, the northern part of the Aral Sea may be on the way to recovery.

CREDITS (TOP TO BOTTOM): ADAPTED FROM J. F. CRETAUX/CNES; C. PALA/*SCIENCE*

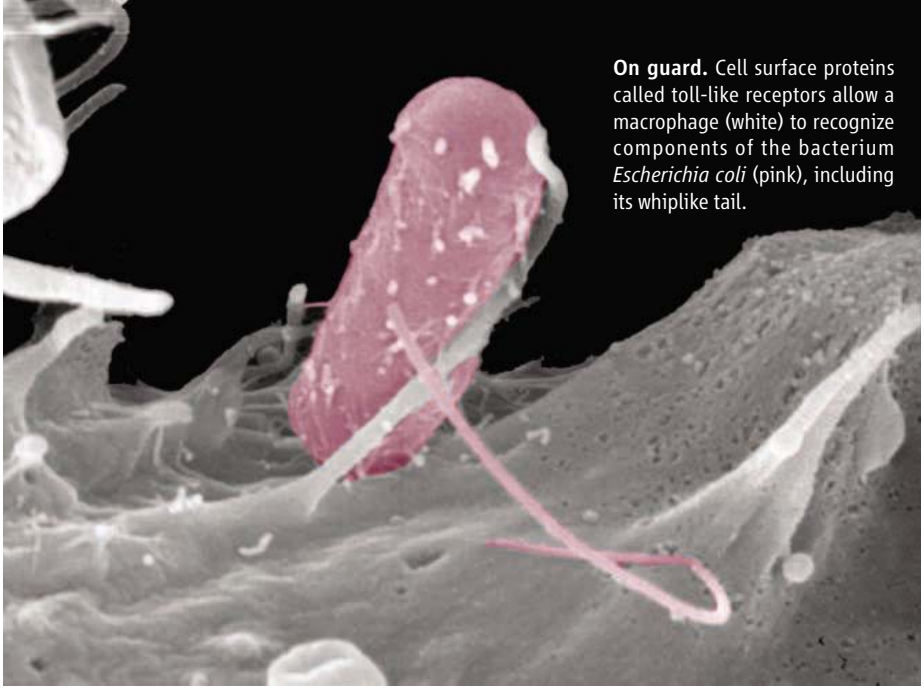

On guard. Cell surface proteins called toll-like receptors allow a macrophage (white) to recognize components of the bacterium *Escherichia coli* (pink), including its whiplike tail.

IMMUNOLOGY

Targeting the Tolls

On the front lines of the body's defense against microbes, toll-like receptors are choice targets for drugs to combat infectious diseases and inflammation

Tens of thousands of horticultural enthusiasts who attended a 1999 flower show in Holland were potentially exposed to something far more insidious than the sight and fragrance of exotic blossoms. *Legionella pneumophila*, the bacterium that causes Legionnaire's disease, contaminated the water in a whirlpool spa on display and a sprinkler system that misted the flowers, which probably dispersed the bacterium widely. More than 100 people fell ill, and 18 died.

The tragedy piqued the curiosity of infectious disease specialist Annelies Verbon of the Academic Hospital Maastricht in the Netherlands. Why did a handful of people get sick, whereas most came away unharmed? Verbon, along with a research team led by immunologist Alan Aderem of the Institute for Systems Biology in Seattle, Washington, and Thomas Hawn, an infectious disease specialist at the University of Washington Medical Center in Seattle, came up with an intriguing answer. When the researchers analyzed the DNA of groups of attendees, they discovered that a higher percentage of those who fell ill carried a single mutation in the gene for an immune cell surface protein called toll-like receptor (TLR) 5. The team found that the mutation cripples the receptor, apparently preventing immune cells from recognizing the whiplike tail of *L. pneumophila* and rendering those with the mutation more susceptible to severe Legionnaire's disease.

That finding, published in 2003, is part of an avalanche of research on TLRs. TLR5 is a member of a family of at least 10 human TLRs discovered within the past 7 years. Their discovery has "revolutionized immunology," in the words of Luke O'Neill, an immunologist at Trinity College in Dublin, Ireland.

Scientists had long known that the immune system has an initial line of defense that triggers the inflammatory response and recruits B and T cells to mount an attack on invading microbes. But they didn't know how that initial alarm was sounded. TLRs have turned out to be the key. "These are the sensors of the microbial world that turn on the immune system," says O'Neill. And more recent evidence suggests that they also play important roles in autoimmunity and inflammatory conditions such as heart disease.

All this has caught the collective fancies of immunologists and biomedical researchers around the globe. Some 3500 papers on these immune sentinels have appeared to date, and at least nine biotech companies have compounds that stimulate or inhibit TLRs in clinical and preclinical trials for illnesses as diverse as hepatitis, cancer, asthma, and allergies. In the past year, big pharma has moved in too, with companies such as GlaxoSmithKline and Novartis buying up or inking deals with smaller firms developing TLR-based drugs. Commercial interest in TLRs is "suddenly hot," says O'Neill, who has himself founded a company, Opsona Therapeutics in Dublin, that is now collaborating with Wyeth Pharmaceuticals on TLR-targeting drugs for inflammatory diseases.

Many more experimental TLR-based drugs are being studied, from cancer vaccines to ones designed to treat or prevent allergies, inflammatory bowel disease, and autoimmune afflictions. Basic researchers, meanwhile, are uncovering a slew of additional drug targets as they identify the cascade of enzymes and other molecules involved in transmitting the messages sent by TLRs to the interior of the cell. In the past 3 years, researchers have unveiled 15 previously unknown proteins activated by TLRs and have now cataloged about 30 of the estimated 40 to 50 components of TLR signaling pathways, says Bruce Beutler, an immunologist at the Scripps Research Institute in San Diego, California.

Of course, many hurdles remain before most of these compounds can be marketed. And some, such as pediatric immunologist Jean-Laurent Casanova of Necker Medical School in Paris, contend that more work must be done to prove the importance of TLRs in human immunity, as most studies on these receptors involve animal models of infection. "Enthusiasm for TLRs is deserved," cautions Casanova, "but it should be tempered."

Weird discovery

The explosion of interest in human TLRs had humble beginnings: the 1988 discovery of a protein involved in fruit fly development. German researchers noted that flies lacking the protein looked *toll*, the German word for "weird" or "far out." The insects' bodies were disordered, with bott`om body parts mixed with parts that belonged on top, and vice versa. It wasn't until 1996 that scientists learned that the protein, Toll, had a second job, helping defend against fungi. Flies with mutated versions of the protein or its signaling partners more readily succumbed to fungal infections, according to work by Jules Hoffmann and colleagues at the National Center for Scientific Research in Strasbourg, France.

That curious finding led immunologists to wonder whether humans have a corresponding protein. Two years earlier, it turned out, Nobuo Nomura and his colleagues at the Kazusa DNA Research Institute in Chiba, Japan, had unveiled a human protein that bore strong resemblance to the fly Toll. It was later dubbed TLR1. In 1997, Yale University scientists unveiled the second human TLR (now called TLR4), and soon thereafter, researchers at DNAX in Palo Alto, California, identified five more TLR proteins in people.

A year later, Beutler and his colleagues provided the first evidence that a TLR plays a part in mammalian immunity: They found that mice with a defective version of TLR4 could survive injections of endotoxin, a cell-wall component of some bacteria that invariably kills normal mice and in humans can incite a deadly inflammatory disorder called sepsis. The work, Beutler says, "proved that TLR4 was the receptor for endotoxin." The receptor

Y. Pagès Proudly Presents, Thx for Support

CREDIT: ADRIAN OZINSKY AND ALAN ADEREM/INSTITUTE FOR SYSTEMS BIOLOGY

suddenly became a hot drug target for sepsis, a killer of 750,000 Americans each year.

After that, discoveries came thick and fast. Immunologist Shizuo Akira of Osaka University in Japan and his colleagues systematically deleted the mouse genes for TLRs to reveal their specific functions. Several groups determined which compounds trigger individual receptors. Akira, in collaboration with Aderem and Hawn, for example, determined that flagellin, a protein in the flagella of bacteria, activates TLR5. Others traced out signaling pathways inside the cell that connect to the TLRs, discovering that triggering these receptors can prompt a range of immune responses. These include the release of cytokines such as interferon—a powerful antiviral agent—and other messenger molecules that stimulate the immune system's storm troopers, T cells and antibody-producing B cells.

The unveiling of TLRs and their specific activities (see chart, right) has given immunologists new respect for the body's frontline defenses, known as the innate immune system. Long considered an evolutionary holdover that provides broad protection before the more specific adaptive immune system of T cells and B cells kicks in, innate immunity is turning out to wield a rather precise set of countermeasures. It is the TLRs that direct the innate immune system's responses, and immunologists are realizing that those responses in turn guide the subsequent adaptive immune reaction that is even more targeted. "The two go hand in glove," says O'Neill. "You wouldn't get any adaptive response without the innate." Adds Kleanthis Xanthopoulos, who heads Anadys Pharmaceuticals, a San Diego firm developing antiviral drugs that target TLRs: "The innate immune system had always been viewed as the 'low-tech immune system.' Only now do we understand that innate immunity has significant molecular specificity."

Revving up immune responses

The more scientists learn about TLRs, the more excited they—and drug company executives—get about the potential of stimulating the receptors to combat everything from infectious diseases to cancer. Among the early targets is the hepatitis C virus. Once the virus sets up a chronic infection, it can be very difficult to dislodge: The current treatment—nearly a year of interferon injections combined with an oral antiviral—clears only about half the infections with the most resistant strain, and its side effects can be debilitating. Anadys recently tested a compound that stimulates TLR7 on 32 patients chronically infected with hepatitis C. The injectable drug lowered blood levels of the virus by 82%—a response comparable to injected interferon—in eight of the 12 patients who received the highest dose daily for a week. Only a few patients had side effects, and those were mild to moderate, Anadys scientists reported in the September 2005 issue of *Hepatology*. The results were promising enough to inspire Novartis to collaborate with Anadys on a pill version of the drug.

Coley Pharmaceutical Group in Wellesley, Massachusetts, a company founded by University of Iowa immunologist Arthur Krieg, has also begun clinical tests of a TLR stimulator aimed at hepatitis C. In a trial with 60 patients, a drug called Actilon that stimulates TLR9 elicited a dose-dependent release of the body's own interferon-α without producing serious side effects, Coley scientists reported at the November 2005 meeting of the American Association for the Study of Liver Diseases. Among the 13 patients who received the highest dose levels of Actilon once or twice a week for 4 weeks, 11 achieved greater than 90% reduction in blood levels of viral RNA.

Krieg started working on TLR stimulators in the mid-1990s—but he wasn't aware of it at the time. He discovered that short sequences of nucleotides containing cytosine (C) followed by guanine (G), which are common in viruses and bacteria, could powerfully activate B cells in mice. At about the same time, immunologist Eyal Raz and cancer biologist Dennis Carson of the University of California, San Diego (UCSD), and their colleagues observed that T cells respond to loops of bacterial DNA called plasmids, which also contain these so-called CpG sequences. In 2001, Akira's group connected both sets of findings to the world of TLRs: The researchers reported that mice lacking TLR9 fail to generate the immune response typically produced by CpG DNA. Since then, several groups, including Krieg's, have used CpG sequences to construct TLR stimulators for a variety of applications, including cancer treatments.

At a cancer meeting last year, Coley scientists and their collaborators reported that one such compound—a 24-base DNA sequence with four CG pairs—plus chemotherapy shrank lung tumors in 37% of 75 patients with advanced forms of lung cancer, compared to just 19% of 37 patients who received chemotherapy alone. The data also show a positive trend toward increased survival after 1 year. The results are "preliminary—but potentially very exciting," says Trinity's O'Neill. Pfizer, which pledged up to $515 million for the rights to develop the Coley drug last year, started large-scale trials in November.

Several companies are using TLR stimulants as adjuvants, boosting the immune system's response to vaccines to increase their efficacy. Coley has developed a CpG-based adjuvant called VaxImmune that seems to improve the human immune response to the anthrax vaccine. GlaxoSmithKline recently bought Corixa, a Seattle-based company devoted to TLR therapeutics, for $300 million and is sponsoring large-scale trials of Corixa's MPL, a derivative of bacterial endotoxin that stimulates TLR4, as an adjuvant in a vaccine against

What the Toll-Like Receptors See

TLR	Natural Ligand
TLR1 (partnered with TLR2)	Bacterial triacyl lipopeptides and certain proteins in parasites
TLR2 (partnered with TLR6)	Bacterial diacyl lipopeptides, lipoteichoic acid from Gram-positive bacteria, and zymosan from the cell wall of yeast
TLR3	Double-stranded RNA from viruses (i.e., West Nile virus)
TLR4	Endotoxin (lipopolysaccaride) from Gram-negative bacteria
TLR5	Flagellin from mobile bacteria
TLR7	Single-stranded RNA from viruses (i.e., HIV)
TLR8 (inactive in mice)	Same as TLR7
TLR9	CpG DNA from bacteria or viruses
TLR10 (found in humans but not mice)	Unknown
TLR11 (found in mice; human form is truncated and thought to be inactive)	Profilin, a protein from the protozoan pathogen *Toxoplasmosis gondii* that can cause miscarriage; may also respond to components of bacteria that cause bladder and kidney infections
TLR12 and TLR13 (found in mice but not humans)	Unknown

Immune recognition. Each toll-like receptor recognizes a specific set of molecular beacons on pathogens. Here are the known natural binding partners for each TLR.

You could be next

Yes, it *can* happen to you:
If you're making inroads in neurobiology research and you've received your M.D. or Ph.D. within the last 10 years, the Eppendorf & *Science* Prize for Neurobiology has been created for YOU!

$25,000 Prize

This annual research prize recognizes accomplishments in neurobiology research based on methods of molecular and cell biology. The winner and finalists are selected by a committee of independent scientists, chaired by the Editor-in-Chief of *Science*. Past winners include post-doctoral scholars and assistant professors.

If you're selected as next year's winner, you will receive $25,000, have your work published in the prestigious journal *Science* and be invited to visit Eppendorf in Hamburg, Germany.

What are you waiting for? Enter your research for consideration!

Deadline for entries:
June 15, 2006

For more information:
www.eppendorf.com/prize
www.eppendorfscienceprize.org

"It was a great honor to be the first recipient of the Prize. This prize highlights the valuable role that the scientific community can play in fostering the promise of developing researchers."

Anjen Chenn, M.D., Ph.D.
Assistant Professor
Northwestern University
2002 Winner

YYePG Proudly Presents, Thx for Support

eppendorf & Science
PRIZE FOR NEUROBIOLOGY

human papillomavirus, which causes cervical cancer. And scientists at Dynavax in Berkeley, California, are conducting large-scale human trials of a hepatitis B vaccine in which a CpG DNA sequence is linked to a surface protein from the virus. Early trials suggest that the adjuvant generates a more robust immune response in older adults—and a faster response in young adults—than does the current vaccine.

Dampening immunity

In addition to revving up immune defenses, researchers are also investigating ways of using TLRs to turn them down. One such strategy may provide faster and safer immunotherapy for allergic conditions.

Current allergy immunotherapy regimens are cumbersome, requiring weekly or monthly shots for 3 to 5 years. They can also be dangerous, causing symptoms from swelling to anaphylaxis in some patients. UCSD's Raz and Carson have discovered that bacterial CpG DNA may offer another solution. By stimulating TLR9, such DNA spurs macrophages and other innate immune cells to kill the so-called T helper 2 (T_H2) cells whose overzealous activity characterizes allergy and asthma. Following up on the UCSD team's work, Dynavax is developing medication that may safely prevent allergies in just 6 weeks. The compound—a CpG molecule bound to DNA encoding the culprit allergen—elicits an anti-T_H2 response in animals that is stronger than that from separately administered CpG DNA. The company has already sponsored some clinical tests of this strategy and at the March meeting of the American Association of Allergy, Asthma & Immunology reported promising results for ragweed-allergic adults.

A more obvious way of taming the immune system through TLRs is to block one or more of the receptors. This may be useful for inflammatory conditions such as the autoimmune disorder lupus and sepsis. Last year, for example, Seattle's Hawn and Aderem reported that the nonworking TLR5 variant they had implicated as a risk factor in Legionnaire's disease was about half as common in lupus patients as it was in their unaffected relatives, suggesting that inactivating TLR5 may protect people against the disorder. And researchers at Eisai Inc. in Teaneck, New Jersey, are already testing a TLR-blocking compound against sepsis. The compound, dubbed eritoran, is a molecular mimic of a portion of the endotoxin molecule; it binds with TLR4 but does not activate it. In a trial of nearly 300 hospital patients diagnosed with sepsis, a large dose of eritoran reduced the death rate by 12%, compared to a placebo, in the 80% of participants who fully complied with the regimen. In the patients at highest risk for death, a large eritoran dose reduced the death rate by 18%, Eisai announced in August. Beutler calls the results "encouraging," given how hard it is to administer a drug soon enough to save sepsis patients. The work also shows that TLR blockers are possible. "It sets a precedent for making small molecule antagonists to other TLRs," he says.

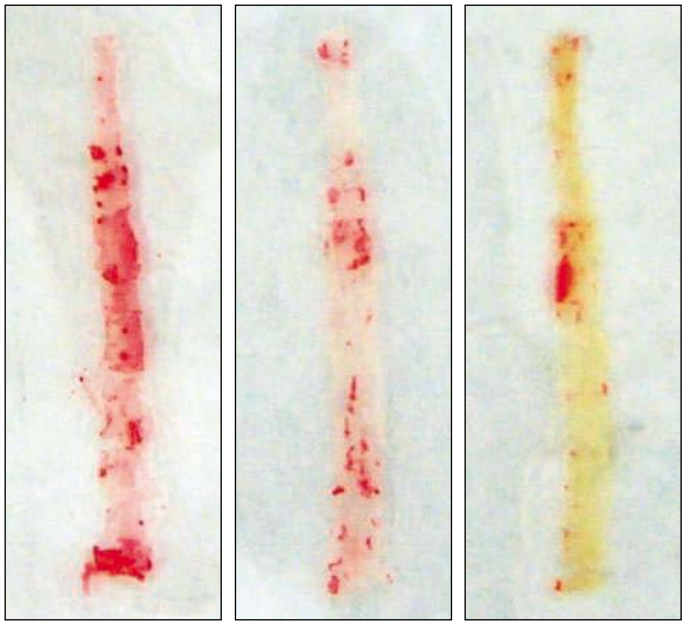

Unplugging aortas. Lipid (red, *left*) clogs an aorta from an atherosclerosis-prone mouse fed a high-fat diet. By contrast, far less fat appears in the aortas of similar mice lacking one (*middle*) or two (*right*) copies of the gene for the TLR adapter protein MyD88.

CREDIT: K. S. MICHELSEN *ET AL.*, *PNAS* **101**, 29 (20 JULY 2004)

Hope for the heart

Drugs that hinder TLRs might one day treat heart disease as well. Accumulating evidence suggests that TLR activity contributes to atherosclerosis, perhaps by stimulating inflammation.

Hints of this role appeared in 2001 when Moshe Arditi, an infectious disease specialist at Cedars-Sinai Medical Center in Los Angeles, California, and his colleagues found that TLR4 was abundant in atherosclerotic plaques from the coronary arteries of five patients needing bypass surgery but scarce in four normal arteries. More recently, they have found that atherosclerosis-prone mice lacking the *TLR4* gene developed arterial lesions that were about 25% smaller than those in the same mice with the *TLR4* gene. And if such mice lacked the gene for MyD88, which is involved in the signaling of several TLRs, the atherosclerosis in their aortas dropped by nearly 60%, the researchers reported in 2004. The study "really shows that TLR4 and MyD88 play a role in the production of atherosclerosis," says Arditi.

TLR1 and TLR2 are also implicated. These receptors are more prevalent in plaque-pocked human arteries than in normal ones. And when immunologist Linda Curtiss and her colleagues at The Scripps Research Institute deleted the *TLR2* gene in atherosclerosis-prone mice, the animals' arterial lesions shrank by almost 50% compared to similar mice that retained the *TLR2* gene. What's more, injecting susceptible mice with a compound that activates TLR2 greatly worsened their lesions.

"It looks like the innate immune system is going to be very clearly involved in the pathogenesis of atherosclerosis," says Arditi. If so, new treatments could include drugs that block TLR4, TLR2, and MyD88. Such drugs might cripple a person's infection-fighting ability if delivered systemically, but administering them locally to the arteries could reduce that risk, Arditi suggests.

Lingering doubts

Despite this flurry of activity, there is still uncertainty about the receptors' role in human immunity. There are rare cases in which people have a mutation in an enzyme in the signaling pathway shared by TLRs and the interleukin-1 (IL-1) receptor, making the receptors useless, and yet these people still seem to resist most types of viral, fungal, and parasitic infections, Necker Medical School's Casanova and his colleagues reported in *Science* in 2003 (28 March 2003, p. 2076). What immune impairment these people do experience could conceivably be caused by an IL-1 pathway defect, Casanova suggests. Because there is no human genetic defect that selectively impacts the TLRs, Casanova says, "there is so far no conclusive evidence that human TLRs are critical, nonredundant players in protective immunity in infection."

Even if TLRs are vital and unique players in human immunity, as many researchers believe, almost all of the TLR-based experimental therapies must undergo further testing. It's also worth remembering that turning up or down the volume of the human immune system—by means of TLRs or any other method—is a risky proposition. Attempts to dampen dangerous inflammatory responses by means of TLRs could cripple the immune system and cause patients to succumb more easily to infectious diseases, for example. On the other hand, TLR-stimulating compounds could rev up the immune system too much or for too long, leading to sepsis or autoimmune diseases.

"These are huge challenges," says Beutler. "But they could have rich payoffs." A growing number of companies are betting on that.

–INGRID WICKELGREN

Call for Sustainability Science papers

PNAS is pleased to announce the launch of a section on Sustainability Science, a vibrant area encompassing fundamental research on interactions between human and environmental systems, as well as sustainability challenges relating to agriculture, biodiversity, cities, energy, health, and water.

Why Submit to PNAS?

- Premier multidisciplinary science journal
- Fast online submission and peer review
- No need for Academy Member sponsorship
- Worldwide authors and readers

Submit your manuscript today

Contact Dr. Jennifer Byers at jbyers@nas.edu for more information.

www.pnas.org/misc/sustainability.shtml

PNAS

Proceedings of the National Academy of Sciences of the United States of America

COMPUTER SCIENCE

Life in Silico: A Different Kind Of Intelligent Design

Engineers and computer scientists are trying to establish a standard tool kit for an emerging field of biology

A biologist sits in front of her computer screen, staring at a model of a bacterium, pondering which metabolic pathway it would use if it were buried deep in the ice of Jupiter's moon Europa. She goes online and searches a database. Within seconds, she finds what she's looking for: Models of three metabolic pathways have been designed and archived by other biologists from past projects. She downloads them, plugs them into her bacterium, programs in the icy environmental conditions, and starts the model running to see which works best.

Futuristic? Yes. But a growing cadre of systems biologists and computer scientists believes it's possible. Just as engineers use the program AutoCad to create structures in virtual space, if an enterprising team of researchers has its way, biologists will have their own software to design and assemble models of organisms and their components. One group has already ventured into this exotic territory—a computer group at Harvard University led by mathematician Jeremy Gunawardena. They soon plan to unveil what they consider the first truly modular program for bio design, called "Little b."

The name is a play on a powerful computer programming language called C. (Gunawardena's group had planned to call their software "B," for biology, but realized the name was already taken by C's predecessor.) Gunawardena outlined the program and some of its uses in talks last October at the Council for the Advancement of Science Writing meeting. One of his goals is to bring more consistency to the young field of computer simulation of biological systems. Although biological modeling has shown early promise in pharmaceutical research and the study of complex diseases, he believes it is still a "cottage industry" in sore need of standardization. Existing model systems are "not proper scientific objects," because they're not easy to reproduce or build upon.

Several other efforts to standardize biological models for easy sharing are under way. The European Bioinformatics Institute (EBI) in Hinxton, U.K., for example, has gathered more than 50 models in its online collection, called BioModels Database (www.ebi.ac.uk/biomodels). It makes them freely available for downloading. Models in this collection are validated for internal consistency and annotated for legibility. But Gunawardena and his collaborators have something more ambitious in mind: a future in which not just biological models but all the pieces of models should be sharable. In this utopia, models should be able to swap computer code for protein cascades as easily as Mr. Potato Head swaps noses.

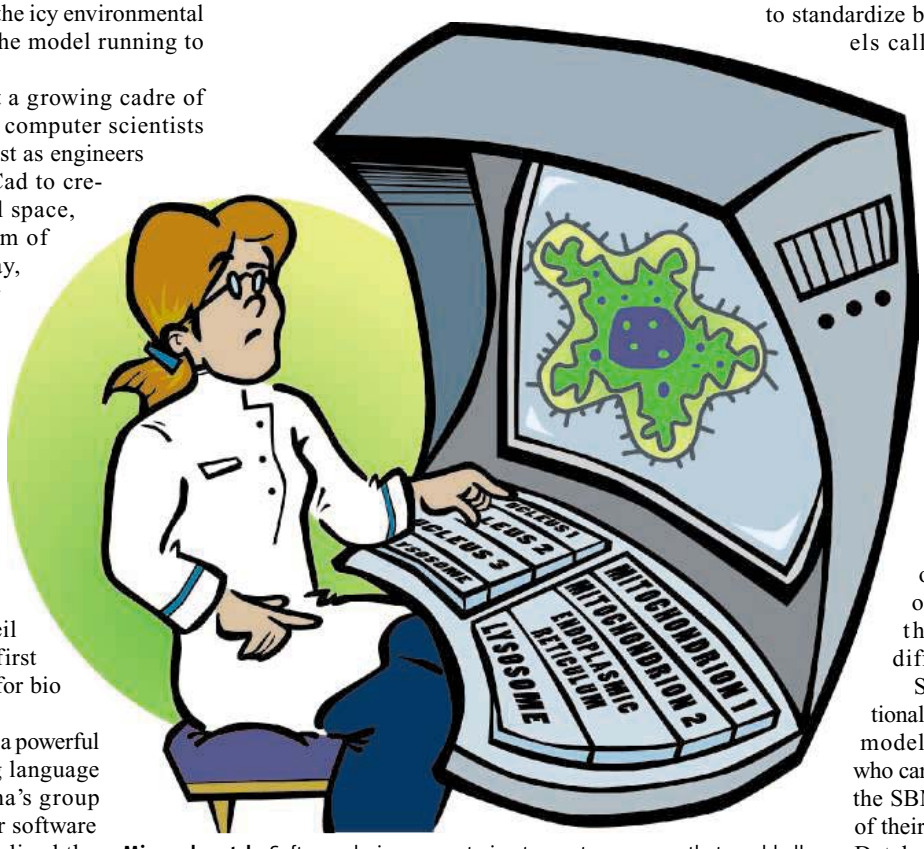

Mix and match. Software designers are trying to create programs that would allow scientists to execute designs using standard biological components.

In concept, Little b bears a resemblance to computer-aided design (CAD) software, which allows engineers to model a new machine in virtual space by combining different parts from a menu of possibilities. The engineer can take the best stock part and tweak it if necessary to make the best fit. Similarly, Little b would allow biologists to build a reaction chain, cell, or organism in silico, picking and choosing proteins and cell parts from a menu of modular parts. If a novel part is needed, the modeler could alter an existing module or write a new one. Once finished, the new module could just be plugged in.

Modularity is a fairly sophisticated software concept. The Little b group "is looking at this from the standpoint … of software engineering," which is a good thing, says Michael Hucka, a computer scientist at the California Institute of Technology in Pasadena. "They're ahead of the curve." Both Hucka and Herbert Sauro, a systems biologist and software engineer at the Keck Graduate Institute in Claremont, California, are principal engineers on another effort to standardize biological systems models called the SBML project, for Systems Biology Markup Language. In the past 5 years, SBML has become the standard—and pretty much the only—way for computational biologists to exchange models in a mutually readable format. SBML and Little b are entirely different beasts, however; Little b is a modeling language, whereas SBML is a file format. Like a Word document or pdf, it's simply a way of encoding a model so that it is readable by different machines.

SBML allows computational biologists to e-mail their models to other researchers, who can then run the models on the SBML-compatible software of their choice. The BioModels Database at EBI has collected and curated the best SBML-compatible models. Several journals, including *Nature*, now require all biological models described in their articles to be submitted to the BioModels Database as well. But neither the database nor SBML requires modularity, as Little b does.

This aspect of Little b promises a unique mix-and-match flexibility. Consider how the program deals with the cell lattice, a construct that describes how cells connect to one another in two or three dimensions. A conventional computer simulation that explores the effect of different cell lattices on embryo development, for example,

ILLUSTRATION: TIM SMITH

treats the lattice structure as an integral part of the model. It would be difficult to change from a square to an irregular grid without altering the entire program. The connectivity in lattices can affect a number of conditions—the shape of the cell, which chemical signals it is exposed to, how much light it gets—altering development.

Gunawardena's group has created a model of embryonic development but made the lattice a flexible module. In Little b, it can be altered or replaced without reprogramming any other part, allowing the same experiment to be run on a wide array of cell-lattice patterns.

Little b can also be used to model complete organisms. There's a *Drosophila melanogaster* living in silico on a laptop at Harvard Medical School, designed completely by Gunawardena's group in Little b. Many research groups are modeling entire organisms and might well make use of a modular approach.

Although it doesn't aim to model whole organisms, the integrative cancer biology program of the National Cancer Institute (NCI) in Bethesda, Maryland, is considering a modular approach to modeling. "It's the Holy Grail to take all these individual modeling components, plug them together, and get a comprehensive view of what's going on," says Daniel Gallahan, the associate director of NCI's division of cancer biology.

Other researchers agree that modularity is necessary if computational biology is to advance. Sauro, for one, decries the "huge waste of grant money" in the "chronic reinvention" of computer tools that employ one-off models. The redundancy is amazing, he says. For example, the BioModels Database has tens of models just of the MAP kinase cascade, a signal pathway in mammalian cells. And no matter how many MAP kinase cascade models there are available, or how well curated they may be, without modularity they're next to useless to a researcher who wants one ready-made to integrate into a larger model. There's simply no way to plug it in.

Whether Little b succeeds will depend in part on how it evolves and how widely it is accepted. Not everyone is enchanted with it, because it's based on an abstract language called LISP originally devised for artificial intelligence applications. Sauro suggests that the best way to get biologists to adopt a modeling language like this would be to give it a friendly graphical interface. No one has started a project like that, to his knowledge. Several computational biologists also say Little b's developers have not shared much information about their efforts thus far. Without input from the biology community, they ask, how can it satisfy everyone's needs?

Gunawardena says his group plans to begin teaching Little b to students at Harvard soon; he's preparing a paper that he hopes to publish this year. Then the test of community acceptance will begin in earnest.

–KIM KRIEGER

Kim Krieger is a writer in Washington, D.C.

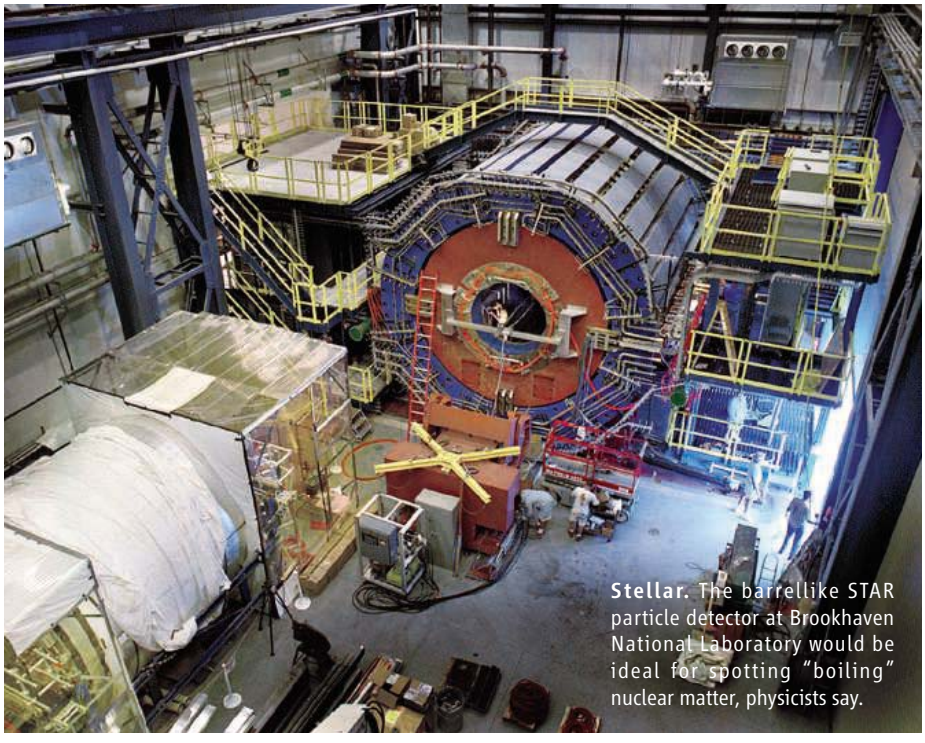

Stellar. The barrellike STAR particle detector at Brookhaven National Laboratory would be ideal for spotting "boiling" nuclear matter, physicists say.

CREDIT: BROOKHAVEN NATIONAL LABORATORY

NUCLEAR PHYSICS

Scheme for Boiling Nuclear Matter Gathers Steam at Accelerator Lab

Physicists hope to glimpse that violent transformation by running a gargantuan particle collider in lowest gear

UPTON, NEW YORK—Coiling through the woods and buried beneath meters of sandy Long Island loam, a vast atom smasher here at Brookhaven National Laboratory (BNL) has transported physicists back to the big bang. Since 2000, researchers have used the 4-kilometer-long Relativistic Heavy Ion Collider (RHIC) to produce a superhot, ultrathin soup of fundamental particles called quarks and gluons (*Science*, 22 April 2005, p. 479). The observation of the quark-gluon plasma sheds light on the type of matter that filled the infant universe and has opened a new frontier in nuclear physics. To explore it, though, researchers need a landmark—and they hope to find it by boiling nuclei like water in a kettle.

Imagine a map of nuclear matter with temperature increasing to the north and density increasing to the east. Ordinary nuclei fill a spot on the chilly southern edge, and RHIC has explored the low-density, high-temperature western border (see diagram, p. 191). Most theorists believe that somewhere to the north and east in the "phase diagram" lies a special point beyond which the transformation from ordinary matter to a mixture of quarks and gluons becomes violent, like the boiling of water. RHIC might be able to reach that "critical point," and in March, more than 50 physicists gathered here to consider whether to try.

The critical point is "*the* landmark on the phase diagram," says Krishna Rajagopal, a theorist at the Massachusetts Institute of Technology in Cambridge and Lawrence Berkeley National Laboratory in California. "If it's not there, then we don't have even a qualitative understanding of the diagram," which also predicts an exotic "color superconductor" state of nuclear matter in neutron stars. Others say the discovery of the critical point would merit a Nobel Prize.

Searching for the critical point may be tricky, however. Pressing eastward on the phase diagram means producing higher density nuclear matter. That requires ratcheting RHIC's energy *down* to as little as 1/40 of its normal level—a challenge akin to driving a Formula 1 race car at jogging pace without stalling. And nobody knows exactly where the critical point should be or how experimenters will recognize it.

Still, previous experiments may have spotted hints of it, and researchers here are eager for

the search. "It's something that's definitely going to happen at some time," says BNL's Timothy Hallman, spokesperson for STAR, one of three ongoing particle-detector experiments at RHIC (see photo, p. 190). William Zajc, a physicist at Columbia University and spokesperson for a second experiment, called PHENIX, says the project would add a new dimension to research at RHIC. "By going down in energy, not only do you have the potential for discovery, you're going out in a whole new direction," he says.

Glued together with gluons, quarks ordinarily bind so tightly that they're always found either in groups of three—as in the protons and neutrons in atomic nuclei—or in quark-antiquark pairs in fleeting particles called mesons. To liberate quarks, RHIC smashes gold nuclei with such energy that they rip through each other and leave behind a tiny volume of vacuum heated to a million billion degrees. From the void, unfettered gluons, quarks, and antiquarks emerge like violets blooming in spring. In an instant, the wispy plasma cools, and the quarks and antiquarks bind into the particles that spray into RHIC's particle-detector experiments.

As far as RHIC researchers can tell, however, the transition they've observed from ordinary particles to plasma and back is smooth. Conceptually, bound-up nuclear matter and quark-gluon plasma resemble water and steam. Squeeze water to 218 times atmospheric pressure, and the distinction between liquid and vapor blurs, so that it's possible to go smoothly from one state to the other by raising the temperature past 374°C. In the same way, at low densities, the transition from bound to unbound quarks is seamless.

But that transition should be more dramatic in higher-density plasmas, theorists predict, just as at lower pressures water boils violently to become steam and then condenses into distinct droplets to return to the liquid state. If researchers can increase the density of the plasma, then nuclear matter should essentially boil in the collisions and condense as the plasma cools—a process known as a "first-order phase transition." The critical point is the density and temperature at which those effects kick in, Rajagopal says. "You want to go to the place where you start seeing the formation of droplets" in the cloud of plasma, he says.

To make a denser plasma, RHIC researchers must collide nuclei at energies much lower than normal. That would leave matter from the nuclei lingering in the hot vacuum, driving up the density. RHIC's two overlapping circular accelerators speed ions in opposite directions and crash them together inside the particle detectors spaced around the ring. The accelerators typically boost gold nuclei to energies of 100 billion electron volts (100 GeV) per nucleon—that is, 100 GeV for every proton and neutron in the nucleus. To reach the densities hoped for, RHIC would have to accelerate ions to just 2.5 GeV per nucleon.

Turning the energy that low may push the limits of the equipment, says BNL accelerator physicist Todd Satogata. "It's like doing the limbo," he says. "How much do your knees hurt as you go lower and lower?" RHIC uses magnets to focus and guide the beams, and those magnets have never been tested at the low fields needed to control such low-energy beams, Satogata says.

Making the beams collide may also pose a problem, says BNL accelerator physicist Angelika Drees. Ordinarily, accelerator operators guide the beams into each other by sensing neutrons from the collisions. But low-energy neutrons won't trigger the neutron detectors, Drees says: "If we don't have a signal to steer with, you may not have collisions at all."

Nevertheless, accelerator physicists see no insurmountable hurdles to running RHIC at very low energies. For example, Drees says, RHIC's particle detectors could be outfitted with new monitors for steering. And Satogata says accelerator physicists should be able to tell what they're up against after just a single day of test runs.

Even if RHIC can deliver the collisions, experimentalists see data [illegible] the [illegible] critical point when they reach it. The signs of the quark-gluon plasma itself are quite subtle. The minuscule puff of plasma blinks out of existence in less than a billionth of a billionth of a second, leaving visible only the thousands of ordinary particles gushing in all directions.

But in that torrent of particles, researchers have found evidence of the plasma of unbound quarks and gluons. For example, an elongated puff rebounds so that it quickly becomes shorter and fatter, like a squeezed water balloon returning to its round shape. Such "hydrodynamic flow" is a hallmark of the quark-gluon plasma. Researchers have also shown that the tiny cloud appears to drag on jets of highly energetic particles moving through it and snuff them out. That "jet quenching" is another sign of the plasma.

The signs of the critical point would be subtler still. For example, the flow should cease when the transition from bound quarks to free quarks becomes violent like boiling, says Horst Stoecker, a theorist at Johann Wolfgang Goethe University in Frankfurt am Main, Germany. More generally, near the critical point, conditions within the superhot cloud of nuclear matter should begin to fluctuate wildly, leading to event-to-event variations in the number of particles such as π mesons, K mesons, and protons and in other variables.

In fact, researchers working on another experiment may have already glimpsed signs of the first-order transition. From 1996 to 2002, researchers at the European particle physics laboratory CERN near Geneva, Switzerland, slammed lead nuclei into a stationary lead target. At energies of about 7 GeV per nucleon, the ratio of K mesons to π mesons peaked dramatically. That and other signs suggest that the collisions pushed around the east side of the critical point, says Marek Gazdzicki, an experimenter at the University of Frankfurt and the Swietokrzyska Academy in Kielce, Poland. He has proposed taking more data at CERN, although that won't happen for at least 3 years, he says. Meanwhile, researchers at Germany's GSI laboratory in Darmstadt are developing an accelerator that could also take up the search in 2012.

Still, Gazdzicki and others agree that with its wide energy range and two large particle detectors, RHIC is ideally suited to hunt for the critical point. The best opportunity should come after researchers upgrade the STAR detector in 2009. In the meantime, interest in the critical point is building like pressure in a boiling tea kettle.

–ADRIAN CHO

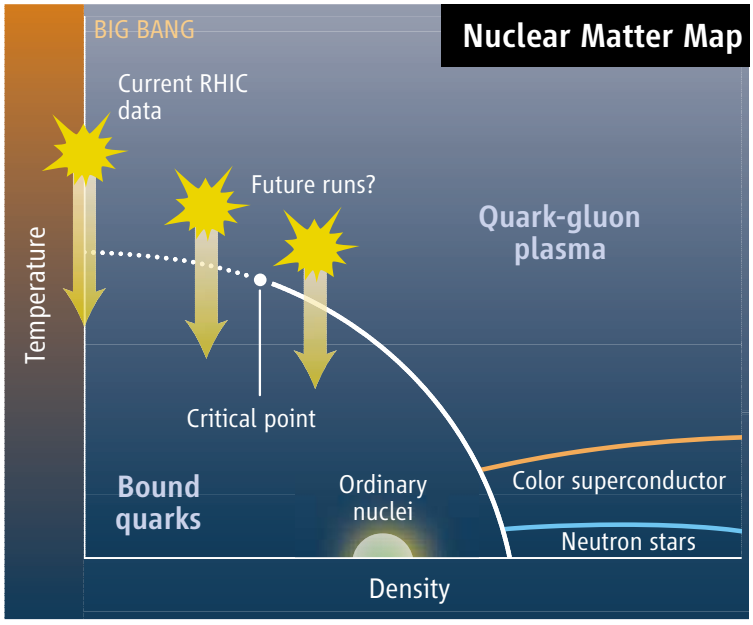

Landmark study. Physicists have seen a smooth transition from bound quarks to quark-gluon plasma (dotted line). They now hope to find the point beyond which the transition becomes violent (white line).

EDITED BY YUDHIJIT BHATTACHARJEE

In the Media

TUNED OUT. Charges of plagiarism have driven off the air one of Britain's best known psychiatrists: Raj Persaud of the Institute of Psychiatry at King's College London. Persaud "stepped down" as host of BBC's popular radio show *All in the Mind*, the company announced last week, "because of continuing allegations of plagiarism." King's College is investigating the charges.

More than a year ago, psychologist Thomas Blass of the University of Maryland, Baltimore County, complained to *Progress in Neurology and Psychiatry* that Persaud had failed to credit him in a February 2005 commentary on Stanley Milgram's work on obedience. Last fall, the journal retracted the article. In December, the *British Medical Journal* (*BMJ*) also retracted Persaud's review of Blass's biography of Milgram, published on 6 August, "owing to unattributed use of text from other published sources."

The Guardian quoted a letter from Persaud saying that his acknowledgement of Blass was deleted by *BMJ* during editing. *BMJ* then posted Persaud's unedited draft and wrote to *The Guardian* that Persaud's text "borrows almost verbatim" from Blass's writing without attributing the material to him (bmj.bmjjournals.com/cgi/content/full/331/7512/356/DC1). Persaud could not be reached for comment.

ON CAMPUS

BOGUS BACKGROUND. Liu Hui, assistant dean and professor of Qinghua University Medical School, has been fired for falsifying the résumé he used to land his job 2 years ago.

University officials said in a statement that an investigation of Liu's credentials found that "the résumé and academic achievements provided by Liu Hui … were gravely untrue and constituted academic misconduct."

Liu, 46, educated in China and Japan, said he had worked in New York for a decade and was director of the Center for Surgical Research and associate professor of surgery at New York University's (NYU's) School of Medicine. But there is no such center, according to NYU officials, and Liu was never an employee.

Shi-min Fang, a U.S.-based biochemist who crusades against "academic corruption" in China (*Science*, 10 August 2001, p. 1039), first questioned Liu's credentials on his Chinese-language New Threads Web site (www.xys.org). Fang also reported Liu's dismissal last month.

FACE-OFFS

WHAT GOES AROUND … Representative Frank Wolf (R–VA) tried to play gotcha with presidential science adviser John Marburger during a 4 April hearing on the proposed 2007 budget for Marburger's Office of Science and Technology Policy and the government's investment in research. But both men wound up with egg on their faces.

Wolf wanted to show that the Bush Administration should be doing more to retain the country's top scientific talent. "Do you know Daniel James?" he asked, referring to a 42-year-old physicist who helped pioneer the field of quantum information while at the Department of Energy's Los Alamos National Laboratory. Marburger's negative reply deflated Wolf, but only momentarily. "Well, now he's a professor at the University of Toronto. That's not in the United States," Wolf proclaimed. Marburger's weak rejoinder, "It's close," seemed ill advised.

Unfortunately for Wolf, James is a British citizen born in Manchester, U.K., who came to the United States for postdoctoral training but became disillusioned with the "poor leadership … and low morale" at the New Mexico weapons lab. James told *Science* last week that, ironically, "I was ready to get naturalized" when Toronto came calling in spring 2005 with a generous offer that included a chaired professorship.

MOVERS

CROSSING THE PACIFIC. A high-profile U.S. husband-and-wife team is decamping for Singapore to help launch the country's translational medicine research efforts. Edward Holmes, 65, dean of the School of Medicine at the University of California, San Diego (UCSD), will help steer national policy as deputy chair of clinical-translational sciences at Singapore's Biomedical Research Council. His wife, Judith Swain, 58, UCSD's dean of translational medicine, will head a new Institute for Clinical Sciences.

Swain says she was attracted by the challenge of starting a translational medicine institution from scratch. To Holmes, moving from day-to-day institutional management to higher level policy-making "sounds like a job made in heaven."

HEALTH OF THE WORLD. The National Institutes of Health (NIH) has recruited an expert in infectious diseases from another federal agency to head the Fogarty International Center. Roger I. Glass has spent most of the past 3 decades at the Centers for Disease Control and Prevention in Atlanta, Georgia. He worked to introduce rotavirus vaccines in developing countries, where diarrhea caused by the virus kills some 600,000 children a year.

The smallest NIH institute or center, with a 2006 budget of $66 million, Fogarty is best known for training scientists from developing countries. In a 31 March press release, Glass praised the center's ability to anticipate "emerging global health problems."

CREDITS (TOP TO BOTTOM): COLIN MCPHERSON; HOLMES AND SWAIN; C. MEASHAM

Got a tip for this page? E-mail people@aaas.org

Vinton G. Cerf
Vice President and Chief Internet Evangelist
Google

Amy Wu
Computer Science Student
Stanford University

Benjamin Mako Hill
Research Assistant
MIT Media Laboratory

Maria Klawe
Dean of Engineering
Princeton University

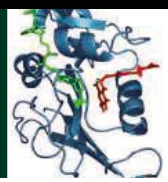

LETTERS

edited by Etta Kavanagh

Retraction

WE WISH TO RETRACT THE REPORT "SINGLE-MOLECULE STUDIES OF HETEROGENEOUS DYNAMICS in polymer melts near the glass transition" (*1*). The majority of the conclusions of this Report were based on the correlation functions of the transient single-molecule data. The Vanden Bout research group has recently reanalyzed these data and found that the correlation functions utilized for the Report do not correspond to the true correlation functions of the transient data. Moreover, the Vanden Bout research group has been unable to reproduce the transient data in either of the polymer systems investigated in the Report. Given that the analysis is flawed and that even the qualitative features of the data cannot be reproduced, we are compelled to retract this Report in its entirety. This retraction is occurring simultaneously with the retraction of all related articles (*2*, *3*). We sincerely regret any inconvenience that the publication of these results has caused for others.

DAVID A. VANDEN BOUT[1] AND LAURA A. DESCHENES[2]

[1]Department of Chemistry and Biochemistry, University of Texas at Austin, Austin, TX 78712, USA. [2]Pfizer Global R&D, Michigan Labs, Ann Arbor, MI 48105, USA.

References

1. L. A. Deschenes, D. A. Vanden Bout, *Science* **292**, 255 (2001).
2. L. A. Deschenes, D. A. Vanden Bout, *J. Phys. Chem. B.* **105**, 11978 (2001).
3. L. A. Deschenes, D. A. Vanden Bout, *J. Chem. Phys.* **116**, 5850 (2002).

Marketing Drugs Too Early in Testing

THE U.S. FOOD AND DRUG ADMINISTRATION has had the authority to approve new drugs for sale in the United States on the basis of their demonstrated safety and efficacy since 1962. Since that time, the agency has regularly come under attack by those who believe that access to drugs should be governed by market forces rather than the scientific evaluation of the balance of their benefits and risks. This view has now entered the political domain in the form of a bill before the U.S. Senate, entitled the "Access, Compassion, Care and Ethics for Seriously Ill Patients Act," sponsored by Senators Brownback (R-KS) and Inhofe (R-OK) (*1*). This bill, if it becomes law, will permit marketing of drugs for serious illnesses on the basis of results from nonhuman studies and a Phase I trial, a trial solely designed to establish a tolerable dose, but not designed to assess whether the drug is actually effective or to develop an understanding of its risks.

This bill has caused much consternation in the scientific community, and its demerits are described in detail in a Position Statement from the Society for Clinical Trials (*2*). The vast majority of drugs that enter Phase I testing turn out to be either ineffective or toxic. Consequently, if the bill becomes law, the market could be flooded with ineffective and possibly harmful agents. Patients gravely ill with cancer and other life-threatening diseases, whose rights of access to experimental agents is the ostensible purpose of the legislation, will likely be faced with a wide array of marketed agents, the vast majority of which will be ineffective, a prospect that thoughtful members of the patient advocacy community recognize to be highly undesirable (*3*). Members of the scientific community and the public should be seriously concerned about this issue.

CREDIT (BOTTOM): CHAD BAKER/PHOTODISC GREEN/GETTY IMAGES

COLIN B. BEGG,[1] OTIS BRAWLEY,[2] ROBERT M. CALIFF,[3] DAVID L. DEMETS,[4] SUSAN S. ELLENBERG,[5] RICHARD S. KAPLAN[6]

[1]Memorial Sloan-Kettering Cancer Center, 307 East 63rd Street, New York, NY 10021, USA. [2]Winship Cancer Institute, Emory University, 201 Dowman Drive, Atlanta, GA 30322, USA. [3]Duke Clinical Research Institute, Duke University, Durham, NC 27708, USA. [4]University of Wisconsin, K6-446a Clinical Sciences Center, 600 Highland Avenue, Madison, WI 53792, USA. [5]University of Pennsylvania School of Medicine, 611 Blockley Hall, 423 Guardian Drive, Philadelphia, PA 19104, USA. [6]National Cancer Research Network, Arthington House, Cookridge Hospital, Hospital Lane, Leeds LS16 6QB, UK.

References

1. See www.govtrack.us/data/us/bills.text/109/s1956.pdf.
2. *Clin. Trials* **3**, 154 (2006).
3. *Clin. Trials* **3**, 149 (2006).

Life-Span Extension in Yeast

THE PERSPECTIVE BY JASPER RINE ("TWISTS IN THE tale of the aging yeast," 18 Nov. 2005, p. 1124) shows a serious lack of knowledge about the history and ideas of the aging field. Rine attempts to reconcile recent contrasting claims about yeast replicative aging and calorie restriction (CR). Several labs have shown that *SIR2* and its paralogs are essential for the longevity induced by CR (*1*, *2*), whereas Kaeberlein *et al*. have suggested that it is not SIR2, but rather the TOR pathway, that is essential (*3*).

There are several flaws and omissions in Rine's analysis of these results. First, Kaeberlein *et al*. (*3*) used 0.05% glucose instead of our previously established 0.5%. Yeast grow quite well on the standard 0.5% used for CR, but are starved and slow growing at 0.05%. This difference may explain the different pathways that are engaged, which Rine fails to point out.

Second, Rine concludes that our failure to

see CR-induced longevity in *sir2* strains is due to an excess of ribosomal DNA (rDNA) circles, which mask effects on CR. But we have also knocked out the circle-promoting gene, *FOB1*, in *sir2* mutants to mitigate effects of circles (*1*), and there is no existing data showing that our strains with *SIR2* and *FOB1* deleted have more circles than wild-type strains have.

Third, Rine surmises that if *SIR2* extends life span by reducing rDNA circles, which may be yeast specific, its role in CR-induced longevity cannot extend beyond yeast. This argument would be deeply flawed even if Rine were correct about circles in our strains. However, causes of aging (e.g., circles) are not likely to be conserved from one organism to another, because they are not adaptive. The regulation of life span in response to environmental conditions, in contrast, is adaptive and therefore very likely conserved. *SIR2* orthologs extend life span in *C. elegans* and *Drosophila*, which are not limited by rDNA circles, and are required for CR-induced longevity in *Drosophila* (*4*), a fact missed by Rine. *SIR2* genes are uniquely suited to respond to CR because they encode NAD-dependent deacetylases (*5*–*7*), which promote longevity by functioning on substrates and pathways that are organism specific. The fact that *SIR2* suppresses circles in response to CR in yeast in no way negates its generality as a mediator of CR-induced longevity in other organisms. Thus, Rine is inaccurate in his description of the differences reported in the yeast studies, as well as implications for *SIR2* genes as mediators of CR in higher organisms.

DAVID A. SINCLAIR,[1] SU-JU LIN,[2] LEONARD GUARENTE[3]*

[1]Department of Pathology, Harvard Medical School, 77 Avenue Louis Pasteur, Boston, MA 02115, USA. [2]Center for Genetics and Development and Section of Microbiology, University of California, Davis, Davis, CA 95616, USA. [3]Department of Biology, Massachusetts Institute of Technology, Cambridge, MA 02139, USA.

*To whom correspondence should be addressed. E-mail: leng@mit.edu

References

1. S. J. Lin *et al*., *Nature* **418**, 344 (2002).
2. D. W. Lamming *et al*., *Science* **309**, 1861 (2005).
3. M. Kaeberlein *et al*., *Science* **310**, 1193 (2005).
4. B. Rogina, S. Helfand, *Proc. Natl. Acad. Sci. U.S.A.* **101**, 15998 (2004).
5. S. Imai *et al*., *Nature* **403**, 795 (2000).
6. J. Landry *et al*., *Proc. Natl. Acad. Sci. U.S.A.* **97**, 5807 (2000).
7. R. M. Anderson *et al*., *Nature* **423**, 181 (2003).

Response

MY PERSPECTIVE FOCUSED ON TWO PAPERS that investigated whether the life-span extension caused by caloric restriction (CR) requires the function of Sir2p and one of its paralogs, Hst2p. Sinclair *et al*. conclude that Sir2p and Hst2p mediate the extension in yeast life span by CR as reported in Lamming *et al*. (*1*), whereas Kaeberlein *et al*. concluded that yeast life-span extension by CR is independent of Sir2p, depending instead upon Tor and Sch9 proteins (*2*). The challenge is finding the most parsimonious explanation for this discrepancy.

Sinclair *et al*. emphasize the differences in growth media used in the two studies [0.5% glucose (*1*) versus 0.05% glucose (*2*)]. I agree that the yeast growth medium with 0.5% glucose, rather than the conventional 2% glucose, represents CR for yeast. Thus, the 0.05% glucose used by Kaeberlein *et al*. must also represent CR, especially considering that growth at 0.05% glucose is accompanied by extended life span, rather than a shorter life span that might reflect inadequate calories to support viability. Perhaps the extent of CR influences which genes mediate replicative longevity.

In earlier studies, Guarente and colleagues elegantly demonstrated that recombination in the ribosomal DNA (rDNA) repeats leads to extrachromosomal rDNA circles that decrease the life span of yeast (*3*). The elevated recombination in the rDNA evident in *sir2* mutants appears to prevent CR from extending life span (*4*). As Kaeberlein *et al*. reported in an earlier

paper, reducing rDNA recombination in *sir2* mutants by using the *fob1* mutation allows CR to extend life span in the *sir2 fob1* double mutant (*4*). Thus, the effect of CR on life-span extension can be masked when rDNA recombination leads to extrachromosomal circles. Sinclair *et al*. argue that they also used the *fob1* mutation to mitigate against elevated rDNA recombination in *sir2* mutants. However, the critical issue is whether *HST2*, a paralog of *SIR2*, is necessary for life-span extension in response to CR, as concluded by Lamming *et al*., or whether other interpretations are possible. Unfortunately, although the *fob1* mutation can block the elevated rDNA recombination evident in *sir2* mutants, Lamming *et al*. report that *fob1* is unable to block elevated rDNA recombination in a *sir2*, *hst2*, *fob1* triple mutant (*1*). Thus, it is possible that what appears to be CR extending life span in a way that depends on *HST2* and *SIR2* is actually increased rDNA recombination blocking CR from extending the life span of this *sir2*, *hst2*, *fob1* triple-mutant strain. It seems important to learn whether the elevated rDNA recombination in this triple mutant does indeed lead to increased levels of rDNA circles.

Kaeberlein *et al*. showed that the life-span extension produced by CR (0.05% glucose) requires *SCH9* and *TOR1* but not *SIR2* (*2*). However, whether life-span extension in this context depends on *HST2* has not yet been reported.

Sinclair *et al*. characterize my view as surmising that *SIR2* orthologs cannot be mediators of CR effects on longevity in other species. That characterization is incorrect. As a discoverer of the *SIR* genes, I am delighted by the emerging role of *SIR2* orthologs in promoting longevity of other species, potentially in response to CR (*5*), regardless of whether *SIR2* and its paralogs mediate CR effects on aging in yeast.

JASPER RINE

Department of Molecular and Cell Biology, University of California, Berkeley, Berkeley, CA 94720, USA. E-mail: jrine@berkeley.edu

References

1. D. W. Lamming *et al.*, *Science* **309**, 1861 (2005).
2. M. Kaeberlein *et al.*, *Science* **310**, 1193 (2005).
3. D. A. Sinclair, L. Guarente, *Cell* **91**, 1033 (1997).
4. M. Kaeberlein *et al.*, *PLoS Biol.* **2**, E296 (2004).
5. B. Rogina, S. Helfand, *Proc. Natl. Acad. Sci. U.S.A.* **101**, 15998 (2004).

Letters to the Editor

Letters (~300 words) discuss material published in *Science* in the previous 6 months or issues of general interest. They can be submitted through the Web (www.submit2science.org) or by regular mail (1200 New York Ave., NW, Washington, DC 20005, USA). Letters are not acknowledged upon receipt, nor are authors generally consulted before publication. Whether published in full or in part, letters are subject to editing for clarity and space.

Archaeopteryx: The Lost Evidence

IT SEEMS THAT *ARCHAEOPTERYX* FINDINGS have always been accompanied by mysterious circumstances. The first complete specimen discovered in Bavaria in 1861 was sold by its anonymous finder to a wealthy buyer, kept secret, and eventually sold to the Natural History Museum in London (*1*).

The tenth, and most recent, specimen is no exception. Also found in Bavaria, by an unknown person (allegedly in the 1970s), it was sold to an unknown third party in Switzerland, ending up in a small private museum in Thermopolis, Wyoming, USA. The finding was published in *Science* (G. Mayr *et al.*, "A well-preserved *Archaeopteryx* specimen with therapod features," Reports, 2 Dec. 2005, p. 1483), along with the description of a failed attempt to buy the specimen by the Senckenberg Natural History Museum in Frankfurt, Germany, where it is being studied (E. Stokstad, "Best *Archaeopteryx* fossil so far ruffles a few feathers," News Focus, 2 Dec. 2005, p. 1418).

The remains of *Archaeopteryx* are probably the most important fossils in the world, the petrified evidence for Darwin's postulate of the existence of missing links. The preservation of the 10th specimen is spectacular, rivaled only by the second specimen. It might seem appropriate that it should find a home in the creationism-shaken and intelligent design–rattled United States. I am concerned, though, that because it is a private museum, researchers may not always have unrestricted and timely access.

As a paleontologist and the former director of the Bavarian State Collections of Paleontology and Geology, which bought *Archaeopteryx* 7 from its legal owner in 1999, I am frequently asked why there was no joint venture attempt to keep *Archaeopteryx* 10 in Bavaria, or at least in Germany. My answer is that no one who might have taken part in such a venture knew about the specimen until the *Science* Report was published. It is understandable that the Senckenberg's attempted purchase was kept secret to prevent the price from skyrocketing, but it is unfortunate that the correct time to ask the rest of the community for a joint purchasing campaign was missed.

Much less understandable is why *Archaeopteryx* 10 has not been protected as a national cultural heritage, as have all previous specimens not owned by public institutions. The State of Bavaria would have requested this status for *Archaeopteryx* 10 if it had known about the find in time: German law stipulates that the state housing an object is responsible for applying to the federal authorities for such protection. Because *Archaeopteryx* 10 is presently in the State of Hessen, Hessen authorities would have to do so. However, to have a chance to obtain the fossil for scientific studies, Hessen has issued a clearance statement that grants re-export of *Archaeopteryx* 10 if it is, why for sure, not

apply for the status of *Archaeopteryx* 10 as a national cultural heritage, because this would jeopardize the guaranty given by its own authorities that the fossil may leave Germany again.

As Speaker of the Board of Directors of the German Natural History Research Collections, I believe that *Archaeopteryx* 10 is an important part of German cultural heritage and should preferably be kept in a German public research collection or in a large, public natural history research museum in the United States. Unlimited access for scientific researchers must be the primary goal. I strongly encourage the present owner to permanently deposit *Archaeopteryx* 10 either in the Senckenberg Museum or in one of the other public natural history research museums in Germany or the United States. This would be an honorable acknowledgment of the immeasurable cultural and scientific value of *Archaeopteryx* 10.

REINHOLD LEINFELDER

Director General, Museum of Natural History, Humboldt-University, Invalidenstrasse 43, Berlin D-10115, Germany. Speaker, Board of Directors, German Natural History Research Collections (Direktorenkonferenz der Naturwissenschaftlichen Forschungssammlungen Deutschlands/DNFS). E-mail: leinfelder@museum.hu-berlin.de

Reference

1. P. Chambers, *Bones of Contention* (Murray, London, 2002).

CORRECTIONS AND CLARIFICATIONS

NetWatch: "Quick-change act" (10 Feb., p. 751). The item incorrectly stated that becquerels, a measure of an isotope's radioactivity, can be converted into rads, a measure of absorbed dose.

TECHNICAL COMMENT ABSTRACTS

Comment on "The Illusion of Invariant Quantities in Life Histories"

Van M. Savage, Ethan P. White, Melanie E. Moses, S. K. Morgan Ernest, Brian J. Enquist, Eric L. Charnov

Nee *et al*. (Reports, 19 August 2005, p. 1236) used a null model to argue that life history invariants are illusions. We show that their results are largely inconsequential for life history theory because the authors confound two definitions of invariance, and rigorous analysis of their null model demonstrates that it does not match observed data.

Full text at www.sciencemag.org/cgi/content/full/312/5771/198b

Response to Comment on "The Illusion of Invariant Quantities in Life Histories"

Sean Nee, Nick Colegrave, Stuart A. West, Alan Grafen

Savage *et al*. describe two different kinds of invariant. The kind they claim to have the greatest biological importance allows the invariant quantities to vary widely, even randomly, between different species. We do not agree that such quantities reveal any deep constraints on evolution.

Full text at www.sciencemag.org/cgi/content/full/312/5771/198c

SCHOLARLY PUBLISHING

Who Needs Books?

Sam Elworthy

In May 1859, Charles Darwin badly needed a publisher. He was relieved when, with some encouragement from his friend Sir Charles Lyell, the London publisher John Murray agreed to take on *The Origin of Species*. A publisher could do many things that Darwin could not. John Murray took his handwritten manuscript and turned it into type and pages, worked with a nearby printer to turn out 1250 finished books, solicited reviews, placed advertisements in major magazines and newspapers, and sold the books to shops and circulating libraries. Even better, the publisher did all this with its own money. Darwin inhabited a heterogeneous intellectual environment peopled by everyone from clergy to cow breeders, poor plant collectors to gentlemen philosophers. To propagate his ideas among that diverse audience, a book and a publisher were crucial.

Books in the Digital Age
The Transformation of Academic and Higher Education Publishing in Britain and the United States

by John B. Thompson

Polity, Cambridge, 2005. 480 pp. $79.95, £65. ISBN 0-7456-3477-X. Paper, $29.95, £19.99. ISBN 0-7456-3478-8.

Would Darwin need a publisher now? Would he even write a book? Over the past 25 years, advances in technology have revolutionized what authors can do themselves. We all now create type, and most of us can post what we write to a Web site that can be accessed by a billion or so people all over the world. We can even get a self-publishing outfit to print a decent-looking book and make it available through Internet booksellers. And we can do all of this with computers that we already own and a few hundred dollars. In 2006, the publisher no longer holds a monopoly over the ability to produce and disseminate a book. At the same time, the audience for scientific ideas has become much more homogeneous and easy to reach than it was in Darwin's time. The rise of modern universities, academic disciplines, and professional societies means that we no longer expect a biology book to reach cow breeders or clergy. A well-placed article in a professional journal or an e-mail to a key listserv may be sufficient to get across a major new idea to the audience that matters. Who, then, needs book publishers?

John Thompson gives us a partial answer to that question. In *Books in the Digital Age*, he systematically examines the changing economics of academic and textbook publishing and the social role that books play for publishers and scholars today. Thompson, a professor of sociology at Cambridge and a founder of Polity Press, brings great credentials to the job, and he has done prodigious homework. After interviewing over 200 key publishers and wading through great piles of data, Thompson has soaked himself in publishing fact and lore. His findings are not startling or outrageous, but they are consistently reliable.

Thompson argues, with perhaps a little hyperbole, that book publishing is now undergoing its most fundamental transformation since Gutenberg. What is changing? Thompson identifies four key factors. (*i*) The rise of computers and the Internet has changed publishing in myriad ways—from the way publishers edit, typeset, and print books to the way people buy, read, and process information. (*ii*) Booming sales through Internet booksellers and shriveling budgets for books at academic libraries have reshaped the book market. (*iii*) The number of commercial scholarly publishers has shrunk even as the number of books published grows every year. (*iv*) Publishing now takes place in a global environment where students at Yale can find themselves buying textbooks that have been acquired from a Dutch professor by an English publisher, composed in India, printed in China, sold in cheap versions to Pakistani students, and then sold back to Yale students on the hunt for a bargain.

Publishers are finding various ways to weather these storms, but Thompson sees a fundamental crisis of legitimacy in publishing. As he acknowledges, publishers now routinely work from authors' electronic files; they usually hand off copy editing, composition, and printing to outside firms; and they often rely on others even for sales and distribution. What distinctive value or expertise, then, is the publisher adding? Thompson argues, rightly I think, that publishing is at its heart about intellectual and financial risk-taking. Good publishers see an extraordinary idea that might take hold of a field. Or they spot an outstanding young scientist, and they take a risk on that hunch—investing a few thousand dollars to edit, design, produce, and promote a book. Frequently the book is a failure. The idea doesn't take off, the scientist doesn't get recognized, and the publisher loses money. But when a book succeeds, it can recoup the publisher's initial investment many times over and turn a bright idea into an intellectual movement. That fundamental role of the publisher has not changed much since John Murray took a gamble on *The Origin of Species*. The publisher brings an understanding of scholars and ideas as well as some cash to engage in the educated risk-taking that allows new ideas to take off.

The reviewer is at Princeton University Press, 41 William Street, Princeton, NJ 08540–5237, USA. E-mail: sam_elworthy@pupress.princeton.edu

BROWSING

CREDIT: (LEFT) MARK KLETT WITH MICHAEL LUNDGREN; (RIGHT) GROVE KARL GILBERT, U.S. GEOLOGICAL SURVEY

After the Ruins, 1906 and 2006. Rephotographing the San Francisco Earthquake and Fire. Mark Klett, with Michael Lundgren. University of California Press, Berkeley, CA, and the Fine Arts Museums of San Francisco, 2006. 140 pp. $49.95, £32.50. ISBN 0-520-24434-6. Paper, $24.95, £15.95. ISBN 0-520-24556-3.

This volume—from an exhibition running at San Francisco's Legion of Honor through 4 June—pairs archival images from 1906 with modern photos showing the same locations today. Essays by historian Philip Fradkin and writer Rebecca Solnit discuss the quake and fire and their place in the city's history and landscape. Although most of Klett's pairings depict urban sites (see page 203), the series ends with two views of the fault trace near Olema.

But what about books? As Thompson makes clear, books are so central to faculty tenure and promotion in the humanities and most of the social sciences that the flood of new titles is unstoppable. But might not journal articles and conference papers suffice for the dissemination of scholarship? Thompson is not quite so useful here. In science, where scholars don't write books for professional advantage, we may have a clearer window into what role, if any, books actually play in modern scholarship. In some scientific disciplines the answer seems to be none. Authored scholarly books (apart from textbooks) are essentially extinct in fields like chemistry and molecular biology. But in disciplines from math to astrophysics to ecology, the book still plays a key role. To lay out a sustained argument for a new way of understanding the distribution of species, Robert MacArthur and Ed Wilson really needed a book (*1*). To explain to students and general readers how different the world might look from a gene's perspective, Richard Dawkins had to write a book (*2*). To fully develop a big idea and to convey it to an audience beyond a narrow circle of specialists, books and publishers still play a key role. But of course, I am a book publisher.

References

1. R. H. MacArthur, E. O. Wilson, *The Theory of Island Biogeography* (Princeton Univ. Press, Princeton, NJ, 1967).
2. R. Dawkins, *The Selfish Gene* (Oxford Univ. Press, Oxford, 1976).

10.1126/science.1119715

SCIENTIFIC PUBLISHING

Considering Multiple Flavors

John E. Enderby

I must declare both a personal and professional interest. Until recently, I was vice president of the Royal Society and lead officer for its publishing activity, which depends for its income on the subscription model. I am also president of the Institute of Physics (IOP), which, as with many other learned societies, uses the profits from its publishing activities to promote and support its discipline, both within the United Kingdom and beyond. In addition, I am a paid adviser to the IOP's publishing company and therefore have a strong interest in the sustainability of any new business model for scholarly journals.

I inwardly groaned when I was asked to review John Willinsky's *The Access Principle: The Case for Open Access to Research and Scholarship*. I suspected that here was another polemic pointing out the iniquities of publishers by making scholars pay twice (in page charges and subscription fees) for access to work and pocketing huge profits in the process. In fact, my fears were unfounded. Willinsky, the director of the Public Knowledge Project at the University of British Columbia, offers a well-researched and scholarly account of the issues surrounding the publication of research. The book is both balanced and fair in its discussion of the various models and responses to concerns about the accessibility of publicly funded research. Perused in conjunction with the research report of the Association of Learned and Professional Society Publishers (ALPSP) on open-access publishing (*1*), it makes important reading for publishers, research funders, politicians, and senior policy-makers.

The Access Principle
The Case for Open Access to Research and Scholarship

by John Willinsky

MIT Press, Cambridge, MA, 2005. 307 pp. $34.95, £22.95. ISBN 0-262-23242-1. Digital Libraries and Electronic Publishing.

Early on in *The Access Principle*, Willinsky makes the crucial distinction between open access and free access. Take, for example, the notion that human rights include "the right to know," a theme the author touches on in both philosophical and political terms. Let us ignore an argument that there is in fact a hierarchy of rights with perhaps clean water, food, clothing, and shelter at the top. None of these is free, even though freedom from hunger is, I would argue, a fundamental right. The apparent contradiction is, at least in developed countries, resolved by a model in which those who can pay for food and shelter do so, and those who cannot are provided with welfare payments of one form or another. Government subsidies to producers might well mask the true cost of, say, food—such payments can and do distort the market and lead to unforeseen consequences for developing countries.

Thus once it is recognized that access to reliable information will have a cost, the question arises as to who will pay for validation and dissemination. Willinsky does not duck this issue and points to the many different business models that he categorizes into "ten flavors of open access." For example, the Health Inter-Network Access to Research Initiative and International Network for the Availability of Scientific Publications projects deliver free or heavily discounted journals to developing countries. Some publishers make material available after a delay, typically six months or one year. The IOP puts all its journals on the Web free of charge for 30 days. Others charge the authors either at submission or at publication.

As Willinsky points out, estimates of the charges that must be levied to create a sustainable business model vary hugely. The ALPSP study (*1*) suggests that the cost of the peer review process is $400 per published paper. The Public Library of Science, on the other hand, charges authors $1500 per paper while also drawing on an initial grant of $9 million from a foundation. Why the difference? Part of the answer is that the charge to successful authors must be enough to cover the costs of processing papers that do not meet the quality threshold and to provide a subsidy for authors who cannot pay.

I actually think that the growth of the open-access movement and the publishers' response to it reflect the fact that market forces will, in the end, lead to a variety of models, each well suited to particular disciplines. I am therefore uneasy about the prospects of funding organizations imposing new rules on authors because these could lead to unforeseen distortions. I would much prefer to see encouragement to use the new freedoms generated by the Web and by the more relaxed view of copyright that many publishers are now adopting (as Willinsky explains in detail). Self, institutional, or topical repositories have not, it seems, significantly affected the subscription base of non–open-access journals, but this might well change if there were less diversity in the market.

The irony is, as Willinsky is the first to admit, that here we find a book on open access, the fourth page of which carries the usual "© 2006.… All rights reserved. No part of this book may be reproduced," etc. The author fairly points out that versions of most of the chapters have already appeared on the Web, but he explains that he has "now chosen to thoroughly revise the body of this work in book form." In other words, the version of record is available to those who pay. A well-edited and -presented book of this quality, which has involved scholarly work of high order, costs money to write and to produce. But the same is true for review articles and commentary sections of scientific journals. I can see no moral argument for the cost to fall on the producer rather than the consumer (and neither does Willinsky), but there may be powerful arguments involving public engagement and support of science that need to be considered.

Lastly, it must be said that many of the myths surrounding open-access and non–open-access publications have been exposed both by Willinsky and the ALPSP research report. Whereas there might be slightly less copy editing in open-access journals, there is no evidence that quality control mechanisms are less rigorous. But in the end, it must be for each scientific community to decide how best to organize the publication of its research. I do not believe that one size fits all.

Reference and Note

1. Kaufman-Willis Group LLC, *The Facts About Open Access* (Association of Learned and Professional Society Publishers, Worthing, West Sussex, UK, 2005; www.alpsp.org/publications/pub11.htm). This report was sponsored by ALPSP, Highwire Press, and AAAS.

10.1126/science.1125228

The reviewer is at the Department of Physics, University of Bristol, Tyndall Avenue, Bristol BS8 1TL, UK. E-mail: j.e.enderby@bristol.ac.uk

SCIENCE COMMUNICATION

Environmental Science Adrift in the Blogosphere

Weblogs are a growing global phenomenon with important consequences for science policy and communication. A survey of blogs on environmental topics shows that they vary greatly in accuracy, which indicates a need for participation by informed scientists.

Alison Ashlin* and Richard J. Ladle

One of the latest challenges to face science communicators is the rise of weblogs or blogs; "frequently updated websites consisting of personal observations, excerpts from other sources, typically run by a single person, and usually with hyperlinks to other sites; online journals or diaries" (*1*). Writing or maintaining a weblog (blogging) has become a hugely popular Internet phenomenon. There are now more than 11.7 million weblogs, and it is estimated that this number is doubling every 5 months (*2*) with one new weblog being created every second (*3*).

Enhanced online at www.sciencemag.org/cgi/content/full/312/5771/201

When linked together into intertwining communities or blogospheres, weblogs provide a communication platform of incredible power and complexity. Information and opinions are exchanged, transformed, and reworked with astounding rapidity across international boundaries and time zones (*2*).

Discussions in the traditional news media about the blogging phenomenon have ranged from the untapped potential of the blogosphere for collaborative learning (*4*) and the power and reach of weblogs to the public relations potential for voluntary sector operations (*5*). Not only is the Internet emerging as a vehicle for enhanced civic involvement (*6*), but many weblog users judge weblogs to be highly credible, even more so than traditional print media or other online sources (*7*). Although the general public is embracing weblogs, many scientists are not, possibly because of the association of blogging with Internet chat-rooms or even the fear of intellectual property theft (*7*).

Accurate representation of environmental science is vitally important for the current and continued support of public policy. Currently, there are roughly 400,000 weblogs featuring discussions on environmental and conservation-related issues, which makes it difficult to assess the general quality of scientific information on weblogs (table S1). To provide a snapshot of scientific representation in the blogosphere, we explored current predictions for global extinction rates as cited within 30 sites (see figure above). There is still uncertainty, but the scientific consensus puts the maximum predicted rate between 74 and 150 species going extinct every day [27,000 to 55,000 per year (*8*)]. Roughly 40% of the sites we examined indicated that extinctions are occurring at rates greater than 200 per day (73,000 per year). The daily extinction rates ranged from one to several thousand per day!

Whereas scientists are used to spotting and correcting errors in traditional communication media, many remain unaware of the blogging discourse. If environmental scientists ignore online communication platforms such as weblogs, we run the risk of creating a generation of eco-illiterate consumers and voters at a crucial time for the Earth's diminishing resources. How should we respond to the challenges and opportunities presented by the blogosphere? We suggest the following responses, which are potentially applicable to all scientific disciplines.

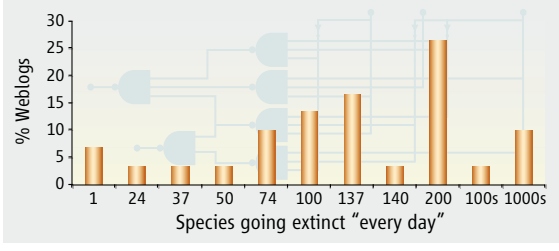

A representation of global species extinction estimates in the blogosphere. The 30 weblogs on daily extinction rates were identified with Google Blog Search and search phrases "extinct per day" and "extinct every day."

Environmental scientists should actively engage in blogging to increase the presence of informed opinions in the blogosphere. Research supervisors should encourage students to blog while providing training in science communication and dissemination. Senior scientists should set up their own high-profile weblogs to help allay fears that blogging is somewhat disreputable. Blogging should be part of a portfolio of public engagement activities, even to the extent of including blogging as part of a researcher's job specification. Examples of excellent, informative sites can readily be found (table S2), but more are needed.

Environmental research groups and peer groups should create weblogs for the discussion of new ideas and the dissemination of research findings. Such weblogs could act as platforms for brainstorming new concepts and generating ideas (*9*). The interactive characteristics of weblogs could also provide an alternative mechanism for gaining feedback in the early stages of a research project. Additionally, group weblogs could be used for public engagement and interpreting peer-reviewed literature.

Environmental scientists should use weblogs for reporting and commenting on international conferences. For example, the IDS Climate Change and Disasters Group effectively used their weblog to report back live from the United Nations 2005 Climate Change Conference in Montreal (*10*).

Field-based environmental scientists should blog as a mechanism for inspiring future environmentalists and to provide a real-time platform for sharing their expertise. Blogging is an excellent way to communicate the excitement of working and living in the field. Furthermore, new wireless communication systems and solar technology now make real-time blogging possible from the remotest of locations.

Some commentators have suggested that weblogs will only increase in popularity among the scientific community once a peer review mechanism has been implemented (*9*). As this is highly unlikely to happen and because much of the appeal of blogging lies in its spontaneity and interactivity, we believe that researchers should not adopt a wait-and-see policy. As citizen-scientists, we have a responsibility to contribute informed opinions to environmental debates and to develop a collective presence in the blogosphere, thereby increasing its inherent credibility. With sites that make the process of creating a weblog quick and easy (*11*), environmental science no longer needs to be adrift in the blogosphere.

The authors are at the Oxford University Centre for the Environment, University of Oxford, South Park Road, Oxford OX1 3QY, UK. *E-mail: aashlin@ouce.ox.ac.uk

References and Notes

1. Oxford English Dictionary (Oxford Univ. Press, Oxford, 2005).
2. J. Cherkoff, *Independent*, 27 June 2005, p. 16.
3. O. Gibson, *Guardian*, 7 October 2005, pp. 1 and 9.
4. D. Buckley, *Times Educational Suppl.*, 16 September 2005, p. 11.
5. "CRISIS co-hosts symposium on value of blogging," *PR Week*, 8 July 2005, p. 7.
6. M. R. Kerbel, A. D. Bloom, *Harvard Int. J. Press-Polit.* **10**, 3 (2005).
7. T. J. Johnson, B. K. Kaye, *Journalism Mass Commun. Q.* **81**, 622 (2004).
8. J.J.Sepkoski, *J. Paleontol.* **71**, 533 (1997).
9. D. Butler, *Nature* **438**, 548 (2005).
10. Live report link (http://community.eldis.org/webx?14@319.iuXYaoDTkR5.0@.ee9f0e1!discloc=.eeca564).
11. Blogger (www.blogger.com).

Supporting Online Material

www.sciencemag.org/cgi/content/full/312/5771/201/DC1

10.1126/science.1124197

Invest in Italy

ITALY'S LIFE SCIENCES SECTOR IS GAINING MOMENTUM

A breeding ground for biotech companies

Italy's Life Sciences industry is becoming ever more appealing for multinational companies seeking to pursue biotechnology and pharmaceutical research. The sector is spurred on by the strong interaction between academia and business environment, a vibrant medical and hospital system, the capacity of world class scientists to produce leading-edge research as well as government support.

Italy's upsurge in the Life Sciences is also proved by a strong performance in the product pipeline with 21 drugs in clinical trials (particularly in Oncology and Neurosciences), which makes it rank ahead of some major European countries like France, Germany and Sweden, if we compare the number of companies with products in pipeline.

Performance Index of Biotech Companies

(Number of products/Number of companies)

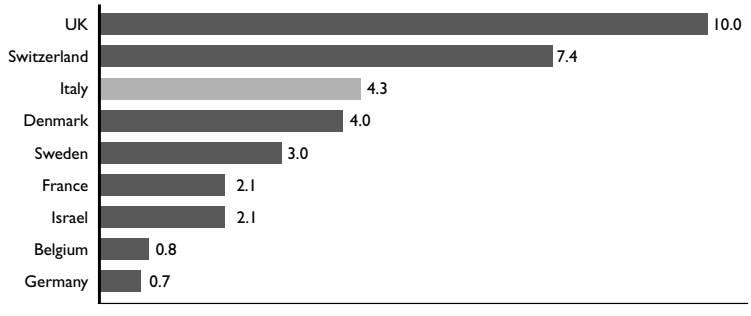

Source: InvestInItaly based on NES, Assobiotec – 2005

Competitive advantages for international investors

Italy's competitive advantage for international investors is also represented by the skilled workforce. Its R&D professionals – 6,000 researchers employed by businesses, a pool of 20,000 university researchers, 200,000 students and 35,000 graduates annually in Biotechnology, Pharmacy and Medicine – are extremely productive, with creativity second to no competitor country worldwide. As a proof, Italy ranks top in Europe for patent productivity and impact rate of publications.

Start-ups and new business initiatives can count on the support of a network of science parks specialized in life sciences, with a track record of excellence in Biotechnology, Biomedical technology, Diagnostics, Genomics. Besides, labor, business and clinical trials costs are internationally competitive with respect to USA, UK, France and Germany.

Innovation Spotlight

Italy to Launch Europe's First Institute for Regenerative Medicine

Modena – The University of Modena and the Eye Bank Foundation of Venice have joined forces to create a public/private partnership forming the Research Center for Regenerative Medicine. It will become the first such center in Europe focused on stem cell therapy for treating vision disorders caused by tissue/organ damage and genetic defects.

Italy Leads Development of Gene Expression Atlas

Naples – The Telethon Institute of Genetics and Medicine (TIGEM) is spearheading a team made up of 12 major European research institutes to develop the first comprehensive atlas of gene expressions with an estimated identification of 30,000 genes.

Italian and American Researchers Team Up on Heart Stem Cell Breakthrough

Rome – Researchers at La Sapienza University in Rome recently teamed up with John Hopkins University to conduct the first study using stem cells to repair the same type of organ from which they were derived. The promising results were presented at the American Cardiology Congress (ACC).

ITALIAN BIOTECH DATABASE

www. italianbiotech.com

The complete on line directory - sponsored by InvestInItaly - to find out more about the Italian Biotech community.

SviluppoItalia

Italian Trade Commission

InvestInItaly is the Italian organization for investment promotion created by Sviluppo Italia, the National Agency for Enterprise and Inward Investment Development and the Italian Trade Commission, the Government Agency which promotes the internationalization of Italian companies. It aims to provide a single and reliable national reference point to current and new foreign investors.

A Year of Products, Presents, Thanks for Support

www.investinitaly.com info@investinitaly.com

EARTHQUAKE ANNIVERSARY

Halfway Through Reid's Cycle and Counting

100 years ago, San Francisco was hit by a great earthquake. The subsequent simple models of cyclical fault rupture have not yielded useful predictions; long-term study of seismic mechanisms are still required.

William L. Ellsworth

As dawn broke across coastal northern California on 18 April 1906, the San Andreas Fault yielded to tectonic forces and ruptured along its northernmost 470 km in a great earthquake measuring 7.9 on the moment magnitude scale. From its epicenter west of the Golden Gate, the rupture spread north and south at speeds exceeding 3 km s^{-1}, releasing stored elastic strain energy in the form of seismic waves that wrought a broad swath of destruction from San Jose in the south to Santa Rosa and Ferndale in the north.

The earthquake also broke the dawn for earthquake science in the United States. Many of the leading earth scientists of the day, including A. C. Lawson, G. K. Gilbert, and H. F. Reid, embarked on a comprehensive investigation of the earthquake, published in 1908 and 1910 (*1*), that continues to be the primary reference and data source for modern studies that continue to probe the quake's inner secrets.

Among their many findings, recently summarized by Zoback (*2*), evidence of crustal distortion caused by the earthquake led Reid (*1*) to formulate the theory of elastic rebound that today forms the foundation of physical theories of earthquakes. Reid deduced that the energy released in the quake had been stored as elastic strain in the crust along the fault and that during the quake the opposite sides of the fault moved in response to the applied stresses to release the stored strain energy. Both he and Gilbert understood that strain accumulated slowly and that a long time would be needed to rebuild the strain shed by the 1906 quake.

A path to earthquake prediction looked straightforward to Reid. Simply track the accumulation of elastic strain along a fault until it approaches the breaking strength. Indeed, long-term forecasts of earthquakes apply the earthquake cycle concept through renewal models to estimate the likelihood of strong earthquakes. For the northern San Andreas Fault, about half of the strain has reaccumulated in the past century, leading to the expectation that another great earthquake there is not imminent (*3*).

The potential for smaller but deadly earthquakes is high, however [62% chance in the greater San Francisco Bay area of moment magnitude (M) ≥ 6.7 by 2031 (*3*)], and northern Californians cannot afford to be complacent. As with people facing natural hazards everywhere, taking ownership of the problem by developing a culture of preparedness, investing in mitigation, and planning for response and recovery will save lives and reduce economic losses.

Now and then. (**Left**) Market Street, San Francisco, today, in a split composite photograph and (**right**) on 18 April 1906 as fire began to consume the Call Building (in center of photo). The building's steel frame was apparently undamaged by the earthquake, and it remains in use today. Note the debris from collapsed masonry buildings further up Market Street. [1906 photo by W. J. Street, courtesy Bancroft Library, Univ. of California, Berkeley. Rephotography by M. Klett with M. Lungren (*8*).]

There is a cultural tendency, however, to prefer the quick fix: Just tell me when the quake will happen and I'll find time to get ready. But as we saw with Hurricane Katrina, the time to prepare is not when the storm is bearing down but in the long calm beforehand, as the exposed vulnerabilities are years in the making.

The reality is that short-term earthquake prediction continues to elude our grasp, and though some continue to search for a silver bullet, the overwhelming consensus is that more needs to be known about the physics of earthquakes and the seismogenic crust before the limits of predictability will be understood (*4*). This strategy requires patience, as the cycle is long for the large earthquakes that matter most to society.

The patience required to mount long-term experiments also taxes funding agencies. My own experience with the Parkfield Earthquake Experiment, beginning in 1982, has been that it is hard to gouge long-term support for the ground, harder to maintain them when competition comes from short-term needs, and hardest to grow them once underway. We were very fortunate that after two decades of steadfast monitoring, the San Andreas Fault produced the anticipated M = 6.0 earthquake at Parkfield in 2004 (*5*) in the middle of the network designed to catch it. Among the results, entire classes of hypothesized deformation and electromagnetic precursors failed to materialize.

Perhaps the most important data caught in the Parkfield trap were 40 near-field strong motion recordings of the propagating rupture (*5*). These accelerograms more than doubled the global database of observations within 10 km of the fault for M ≥ 6, where the strongest shaking occurs. Together with data from the entire suite of experiments, they form a rich harvest of information that will fuel research on earthquake physics and engineering seismology for years to come.

Parkfield alone, however, is insufficient to answer pressing questions on the severity of shaking in the largest earthquakes. We know little about the motions that occur during great

The author is at the U. S. Geological Survey, Menlo Park, CA 94025, USA. E-mail: ellsworth@usgs.gov

earthquakes, because direct measurements in the near field are rare. Exactly one on-scale recording of motion has been collected within 10 km of the rupture plane for great earthquakes ($M \geq 7.9$) worldwide, and only five have been collected within 25 km. No accelerograms exist within 1000 km of either great Sumatran earthquake of 2004 and 2005. Uncertainty in the severity of motion drives conservatism in building codes and hence the cost of seismic safety.

A recently published report by the National Research Council assessed the economic benefits of improved seismic monitoring proposed under the Advanced National Seismic System (ANSS) program of the U.S. Geological Survey (USGS) (*6*). The report concluded that full deployment of the ANSS would reduce the annualized losses in earthquakes of $5.6 billion "by providing critical information for land-use planning, building design, insurance, warnings, and emergency preparedness and response." The report also noted that the annual cost of a fully deployed ANSS is substantially less than the estimated annual benefits of more than $140 million derived just from design and construction savings enabled by reduced uncertainty in earthquake motions.

The Parkfield experiment began about halfway into the earthquake cycle for that segment of the fault, after much of the rapid post-1966 quake adjustments were over, and was monitored by an evolving suite of deformation measurement technologies that spanned the 19th and 20th centuries. The new cycle, which began when the ground motion from the 2004 earthquake ceased, has been captured by the state of the art in Global Positioning System satellite technology, at least as we practice it in the early 21st century. Improvements will come as the Plate Boundary Observatory component of the National Science Foundation EarthScope project connects to the existing USGS networks, and thus there is hope for continued observation of this best-instrumented fault segment in the United States.

All earthquakes begin small and grow at seismic speeds along the fault plane until they either run out of fault or driving stress. Virtually all earthquake nucleations end up as microearthquakes. For every $M = 9$ quake that occurs globally once every few decades, tens of trillions of nucleation events happen. Is there a way to tell them apart at the start? As long as we restrict our study of earthquakes to measurements made at the Earth's surface, we will be blind to inelastic and chemical processes that are part and parcel of the loading cycle, nucleation process, and dynamics of rupture.

This past summer, the inclined main drill hole of the EarthScope's San Andreas Fault Observatory at Depth (SAFOD) (*7*) cut through the entire fault zone at depths between 2.7 and 3.1 km just northwest of the Parkfield earthquake. The hole intersects the fault in the source region of a pair of repeating $M = 2$ earthquakes. Each football field–sized patch on the fault's surface accumulates elastic strain for a few years and suddenly releases it in nearly identical earthquakes. This process has been going on since at least the start of intensive seismic monitoring at Parkfield in the early 1980s, and the postseismic adjustments from the 2004 earthquake have only shortened the length of the earthquake cycle, presently about 1 year.

SAFOD gives us a window into the nonlinear zone where earthquakes nucleate. Physical samples of fault zone materials, extensive geophysical measurements of in situ chemical and physical conditions including the stresses driving the fault, and direct observation of the transition from quasistatic to dynamic slip, presently known only from laboratory analogs and theoretical considerations, will teach us much about the earthquake cycle discovered by Reid a century ago. Whether short-term prediction proves to be achievable even on this scale, the improved understanding of the earthquake cycle will translate into reduced uncertainty in long-term forecasts and probabilistic seismic hazard assessments that are the foundation of building codes and land-use plans. That will be money in the bank.

References

1. A. C. Lawson, Ed., *The California Earthquake of April 18, 1906: Report of the State Earthquake Investigation Commission* (Carnegie Institution of Washington Publ. 87, Washington, DC, 1908 and 1910).
2. M. L. Zoback, *GSA Today* **16**, 4 (April-May 2006).
3. Working Group on California Earthquake Probabilities, *U.S. Geological Survey Open-File Rep. 03-214* (2003).
4. T. H. Jordan, *Seismol. Res. Lett.* **77**, 3 (2006).
5. W. H. Bakun *et al.*, *Nature* **437**, 969 (2005).
6. *Improved Seismic Monitoring, Improved Decision-Making: Assessing the Value of Reduced Uncertainty* (National Research Council, National Academies Press, Washington, DC, 2006).
7. S. H. Hickman *et al.*, *Geophys. Res. Lett.* **31**, L12S01 (2004).
8. M. Klett, M. Lundgren, *After the Ruins, 1906 and 2006: Rephotographing the San Francisco Earthquake and Fire*: (Univ. of California Press and the Fine Arts Museums of San Francisco, 2006).

10.1126/science.1124890

EARTHQUAKE ANNIVERSARY

Can Buildings Be Made Earthquake-Safe?

Earthquake resistant building design has improved greatly since the 1906 San Francisco temblor. However, low-tech solutions for structures in the developing world are sorely needed.

Mary C. Comerio

The 100th anniversary of the 1906 San Franciso earthquake provides an opportunity to reflect on what we have learned about earthquake-resistant design and how research in the field can be used to build better in the future (*1*). During a major earthquake, ground shaking under an urbanized area can cause serious damage or even the collapse of buildings and bridges, freeways, power lines, and other critical infrastructure. The damage can lead to a disaster threatening thousands of lives, and affecting the economic well-being of the epicentral region. Over the past 100 years, architects and engineers have developed tools to assess the earthquake hazard, as well as the stability of individual designs. Building codes provide the key policy mechanism for regulating a standard of safety. However, the death toll in recent earthquakes in Pakistan, Iran, Turkey, and India, and the economic losses in Japan and the United States, suggest that the technical capacity to design buildings to withstand earthquake forces may not be all that is needed to make society safe in earthquakes (*2*).

Throughout history, designers and builders have attempted to learn from earthquake damage in order to improve the stability of their structures. The Roman scientist, Pliny the Elder, suggested bigger buildings, to increase earth's trapped air. When Lima was leveled by an earthquake in 1746, authorities limited the height of buildings and required *quincha* (adobe reinforced with bamboo) construction. In Portugal, the *gaiola*, a masonry building reinforced with a wooden framework, was perfected after the 1755 Lisbon earthquake. Between 1850 and 1906, architects and civil engineers in San Francisco attempted a variety of design innovations to reinforce their buildings for seismic stability. In one case, a raft of redwood logs was used to "float" a foundation on bay mud; other inventors patented "earthquake-proof" technologies (see the figure) (*3*). Others used iron tie-rods secured to the masonry walls to ensure that the exterior walls would not fail. In fact, photos of the destruction

The author is in the Department of Architecture, University of California, Berkeley, Berkeley, CA 94720–1800, USA. E-mail: mcomerio@berkeley.edu

wrought by the 1906 earthquake and fire also show that numerous major brick buildings survived the shaking intact. All were designed by professionals who were extremely cognizant of the possibility of damage from lateral forces (*4*).

Still, the assessment of damage after the 1906 earthquake and fire forced architects and engineers to reassess the dangers and limits of unreinforced masonry (brick, stone, or adobe) construction, and to look to concrete and steel—new materials with the capacity to provide larger interior spaces, large openings for better light, as well as more efficient and safer construction for urban buildings. At the same time that the modern movement in architecture created the thin column and light slab for aesthetic and functional simplicity, engineers developed an understanding of the site effects and ground failures caused by earthquakes; and structural engineering began to understand the relation between strong motion, building configuration, and building performance. If it is possible to summarize the achievements of 20th-century earthquake engineering in a sentence, it would be to say that intuitive understandings of building behavior were replaced with scientific tools to measure ground shaking and mathematical models to analyze and predict structural behavior.

These included instruments designed to measure strong motion, laboratory shaking tables designed to simulate and test the response of building components to strong shaking, and mathematical (and later digital) models for calculating the strength of materials, building components, and joints. The development of the tools to collect data on the hazard and the use of analytic procedures to predict structural behavior under earthquake loads, combined with systematic investigations of building failures after events, led to an understanding of how to build both "strength" and "toughness" into buildings and other structures. Strengthening often requires making a building stiff, but stiffness can transfer the load to other building systems, causing extensive damage to partitions, mechanical systems, or contents. As such, design for seismic forces requires balancing the probable ground motions at the site and soil conditions with building configuration, height, materials, and structural system to meet a code standard or a client's performance expectations.

A downtown office building built by a developer will be designed per the code to provide safety for its occupants, and the owner accepts that certain systems may sustain damage and require time for repairs after an earthquake. However, an art museum, or a high-technology manufacturing facility, may require a design that protects the contents from damage and provides continued operations after an event. To meet such performance needs, new technologies have been developed in recent years. For example, base-isolation uses rubber or neoprene bearings to decouple the ground motion from the building structure. Dampers can be used in a structural frame to act as shock absorbers—again, to lessen the transmission of forces and limit damage.

Public-policy mechanisms are also a key component in limiting earthquake damage. Although building codes promote "safe development" in general, special requirements for schools, hospitals, and emergency-service facilities acknowledge the need for higher standards in certain public buildings. Land-use policies also reduce risk by restricting development in fault zones or on specific soil types. Similarly, government programs aimed at preparedness and hazards mitigation contribute to the reduction of losses.

Performance-based earthquake engineering is a relatively new concept that challenges engineers to rethink the parameters by which they measure good seismic design, and it challenges the policy-makers to rethink safety standards (*5*). The goal of performance-based earthquake engineering is to design facilities with predictable levels of seismic performance, using casualties, cost, and downtime as metrics. Current research at the Pacific Earthquake Engineering Research (PEER) Center combines a probabilistic assessment of the hazard, using suites of ground motions, with nonlinear dynamic analyses of building responses to determine a range of possible outcomes. Although seemingly straightforward, the methodology requires substantial data to adequately model the performance of all building components, and it requires critical judgment in quantifying uncertainty. Equally important, performance-based earthquake engineering requires consumers to specify clear performance goals, and local and state governments to adopt very different approaches to regulating construction. Performance-based earthquake engineering is both inspiring and daunting, but it will unquestionably change the way we design and build in the next 50 years.

The influence of computational technologies on design cannot be underestimated. Not only can designers analyze the technical performance of structures, but they can also use computational technologies to better design the day-lighting and thermal comfort zones in buildings, and to manage maintenance and operations. Computational tools are also changing the form of structures. The new technologies do not require space to be rectilinear for computational purposes. Digital design means that complex curved spaces can be represented, analyzed, and built to the highest seismic standards. The new de Young fine arts museum in San Francisco, and the Walt Disney Concert Hall in Los Angeles, are only two examples.

Unfortunately, the exciting developments in design and engineering do not translate into an overall reduction of losses from earthquakes. On average, every year there are more than 1000 earthquakes of magnitude 5 (M = 5) or greater worldwide. There are 100 earthquakes of M = 6 or greater, and 10 of M = 7 or greater. On 8 October 2005, a M = 7.6 earthquake in the Kashmiri region of Pakistan and India left over 80,000 dead and 4 million homeless. The 26 December 2004 undersea earthquake and tsunami affected 20 countries, killing nearly 300,000 and displacing more than 1 million people. The Bhuj, India, earthquake of 2001 and similar events in Turkey in the

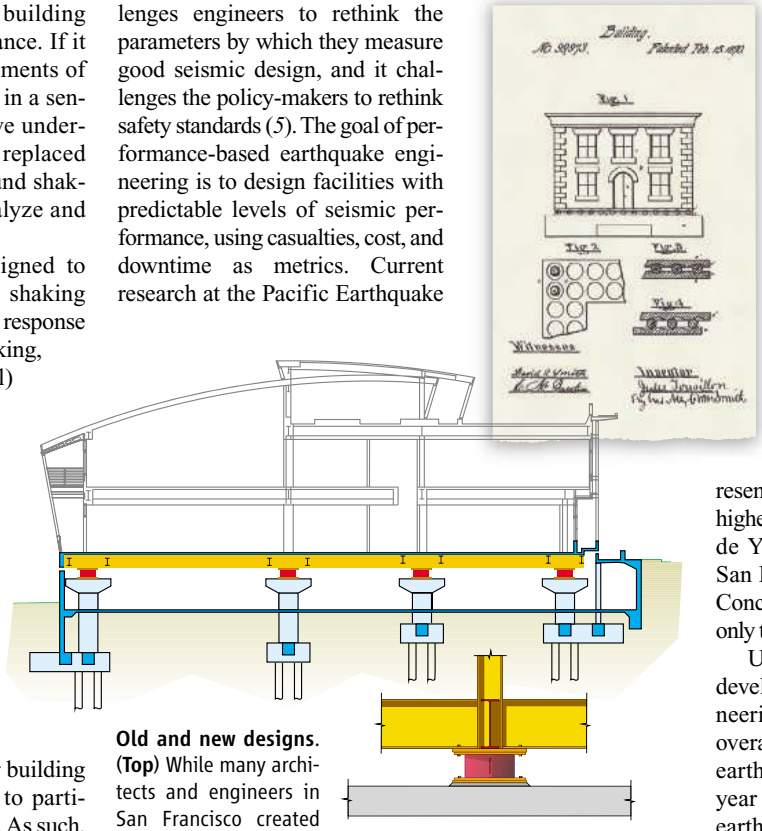

Old and new designs. (**Top**) While many architects and engineers in San Francisco created unique structural details to withstand earthquake forces, the most avant-garde proposal was Jules Touaillon's system of base isolation. He proposed that brick structures be built on platforms that rested on balls, each free to roll within its own space. Touaillon, a San Francisco resident, patented his system in 1870. Little is known about who he was or what prompted his invention. (**Bottom**) Today, the common meaning of isolating a structure is to support its superstructure on extremely hard and dense rubber bearings. Research on this technology began in the 1970s at the Earthquake Engineering Research Center (now the Pacific Earthquake Engineering Center) at the University of California, Berkeley. Forell/Elsesser Engineers, based in San Francisco, and specialists in seismic and innovative engineering, were early adopters of this technology in the retrofits of existing buildings and design of new facilities such as the San Francisco 911 Emergency Communications Center.

CREDIT: MODERN BASE ISOLATOR IMAGE COURTESY FORELL/ELSESSER, ENGINEERS, INC., SAN FRANCISCO, CA

past decade have caused tens of thousands of deaths and in each case, millions were left homeless. In developed countries, such as the United States, Japan, and others, the number of deaths and injuries are typically lower because building standards are enforced and construction quality is higher. However, the economic losses from the 1994 Northridge (Los Angeles) and the 1995 Kobe, Japan, earthquakes were $40 billion and $150 billion, respectively.

Although performance-based earthquake engineering holds the promise of reducing the economic cost of earthquake damage for new and existing buildings in developed countries, low-tech solutions to improve the performance of adobe, rammed earth, and stone construction in developing countries receive little research support, and rely on the volunteer efforts of academics and professionals. For example, the Earthquake Engineering Research Institute supports the World Housing Encyclopedia (*2*), where volunteers share information on good housing construction practices. The Getty Conservation Institute sponsors the Seismo-Adobe project, using volunteers to assist with the preservation of housing and cultural heritage sites around the world. These are laudable efforts, but to genuinely reduce earthquake losses throughout the world, the scientific, design, and engineering communities need to make research on safety in housing construction a global priority. Architects and engineers are creating sophisticated analytic tools for cutting-edge high-tech designs, but if a portion of the research effort went to providing safer solutions for housing, the world's most vulnerable populations would see real progress in earthquake safety.

References

1. M. C. Comerio, *Disaster Hits Home: New Policy for Urban Housing Recovery* (Univ. of California Press, Berkeley, CA,1998).
2. Earthquake Engineering Research Institute, World Housing Encyclopedia (2006); www.world-housing.net/
3. J. Touaillon, U.S. Patent 99,973 (1870).
4. S. Tobriner, *Bracing for Disaster: Earthquake Resistant Architecture and Engineering in San Francisco 1838-1933* (Heyday Books, Berkeley, CA, 2006).
5. P. Fajfar, H. Krawinkler, Eds. *Performance-Based Seismic Design Concepts and Implementation*, PEER Report 2004/05 (Pacific Earthquake Engineering Research Center, Univ. of California, Berkeley, CA, 2004).

10.1126/science.1126302

IMMUNOLOGY

Thoracic Thymus, Exclusive No Longer

T cell production in mice occurs in the chest thymus. A similar second thymus in the neck has now been shown to also make T cells, raising questions about earlier experiments.

Harald von Boehmer

Ancient Greeks considered the thymus "the seat of the soul," probably because of its location near the heart. Anatomists came to regard it as a hormone-producing gland. But in the early 1960s, removal of the thymus in newborn mice provided evidence for its role in lymphopoiesis (*1*, *2*). However, doubts about the exclusive role of the thymus in lymphocyte production persisted because removal of the organ from the thoracic cavity of newborn mice has not always resulted in immunodeficiency (*3*). These results were recently reconsidered, and it was hypothesized that a lymphoid organ with thymus-like histology in the mouse neck (*4*) could be responsible for lymphopoiesis in the absence of the thoracic thymus (*3*). On page 284 in this issue, Terszowski *et al*. (*5*) provide a conclusive answer to this puzzle by showing that a tissue in the mouse neck exhibits all the structural and functional features of a thoracic thymus, including lymphocyte production and selection (see the figure).

The mammalian thymus is not only an organ of intense lymphopoiesis (*1*, *2*, *6*), but also a key locale for the developing immune system to adapt to the organism. The immune system learns to recognize the organism's own cells to avoid mounting an immune response against them. The organism's major histocompatibility complex antigens in the thymus bind to receptors on the surface of developing T cells. This association determines, through differential signaling in the T cells, which lymphocytes will die and which will survive as T helper cells ($CD4^+$), T killer cells ($CD8^+$), natural killer cells, or regulatory T cells. Thus, acquisition of self-tolerance and lymphocyte lineage commitment are important hallmarks of thymus function (*7*). Because of this rather intense T cell receptor–dependent lymphocyte selection process, the thymus is also a major graveyard for lymphocytes that die. In mammals, only a few selected T cells exit the thymus every day and colonize peripheral lymphoid tissues, where they survive

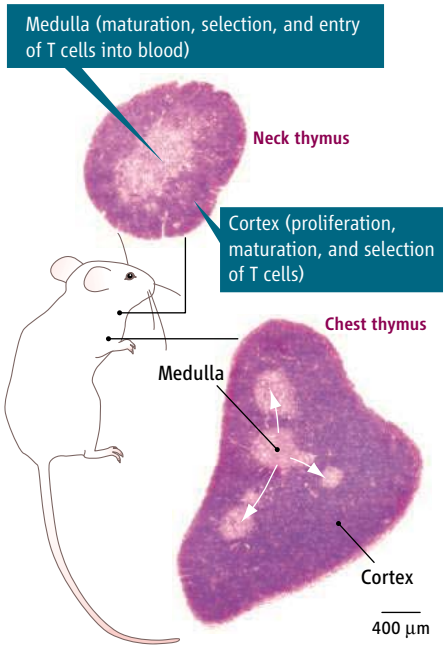

A second thymus. Morphology of neck thymus and chest thymus in a mouse, visualized by May-Grünwald staining of histological sections. In the neck thymus, the cortex-to-medulla size ratio is reduced, corresponding to reduced percentages of cortical T cells compared with those of the thoracic thymus. Images are not representative of the absolute size differences between both organs.

that circulate from blood to lymph and initiate immune responses. Once this peripheral T cell pool is established, the thymus appears to be no longer required, as its removal from the adult has little effect on the peripheral immune system even though the de novo generation of naïve T cells is reduced. The thymus involutes after sexual maturity, but this is counterproductive in situations where a functional thymus is required in adult life—for example, after destruction of lymphocytes by cancer drugs, toxins, or irradiation. Hence, intense efforts are under way to restore thymus function in the adult.

In this context, immunologists have long suspected that T cells are generated in extrathymic tissues such as the bone marrow, skin, and gut. However, recent experiments in mice suggest that T cell production in the gut requires the exit of "committed" T cell precursors from the thymus. Thus, the thymus appears to export not only mature but also immature T cells (*8*). Such commitment steps in T cell development may occur very inefficiently outside of the thymus, as observed in genetically deficient "nude" mice that lack a proper thymus (*9*) but still harbor a few bona fide

The author is at Harvard Medical School, Dana-Farber Cancer Institute, 44 Binney Street, Boston, MA 02115, USA. E-mail: harald_von_boehmer@dfci.harvard.edu

T cells. However, there are too few T cells to permit effective immune responses.

The discovery over 40 years ago that some mice lacking a thoracic thymus still exhibit immunocompetence was a major blow to the assumed exclusive role of the thymus in lymphopoiesis (*3*). Since then, other sources of T cells have been contested, and it was recently postulated that in these unusual cases, a neck thymus may be responsible for T cell production (*3*). However, conclusive functional proof of a second thymus was lacking.

Verification of this idea is now presented by Terszowski *et al*., who were investigating the significance of lymphoid structures in the neck of mice. Their analysis reveals that epithelial and lymphoid components of these neck structures correspond to those seen in the thoracic thymus. Importantly, hematological markers displayed by immature, but not mature, T cells are present, indicating ongoing T cell lymphopoiesis. Epithelial cells expressing cytokeratin, a protein present in thoracic thymus but not in lymph nodes, were also apparent, as was the expression of Foxn1, a protein crucial for proper epithelial cell function (*9*). Finally, functional studies with precursor T cells that express a transgenic T cell receptor showed that lymphocyte selection in the neck thymus occurs as in the thoracic thymus. Furthermore, transplants of the neck thymus into nude mice conferred immunocompetence. These results leave no doubt that the neck thymus functions as a primary lymphoid organ. Other observations by Terszowski *et al*. suggest that during development, the neck thymus branches off from the common thymus anlage before the descent of the thoracic thymus into the chest cavity, and that the structure of the neck thymus matures only after birth. This scenario appears consistent with the delayed onset of lymphopoiesis in the neck thymus as compared with the thoracic thymus.

For several decades, the mouse has been the model organism for studying the mammalian immune system, so it is surprising that the functional relevance of a thymus-like organ in the neck has not been fleshed out earlier. The neck thymus is present in strains of mice that are commonly used in experiments (most BALB/c and about half of C57BL/6 mice have it) (*5*). A thymus-like neck structure has also been observed in adult humans, though its presence is considered pathological.

The experiments of Terszowski *et al*. raise concerns about experiments in which the thoracic thymus is removed to study thymus-independent features of the peripheral T cell pool, such as lymphocyte turnover or lymphocyte production in extrathymic tissue. Likewise, the role of the neck thymus in autoimmune disease that occurs after removal of the thoracic thymus shortly after birth needs to be considered. Confirmation of a second mammalian thymus may have settled one debate, but it likely has generated other important questions not previously considered.

References

1. J. F. Miller, *Lancet* **2**, 748 (1961).
2. R. A. Good *et al.*, *J. Exp. Med.* **116**, 733 (1962).
3. J. F. Miller, *Nat. Immunol.* **7**, 3 (2006).
4. L. W. Law, T. B. Dunn, N. Trainin, R. H. Levey, paper presented at the the Wistar Institute Symposium, Philadelphia, PA, 1962.
5. G. Terszowski *et al.*, *Science* **312**, 284 (2006); published online 2 March 2006 (10.1126/science.1123497).
6. M. Matsuyama, M. N. Wiadrowski, D. Metcalf, *J. Exp. Med.* **123**, 559 (1966).
7. H. von Boehmer, *Adv. Immunol.* **84**, 201 (2004).
8. F. Lambolez *et al.*, *Nat. Immunol.* **7**, 76 (2006).
9. T. Boehm, C. C. Bleul, M. Schorpp, *Immunol. Rev.* **195**, 15 (2003).

10.1126/science.1126403

MOLECULAR BIOLOGY

Managing Associations Between Different Chromosomes

Genes present on different chromosomes can be coordinately expressed through a transcription regulatory factor that brings them together in a region of active transcription in the nucleus.

Charalampos G. Spilianakis and Richard A. Flavell

The genetic information of higher organisms is encoded in DNA that is not randomly dispersed within the cell nucleus, but is organized with nucleoproteins into different kinds of chromatin, the building blocks of the chromosomes. Each chromosome resides in a specific region of the nucleus when the cell is not undergoing cell division, and usually genes that are actively being expressed loop out from their condensed chromatin territory and localize to a region of transcriptional activity. These "transcription factory" areas are thus abundant with protein factors that initiate and regulate gene expression (*1*). Although it is well known that expression of a gene is controlled by regulatory elements located in the same region of the same chromosome (in cis), interchromosomal gene regulation has been recently observed in which the transcription of genes located on one chromosome is controlled by regulatory elements located on another chromosome (in trans) (*2*). Now, on page 269 of this issue, Ling *et al.* (*3*) show that a maternal locus on mouse chromosome 7 harboring two adjacent imprinted genes localizes with a paternal locus on chromosome 11 that contains two different genes. This interaction depends on genetic regulatory elements on chromosome 7 and on a protein called the CCCTC-binding factor (CTCF) (see the figure). The result is regulated expression of the two genes on chromosome 11.

Diploid organisms possess two alleles (alternate versions of a gene, maternally and paternally derived) of the same genetic locus. Each allele is thought to function independently of the other, although there are certain phenomena that implicate coordinated or alternate transcriptional regulation of certain loci. Regulatory elements located on one chromosome generally operate in cis on adjacent genes located on the same chromosome, but there are examples of trans-regulation by such regulatory elements on genes located on another chromosome. Such examples include transvection in the fruit fly *Drosophila melanogaster*, a process in which homologous chromosomes come together in a "synapse" and influence gene expression through enhancer elements that act in trans. Another phenomenon, known as X chromosome inactivation, present in many organisms, to ensure that males and females have comparable doses of expressed genes. Interchromosomal pairing of the two homologous X chromosomes allows communication between them, resulting in the mutually exclusive silencing of genes on one X chromosome (*4*, *5*). Similarly, in the plant *Zea mays*, the process of paramutation enables one allele to silence its homolog (*6*).

One allele can sense the presence of the other allele and initiate the above-mentioned processes through epigenetic changes that mark the loci to be regulated. One such epigenetic change involves DNA methylation and demethylation. This modification, known as "genomic imprinting," occurs when both maternal and paternal alleles are present but only one will be expressed. The recently developed chromosome conformation capture technique has revealed (*7*, *8*) that the onset of transcription at an imprinting locus on mouse chromosome 7 depends on the methylation status of an imprinting control region of the locus. It also depends on the looping out of DNA that contains this region, located between the enhancer element of one gene (*H19*) and the promoter element of another gene (*Igf2*). Ling *et al.* applied an alterna-

The authors are in the Section of Immunobiology, Yale University School of Medicine, New Haven, CT 06520, USA; E-mail: richard.flavell@yale.edu

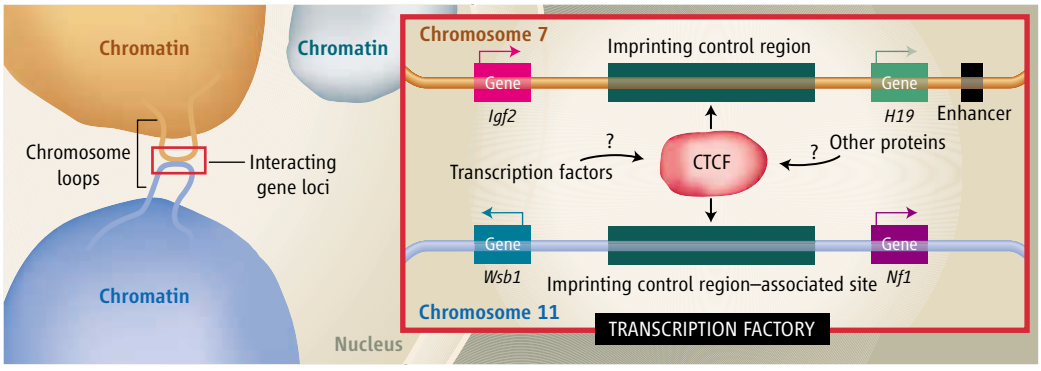

Interchromosomal rendezvous. The interaction between two different gene loci on two different chromosomes is mediated by the transcription regulatory factor CTCF and perhaps other factors. This may occur in regions of the nucleus that are enriched with transcription machinery whereby the genetic elements on one chromosome regulate expression of genes on the partnering chromosome.

tive chromosome conformation capture technique on mouse fibroblast-like cells and identified new chromosomal interacting partners with the imprinting control region of the *H19*/*Igf2* locus. Fluorescence in situ hybridization (FISH) experiments confirmed the overlapping localization in the nucleus of the mouse chromosome 7 *H19*/*Igf2* locus with a locus on chromosome 11 harboring the genes *Wsb1* and *Nf1*. CTCF, a factor that regulates DNA methylation in mammals by binding to the imprinting control region of the maternal *H19*/*Igf2* locus and the paternal loci of *Wsb1*/*Nf1*, is responsible for driving this interchromosomal interaction. Knockdown of the expression of this factor ablated the overlapping localization of the interacting alleles and impaired the transcriptional transactivation of the *Wsb1* and *Nf1* genes by regulatory elements of the *H19*/*Igf2* locus. The allele specific requirement for CTCF binding on the maternal allele was confirmed by the loss of the interchromosomal interaction when the maternal imprinting control region was deleted. The interaction was preserved when the paternal imprinting control region was deleted. Because there is parental allele specificity for CTCF binding (paternal chromosome 11 and maternal chromosome 7), we could assume that the interchromosomal association is implicated in the imprinting process. There was loss of maternal *Igf2* imprinting in cells lacking CTCF and in cells in which the maternal imprinting control region was deleted. The study suggests that a protein factor is critical to mediating the interaction of the two loci into a common nuclear compartment where transcription may be regulated.

The exact nuclear compartment where these interactions occur remains to be characterized by means of a combination of FISH to visualize DNA loci and immunofluorescence techniques to visualize the cell's transcription machinery. Is the colocalization and physical interaction of loci from different chromosomes a static or a dynamic process in which chromosomal partners transiently associate to be transcriptionally regulated? Interchromosomal interactions are more likely to be a dynamic process in which gene loci enter and leave a specific nuclear environment, possibly changing or exchanging interacting partners. The integration of multiple copies of a specific binding site for a fluorescently labeled protein, within a specific locus, will also permit monitoring the movement of the labeled locus in a living cell, and in real time. RNA FISH experiments, in which newly transcribed RNA on the locus of interest is detected, may also provide answers to such questions. And what about the mechanism by which homologous, associated gene loci exchange epigenetic information? Is it RNA-mediated? Or is it based, as the Ling *et al.* study suggests, on transcription factors (and perhaps homo- or heterotypic interactions between them) that bind each genetic locus?

Gene regulation through interchromosomal interactions may well be a general phenomenon with paradigms in different systems. It has now been implicated in the regulation of alternatively expressed genes in T cells (*2*), for α- and β-globin genes in erythroblasts (*9*), for loci that regulate X chromosome inactivation (*4*, *5*), and in the regulation of imprinting loci (*3*). It is likely that clusters of genes with coordinate or alternate regulation of expression may be controlled by interchromosomal interactions. A genome-wide analysis will reveal interacting chromosome partners with functional consequences in the regulation of gene expression, with possible implications in disease.

References

1. D. L. Spector, *Annu. Rev. Biochem.* **72**, 573 (2003).
2. C. Spilianakis, M. Lalioti, T. Town, G. R. Lee, R. A. Flavell, *Nature* **435**, 637 (2005).
3. J. Q. Ling *et al.*, *Science* **312**, 269 (2006).
4. N. Xu, C.-L. Tsai, J. T. Lee, *Science* **311**, 1149 (2006); published online 19 January 2006 (10.1126/science.1122984).
5. C. P. Bacher *et al.*, *Nat. Cell Biol.* **8**, 293 (2006).
6. V. L. Chandler, M. Stam, *Nat. Rev. Genet.* **5**, 532 (2004).
7. J. Dekker, K. Rippe, M. Dekker, N. Kleckner, *Science* **295**, 1306 (2002).
8. B. Tolhuis, R.-J. Palstra, E. Splinter, F. Grosveld, W. de Laat, *Mol. Cell* **10**, 1453 (2002).
9. J. M. Brown *et al.*, *J. Cell Biol.* **172**, 177 (2006).

10.1126/science.1126689

BIOCHEMISTRY

Enzyme Motions Inside and Out

Stephen J. Benkovic and Sharon Hammes-Schiffer

In one enzyme, short-range thermal motions are sufficient to explain the transfer of a hydrogen by tunneling—a transition through a classically forbidden energy state.

A long-standing question in biochemistry is how enzymes catalyze chemical reactions at rates that are, in some cases, millions of times faster than the reaction rate in their absence. The quest for the source of this extraordinary ability has been augmented by recent advances in structural methods [particularly nuclear magnetic resonance (NMR)] (*1*–*3*), in computational power (*4*), and in the sophistication of physical chemical experiments (*5*). The key question is simple: How does the enzyme reduce the free-energy barrier for the chemical transformation? We have reviewed the progression of hypothetical answers to this question (*6*, *7*) and identified a common feature of the various rationales—namely, the requirement for conformational flexibility within the enzyme and substrates—and we noted the diversity of time scales for these movements. On page 237 of this issue, Masgrau *et al.* (*8*) examine the importance of dynamics for catalysis by the enzyme aromatic amine dehydrogenase in the oxidation of tryptamine.

The pathway for oxidation proceeds through a series of intermediates that have been characterized by x-ray crystallography. The step that is the focus of Masgrau and coworkers' study is a proton transfer from the carbon of a Schiff base intermediate to a car-

The authors are in the Department of Chemistry, Pennsylvania State University, University Park, PA 16802, USA. E-mail: sjb1@psu.edu (S.J.B.), shs@chem.psu.edu (S.H.-S.)

CREDIT: P. HUEY/SCIENCE

boxylate oxygen of Asp[128]. Stopped-flow kinetics with protio and deutero substrates showed a kinetic isotope effect of ~55, which is well above the semiclassical limits that do not include tunneling, and hence it is consistent with a hydrogen tunneling process. Variational transition-state theory with semiclassical tunneling contributions was used to illustrate the importance of hydrogen tunneling. Analyses based on classical molecular-dynamics simulations of the reactant complex suggest that the motion of the transferring hydrogen is not strongly coupled to neighboring atoms and that short-range local motion decreases the proton donor-acceptor distance to facilitate hydrogen tunneling. The authors conclude that long-range coupled motions are not required to promote hydrogen tunneling in this enzyme.

How hydrogen tunneling processes are facilitated by conformational changes within the active site and how these local changes are coupled to longer range conformational changes is a highly debated topic (*6–10*). Most experimental and theoretical studies of tunneling investigate enzyme motions that are in thermal equilibrium. Exceptions include the calculation of transmission coefficients that account for dynamical barrier recrossings and the calculation or measurement of time-dependent properties under nonequilibrium conditions. To our knowledge, the direct contribution of nonequilibrium motions to tunneling in enzymes has not been proven. Thermal equilibrium motions tend to be stochastic or Brownian in nature and are often much faster than the millisecond time scale of most enzyme-catalyzed reactions. Nevertheless, thermal motions occurring within the confines of the protein structure can lead to conformational sampling of configurations that facilitate the chemical reaction.

A general perspective of the impact of enzyme motion on a hydrogen tunneling process is illustrated schematically in the figure. In this framework (*11*, *12*), the transferring hydrogen nucleus is represented by a quantum-mechanical wave function, and the collective reaction coordinate corresponds to conformational changes of the enzyme and ligands. Thermal equilibrium motions lead to conformational sampling of configurations that facilitate the hydrogen tunneling process by providing a favorable electrostatic environment (that is, leading to degeneracy of a pair of localized proton vibrational states) and decreasing the average proton donor-acceptor distance. The free-energy barrier is a consequence of the difference between the probabilities of sampling those configurations that are conducive to hydrogen tunneling and the configurations corresponding to the initial enzyme-ligand(s) reactant complex. A network of coupled thermal equilibrium motions can lead to overall conformational changes that occur on the millisecond time scale of the rate measured in the stopped-flow experiments. Of course, the actual hydrogen tunneling process is virtually instantaneous relative to the millisecond overall conformational changes. Substantial kinetic isotope effects can arise mainly from differences in tunneling probabilities between hydrogen and deuterium for the configurations at which tunneling occurs, as well as differences in zero point energies.

That short-range subpicosecond thermal motions alone are sufficient to explain the tunneling in amine dehydrogenase (*8*) is suprising and at variance with other systems. For example, the hydride transfer reaction catalyzed by dihydrofolate reductase involving the reduced form of nicotinamide adenine dinucleotide phosphate (NADPH) cofactor has been shown by various experimental methods (*2*, *5*)—complemented by computer simulations (*6*, *7*)—to involve long-range motions that extend throughout the enzyme. In this case, relatively slow conformational changes lead to the configurations that enable hydrogen tunneling. Moreover, these conformational changes arise from a network of equilibrium-coupled motions that extend throughout the enzyme (*6*, *7*).

Although Masgrau *et al.* (*8*) show that short-range motions are sufficient to explain tunneling in the enzyme aromatic amine dehydrogenase, they do not rule out a role for long-range motions. Their covariance analysis of the relatively fast classical hydrogen vibrational motion in the reactant complex does not allow the identification of slower conformational changes composed of long-range coupled motions along the collective reaction coordinate. Thus, the role of these types of conformational changes in aromatic amine dehydrogenase remains to be seen. Their work gives fresh insight into the importance of fast, short-range motions, but looking outward from the active site may reveal a more complex picture.

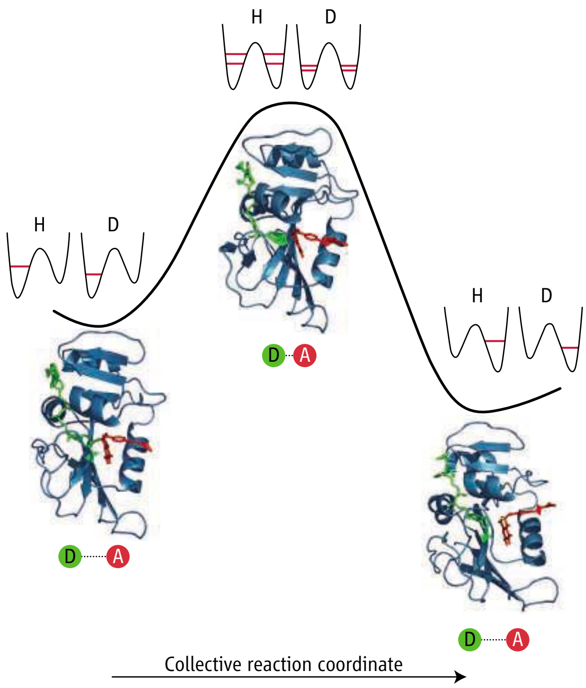

Path of hydrogen transfer. Schematic depiction of the free-energy profile along a collective reaction coordinate for a hydrogen transfer reaction catalyzed by an enzyme. The thermally averaged equilibrium conformations and the associated average donor-acceptor (D···A) distances along the reaction pathway are shown (*13*). The double-well potential-energy curves along the hydrogen (or deuterium) coordinate and the associated hydrogen and deuterium vibrational quantum states are also shown (*14*). The free-energy profile corresponds to only the ground hydrogen vibrational state (*15*, *16*).

References and Notes

1. A. Mittermaier, L. E. Kay, *Science* **312**, 224 (2006).
2. J. R. Schnell, H. J. Dyson, P. E. Wright, *Annu. Rev. Biophys. Biomol. Struct.* **33**, 119 (2004).
3. E. Z. Eisenmesser, D. A. Bosco, M. Akke, D. Kern, *Science* **295**, 1520 (2002).
4. M. Garcia-Viloca, J. Gao, M. Karplus, D. G. Truhlar, *Science* **303**, 186 (2004).
5. N. M. Antikainen, R. D. Smiley, S. J. Benkovic, G. G. Hammes, *Biochemistry* **44**, 16835 (2005).
6. S. J. Benkovic, S. Hammes-Schiffer, *Science* **301**, 1196 (2003).
7. S. Hammes-Schiffer, S. J. Benkovic, *Annu. Rev. Biochem.* **75**, 519 (2006).
8. L. Masgrau *et al.*, *Science* **312**, 237 (2006).
9. A. Kohen, J. P. Klinman, *Acc. Chem. Res.* **31**, 397 (1998).
10. J. Villa, A. Warshel, *J. Phys. Chem. B* **105**, 7887 (2001).
11. R. A. Marcus, N. Sutin, *Biochim. Biophys. Acta* **811**, 265 (1985).
12. P. M. Kiefer, J. T. Hynes, *Solid State Ionics* **168**, 219 (2004).
13. In addition to changes in the average donor-acceptor distance, this mode vibrates on a relatively fast time scale due to thermal fluctuations, and it could be treated quantum mechanically. The dominant donor-acceptor distance for tunneling may differ for hydrogen and deuterium.
14. In the figure, the double-well proton potential becomes symmetric to enable hydrogen tunneling, but tunneling involving excited vibrational states is possible for an asymmetric proton potential.
15. This free-energy barrier is expected to be slightly higher for deuterium than for hydrogen because of zero point energy effects. If the reaction is adiabatic (that is, the system remains in the vibrational ground state), then this difference in free-energy barriers leads to a moderate kinetic isotope effect. If the reaction is vibrationally nonadiabatic (that is, excited vibrational states participate substantially), then the rate is approximately proportional to the square of the tunneling splitting, which is the energy difference between the lowest two vibrational states in the approximately symmetric double-well hydrogen potential at the top of the barrier. The smaller splitting for deuterium than for hydrogen can lead to a large kinetic isotope effect for these types of reactions. The reaction is assumed to occur in the ground electronic state.
16. Although the thermally averaged structures shown in the figure correspond to dihydrofolate reductase, here they represent a generic enzyme. The double-well potentials and associated quantum states are drawn qualitatively and will differ for each enzyme system.
17. This work was supported by NIH grant GM56207 (S.H.S.) and GM24129 (S.J.B.).

10.1126/science.1127654

SCIENCE & ENGINEERING

VISUALIZATION CHALLENGE

CALL FOR ENTRIES

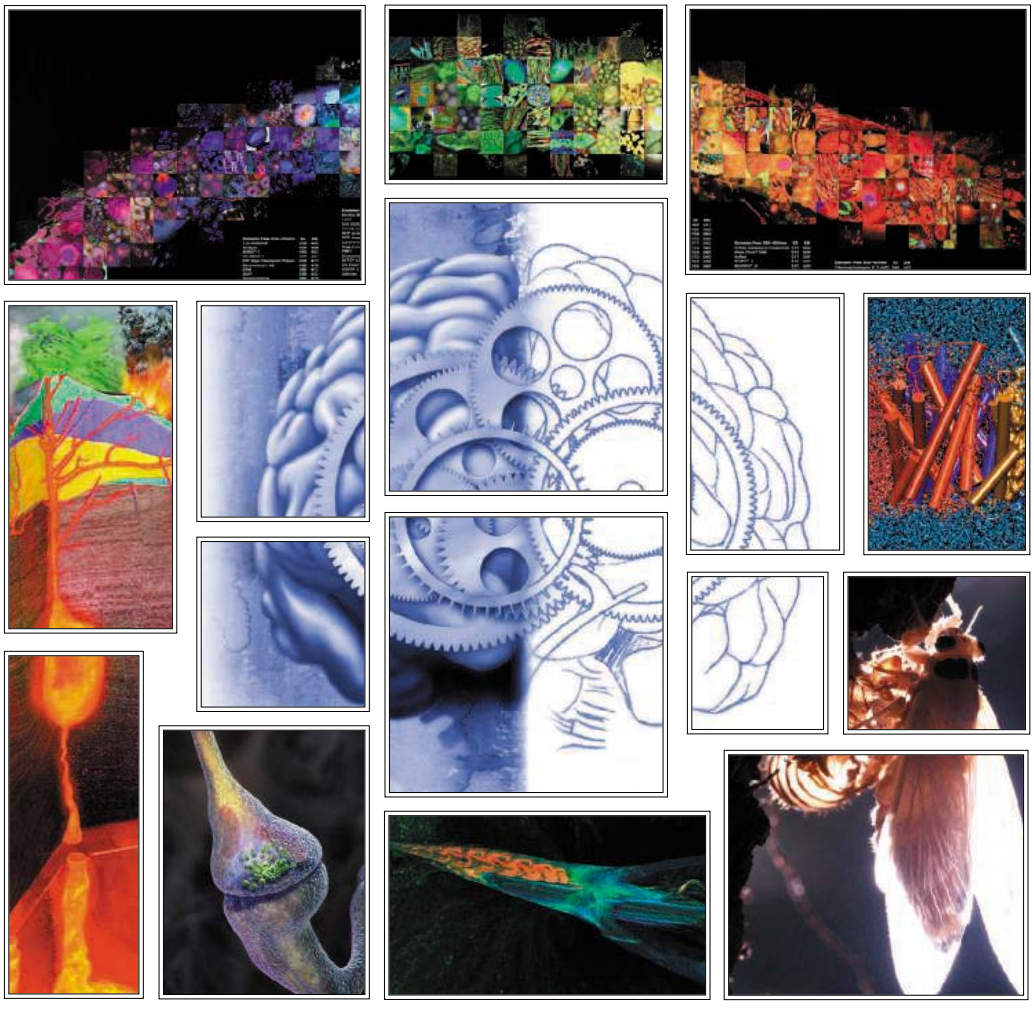

SCIENCE AND ENGINEERING'S MOST POWERFUL STATEMENTS ARE NOT MADE FROM WORDS ALONE

When the left brain collaborates with the right brain, science emerges with art to enhance communication and understanding of research results—illustrating concepts, depicting phenomena and drawing conclusions.

The National Science Foundation (NSF) and the journal *Science*, published by the American Association for the Advancement of Science, invite you to participate in the fourth annual Science and Engineering Visualization Challenge. The competition recognizes scientists, engineers, visualization specialists and artists for producing or commissioning innovative work in visual communication.

ENTRY DEADLINE: MAY 31, 2006

Award categories: Photographs, Illustrations, Interactive Media, Non-Interactive Media and Informational Graphics. Winners in each category will be published in the Sept. 22, 2006 issue of *Science* and *Science* Online, and will be displayed on the NSF Web site.

Complete Entry Information: www.nsf.gov/news/special-reports/scivis/index AND www.sciencemag.org/prizes/

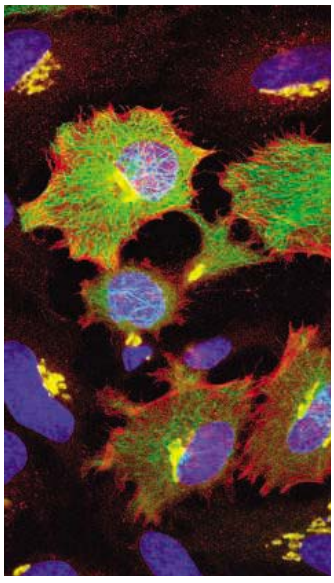

INTRODUCTION

Proteins at Work

IMPORTANT INSIGHTS INTO BIOLOGICAL PROCESSES HAVE COME FROM TRADITIONAL in vitro biochemistry experiments and from static structures determined by x-ray crystallography and nuclear magnetic resonance (NMR) spectroscopy. Now scientists seek to gain a quantitative understanding of how dynamic macromolecules function inside of cells. This special issue highlights technological advances that are facilitating progress in this field.

Knowing the players is fundamental to a quantitative understanding of cellular processes. To this end, the field of proteomics is aimed at the systematic analysis of all proteins in a cell or tissue. Mass spectrometry is central to most proteomic strategies, and Domon and Aebersold (p. 212) describe how recent advances in mass spectrometry instrumentation are allowing not only descriptive studies that identify proteins and characterize posttranslational modifications, but also quantitative studies looking at changes in protein concentration between samples. But a cast list, even with exits and entrances marked, cannot tell the whole story. Ultimately, we would like to view the action as it happens. Giepmans *et al*. (p. 217) discuss developments in fluorescent probes and techniques to determine protein expression, activity, and function in fixed and live cells; and Xie *et al*. (p. 228) provide examples where single-molecule imaging techniques are used to follow gene expression, active transport, and metabolism in live cells.

Exciting as this global view is, it does not show us how each protein works. It has become clear that protein motions are important for function, with much of the experimental data coming from NMR spectroscopy. Mittermaier and Kay (p. 224) give an overview of NMR methods that allow internal motions to be probed with very high time and spatial resolution. Some of these methods were used by Koglin *et al.* (p. 273) to show that a protein that acts in nonribosomal peptide synthesis displays a double two-state conformational equilibrium that is important to its function. Computational methods provide additional tools to study dynamics. Masgrau *et al*. (p. 237) used a combination of kinetic and crystallographic experiments and computer simulation to show that in one enzyme, short-range thermal motions are sufficient to explain hydrogen tunneling. An associated Perspective by Benkovic and Hammes-Schiffer (p. 208) suggests that looking outward from the active site may reveal a more complex picture.

In related online resources, *Science*'s Signal Transduction Knowledge Environment (STKE) (http://stke.sciencemag.org/) features a Protocol by England on monitoring AMPA receptor trafficking and a Review by Vogel *et al*. discussing how to overcome potential pitfalls of fluorescence resonance energy transfer (FRET) analysis.

We look to a future where the tools described here, and those yet to come, will allow us to watch biochemical reactions in live cells and understand how each molecule plays its role.

– VALDA J. VINSON

Tools for Biochemistry

CONTENTS

Reviews

Perspective

See also related Perspective page 208; Research Article page 237; Report page 273; STKE material page 153 or at www.sciencemag.org/sciext/biochemtools/

CREDIT: B. GIEPMANS *ET AL.*

REVIEW

Mass Spectrometry and Protein Analysis

Bruno Domon[1] and Ruedi Aebersold[1,2,3]

Mass spectrometry is a central analytical technique for protein research and for the study of biomolecules in general. Driven by the need to identify, characterize, and quantify proteins at ever increasing sensitivity and in ever more complex samples, a wide range of new mass spectrometry–based analytical platforms and experimental strategies have emerged. Here we review recent advances in mass spectrometry instrumentation in the context of current and emerging research strategies in protein science.

The ability to identify proteins and to determine their covalent structures has been central to the life sciences. The amino acid sequence of proteins provides a link between proteins and their coding genes via the genetic code, and, in principle, a link between cell physiology and genetics. The identification of proteins provides a window into complex cellular regulatory networks.

Before the genomics revolution, chemical or enzymatic methods were used to probe the covalent structure of single, highly purified proteins, and typically, the products of such reactions were detected by ultraviolet (UV) absorbance or fluorescent spectroscopy. For example, polypeptides were sequenced by stepwise chemical degradation from the N terminus to the C terminus (Edman degradation), with subsequent identification of the released amino acid derivatives by UV absorbance spectroscopy. Gradually over the past two decades, mass spectrometers were interfaced with a number of protein chemistry assays to create detectors providing superior information. With the increased performance and versatility of the instrumentation, new protein analytical strategies have emerged in which mass spectrometry is the central element. For example, by the mid-1990s, a variety of mass spectrometry–based strategies had essentially replaced the Edman degradation as the mainstream method for determining the amino acid sequences of polypeptides.

The trend toward mass spectrometry as the technique of choice for identifying and probing the covalent structure of proteins was accelerated by the genome project. Genomics demonstrated the power of high-throughput, comprehensive analyses of biological systems. Genomics also provides complete genomic sequences, which are a critical resource for identifying proteins quickly and robustly by the correlation of mass-spectrometric measurements of peptides with sequence databases. The systematic analysis of all the proteins in a tissue or cell was popularized under the name proteomics, with mass spectrometry central to most proteomic strategies.

The analysis of a full proteome presents a formidable task and, in spite of recent technical developments, remains to be achieved for any species. The task is challenging because proteomes have a large and unknown complexity. What is certain is that the number of proteins in a species' proteome exceeds by far the number of genes in the corresponding genome. This diversity arises from the fact that a particular gene can generate multiple distinct proteins as a result of alternative splicing of primary transcripts, the presence of sequence polymorphisms, post-translational modifications, and other protein-processing mechanisms. Moreover, proteins span a concentration range that exceeds the dynamic range of any single analytical method or instrument. For example, it has been estimated that the concentration range of serum proteins exceeds 10 orders of magnitude (*1*). Although these challenges are daunting, they have stimulated advances in technologies for the analysis of proteins and proteomes. Here we describe a range of mass-spectrometric techniques, discuss their utility for protein analysis, and assess their ability to support or interface with a range of proteomic strategies.

MS Instruments and Their Use

Mass spectrometry was restricted for a long time to small and thermostable compounds because of the lack of effective techniques to softly ionize and transfer the ionized molecules from the condensed phase into the gas phase without excessive fragmentation. The development in the late 1980s of two techniques for the routine and general formation of molecular ions of intact biomolecules—electrospray ionization (ESI) (*2*) and matrix assisted laser desorption/ionization (MALDI) (*3*)—dramatically changed this situation and made polypeptides accessible to mass-spectrometric analysis. This catalyzed the development of new mass analyzers and complex multistage instruments [for instance, hybrid quadrupole time-of-flight (Q-Q-ToF) and tandem time-of-flight (ToF-ToF) instruments] (Table 1) designed to tackle the challenges of protein and proteome analysis (*4*, *5*). Mass spectrometers are used either to measure simply the molecular mass of a polypeptide or to determine additional structural features including the amino acid sequence or the site of attachment and type of posttranslational modifications. In the former case, single-stage mass spectrometers are used, acting essentially as balances to weigh molecules. In the latter case, after the initial mass determination, specific ions are selected and subjected to fragmentation through collision. In such experiments, referred to as tandem mass spectrometry (MS/MS), detailed structural features of the peptides can be inferred from the analysis of the masses of the resulting fragments. The types of mass spectrometers described below are most commonly used to support a range of research strategies in the protein sciences. They differ in their physical principles, their performance standards, their mode of operation, and their ability to support specific analytical strategies.

Table 1. Characteristics and performances of commonly used types of mass spectrometers. Check marks indicate available, check marks in parentheses indicate optional. +, ++, and +++ indicate possible or moderate, good or high, and excellent or very high, respectively. Seq., sequential.

	IT-LIT	Q-Q-ToF	ToF-ToF	FT-ICR	Q-Q-Q	QQ-LIT
Mass accuracy	Low	Good	Good	Excellent	Medium	Medium
Resolving power	Low	Good	High	Very high	Low	Low
Sensitivity (LOD)	Good		High	Medium	High	High
Dynamic range	Low	Medium	Medium	Medium	High	High
ESI	✓	✓		✓	✓	✓
MALDI	(✓)	(✓)	✓			
MS/MS capabilities	✓	✓	✓	✓	✓	✓
Additional capabilities	Seq. MS/MS			Precursor, Neutral loss, MRM		
Identification	++	++	++	+++	+	+
Quantification	+	+++	++	++	+++	+++
Throughput	+++	++	+++	++	++	++
Detection of modifications	+	+	+	+		+++

[1]Institute of Molecular Systems Biology, ETH Zurich, CH-8093 Zurich, Switzerland. [2]Faculty of Sciences, University of Zurich, CH-8006 Zurich, Switzerland. [3]Institute for Molecular Systems Biology, Seattle, WA 98103, USA.

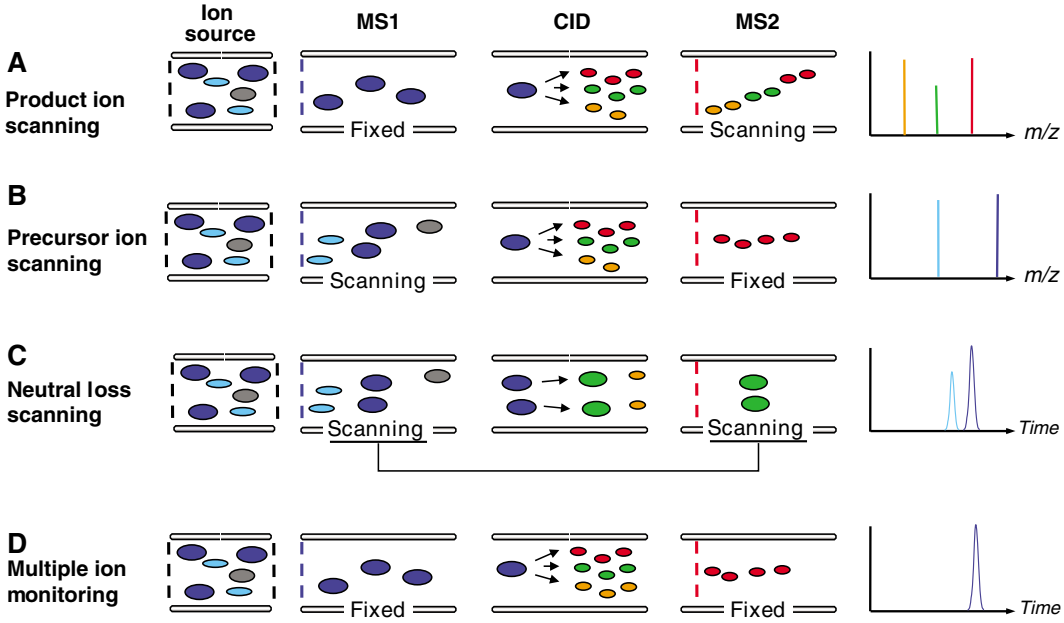

Fig. 1. Schematic representation of various types of tandem mass spectrometry experiments. (**A**) Product ion scanning is the most common MS/MS experiment in proteomics. Its purpose is the generation of fragment ion spectra for the identification of the amino acid sequence of specific peptides. In this experiment, the first analyzer (MS1) is set to a value that selects one specific precursor ion at a time. The selected ion undergoes CID in the collision cell, and the resulting fragments are analyzed by the second analyzer (MS2). This process is repeated for different precursors. (**B**) Precursor ion scanning sets the second analyzer (MS2) to transmit only one specific fragment ion to the detector. MS1 is scanned to detect all the precursor ions that generate this fragment. Typically, this method is used to detect a subset of peptides in a sample that contain a specific functional group, for instance a phosphate ester or a carbohydrate modification. (**C**) Neutral loss scanning scans both analyzers in a synchronized manner, so that the mass difference of ions passing through MS1 and MS2 remains constant. The mass difference corresponds to a neutral fragment that is lost from a peptide ion in the collision cell. The neutral loss scan is therefore used to detect those peptides in a sample that contain a specific functional group. A common application of this method is the detection of peptides phosphorylated at serine or threonine residues via a loss of phosphoric acid. (**D**) MRM consists of a series of short experiments in which one precursor ion and one specific fragment characteristic for that precursor are selected by MS1 and MS2, respectively. Typically, the instrument cycles through a series of transitions (precursor-fragment pair) and records the signal as a function of time (chromatographic elution). MRM is used for the detection of a specific analyte with known fragmentation properties in complex samples.

Time-of-flight (ToF) and hybrid ToF instruments. In ToF analyzers, the mass-to-charge ratio of an analyte ion is deduced from its flight time through a tube of specified length that is under vacuum. The performance of ToF analyzers has greatly improved, in particular in terms of resolution and mass accuracy (*6*). A resolving power exceeding 12,000 has become routine on many instruments, and with a proper mass calibration protocol, mass accuracies in the low–parts per million (ppm) range are achievable. ToF mass analyzers are the basis for analytical platforms operated with both ESI and MALDI. The Q-Q-ToF instruments exhibit high resolution and mass accuracy in MS and MS/MS mode. In the MS mode, the quadrupole acts as an ion guide to the ToF analyzer where the mass analysis takes place. In the MS/MS mode, the precursor ions (typically a multiply charged ion in ESI) are selected in the first quadrupole and undergo fragmentation through collision-induced dissociation in the second quadrupole. The product ions are analyzed in the ToF device. Spectra obtained in both full-scan and MS/MS modes exhibit good mass accuracy and high resolution, yielding an increased number of peptides detected and allowing for the determination of the charge state and unambiguous assignment of the mono-isotopic signal. All of these factors simplify the identification of peptides via database searches by tightening the search parameters and augmenting the confidence in the results. Finally, Q-Q-ToF instruments perform well for quantitative analyses and for the identification of posttranslational modifications.

MALDI remains a valuable alternative ionization technique for peptides and proteins and is often used to complement results obtained by ESI MS. MALDI MS is very sensitive and more tolerant than ESI to the presence of contaminants such as salts or small amount of detergent. The MALDI technique has primarily been used in conjunction with ToF analyzers for molecular mass determination. It has been implemented on Q-Q-ToF or ToF-ToF mass spectrometers to provide true MS/MS capabilities. The resulting spectra characterized by singly charged precursor ions and those obtained on ToF-ToF instruments present high-energy collision fragments (cleavages of the peptidic bonds and side chains), which are readily interpretable (*7*).

Ion trap (IT) mass analyzers. In IT analyzers, ions are trapped and can therefore be accumulated over time in a physical device. The IT technology is characterized by MS/MS capabilities (*8*) with unmatched sensitivity and fast data acquisition. Used in conjunction with data-dependent acquisition (*9*), IT technology allows high-throughput analyses. However, IT analyzers have limited-resolution, low–ion trapping capacity, and space-charging effects result in mass measurements lacking accuracy. The development of linear ion trap (LIT) analyzers with higher ion-trapping capacities has expanded the dynamic range and the overall sensitivity of this technique, and LITs have been replacing classical quadrupole trapping devices. Typically, LIT instruments have an optional slow scanning function to increase resolution. They also have multiple-stage sequential MS/MS capabilities, in which fragment ions are iteratively isolated and further fragmented, a strategy that has proven to be very useful for the analysis of posttranslational modifications such as phosphorylation (*10*).

LIT devices have been implemented on triple quadrupole–type instruments (i.e., the second analyzer is substituted by a LIT) to offer a unique set of functionalities (*11*). The Q-Q-LIT geometry offers the scanning capabilities of a triple quadrupole instrument, including precursor ion and neutral loss scanning (Fig. 1, B and C), and increased sensitivity. These instruments therefore offer unique capabilities for the analysis of modifications. In addition, the multiple reaction monitoring (MRM) capability of Q-Q-LIT instruments (Fig. 1D) allows the detection of specific transitions between the precursor and one fragment of a given peptide. The selectivity resulting from two stages of analyzer combined with the high duty cycle results in quantitative analyses with unmatched sensitivity.

Ion cyclotron resonance and orbitrap mass analyzers. The development and commercialization of robust Fourier transform–ion cyclotron resonance (FT-ICR) mass spectrometers with external ion sources (*12*) represented a breakthrough in terms of resolving power and

mass accuracy. Measurements in the low ppm–sub ppm range can be achieved. The high resolution of this instrument not only accounts for better data quality, but it also increases the peak capacity and thus allows for the detection of more signals compared with instruments with lower resolving power. The development of hybrid FT-ICR instrument with an external LIT device has added robustness to this platform and allowed routine generation of low-resolution MS/MS spectra with accurate mass of the precursor ions. FT-MS performed on an LIT-ICR hybrid instrument allows true parallel full mass spectrum (MS1) and tandem mass spectrum (MS2) acquisition (not sequential), and it yields high-quality MS1 data that can be used for quantification. The only drawback of that approach is the relatively slow acquisition rate (several s per cycle) and the limited dynamic range of IT devices.

Very recently, a new type of mass analyzer called orbitrap (*13*, *14*) has emerged. It is the first analyzer introduced to the market in three decades that is based on a new physics principle (the separation of ions in an oscillating electric field). This instrument presents characteristics similar to an FT-ICR spectrometer in terms of resolution and mass accuracy but without the burden of an expensive superconducting magnet.

MS/MS modes of operation. Tandem mass spectrometry is commonly used in the product ion mode (Fig. 1A) to determine the amino acid sequence of a specific peptide. This technique is available on all instruments equipped with MS/MS capabilities. However, more specialized instruments (Table 1) allow other types of MS/MS experiments. Experiments to detect a subset of peptides that contain a specific functional group requiring precursor-ion or neutral-loss scans (Fig. 1, B and C, respectively) can only be performed effectively on triple quadrupole (Q-Q-Q) or quadrupole ion trap (Q-Q-LIT) instruments. For instance, phosphorylation and glycosylation can be detected very effectively in complex mixtures by generating specific reporter ions in the collision cell that can be detected by the specific scan functions (*15*–*17*). In a typical experiment, the precursor or neutral loss scan will detect the components of interest and then trigger a conventional MS/MS (product ion scan) to identify the amino sequence and localize the modifications.

Triple quadrupole–derived technologies also allow quantitative analyses with very high sensitivity in the MRM mode. Known (or suspected) analytes can be detected and quantified with a high degree of sensitivity and selectivity (Fig. 1D). The high selectivity results from monitoring one pair of precursor/fragment ions characteristic of a single peptide. In addition, the two levels of mass selection in MRM experiments result in a substantial increase in sensitivity, because the first mass filter only transmits a small ion population, and thus minimizes the overall chemical background. The collision-induced dissociation (CID) fragment ions derived from the precursor ions produce discrete signals, whereas chemical noise is randomly distributed. Finally, the nonscanning nature of this technique (high dwell time) increases in sensitivity by several orders of magnitude compared with the limit of detection (LOD) achieved by product ion scans.

Instrument performance. The pertinent characteristics of the various instrument types are summarized in Table 1. Instrument performance in terms of resolving power, LOD (sensitivity), and mass accuracy depends on the instrument type, the ionization method, and the scanning capabilities used. At this point, no instrument offers all capabilities simultaneously, and trade-offs need to be made based on the type of analysis to be performed.

The comparison of instrument performance is potentially a controversial subject, because specifications very much depend on the type of application, the sample analyzed, and the experimental setup. Very low LOD is often reported for individual peptides; however, for biological samples with high matrix background, the practical limits are often off by several orders of magnitude. Discrepancies in performance are often observed between an instrument performing under optimum conditions (typically above manufacturer specifications) and a routine, high-throughput operation. Whether the application focuses on identification or quantification will determine which platform and strategy is preferred. In the former case, resolving power (to improve separation of the various components) and mass accuracy are important factors, whereas in the latter case, the emphasis is on sensitivity, dynamic range, and MRM capabilities. Thus, biological questions to be addressed together with the experimental design should define the type of instrumental platform required.

The simultaneous collection of quantitative data (full scan mode) and qualitative data (MS/MS mode) is often difficult. Parallel data acquisition in some hybrid instruments (LIT-ICR) partially solves the problem. Precise quantification requires high-quality data characterized by intense signals and a high signal-to-noise ratio collected across the entire elution profile. Data quality is very much dependent on the data acquisition parameters (scanning time or dwell time for nonscanning instruments). Thus, usually trade-offs have to be made between data quality and throughput.

Latest developments. A number of recent developments are opening new opportunities for the characterization of biomolecules. Alternate fragmentation techniques to CID that are based on electron transfer of the ions present in the collision cell have been developed to improve peptide sequencing. In particular, electron capture dissociation (ECD) (*18*) and electron transfer dissociation (ETD) (*19*) have been implemented on FT-ICR and LIT instruments, respectively. These two techniques yield fragments that are complementary to the classical CID fragmentation. They tend to be more evenly distributed over the entire peptide backbone and are particularly useful in localizing posttranslational modifications. ECD and ETD are also applicable to large peptides and proteins. The ability to fragment and analyze intact proteins opens new possibilities for the direct analysis of intact proteins by mass spectrometry (called top-down approaches), which yield full amino acid coverage and precise identification and localization of modifications (*20*).

Classical and Emerging Proteomic Strategies

Although no proteomic strategies are currently capable of completely and routinely analyzing a proteome, the techniques are robust and their potential for complete proteome analysis is increasing rapidly. Moreover, the analysis of specific subproteomes, such as the proteins contained in organelles or subcellular fractions, has become routine. Proteomic studies also differ in their objectives. Many studies are descriptive, focusing on the identification of the proteins in a sample and the characterization of their posttranslational modifications. More recently, quantitative measurements of either absolute protein quantities or quantitative changes of proteins between samples have been performed.

Virtually every mass spectrometry–based proteomic workflow consists of three distinct stages: (i) Protein samples are isolated from their biological source and optionally fractionated. The final protein sample is then digested and the resulting peptide sample is further fractionated. (ii) The peptides are subjected to qualitative and quantitative mass-spectrometric analysis. (iii) The large data sets generated are analyzed by suitable software tools to deduce the amino acid sequence and, if applicable, the quantity of the proteins in a sample. The peptide identity is assigned to the MS/MS spectra through database searching (*21*), which is performed according to established guidelines to generate consistent results (*22*). A subsequent statistical analysis of the search results is critical to ensure confidence in the identifications (*23*).

MS analysis of substantially purified proteins. This approach is exemplified by the original proteomic approach: two-dimensional (2D) gel electrophoresis followed by the mass-spectrometric identification of the protein(s) in a single gel spot (Fig. 2A). The targeted proteins are digested and identified by mass spectrometry, usually peptide mass fingerprinting using a MALDI-ToF instrument. More recently, variants of this approach have been developed in which various combinations of sequential electrophoretic or chromatographic separation methods are combined to achieve sufficient peak capacity to resolve complex samples (*24*, *25*). Quantification is achieved at the protein level by comparing the signal intensities of identical proteins in different

samples. The strength of these methods is their ability to resolve related proteins, such as differentially modified forms, and the low degree of complexity of the samples generated for mass spectrometry analysis. The methods suffer from limited dynamic range, insufficient power to resolve proteomes, and limited sample throughput. Furthermore, important classes of proteins, including membrane proteins, are difficult to analyze by these methods, which are best suited for the analysis of protein samples of limited complexity and for studies where specific proteins need to be extensively characterized.

MS analysis of complex peptide mixtures. In this method, also referred to as shotgun proteomics, complex protein samples are digested, and the resulting peptide samples are extensively fractionated and analyzed by automated MS/MS, typically using rapidly scanning analyzers such as IT mass spectrometers (Fig. 2B). Protein samples analyzed by this method include complete cell lysates or tissue extracts, subcellular fractions, isolated organelles, or other subproteomes.

If samples are labeled with stable isotopes, the ratio of signal intensities of differentially labeled but chemically identical analytes can be used to determine accurately their relative abundance in different samples (Fig. 3A). Multiple analyses can be performed concomitantly by using tandem mass tags (Fig. 3B). Alternately, the absolute quantity of peptide can be determined by adding calibrated amounts of isotopically labeled peptides into the sample before the MS analysis (Fig. 3C).

The strength of the shotgun approach is its conceptual and experimental simplicity, increased proteomic coverage compared with the method described above, and accurate quantification. The shotgun method suffers from limited dynamic range, informatics challenges related to inferring peptide and protein sequence identities from the large number of acquired mass spectra, a high redundancy, and the enormous complexity of the generated peptide samples. These limitations have been addressed, in part, by the use of fractionation that reduces the complexity of the peptide sample. Popular fractionation methods target information-rich subsets of the proteome, such as the cysteine-containing peptides (*26*), phosphorylated peptides (*27*, *28*), or glycosylated peptides (*29*). Shotgun proteomics is most suitable for the rapid identification of the components of complex sample mixtures and for the comparative quantitative analysis of the proteins contained in different samples. Because the connection between the peptides that are analyzed in the mass spectrometer and the protein(s) from which the peptides originate is lost during proteolysis, this approach is less well suited for the extensive characterization of proteins with multiple modifications.

Comparative pattern analysis. Comparative peptide pattern analysis (Fig. 2C) is conceptually

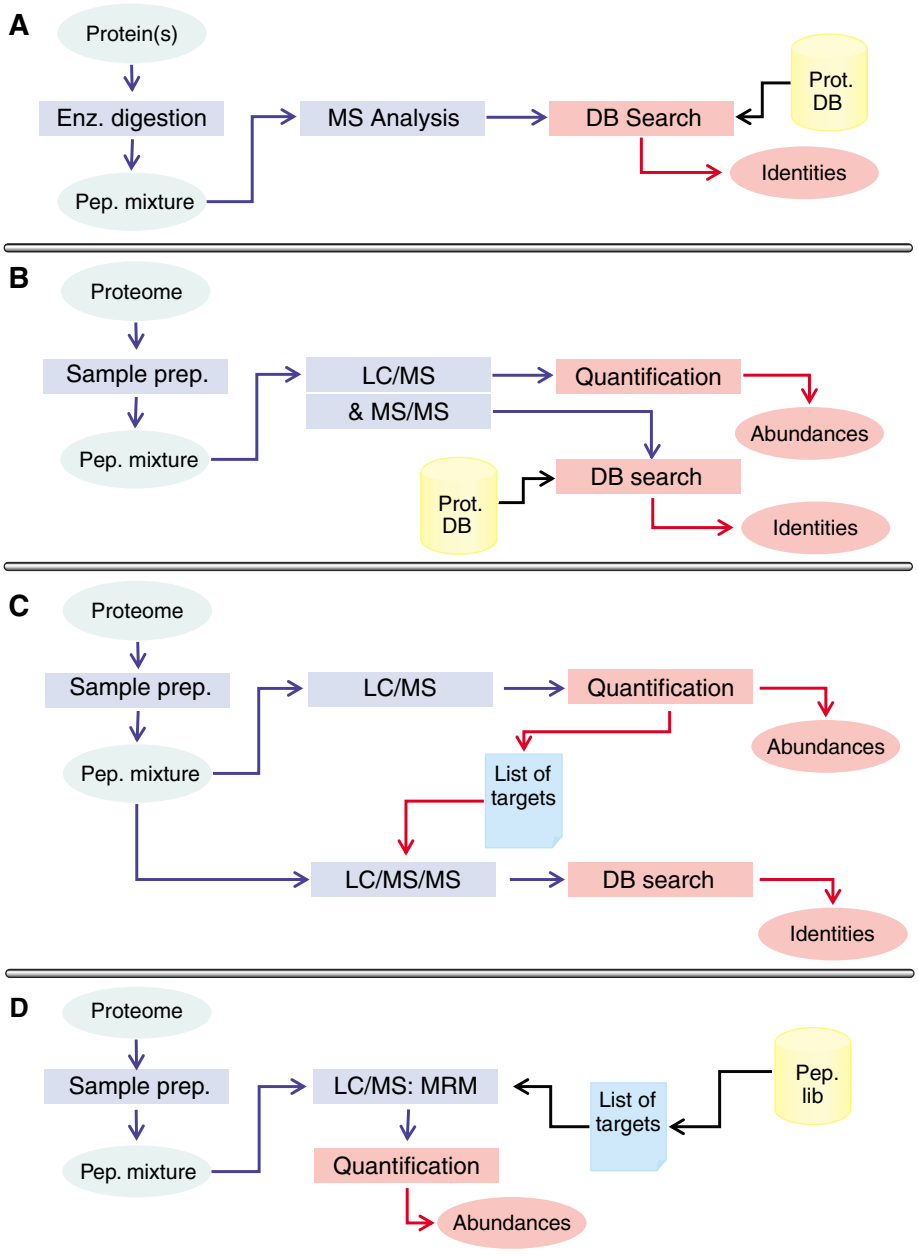

Fig. 2. Proteomics strategies. (**A**) Identification of simple protein (prot.) mixtures from 2D gel electrophoresis or pull-down experiments is carried out by enzymatic (enz.) digestion and by mass spectrometry analysis of the resulting peptides (pep.) (in ESI or MALDI mode). Peptide masses allows their identification (and that of the parent proteins) using peptide mass fingerprinting (PMF). Additional MS/MS data are also used for the peptide identification. (**B**) Random protein identification and quantification, also referred to as shotgun proteomics, couples identification and quantification of specific peptides in a sample. Selected peptides are subjected to product ion scanning (Fig. 1A) in a tandem mass spectrometer. The precursor ions are selected randomly, and typically only a fraction of the precursor ions detected are selected (undersampling). The ion intensities in MS1 are used to quantify the analytes by relating the signal intensity of the selected analyte to the signal intensity of a suitable reference molecule (frequently, a reference peptide labeled with heavy stable isotopes). (**C**) Quantification-driven identification decouples quantification and identification of peptides. In a first step, peptides that quantitatively differ between samples are detected by comparing the MS1 peptide patterns (mass versus chromatographic retention time) between samples, allowing for a more extensive analysis of the peptide patterns. Candidate peptides that show interesting quantitative properties are subjected to MS/MS sequencing in a second step using an inclusion list resulting from the primary analysis. (**D**) Hypothesis-driven peptide identification measures with high precision the abundance of a series of predetermined peptides. The targeted peptides, usually identified from previous experiments, are subjected to MRM (Fig. 1D). Accurate quantification is achieved by adding a suitable calibrated reference peptide.

similar to the 2D gel electrophoresis method in that 2D patterns of features are generated for each sample, and the patterns are compared to identify quantitative or qualitative changes. Such features are then further characterized, for example, by sequencing or by determining their posttranslationally modified state. However, in MS-based pattern analysis methods, protein samples are proteolyzed, fractionated, and the resulting peptides are analyzed by liquid chromatography (LC)/MS. The two dimensions to describe a peptide ion are chromatographic elution time and mass. Quantification of the detected features is achieved by integrating the ion counts of each signal. The main advantage of this method is that all the features that are detectable by MS can be quantified. This is in contrast with the shotgun methods, in which only identified peptides are quantified. However, in practice, it is extraordinarily challenging to generate highly reproducible patterns and to develop software tools that reliably match related patterns (*30*, *31*). Such analyses result in a list of features that represents putative peptide ions, with the following attributes: mass-to-charge ratio (*m*/*z*), charge state, elution time, and ion intensity. The peptides that need to be sequenced (for instance, features indicating different expression between two samples) are included in a list and then submitted to a new, directed mass-spectrometric experiment to collect MS/MS spectra of these features exclusively. This type of analysis is also well suited for the MALDI/MS/MS platform, because the samples are "immobilized" on the sample plate and can therefore be interrogated sequentially and without any time constraints.

Hypothesis-driven strategies. It can be expected that incremental improvements in instrument performance will continue to translate into more-sensitive, faster, and more-reliable proteomic analyses. However, it is not clear whether such advances will be sufficient to eliminate the major bottlenecks encountered in the current proteomics approaches. We have argued before (*32*) that proteomics needs to undergo a paradigm shift to reach the goal of robustly and globally analyzing proteomes. The essence of this shift is the transformation of proteomics from a mode where in every experiment, the proteome is rediscovered, to a mode in which the information from prior proteomic experiments is used to guide the present experiments. Specifically, it can be anticipated that extensive (complete) proteome maps containing all the peptides of a species that are observable by mass spectrometry will be generated and that future strategies will aim at the targeted, nonredundant analysis of information-rich peptides. For mass spectrometry instrumentation and strategy, this shift of paradigm requires the development of instruments and data acquisition protocols that support the fast, sensitive, and robust analysis of previously generated lists of target peptides. Databases that allow the extraction of peptides that uniquely identify a specific protein or a specific modified form of a protein and that are easily detectable by

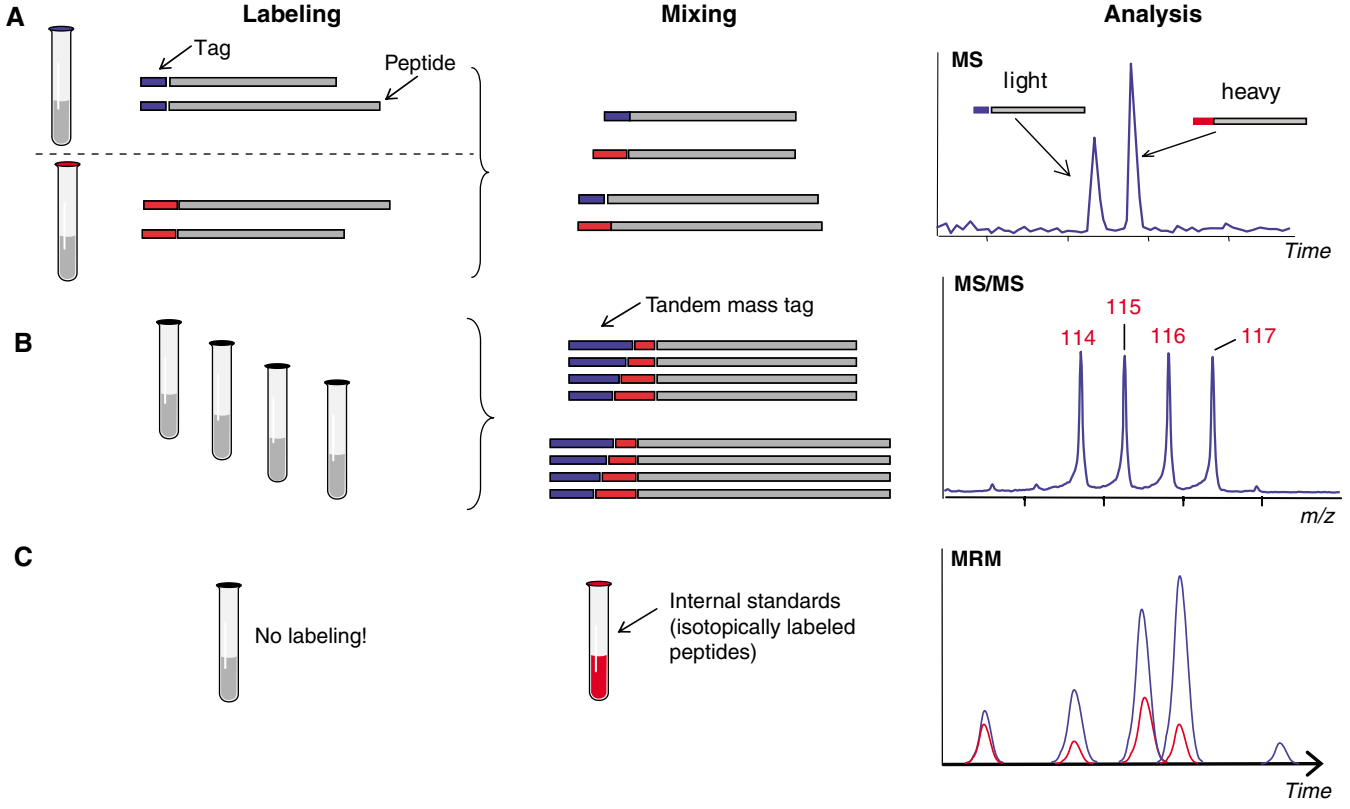

Fig. 3. Strategies for quantitative peptide analyses. (**A**) Quantification using isotope dilution is widely used and accepted in the proteomics community. It is based on the incorporation of a stable isotope signature into all of the proteins of one sample and the incorporation of a different stable isotope signature in all proteins of a second sample. The samples are then combined to serve as mutual references. Stable isotope incorporation has been achieved by chemical modification of proteins using suitable isotope coded labeling reagents (*26*), metabolic labeling (*35*), or by enzyme reactions (*36*). The method is schematically illustrated here. (**B**) Quantification using tandem mass tags relies on variants of stable isotope labeling reagents (*37*, *38*). They consist of two isotopically labeled elements, which have an overall constant mass. Currently, these reagents can be multiplexed to four channels. Quantification is performed in the MS/MS mode by measuring the relative intensity of the reporter group attached at the N terminus and observed in low mass range of the CID spectrum. (**C**) Quantification using internal standards is a variant of isotopic dilution in which a subset of isotopically labeled peptides is added to the sample at defined concentrations to perform precise quantification using calibration curves. Although it is more demanding in terms of sample preparation, this method is likely to gain importance in the future in the more directed approach indicated above for quantifying proteins in a larger number of samples. It may also be a more effective way to perform hypothesis-driven studies by screening for known or putative proteins (i.e., peptides) present in samples.

mass spectrometry are just emerging (*33*). It can be anticipated that biological hypotheses will generate lists of proteins that need to be characterized and quantified in a particular study. Such lists of proteins can then be submitted to the database to produce the minimal set of peptides required to test the hypothesis. This set of peptides can then be measured by targeted methods, including MRM (Fig. 2D). The directed nature of this approach allows the mass spectrometer to focus on a nonredundant set of targets and therefore leads to a substantial gain in throughput and sensitivity. By adding calibrated, isotopically labeled reference peptides, precise quantitative information can be obtained.

Such strategies are best implemented on mass spectrometers with Q-Q-LIT geometry related to the triple quadrupole instrument that has been used for decades to quantify small molecules drugs and their metabolites in serum. The same type of protocols can be applied to proteomics studies.

As a variant of this approach, Smith developed the concept of using accurate mass tags to identify peptides by matching accurately measured peptide masses with those calculated for peptides present in a database (*34*), thus obviating the need to sequence each peptide in each sample. With the rapid increase in accessible data from prior proteomic experiments and the development of mass spectrometer control software that supports large inclusion lists for targeted analyses, the use of the hypothesis-driven strategies can be expected to increase.

Outlook and Conclusion

Protein analysis and, more specifically, proteomics have driven the development of mass spectrometry for the past decade. Technological advances have translated into major improvements in mass accuracy, resolving power, LOD, and accuracy of quantification and new experimental strategies aimed at the routine and comprehensive analysis of whole proteomes. New mass-spectrometric strategies to analyze intact proteins, protein complexes, and low-redundancy target workflows are emerging. Although these mass spectrometry technologies have been driven by protein research; once developed, they will equally effect the analysis of other types of biomolecules, including metabolites, lipids, and carbohydrates. It can therefore be anticipated that the use of mass spectrometry in the life sciences will become even more prevalent and diversified.

References and Notes

1. N. L. Anderson, N. G. Anderson, *Mol. Cell. Proteomics* **1**, 845 (2002).
2. J. B. Fenn, M. Mann, C. K. Meng, S. F. Wong, C. M. Whitehouse, *Science* **246**, 64 (1989).
3. M. Karas, F. Hillenkamp, *Anal. Chem.* **60**, 2299 (1988).
4. R. Aebersold, D. R. Goodlet, *Chem. Rev.* **101**, 269 (2001).
5. R. Aebersold, R. M. Mann, *Nature* **422**, 198 (2003).
6. Mass accuracy and resolving power are two key characteristics of a mass spectrometer. Resolving power characterizes the ability to separate two ions that are close in mass (and it is defined by the ratio mass/mass difference). Mass accuracy is expressed either in absolute terms (difference between the observed and calculated values) or in relative terms expressed in ppm.
7. K. F. Medzihradszky *et al.*, *Anal. Chem.* **72**, 552 (2000).
8. R. G. Cooks, G. L. Glish, S. A. McLuckey, R. E. Kaiser, *Chem. Eng. News* **69**, 26 (1991).
9. In data (or information)-dependent acquisition, the data system will use information collected on the flight in full scan mode (MS1) to trigger the subsequent MS/MS experiments.
10. J. V. Olsen, M. Mann, *Proc. Natl. Acad. Sci. U.S.A.* **101**, 13417 (2004).
11. J. W. Hager, *Rapid Commun. Mass. Spectrom.* **16**, 512 (2002).
12. M. W. Senko, C. L. Henderickson, M. R. Emmett, S. D. Shi, A. G. Marshall, *J. Am. Soc. Mass Spectrom.* **8**, 970 (1997).
13. M. Hardmanand, A. Makarov, *Anal. Chem.* **75**, 1699 (2003).
14. Q. Hu *et al.*, *J. Mass Spectrom.* **40**, 430 (2005).
15. M. J. Huddleston, M. F. Bean, S. A. Carr, *Anal. Biochem.* **239**, 180 (1996).
16. J. C. Le Blanc *et al.*, *Proteomics* **3**, 859 (2003).
17. M. J. Huddleston, R. J. Annan, M. F. Bean, S. A. Carr, *Anal. Chem.* **65**, 877 (1993).
18. R. A. Zubarev, N. L. Kelleher, F. W. McLafferty, *J. Am. Chem. Soc.* **120**, 3265 (1998).
19. J. E. P. Syka, J. J. Coon, M. J. Schroeder, J. Shabanowitz, D. F. Hunt, *Proc. Natl. Acad. Sci. U.S.A.* **101**, 9528 (2004).
20. N. L. Kelleher, *Anal. Chem.* **76**, 197A (2004).
21. M. A. Baldwin, *Mol. Cell. Proteomics* **3**, 1 (2004).
22. S. Carr *et al.*, *Mol. Cell. Proteomics* **3**, 531 (2004).
23. A. Keller, A. I. Nesvizhskii, E. Kolker, R. Aebersold, *Anal. Chem.* **74**, 5383 (2002).
24. H. Wang *et al.*, *Mol. Cell. Proteomics* **4**, 618 (2005).
25. S. Hu *et al.*, *Anal. Chem.* **76**, 4044 (2004).
26. S. P. Gigy *et al.*, *Nat. Biotechnol.* **17**, 994 (1999).
27. H. Zhou *et al.*, *Nat. Biotechnol.* **19**, 375 (2001).
28. S. Ficarro *et al.*, *Nat. Biotechnol.* **20**, 301 (2002).
29. H. Zhang, X. J. Li, D. B. Martin, R. Aebersold, *Nat. Biotechnol.* **21**, 660 (2003).
30. P. Kearney, P. Thibault, *J. Bioinform. Comput. Biol.* **1**, 183 (2003).
31. X. J. Li *et al.*, *Anal. Chem.* **76**, 3856 (2004).
32. B. Kuster, M. Schirle, P. Mallick, R. Aebersold, *Nat. Rev. Mol. Cell Biol.* **6**, 577 (2005).
33. F. Desiere *et al.*, *Genome Biol.* **6**, R9 (2004).
34. R. D. Smith, G. A. Anderson, M. S. Lipton, *Proteomics* **2**, 513 (2002).
35. S. E. Ong *et al.*, *Mol. Cell. Proteomics* **1**, 376 (2002).
36. X. Yao, A. Freas, J. Ramirez, P. A. Demirev, C. Fenselau, *Anal. Chem.* **73**, 2836 (2001).
37. A. Thompson *et al.*, *Anal. Chem.* **75**, 1895 (2003).
38. P. L. Ross *et al.*, *Mol. Cell. Proteomics* **3**, 1154 (2004).

39. We gratefully acknowledge funding with federal funds from the National Heart, Lung, and Blood Institute of the NIH under contract no. N01-HV-28179.

10.1126/science.1124619

REVIEW

The Fluorescent Toolbox for Assessing Protein Location and Function

Ben N. G. Giepmans,[1,2] Stephen R. Adams,[2] Mark H. Ellisman,[1] Roger Y. Tsien[2,3]*

Advances in molecular biology, organic chemistry, and materials science have recently created several new classes of fluorescent probes for imaging in cell biology. Here we review the characteristic benefits and limitations of fluorescent probes to study proteins. The focus is on protein detection in live versus fixed cells: determination of protein expression, localization, activity state, and the possibility for combination of fluorescent light microscopy with electron microscopy. Small organic fluorescent dyes, nanocrystals ("quantum dots"), autofluorescent proteins, small genetic encoded tags that can be complexed with fluorochromes, and combinations of these probes are highlighted.

Fluorescence has long been used to visualize cell biology at many levels, from molecules to complete organisms. Originally, fluorescence was mainly observed from small organic dyes attached by means of antibodies to the protein of interest. However, antibody targeting of intracellular proteins normally requires cell fixation and permeabilization. Later, fluorophores could directly recognize organelles, nucleic acids, and certain important ions in living cells. In the past decade, fluorescent proteins have enabled noninvasive imaging in living cells and organisms of reporter gene expression, protein trafficking, and many dynamic biochemical signals. Hybrid systems in which small organic fluorophores are genetically targeted are filling other useful niches including determination of protein age, correlative electron-microscopic localization, and rapid photoinactivation of selected proteins. Meanwhile, semiconductor nanocrystals have been developed with higher brightness and photostability than previous fluorophores, but their targeting currently remains challenging. This review will discuss recent developments in fluores-

[1]National Center for Microscopy and Imaging Research, Center for Research in Biological Systems, Department of Neurosciences; [2]Department of Pharmacology; [3]Department of Chemistry and Biochemistry and Howard Hughes Medical Institute, University of California, San Diego, La Jolla, CA 92093, USA.

*To whom correspondence should be addressed. E-mail: rtsien@ucsd.edu

cent probes and techniques to determine protein expression, activity, and function.

Fluorophores

Small organic dyes. Small organic fluorophores (<1 kD) for covalent labeling of macromolecules have undergone industrial optimization of wavelength range, brightness (extinction coefficient for absorbance × quantum yield of fluorescence), photostability, and reduction in self-quenching. Molecular strategies have included extension of double-bond conjugation, rigidification through extra rings, and decoration with electron-withdrawing or obligatorily charged substituents such as fluorines or sulfonates. Hundreds of such dyes are commercially available (*1*), and further progress is likely to be incremental. Because these dyes lack specificity for any particular protein, most applications use antibodies (Fig. 1, A to C) in fixed and permeabilized cells.

Fluorescent proteins. The first fluorescent proteins to become useful in cell biology were phycobiliproteins, photosynthetic antenna pigments extracted from cyanobacteria (*2*). Each macromolecule contains multiple bilin chromophores encapsulated in a matrix evolved to minimize quenching, making phycobiliproteins up to two orders of magnitude brighter than small organic fluorophores. However, their size (200 kD) limits diffusion, so their application has been mainly in antibody conjugates for surface labeling in flow cytometry and enzyme-linked immunosorbent assay (ELISA) [reviewed in (*3*)]. They could become much more widely useful if genetically expressed in situ, but the problem is that bilin chromophores have to be supplied and inserted into the apoproteins. Fortunately, much progress has been made (*4*, *5*).

A revolution in cell biological imaging has resulted from the discovery (*6*), gene cloning (*7*), and heterologous expression of the green fluorescent protein (GFP) from the jellyfish *Aequorea victoria* [reviewed in (*8*)]. Expression of GFP alone or in most genetic fusions with other proteins results in visible fluorescence (Fig. 1, C and D) without requiring any cofactors other than O_2, because the chromophore is generated by spontaneous cyclization and oxidation of three amino acids buried at the heart of the 2.4- by 4-nm beta barrel. GFP is just one member of a large family of homologous fluorescent proteins (FPs) (*9*, *10*), mostly from marine coelenterates, with different colors from variations in chromophore covalent structure and noncovalent environment (*11*). Laboratory mutagenesis has further diversified FPs' spectra, increased their brightness and folding efficiencies (*12*), and decreased oligomerization [reviewed in (*11*)]. Mutation can either increase the photostability for standard fluorescence observation or conversely generate FPs that are photoswitchable from dark to bright or from one color to another [reviewed in (*13*)]. Such photoswitching can be reversible or irreversible and is useful for monitoring protein diffusion, trafficking, and age. Although FPs generate stoichiometric amounts of H_2O_2 during chromophore formation (*8*), they seem to generate relatively little reactive oxygen species (ROS) during illumination, which is not

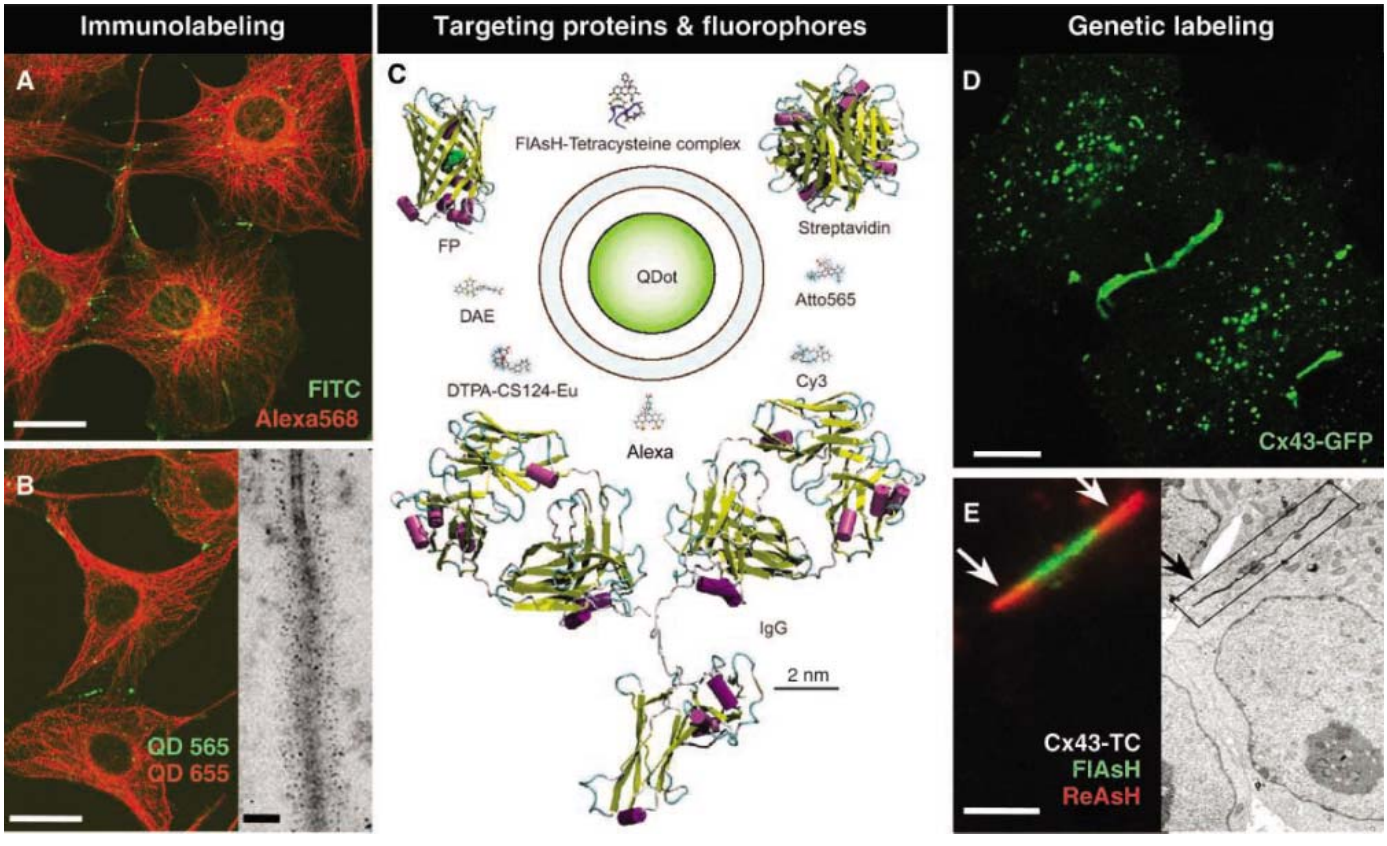

Fig. 1. Characteristics and applications of types of fluorophores in protein detection. Applications of different targeting methods and types of fluorophores are illustrated on connexin43 (green) and α-tubulin (red) in fibroblasts (**A** and **B**) and connexin43 in HeLa cells (**D** and **E**) as indicated. The structures of different types of targeting proteins and fluorophores (**C**) are shown to scale. [Scale bar is 2 nm; reproduced from (*58*).] Endogenous proteins are labeled using primary antibodies followed by secondary antibodies conjugated to small organic dyes (A) or Fab fragments attached to QDs (B), which are also detected at the EM level; (B) (right), QD 565 at connexin43–based gap junction. Genetically encoded intrinsic FPs (D) or tetracysteine tags labeled with biarsenicals (E) rely on ectopic expression. Tetracysteines on connexin43 were pulse-labeled with FlAsH (green) and subsequently ReAsH (red), thus distinguishing old from new connexins, respectively. ReAsH is also visualized in EM using photooxidation (E) (right). [Reproduced from (*37*).] Scale bars in (A), (B), and (D), 20 μm (LM); (B), 50 nm (EM); (C), 2 nm; (E), 2 μm.

surprising given their evolution within organisms exposed to sunlight. Nevertheless, it has been possible to mutate FPs to generate ROS for photodestruction of cells (*14*). The fluorescence of FPs is normally rather insensitive to their biochemical environment except for quenching by acid pH or denaturation, but they have been engineered for enhanced pH sensitivity or responsiveness to metal or halide ions and thiol-disulfide redox potentials [reviewed in (*10*, *15*)].

Quantum dots. Quantum dots (QDs) are inorganic nanocrystals that fluoresce at sharp and discrete wavelengths depending on their size, have high extinction coefficients (10 to 100 times those of small fluorophores and FPs), and have good quantum yields. QDs typically contain a CdSe or CdTe core and ZnS shell (Fig. 1C). Their absorbance extends from short wavelengths up to just below the emission wavelength, so that a single excitation wavelength readily excites QDs of multiple emission maxima. Crucial for biological applications was the development of coatings that make QDs water soluble, prevent quenching by water, and allow conjugation to protein-targeting molecules such as antibodies and streptavidin (Fig. 1B) (*16*–*20*). The large size of QDs conjugated to biomolecules (~10 to 30 nm) prevents efficient traversal of intact membranes, which restricts their use to permeabilized cells or extracellular or endocytosed proteins. The photostability of QDs allows repeated imaging of single molecules, and their size and electron-density permits correlated electron microscopy (EM) (*21*).

Gold and silver nanodots formed within hydrophilic dendrimers are also highly fluorescent and wavelength tunable (*22*). Their derivatization and application in cell biology is eagerly awaited.

Techniques to Tag Proteins

Immunolabeling. Immunolabeling and other techniques for tagging proteins are summarized in Table 1. The most widespread technique to detect endogenous proteins using fluorescence is labeling with a primary antibody followed by amplification with a secondary antibody conjugated to small organic dyes, a phycobiliprotein, or a QD (Fig. 1. A to C). Alternatively, primary antibodies can be directly conjugated to fluorophores or to biotin, which is then detected using streptavidin. Direct conjugation is especially useful when injecting antibodies into live cells or to increase spectral diversity when analyzing multiple proteins. When high-quality antibodies to the target protein are not available, the target can be recombinantly expressed with an epitope tag, although it is no longer completely endogenous. Of course, the accuracy of protein recognition depends on the specificity of the primary antibodies, so this should be validated using parallel methods. Disadvantages of immunofluorescence are that it is usually restricted to permeabilized cells or extracellular or endocytosed proteins, and the multivalency of these probes might lead to oligomerization of target proteins on live cells. In standard immunolabeling, the size of the fluorophore-targeting complex typically exceeds 200 kD and might interfere with multiprotein recognition in protein complexes.

Genetic tagging. A key advantage of genetically encoded FPs is that they can be covalently fused to the protein of interest, so that targeting is precise (Fig. 1, C and D). Transfection and transgenic techniques often make exogenous DNA easier than dyes to deliver to cells or organisms. Limitations include the need for ectopic expression, the significant size of FPs, the possibility that the fusion may interfere with the function of the protein of interest, and the restriction to fluorescence as the only useful property. Therefore, several hybrid systems have been described by which small molecules can be covalently targeted to genetically specified proteins inside or on the surface of living cells, either by spontaneous attachment or enzymatic ligation [reviewed in (*23*–*25*)]. Most of these techniques are too new to have had much cell biological application. The most developed is the tetracysteine-biarsenical system (*26*), which requires modification of the target protein by a 12-residue peptide sequence that includes four cysteines, which binds membrane-permeable biarsenical molecules, notably the green and red dyes "FlAsH" and "ReAsH" (*27*), with picomolar affinity (Fig. 1, C and E). Small dithiol antidotes are coadministered to minimize binding and toxicity to endogenous proteins. The tetracysteine motif has undergone multiple rounds of improvement to increase its affinity for the biarsenical dyes, enabling lower dye concentrations and higher antidote concentrations to reduce background staining (*28*). Examples where protein function is less perturbed by the small tetracysteine-biarsenical combination than by FP fusions include tubulin in yeast (*29*), coupling of receptors to heterotrimeric guanine nucleotide–binding proteins (G proteins) (*30*), translocation to the nucleus (*31*), and type III secretion of pathogenic proteins from bacteria into eukaryotic cells (*32*). Tetracysteine-biarsenicals also enable manipulations not readily possible with FPs, such as affinity purification (*27*), fluorophore-assisted light inactivation (*33*, *34*), cotranslational detection of protein synthesis (*35*, *36*), pulse-chase labeling (*37*, *38*), and correlative EM localization (*37*). However, the biarsenical dyes give higher background fluorescence and poorer contrast than FPs, have not yet been demonstrated in intact transgenic animals, require the cysteines to be reduced during labeling, and do not permit two different proteins in the same compartment to be simultaneously labeled with different colors. The tetracysteine sequence occasionally provides a palmitoylation site, although such modification can sometimes be

Table 1. Applications of fluorophores in protein detection. Applicability ranges from most optimal (++) to generally not applicable (–), and (+/–) indicates applicable in some cases.

Fluorophores for examination of	Small organic dyes (antibody-targeted)	Quantum dots (antibody-targeted)	Fluorescent proteins	Genetic tags with small dyes
Endogenous proteins	++	+	–	–
Clinical specimens	++	+	–	–
Animals	Ex vivo	Ex vivo	Transgene live	Transgene ex vivo
Primary tissues	++	+	Transgene/virus	Transgene/virus
Live cells in culture	Surface	Surface	++	+
Multiple proteins at once	++	++	++	–
Dynamic interactions	+/–	+/–	++	Combination with FP
Turnover/synthesis	–	–	+	+
Activation state	Phospho-specific	Phospho-specific	FRET sensors	Combination with FP
CALI	+	–	+	++
EM	+/–	++	+/–	+
Protein microarrays	++	+	–	–
In gel fluorescence	–	–	+	+
Western blot	–	+	–	–
Major advantages	Diversity of properties	Bright and photostable	Live cells and specificity	Live cells and small size
Major limitations	Targeting in live cells	Targeting and penetration	Ectopic expression	Ectopic expression, background staining
Improvements expected	Generic conjugated primary antibodies	Smaller, diversity of properties	Better properties, generic sensors	New applications

prevented by a preceding epitope tag (*28*). Genetic tags have unique applications, but other methods should be used in parallel to decide whether tagging or ectopic expression levels are perturbing protein function or localization.

Studying Protein Expression and Localization in Primary Cells and Fixed Tissues

Expression and activity profiling with flow cytometry. To study endogenous proteins, immunofluorescence approaches are usually most suitable. Fluorophore-conjugated antibodies specific for phosphoproteins conjugated to fluorophores enable visualization of the activation state of endogenous proteins and are crucial in single-cell profiling of the activity of multiple cytoplasmic proteins simultaneously using fluorescent flow cytometry (*39*). Single-cell profiling can delineate signaling networks in cells (*40*) and might be extendable to clinical drug testing on patients' blood cells in ex vivo experiments. For cytoplasmic proteins, small dyes are currently preferable to QDs because of the better penetration in fixed and mildly permeabilized cells (Table 1). However, the brightness of QDs improves the detection limit, and the different spectral characteristics aid in multilabel separation. Using small dyes, phycobiliproteins, and QDs, 17 fluorophores have been detected simultaneously in a flow cytometer (*41*).

Protein localization at light and EM levels. The best information on localization of proteins in the context of organelles and other subcellular structures is achieved by EM. Most naked fluorophores upon illumination generate some singlet oxygen, which not only tends to bleach the fluorophore itself but can locally oxidize diaminobenzidine (DAB) to an osmiophilic polymer identifiable by EM. This process of "photoconversion" was first shown with Lucifer Yellow (*42*) and later improved by eosin immunostaining (*43*). Recently, tetracysteine-tagged proteins labeled with the biarsenical dye ReAsH were shown to photoconvert DAB in protocols that allow stringent fixation and optimal preservation of ultrastructure (Figs. 1E and 2H). Moreover, the technique allows pulse-chase distinction between young and old copies of a given protein at the EM level (Fig. 1E) (*37*). GFP has been claimed to photoconvert DAB (*44*), albeit with much lower efficiency than ReAsH.

Photoconversion works best for proteins concentrated in subcellular structures. To detect multiple or more diffuse proteins, QDs are a promising tool for protein detection at the light microscope (LM) and EM levels (Fig. 1B). The electron-dense core and the size of QDs make them visible at the EM level, and this visibility can be enhanced by silver staining (*45*). Correlated LM and EM was shown by postsectioning labeling of a nuclear protein with QDs (*46*). Recently a straightforward application to label multiple endogenous proteins simultaneously for correlated LM-EM in cells and tissues using immunolabeling with QDs has been reported (*21*). QDs permit quick LM prescreening of labeling efficiency and areas of interest before EM examination. Because of the different sizes of QDs, three different proteins can be easily discriminated (*21*). Because every QD that fluoresces should be visible in EM, all fluores-

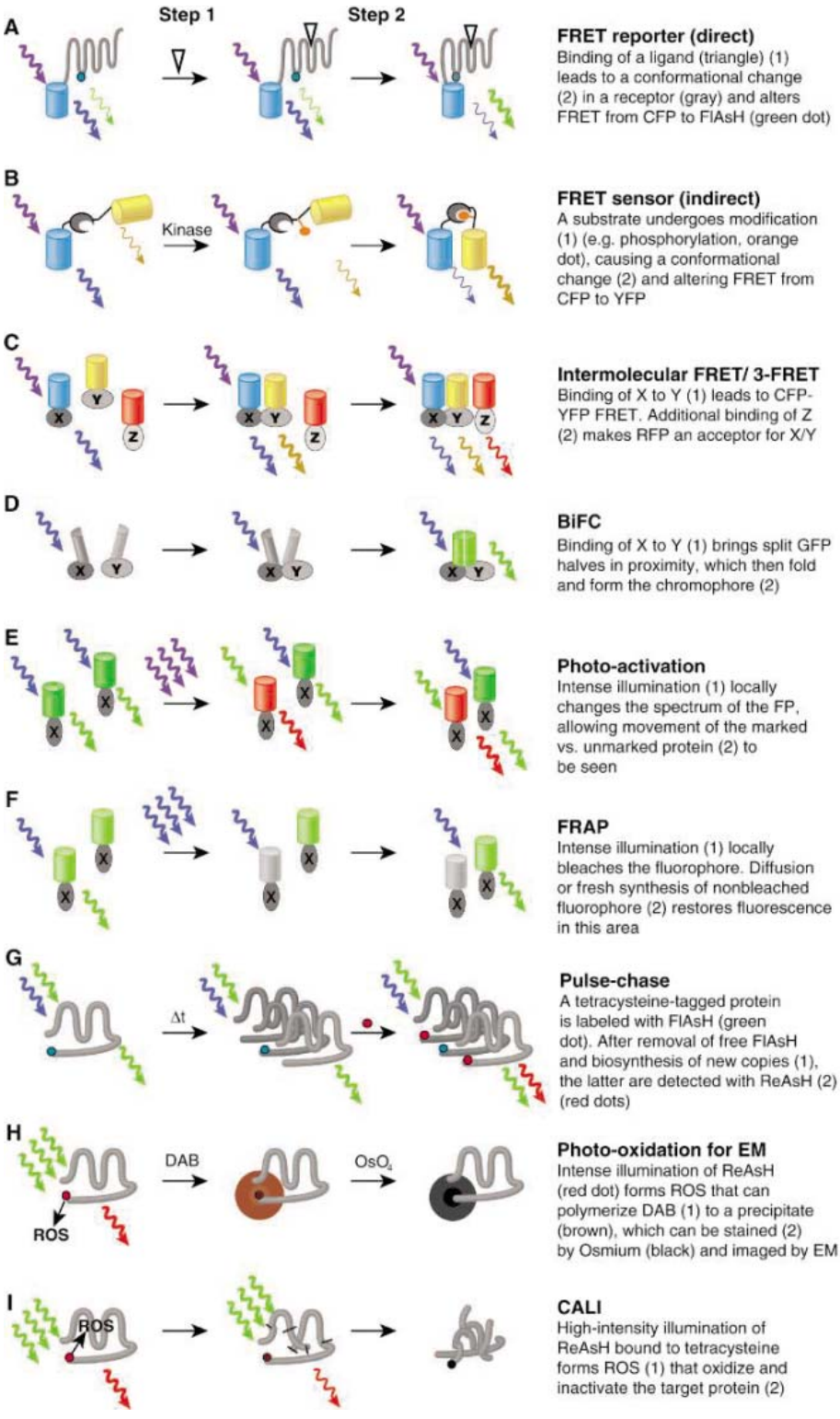

Fig. 2. Advanced fluorescent applications with genetic tags. (**A** to **I**) Principles of advanced techniques are depicted and explained. Barrels represent cyan, green, yellow, and red fluorescent proteins. X, Y, and Z represent target proteins. Light intensity is indicated by the thickness of the waves. See text for further details.

Excitation (nm):	800 (2 photon)	488	432	568	637
Emission (nm):	410-490	500-530	555-565	580-620	>660
Fluorophore:	Hoechst	GFP	QD565	ReAsH	Cy5
Targeting:	direct affinity	genetic	immuno	genetic	immuno
Target:	DNA	α-tubulin	giantin	β-actin	Cytochrome c
Structure:	nuclei	microtubules	golgi	stress fibers	mitochondria

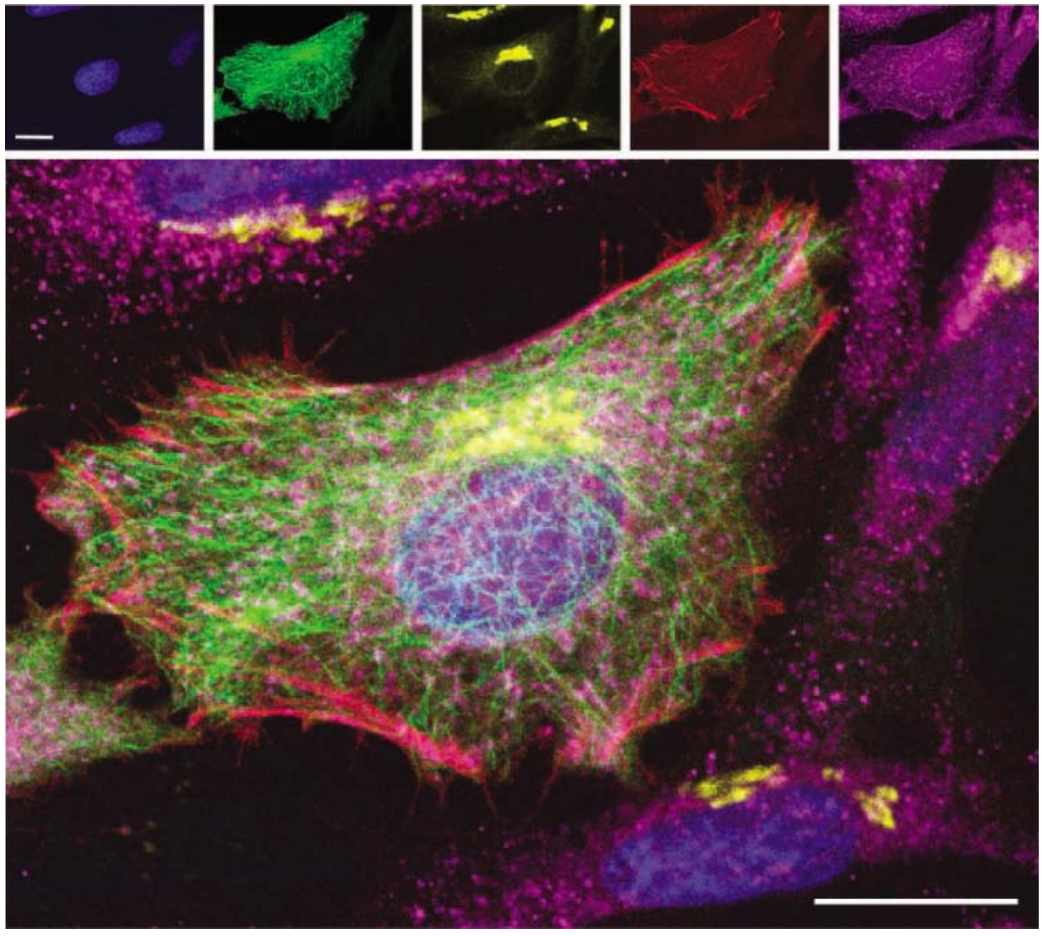

Fig. 3. Parallel application of targeting methods and fluorophores. HeLa cells transfected with GFP–α-tubulin and tetracysteine–β-actin were stained with ReAsH. After fixation, cells were immunolabeled for the Golgi matrix protein giantin with QDs and for the mitochondrial enzyme cytochrome c with Cy5 as indicated. DNA was stained with Hoechst 33342. Images were acquired from Z planes that best represent each structure using excitation and emission wavelengths as indicated. Individual channels are false-colored (middle) and merged (bottom). Scale bars, 20 μm.

cent studies using QDs could, in principle, be followed up at the EM, including nonantibody techniques such as using biotin ligase to tag cell surface proteins for detection by streptavidin-conjugated QDs (*47*). Because preembedding immunolabeling requires permeabilization and does not allow direct stringent fixation, the ultrastructure is less well preserved than when using tetracysteine-based correlated microscopy.

Protein Dynamics in Live Cells

Protein diffusion and trafficking. When a labeled protein undergoes major net redistribution, direct imaging can see this motion. Such translocation can be deliberately engineered as a readout for protein activation or second messengers, e.g., translocation of FP-tagged pleckstrin homology domains to monitor accumulation of polyphosphoinositides in the plasma membrane [reviewed in (*15*, *48*)]. But even at steady state, proteins are typically undergoing diffusion or intercompartmental exchange. Three general approaches for measuring such normally invisible fluxes are single-particle tracking, correlation spectroscopy, and photomarking methods. In single-particle tracking, the individual molecules, aggregates, or organelles must be both bright and sparse enough to be tracked from one video frame to the next, preferably by automated software. For example, low concentrations (<0.5%) of fluorescent-conjugated actin or tubulin form fluorescent speckles in filamentous actin or microtubules, respectively. The assembly, flow, and turnover within the macromolecular structure is reflected by the dynamic movement of the fluorescent speckles [reviewed in (*49*)]. Fluorescence correlation spectroscopy statistically analyzes the intensity fluctuations resulting from migration of fluorescent objects into and out of a small volume at the focus of a laser (*50*–*52*). Extensions include image correlation spectroscopy, which measures changes in fluorescence from microscopic images and thus allows more global mapping of interactions and dynamics of labeled constituents in living cells (*53*, *54*). Photochemical sensitivity of the fluorophore is undesirable in the above techniques, whereas it is essential for photomarking, another set of techniques to image protein dynamics. Various FPs (*10*, *11*, *13*) can be destroyed (Fig. 2F), dequenched, or changed in color, as by photoactivation (Fig. 2E) in a subcellular area with the use of intense local illumination (*55*). The subsequent fate of the marked molecules can then be imaged directly. For active transport, the size of the fluorescent tag is usually not very important, but for passive diffusion, small tags are much less likely to cause perturbations.

Single QDs can be imaged repeatedly because of their brightness and resistance to photobleaching, but the difficulty in targeting cytoplasmic proteins in live cells is a major limitation. For cell surface proteins, however, QDs are advancing single-molecule live-cell imaging. Glycine receptor diffusion was followed by immunotargeted streptavidin-QDs (*45*). More than a thousand high-quality images could be acquired from endogenous receptors in living neurons, which revealed that glycine receptors diffuse with different rates in extrasynaptic, perisynaptic,

and synaptic domains. Lidke and co-workers recently obtained new insight into epidermal growth factor (EGF) signaling using a combination of many of the probes and techniques reviewed here. They found that EGF-conjugated QDs specifically colocalize with an ErbB1-GFP receptor chimera and activate the receptor, as determined by Cy5-conjugated antibodies against activated ErbB1. The complex was internalized by a clathrin-dependent process, as shown by colocalization of Alexa-labeled transferrin (*56*). Retrograde transport of single EGF-QD bound to the receptor was found to depend on receptor oligomerization, as shown using spectrally distinct EGF-QDs. Fluorescence recovery after photobleaching (FRAP) of GFP-actin revealed that retrograde receptor transport and actin flow was at the same rate. Receptors did not internalize on filopodia, but at the cell body, as was found by specific quenching of extracellular EGF-QDs-streptavidin by using impermeable biotin-Alexa. Thus, filopodia might serve as antennae and could regulate transport of activated receptors to the cell body (*57*).

Conformational changes. One of the most general ways to detect dynamic conformational changes with spatiotemporal resolution is to sandwich the protein domain between two fluorophores (most commonly cyan and yellow FPs, CFP and YFP, respectively) and monitor fluorescence resonance energy transfer (FRET) [reviewed in (*15*, *58*, *59*)] (Fig. 2, A to C). A typical FRET-based sensor is shown in Fig. 2B. FRET efficiency depends both on the distance and the orientation between donor and acceptor. FRET responses to internal conformational changes most often result from reorientation rather than distance changes, because circular permutation of one of the FPs (*60*) or small changes in linker length alter the FRET response much more drastically than can be explained by any alteration in the distance between the FPs. The protein linking the FPs can itself be engineered to change conformation in response to important biochemical signals. These sensors can be targeted to specific subcellular compartments when fused to an appropriate localization signal. In this way, FRET-based indicators have been developed to measure several ions, cyclic nucleotides, metabolites, neurotransmitters, the balance between protein kinase and phosphatase activities, and activities of proteases, small G proteins, and histone acetylases (*15*, *58*, *59*).

Protein-protein interactions. FRET can also detect dynamic protein-protein interaction in live cells of ectopically expressed FP-tagged proteins (Fig. 2C), provided that the FPs get within 6 to 8 nm of each other. Recently, the possibility of using three fluorescent proteins to study higher order complexes has been addressed by adding a monomeric red fluorescent protein (mRFP) to the CFP/YFP pair. In trimeric complexes, CFP is the FRET donor for YFP; subsequently, YFP can act as a FRET donor for mRFP (Fig. 2C). 3-FRET has been shown in multiprotein complexes (*61*) and in protein trimerization (*62*). Further optimization of a higher wavelength FRET pair, as well as spectral deconvolution, might improve the 3-FRET technique.

FPs split at appropriate sites can fold and reconstitute the chromophore when the two halves are fused to interacting partners (*63*), a two-hybrid system termed bimolecular fluorescence complementation (BiFC) (Fig. 2D). Self-assembling fragments of GFP have also been reported (*64*), in which the two fragments only have to exist in the same compartment to generate fluorescence, without requiring splinting by other protein-protein interactions. BiFC can be used to study gene expression of at least two promotors, as has been demonstrated in *Caenorhabditis elegans* (*65*). BiFC has a high signal-to-background ratio, because it creates new fluorescence rather than modulating existing fluorescence. Multiple protein-protein interactions can be studied in parallel using spectrally distinct split FPs (*65*, *66*). However, BiFC is slow (hours to days) and irreversible, and the geometrical and affinity requirements for the protein-protein interaction have not yet been characterized.

In some cases, simple colocalization can be sufficient to indicate protein-protein interaction. For example, if the regulatory subunit of protein kinase A is targeted to the plasma membrane and a fluorescently tagged catalytic subunit is coexpressed, the latter is dragged to the plasma membrane but released when elevation of adenosine 3′,5′-monophosphate (cAMP) dissociates the subunits (*31*). Two-color fluorescence correlation spectroscopy can also show when partners with differently colored tags diffuse in pairs and are therefore likely to be interacting (*51*).

Protein synthesis and turnover. The determination of protein turnover requires discriminating old from new copies of the protein, typically by irreversibly labeling with one color all copies made up to a certain time. Optionally, proteins made later can be labeled with a different color after a delay. Endogenous, extracellularly exposed epitopes or receptors can be tagged with high-affinity ligands or antibodies conjugated to a fluorophore. Tetracysteine motifs can be labeled with one biarsenical, followed with another biarsenical, to study synthesis of assembled protein structures (*37*) (Figs. 1E and 2G) or to determine the subcellular site of protein translation (*38*). Chimeric proteins tagged with photomarkable FPs can be photoactivated or bleached to highlight proteins synthesized before (*13*) (Fig. 2E) or after (Fig. 2F) illumination. Some FP mutants irreversibly misfold above a critical threshold temperature, so a temperature shift can also serve as the triggering event (*67*). Yet others spontaneously change color from green to red as they complete their chromophore maturation, so that no external stimulus is required (*68*). In this case, the time resolution is modest because the color change in a population of molecules takes place over hours.

Manipulation of protein activity using chromophore-activated light inactivation. The ability of illuminated fluorophores to generate ROS, especially singlet oxygen (see EM section), can be used to inactivate the protein of interest (Fig. 2I) with much better spatiotemporal control than possible with genetic knockouts or RNA interference. This technique, chromophore-activated light inactivation (CALI), was introduced using the dye malachite green immunotargeted to the protein of interest (*69*). To avoid the difficulties of delivering dye-conjugated antibodies into living cells, the use of genetic tags for CALI has been explored. GFP (*70*), tetracysteine-bound biarsenical dyes FlAsH (*33*) and ReAsH (*34*), and a fluorescein conjugate targeted to the FK506-binding protein–12 FKBP12(F36V) (*71*) have been used to specifically destroy ectopically expressed proteins in living cells, with an order of efficiency ReAsH > FlAsH ~ fluorescein ≫ malachite green ~ GFP (*33*, *34*). Nonspecific toxic effects can be further minimized by multiphoton excitation at longer, less damaging wavelengths (*72*). "KillerRed," recently identified in a screen for phototoxic FPs (*14*), is a promising prototype of a wholly genetically encoded sensitizer for CALI and photoconversion, but it is an obligate dimer and its current CALI efficiency is less than that of ReAsH (*14*).

Seeing endogenous enzyme activity. Antibody recognition and genetic fusion are essentially stoichiometric, i.e., each target associates with one or, at most, a small number of fluorophores. Fluorogenic substrates (*1*) for endogenous enzymes offer much greater amplification and detect whether the enzyme is in an activated versus latent or inhibited state. The latter distinction is particularly important for proteases, because for many proteases only a small fraction of the total pool is active. Because of the great importance of proteases in infectious diseases, apoptosis, inflammation, tumor development, and metastasis, several approaches have recently been developed for imaging protease activity in intact animals (*73*), including disruption of FRET or other fluorescence quenching on multiply labeled substrates (*74*), and activation of cationic cell penetrating peptides to carry fluorophores onto and into cells (*75*).

Increasing spatial resolution and depth penetration. Because so many molecular and cell biological phenomena operate over distances

from one to a few hundred nanometers, much effort has been devoted to increasing the spatial resolution of fluorescence microscopy beyond the limits (~200 nm) set by classical diffraction theory. When an emitter is known to be a single point, its position can be determined with subnanometer accuracy if enough photons can be collected. Such measurements have been particularly valuable in deciphering step sizes of motor proteins and processive enzymes in vitro (*52*, *76*). A recent extension to live cells revealed that the step size of GFP-labeled peroxisomes along microtubules is ~8 nm (*77*). For more complex objects of unknown size and shape, several optically innovative approaches such as structured illumination, coherent observation with diametrically opposed objectives, and stimulated emission depletion are showing great promise (*78*–*80*).

For high-resolution imaging in scattering tissue at depths up to ~1 mm, multiphoton excitation with pulsed infrared is the method of choice because scattering is weakest in the infrared and because all of the collected emission photons must have originated from the illumination focus, even if they have suffered scattering (*81*, *82*). Fluorescence imaging at even greater depths is possible using novel serial reconstruction techniques in fixed tissue (*83*) or by tomography in live tissues, albeit with reduced resolution (*84*, *85*).

Further Considerations and Concluding Remarks

The power of fluorescence imaging is expanding rapidly because of synergistic advancements in fluorescent probes, targeting strategies, instrumentation, and data analysis, enabling high-throughput screens, single-molecule detection, multiprotein and live-cell imaging. The ecological diversity of natural FPs, further expanded by deliberate engineering by rational or randomly combinatorial mutagenesis, is producing an amazing range of useful phenotypes, although no one mutant combines all desirable properties. Reporters for many key metabolites, regulatory enzymes, and biochemical processes have already been developed, with no obvious limit in sight. Although genetic tagging is an unprecedented tool in live-cell protein imaging, other methods should be used in parallel (Figs. 1 and 3) to address whether tags perturb endogenous protein function. These include fluorophores conjugated to well-characterized antibodies, often specific for given posttranslational modifications, as well as genetic knock-in experiments to test whether the modified protein is an adequate in vivo replacement for its endogenous parent. Conversely, immunofluorescence labeling of FP-tagged target proteins tests the specificity of primary antibodies. Immunodetection using bright and stable QDs lowers the detection limit, increases the feasibility of multiprotein detection, and can be applied in correlated EM studies and in vitro assays that currently rely on enzymatic activity, such as Western blots and ELISA (Table 1). But better targeting and penetration will be required for QDs to reach their fullest potential.

Fluorescence detection will also be increasingly applied in clinical assays like protein-activity profiling in patient cells and biopsies, and to study effects of drugs on cell signaling in individual patients. Fluorescence assays are well suited for high-throughput drug screening both in biochemical assays such as protein microarrays and in functional assays in live cells or animals (*86*). The unique combination of high spatial and temporal resolution, nondestructive compatibility with living cells and organisms, and molecular specificity insure that fluorescence techniques will remain central in the analysis of protein networks and systems biology.

References and Notes

1. R. P. Haugland, *The Handbook—A Guide to Fluorescent Probes and Labeling Technologies* (Molecular Probes, Eugene, OR, 10th ed., 2005).
2. A. N. Glazer, *J. Biol. Chem.* **264**, 1 (1989).
3. A. Waggoner, *Curr. Opin. Chem. Biol.* **10**, 62 (2006).
4. A. J. Fischer, J. C. Lagarias, *Proc. Natl. Acad. Sci. U.S.A.* **101**, 17334 (2004).
5. A. J. Tooley, A. N. Glazer, *J. Bacteriol.* **184**, 4666 (2002).
6. O. Shimomura, F. H. Johnson, Y. Saiga, *J. Cell. Comp. Physiol.* **59**, 223 (1962).
7. D. C. Prasher, V. K. Eckenrode, W. W. Ward, F. G. Prendergast, M. J. Cormier, *Gene* **111**, 229 (1992).
8. R. Y. Tsien, *Annu. Rev. Biochem.* **67**, 509 (1998).
9. M. V. Matz, Y. A. Labas, J. Ugalde, *Methods Biochem. Anal.* **47**, 139 (2006).
10. D. M. Chudakov, S. Lukyanov, K. A. Lukyanov, *Trends Biotechnol.* **23**, 605 (2005).
11. N. C. Shaner, P. A. Steinbach, R. Y. Tsien, *Nat. Methods* **2**, 905 (2005).
12. J. D. Pedelacq, S. Cabantous, T. Tran, T. C. Terwilliger, G. S. Waldo, *Nat. Biotechnol.* **24**, 79 (2006).
13. K. A. Lukyanov, D. M. Chudakov, S. Lukyanov, V. V. Verkhusha, *Nat. Rev. Mol. Cell Biol.* **6**, 885 (2005).
14. M. E. Bulina *et al.*, *Nat. Biotechnol.* **24**, 95 (2006).
15. J. Zhang, R. E. Campbell, A. Y. Ting, R. Y. Tsien, *Nat. Rev. Mol. Cell Biol.* **3**, 906 (2002).
16. X. Michalet *et al.*, *Science* **307**, 538 (2005).
17. J. K. Jaiswal, S. M. Simon, *Trends Cell Biol.* **14**, 497 (2004).
18. X. Gao *et al.*, *Curr. Opin. Biotechnol.* **16**, 63 (2005).
19. A. P. Alivisatos, W. Gu, C. Larabell, *Annu. Rev. Biomed. Eng.* **7**, 55 (2005).
20. F. Pinaud *et al.*, *Biomaterials* **27**, 1679 (2006).
21. B. N. Giepmans, T. J. Deerinck, B. L. Smarr, Y. Z. Jones, M. H. Ellisman, *Nat. Methods* **2**, 743 (2005).
22. T. H. Lee, J. I. Gonzalez, J. Zheng, R. M. Dickson, *Acc. Chem. Res.* **38**, 534 (2005).
23. T. Gronemeyer, G. Godin, K. Johnsson, *Curr. Opin. Biotechnol.* **16**, 453 (2005).
24. L. W. Miller, V. W. Cornish, *Curr. Opin. Chem. Biol.* **9**, 56 (2005).
25. I. Chen, A. Y. Ting, *Curr. Opin. Biotechnol.* **16**, 35 (2005).
26. B. A. Griffin, S. R. Adams, R. Y. Tsien, *Science* **281**, 269 (1998).
27. S. R. Adams *et al.*, *J. Am. Chem. Soc.* **124**, 6063 (2002).
28. B. R. Martin, B. N. Giepmans, S. R. Adams, R. Y. Tsien, *Nat. Biotechnol.* **23**, 1308 (2005).
29. M. Andresen, R. Schmitz-Salue, S. Jakobs, *Mol. Biol. Cell* **15**, 5616 (2004).
30. C. Hoffmann *et al.*, *Nat. Methods* **2**, 171 (2005).
31. O. Dyachok, Y. Isakov, J. Sagetorp, A. Tengholm, *Nature* **439**, 349 (2006).
32. J. Enninga, J. Mounier, P. Sansonetti, G. Tran Van Nhieu, *Nat. Methods* **2**, 959 (2005).
33. K. W. Marek, G. W. Davis, *Neuron* **36**, 805 (2002).
34. O. Tour, R. M. Meijer, D. A. Zacharias, S. R. Adams, R. Y. Tsien, *Nat. Biotechnol.* **21**, 1505 (2003).
35. M. C. Rice, M. Bruner, K. Czymmek, E. B. Kmiec, *Mol. Microbiol.* **40**, 857 (2001).
36. M. C. Rice, K. Czymmek, E. B. Kmiec, *Nat. Biotechnol.* **19**, 321 (2001).
37. G. Gaietta *et al.*, *Science* **296**, 503 (2002).
38. W. Ju *et al.*, *Nat. Neurosci.* **7**, 244 (2004).
39. E. A. Danna, G. P. Nolan, *Curr. Opin. Chem. Biol.* **10**, 20 (2006).
40. K. Sachs, O. Perez, D. Pe'er, D. A. Lauffenburger, G. P. Nolan, *Science* **308**, 523 (2005).
41. S. P. Perfetto, P. K. Chattopadhyay, M. Roederer, *Nat. Rev. Immunol.* **4**, 648 (2004).
42. A. R. Maranto, *Science* **217**, 953 (1982).
43. T. J. Deerinck *et al.*, *J. Cell Biol.* **126**, 901 (1994).
44. M. Grabenbauer *et al.*, *Nat. Methods* **2**, 857 (2005).
45. M. Dahan *et al.*, *Science* **302**, 442 (2003).
46. R. Nisman, G. Dellaire, Y. Ren, R. Li, D. P. Bazett-Jones, *J. Histochem. Cytochem.* **52**, 13 (2004).
47. M. Howarth, K. Takao, Y. Hayashi, A. Y. Ting, *Proc. Natl. Acad. Sci. U.S.A.* **102**, 7583 (2005).
48. N. A. O'Rourke, T. Meyer, G. Chandy, *Curr. Opin. Chem. Biol.* **9**, 82 (2005).
49. C. M. Waterman-Storer, G. Danuser, *Curr. Biol.* **12**, R633 (2002).
50. S. T. Hess, S. Huang, A. A. Heikal, W. W. Webb, *Biochemistry* **41**, 697 (2002).
51. E. Haustein, P. Schwille, *Curr. Opin. Struct. Biol.* **14**, 531 (2004).
52. S. Weiss, *Science* **283**, 1676 (1999).
53. P. W. Wiseman *et al.*, *J. Cell Sci.* **117**, 5521 (2004).
54. P. W. Wiseman, J. A. Squier, M. H. Ellisman, K. R. Wilson, *J. Microsc.* **200**, 14 (2000).
55. T. H. Ward, J. Lippincott-Schwartz, *Methods Biochem. Anal.* **47**, 305 (2006).
56. D. S. Lidke *et al.*, *Nat. Biotechnol.* **22**, 198 (2004).
57. D. S. Lidke, K. A. Lidke, B. Rieger, T. M. Jovin, D. J. Arndt-Jovin, *J. Cell Biol.* **170**, 619 (2005).
58. E. A. Jares-Erijman, T. M. Jovin, *Nat. Biotechnol.* **21**, 1387 (2003).
59. H. Wallrabe, A. Periasamy, *Curr. Opin. Biotechnol.* **16**, 19 (2005).
60. T. Nagai, S. Yamada, T. Tominaga, M. Ichikawa, A. Miyawaki, *Proc. Natl. Acad. Sci. U.S.A.* **101**, 10554 (2004).
61. E. Galperin, V. V. Verkhusha, A. Sorkin, *Nat. Methods* **1**, 209 (2004).
62. L. He, X. Wu, J. Simone, D. Hewgill, P. E. Lipsky, *Nucleic Acids Res.* **33**, e61 (2005).
63. T. J. Magliery, L. Regan, *Methods Biochem. Anal.* **47**, 391 (2006).
64. S. Cabantous, T. C. Terwilliger, G. S. Waldo, *Nat. Biotechnol.* **23**, 102 (2005).
65. S. Zhang, C. Ma, M. Chalfie, *Cell* **119**, 137 (2004).
66. C. D. Hu, T. K. Kerppola, *Nat. Biotechnol.* **21**, 539 (2003).
67. C. Kaether, H. H. Gerdes, *FEBS Lett.* **369**, 267 (1995).
68. A. Terskikh *et al.*, *Science* **290**, 1585 (2000).
69. D. G. Jay, T. Sakurai, *Biochim. Biophys. Acta* **1424**, M39 (1999).
70. Z. Rajfur, P. Roy, C. Otey, L. Romer, K. Jacobson, *Nat. Cell Biol.* **4**, 286 (2002).
71. K. M. Marks, P. D. Braun, G. P. Nolan, *Proc. Natl. Acad. Sci. U.S.A.* **101**, 9982 (2004).
72. T. Tanabe *et al.*, *Nat. Methods* **2**, 503 (2005).
73. K. Shah, R. Weissleder, *NeuroRx* **2**, 215 (2005).
74. D. Stockholm *et al.*, *J. Mol. Biol.* **346**, 215 (2005).
75. T. Jiang *et al.*, *Proc. Natl. Acad. Sci. U.S.A.* **101**, 17867 (2004).
76. A. Yildiz *et al.*, *Science* **300**, 2061 (2003).
77. C. Kural *et al.*, *Science* **308**, 1469 (2005).

78. M. Hofmann, C. Eggeling, S. Jakobs, S. W. Hell, *Proc. Natl. Acad. Sci. U.S.A.* **102**, 17565 (2005).
79. A. Egner, S. W. Hell, *Trends Cell Biol.* **15**, 207 (2005).
80. M. G. Gustafsson, *Proc. Natl. Acad. Sci. U.S.A.* **102**, 13081 (2005).
81. W. R. Zipfel, R. M. Williams, W. W. Webb, *Nat. Biotechnol.* **21**, 1369 (2003).
82. F. Helmchen, W. Denk, *Nat. Methods* **2**, 932 (2005).
83. P. S. Tsai *et al.*, *Neuron* **39**, 27 (2003).
84. P. J. Keller, F. Pampaloni, E. H. Stelzer, *Curr. Opin. Cell Biol.* **18**, 117 (2006).
85. V. Ntziachristos, J. Ripoll, L. V. Wang, R. Weissleder, *Nat. Biotechnol.* **23**, 313 (2005).
86. P. A. Clemons, *Curr. Opin. Chem. Biol.* **8**, 334 (2004).

87. We apologize that many original research papers could not be cited because of space limitations. Work by the authors directly related to this review is supported by NIH RR04050, NS27177, GM 72033, and by the Howard Hughes Medical Institute.

10.1126/science.1124618

REVIEW

New Tools Provide New Insights in NMR Studies of Protein Dynamics

Anthony Mittermaier[1] and Lewis E. Kay[2]

There is growing evidence that structural flexibility plays a central role in the function of protein molecules. Many of the experimental data come from nuclear magnetic resonance (NMR) spectroscopy, a technique that allows internal motions to be probed with exquisite time and spatial resolution. Recent methodological advancements in NMR have extended our ability to characterize protein dynamics and promise to shed new light on the mechanisms by which these molecules function. Here, we present a brief overview of some of the new methods, together with applications that illustrate the level of detail at which protein motions can now be observed.

NMR spectroscopy is an experimental tool developed over half a century ago by physicists who were interested in exploring fundamental properties of matter. They could have hardly imagined the wide utility of their creation. One such example is in the area of structural biology, where since the early 1970s the technique has been used to study the interplay between biomolecular structure, dynamics, and function. An early experiment by Wagner and Wüthrich (*1*) foreshadowed the importance of NMR in protein science. In this seminal contribution, the authors studied the positions and intensities of peaks in one-dimensional (1D) ^{1}H NMR spectra of aromatic residues in a small globular protein as a function of temperature and found compelling evidence for rotation of bulky aromatic side chains within the hydrophobic core. This showed that proteins were in fact dynamic over a spectrum of time scales and complemented the beautiful and static pictures of protein structure that were already emerging from x-ray diffraction. We now know that there is an intimate relation between dynamics and molecular function. For example, protein dynamics contribute to the thermodynamic stability of functional states and play an important role in catalysis, where conformational rearrangements can juxtapose key catalytic residues; in ligand binding, which often involves the entry of molecules into areas that would normally be occluded; in molecular recognition processes, which are often fine-tuned by disorder-to-order transitions; and in allostery, where coupled structural fluctuations can transmit information between distant sites in a protein. NMR spectroscopy is uniquely suited to study many of these dynamic processes, because site-specific information can be obtained for motions that span many time scales, from rapid bond librations (picoseconds) to events that take seconds (*2*, *3*). Here, we review a number of recent advances in solution NMR spectroscopy that have substantially extended our ability to measure protein motions and that promise to improve our understanding of protein dynamics and their relation to biological activity.

Investigating Micro- to Millisecond Time Scale Dynamics

Many biochemical events occur on the microsecond to millisecond time scale, and it is of considerable interest to characterize the conformational transitions that are involved in such processes. However, intermediates are often formed only transiently and are populated at levels that are not amenable to traditional structural approaches. Figure 1 illustrates the situation schematically for the case of a protein that can exist in two distinct conformational states, $A \underset{k_{BA}}{\overset{k_{AB}}{\rightleftharpoons}} B$, with one state substantially more populated than the other. Because the frequency of the magnetic energy absorbed by each nucleus depends on its chemical environment, a given probe will likely have distinct chemical shifts in each conformation, separated by $\Delta\nu$ (Fig. 1A). If the exchange rate, $k_{ex} = k_{AB} + k_{BA}$, between conformers is very much less than $2\pi\Delta\nu$, then separate peaks may be observed for a single site in each of the conformations, so long as the population of the minor species is on the order of a few percent. However, for systems where k_{ex} is not much smaller than $2\pi\Delta\nu$, peaks derived from the weakly populated conformer (excited state) are most often not observed, because the transient nature of this state leads to substantial peak broadening. As a result, a spectrum is obtained (Fig. 1B) where for each probe a peak is observed only from the more populated state, slightly shifted from its position in the absence of a slow exchange limit. How, then, does one obtain information about the excited state when it is essentially invisible in NMR spectra?

One way is to use an experimental approach, based on an idea from Erwin Hahn in the 1950s, called a spin echo. The basic phenomenon can be explained as follows. Imagine that a group of runners, composed of both slow and fast individ-

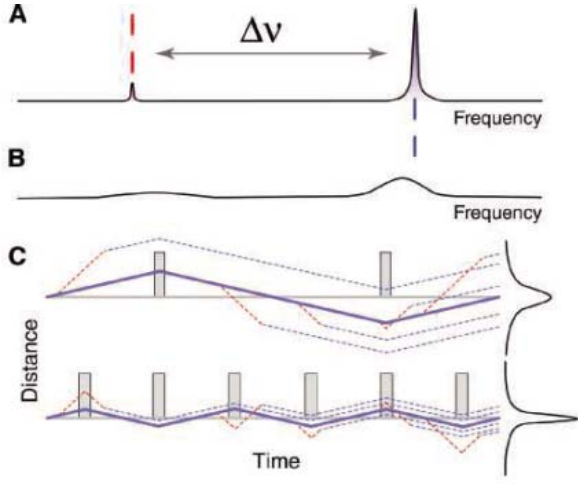

Fig. 1. Spectra from a single protein site undergoing (**A**) slow conformational exchange, $k_{ex} \ll 2\pi\Delta\nu$, and (**B**) intermediate conformational exchange, $k_{ex} \approx 2\pi\Delta\nu$. (**C**) Schematic representation of signal dephasing during CPMG pulse trains based on the analogy to the runners described in the text, where the *y* axis plots the distance of the runners from the starting position. A blue or red line indicates a spin in the major or minor state, respectively. Dashed lines correspond to spins experiencing at least one conformational transition, whereas the solid lines correspond to no transitions.

[1]Department of Chemistry, McGill University, Montreal, Quebec H3A 2K6, Canada. E-mail: anthony.mittermaier@mcgill.ca [2]Department of Medical Genetics, Department of Biochemistry, and Department of Chemistry, University of Toronto, Toronto, Ontario M5S 1A8, Canada. E-mail: kay@pound.med.utoronto.ca

uals, start a race at the same time. If at the halfway point of the race all runners are made to stop, turn around, and run back to the starting position, it is clear that both slow and fast individuals will cross the starting line at the same time, giving rise to a spontaneous ordering referred to as an echo. Now suppose that the runners can interconvert stochastically during the course of the race, in the sense that a slow runner can become fast and vice versa (corresponding to molecules interconverting between a pair of states). Although the positions of the runners at the end will depend on the details of the exchange process, in general they will not all finish the race simultaneously, and a plot of the distribution of runners crossing the starting line versus time gives rise to a peak that is broader than that observed in the absence of exchange. The breadth of the peak provides information about the relative numbers of fast and slow runners (thermodynamics), their rate of interconversion (kinetics), and the difference in running speeds between the two groups (analogous to chemical shift differences between exchanging conformations, which relate to structure). The basic NMR experiment [so-called Carr-Purcell-Meiboom-Gill (CPMG) relaxation dispersion (*3*)] builds on this concept by applying a variable number of refocusing pulses during a fixed time interval, where each pulse corresponds to runners stopping and turning around in the analogy above. If the rate of application of pulses is such that the runners are allowed to get out of phase with each other, then the exchange process leads to broad lines as described above (Fig. 1C, top). In contrast, when the pulses are applied at a fast rate the effects of the interconversion are reduced and narrower peaks are obtained (Fig. 1C, bottom). The dependence of line width on pulsing rate (the relaxation dispersion profile) is subsequently fit to extract the exchange parameters (*3*).

As mentioned above, the basic CPMG scheme dates back to the formative days of NMR spectroscopy. However, the routine application of the method to proteins had to await a number of advances. One such advance was the development of multidimensional spectroscopy, where the great majority of sites in the protein can, in principle, be visualized in the form of cross peaks in ^{1}H-^{15}N or ^{1}H-^{13}C correlation spectra. Such spectra provide the site-specific information that distinguishes modern NMR from so many other physical techniques. The second breakthrough was due to Loria and Palmer, who developed a clever scheme for allowing slow dynamical processes to be characterized without interference from interactions between the nucleus of interest and directly bonded NMR-active nuclei (*3*). CPMG relaxation dispersion experiments most often make use of backbone amide ^{1}H or ^{15}N spin probes (*4*–*6*), focusing on proton or nitrogen magnetization (single-quantum transitions), respectively. However, in the context of a ^{1}H-^{15}N spin pair, there are additional transitions that can be explored to gain further insight into the dynamics. A comparison of experimental dispersion profiles for the same amide site but derived from experiments that monitor different transitions (Fig. 2A) emphasizes that the same exchange process can lead to very different dispersion shapes (*7*, *8*). Here $R_{2,\mathrm{eff}}$ (peak line width) is plotted along *y*, versus ν_{CPMG} (proportional to the number of refocusing pulses applied) along *x*.

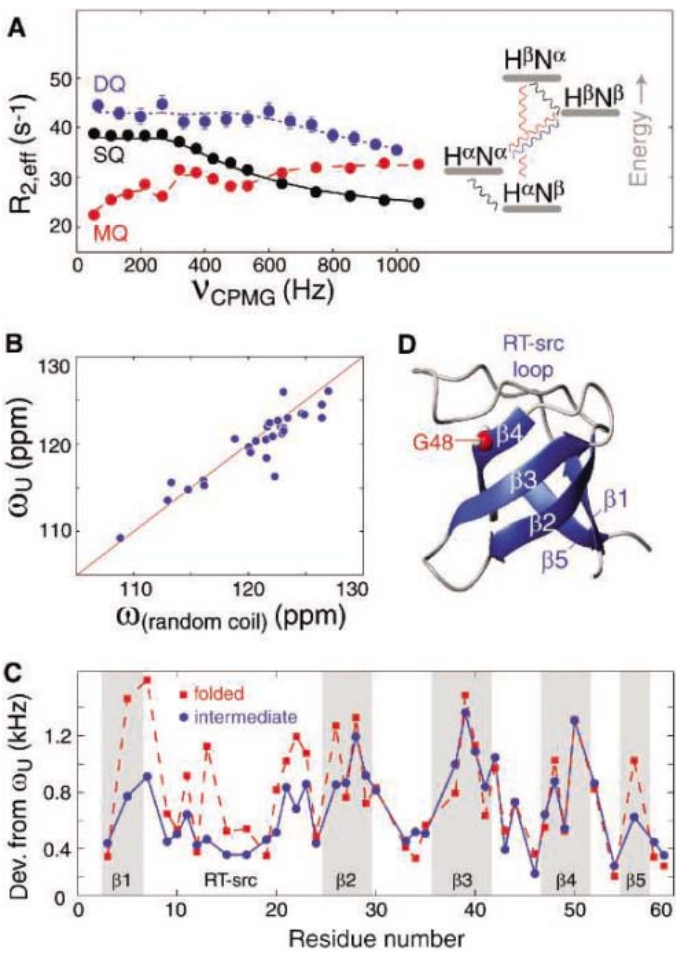

Fig. 2. (**A**) Experimental relaxation dispersion profiles for amide ^{1}H-^{15}N single-quantum (SQ), double-quantum (DQ), and multiple-quantum (MQ) coherences of Glu^{11} in the G48M mutant of the Fyn SH3 domain (*8*). Fits to a global three-site model of exchange are indicated by lines. (Inset) An energy level diagram for a ^{1}H-^{15}N spin pair with SQ, DQ, MQ coherences indicated by black, blue, and sum of red lines, respectively. (**B**) The ^{15}N chemical shifts of the G48M U state calculated from relaxation dispersion data plotted as a function of corresponding random coil chemical shifts. (**C**) Deviations from unfolded (*U*) state backbone chemical shifts, $[[\Delta\omega(^{15}\mathrm{N})]^2 + [\Delta\omega(^{1}\mathrm{H})]^2]^{0.5}$, calculated in absolute frequency units (800-MHz spectrometer) for intermediate (*I*, solid blue) and folded (*F*, dashed red) states, plotted as a function of residue number (*8*). (**D**) Structure of the wild-type Fyn SH3 domain (1SHF) with the location of Gly^{48} indicated in red.

CPMG relaxation dispersion experiments in which exchange effects are quenched through the application of pulses are often the method of choice for the study of millisecond dynamics in proteins (*3*). A similar quenching effect can be achieved by applying a continuous radio-frequency field that is allowed to vary both in magnitude and in frequency (*3*), and this approach is used to study faster processes (k_{ex} up to $\approx$ 100,000 s^{-1}).

In order to illustrate the utility of the dispersion methodology, we focus on a single application in the area of protein folding that makes use of the CPMG method (*9*); additional studies can be found in the literature, with the work of Kern and colleagues relating protein dynamics to enzyme catalysis being particularly noteworthy (*10*–*14*). The present example concerns several Gly^{48} mutants of the Fyn SH3 domain that had been shown with use of stopped-flow fluorescence denaturation and renaturation measurements to fold with a two-state mechanism, $F \underset{k_{UF}}{\overset{k_{FU}}{\rightleftharpoons}} U$. The exchange parameters obtained by using fluorimetry are well within the ranges of k_{ex} values (several hundred to a few thousand s^{-1}) and excited state populations ($p_U > \sim 0.5\%$) that are necessary for the measurement of NMR relaxation dispersions. Yet ^{15}N CPMG studies of a pair of these mutants, Gly^{48}→Met^{48} (G48M) and Gly^{48}→Val^{48} (G48V), performed in the absence of denaturant, are inconsistent with a two-state folding mechanism (*9*). Folding and unfolding rates obtained on a per-residue basis from fits of the dispersion profiles to a two-state folding model do not give the same values at each site, with differences as large as a factor of 10 in some cases; for cooperative folding, k_{UF} and k_{FU} values

are expected to be uniform among all sites in the protein. However, the data for all of the sites in both mutants can be well fit globally to a three-site model of conformational exchange, $F \underset{k_{IF}}{\overset{k_{FI}}{\rightleftharpoons}} I \underset{k_{UI}}{\overset{k_{IU}}{\rightleftharpoons}} U$ (Fig. 2A). The temperature dependence of the four rates allows values of free energy, enthalpy, and entropy differences to be extracted between pairs of states as well as activation barriers, assuming that the temperature dependence of the rates obeys transition state theory (*9*).

Further information is obtained in the form of chemical shift differences between the *F*, *I*, and *U* states. In fits of the dispersion data, no assumption is made a priori as to the positions of the *I* and *U* states along the reaction scheme; the chemical shifts obtained for an end point state are found to correspond to those of an unfolded protein (i.e., the *U* state) (Fig. 2B). It is well known that chemical shifts are sensitive indicators of molecular structure, and a long-standing goal is to exploit shifts of NMR "invisible" excited states so that structural information can be obtained. The deviations in chemical shifts of the *I* and *F* states from those of *U*, obtained for the G48M Fyn SH3 domain (Fig. 2C), show that the central β sheet is largely formed in the *I* state (β2, β3, and β4) but that there is considerably less structure at the termini of the domain. For reference, the *F* state structure of the domain is also illustrated (Fig. 2D).

Measuring Dynamics on the Pico- to Nanosecond Time Scale

Consider a protein that is tumbling in solution such that every orientation is equally probable. For the moment, let us focus on a single bond vector in the molecule that connects a pair of NMR active spins, such as a ^{1}H-^{15}N spin pair. When internal motions and molecular tumbling cause reorientation of the ^{1}H-^{15}N bond vector with respect to the external magnetic field, the local magnetic field at the site of the ^{15}N spin that derives from the directly attached ^{1}H magnetic dipole fluctuates (Fig. 3A). It can be shown that, although the local dipolar interaction between ^{1}H and ^{15}N spins averages to zero because of the molecular tumbling, the time-dependent variations in the field lead a spin system that has been perturbed by radio-frequency pulses to return, or relax, to thermal equilibrium. Because the fluctuations of the local magnetic fields are sensitive to internal motions, measurement of NMR relaxation rates provides a direct avenue to extracting dynamics parameters.

A pair of basic nitrogen spin relaxation experiments are used to probe backbone dynamics in proteins (*2*) (Fig. 3B). Although a large arsenal of different methods have now been developed, most are fundamentally similar to this example. The ^{15}N relaxation experiments monitor either the recovery of ^{15}N Z-magnetization to its equilibrium position (T_1) or the decay of magnetization orthogonal to the Z axis to its zero equilibrium value (T_2). The ^{1}H spin has a magnetogyric ratio (γ) that is 10 times larger than that of ^{15}N, and the inherent sensitivity of the NMR experiment scales as $\gamma^{5/2}$; therefore experimental sensitivity is optimized by shuffling magnetization from an amide ^{1}H to its directly coupled ^{15}N and then back again to ^{1}H for detection as a 2D data set. Here, one peak is obtained for each (^{1}H-^{15}N) pair in the protein, with an intensity proportional to $\exp(-\tau/T_i)$ where T_i is the T_1 or T_2 value of the particular ^{15}N nucleus and τ is a variable relaxation delay; relaxation times are measured by recording a series of spectra and fitting the peak intensities as a function of τ. The values of T_i so obtained are usually interpreted in terms of generalized order parameters that describe the amplitude of bond vector motions and time constants that indicate the time scale of the internal motions (*15*), but specific models can be used as well (*16*). In addition, many experiments that provide complementary information to the ^{15}N studies described above have been developed, such as those that measure correlated motions of successive residues in proteins (*17*, *18*) or the dynamics of backbone carbonyl-Cα bonds (*19*).

Side chain motions in proteins are also amenable to study with the use of spin relaxation techniques (*20*, *21*). In particular, the use of the ^{2}H nucleus as a probe of side chain methyl group dynamics has seen substantial advances in recent years. It has long been known that the deuterium spin is an excellent probe of molecular motion, but applications in the solution state were limited, primarily because the poor resolution of ^{2}H spectra make site-specific studies extremely difficult. This is illustrated by protein spectra in Fig. 3C, where the broad, featureless 1D ^{2}H spectrum may be compared with the high resolution ^{1}H spectrum. The deuteron can be exploited as a probe of molecular dynamics, however, by preparing uniformly ^{13}C labeled, fractionally deuterated protein and using the scheme illustrated in Fig. 3D that can be "tuned" to select, in this case, for $^{13}CH_2D$ methyl groups. A series of high resolution ^{13}C-^{1}H maps are produced, with ^{2}H relaxation rates encoded by the intensities of the cross peaks.

One of the most exciting applications of the methodology described above is in the use of

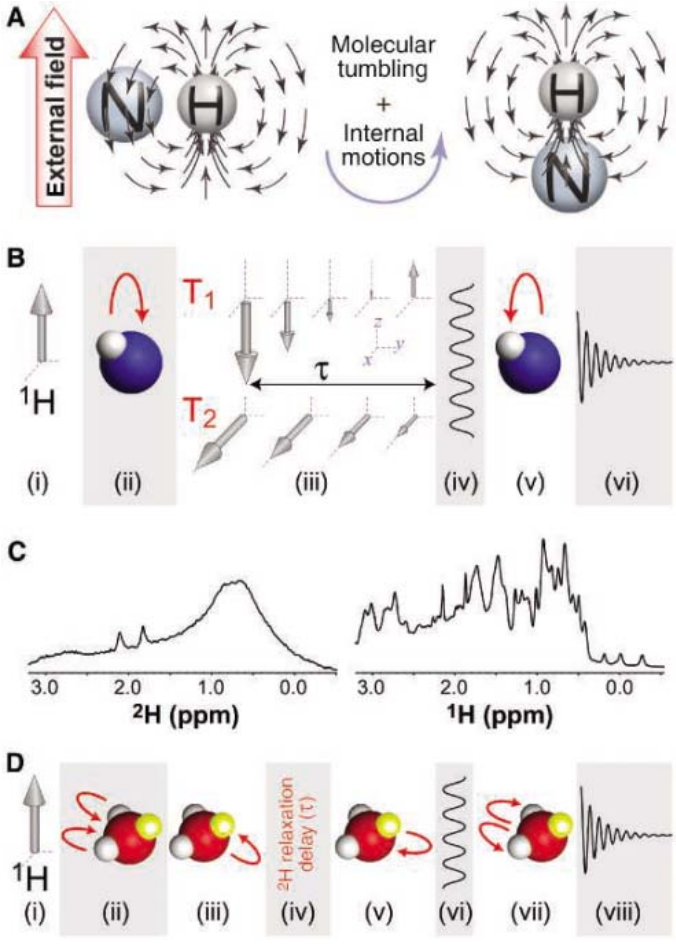

Fig. 3. (**A**) Illustration of the orientation-dependent magnetic field experienced by an amide ^{15}N nucleus due to the directly bonded proton. A pair of orientations have been chosen arbitrarily for illustration. (**B**) Schematic representation of an amide ^{15}N relaxation experiment (*2*): (i) equilibrium ^{1}H magnetization, (ii) ^{1}H to ^{15}N transfer, (iii) relaxation delay, (iv) indirect ^{15}N chemical shift detection, (v) ^{15}N to ^{1}H transfer, and (vi) direct ^{1}H chemical shift detection. (**C**) 1D ^{2}H and ^{1}H spectra of perdeuterated and protonated spectrin SH3 domains, respectively. (**D**) Schematic representation of a methyl ^{2}H relaxation experiment (*21*): (i) equilibrium ^{1}H magnetization, (ii) ^{1}H to ^{13}C transfer, (iii) ^{13}C to ^{2}H transfer, (iv) relaxation delay, (v) ^{2}H to ^{13}C transfer, (vi) indirect ^{13}C chemical shift detection, (vii) ^{13}C to ^{1}H transfer, and (viii) direct ^{1}H chemical shift detection.

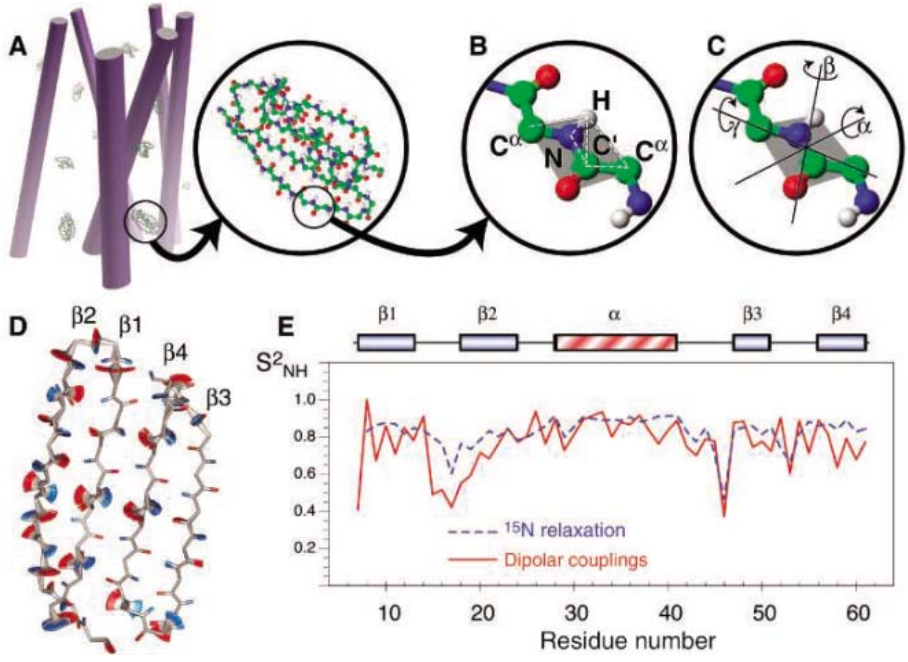

Fig. 4. (**A**) Representation of protein G B1 domain molecules dissolved in an anisotropic medium, with cylinders corresponding to filamentous phage particles aligned with respect to the static magnetic field. (**B**) Peptide plane with spin pairs, for which residual dipolar coupling data was obtained, identified by dashed white lines. (**C**) The three axes of rotation for a GAF model of rigid-body peptide plane dynamics. (**D**) Visualization of γ rotations for peptide planes in the β sheet. (**E**) Comparison of ^{15}N relaxation-derived "fast motion" order parameters and residual dipolar coupling-derived order parameters. [Figure adapted from Bouvignies *et al.* (*28*); copyright (2005), National Academy of Sciences, United States]

order parameters as restraints in molecular dynamics calculations to produce an ensemble of structures that satisfies both structural and dynamical NMR data. In one such study involving ubiquitin, it was found that many side chains, even those in the core of the protein, occupy multiple rotameric states and can be considered to have liquidlike characteristics (*22*).

Probing Dynamics Spanning a Broad Time Scale Range by Using Residual Dipolar Couplings

Let us return to the example of the ^{1}H-^{15}N spin pair in Fig. 3A, but now suppose that the protein is not dissolved in isotropic solution but rather in a media that leads to fractional alignment (typically about 0.1%) (*23*) (Fig. 4A). In this case, the dipolar interaction considered above does not average to zero. Instead, for a fixed orientation of the ^{1}H-^{15}N spin vector, the effective magnetic field at the ^{15}N spin is either increased or decreased depending on the ^{1}H spin state, leading to dipolar splittings (^{15}N peak doublets) in spectra. These splittings are a rich source of structural information, because they report on the orientation of bond vectors with respect to an external coordinate frame (the magnetic field) (*23*). However, there is also potential for studies of biomolecular dynamics because motions that modulate local fields over a broad time regime (picosecond to millisecond) can affect dipolar splittings (*24*–*27*). Here, we focus on one such study by Blackledge and co-workers that highlights beautifully the power of the dipolar coupling approach (*28*).

In this study, the authors used an extensive set of dipolar couplings recorded on the immunoglobulin-binding B1 domain of streptococcal protein G (protein G). Data from experiments performed in a number of different alignment media were pooled to obtain as many as 27 measurements per residue, with six different types of dipolar couplings measured per peptide plane (Fig. 4B). The dipolar coupling data were interpreted by using the x-ray structure of the protein along with a 3D Gaussian axial fluctuation model (GAF) of the motion (Fig. 4C) (*16*). A remarkable distribution of motion about the γ axis was found for residues throughout the β sheet of the protein (Fig. 4D), with hydrogen-bonded residues on adjacent strands experiencing similar levels of dynamics. In order to address whether the motions of interacting peptide planes are correlated, the authors recorded three-bond ^{15}N-^{13}C′ scalar couplings (^{15}N-^{1}H···O-^{13}C′), which depend on lengths and angles of H···O hydrogen bonds. Experimental couplings were compared with values calculated by using the GAF fluctuation amplitudes from the dipolar coupling measurements, assuming either correlated, anticorrelated, or uncorrelated motion. Significantly better agreement between computed and experimental couplings was obtained for the correlated motional model compared with the other two models. Although dipolar coupling data per se do not report on the time scale of motion, information can be obtained by comparing the per-residue generalized order parameters from the 3D GAF model of dynamics with order parameters extracted from backbone ^{15}N spin relaxation data (see above) that report on pico- to nanosecond time scale motions (Fig. 4E). For the sites involved in the correlated dynamics described above, dipolar coupling–derived generalized order parameters are lower than those obtained from ^{15}N relaxation experiments, implying that the correlated dynamics involve motional time scales that are slower than the pico- to nanosecond range.

Lastly, we to note that the residues with the highest level of dynamics are those that interact with the protein G binding partner and that the direction of the motion (about the γ axis) coincides with the conformational adjustment needed for molecular recognition and for the formation of a hydrogen bonded complex.

Concluding Remarks

Over the past several years, new NMR experiments have been developed to provide site-specific information about protein motions spanning a range of time scales. Some of the most exciting new applications involve large molecular complexes, where motion is likely to be critical for function. NMR methods exploiting the TROSY (transverse relaxation optimized spectroscopy) principle (*29*) have emerged for both backbone positions and side chain methyl groups, allowing site-specific studies of dynamics to be performed on large protein complexes such as the GroEL-GroES chaperone (*30*) and the ClpP protease (*31*). It is clear from these studies, and from the applications to the smaller proteins described above, that the insights obtained from NMR dynamics studies will have important implications for our understanding of biological function.

References

1. K. Wuthrich, G. Wagner, *Trends Biochem. Sci.* **3**, 227 (1978).
2. L. E. Kay, D. A. Torchia, A. Bax, *Biochemistry* **28**, 8972 (1989).
3. A. G. Palmer, C. D. Kroenke, J. P. Loria, *Methods Enzymol.* **339**, 204 (2001).
4. J. P. Loria, M. Rance, A. G. Palmer, *J. Am. Chem. Soc.* **121**, 2331 (1999).
5. R. Ishima, D. Torchia, *J. Biomol. NMR* **25**, 243 (2003).
6. M. Tollinger, N. R. Skrynnikov, F. A. A. Mulder, J. D. Forman-Kay, L. E. Kay, *J. Am. Chem. Soc.* **123**, 11341 (2001).
7. D. M. Korzhnev, P. Neudecker, A. Mittermaier, V. Y. Orekhov, L. E. Kay, *J. Am. Chem. Soc.* **127**, 15602 (2005).
8. A. Mittermaier, D. M. Korzhnev, L. E. Kay, *Biochemistry* **44**, 15430 (2005).
9. D. M. Korzhnev *et al.*, *Nature* **430**, 586 (2004).

10. R. Ishima, J. M. Louis, D. A. Torchia, *J. Mol. Biol.* **305**, 515 (2001).
11. M. J. Grey, C. Y. Wang, A. G. Palmer, *J. Am. Chem. Soc.* **125**, 14324 (2003).
12. F. A. A. Mulder, A. Mittermaier, B. Hon, F. W. Dahlquist, L. E. Kay, *Nat. Struct. Biol.* **8**, 932 (2001).
13. M. Wolf-Watz *et al.*, *Nat. Struct. Mol. Biol.* **11**, 945 (2004).
14. E. Z. Eisenmesser *et al.*, *Nature* **438**, 117 (2005).
15. G. Lipari, A. Szabo, *J. Am. Chem. Soc.* **104**, 4546 (1982).
16. T. Bremi, R. Brüschweiler, *J. Am. Chem. Soc.* **119**, 6672 (1997).
17. P. Pelupessy, S. Ravindranathan, G. Bodenhausen, *J. Biomol. NMR* **25**, 265 (2003).
18. P. Lundstrom, F. A. Mulder, M. Akke, *Proc. Natl. Acad. Sci. U.S.A.* **102**, 16984 (2005).
19. T. Wang, K. K. Frederick, T. I. Igumenova, A. J. Wand, E. R. Zuiderweg, *J. Am. Chem. Soc.* **127**, 828 (2005).
20. D. M. LeMaster, D. M. Kushlan, *J. Am. Chem. Soc.* **118**, 9255 (1996).
21. D. R. Muhandiram, T. Yamazaki, B. D. Sykes, L. E. Kay, *J. Am. Chem. Soc.* **117**, 11536 (1995).
22. K. Lindorff-Larsen, R. B. Best, M. A. Depristo, C. M. Dobson, M. Vendruscolo, *Nature* **433**, 128 (2005).
23. N. Tjandra, A. Bax, *Science* **278**, 1111 (1997).
24. J. R. Tolman, J. M. Flanagan, M. A. Kennedy, J. H. Prestegard, *Nat. Struct. Biol.* **4**, 292 (1997).
25. G. M. Clore, C. D. Schwieters, *Biochemistry* **43**, 10678 (2004).
26. J. Meiler, J. J. Prompers, W. Peti, C. Griesinger, R. Bruschweiler, *J. Am. Chem. Soc.* **123**, 6098 (2001).
27. J. J. Chou, D. A. Case, A. Bax, *J. Am. Chem. Soc.* **125**, 8959 (2003).
28. G. Bouvignies *et al.*, *Proc. Natl. Acad. Sci. U.S.A.* **102**, 13885 (2005).
29. K. Pervushin, R. Riek, G. Wider, K. Wüthrich, *Proc. Natl. Acad. Sci. U.S.A.* **94**, 12366 (1997).
30. R. Horst *et al.*, *Proc. Natl. Acad. Sci. U.S.A.* **102**, 12748 (2005).
31. R. Sprangers, A. Gribun, P. M. Hwang, W. A. Houry, L. E. Kay, *Proc. Natl. Acad. Sci. U.S.A.* **102**, 16678 (2005).

10.1126/science.1124964

PERSPECTIVE

Living Cells as Test Tubes

X. Sunney Xie,* Ji Yu, Wei Yuan Yang

The combination of specific probes and advanced optical microscopy now allows quantitative probing of biochemical reactions in living cells. On selected systems, one can detect and track a particular protein with single-molecule sensitivity, nanometer spatial precision, and millisecond time resolution. Metabolites, usually difficult to detect, can be imaged and monitored in living cells with coherent anti-Stokes Raman scattering microscopy. Here, we describe the application of these techniques in studying gene expression, active transport, and lipid metabolism.

Much of our quantitative understanding of molecular reactions in cells has come from traditional biochemistry—experiments done in test tubes with purified biomolecules. Although this approach is extremely productive, we understand that the milieu of the cell is fundamentally different from an in vitro solution in several ways: (i) DNA, many mRNA molecules, and some enzymes exist in low copy numbers and participate in stochastic reaction events in the cell that are hidden in test tubes with large numbers of molecules. (ii) Reactions are often at nonequilibrium steady state in the cell, with a constant supply of free energy and reactants. (iii) Many reactions are coupled in the cell, resulting in networks of complex interactions. Consequently, a biochemical reaction in a single cell could have different thermodynamic and kinetic properties from the same biochemical reaction in a test tube. The challenge now is to observe the biochemical reactions in living cells, and techniques are in place to do this in selected systems. Central to these techniques is optical imaging, which offers millisecond time resolution and nanometer spatial precision, single-molecule sensitivity, and most importantly, biochemical specificity. Here, we highlight advances that allow investigation of gene expression, active transport, and metabolism in living cells.

Department of Chemistry and Chemical Biology, Harvard University, Cambridge, MA 02138, USA.

*To whom correspondence should be addressed. E-mail: xie@chemistry.harvard.edu

In an individual cell, gene expression is a single-molecule problem. On genomic DNA, a particular gene only exists in one (or a few) copy, switching on and off stochastically to regulate biological functions [for a review, see (*1*)]. Gene expression has been studied by biochemical assays, such as Northern and Western blotting, polymerase chain reaction, and more recently, DNA arrays and mass spectrometry. However, these techniques are not sensitive enough to allow single-cell analysis of genes that are expressed at low levels. Furthermore, these ensemble-averaged methods often mask stochastic gene expression events. Single-molecule experiments in vitro have provided valuable insight into the mechanisms of gene expression machines (*2*–*4*). The next frontier will carry out single-molecule studies in individual living cells.

Imaging of gene expression at a single-molecule level in living cells has been made possible by two developments. At the transcriptional level, single mRNA molecules were detected and tracked in a living cell using multiple copies of a fluorescent mRNA binding protein (*5*, *6*). At the translational level, we have tracked expression of single-protein molecules using a fast-maturing and membrane-targeting yellow fluorescent protein (YFP) (Venus) as a reporter (*7*).

Immobilizing the fluorescent protein reporter on the cell membrane (*7*, *8*) overcame the difficulty in detecting single-protein molecules inside the cytoplasm; the fluorescence distributes throughout the cell because of fast protein diffusion during the image acquisition time and drops below the strong cellular autofluorescence. We monitored repressed expression from the *lac* promoter in *Escherichia coli* (Fig. 1A) and showed that protein expression occurs in small bursts (Fig. 1B), each originating from multiple ribosomes on an mRNA molecule. The protein copy numbers within a burst adhered to a geometric distribution (*7*), which was verified with the use of a different reporter (*9*). These assays provided quantitative details about the stochastic fluctuations in gene expression.

Is there a way to detect a single cytoplasmic protein molecule? The answer is yes, by extending the idea of detection by immobilization. We borrowed a method from strobe photography, which makes it possible to take a sharp picture of a bullet going through an apple (Fig. 1C). The sharpness is achieved because the light flash is so short that the bullet does not move far during the flash. Likewise, we applied an intense laser exposure for a very short duration (~300 μs), during which a protein reporter does not diffuse beyond the diffraction-limited spot. Figure 1D shows detection of single red fluorescent proteins [tdTomato (*10*)] in *E. coli* cytoplasm with a high signal-to-background ratio. The method could be used, for example, to determine the cellular concentration of a weakly expressed protein without calibration. To further develop this method, we need reporters with high photostability and better-controlled photochemistry.

The next step is to probe the expression of multiple genes simultaneously with the use of different colors of reporters (*10*) in order to study their interactions. In addition to transcription and translation, similar live-cell single-molecule assays offer the prospect of studying cellular processes, such as cell signaling (*11*), protein folding, DNA replication, and RNA trafficking (*5*, *12*).

No less important than gene expression is energy transduction in living cells. Motor proteins convert chemical energy in the form of adenosine 5′-triphosphate (ATP) into mechanical work. Kinesin and dynein motors transport organelles along microtubules in opposite directions. Much has been learned about these motors at the single-

molecule level through in vitro experiments with mechanical manipulation and optical detection (*13*, *14*). However, little is known about the workings of motors at the single-molecule level in vivo.

Last year, two groups reported the observation of individual steps of molecular motors in living cells with nanometer spatial precision and millisecond time resolution with the use of sensitive high-speed cameras (*15*, *16*). A key technical concept is that even though diffraction results in a fluorescent spot size of ~270 nm, one can determine the centroid position of an isolated fluorophore with nanometer spatial resolution (*17*–*19*), provided that the optical signal is sufficiently bright. This idea was first applied in vitro to resolve the individual steps of molecular motors (*20*). Presenting an additional challenge, in vivo motor speeds are faster because the cell's ATP concentrations are higher than those used for in vitro measurements. Thus, higher time resolution is required to resolve individual steps.

In the example from our laboratory, Nan *et al.* achieved submillisecond time resolution in resolving the discrete nanometer steps of molecular motors by tracking the motion of endocytic vesicles (*16*) containing quantum dots (QDs). QDs are extremely bright (*21*, *22*), and after introduction into mouse fibroblast cells by endocytosis, the QD-containing vesicle moves on microtubules (Fig. 2A). Steps of 8 nm, each corresponding to a stochastic ATP hydrolysis event, are resolved (Fig. 2B), as evidenced by the 8-nm spacings in the pairwise correlation function (Fig. 2C). Stepwise movements of the QD-containing vesicle are seen in both directions along the microtubule, with some showing steps larger than 8 nm and others exhibiting reversible steps. These observations raise interesting questions regarding how multiple copies and types of motors work collectively in a living cell. These live-cell motility assays are yielding new dynamic information and will be even more productive if force sensing (*23*, *24*) and mechanical manipulation of motors, similar to those implemented in vitro, can be realized in living cells.

Unlike proteins that can often be labeled without altering function, the majority of metabolites are small organic molecules that are difficult to label for imaging without altering their cellular behavior. Raman scattering offers a way to image metabolites without the need for exogenous labels, as it probes intrinsic molecular vibrational frequencies. For example, the Raman spectra of two fatty acid species, eicosapentaenoic acid (EPA) and fully deuterated oleic acid (OA), have two distinct peaks arising from strong $–CH_2$ and $–CD_2$ stretching vibrations contained within the respective acyl-chains of the two fatty acid molecules (Fig. 3A).

For living cells, however, Raman signals are so weak that high excitation powers and long acquisition times (hours) are required to obtain useful images. A noninvasive method in live-cell and animal imaging, coherent anti-Stokes Raman

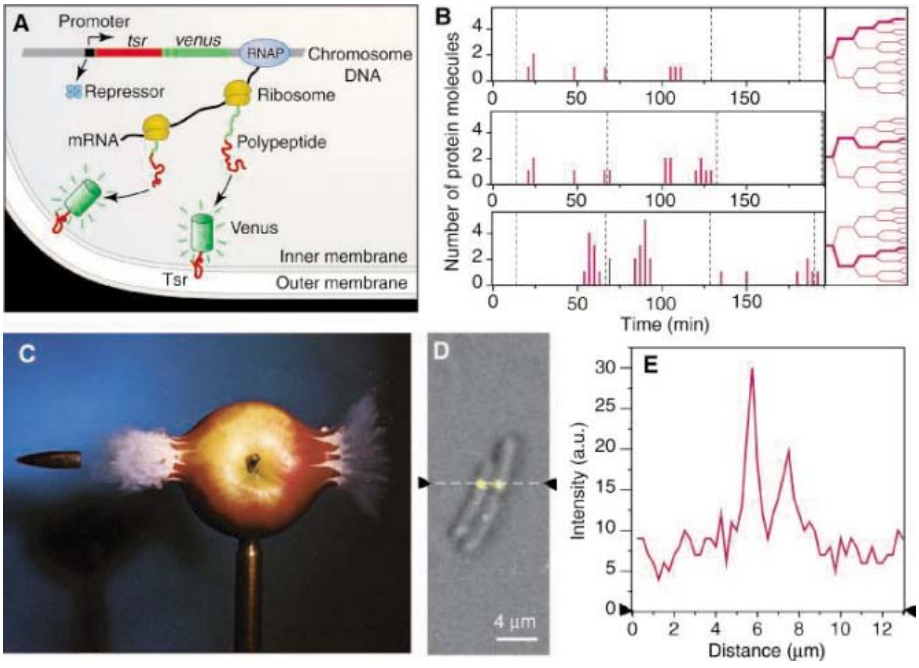

Fig. 1. Imaging protein expression in live *E. coli* cells. (**A**) When a repressor dissociates from the *lac* promoter, RNA polymerase transcribes the gene of a fusion protein Tsr-Venus into an mRNA, on which a few ribosomes bind, each making a fusion protein molecule. Tsr targets Venus, a fast-maturing YFP, to the membrane, allowing detection of Venus one molecule at a time. (**B**) Time traces of the burst production of Tsr-Venus (left) in three cell lineages (right) extracted from the time-lapse recording of protein production. Images with 100-ms exposure, followed by 1000-ms photobleaching, were taken every 3 min and the number of protein molecules synthesized since the last image was counted. The dotted lines mark the cell division times. (**C**) Image of a bullet passing through an apple (*32*), obtained using strobe photography. (**D**) Fluorescence/DIC overlay image of three *E. coli* cells, with two containing single cytoplasmic tdTomato molecules. The fluorescence image was taken with a short (300-μs) and intense (50-kW/cm^2) laser excitation. (**E**) Fluorescence signal with two distinct peaks along the line in (D) due to two single cytoplasmic tdTomato molecules. a.u., arbitrary units.

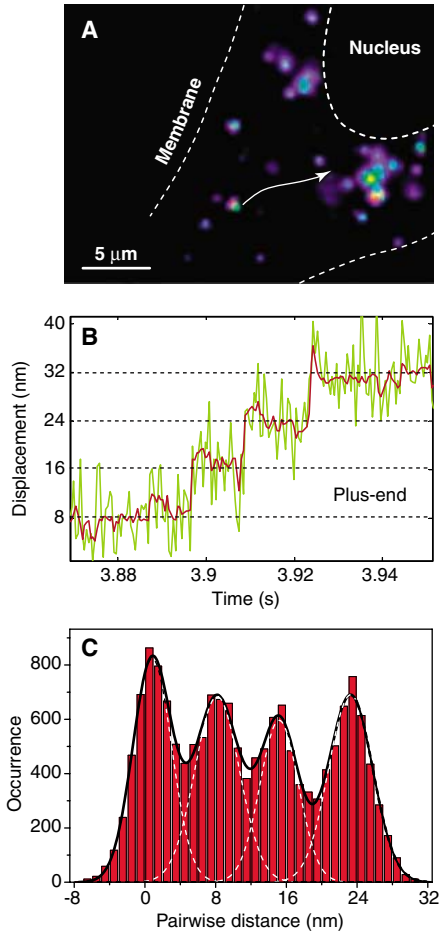

Fig. 2. Observation of individual microtubule motor steps in a live cell with endocytosed quantum dots. (**A**) Live A549 cell with QD-containing endosomes (bright dots), many of which undergo active transport by kinesin (outward movements) or dynein (inward movements, white arrow). (**B**) Displacement trajectory of a outward-going (microtubule plus-end) endosome, exhibiting stepwise movements of the underlying motor (likely kinesin). Green, raw data; red, filtered data. (**C**) Pairwise distance histogram of the filtered displacement trace in (B), with an 8-nm spacing between adjacent peaks.

scattering (CARS) microscopy provides vibrational contrast with a sensitivity that is orders of magnitude higher than conventional Raman microscopy (*25*–*27*). The technique uses two temporally and collinearly overlapped picosecond laser beams at different frequencies, ω_p and ω_s, which are tightly focused onto the sample. When $\omega_p - \omega_s$ matches the vibrational frequency of the molecular species of interest, molecular oscillators are driven coherently, resulting in a resonance-enhanced CARS signal at the anti-Stokes frequency $2\omega_p - \omega_s$. CARS is only generated at the laser focus, allowing three-dimensional sectioning, similar to two-photon fluorescence microscopy (*28*). Although CARS microscopy does not offer the penetration depth of magnetic resonance imaging (MRI), it does offer better time and spatial resolution than MRI, which is key for monitoring living cells. CARS microscopy is particularly powerful in tracking lipid metabolism, due to the large number of CH bonds in lipids.

As an example of an application of CARS microscopy, we monitored how fish oil affects the cellular biochemistry of fat molecules (*29*). It has long been realized that polyunsaturated fatty acids, such as EPA, in fish oil provide health benefits by lowering triglyceride levels. This effect prompted the Food and Drug Administration to issue a qualified health claim in 2004 for fish oil on avoiding heart disorders, diseases often associated with high lipid levels in the blood.

To distinguish the normal fatty acids (i.e., OA) from EPA, we used deuterated OA. This approach is similar to isotope tracking, historically used to identify metabolic pathways (*30*). The deuteration results in a vibrational frequency shift, from 2850 cm^{-1} for $-CH_2$ to 2105 cm^{-1} for $-CD_2$ (Fig. 3A). In cells grown with non-deuterated EPA and deuterated OA in the culturing media, we found that the two fatty acids colocalized in the lysosomes, the digestive organelles of the cell, in the form of triglycerides (Fig. 3, B to F). In contrast, OA is not incorporated into the lysosomes when EPA is absent. This provides an important assay toward the understanding of fish oil's health benefits. Future integration of fluorescence imaging of reporter proteins with CARS microscopy will lead to new understanding of metabolism at the systems level.

Currently, the sensitivity of CARS microscopy is 10^5 vibrational oscillators at the laser focus (*31*). We are working to improve the sensitivity for imaging other small molecules of low concentrations, such as drugs.

New single-molecule and metabolic imaging techniques, when combined with novel reporters and integrated into cellular assays, offer exciting possibilities for unraveling biochemistry in vivo. The application and continuous evolution of these fronts will lead to a quantitative understanding of fundamental biochemical processes in living cells.

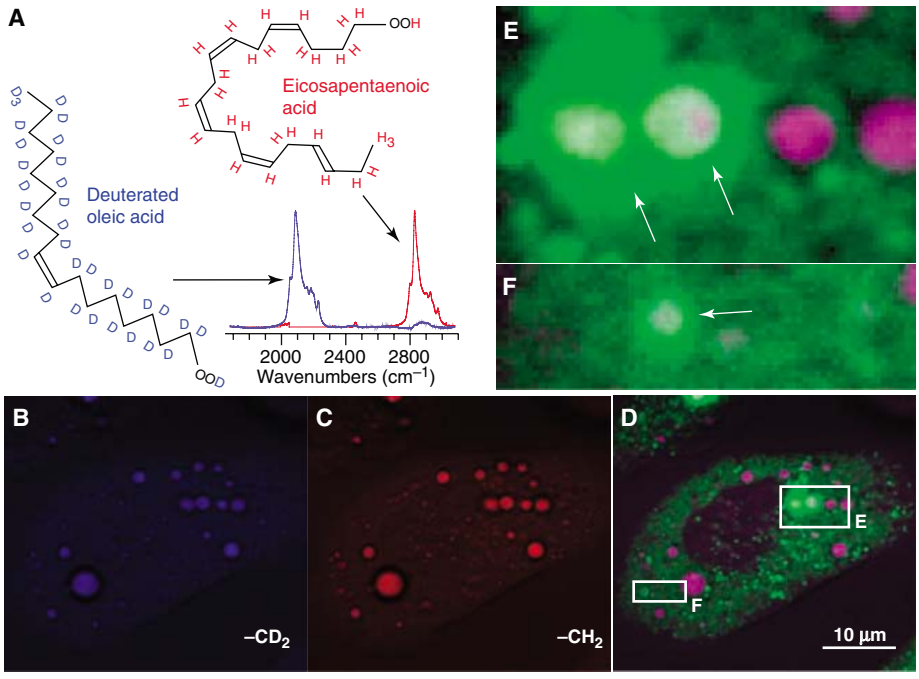

Fig. 3. Effect of fish oil on lipid metabolism studied by metabolic imaging with CARS microscopy. (**A**) Raman spectra of EPA and deuterated OA. (**B** to **F**) Live liver cells were treated with 0.4 mM EPA and 0.2 mM deuterated OA for 7.5 hours and labeled with monodansylcadaverine, a dye for staining degradative organelles. (B) CARS image tuned to $-CD_2$ (blue, deuterated OA). (C) CARS image tuned to $-CH_2$ (red, EPA). (D) Composite image of well-mixed $-CO_2$ and $-CH_2$ (purple) and two-photon fluorescence from monodansylcadaverine (green). [(E) and (F)] Zoomed-in regions in the cell where triglycerides rich in $-CH_2$ and $-CD_2$ are colocalized within degradative compartments (stained by monodansylcadaverine and indicated by arrows).

References and Notes

1. J. M. Raser, E. K. O'Shea, *Science* **309**, 2010 (2005).
2. M. D. Wang *et al.*, *Science* **282**, 902 (1998).
3. R. J. Davenport, G. J. Wuite, R. Landick, C. Bustamante, *Science* **287**, 2497 (2000).
4. S. C. Blanchard, H. D. Kim, R. L. J. Gonzalez, J. D. Puglisi, S. Chu, *Proc. Natl. Acad. Sci. U.S.A.* **101**, 12893 (2004).
5. Y. Shav-Tal *et al.*, *Science* **304**, 1797 (2004).
6. I. Golding, J. Paulsson, S. M. Zawilski, E. C. Cox, *Cell* **123**, 1025 (2005).
7. J. Yu, J. Xiao, X. Ren, K. Lao, X. S. Xie, *Science* **311**, 1600 (2006).
8. J. Deich, E. M. Judd, H. H. McAdams, W. E. Moerner, *Proc. Natl. Acad. Sci. U.S.A.* **101**, 15921 (2004).
9. L. Cai, N. Friedman, X. S. Xie, *Nature* **440**, 358 (2006).
10. N. C. Shaner, P. A. Steinbach, R. Y. Tsien, *Nature Methods* **2**, 905 (2005).
11. M. Ueda, Y. Sako, T. Tanaka, P. Devreotes, T. Yanagida, *Science* **294**, 864 (2001).
12. H. P. Babcock, C. Chen, X. Zhuang, *Biophys. J.* **87**, 2749 (2004).
13. K. Svoboda, C. F. Schmidt, B. J. Schnapp, S. M. Block, *Nature* **365**, 721 (1993).
14. R. D. Vale *et al.*, *Nature* **380**, 451 (1996).
15. C. Kural *et al.*, *Science* **308**, 1469 (2005).
16. X. Nan, P. A. Sims, P. Chen, X. S. Xie, *J. Phys. Chem. B* **109**, 24220 (2005).
17. J. Gelles, B. J. Schnapp, M. P. Sheetz, *Nature* **331**, 450 (1988).
18. E. Betzig, *Opt. Lett.* **20**, 237 (1995).
19. R. E. Thompson, D. R. Larson, W. W. Webb, *Biophys. J.* **82**, 2775 (2002).
20. A. Yildiz *et al.*, *Science* **300**, 2061 (2003).
21. M. Bruchez Jr., M. Moronne, P. Gin, S. Weiss, A. P. Alivisatos, *Science* **281**, 2013 (1998).
22. W. C. Chan, S. Nie, *Science* **281**, 2016 (1998).
23. M. A. Welte, S. P. Gross, M. Postner, S. M. Block, E. F. Wieschaus, *Cell* **92**, 547 (1998).
24. A. Ashkin, K. Schutze, J. M. Dziedzic, U. Euteneuer, M. Schliwa, *Nature* **348**, 346 (1990).
25. A. Zumbusch, G. R. Holtom, X. S. Xie, *Phys. Rev. Lett.* **82**, 4142 (1999).
26. J. X. Cheng, X. S. Xie, *J. Phys. Chem. B* **108**, 827 (2004).
27. C. L. Evans *et al.*, *Proc. Natl. Acad. Sci. U.S.A.* **102**, 16807 (2005).
28. W. Denk, J. H. Strickler, W. W. Webb, *Science* **248**, 73 (1990).
29. G. Thorne-Tjomsland *et al.*, *Mol. Biol. Cell* **14**, 104a (2003).
30. R. Schoenheimer, D. Rittenberg, *Science* **87**, 221 (1938).
31. G. Ganikhanov *et al.*, *Opt. Lett.*, in press.

32. Harold and Esther Edgerton Foundation, 2006, courtesy of Palm Press, Inc.
33. We thank current and former group members, especially X. Nan, J. Xiao, P. Chen, and P. Sims for contributing to the work summarized herein and X. Nan for providing Fig. 2. We acknowledge the fruitful collaboration on lipid metabolism with Z. Yao at the University of Ottawa, G. Thorne-Tjomsland at the University of Manitoba, and their colleagues. This work is supported by a NIH Director's Pioneer Award. The title was inspired by J. Widom's remark: "Living cells are the test tubes of the 21st century."

10.1126/science.1127566

Thermal Preference and Tolerance of Alvinellids

Peter R. Girguis[1]* and Raymond W. Lee[2]*

The thermal tolerance of marine animals has been debated for some time (*1*, *2*). At deep-sea hydrothermal vents, temperatures can exceed 350°C, although nearly all vent animals live at temperatures below 30°C. However, the polychaete worms *Alvinella pompejana* and *Paralvinella sulfincola* (family Alvinellidae) live directly on high-temperature vents in the Eastern and Northeastern Pacific, respectively, where temperatures up to 81° and 90°C have been measured around *A. pompejana* and *P. sulfincola* tube openings (*1*, *3*, *4*). Although it has been suggested that alvinellids thrive at these temperatures (*1*), earlier studies have found that the rapid mixing of hot vent fluids and cold seawater produces a dynamic thermal regime that is difficult to characterize (*3*, *5*). As such, it is impractical to ascertain alvinellid thermotolerance via in situ measurements. To determine directly *P. sulfincola* thermal tolerance and preference, we developed a high-pressure aquarium that mimics the thermal gradients found in situ, allows the worms to occupy their preferred thermal regime, and permits viewing of the worms' distribution within the aquarium (fig. S1). Our results show that *P. sulfincola* are thermotaxic and extremely thermotolerant, preferring temperatures between 40° and 50°C, with individuals surviving 7 hours of chronic exposure to 50°C and 15 min of acute exposure to 55°C (Fig. 1, B and C).

During all trials, *P. sulfincola* were placed at random into the aquarium, and then the aquarium was repressurized to in situ pressures. The aquarium was flushed with seawater resembling vent effluent (*6*) and maintained at room temperature (26°C) for 1 hour. Soon after, worms began moving within the chamber, although their distributions remained haphazard. When the heating and cooling units were activated to establish a stable thermal gradient of 20° to 61°C, *P. sulfincola* rapidly migrated toward warmer regions, and by 45 min, all worms were in regions above 40°C (Fig. 1, A to C). During the second trail, four worms migrated into the 50°C region and remained there for the duration of the experiment (2.25 hours), exhibiting typical behaviors such as gill irrigation (Fig. 1B). One worm migrated into 55°C for 15 min before returning to cooler regions (Fig. 1B). During the third trial, two worms remained at 50°C for 7 hours (the duration of the experiment), once again irrigating their gills (Fig. 1C). At the end of all three trials, temperature was returned to a uniform 26°C and worms migrated to the formerly hotter regions of the aquarium. All worms survived the thermal gradient trials, exhibiting typical behaviors for at least 24 hours. However, when the aquarium was uniformly heated to 55°C for two hours, all worms ($N = 4$) showed signs of physiological dysfunction such as severe contortion, and were not visibly active when temperature was returned to 26°C. When the aquarium was uniformly heated to 60°C, all worms ($N = 5$) died within minutes. In a separate trial, *Paralvinella palmiformis*, a congener that inhabits diffuse vents with cooler temperatures, was subjected to a 20° to 55°C thermal gradient, and the worms consistently avoided temperatures above 35°C (Fig. 1D).

In light of its ability to tolerate high temperatures, *P. sulfincola* is among the most thermotolerant of animals. By comparison, the aquatic ostracod *Potamocypris* sp. exhibited 50% mortality when exposed to 50°C for 1 hour (*7*), and the ant *Cataglyphis bicolor* exhibited systemic dysfunction when exposed to 55°C for 1 min (*8*). The fungi *Chaetomium thermophile* grows at temperatures up to 55°C, making it the most thermotolerant eukaryote known (*9*).

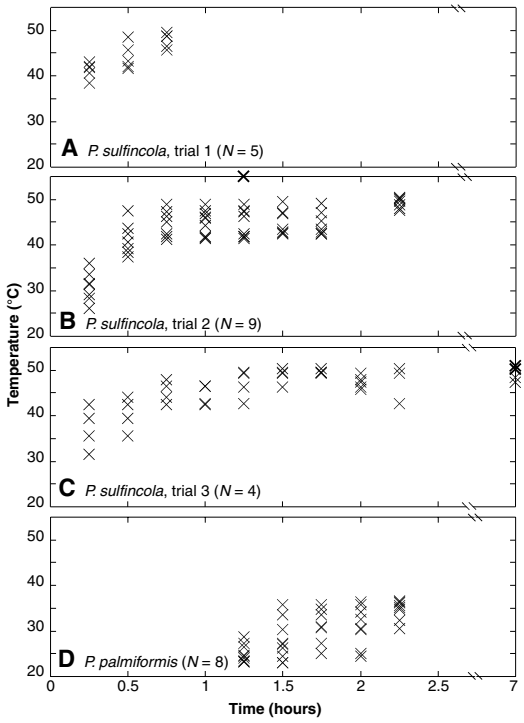

Fig. 1. Distribution of *P. sulfincola* and *P. palmiformis* worms in temperature-gradient experiments. Worms were uniformly dispersed within the aquaria before establishing the temperature gradient. (**A** to **C**) Plots of *P. sulfincola* distributions over time within a 20° to 61°C gradient; $N = 5$, 9, and 4 individuals, respectively. (**D**) Plot of *P. palmiformis* distributions over time within a 20° to 55°C gradient; $N = 8$ individuals.

To our knowledge, *P. sulfincola* is the only animal that prefers chronic exposure to such high temperatures. Although the behaviors and mechanisms underlying this thermo-preference and tolerance remain unknown, this capacity may enable *P. sulfincola* to exploit resources inaccessible to other organisms such as the microbial mats that grow at higher temperatures.

The results presented here are the first direct measure of alvinellid thermotolerance and preference, and they emphasize the difference between acute and chronic tolerance. These results also illustrate the utility of conducting thermal gradient experiments that can provide a more accurate depiction of an organism's thermal biology. Similar experiments may be applied to other species, including *Alvinella pompejana* (*10*). Regardless, all metazoans may be constrained to living in environs below 55°C, the temperature at which mitochondria appear to dysfunction (*11*). Further investigations into alvinellids and other animals that live in thermally challenging environments will help better our understanding of the thermal constraints on metazoan life.

References and Notes

1. S. C. Cary *et al.*, *Nature* **391**, 545 (1998).
2. P. Chevaldonne *et al.*, *Mar. Eco. Prog. Ser.* **208**, 293 (2000).
3. N. Le Bris *et al.*, *Deep Sea Res. I* **52**, 1071 (2005).
4. J. Sarrazin *et al.*, *Cah. Biol. Mar.* **43**, 275 (2002).
5. K. Johnson *et al.*, *Deep Sea Res. A* **35**, 1711 (1988).
6. Materials and methods are available as supporting material on *Science* Online.
7. C. E. Wickstrom, R. W. Castenholz, *Science* **181**, 1063 (1973).
8. R. Wehner *et al.*, *Nature* **357**, 586 (1992).
9. D. Cooney, R. Emerson, *Thermophilic Fungi* (Freeman and Co., San Francisco, CA, 1964), pp. 63–71.
10. B. Shillito *et al.*, *Int. J. High Press. Res.* **24**, 169 (2004).
11. P. Hochachka, G. N. Somero, *Biochemical Adaptation: Mechanism and Process in Physiological Evolution* (Oxford Univ. Press, New York, 2002), pp. 363–366.
12. We thank the crew of the *R.V. Thompson*, the Remotely Operated Vehicle (ROV) Remotely Operated Platform for Ocean Science (ROPOS) group, the New Millennium Observatory group, B. Chadwick, B. Embley, V. Tunnicliffe, A. Bates, J. Marcus, R. Romjue, G. Henry, J. Rutherford, D. Kelley, and J. Delaney. Funding was provided by the NSF, the West Coast and Polar Regions National Undersea Research Center, and the Packard Foundation (Monterey Bay Aquarium Research Institute).

Supporting Online Material

www.sciencemag.org/cgi/content/full/312/5771/231/DC1
Materials and Methods
Fig. S1

23 January 2006; accepted 15 March 2006
10.1126/science.1125286

[1]Department of Organismic and Evolutionary Biology, Harvard University, Cambridge, MA 02138, USA. [2]School of Biological Sciences, Washington State University, Pullman, WA 99164, USA.

*To whom correspondence should be addressed. E-mail: rlee@mail.wsu.edu (R.W.L.); pgirguis@oeb.harvard.edu (P.R.G.)

Nuclear Receptor–Dependent Bile Acid Signaling Is Required for Normal Liver Regeneration

Wendong Huang,[1]* Ke Ma,[1] Jun Zhang,[1]† Mohammed Qatanani,[1]‡ James Cuvillier,[1] Jun Liu,[1] Bingning Dong,[1] Xiongfei Huang,[2] David D. Moore[1]§

Liver mass depends on one or more unidentified humoral signals that drive regeneration when liver functional capacity is diminished. Bile acids are important liver products, and their levels are tightly regulated. Here, we identify a role for nuclear receptor–dependent bile acid signaling in normal liver regeneration. Elevated bile acid levels accelerate regeneration, and decreased levels inhibit liver regrowth, as does the absence of the primary nuclear bile acid receptor FXR. We propose that FXR activation by increased bile acid flux is a signal of decreased functional capacity of the liver. FXR, and possibly other nuclear receptors, may promote homeostasis not only by regulating expression of appropriate metabolic target genes but also by driving homeotrophic liver growth.

Liver regeneration has been studied intensively since the introduction of a rodent partial hepatectomy (PH) model in 1931 (*1*). This process consists of several well-orchestrated phases, with rapid induction of proliferative factors activating the quiescent hepatocytes and priming their subsequent proliferation, followed by reestablishment of normal liver size and renewed quiescence (*2*, *3*). Important early events include the secretion of growth factors and cytokines such as TGFα, produced in hepatocytes, and interleukin-6 (IL-6) and TNFα, produced in nonparenchymal cells. Activation of these signaling pathways increases the expression of many target genes by activating transcription factors, including Stat3, NF-κB, and c-Myc (*4*). Gene knockout studies in mice have confirmed the importance of these pathways in liver regeneration (*3*, *4*), although the requirement for individual factors is generally only partial. One of the most potent is IL-6, the loss of which results in ~75% decrease in DNA synthesis in response to PH (*5*). The absence of its downstream target, Stat-3, has a lesser effect (*6*).

Although many details of the process have been elucidated, the initiation of liver proliferation in response to PH cannot be ascribed to any individual growth factor, cytokine, or specific pathway. Thus, the mechanism by which hepatocytes sense the loss of functional capacity and the identity of the long-sought "regenerative stimulus" that drives regrowth (*7*) have remained elusive.

The primary evidence for such a stimulus is the observation that in rats whose circulatory systems are linked by parabiosis, PH of one animal induces hepatocyte proliferation in the other (*8*). Liver regeneration is thus driven by one or more soluble, circulating factors. Because several nuclear hormone receptor agonists are potent hepatomitogens (*9*), we hypothesized that nuclear receptor activation could contribute to the proliferative response in resected liver. Among candidates for an activating signal, bile acids are attractive because they activate receptors that drive proliferation (*10*). Interrupting enterohepatic biliary circulation also inhibits regeneration (*11*). Moreover, hepatic bile acids comprise less than 5% of the total pool (*12*), and PH stimulates bile flow (*13*). Thus, release of bile from the intact gall bladder and its efficient return through the enterohepatic circulation would expose the much smaller number of remaining hepatocytes to an increase in relative bile acid flux.

Bile acids are sufficient to drive liver growth and necessary for normal regeneration. Bile acids are toxic, and substantial increases in hepatic bile acid levels, as in cholestatic liver disease, induce both apoptosis and necrosis (*14*). To directly test their proliferative effects, wild-type mice were fed a relatively mild diet containing 0.2% cholic acid (CA) for 5 days. This treatment did not induce substantial toxic effects, as indicated by elevated serum alanine aminotransferase levels or histologically apparent liver damage. However, it increased liver size by approximately 30% (Fig. 1A). DNA synthesis also increased, as demonstrated by a marked increase in hepatocyte nuclei staining with BrdU (Fig. 1C). The majority of hepatocytes are 4N under ordinary circumstances, with smaller numbers of both 2N and 8N cells. The 8N population is increased by mitogenic stimuli, including PH and nuclear receptor activation (*15*, *16*). The livers from CA-fed mice showed a more than twofold increase in 8N cell number (Fig. 1B). Thus, modestly elevated bile acid levels are sufficient to drive hepatocyte DNA replication in vivo.

The role of bile acids in liver regeneration was examined more directly in mice in which bile acid pools were either increased by the 0.2% CA diet or decreased by a diet supplemented with the bile acid sequestering resin cholestyramine. CA-fed mice showed an increased rate of liver growth over the first 3 days after PH, and

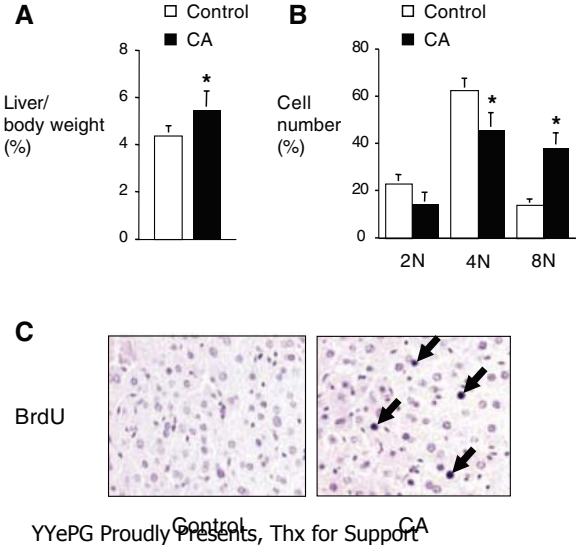

Fig. 1. Bile acid feeding stimulates liver growth. Mice were fed a control diet or a diet containing 0.2% cholic acid (CA) for 5 days. (**A**) Increased liver weight in CA-fed mice. (**B**) Induction of hepatocyte polyploidy by CA feeding. Primary hepatocytes were prepared and stained with propidium iodide, and numbers of diploid (2N), tetraploid (4N), or octoploid (8N) cells were determined by cell sorting. (**C**) Induction of DNA synthesis by CA feeding. Control or CA-fed mice were injected with BrdU, livers were recovered 2 hours later, and incorporation of BrdU was determined histologically. Arrows indicate BrdU-positive nuclei. *, $P < 0.05$.

[1]Department of Molecular and Cellular Biology, Baylor College of Medicine, One Baylor Plaza, Houston, TX 77030, USA. [2]Department of Gene Regulation and Drug Discovery, City of Hope Beckman Research Institute, 1500 East Duarte, Duarte, CA 91010, USA.

*Present address: Department of Gene Regulation and Drug Discovery, City of Hope Beckman Research Institute, 1500 East Duarte, Duarte, CA 91010, USA.

†Present address: Clark Center W252, 318 Campus Drive, Stanford University School of Medicine, Stanford, CA 94305, USA.

‡Present address: Division of Endocrinology, Diabetes, and Metabolism, and University of Pennsylvania School of Medicine, 415 Curie Boulevard, Philadelphia, PA 19104, USA.

§To whom correspondence should be addressed. E-mail: moore@bcm.tmc.edu

the number of BrdU-positive nuclei also increased, particularly at day 1 (Fig. 2, A and B). This stimulatory effect is consistent with results in dogs (*17*) and other studies (*18*, *19*), although distinct bile acids can have different effects. In the cholestyramine-fed mice, both the rate of liver growth and the number of BrdU-positive nuclei decreased (Fig. 2, A and B). This is in accord with the observation that diverting bile flow from the gut decreases liver regrowth and DNA synthesis in PH rats (*11*) and suggests that loss of bile acid signaling accounts for the defect.

Bile acids activate the primary bile acid receptor FXR (*20*–*22*), as well as the xenobiotic receptors CAR (*10*) and PXR (*23*, *24*). Because CAR activation induces a strong liver growth response (*16*, *25*), regeneration was examined in mice lacking each of these receptors and also in mice lacking the orphan receptor SHP, a negative regulator of nuclear receptor and bile acid signaling. No defect was observed in the PXR$^{-/-}$ or SHP$^{-/-}$ mice, whereas CAR$^{-/-}$ mice showed a modest decrease in liver growth at day 1 combined with delayed replication, as demonstrated by a decreased number of 8N cells 3 days after PH (fig. S1). In contrast, liver growth was strongly inhibited in the early stages of regeneration in FXR$^{-/-}$ mice (Fig. 3A). The FXR$^{-/-}$ mice also showed a decrease in BrdU-positive nuclei in the first 3 days after PH (Fig. 3B). At later stages, the FXR$^{-/-}$ livers showed relatively rapid growth, and the weights of the livers from wild-type and knockout mice did not differ significantly at 7 days. This was not associated with a late increase in BrdU incorporation, and the cumulative overall decrease in the FXR$^{-/-}$ animals was approximately 70% relative to wild type (Fig. 3B). The loss of FXR function also prevented the acceleration of regeneration in mice fed the 0.2% diet, and the delay in the FXR$^{-/-}$ mice was not further extended by treatment with the bile acid binding resin (Fig. 2, A and B). The negative effect of the loss of FXR on liver regeneration was also evident from an increase in mortality, which was approximately 5% in sham-treated or hepatectomized wild-type mice or sham-treated FXR$^{-/-}$ mice but was 30% in PH FXR$^{-/-}$ mice (Fig. 3C). Despite this increased mortality, the surviving mice used for these studies did not show elevated liver toxicity as indicated by serum alanine aminotransferase levels or elevated apoptosis (fig. S2).

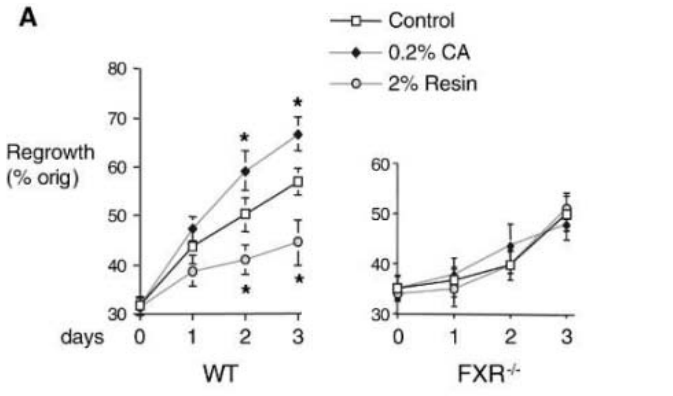

Fig. 2. Bile acids stimulate liver regeneration. PH was performed on mice that had been fed control diets or diets containing 0.2% CA or 2% cholestyramine (resin) for 5 days. At indicated times, the extent of regeneration was assessed by measuring (**A**) liver weight or (**B**) BrdU incorporation. *, $P < 0.05$; **, $P < 0.01$.

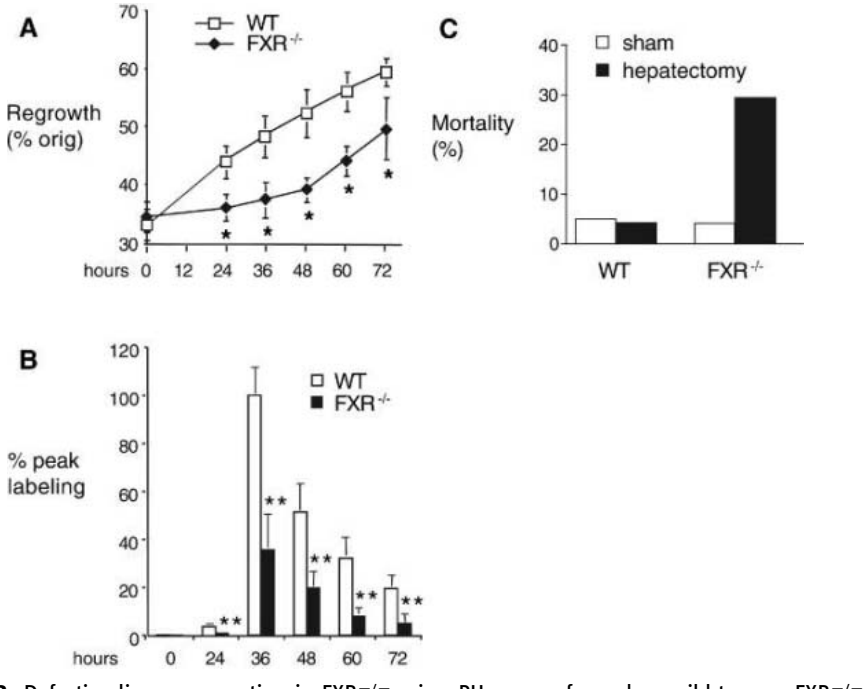

Fig. 3. Defective liver regeneration in FXR$^{-/-}$ mice. PH was performed on wild-type or FXR$^{-/-}$ mice. At indicated times, the extent of regeneration was assessed by measuring (**A**) liver weight or (**B**) BrdU incorporation. (**C**) Increased mortality after PH in FXR$^{-/-}$ mice. Percentage of animals not surviving for 7 days after PH is indicated. *n*, 20 to 40; *, $P < 0.05$; **, $P < 0.01$.

Partial hepatectomy activates bile acid signaling. The prediction that remaining hepatocytes are exposed to increased bile acid flux was examined in both wild-type and FXR$^{-/-}$ mice. Basal serum and hepatic bile acid levels are somewhat elevated in the FXR$^{-/-}$ mice (*26*), and this is not altered by sham surgery or immediately after PH. Wild-type mice show a trend toward increased serum bile acids that does not reach statistical significance at early stages after PH (Fig. 4A). Hepatic bile acid levels decrease, rather than increase, after PH (Fig. 4B), in agreement with previous results and with the increased bile flow from the liver in response to PH (*27*, *28*). In rats, this is associated with increased biliary output of cholic acid, but the contributions of individual bile acids to bile composition are not altered during regeneration (*29*). In contrast to the results with wild-type mice, the FXR$^{-/-}$ animals show

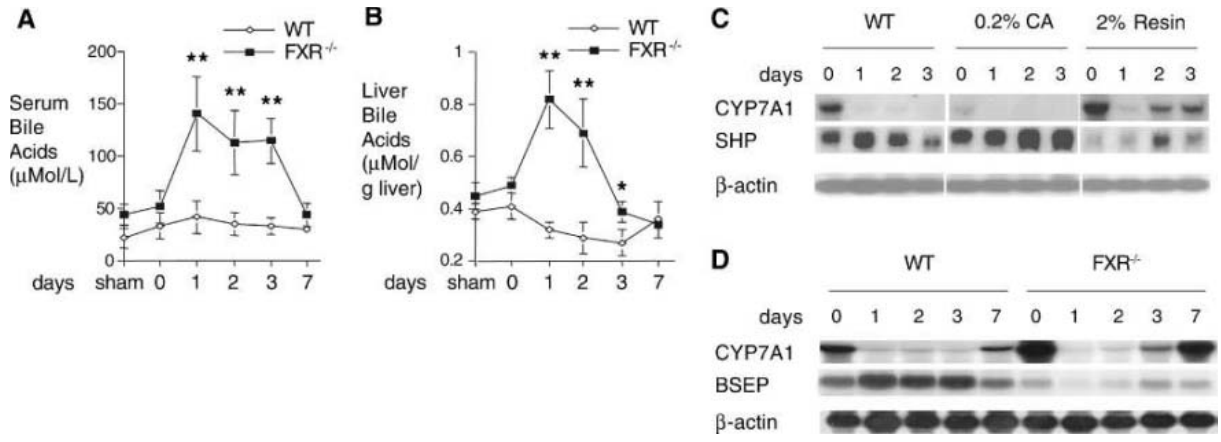

Fig. 4. PH increases bile acid signaling. PH was performed on wild-type or FXR$^{-/-}$ mice. At indicated times after PH, total bile acid levels were measured in (**A**) serum or (**B**) liver. Liver responses of bile acid regulated genes were assessed by Northern blotting at indicated times after PH in (**C**) mice fed control, CA, or cholestyramine diets as in Fig. 2 or (**D**) wild-type and FXR$^{-/-}$ mice as in Fig. 3. *, $P < 0.05$; **, $P < 0.01$.

large increases in both serum and hepatic bile acids on the first day after PH, which decline with time and return to normal at day 7 (Fig. 4, A and B). A simple interpretation of these results is that PH has a potential stimulatory effect on serum and hepatic bile acid levels that is prevented by the potent counterregulatory pathways in wild-type mice but not in those lacking functional FXR (*30*).

This was tested by examining the expression of the primary FXR target gene SHP and the downstream negative target cholesterol 7α hydroxylase, CYP7A1. SHP mRNA expression increased before PH in wild-type mice fed the 0.2% CA diet and decreased in cholestyramine-supplemented mice, with opposite effects for CYP7A1 (Fig. 4C). CYP7A1 mRNA expression was repressed in chow-fed animals after PH, in accord with previous results (*19*, *31*), and SHP expression increased. CA feeding increased SHP expression and eliminated basal CYP7A1 expression, whereas the cholestyramine-fed group showed a more transient decrease in CYP7A1 expression at day 1 and an increase in SHP expression at day 3. These results indicate a rapid increase in bile acid signaling in response to PH in the chow-fed mice that is consistent with the reported transient increase in nuclear bile acids after PH (*32*).

In a longer term experiment, CYP7A1 expression was repressed from day 1 to day 3 after PH in wild-type mice, with partial expression observed at day 7 (Fig. 4D). This repression was more transient in the FXR$^{-/-}$ mice, with CYP7A1 expression reemerging at day 3 in the mutants. Expression of the positive FXR target gene BSEP increased in the wild-type mice on days 1 to 3 and returned to basal on day 7. This inductive response was replaced by a transient inhibition in the FXR$^{-/-}$ mice. Overall, we conclude that the wild-type mice reach a new steady state in response to PH, in which the observed maintenance of normal bile acid levels depends on activation of the powerful mechanisms of bile acid homeostasis (*30*), including both the shut-off of synthesis by CYP7A1 and the induction of export by BSEP. It is the failure of this homeostatic response in the FXR$^{-/-}$ mice that results in the anticipated increase in serum and liver bile acids.

The transient repression of CYP7A1 expression in the FXR$^{-/-}$ mice is consistent with a number of previous studies identifying nuclear receptor–independent pathways for bile acid negative feedback regulation (*33*–*35*). Recent results have also identified a cyclic adenosine monophosphate (cAMP)–coupled transmembrane bile acid receptor (*36*–*38*). It would be interesting to further examine the activation of these pathways in the FXR$^{-/-}$ mice, because we have observed only limited proliferative effects in mice treated with the synthetic FXR agonist GW4064 despite responses of SHP, CYP7A1, and other FXR targets that confirmed the general effectiveness of the treatment. Thus, bile acid activation of stress kinase, cAMP, or other pathways may function to complement FXR activation to elicit proliferative effects.

Relationship of the bile acid pathway to other regenerative pathways. These results identify an FXR-dependent bile acid signaling pathway that is necessary for normal liver regeneration but do not address the relationship of this pathway to the well-defined growth factor and cytokine-dependent pathways. We examined the effects of 3 days of feeding a more potent 1% CA diet to amplify potential effects of bile acids on expression of a number of PH targets, including growth factors, cytokines, and transcription factors. There was an increase in TNFα transcripts in response to dietary CA that was decreased but not absent in FXR$^{-/-}$ mice (fig. S3A). CA feeding also increased c-Myc expression in an FXR-independent manner. The remaining 10 PH targets, including IL-6, IL-1, and their receptors, HGF and TGFα, showed no detectable response. PH-induced serum IL-6 levels at 24 hours were also not significantly affected by dietary CA or the bile acid binding resin. Activation of the major downstream transcription factor Stat3 by PH was also unaffected by the loss of FXR, as indicated by comparable induction of DNA binding in nuclear extracts from wild-type and FXR$^{-/-}$ mice 2 and 8 hours after hepatectomy (fig. S3B). Overall, we conclude that manipulation of the FXR-dependent pathway has little or no impact on the important initial growth factor and cytokine responses to PH.

The early responses are necessary to exit the quiescent G_o state and promote subsequent cell cycle progression, and these effects are dependent on targets such as the general proliferative transcription factors c-Myc and FoxM1b that function at later stages (*3*, *4*). Loss of FXR reduced but did not prevent induction of c-Myc expression, which is consistent with residual proliferative function in the FXR$^{-/-}$ mice, but did block induction of FoxM1b expression (Fig. 5A). A stronger and earlier induction of FoxM1b expression was observed in the CA-fed mice, which show a temporally advanced regenerative response, and this induction was undetectable in the cholestyramine-fed mice (Fig. 5B). Both of these dietary effects were lost in the FXR$^{-/-}$ mice. Although the 0.2% CA diet did not affect FoxM1b expression, the stronger stimulus provided by a 1% CA diet for 3 days increased FoxM1b transcripts in an FXR-dependent manner (Fig. 5C) and also induced expression of the direct FoxM1b target cdc25b (*39*) at the protein level (Fig. 5D).

Conclusions. Normal liver regeneration appears to be dependent on bile acid activation of nuclear receptor–dependent signaling pathways. The current results suggest a simple homeostatic model in which FXR and potentially additional nuclear receptors dynamically regulate the size

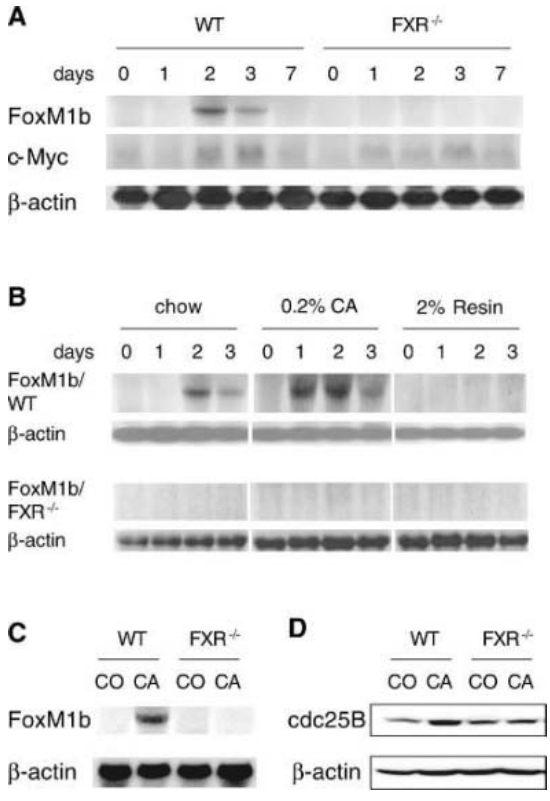

Fig. 5. Bile acid signaling is required for induction of FoxM1b by PH. Liver responses of proliferative target genes were assessed by Northern blotting at indicated times after PH in (**A**) wild-type or FXR$^{-/-}$ mice as in Fig. 3 or (**B**) wild-type or FXR$^{-/-}$ mice fed control, 0.2% CA, or cholestyramine diets as in Fig. 2. (**C**) Expression of FoxM1b in livers of wild-type or FXR$^{-/-}$ mice fed control or 1% CA diets for 3 days was assessed by Northern blotting. (**D**) Expression of the FoxM1b target cdc25b was assessed by Western blotting in liver extracts from wild-type or FXR$^{-/-}$ mice fed control or 1% CA diets for 3 days.

of the adult liver by sensing its functional capacity. When inadequate function causes bile acid levels to build up, the resultant FXR activation not only induces negative feedback pathways that protect hepatocytes from bile acid toxicity but also increases the capacity of the liver to manage the overload by promoting liver growth. This is analogous to the ability of the xenobiotic receptor CAR to promote clearance of potentially toxic foreign compounds by both inducing drug-metabolizing enzymes and rapidly increasing liver size (*16*, *25*). Although a recent report highlighted the distinction between the CAR and growth factor/cytokine pathways (*40*), and loss of CAR has only a modest and transient effect on liver regrowth in response to PH, CAR is activated by both bile acids (*10*) and PH (fig. S1), and the decreased FoxM1b induction and DNA replication in the CAR$^{-/-}$ liver (fig. S1) indicates that the xenobiotic receptor may also contribute to liver regeneration. More broadly, the function of CAR and other nuclear receptor ligands as hepatomitogens (*9*) suggests that additional receptors could also act as both sensors of liver function and mediators of liver growth.

This homeostatic mechanism may also contribute to the termination of regeneration. This process has been attributed to effects of inhibitory cytokines such as TGFβ, although recent studies with mice defective in TGFβ signaling have not supported such a mechanism (*41*, *42*), perhaps as a result of compensatory increases in activin A signaling (*41*, *42*). The homeostatic model suggests that cessation of proliferation is simply due to the loss of the proliferative stimulus as the liver approaches its normal size and the functional deficit is eliminated. The return of expression of FXR target genes to basal levels at day 7 in the wild-type mice is consistent with this idea.

In the context of PH or liver damage, this nuclear receptor–dependent mechanism must function in combination with the important early growth factor and cytokine responses to liver damage thought to prime hepatocytes for later growth (*2*). The mechanisms that initiate these responses are not known, but it has been suggested that the decreased ability of the resected liver to clear endotoxins released by the gut results in Kupffer cell activation (*43*). This activation in response to decreased innate immunity function parallels the activation of FXR by increased bile acid flux. The growth factor and cytokine responses are not lost in the FXR$^{-/-}$ livers and undoubtedly contribute to their eventual regrowth. However, at least the initial stages of many early responses can be observed at the transcriptional level in sham-operated animals (*44*), and recent evidence indicates their primary role may be to maintain the function of the remaining hepatocytes (*3*). We propose that normal liver regeneration requires not only the priming and protective effects of these early responses but also the signal of decreased metabolic functional capacity delivered by the nuclear receptors. We suggest the term ''homeotrophic'' to describe growth to recover functional capacity and reestablish homeostasis.

References and Notes

1. G. M. Higgins, R. M. Anderson, *Arch. Pathol.* **12**, 186 (1931).
2. N. Fausto, *J. Hepatol.* **32**, 19 (2000).
3. R. Taub, *Nat. Rev. Mol. Cell Biol.* **5**, 836 (2004).
4. R. H. Costa, V. V. Kalinichenko, A. X. Holterman, X. Wang, *Hepatology* **38**, 1331 (2003).
5. D. E. Cressman *et al.*, *Science* **274**, 1379 (1996).
6. W. Li, X. Liang, C. Kellendonk, V. Poli, R. Taub, *J. Biol. Chem.* **277**, 28411 (2002).
7. N. L. Bucher, *Int. Rev. Cytol.* **15**, 245 (1963).
8. F. L. Moolten, N. L. Bucher, *Science* **158**, 272 (1967).
9. A. Columbano, G. M. Ledda-Columbano, *Cell Death Differ.* **10** (suppl. 1), S19 (2003).
10. J. Zhang, W. Huang, M. Qatanani, R. M. Evans, D. D. Moore, *J. Biol. Chem.* **279**, 49517 (2004).
11. J. Ueda, K. Chijiiwa, K. Nakano, G. Zhao, M. Tanaka, *Surgery* **131**, 564 (2002).
12. K. D. Setchell *et al.*, *Gastroenterology* **112**, 226 (1997).
13. G. R. Sainz, M. J. Monte, E. R. Barbero, M. C. Herrera, J. J. Marin, *Int. J. Exp. Pathol.* **78**, 109 (1997).
14. G. A. Kullak-Ublick, P. J. Meier, *Clin. Liver Dis.* **4**, 357 (2000).
15. C. Melchiorri *et al.*, *Carcinogenesis* **14**, 1825 (1993).
16. W. Huang *et al.*, *Mol. Endocrinol.* (14 Apr 2005).
17. B. P. Solopaev, *Biull. Eksp. Biol. Med.* **43**, 109 (1957).
18. M. Barone *et al.*, *Hepatology* **23**, 1159 (1996).
19. B. T. Kren, C. M. Rodrigues, K. D. Setchell, C. J. Steer, *Liver Transpl.* **7**, 321 (2001).
20. D. J. Parks *et al.*, *Science* **284**, 1365 (1999).
21. M. Makishima *et al.*, *Science* **284**, 1362 (1999).
22. H. Wang, J. Chen, K. Hollister, L. C. Sowers, B. M. Forman, *Mol. Cell* **3**, 543 (1999).
23. J. Staudinger, Y. Liu, A. Madan, S. Habeebu, C. D. Klaassen, *Drug Metab. Dispos.* **29**, 1467 (2001).
24. W. Xie *et al.*, *Proc. Natl. Acad. Sci. U.S.A.* **98**, 3375 (2001).
25. P. Wei, J. Zhang, M. Egan-Hafley, S. Liang, D. D. Moore, *Nature* **407**, 920 (2000).
26. C. J. Sinal *et al.*, *Cell* **102**, 731 (2000).
27. G. F. Leong, R. L. Pessotti, R. W. Brauer, *Am. J. Physiol.* **197**, 880 (1959).
28. J. J. Garcia-Marin, P. Regueiro, J. C. Perez-Antona, G. R. Villanueva, F. Perez-Barriocanal, *Clin. Sci. (Lond.)* **78**, 55 (1990).
29. M. J. Monte, M. Y. El-Mir, G. R. Sainz, P. Bravo, J. J. Marin, *Biochim. Biophys. Acta* **1362**, 56 (1997).
30. D. W. Russell, *Annu. Rev. Biochem.* **72**, 137 (2003).
31. K. Chijiiwa *et al.*, *Br. J. Surg.* **83**, 482 (1996).
32. M. J. Monte *et al.*, *J. Hepatol.* **36**, 534 (2002).
33. S. Gupta, R. T. Stravitz, P. Dent, P. B. Hylemon, *J. Biol. Chem.* **276**, 15816 (2001).
34. L. Wang *et al.*, *Dev. Cell* **2**, 723 (2002).
35. S. Gupta *et al.*, *J. Biol. Chem.* **279**, 5821 (2004).
36. T. Maruyama *et al.*, *Biochem. Biophys. Res. Commun.* **298**, 714 (2002).
37. Y. Kawamata *et al.*, *J. Biol. Chem.* **278**, 9435 (2003).
38. M. Watanabe *et al.*, *Nature* **439**, 484 (2006).
39. X. Wang, H. Kiyokawa, M. B. Dennewitz, R. H. Costa, *Proc. Natl. Acad. Sci. U.S.A.* **99**, 16881 (2002).
40. A. Columbano *et al.*, *Hepatology* **42**, 1118 (2005).
41. S. Oe *et al.*, *Hepatology* **40**, 1098 (2004).
42. J. Romero-Gallo *et al.*, *Oncogene* **24**, 3028 (2005).
43. M. J. Wiezer *et al.*, *Ann. Surg.* **232**, 208 (2000).
44. A. I. Su, L. G. Guidotti, J. P. Pezacki, F. V. Chisari, P. G. Schultz, *Proc. Natl. Acad. Sci. U.S.A.* **99**, 11181 (2002).

45. We thank F. Gonzalez for the FXR$^{-/-}$ mice. This work was supported by grants R01 DK053366 and U19 DK62434 from the NIH.

Supporting Online Material

www.sciencemag.org/cgi/content/full/312/5771/233/DC1
Materials and Methods
Figs. S1 to S3

17 October 2005; accepted 24 February 2006
10.1126/science.1121435

Atomic Description of an Enzyme Reaction Dominated by Proton Tunneling

Laura Masgrau,[1,2]* Anna Roujeinikova,[1,3] Linus O. Johannissen,[1,2] Parvinder Hothi,[1,3] Jaswir Basran,[4] Kara E. Ranaghan,[5] Adrian J. Mulholland,[5]† Michael J. Sutcliffe,[1,2]† Nigel S. Scrutton,[1,3]† David Leys[1,3]†

We present an atomic-level description of the reaction chemistry of an enzyme-catalyzed reaction dominated by proton tunneling. By solving structures of reaction intermediates at near-atomic resolution, we have identified the reaction pathway for tryptamine oxidation by aromatic amine dehydrogenase. Combining experiment and computer simulation, we show proton transfer occurs predominantly to oxygen O2 of Asp$^{128}\beta$ in a reaction dominated by tunneling over ~0.6 angstroms. The role of long-range coupled motions in promoting tunneling is controversial. We show that, in this enzyme system, tunneling is promoted by a short-range motion modulating proton-acceptor distance and no long-range coupled motion is required.

The physical basis of the catalytic power of enzymes remains contentious despite sustained and intensive research efforts (*1–3*). The question of whether enzymes have evolved to use quantum tunneling to the best advantage has provoked a heated debate (*4–10*). That tunneling occurs is now widely accepted, with conceptual frameworks incorporating protein motion into the enzymic H tunneling process (*11–14*). More controversial is a role for compressive motion to promote H tunneling (*4*), a special property of enzymes that might be endowed by evolutionary pressure. Whereas some studies have suggested a role for protein motion in facilitating tunneling (*15–22*), others have argued that motions that contribute to tunneling are similar in both enzymes and free solution and therefore that the degree of tunneling available in the enzyme system is equivalent to that in free solution (*5–8*, *10*). A number of kinetic studies (*23–31*) are in agreement with environmentally coupled models of H tunneling (*11*, *29*, *32–34*), but atomic-level insight into the tunneling event can only be obtained from high-resolution protein structures of catalytically competent intermediates combined with computer simulation (*35*).

The quinoprotein enzymes, the mechanisms of which are generally well understood (*36*), are ideally suited to studies of H transfer during substrate oxidation (*14*) and are thus excellent model systems for investigating H transfer by nuclear tunneling. Aromatic amine dehydrogenase (AADH) is a tryptophan tryptophyl quinone (TTQ)–dependent quinoprotein (*37*, *38*) and catalyzes H transfer by quantum mechanical tunneling (*24*). It oxidatively deaminates aromatic primary amines to form the corresponding aldehyde (Fig. 1); the electrons released are transferred from AADH to the type I blue copper protein azurin and enter the respiratory chain via a *c*-type cytochrome. We present here an analysis of the oxidative deamination of tryptamine by AADH using a combination of x-ray crystallography and computational and kinetic studies. This has provided a detailed description of the overall reaction pathway and in particular the H-tunneling step.

Crystal structures of key intermediates. The crystal structure of substrate-free AADH was determined at a resolution of 1.2 Å (x-ray exposure reduces the TTQ cofactor to the semiquinone form within the first seconds of data collection, as observed by color change) (*39*). The $\alpha_2\beta_2$ heterotetramer (α molecular mass, 40 kD, and TTQ-containing β, 12 kD) is highly similar in fold to the related TTQ-dependent methylamine dehydrogenase (Fig. 1). The carboxylate of Asp$^{128}\beta$, the proton acceptor in the tunneling step, is in close proximity to and almost perpendicular to the plane of the quinone system. O1 of this carboxylate (Fig. 2) hydrogen bonds to the backbone amide of Trp$^{160}\beta$ (3.0 Å) and a partially occupied (~50% present) water molecule (2.7 Å), and O2 is in close proximity to Thr$^{172}\beta$ hydroxyl (3.4 Å).

Crystal structures of tryptamine-AADH intermediate complexes in the reductive half-reaction (Fig. 2C) were obtained by soaking crystals with substrate and flash-cooling either before, immediately after, or several minutes after complete reduction of the TTQ was observed by visible inspection of the crystals (*39*). Alternatively, crystals of tryptamine-AADH intermediate complexes were prepared by cocrystallization under anaerobic conditions, leading to different space groups (*39*). The high resolution routinely obtained (ranging from 1.6 to

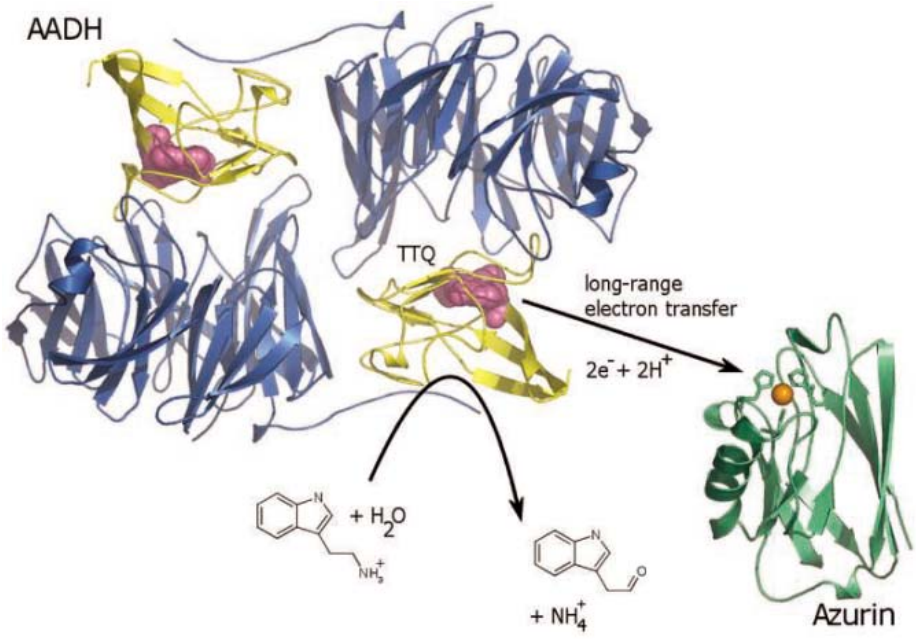

Fig. 1. Schematic overview of the AADH reaction with tryptamine. The AADH structure is represented in cartoon form with the α subunit in blue, the β subunit in yellow, and the TTQ cofactor in magenta spheres. The reductive half-reaction with tryptamine is depicted in detail in Fig. 2. The oxidative half-reaction consists of two consecutive long-range electron transfer events to the single-electron carrier azurin. An azurin from *Pseudomonas putida* (PDB code 1NWO) is depicted in green cartoon with the copper atom as an orange sphere.

[1]Manchester Interdisciplinary Biocentre, [2]School of Chemical Engineering and Analytical Science, [3]Faculty of Life Sciences, University of Manchester, Jackson's Mill, Post Office Box 88, Manchester M60 1QD, UK. [4]Department of Biochemistry, University of Leicester, University Road, Leicester LE1 7RH, UK. [5]School of Chemistry, University of Bristol, Cantocks Close, Bristol BS8 1TS, UK.

*Present address: Unité de Bioinformatique Structurale, Institut Pasteur, 25 Rue du Dr Roux, 75724 Paris, France. †To whom correspondence should be addressed. E-mail: david.leys@manchester.ac.uk (D.L.); michael.sutcliffe@manchester.ac.uk (M.J.S.); adrian.mulholland@bristol.ac.uk (A.J.M.); nigel.scrutton@manchester.ac.uk (N.S.S.)

1.1 Å) allowed unambiguous identification of the intermediates present by inspection of the difference Fourier electron density maps (identification by microspectrophotometry was not possible, because intermediates after TTQ reduction do not absorb in the visible region). Only data sets consistent with a single intermediate present at high occupancy levels in the active site were used for model building and refinement. Key intermediates were observed in both active sites within the asymmetric unit and in distinct space groups, indicating the reaction path is largely independent of crystal packing. The Michaelis complex (intermediate I, Fig. 2) was too short-lived to be observed. However, the crystal structure of the reduced enzyme in complex with tryptamine (I) reveals the indole moiety of the substrate sandwiched between the side chain of Phe$^{97}\alpha$ and the Gly$^{178}\alpha$–Leu$^{179}\alpha$ peptide bond, in a position that is occupied by the Leu$^{179}\alpha$ side chain in other structures (Fig. 2B). Structures of substrate-oxidized AADH complexes obtained at lower resolution by soaking at pH < 5.0 reveal a similar structure. The amine group of the substrate contacts (Fig. 2B) the carbonyl backbone oxygen of Asn$^{156}\beta$ (2.9 Å), Asp$^{84}\beta$ (3.1 Å), and Val$^{158}\beta$ (3.0 Å); the amino group of the aminoquinol (2.9 Å); and a water molecule located close to Asp$^{128}\beta$ O1 (3.2 Å). Assuming this structure is a good model for intermediate I, we postulate that, upon formation of the Michaelis complex, Asp$^{128}\beta$ O1 deprotonates the substrate via a bridging water molecule, initiating attack of the nucleophilic nitrogen on the TTQ O6–C6 bond and leading to formation of a transient carbinolamine intermediate (II). The next step likely involves departure of the hydroxyl group via Asp$^{128}\beta$ acid catalysis, leading to formation of the first Schiff base (or iminoquinone, III) intermediate of the catalytic cycle and ensuring that Asp$^{128}\beta$ is deprotonated (Fig. 2A). We were unable to obtain structural data for this AADH-iminoquinone complex, which formed before the proton transfer (i.e., quantum tunneling) step. However, an analogous complex with the inhibitor phenylhydrazine (containing a phenyl rather than indole side chain) has been characterized in solution (*37*). In the crystal structure, the only notable changes from intermediate I are a slight rotation of the TTQ away from the carboxylate group of Asp$^{128}\beta$ (Fig. 2B) and the concomitant minor repositioning of the side chain of Thr$^{172}\beta$, which now forms a hydrogen bond with Asp$^{128}\beta$ O2 (3.0 Å). The phenylhydrazine nitrogen, which mimics the iminoquinone-reactive C1 donor atom in the catalytic cycle, is within hydrogen-bonding distance of Asp$^{128}\beta$ O1 (2.8 Å) and in van der Waals contact with Asp$^{128}\beta$ O2 (3.2 Å). In principle, either Asp$^{128}\beta$ oxygen could be a proton acceptor for the H-tunneling reaction, leading to two distinct possible intermediates (IV).

We were unable to trap the proposed intermediate (IV) formed immediately after the tunneling event, in which the C1=N bond is expected to be coplanar with the modified indole of Trp$^{109}\beta$ and the proton residing on either O1 or O2. The electron density obtained for crystals flash-cooled immediately after reduction (as identified by color change) is consistent with movement of the C1=N bond out of plane by ~60° to give the enzyme species (V) after proton transfer. This geometry increases the distance between C1 and Asp$^{128}\beta$ O1 and O2 to 3.7 Å and 4.1 Å, respectively. No evidence for protonation of Asp$^{128}\beta$ was observed from the 1.1 Å electron density map, and from the structure it is clear that the enzyme is not configured to stabilize the negative charge on O7 of the TTQ cofactor by hydrogen bonding (i.e., there is no oxyanion hole). We infer that, in the crystal structure of intermediate V, O7 is protonated

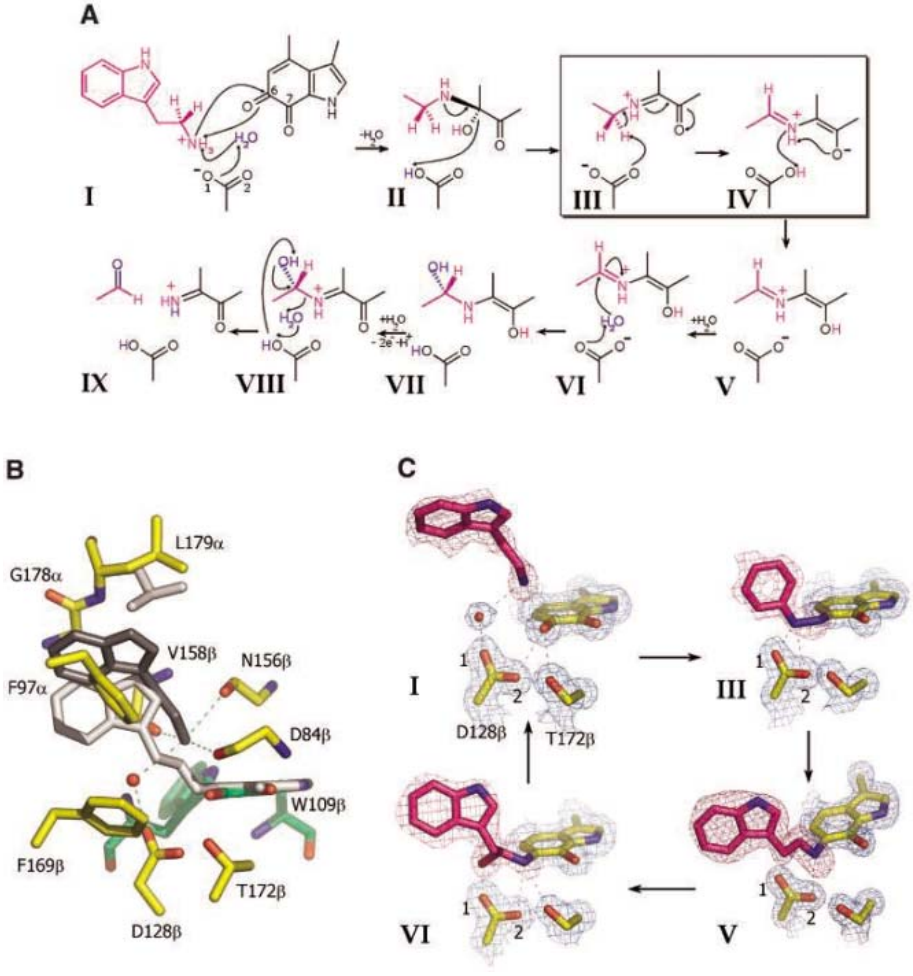

Fig. 2. Reductive half-reaction of AADH with tryptamine. (**A**) Schematic overview of the proposed reaction mechanism. Intermediates are numbered by roman numerals; for clarity only key atoms are represented from intermediate II onward, whereas TTQ atoms C6 and C7 and Asp$^{128}\beta$ O1 and O2 are labeled for intermediate I. Atoms derived from the substrate are depicted in magenta; those derived from water, in blue. All other enzyme-derived atoms are depicted in black. (**B**) AADH active site structure for the ligand-free protein, represented by atom-colored sticks: green carbons, TTQ cofactor; other carbons, yellow. The position occupied by the substrate in complex with the reduced AADH is depicted in dark gray, and the positions in intermediate V of substrate Leu$^{179}\alpha$ and TTQ are in light gray; putative hydrogen bonds are shown as green dashed lines. (**C**) Active site and SigmaA weighted F_oF_c and $2F_oF_c$-electron density of intermediates in the reductive half-reaction with tryptamine. Atoms are colored according to atom type, with substrate-derived carbon atoms in magenta and protein-derived carbon atoms in yellow. For clarity, only substrate- or inhibitor-derived atoms are shown, in addition to the side chain atoms for residues Asp$^{128}\beta$ and Thr$^{172}\beta$ and part of the TTQ cofactor. The $2F_oF_c$ density for these enzyme-derived atoms or water molecules is shown as a blue mesh, whereas F_oF_c density for the substrate- or inhibitor-derived atoms is depicted at 4σ and shown as a magenta mesh. Intermediates are labeled by roman numerals corresponding to (A). The covalent phenylhydrazine-AADH complex is used as a model for intermediate III. For intermediate V, electron density for the $P2_1$ crystal form is shown, whereas intermediate VII is depicted by electron density for the F222 crystal form.

by proton transfer from Asp^{128}β via the nitrogen Schiff base in a two-step process. This is consistent with combined quantum mechanics/molecular mechanics (QM/MM) dynamics simulations, where planarity in intermediate IV is lost after proton transfer to form intermediate V. This step substantially increases the C1–acceptor distances and effectively ensures irreversibility of the H-tunneling step. Our calculations show that the deprotonated Asp^{128}β (V) is stabilized substantially (by ~18 kcal mol^{-1}) relative to the protonated form by electrostatic interactions with Trp^{160}β HN and Thr^{172}β hydroxyl and that deprotonation of either O1 or O2 by the neutral Schiff base nitrogen could occur after rotation around the N–C6 bond. Although the conformation required for proton transfer from O2 to N is highly similar to that observed in the structure of V, efficient proton transfer from O1 requires the N–C6 torsion angle to increase from the observed value of ~60° to beyond ~90°. The latter process would require substantial repositioning of the main chain of Asp^{84}β to avoid a steric clash with the C1 atom, a dynamic process for which no evidence was found in the obtained crystal structures. Regardless, formation of intermediate V allows for both species of IV, either O1 or O2 protonated, to converge to a single intermediate and poises the enzyme for the subsequent hydrolysis steps.

The increased C1–Asp^{128}β distance after formation of V allows for positioning of a water molecule between C1 and O1 (intermediate VI). Transfer of a water molecule from bulk solution to the postulated position in VI requires transient but substantial repositioning of the indole group, which is likely to be hindered within the crystal. Stereospecific attack by this water molecule forms a carbinolamine (VII) containing a chiral center at C1. Analysis of crystals soaked for 5 to 10 min after TTQ reduction reveals electron density that clearly corresponds to intermediate VII in an S enantiomeric configuration, consistent with activation of the water molecule by Asp^{128}β O1 leading to attack of the si face of the C1=N bond. Despite the inherent instability of carbinolamines in water, intermediate VII is stable under anaerobic conditions for several days, as revealed by crystal structures obtained from cocrystallization under anaerobic conditions. We conclude that Asp^{128}β is unable to catalyze C1–N bond breakage by proton abstraction from the hydroxyl of the carbinolamine by O1 and concomitant proton donation to the leaving NH group by O2, because O1 rather than O2 abstracts a proton from the attacking water molecule. In principle, indirect deprotonation of O1 by O2 via the TTQ nitrogen is possible, a process that requires active site motions similar to those invoked for transferring the proton of O1 to N and ultimately to O7 in the step from IV to V. However, this motion does not occur to any significant extent, as indicated by the stability of intermediate VII in the crystals and by mass spectrometric analysis of enzyme incubated with β-substituted aromatic amine substrates, which reveals the presence of a covalent adduct consistent with formation of a stable intermediate VII in solution (*39*). In the case of the reduced AADH-tryptamine complex, the carbinolamine moiety is furthermore protected from water by both enzyme and substrate aromatic groups. After oxidation of the enzyme, we postulate that hydrolysis of the carbinolamine is facilitated by creation of a good leaving group (i.e., the aminoquinone) and the possible introduction of a water molecule between Asp^{128}β O2 and the aminoquinone (intermediate VIII).

Computational analysis of the H-tunneling step (III to IV). To investigate in atomic detail the proton transfer step that leads to intermediate IV, we performed computational simulation studies (*39*). On the basis of the proton-acceptor distances in the modeled complex III structure [d(O1–H1) = 1.74 Å and d(O2–H1) = 2.67 Å, respectively] and in accord with the analogous AADH-phenylhydrazine structure described above, we inferred that the transfer of H1 could occur to either O1 or O2 of Asp^{128}β. Therefore, we have studied both transfers.

With use of a combined QM/MM potential (*40*), we first calculated the free energy of activation for the classical transfer of the proton to O1 and O2 at 300 K ($\Delta G^{\ddagger,\mathrm{classical}}$) (*41*). This magnitude was then corrected to account for H tunneling ($\Delta G^{\ddagger,\mathrm{tunneling}}$), which results in the phenomenological free energy of activation (*11*) at 300 K [$\Delta G^{\mathrm{act}}(300) = \Delta G^{\ddagger,\mathrm{classical}}(300) + \Delta G^{\ddagger,\mathrm{tunneling}}(300)$], from which we estimate the rate constant according to

$$k(T) = \frac{k_B T}{h} \exp[-\Delta G^{\mathrm{act}}(T)/RT]$$

where T is temperature, k_B is Boltzmann's constant, h is Planck's constant, and R is the gas constant. The term $\Delta G^{\ddagger,\mathrm{tunneling}}$ was calculated from the transmission coefficient (κ), often written in the literature (*11*, *42*) as a preexponential factor multiplying the classical rate constant, obtained from variational transition-state theory with small curvature tunneling corrections (*32*, *42*) calculations [$\Delta G^{\ddagger,\mathrm{tunneling}} = -RT\ln(\kappa)$]. We have limited our study to a single temperature (T = 300 K) because, although the first microscopic simulations of the temperature dependence of kinetic isotope effects (KIEs) for enzymic reactions have been presented recently (*7*, *34*, *43*) and are encouraging, they also reflect the difficulties and complexities of addressing this issue computationally.

Despite the shorter initial O1–H1 distance, our simulations show an energetic preference for the transfer to O2 both kinetically ($\Delta G^{\ddagger,\mathrm{classical}}$ = 20.0 kcal mol^{-1} for O1 and $\Delta G^{\ddagger,\mathrm{classical}}$ = 18.1 kcal mol^{-1} for O2) and thermodynamically ($\Delta G^{\mathrm{classical}}_{\mathrm{reaction}}$ = 4.8 kcal mol^{-1} for O1 and $\Delta G^{\mathrm{classical}}_{\mathrm{reaction}}$ = –7.8 kcal mol^{-1} for O2). Breakage of the polarized C–H bond in the AADH:tryptamine adduct is aided by the cationic nature of the iminoquinone and the elevated pK_a [7.1 in free enzyme and 6.0 in the enzyme-substrate complex (*44*)] of Asp^{128}β. The product is stabilized partly by delocalization of the developing negative charge onto the TTQ and partly by hydrogen bonds with the enzyme. The inclusion of H tunneling reduces both barriers by a substantial yet similar amount ($\Delta G^{\ddagger,\mathrm{tunneling}}$ = –4.6 kcal mol^{-1} for O1 and $\Delta G^{\ddagger,\mathrm{tunneling}}$ = –4.9 kcal mol^{-1} for O2), thus not altering the preference for transfer to O2. The experimentally deduced free energy of activation [~12.7 kcal mol^{-1} and k(300) ~ 3500 s^{-1}] therefore agrees well with that calculated for transfer to O2 [13.2 kcal mol^{-1} and k(300) = 1500 s^{-1}] but less well for the much slower transfer to O1 [15.4 kcal mol^{-1} and k(300) = 38 s^{-1}].

As indicated by this $\Delta G^{\ddagger,\mathrm{tunneling}}$ and irrespective of the acceptor oxygen considered, our calculations demonstrate a large H-tunneling component in this proton-transfer step [the catalytic contribution of tunneling cannot be calculated directly here, because this requires comparison with an appropriate reference system (*3*)]. From the calculated transmission factor (*11*), κ, we estimate that in excess of 99.9% of the reaction proceeds via tunneling (i.e., tunneling increases the rate by three orders of magnitude). This suggests that, in the absence of tunneling, C–H bond cleavage (~1 s^{-1}) rather than the oxidative half-reaction (*45*) would be rate limiting in the overall catalytic cycle, emphasizing the critical role of tunneling in this enzyme system. The effect is less pronounced for the deuterated substrate ($\Delta G^{\ddagger,\mathrm{tunneling}}$ = 3.3 kcal mol^{-1} for O1 and $\Delta G^{\ddagger,\mathrm{tunneling}}$ = 3.3 kcal mol^{-1} for O2), resulting in calculated KIEs (42 for O1 and 93 for O2) elevated substantially beyond the semiclassical results (5.0 for O1 and 5.8 for O2, i.e., when no tunneling is considered) and in agreement with the large experimentally observed value (55 ± 6) (Fig. 3A).

Our analysis of tunneling in AADH using computational methods is consistent with our experimental kinetic data obtained by using stopped-flow methods (Fig. 3A and table S1) (*39*). We used dideuterated tryptamine in our kinetic studies. Although secondary KIEs can make substantial contributions to observed KIEs and therefore affect their interpretation, they will have negligible effect in this case, given the highly inflated value of the observed KIE (55 ± 6). A predicted upper value for the secondary KIE is 1.15 for reactions involving a change in hybridization (sp3 to sp2) (*46*), although this might be elevated slightly if there is coupled motion between the primary and α-secondary hydrogens (*47*). Both the

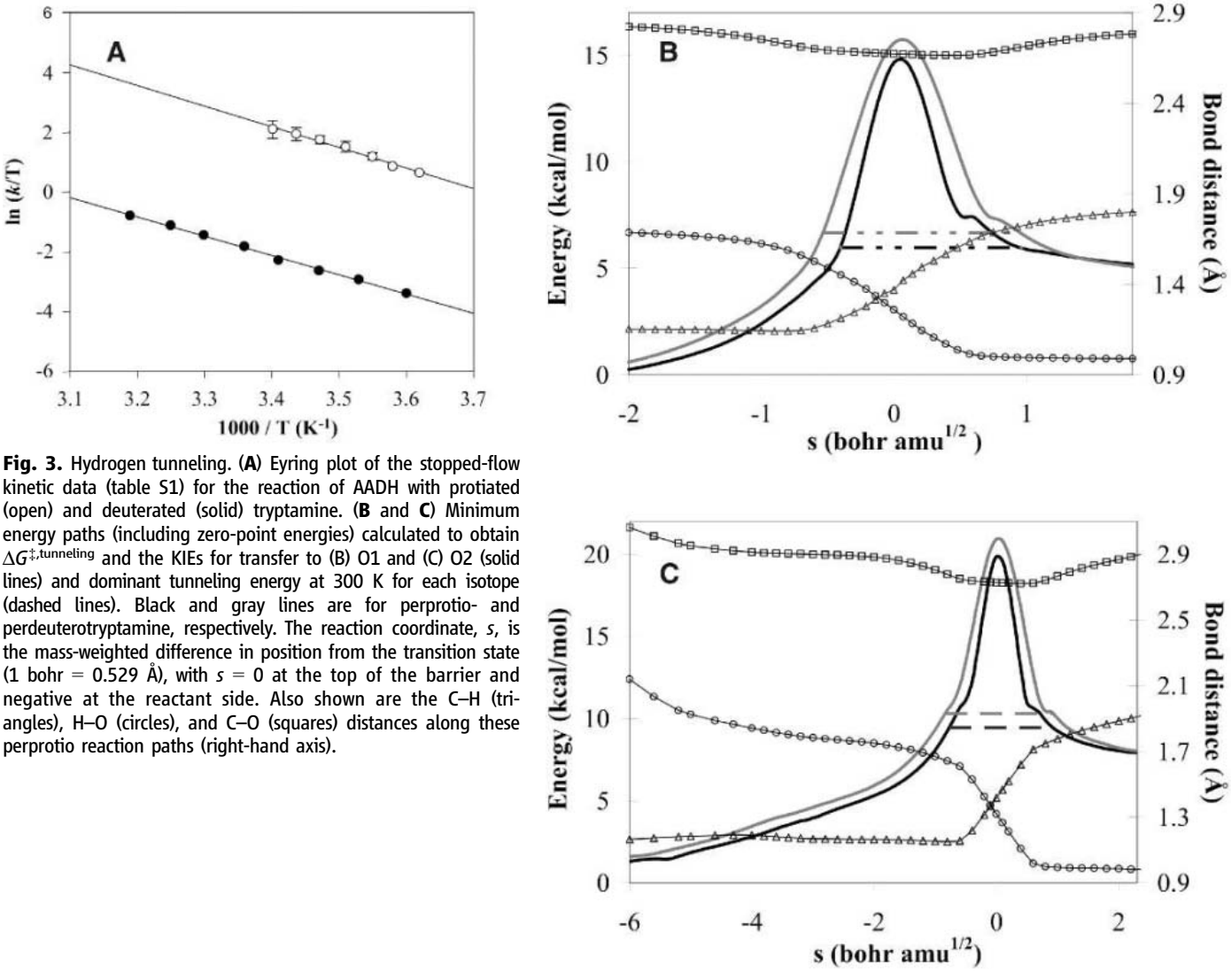

Fig. 3. Hydrogen tunneling. (**A**) Eyring plot of the stopped-flow kinetic data (table S1) for the reaction of AADH with protiated (open) and deuterated (solid) tryptamine. (**B** and **C**) Minimum energy paths (including zero-point energies) calculated to obtain $\Delta G^{\ddagger,\text{tunneling}}$ and the KIEs for transfer to (B) O1 and (C) O2 (solid lines) and dominant tunneling energy at 300 K for each isotope (dashed lines). Black and gray lines are for perprotio- and perdeuterotryptamine, respectively. The reaction coordinate, *s*, is the mass-weighted difference in position from the transition state (1 bohr = 0.529 Å), with $s = 0$ at the top of the barrier and negative at the reactant side. Also shown are the C–H (triangles), H–O (circles), and C–O (squares) distances along these perprotio reaction paths (right-hand axis).

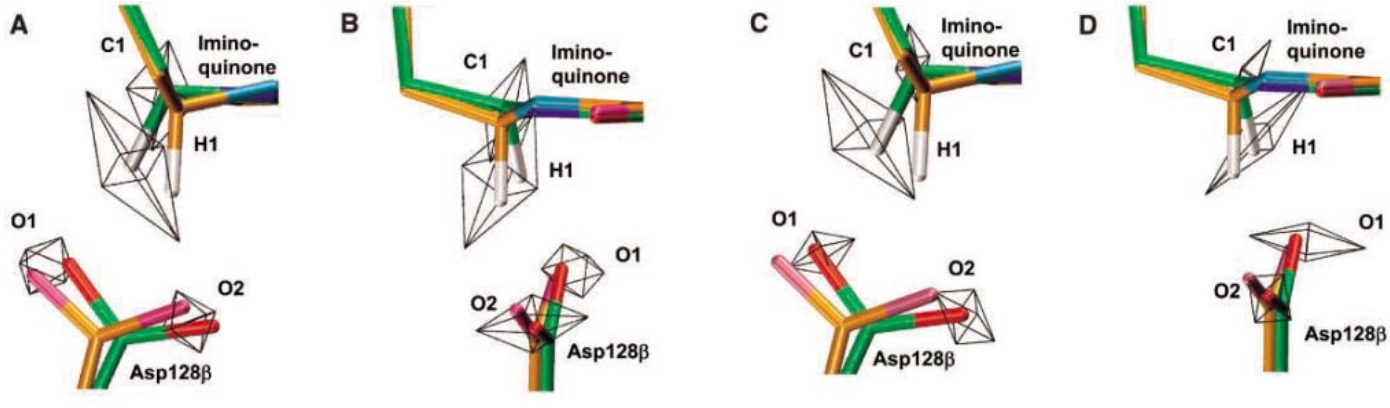

Fig. 4. Orthogonal views (**A** and **B**) illustrating the rotation of the C1 methylene and the movement of the Asp$^{128}\beta$ carboxylate that occurs in passing from reactant (carbon atoms in green) to the representative structure for tunneling to O2 ($s = -0.77$ bohr amu$^{1/2}$ in Fig. 3C; carbon atoms are shown in orange). The cages represent the principal components, scaled according to the respective eigenvalues, for the motion of the respective atom in the molecular dynamics simulation. Percentages of motion along the first principal component are as follows: C1, 48%; H1, 54%; O1, 40%; and O2, 50%. Corresponding orthogonal views (**C** and **D**) illustrating the three-dimensional nature of the vibration at ~165 cm^{-1}. The cages represent the principal components of the motion of the respective atoms after removal, by digital filtering, of motions outside the frequency window of 140 to 190 cm^{-1}.

highly inflated KIE (≫7) and the magnitude of the prefactor ratio (≫1) derived from temperature analysis of reaction rates with protiated and deuterated tryptamine are consistent with H transfer by quantum mechanical tunneling. We infer this temperature-dependent H transfer indicates an environmental reorganization that serves to bring the H energy levels into resonance.

The picture of the reaction emerging from our results is as follows: The reacting moieties first approach by classical activation to a H1–O1 and H1–O2 separation of ~1.51 Å and ~1.64 Å, respectively; before this point (Fig. 3, B and C), the reaction coordinate is dominated by heavy atom motions, especially for the transfer to O2. From this point [s = –0.40 bohr amu$^{1/2}$ for O1 and s =–0.77 bohr amu$^{1/2}$ for O2; the reaction coordinate, s, is the mass-weighted difference in position from the transition state (1 bohr = 0.529 Å), with s = 0 at the top of the barrier and negative at the reactant side], the proton tunnels a distance of ~0.49 Å and ~0.59 Å (for O1 and O2, respectively) through the barrier at a dominant tunneling energy of ~8.7 kcal mol^{-1} (for O1) and ~10.4 kcal mol^{-1} (for O2) below the top of the barrier; proton motion is highly dominant in this region of the reaction coordinate because the proton-donor bond breaks (and the proton tunnels) (Fig. 3, B and C). From the initial complex III structure, with H1 hydrogen bonded to O1, transfer to O2 requires more structural rearrangements to attain a configuration from which the proton can tunnel than does transfer to O1. However, inspection of the classical free energy profile reveals that early in the reaction, the H1–O2 average distance shortens to ~2.0 Å [i.e., more similar to d(O1–H1)] at a relatively low energetic cost (<2 kcal mol^{-1}), in part by maintaining a short O1–H1 distance while shortening the O2–H1 distance. This shortening of the O2–H1 distance is accompanied by repositioning of the Asp^{128}β carboxylate and rotation of the C1 methylene (Fig. 4). Although a recent study with lipoxygenase suggests that such a shortening of the proton-acceptor distance decreases tunneling (*48*), it is generally associated with the promotion of tunneling (*1*).

To investigate further protein motions and in particular those that could reduce the proton-acceptor distance and thereby promote tunneling, we performed molecular dynamics simulations of our modeled complex III. These simulations also suggest that the O2–H1 distance, critical for tunneling, can be shortened by rotation of H1 toward O2 and repositioning of the Asp^{128}β carboxylate; in particular, the motion of H1 is focused on modulating the O2–H1 distance (Fig. 4, A and B). The C1 and H1 spectral densities (*21*, *49*) derived from the dynamics simulations share a common peak at ~165 cm^{-1}, the frequency of a short-range motion that reduces the proton-acceptor distance, predominantly through motion of H1 (Fig. 4, C and D). However, cross-correlation analysis suggests that the motion of H1 is not strongly coupled to O2 (fig. S1, A and B) or any other neighboring atom; this is further supported by principal component analysis of the covariance (table S2). The motion of O2 is (with the use of a low cutoff value of 0.5) only coupled to its hydrogen-bonding partner, Thr^{172}β (fig. S1, C and D). In turn, the motion of Thr^{172}β is additionally only coupled to Cys^{171}β, which is not correlated with O2. Thus, our results show no network of coupled long-range motions that modulate the O2–H1 distance (*50*); modulation of the proton transfer distance in AADH involves only short-range motion.

References and Notes

1. S. J. Benkovic, S. Hammes-Schiffer, *Science* **301**, 1196 (2003).
2. M. Garcia-Viloca, J. Gao, M. Karplus, D. G. Truhlar, *Science* **303**, 186 (2004).
3. J. Villa, A. Warshel, *J. Phys. Chem. B* **105**, 7887 (2001).
4. P. Ball, *Nature* **431**, 396 (2004).
5. J. K. Hwang, Z. T. Chu, A. Yadav, A. Warshel, *J. Phys. Chem.* **95**, 8445 (1991).
6. J. K. Hwang, A. Warshel, *J. Am. Chem. Soc.* **118**, 11745 (1996).
7. M. H. M. Olsson, P. E. M. Siegbahn, A. Warshel, *J. Am. Chem. Soc.* **126**, 2820 (2004).
8. K. M. Doll, B. R. Bender, R. G. Finke, *J. Am. Chem. Soc.* **125**, 10877 (2003).
9. K. M. Doll, R. G. Finke, *Inorg. Chem.* **42**, 4849 (2003).
10. W. Siebrand, Z. Smedarchina, *J. Phys. Chem. B* **108**, 4185 (2004).
11. D. G. Truhlar *et al.*, *Int. J. Quantum Chem.* **100**, 1136 (2004).
12. A. M. Kuznetsov, J. Ulstrup, *Can. J. Chem.* **77**, 1085 (1999).
13. M. J. Knapp, J. P. Klinman, *Eur. J. Biochem.* **269**, 3113 (2002).
14. L. Masgrau, J. Basran, P. Hothi, M. J. Sutcliffe, N. S. Scrutton, *Arch. Biochem. Biophys.* **428**, 41 (2004).
15. C. Alhambra, J. Corchado, M. Sanchez, J. Gao, D. Truhlar, *J. Am. Chem. Soc.* **122**, 8197 (2000).
16. P. F. Faulder *et al.*, *J. Am. Chem. Soc.* **123**, 8604 (2001).
17. C. Alhambra, M. L. Sanchez, J. Corchado, J. L. Gao, D. G. Truhlar, *Chem. Phys. Lett.* **347**, 512 (2001).
18. C. Alhambra, M. L. Sanchez, J. Corchado, J. L. Gao, D. G. Truhlar, *Chem. Phys. Lett.* **355**, 388 (2002).
19. G. Tresadern, H. Wang, P. F. Faulder, N. A. Burton, I. H. Hillier, *Mol. Phys.* **101**, 2775 (2003).
20. P. K. Agarwal, S. R. Billeter, P. T. Rajagopalan, S. J. Benkovic, S. Hammes-Schiffer, *Proc. Natl. Acad. Sci. U.S.A.* **99**, 2794 (2002).
21. S. Caratzoulas, J. S. Mincer, S. D. Schwartz, *J. Am. Chem. Soc.* **124**, 3270 (2002).
22. D. Antoniou, S. D. Schwartz, *J. Phys. Chem. B* **105**, 5553 (2001).
23. J. Basran, M. J. Sutcliffe, N. S. Scrutton, *Biochemistry* **38**, 3218 (1999).
24. J. Basran, S. Patel, M. J. Sutcliffe, N. S. Scrutton, *J. Biol. Chem.* **276**, 6234 (2001).
25. R. J. Harris, R. Meskys, M. J. Sutcliffe, N. S. Scrutton, *Biochemistry* **39**, 1189 (2000).
26. J. Basran, M. J. Sutcliffe, N. S. Scrutton, *J. Biol. Chem.* **276**, 24581 (2001).
27. J. Basran, R. J. Harris, M. J. Sutcliffe, N. S. Scrutton, *J. Biol. Chem.* **278**, 43973 (2003).
28. A. Kohen, R. Cannio, S. Bartolucci, J. P. Klinman, *Nature* **399**, 496 (1999).
29. M. J. Knapp, K. Rickert, J. P. Klinman, *J. Am. Chem. Soc.* **124**, 3865 (2002).
30. W. A. Francisco, M. J. Knapp, N. J. Blackburn, J. P. Klinman, *J. Am. Chem. Soc.* **124**, 8194 (2002).
31. N. Agrawal, B. Hong, C. Mihai, A. Kohen, *Biochemistry* **43**, 1998 (2004).
32. D. G. Truhlar, B. C. Garrett, S. J. Klippenstein, *J. Phys. Chem.* **100**, 12771 (1996).
33. Z. X. Liang, T. Lee, K. A. Resing, N. G. Ahn, J. P. Klinman, *Proc. Natl. Acad. Sci. U.S.A.* **101**, 9556 (2004).
34. J. Z. Pu, S. H. Ma, J. L. Gao, D. G. Truhlar, *J. Phys. Chem. B* **109**, 8551 (2005).
35. Warshel and co-workers realized and demonstrated that an understanding of tunneling requires computer simulations. A recent analysis is presented in (*6*). Others have also made important contributions in this area, and these have been reviewed recently (*2*).
36. M. Mure, S. A. Mills, J. P. Klinman, *Biochemistry* **41**, 9269 (2002).
37. S. Govindaraj *et al.*, *J. Bacteriol.* **176**, 2922 (1994).
38. Y. L. Hyun, V. L. Davidson, *Biochim. Biophys. Acta* **1251**, 198 (1995).
39. Materials and methods are available as supporting material on *Science* Online.
40. A. Warshel, M. Levitt, *J. Mol. Biol.* **103**, 227 (1976).
41. L. Ridder, I. M. C. M. Rietjens, J. Vervoort, A. J. Mulholland, *J. Am. Chem. Soc.* **124**, 9926 (2002).
42. D. G. Truhlar, A. D. Isaacson, B. C. Garret, in *Theory of Chemical Reaction Dynamics*, M. Baer, Ed. (CRC Press, Boca Raton, FL, 1985), vol. IV, pp. 65–136.
43. E. Hatcher, A. V. Soudackov, S. Hammes-Schiffer, *J. Am. Chem. Soc.* **126**, 5763 (2004).
44. P. Hothi, K. A. Khadra, J. P. Combe, D. Leys, N. S. Scrutton, *FEBS J.* **272**, 5894 (2005).
45. Y. L. Hyun, V. L. Davidson, *Biochemistry* **34**, 12249 (1995).
46. J. P. Klinman, *Adv. Enzymol. Relat. Areas Mol. Biol.* **46**, 415 (1978).
47. W. P. Huskey, R. L. Schowen, *J. Am. Chem. Soc.* **105**, 5704 (1983).
48. A. Warshel, M. H. M. Olsson, J. Villa-Freixa, in *Isotope Effects in Chemistry and Biology*, A. Kohen, H. H. Limbach, Eds. (CRC Press, Boca Raton, FL, 2006), pp. 621–644.
49. A. Warshel, Z. T. Chu, W. W. Parson, *Science* **246**, 112 (1989).
50. We cannot rule out a possible role for long-range motions in causing fluctuations in electrostatic interactions that control the energy difference between reactants and products; see, for example, (*48*).

51. This work was supported by the Lister Institute of Preventive Medicine (NSS), by the Biotechnology and Biological Sciences Research Council (BBSRC), and by the Engineering and Physical Sciences Research Council (EPSRC). A.J.M. thanks the IBM High Performance Computing Life Sciences Outreach Programme for support. M.J.S. gratefully acknowledges use of the University of Leicester Mathematical Modelling Centre's supercomputer, which was purchased through the EPSRC Strategic Equipment Initiative. D.L. is a Royal Society University Research Fellow and a European Molecular Biology Organisation (EMBO) Young Investigator. We gratefully acknowledge access to European Synchrotron Radiation Facility and to EMBL–Deutches Electronen Synchrotron beamlines with support from the European Community contract number RII3/CT/2004/5060008. Atomic coordinates and structure factor amplitudes have been deposited in the Protein Data Bank (PDB) (accession codes: 2AH1 for the free enzyme; 2AGL for the phenylhydrazine adduct; 2AGY and 2AGX for the Schiff-base intermediate in the form A and B crystals, respectively; 2AHO and 2AGZ for the carbinolamine intermediate in the form A and C crystals, and 2AGW for the tryptamine-reduced AADH).

Supporting Online Material

www.sciencemag.org/cgi/content/full/312/5771/237/DC1
Materials and Methods
SOM Text
Figs. S1 and S2
Tables S1 to S4

9 February 2006; accepted 20 March 2006
10.1126/science.1126002

Piezoelectric Nanogenerators Based on Zinc Oxide Nanowire Arrays

Zhong Lin Wang[1,2,3]* and Jinhui Song[1]

We have converted nanoscale mechanical energy into electrical energy by means of piezoelectric zinc oxide nanowire (NW) arrays. The aligned NWs are deflected with a conductive atomic force microscope tip in contact mode. The coupling of piezoelectric and semiconducting properties in zinc oxide creates a strain field and charge separation across the NW as a result of its bending. The rectifying characteristic of the Schottky barrier formed between the metal tip and the NW leads to electrical current generation. The efficiency of the NW-based piezoelectric power generator is estimated to be 17 to 30%. This approach has the potential of converting mechanical, vibrational, and/or hydraulic energy into electricity for powering nanodevices.

Wireless devices may allow in situ, real-time biomedical monitoring and detection, but such devices still require a power source. Ideally, such devices should be self-powered and not dependent on a battery. The body provides numerous potential power sources: mechanical energy (such as body movement, muscle stretching, blood vessel contraction), vibrational energy (acoustic waves), chemical energy (glucose), and hydraulic energy (body fluid and blood flow), but the challenge is their efficient conversion into electrical energy. If accomplished on the nanoscale, such power sources could greatly reduce the size of integrated nanosystems for optoelectronics (*1*), biosensors (*2*), resonators (*3*), and more.

We demonstrate an approach to converting mechanical energy into electric power with the use of aligned zinc oxide (ZnO) nanowires (NWs). The mechanism of the power generator relies on the coupling of piezoelectric and semiconducting properties of ZnO as well as the formation of a Schottky barrier between the metal and ZnO contacts. The nanogenerator has the potential of harvesting energy from the environment for self-powered nanotechnology.

Among the known one-dimensional (1D) nanomaterials, ZnO has three key advantages. First, it exhibits both semiconducting and piezoelectric (PZ) properties that can form the basis for electromechanically coupled sensors and transducers. Second, ZnO is relatively biosafe and biocompatible (*4*), and it can be used for biomedical applications with little toxicity. Finally, ZnO exhibits the most diverse and abundant configurations of nanostructures known so far, such as NWs (*5*), nanobelts (NBs) (*6*), nanosprings (*7*), nanorings (*8*), nanobows (*9*), and nanohelices (*10*). Although numerous studies have demonstrated novel nanodevices and applications based on NWs and NBs, little work has been done to address the power needs of these nanosystems.

Our study is based on aligned ZnO nanowires grown on *c* plane–oriented α-Al_2O_3 substrate, using Au particles as a catalyst, by the vapor-liquid-solid (VLS) process (*11*, *12*). An epitaxial relation between ZnO and α-Al_2O_3 allows a thin, continuous layer of ZnO to form at the substrate, which serves as a large electrode connecting the NWs with a metal electrode for transport measurement (Fig. 1A). The NW grows along the [0001] direction and has side surfaces of $\{01\bar{1}0\}$ (Fig. 1B). Most of the Au particles at the tips of the NWs either evaporate during the growth or fall off during scanning by the atomic force microscope (AFM) tip (fig. S1). For most of the NWs, the growth front is free of Au particles or has a small hemispherical Au particle that covers only a fraction of the top (inset, Fig. 1B). For the purpose of our measurements, we have grown NW arrays that have relatively less density and shorter length (0.2 to 0.5 μm), so that the AFM tip can exclusively reach one NW without touching another.

The measurements were performed by AFM using a Si tip coated with Pt film, which has a cone angle of 70°. The rectangular cantilever had a calibrated normal spring constant of 0.76 N/m (Fig. 1C). In the AFM contact mode, a constant normal force of 5 nN was maintained between the tip and sample surface. The tip scanned over the top of the ZnO NW, and the tip's height was adjusted according to the surface morphology and local contacting force. The thermal vibration of the NWs at room temperature was negligible. For the electric contact at the bottom of the nanowires, silver paste was applied to connect the (large) ZnO film on the substrate surface with the measurement circuit. The output voltage across an outside load of

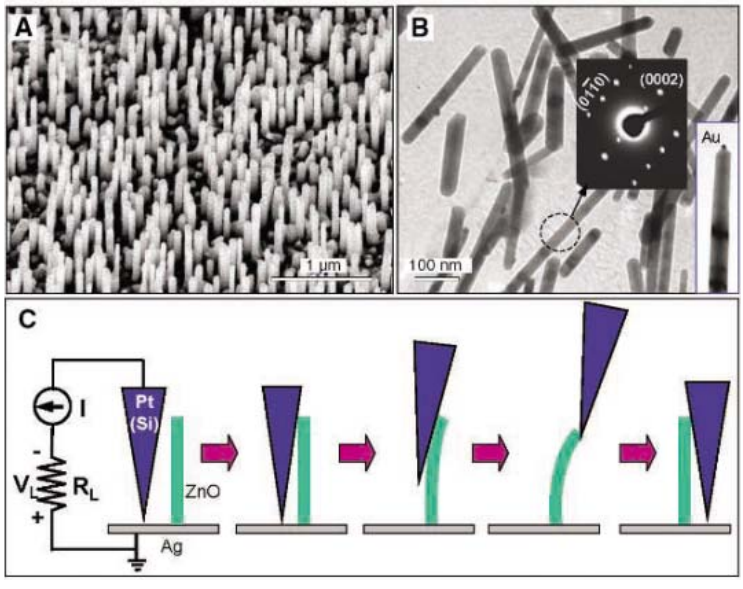

Fig. 1. Experimental design for converting nanoscale mechanical energy into electrical energy by a vertical piezoelectric (PZ) ZnO NW. (**A**) Scanning electron microscopy images of aligned ZnO NWs grown on α-Al_2O_3 substrate. (**B**) Transmission electron microscopy images of ZnO NWs, showing the typical structure of the NW without an Au particle or with a small Au particle at the top. Each NW is a single crystal and has uniform shape. Inset at center: an electron diffraction pattern from a NW. Most of the NWs had no Au particle at the top. Inset at right: image of a NW with an Au particle. (**C**) Experimental setup and procedures for generating electricity by deforming a PZ NW with a conductive AFM tip. The base of the NW is grounded and an external load of R_L is applied, which is much larger than the resistance R_s of the NW. The AFM scans across the NW arrays in contact mode.

[1]School of Materials Science and Engineering, Georgia Institute of Technology, Atlanta, GA 30332, USA. [2]Department of Advanced Materials and Nanotechnology, College of Engineering, Peking University, Beijing 100871, China. [3]National Center for Nanoscience and Technology, Beijing 100080, China.

*To whom correspondence should be addressed. E-mail: zhong.wang@mse.gatech.edu

resistance R_L = 500 megohms was continuously monitored as the tip scanned over the nanowires (note the defined polarity of the voltage signal). No external voltage was applied in any stage of the experiment.

Experimentally, both the topography (feedback signal from the scanner) (Fig. 2A) and the corresponding output voltage (V_L) images across the load (Fig. 2B) were recorded simultaneously when the AFM tip was scanned over the aligned NW arrays. In contact mode, as the tip scanned over the vertically aligned NWs, the NWs were bent consecutively. The bending distance was directly recorded in the topography image, from which the maximum bending deflection distance and the elastic modulus of the NW as well as the density of NWs that have been scanned by the tip were directly derived (*13*).

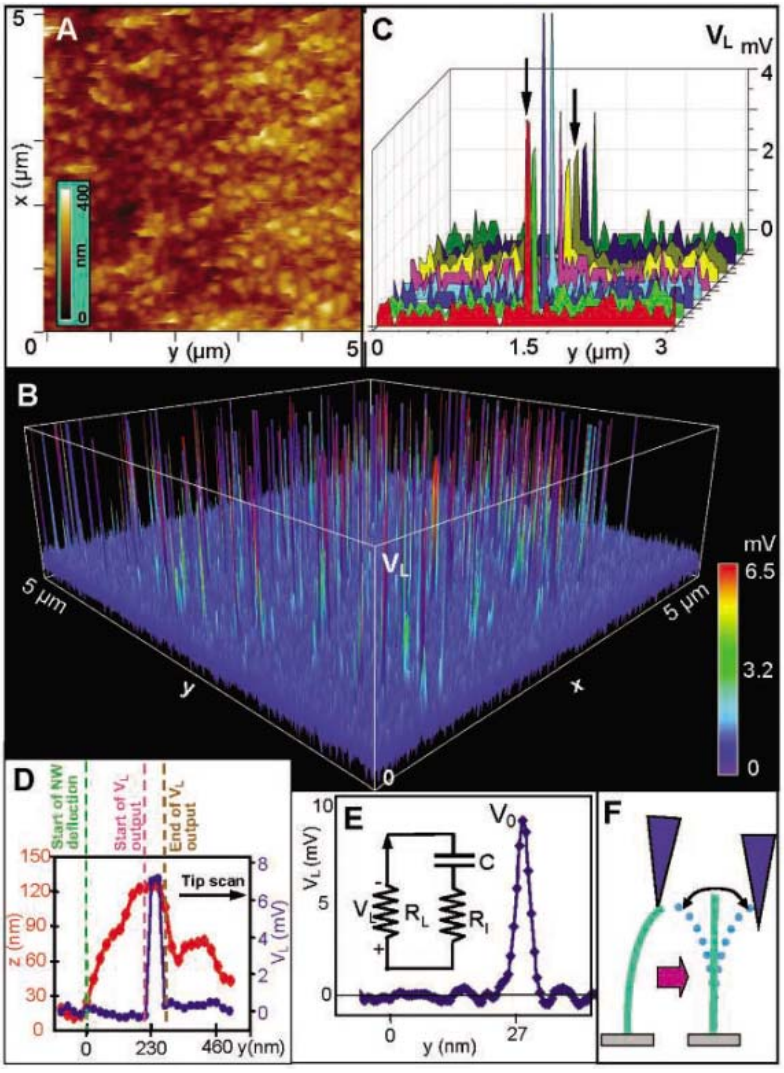

Fig. 2. Electromechanically coupled discharging process of aligned piezoelectric ZnO NWs observed in contact mode. (**A** and **B**) Topography image (A) and corresponding output voltage image (B) of the NW arrays. The discharging process was so rapid that each discharge event was characterized by only a couple of data points, which made it difficult to display the data by rainbow color (see fig. S2). (**C**) A series of line profiles of the voltage output signal when the AFM tip scanned across a vertical NW at a time interval of 1 min. The data show the registration of the electric signal with the location of the NW and the reproducibility of the event over an extended period of time. Colors represent the outputs required for a series of scans. In (A) to (C), the scanning speed of the tip was 12.081 μm/s, and the time spent to acquire and output one scan point was 2 ms. (**D**) Line profiles from the topography (red) and output voltage (blue) images across a NW. The peak of the voltage output corresponds approximately to the maximum deflection of the NW, indicating that the discharge occurs when the tip is in contact with the compressed side of the NW. When the tip touches the NW, PZ charges start to accumulate but no discharge occurs. Discharge occurs when the deflection reaches nearly the maximum y_m. Note that the lateral deflection y includes the shape and contact geometry of the tip, which must be subtracted to derive the true deflection of the NW. (**E**) Line profile of the voltage output signal when the AFM tip scans across a vertical NW at 12.394 μm/s. The time spent to acquire and output one scan point was 0.05 ms, which was achieved at the maximum scan frequency of the AFM. The inset is an equivalent circuit of the measurement to be used for simulating the discharging process. (**F**) The resonance vibration of a NW after being released by the AFM tip, showing that the stored elastic energy is transferred mainly into vibrational energy after creating the PZ discharge event.

In the V_L image, many sharp output peaks (like discharge peaks) were observed. These peaks, typically about 4 to 50 times the noise level, are rather sharp and narrow, and sometimes one or two pixels represent one voltage peak because of the limited scanning speed of the AFM tip, so that the color distribution in the plot is not easy to display (fig. S2). By reducing the scan range and increasing the scan frequency, more complete profiles of the discharge peaks were captured (fig. S3). Most of the voltage peaks are ~6 to 9 mV in height. The density of NWs contacted by the tip is counted from Fig. 2A to be ~20/μm^2, and the average density of NWs whose voltage output events had been captured by the tip in Fig. 2B is ~8/μm^2, thus ~40% of the NWs were contacted.

The location of the voltage peak is directly registered at the site of the NW. A time series of the voltage output line profiles across one NW acquired at a time interval of 1 min is shown in Fig. 2C. Because the dwell time for each data point (or pixel) is 2 ms, which is longer than the average lifetime of the voltage peak of ~0.6 ms (Fig. 2D), the peak at which V_L reached the maximum was possibly missed by the "slow" scanning tip, so that V_L shows a chopped top (arrows in Fig. 2C). A sharp peak can be identified continuously at the location of the NW and in the NW output voltage in each scan of the tip. When the tip started to deflect the NW, no voltage output was observed (Fig. 2D); V_L was detected when the deflection of the NW approached its maximum. When the NW was released by the AFM tip, V_L dropped to zero, indicating that the output of piezoelectricity was detected toward the end of the AFM scan over the NW.

The shape of the discharge peak can be further improved and analyzed by maximizing the tip scanning frequency and reducing the scanning range. Shown in Fig. 2E is a line profile of V_L when the tip was scanned over a single NW at a scanning velocity of 12.394 μm/s. The full width at half maximum (FWHM) of the voltage peak was estimated to be $\tau \sim 0.6$ ms. The damping behavior of the voltage peak can be qualitatively described with an equivalent circuit (*14*) (Fig. 2E). The NW is approximated as a resistor R_I and a capacitor C (including the contribution from the system). The lifetime of the output voltage V_L across the load R_L (note the polarity of the voltage) is $\tau = (R_L + R_I)C$ (*15*). For the experiment we have designed, the resistance of the NW R_I is negligible relative to R_L (*16*, *17*). Thus, the equivalent capacitance of the NW and the system is $C \approx \tau/R_L \approx 1.2$ pF.

The observed sharp voltage output for ZnO NWs was not observed for metal film (fig. S4), aligned carbon nanotubes (fig. S5), or aligned WO_3 NWs (fig. S6) under identical or similar experimental conditions. These data rule out the possibility of friction or contact potential as the source of the observed V_L response.

The efficiency of the electric power generated by this process can be calculated as follows. The output electrical energy from one NW in one piezoelectric discharge (PZD) event is $\Delta W_{PZD} = V_0^2 C/2$ (*15*), where V_0 is the peak voltage of the discharge output. For simplicity, we approximately take the NW as a 2D object for easy analytical calculation. The elastic deformation energy (W_{ELD}) created by the AFM tip for displacing the NW is $W_{ELD} = 3YIy_m^2/2L^3$ (*15*), where Y is the elastic modulus, I is the moment of inertia, L is the length of the NW, and y_m is the maximum deflection of the NW. Dissipation of W_{ELD} mainly occurs in three ways: (i) mechanical resonance/vibration after releasing the NW (Fig. 2F); (ii) PZ discharge (ΔW_{PZD}) for each cycle of the vibration; and (iii) friction/viscosity from the environmental medium. The mechanical resonance of the NW continues for many cycles, but it is eventually damped by the viscosity of the medium. Each cycle of the vibration generates ΔW_{PZD}, but the AFM tip in the present experimental design catches only the energy generated in the first cycle of vibration. Taking into account the energy dissipated by the NW in the first cycle of vibration ΔW_{ELD} (*15*), the efficiency of converting mechanical energy to electrical energy is $\Delta W_{PZD}/\Delta W_{ELD}$. Therefore, an efficiency of 17 to 30% has been received for a cycle of the resonance (table S1). The large efficiency is likely due to the extremely large deformation that can be borne by the nanowire (*18*).

The physical principle for creating the PZ discharge energy arises from how the piezoelectric and semiconducting properties of ZnO are coupled. For a vertical, straight ZnO NW (Fig. 3A), the deflection of the NW by an AFM tip creates a strain field, with the outer surface being stretched (positive strain ε) and the inner surface compressed (negative ε) (Fig. 3B). An electric field E_z along the NW (z direction) is then created inside the NW volume through the PZ effect, $E_z = \varepsilon_z/d$, where d is the PZ coefficient (*19*) along the NW direction that is normally the positive c axis of ZnO, with the Zn atomic layer being the front-terminating layer (*20*, *21*). The PZ field direction is closely parallel to the z axis (NW direction) at the outer surface and antiparallel to the z axis at the inner surface (Fig. 3C). Under the first-order approximation, across the width of the NW at the top end, the electric potential distribution from the compressed to the stretched side surface is approximately between V_s^- to V_s^+ [with $V_s^\mu = \mu 3T|y_m|/4Ld$ (*15*), where T is the thickness of the NW). The electrode at the base of the NW is grounded. Note that V_s^+ and V_s^- are the voltages produced by the PZ effect, which are each typically larger than a few tens of volts (*22*). The potential is created by the relative displacement of the Zn^{2+} cations with respect to the O^{2-} anions, a result of the PZ effect in the wurtzite crystal structure; thus, these ionic charges cannot freely move and cannot recombine without releasing the strain (Fig. 3D). The potential difference is maintained as long as the deformation is in place and no foreign free charges (such as from the metal contacts) are injected.

The contacts at the top and the base of the NW are nonsymmetric; the bottom contact is to the ZnO film in contact with Ag paste, so the effective contact is between ZnO and Ag. The electron affinity (E_a) of ZnO is 4.5 eV (*23*) and the work function (ϕ) of Ag is 4.2 eV; there is no barrier at the interface, so the ZnO-Ag contact is ohmic. At the tip of the NW, Pt has ϕ = 6.1 eV, and the Pt-ZnO contact is a Schottky barrier (*24*, *25*) and dominates the entire transport process. Because the compressed side of the semiconductor ZnO NW has negative potential V_s^- and the stretched side has positive potential (V_s^+), two distinct transport processes will occur across the Schottky barrier.

We now consider the case of a ZnO NW without an Au particle at the top. In the first step, the AFM conductive tip that induces the deformation is in contact with the stretched surface of positive potential V_s^+ (Fig. 3, D and E). The Pt metal tip has a potential of nearly zero, $V_m = 0$, so the metal tip–ZnO interface is negatively biased for $\Delta V = V_m - V_s^+ < 0$. Because the as-synthesized ZnO NWs behave as n-type semiconductors, the Pt metal–ZnO semiconductor (M-S) interface in this case is a reverse-biased Schottky diode (Fig. 3E), and little current flows across the interface. In the second step, when the AFM tip is in contact with the compressed side of the NW (Fig. 3F), the metal tip–ZnO interface is positively biased for $\Delta V = V_L = V_m - V_s^- > 0$. The M-S interface in this

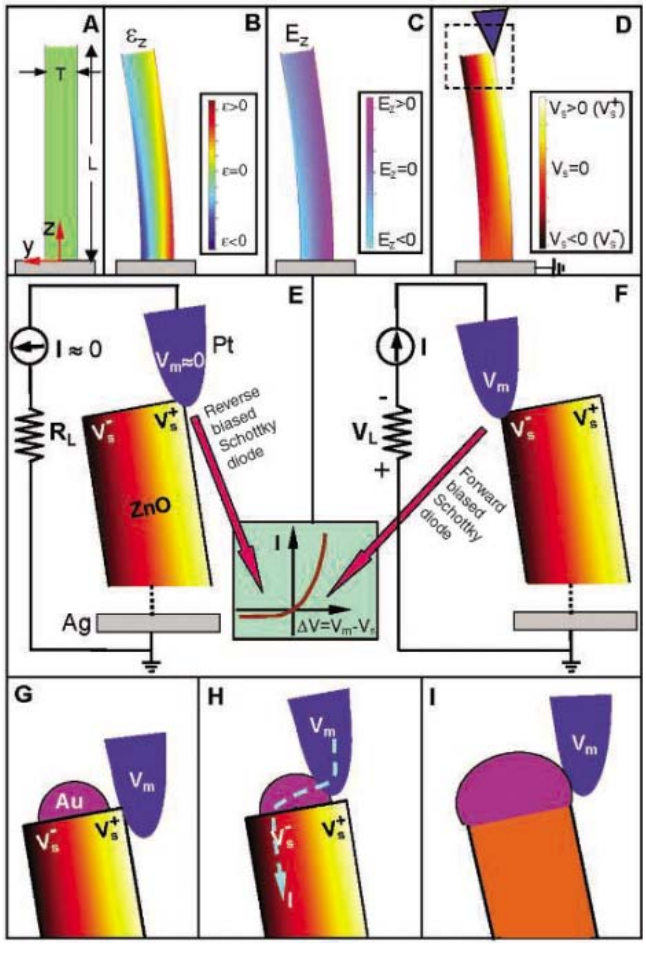

Fig. 3. Transport is governed by a metal-semiconductor Schottky barrier for the PZ ZnO NW (see movies S1 and S2). (**A**) Schematic definition of a NW and the coordination system. (**B**) Longitudinal strain ε_z distribution in the NW after being deflected by an AFM tip from the side. The data were simulated by FEMLAB for a ZnO NW of length 1 μm and an aspect ratio of 10. (**C**) The corresponding longitudinal PZ-induced electric field E_z distribution in the NW. (**D**) Potential distribution in the NW as a result of the PZ effect. (**E** and **F**) Contacts between the AFM tip and the semiconductor ZnO NW [boxed area in (D)] at two reversed local contact potentials (positive and negative), showing reverse- and forward-biased Schottky rectifying behavior, respectively (see text). This oppositely biased Schottky barrier across the NW preserves the PZ charges and later produces the discharge output. The inset shows a typical current-voltage (*I-V*) relation characteristic of a metal-semiconductor (n-type) Schottky barrier. The process in (E) is to separate and maintain the charges as well as build up the potential. The process in (F) is to discharge the potential and generates electric current. (**G** and **H**) Contact of the metal tip with a ZnO NW with a small Au particle at the top. The PZ potential is built up in the displacing process (G), and later the charges are released through the compressed side of the NW (H). (**I**) Contact of the metal tip with a ZnO NW with a large Au particle at the top. The charges are gradually "leaked" out through the compressed side of the NW as soon as the deformation occurs; thus, no accumulated potential will be created.

case is a positively biased Schottky diode, and it produces a sudden increase in the output electric current. The current is the result of ΔV-driven flow of electrons from the semiconductor ZnO NW to the metal tip. The flow of the free electrons from the loop through the NW to the tip will neutralize the ionic charges distributed in the volume of the NW and thus will reduce the magnitudes of the potential V_s^- and V_s^+. Thus, V_L starts to drop and reaches zero after all of the ionic charges in the NW are fully neutralized. This mechanism explains why the discharge curve in Fig. 2E is nearly symmetric. According to the model, the discharge occurs when the NW is bent nearly to its maximum deflection, so V_L should have a small offset in reference to the corresponding topography peak along the direction of tip scan, as is observed experimentally in Fig. 2D.

We next consider the case of a ZnO NW with a small Au particle at the top as a result of VLS growth (Fig. 3, G and H). In the first step of the AFM tip displacing the NW, the tip is directly in contact with the ZnO NW but not the Au particle (Fig. 3G) because of its small size and hemispherical shape (Fig. 1B and fig. S1). A process similar to that described in Fig. 3E occurs, and no output voltage will be observed. When the tip is in contact with the Au particle, the tip is integrated with the particle as one metal contact, and at the local interface between the Au particle and the negatively charged, compressed side of the ZnO NW (V_s^-), a forward-biased Schottky diode is formed; thus, the current flows from the tip through the Au particle to the interface region with negative PZ voltage (V_s^-) (Fig. 3H). A discharge process similar to that shown in Fig. 3F occurs, and a sharp voltage output is produced.

In the case of a NW with a large Au particle that fully covers its top (Fig. 3I), the metal tip is directly in touch with the Au tip at the beginning of the forced displacement. Because of the conducting channel at the compressed side of the NW, the polar charges produced by the displaced Zn^{2+} and O^{2-} ions caused by the PZ effect are immediately neutralized by external free charges as soon as they are produced by the deformation. Therefore, no accumulative potential profile is formed at the M-S interface, and no measurable output voltage is detected in the experimental setup we have designed (Fig. 1C).

We also measured the PZ voltage output for the same samples of aligned ZnO NWs in the AFM tapping mode. In this case, the deformation occurred longitudinally and there was no side displacement. The NW was vertically compressed, so the voltage created at the top of the NW was negative V_s^- so long as the base electrode was grounded (Fig. 4A). There was no voltage drop across the width of the NW. Thus, across the metal tip–ZnO interface, a positively biased Schottky diode formed and the electrons could freely flow across the interface. Electrons flowed as the deformation occurred, and there was no accumulation of net charge in the NW volume. This type of slowly "leaked" current produces no detectable signal. Therefore, for the ZnO NWs whose AFM image in tapping mode is shown in Fig. 4B, no output voltage V_L was detected beyond the noise level (Fig. 4C).

We now estimate the possibility of powering nanodevices with the NW-based power generator. From table S1, the PZ energy output by one NW in one discharge event is ~0.05 fJ, and the output voltage on the load is ~8 mV. For a NW of typical resonance frequency ~10 MHz, the output power of the NW would be ~0.5 pW. If the density of NWs per unit area on the substrate is 20/μm², the output power density is ~10 pW/μm². By choosing a NW array of size 10 μm × 10 μm, the power generated may be enough to drive a single NW/NB/nanotube-based device (*26*–*28*). If we can find a way to induce the resonance of a NW array and output the PZ-converted power generated in each cycle of the vibration, a significantly strong power source may be possible for self-powering nanodevices. Furthermore, if the energy produced by acoustic waves, ultrasonic waves, or hydraulic pressure/force could be harvested, electricity could be generated by means of ZnO NW arrays grown on solid substrates or even on flexible polymer films (*29*). The principle and the nanogenerator demonstrated could be the basis for new self-powering nanotechnology that harvests electricity from the environment for applications such as implantable biomedical devices, wireless sensors, and portable electronics (*29*).

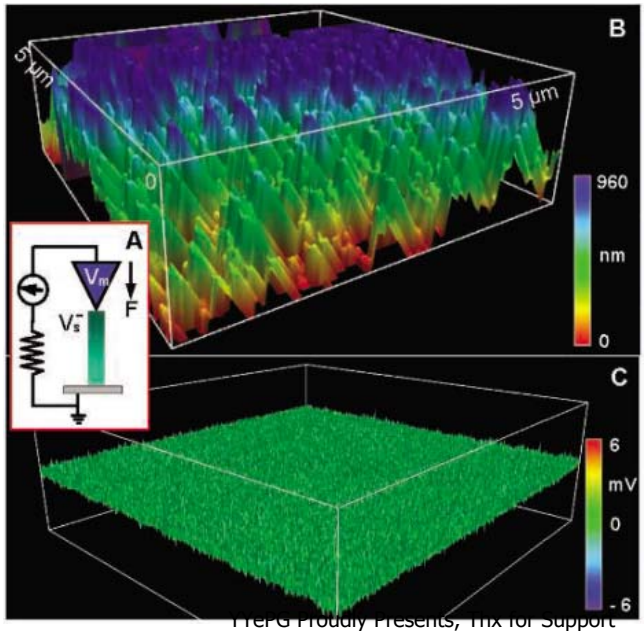

Fig. 4. Electromechanically coupled discharging process of aligned piezoelectric ZnO NWs observed in tapping mode. (**A**) Experimental setup. (**B** and **C**) Topography image (B) and corresponding output voltage image (C) of the NWs. The tapping force was 5 nN, tapping frequency 68 KHz, and tapping speed 6 μm/s. The voltage output contains no information but noise, proving the physical mechanism demonstrated in Fig. 3.

References and Notes

1. X. F. Duan, Y. Huang, R. Agarwal, C. M. Lieber, *Nature* **421**, 241 (2003).
2. G. F. Zheng, F. Patolsky, Y. Cui, W. U. Wang, C. M. Lieber, *Nat. Biotechnol.* **23**, 1294 (2005).
3. X. D. Bai, P. X. Gao, Z. L. Wang, E. G. Wang, *Appl. Phys. Lett.* **82**, 4806 (2003).
4. J. Zhou, N. S. Xu, Z. L. Wang, unpublished data.
5. M. H. Huang *et al.*, *Adv. Mater.* **13**, 113 (2001).
6. Z. W. Pan, Z. R. Dai, Z. L. Wang, *Science* **291**, 1947 (2001).
7. X. Y. Kong, Z. L. Wang, *Nano Lett.* **3**, 1625 (2003).
8. X. Y. Kong, Y. Ding, R. Yang, Z. L. Wang, *Science* **303**, 1348 (2004).
9. W. L. Hughes, Z. L. Wang, *J. Am. Chem. Soc.* **126**, 6703 (2004).
10. P. X. Gao *et al.*, *Science* **309**, 1700 (2005).
11. X. D. Wang, C. J. Summers, Z. L. Wang, *Nano Lett.* **3**, 423 (2004).
12. X. D. Wang *et al.*, *J. Am. Chem. Soc.* **127**, 7920 (2005).
13. J. H. Song, X. D. Wang, E. Riedo, Z. L. Wang, *Nano Lett.* **5**, 1954 (2005).
14. A piezoelectric material can be approximately characterized by a capacitor and a resistor. The capacitor represents the piezoelectric charges accumulated in the volume, and the resistor represents its inner resistance.
15. See supporting material on *Science* Online.
16. From our recent measurements of ZnO nanowires, the resistivity is from 10^{-2} to 10 ohm·cm (*17*) depending on the contacts at the electrodes and the concentration of oxygen vacancies. For a NW of length 0.2 μm and diameter 40 nm, the resistance is between 16 kilohms and 16 megohms, which is much smaller than the applied external load of 500 megohms. Here we ignored the resistance produced by the ZnO film at the bottom of the nanowires because it is very large and covers the entire area of the substrate; thus, the inner resistance is dominated by the NW.
17. J. H. He, C. S. Lao, L. J. Chen, D. Davidovic, Z. L. Wang, *J. Am. Chem. Soc.* **127**, 16376 (2005).
18. W. L. Hughes, Z. L. Wang, *Appl. Phys. Lett.* **86**, 043106 (2005).
19. M. H. Zhao, Z. L. Wang, S. X. Mao, *Nano Lett.* **4**, 587 (2004).
20. The wurtzite-structured ZnO can be described as a number of alternating planes composed of tetrahedrally coordinated O^{2-} and Zn^{2+} ions stacked alternatively along the *c* axis. The oppositely charged ions produce positively charged (0001)-Zn and negatively charged $(000\bar{1})$-O polar surfaces. The Zn-terminated surface is at the growth front (positive *c*-axis direction) because of its higher catalytic activity (*19*).
21. Z. L. Wang, X. Y. Kong, J. M. Zuo, *Phys. Rev. Lett.* **91**, 185502 (2003).

22. A simple calculation indicates that the magnitudes of V_s^+ and V_s^- are on the order of a few tens to hundreds of volts. In practice, if we consider the polarization and dielectric screening in the calculation, the local potential is much smaller than the numbers given by the equations here. An accurate calculation of the potential distribution as a result of the ionic charges introduced by the PZ effect and the surface charges caused by boundaries must be solved numerically and self-consistently. In our analysis, a correct magnitude and sign of the potential is sufficient for illustrating the physical model.
23. S. Hasegawa, S. Nishida, T. Yamashita, H. Asahi, *J. Ceramic Proc. Res.* **6**, 245 (2005).
24. R. F. Pierret, *Semiconductor Device Fundamentals* (Addison-Wesley, Reading, MA, 1996), chapter 14.
25. W. I. Park, G. C. Yi, J. W. Kim, S. M. Park, *Appl. Phys. Lett.* **82**, 4358 (2003).
26. Y. Huang *et al.*, *Science* **294**, 1313 (2001).
27. A. Bachtold, P. Hadley, T. Nakanishi, C. Dekker, *Science* **294**, 1317 (2001); published online 4 October 2001 (10.1126/science.1065824).
28. J. Chen *et al.*, *Science* **310**, 1171 (2005).
29. U.S. patent pending.
30. Supported by NSF grant DMR 9733160, the NASA Vehicle Systems Program and Department of Defense Research and Engineering, and the Defense Advanced Research Projects Agency. We thank X. Wang, W. L. Hughes, J. Zhou, and J. Liu for their help.

Supporting Online Material
www.sciencemag.org/cgi/content/full/312/5771/242/DC1
SOM Text
Figs. S1 to S6
Table S1
Movies S1 and S2

19 December 2005; accepted 10 March 2006
10.1126/science.1124005

Control of Electron Localization in Molecular Dissociation

M. F. Kling,[1] Ch. Siedschlag,[1] A. J. Verhoef,[2] J. I. Khan,[1] M. Schultze,[2] Th. Uphues,[3] Y. Ni,[1] M. Uiberacker,[4] M. Drescher,[3,5] F. Krausz,[2,4] M. J. J. Vrakking[1]

We demonstrated how the subcycle evolution of the electric field of light can be used to control the motion of bound electrons. Results are presented for the dissociative ionization of deuterium molecules ($D_2 \rightarrow D^+ + D$), where asymmetric ejection of the ionic fragment reveals that light-driven intramolecular electronic motion before dissociation localizes the electron on one of the two D^+ ions in a controlled way. The results extend subfemtosecond electron control to molecules and provide evidence of its usefulness in controlling reaction dynamics.

Few-cycle laser light with a controlled evolution of the electric field $E(t) = a(t) \times \cos(\omega t + \varphi)$, with amplitude $a(t)$, frequency ω, and carrier envelope phase φ (*1*), has recently allowed the steering of the motion of electrons in and around atoms on a subfemtosecond time scale. Manifestations of this control include the reproducible generation and measurement of single subfemtosecond pulses (*2*, *3*) and controlled electron emission from atoms (*4*, *5*). Here we address the question of whether this control can be extended to electron wave packets in molecules and, if so, can light-field–driven electronic motion affect reaction dynamics?

Many of the processes in terms of which strong-field molecular interactions are presently interpreted (such as bond softening and enhanced ionization) were discovered in experimental and theoretical work on H_2 and its isotopes HD and D_2 [see (*6*) and references therein]. The role of phase control in the dissociation of hydrogen has recently been addressed in a few theoretical studies (*7*–*9*). We present experiments on the dissociation of D_2^+ into $D^+ + D$ by intense few-cycle laser pulses with controlled field evolution and report a pronounced dependence of the direction of the D^+ ejection (and hence of the localization of the electron in the system) on the waveform driving the reaction. Quantum-classical computations reveal that light-field control of molecular electron dynamics is responsible for the observed phenomenon.

The dynamics of molecules in intense laser fields typically includes ionization and dissociation. The dissociation of D_2 in intense laser fields is known to involve several pathways whose relative importance depends on intensity and pulse duration (*6*). The formation of fragment ions occurs via a two-step mechanism (Fig. 1A) in which initially the molecule is ionized by the laser field (Fig. 1A, red arrow) and a vibrational wave packet is launched in the $1s\sigma_g^+$ state. Breakup of the D_2^+ ion is triggered by excitation to a repulsive state or after double ionization.

In the single-ionization pathways, excitation of bound D_2^+ (such as to the $2p\sigma_u^+$ state in Fig. 1A) by recollision of the first electron [recollision excitation (RCE), green line] or directly by the laser field [sequential excitation (SE), blue line] leads to dissociation and the formation of a D^+ ion and a D atom. For example, in recent molecular clock studies, vibrational motion in D_2^+ was time-resolved by exploiting RCE (*10*, *11*). Additional dissociation mechanisms can be understood by considering that molecular potentials are modified by strong laser fields. Bond softening (BS, purple line) (*12*) occurs when energy gaps open up at avoided crossings between adiabatic field-dressed potential energy curves.

In double-ionization pathways, the formation of D_2^+ is followed by a second ionization

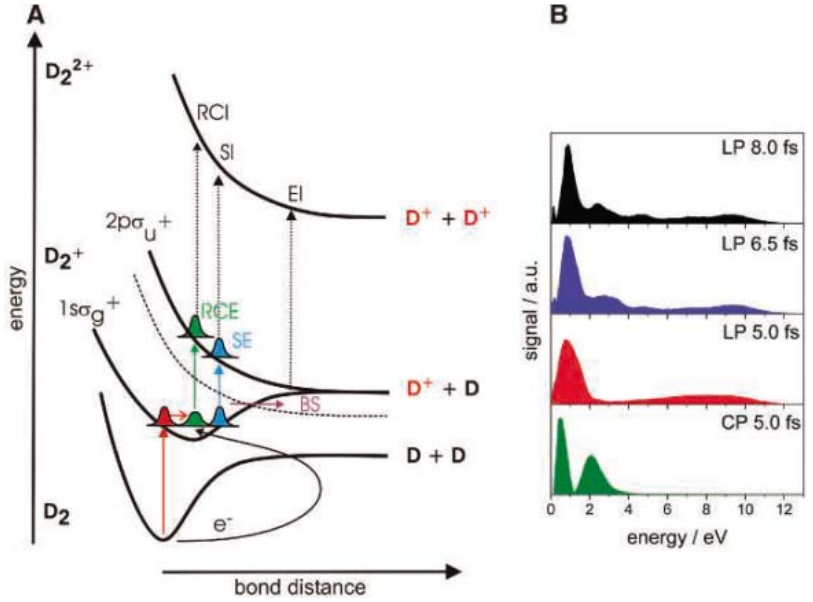

Fig. 1. (**A**) Pathways for the production of D^+ ions from D_2 by dissociation of the molecular ion (through BS, SE, or RCE) or by Coulomb explosion (through RCI, SI, or EI). BS occurs when the avoided crossing between diabatic potentials that are dressed by the laser field gives rise to dissociation from vibrational levels that were originally bound (*12*). (**B**) D^+ kinetic energy spectra for dissociation of D_2 by 5- to 8-fs linearly polarized (LP) and 5-fs circularly polarized (CP) laser pulses without phase stabilization, at $I = 1.2 \pm 0.2 \times 10^{14}$ W cm^{-2} and $I = 2.4 \pm 0.2 \times 10^{14}$ W cm^{-2}, respectively.

[1]FOM Instituut voor Atoom en Molecuul Fysica (AMOLF), Kruislaan 407, 1098 SJ Amsterdam, Netherlands. [2]Max-Planck-Institut für Quantenoptik, Hans-Kopfermann-Strasse 1, D-85748 Garching, Germany. [3]Fakultät für Physik, Universität Bielefeld, Universitätsstrasse 25, D-33615 Bielefeld, Germany. [4]Department für Physik, Ludwig-Maximilians-Universität München, Am Coulombwall 1, D-85748 Garching, Germany. [5]Institut für Experimentalphysik, Universität Hamburg, Luruper Chaussee 149, D-22761 Hamburg, Germany.

step via recollision [recollision ionization (RCI)] or via the laser field [sequential ionization (SI)]. Enhanced ionization (EI) takes place when the vibrational wave packet reaches a transition region where electron localization occurs and where (anti)-bonding molecular orbitals turn into atomic orbitals. Double ionization (via RCI, SI, or EI) leads to the breakup of the molecule by Coulomb repulsion between the two D^+ ions. Two momentum-matched D^+ ions are emitted symmetrically along the molecular axis, irrespective of the shape of the driving fields. To address the feasibility of reaction control by means of steering electronic motion, we therefore have to investigate the BS, SE, and RCE pathways and keep double ionization at a minimum.

We have studied the dissociation of D_2^+ in a few-cycle laser field by measuring the emission of D^+ as a probe of the location (or absence) of the electron. D^+ fragment kinetic energy and angular distributions were retrieved using the velocity-map imaging technique (*13*). For a description of the experimental apparatus, see the supporting online material (SOM). In general, all the pathways illustrated in Fig. 1 contribute to the D^+ kinetic energy spectra. Their relative importance sensitively depends on the intensity and duration of the laser (*6*). Figure 1B shows D^+ kinetic energy spectra recorded for linearly and circularly polarized laser pulses with durations of 5 to 8 fs at peak intensities (I) of $I = 1.2 \pm 0.2 \times 10^{14}$ W cm^{-2} and $I = 2.4 \pm 0.2 \times 10^{14}$ W cm^{-2}, respectively.

Previous studies (*14*–*16*) suggest that D^+ ions with energies below 3 eV originate from BS (at ~ 0.9 eV) and EI (at ~ 2.5 eV). Above 3 eV, contributions may arise from SE/SI and RCE/RCI. In our experiment, the disappearance of the D^+ signal above 3 eV upon changing the polarization from linear to circular (while maintaining the peak electric field of the laser) indicates that recollision is responsible for the creation of the high-energy fragments (Fig. 1B). Decreasing the pulse duration from 8 to 5 fs suppresses spectral components assigned to double ionization. Light-field control of molecular dissociation was therefore pursued with phase-stabilized 5-fs laser pulses.

Figure 2 shows a cut through the D^+ three-dimensional momentum distribution in Cartesian coordinates (p_x, p_y) at $p_z = 0$, for a 5-fs, 1×10^{14} W cm^{-2} laser field without phase stabilization. The laser propagated along the x axis ($\theta = 90°/270°$) and was polarized along the y axis ($\theta = 0°/180°$). In agreement with previous studies (*17*), the BS (0 to 2 eV) and the weak EI channel (2 to 3 eV) that appear in the center of the image show relatively narrow angular distributions. A nearly isotropic distribution is measured for higher energies (3 to 10 eV) and is a typical signature of recollision-induced fragmentation (*15*). No difference in the up versus down emission of D^+ ions (along the laser polarization axis) is observed without phase stabilization.

In an attempt to control and probe the final location of the electron in the D_2^+ dissociation, D^+ images were recorded while changing the carrier envelope phase φ. The angle-integrated asymmetry in the D^+ emission was evaluated as a function of energy $W = p^2/2m$ and φ via

$$A(W,\varphi) = \frac{P_{up}(W,\varphi) - P_{down}(W,\varphi)}{P_{up}(W,\varphi) + P_{down}(W,\varphi)}$$

with

$$P_{up}(W,\varphi) = \int_{330}^{360} d\theta \int_{0}^{360} d\phi\, P(W,\theta,\phi,\varphi)\sin\theta + \int_{0}^{30} d\theta \int_{0}^{360} d\phi\, P(W,\theta,\phi,\varphi)\sin\theta$$

and

$$P_{down}(W,\varphi) = \int_{150}^{210} d\theta \int_{0}^{360} d\phi\, P(W,\theta,\phi,\varphi)\sin\theta$$

with θ and ϕ being the polar and azimuthal angles, respectively.

We chose to analyze the ion emission within a restricted angular range because (as will become clear) our ability to control electron motion in D_2^+ requires that the laser couple the two lowest-lying electronic states. For molecules aligned orthogonally to the laser polarization axis, this coupling is absent.

Figure 3A depicts the angle-integrated D^+ energy spectrum obtained with 5-fs laser pulses with a peak intensity of $I = 1 \times 10^{14}$ W cm^{-2} and a randomly varying carrier envelope phase. Figure 3B reveals how phase locking results in a nonzero asymmetry $A(W,\varphi)$ as a function of the kinetic energy W of the D^+ fragments (y axis) and the laser phase φ (x axis). Regions where the asymmetry oscillates as a function of the phase represent conditions where the direction of the D^+ emission, and hence the localization of the electron in the dissociation process, is effectively controlled by the subcycle evolution of the laser field driving the dissociation. The extent of the control is further illustrated in Fig. 3C, which displays a series of curves where $A(W,\varphi)$ is integrated over selected energy intervals. The highest degree of asymmetry with a modulation depth of ~50% is observed between 3 and 8 eV. A very small phase dependence is seen between 0 and 3 eV. Asymmetric D^+ ejection is observed predominantly at kinetic energies that are virtually absent in a circularly polarized field, suggesting that electron-ion recollision is a vital element in the mechanism responsible for the observed phase control.

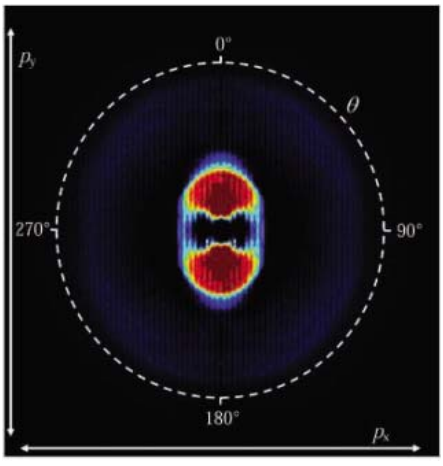

Fig. 2. Two-dimensional D^+ momentum image for D_2 dissociation in a 5-fs, 1×10^{14} W cm^{-2} laser field without phase stabilization.

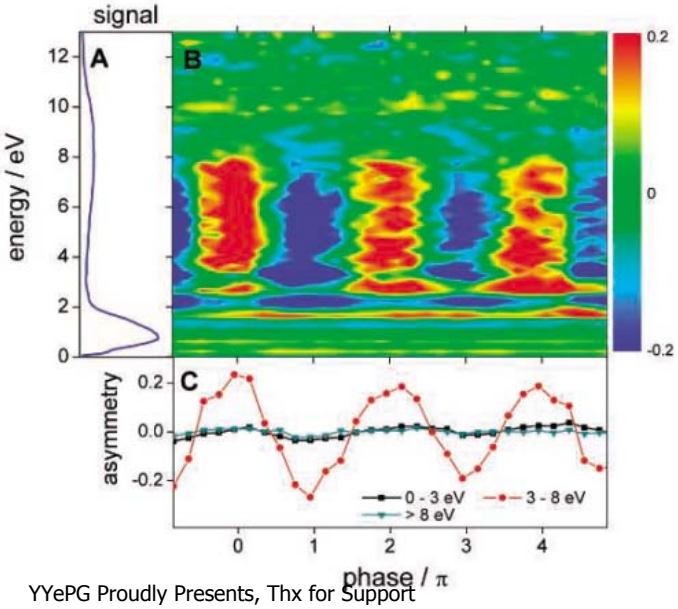

Fig. 3. (**A**) D^+ kinetic energy spectrum for D_2 dissociation with 5-fs, 1×10^{14} W cm^{-2} laser pulses without phase stabilization. (**B**) Map of asymmetry parameter $A(W,\varphi)$ as a function of the D^+ kinetic energy and carrier envelope phase φ (measured over a range of 6π with a step size of $\Delta\varphi = 0.1\pi$). (**C**) Integrated asymmetry over several energy ranges versus carrier envelope phase φ.

To gain qualitative insight into the mechanism responsible for the observed phase-controlled asymmetry in the dissociation of D_2^+, we modeled the laser-driven motion of the two nuclei and the bound electron by numerically solving the time-dependent Schrödinger equation (see the SOM for details). As in previous studies (*18*), the process is modeled in terms of the $1s\sigma_g^+$ and $2p\sigma_u^+$ electronic states, and the molecule is assumed to be aligned along the laser polarization axis.

In our modeling, the D_2^+ molecular ion is formed in a single ionization event that occurs at the maximum of the laser electric field. This ionization produces a vibrational wave packet in the $1s\sigma_g^+$ ground electronic state that mimics the ($v = 0$) vibrational wave function of the D_2 ground state. Population transfer from the $1s\sigma_g^+$ ground electronic state to the $2p\sigma_u^+$ excited electronic state is introduced at a delay of 1.7 fs after ionization [corresponding to the first recollision time (*10*)]. Later recollision events are efficiently suppressed with short laser pulses (*15*). Because of the strongly repulsive nature of the $2p\sigma_u^+$ state, the excited D_2^+ molecule dissociates and the momentum-matched D and D^+ fragments acquire a large kinetic energy (E_k up to 10 eV). During the dissociation, the laser field transfers part of the $2p\sigma_u^+$ population to the $1s\sigma_g^+$ state, producing a dissociative wave packet with a large excess kinetic energy. The emerging coherent superposition of the two electronic states results in a time-dependent localization of the electron density on the upper or lower nucleus due to the gerade and ungerade nature of the two states (*7*, *9*, *19*).

In Fig. 4, the temporal evolution of the laser field and the occupations of the $1s\sigma_g^+$ and $2p\sigma_u^+$ electronic states are depicted in (A) and (B), respectively. A time-dependent electron localization parameter quantifying the localization on the upper/lower nucleus (for definition, see the SOM) is displayed in (C). By the time the molecule has dissociated (with the internuclear distance reaching ~15 atomic units), the electron density is found to localize predominantly on the lower D atom. A simple shift of the carrier envelope phase φ by π reverses the field and turns the direction of emission of the ionic/atomic fragment opposite, in agreement with our experimental observation. To the best of our knowledge, this is the first demonstration of direct light-field control of a chemical reaction via the steering of electronic motion.

Let us consider the electron localization dynamics after the recollision in more detail. Initially, the $1s\sigma_g^+$ state is hardly populated by the laser-induced coupling, and the energy gap $\Delta W(t) = \hbar\omega(t)$ between the binding $1s\sigma_g^+$ and repulsive $2p\sigma_u^+$ states is much larger than the laser photon energy. Hence, the electronic wave function can respond nearly instantaneously to changes in the laser field, and the electron localization parameter (Fig. 4C) oscillates with a small amplitude at the frequency of the light pulse. As the eigenfrequency $\omega(t)$ of the two-level system decreases because of the increasing bond length, the laser field starts populating the lower state substantially, strongly increasing the extent of electron localization. In our calculations, the electron wave packet keeps evolving with the instantaneous eigenfrequency $\omega(t)$ as the laser field strength approaches zero (for $t > 7$ fs). The oscillation of the electron localization ceases when the interatomic barrier that builds up between the two D^+ ions can no longer be overcome by the electron. In the experiment, because of a nonzero background of the few-cycle pulses (<10% in intensity), a laser field may still be present when the molecule breaks up and contribute to the asymmetry (*20*).

The field-controlled electron dynamics demonstrated in this work does not rely on electron recollision. In fact, control of electron dynamics in molecules can also be achieved by preparing a coherent electronic superposition state by photoexcitation (*7*, *19*, *21*, *22*). In contrast with the current experiment, the photoexcitation will permit the creation of an electron wave packet at the beginning of the reaction, thereby offering a greater flexibility for its subsequent light-field control. This approach will also be applicable in neutral molecules.

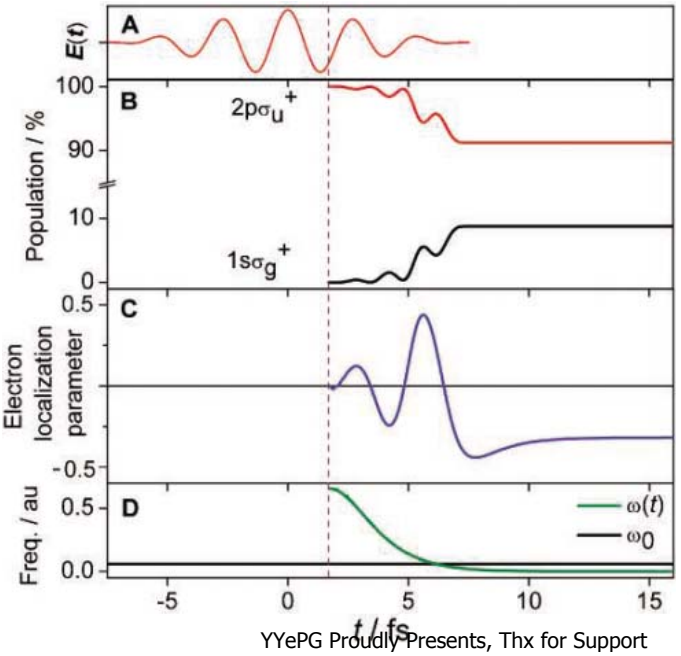

Fig. 4. **(A)** Electric field of the 5-fs, $1 \cdot 10^{14}$ W cm^{-2} pulse used in the calculations, with carrier envelope phase $\varphi = 0$. **(B)** Time-dependent populations of the $1s\sigma_g^+$ and $2p\sigma_u^+$ states of D_2^+ after excitation through recollision. **(C)** Temporal evolution of the electron localization parameter starting from the time of recollision. **(D)** Time dependence of the eigenfrequency $\omega(t)$ of the two-level system versus the laser frequency ω_0 (frequencies are given in atomic units). The vertical dashed purple line marks the time of recollision in all panels.

References and Notes

1. A. Baltuška *et al.*, *Nature* **421**, 611 (2003).
2. R. Kienberger *et al.*, *Nature* **427**, 817 (2004).
3. E. Goulielmakis *et al.*, *Science* **305**, 1267 (2004).
4. G. G. Paulus *et al.*, *Phys. Rev. Lett.* **91**, 253004 (2003).
5. F. Lindner *et al.*, *Phys. Rev. Lett.* **95**, 040401 (2005).
6. J. H. Posthumus, *Rep. Prog. Phys.* **67**, 623 (2004).
7. A. D. Bandrauk, S. Chelkowski, H. S. Nguyen, *Int. J. Quant. Chem.* **100**, 834 (2004).
8. V. Roudnev, B. D. Esry, I. Ben-Itzhak, *Phys. Rev. Lett.* **93**, 163601 (2004).
9. H. Niikura, D. M. Villeneuve, P. B. Corkum, *Phys. Rev. A* **73**, 021402 (2006).
10. H. Niikura *et al.*, *Nature* **417**, 917 (2002).
11. H. Niikura *et al.*, *Nature* **421**, 826 (2003).
12. P. H. Bucksbaum, A. Zavriyev, H. G. Muller, D. W. Schumacher, *Phys. Rev. Lett.* **64**, 1883 (1990).
13. A. T. J. B. Eppink, D. H. Parker, *Rev. Sci. Instr.* **68**, 3477 (1997).
14. A. S. Alnaser *et al.*, *Phys. Rev. Lett.* **91**, 163002 (2003).
15. A. S. Alnaser *et al.*, *Phys. Rev. Lett.* **93**, 183202 (2004).
16. H. Sakai *et al.*, *Phys. Rev. A* **67**, 063404 (2003).
17. K. Sändig, H. Figger, T. W. Hänsch, *Phys. Rev. Lett.* **85**, 4876 (2000).
18. I. Kawata, H. Kono, Y. Fujimura, *J. Chem. Phys.* **110**, 11152 (1999).
19. G. L. Yudin, S. Chelkowski, J. Itatani, A. D. Bandrauk, P. B. Corkum, *Phys. Rev. A* **72**, 051401 (2005).
20. M. Y. Ivanov, P. B. Corkum, P. Dietrich, *Laser Phys.* **3**, 375 (1993).
21. H. Niikura, D. M. Villeneuve, P. B. Corkum, *Phys. Rev. Lett.* **94**, 083003 (2005).
22. P. Krause, T. Klamroth, P. Saalfrank, *J. Chem. Phys.* **123**, 074105 (2005).

23. We thank J. Rauschenberger for experimental support and acknowledge valuable discussions with B. Esry, P. Corkum, and H. Niikura. We are grateful for financial support from the Marie Curie Research Training Network XTRA (grant no. MRTN-CT-2003-505138) and a Marie Curie Intra-European Fellowship (no. MEIF-CT-2003-500947) (M.F.K.). The research of M.F.K., Ch.S., J.I.K., Y.N., and M.J.J.V. is part of the research program of the Stichting voor Fundamenteel Onderzoek der Materie (FOM), which is financially supported by the Nederlandse Organisatie voor Wetenschappelijk Onderzoek (NWO).

Supporting Online Material

www.sciencemag.org/cgi/content/full/312/5771/246/DC1
SOM Text
Figs. S1 and S2
References

15 February 2006; accepted 15 March 2006
10.1126/science.1126259

Hardening by Annealing and Softening by Deformation in Nanostructured Metals

Xiaoxu Huang,[1]* Niels Hansen,[1] Nobuhiro Tsuji[2]

We observe that a nanostructured metal can be hardened by annealing and softened when subsequently deformed, which is in contrast to the typical behavior of a metal. Microstructural investigation points to an effect of the structural scale on fundamental mechanisms of dislocation-dislocation and dislocation-interface reactions, such that heat treatment reduces the generation and interaction of dislocations, leading to an increase in strength and a reduction in ductility. A subsequent deformation step may restore the dislocation structure and facilitate the yielding process when the metal is stressed. As a consequence, the strength decreases and the ductility increases. These observations suggest that for materials such as the nanostructured aluminum studied here, deformation should be used as an optimizing procedure instead of annealing.

From the beginning of our civilization, metalworkers have known that when a metal becomes too hard—for example, when forged—it can be softened by annealing. By choosing the right combination of annealing temperature and time, a desired combination of strength and ductility can be achieved. The current focus is on nanostructured metals that have extreme strength but limited ductility and formability, which reduces their applicability. The extreme strength is obtained through a structural refinement of the grains down to nanometer dimensions, and an optimization of ductility has been sought through annealing. It has been shown (*1*) that when annealing under conditions that produce a structure with bimodal distribution of grain sizes from nanometer to micrometer scales, the strength of nanostructured metals decreases slightly but the deformation-induced hardening (i.e., work hardening) of the coarse grains in the structure gives ductility. It has been also discovered that during annealing at low temperatures, which does not cause excessive and heterogeneous coarsening of the nanostructure, nanostructured metals may harden rather than soften—as observed, for example, in metals produced by inert gas condensation (*2*–*4*), electrodeposition (*5*, *6*), and plastic deformation to very high strains (*7*–*10*). Associated with the hardening, a decrease in the tensile ductility has been reported (*5*, *9*, *10*) where tensile tests were carried out to evaluate the mechanical properties. This unusual, annealing-induced hardening has been related to changes in structural characteristics [e.g., the grain boundary structure (*11*)], but various hypotheses have not been verified. The present work has two objectives: to improve our understanding of the changes in properties and structure when a nanostructured metal is annealed, and to use such findings to inspire the development of new optimization processes.

We investigated annealing behavior in a fully dense, nanostructured aluminum of commercial purity (99.2%) that was prepared by a high-strain rolling deformation known as accumulative roll bonding (ARB) (*12*). Aluminum sheets of a final thickness of 1 mm were produced by a six-cycle ARB processing to an equivalent strain of 4.8 (*13*). The ARB-processed state showed a weak crystallographic texture and a lamellar microstructure of dislocation boundaries and grain boundaries characteristic of high-strain rolling of metals and alloys. The lamellar boundaries are parallel to the rolling plane, with an average spacing of 180 nm. This lamellar morphology and the relatively coarse boundary spacing ensure the elimination of grain boundary sliding during tensile testing. Tensile specimens of gauge dimensions 10 mm by 5 mm were machined from the sheets and tested at room temperature. The engineering stress-strain curve of the ARB sample (Fig. 1, curve 1) shows a very high yield stress (259 MPa) and ultimate tensile stress (UTS, 334 MPa) and a reasonably good tensile ductility, as expressed by total elongation (7%) and uniform elongation (1.8%). This yield stress is nearly 10 times that of a coarse-grained material with a grain size of 50 μm (~28 MPa). When the ARB sample was annealed at 150°C for 30 min, the yield stress increased by 8.9% to 281 MPa (curve 2, Fig. 1) and the total elongation decreased markedly, making the material almost brittle. This is in contrast to the expected behavior after annealing—a decrease in strength and an increase in elongation or ductility.

An increase in flow stress during annealing of a deformed metal is typical if the metal contains alloying elements in solid solution that precipitate when the metal is annealed. This so-called precipitation hardening was not expected in the aluminum, which had a purity of 99.2%. However, other stable impurities might have dissolved during processing and reprecipitated during annealing. To prove that this was not the case, we carried out an experiment using 99.99% pure aluminum as the starting material. As with the 99.2% pure aluminum, specimens were produced by a six-cycle ARB processing to an equivalent strain of 4.8, followed by annealing at 150°C for 30 min. The specimens were tested under the same conditions. The results showed that, as expected, both the yield stress and the UTS were substantially reduced relative to the 99.2% Al, but the key phenomena (i.e., the hardening by annealing and the decrease in ductility) were reproduced. For example, an increase of about 9% in the yield stress was observed after annealing. Therefore, the dissolution and reprecipitation of impurities, if it occurred, did not contribute to the annealing-induced property changes.

We used transmission electron microscopy (TEM) and high-resolution TEM (HRTEM) to characterize the structural parameters of ARB samples before and after annealing. The initial structure (Fig. 2A) is delineated by lamellar boundaries parallel to the rolling direction (RD) and interconnecting boundaries parallel to the normal direction (ND). Table 1 shows the quantified structural parameters that are thought to contribute to the mechanical properties. Slight coarsening occurred during annealing (Fig. 2B) for both the lamellar boundary spacing D_{LB} and the interconnecting boundary spacing D_{ICB}, which produced a reduction of boundary surface area per unit volume.

Statistical measurements of misorientation angles across the lamellar boundaries and interconnecting boundaries were made by Kikuchi diffraction. Misorientation angles in both samples show a bimodal distribution, with one peak located in the range below 3° and the other located between 40° and 55°. More than 60% of the boundaries were high-angle boundaries (>15°) in the ARB samples both before and after annealing. This high density, in combination with the small boundary spacing, results in

Table 1. Structural parameters in samples of different conditions. $f_{<3°}$, fraction of boundaries with misorientation angles less than 3°; $f_{3–15°}$, fraction of boundaries with misorientation angles between 3° and 15°; $f_{>15°}$, fraction of high-angle boundaries (>15°).

Sample	ρ_0 (m^{-2})	D_{LB} (nm)	D_{ICB} (nm)	$f_{<3°}$ (%)	$f_{3–15°}$ (%)	$f_{>15°}$ (%)
ARB	1.33×10^{14}	180	600	17.5	16.2	66.3
ARB annealed at 150°C for 30 min	0.53×10^{14}	225	640	12.8	23.3	63.9

[1]Center for Fundamental Research: Metal Structures in Four Dimensions, Materials Research Department, Risø National Laboratory, DK 4000 Roskilde, Denmark. [2]Department of Adaptive Machine Systems, Graduate School of Engineering, Osaka University, 2-1 Yamada-Oka, Suita, Osaka 565-0871, Japan.

*To whom correspondence should be addressed. E-mail: xiaoxu.huang@risoe.dk

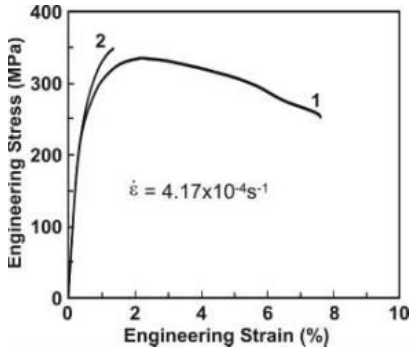

Fig. 1. Engineering stress-strain curves for 99.2% pure Al. Curve 1: processed by six ARB cycles to an equivalent strain of 4.8. Curve 2: same material as 1, plus annealing at 150°C for 30 min. The strain rate $\dot{\varepsilon}$ used for the tensile test is indicated. Refer to table S2 for sample numbering.

a very large area per unit volume (S_V) of high-angle boundaries, which can act as dislocation sinks. As an example, S_V in the ARB sample before annealing is $\sim 5.6 \times 10^6$ m^{-1}, which is about 100 times the S_V for a typical polycrystalline material with a grain size of 50 μm. In the bright-field images (Fig. 2), it is seen that a series of alternating bright and dark thickness contours characterize individual high-angle boundaries, most of which correspond to the lamellar boundaries. HRTEM observations show that the lattice images on both sides of a lamellar boundary extend all the way to the boundary; no special region with a disordered structure is detected along the boundary. The low-angle boundaries exhibit a certain width in the deformed state, but they become sharper and better defined upon annealing, which suggests the occurrence of a recovery process by rearrangement of dislocations in these boundaries. The most remarkable change observed was the decrease in the density of interior dislocations, ρ_0, that exist in the volume between the boundaries (Fig. 2). A determination of the interior dislocation density showed that it decreased from 1.33×10^{14} m^{-2} in the deformed state to 0.53×10^{14} m^{-2} after annealing (Table 1).

In previous strength-structural analysis of lamellar structures, two additive strengthening mechanisms have been proposed: (i) forest hardening caused by the dislocations in the low-angle boundaries and in the volume between the boundaries (*14*), and (ii) grain boundary hardening caused by the high-angle boundaries (*14*, *15*) taken to be inversely proportional to the square root of the boundary spacing [i.e., a Hall-Petch relationship (*16*, *17*)]. Not included is a contribution from texture strengthening, as the texture change during annealing is negligible. Therefore, the observed coarsening and decrease in the dislocation density in the volume between the boundaries and the decrease in the low-angle boundary fraction suggest a decrease in strength, which is opposite to the hardening observed experimentally.

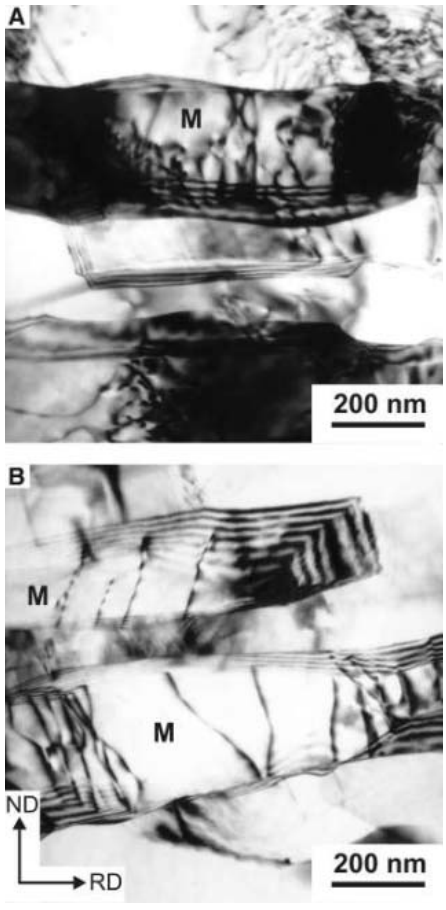

Fig. 2. TEM images showing the lamellar structural morphology and dislocation configuration in two ARB samples, (**A**) before annealing and (**B**) after annealing at 150°C for 30 min. The micrographs were recorded when at least one lamella (M) in the area was under multiple-beam condition with the beam direction parallel to the [001] zone axis of the lamella to reveal the interior dislocations. In (A), dislocation tangles are seen within the lamella marked M. In (B), dislocation tangles are replaced by fewer dislocations, many of which are pinned by the lamellar boundaries.

When a deformed structure is annealed at a temperature that does not cause recrystallization, typical effects include a coarsening of boundary spacing, recovery of low-angle boundaries, and reduction in the dislocation density in the grain interior, at grain boundaries and triple junctions. In conventional materials with medium to large grain sizes, these changes will cause softening by a reduction in dislocation hardening and grain boundary strengthening. However, the changes in the dislocation structure occurring in a nanostructured metal may play a distinct and different role. As a hypothesis, it is suggested that the many dislocation sinks available in the form of closely spaced high-angle boundaries will reduce the number of dislocation sources during annealing. This may lead to an increase in the yield stress

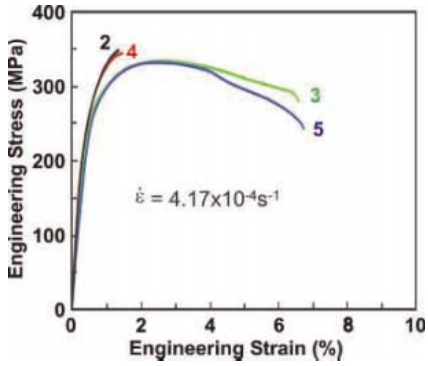

Fig. 3. Engineering stress-strain curves for 99.2% pure Al. Curve 2: ARB annealed at 150°C for 30 min (the same curve 2 as shown in Fig. 1). Curve 3: same as 2 but deformed 15% by cold rolling. Curve 4: same as 3 but again annealed at 150°C for 30 min. Curve 5: same as 4 but deformed 15% by cold rolling. Refer to table S2 for sample numbering.

in order to activate new dislocation sources during straining. Such a correlation between the density of dislocation sources and the strength is typically observed in nanoscale metals, both experimentally (*18*) and by atomic-scale modeling (*19*). Furthermore, the decrease in the density of interior dislocations that can carry the strain may efficiently reduce the elongation. These different effects are reflected in Fig. 1.

A critical test for the above hypothesis is to see whether a softening and an increase in elongation occur if dislocations are generated in the annealed sample. An annealed sample was deformed 15% by cold rolling and tested under the same conditions. The tensile curve for this test is plotted as curve 3 in Fig. 3. It is seen that the stress-strain behavior of this redeformed sample returns to that of the initial ARB sample (Fig. 1), as do the values for the measured yield stress (256 MPa), UTS (333 MPa), total elongation (6.6%), and uniform elongation (2.0%). The similarity in mechanical behavior between this 15% cold-rolled sample and the original ARB sample suggests that applying 15% cold rolling has modified the structure in the annealed sample to be similar to the structure in the initial ARB sample. TEM characterization shows that a large number of dislocations are indeed introduced again in the volume between the boundaries (Fig. 4) and at triple junctions and grain boundary regions. As a result, the dislocation configuration is very similar to that observed in the original ARB sample (Fig. 2A). We obtained an interior dislocation density of 1.14×10^{14} m^{-2} and boundary spacings of 200 nm (D_{LB}) and 650 nm (D_{ICB}) in this sample. These parameters are close to the values measured for the original ARB sample (Table 1).

To further verify this hypothesis, we carried out further annealing and deformation experiments as well as tensile tests. Repeated hardening and decrease in the elongation by low-temperature annealing, and softening and in-

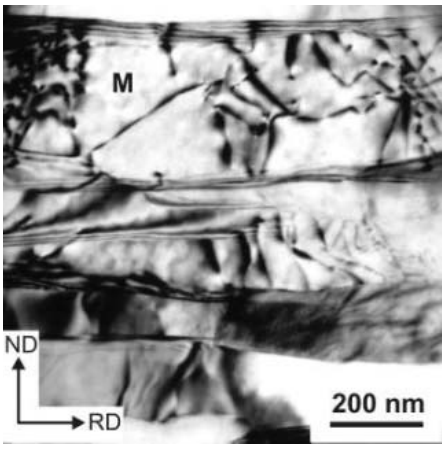

Fig. 4. TEM image showing the lamellar structural morphology and dislocation configuration in the ARB sample processed by annealing at 150°C for 30 min, then deformed 15% by cold rolling. A dislocation structure similar to that in the original ARB sample (Fig. 2A) is introduced in the lamellae.

crease in the elongation by a low level of deformation, are obtained, as shown by curves 4 and 5 in Fig. 3. This repeated mechanical behavior, combined with the structural characterization, confirms that the removal of dislocations by annealing and their introduction by slight deformation are the cause of the changes in the mechanical properties. The deformation induced relatively small decreases in yield stress and UTS, and a large increase in the elongation greatly improves the applicability of the material. A further test of the beneficial effect of deformation as a final processing step is to deform the initial ARB sample 15% by cold rolling. The reason is that this sample has been

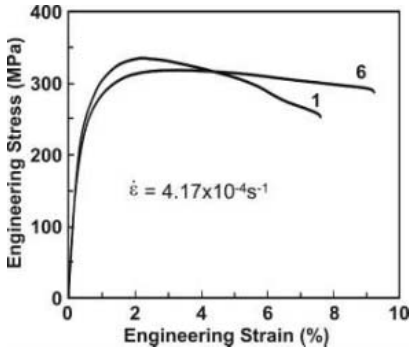

Fig. 5. Engineering stress-strain curves for 99.2% pure Al. Curve 1: same as curve 1 in Fig. 1. Curve 6: same as 1 but deformed 15% by cold rolling. Refer to table S2 for sample numbering.

processed by rolling to a large strain per pass and some adiabatic heating may have taken place (i.e., the material may be in a recovered state) (*20*). Such conditions are also typical of industrial processing. In accordance with the present hypothesis, it is assumed that a light deformation of an ARB sample in the as-delivered state may induce a small decrease in strength followed by an increase in ductility. Curves 1 and 6 in Fig. 5 confirm this assumption.

The present investigation has focused on aluminum. The strategy described above may also apply to metals such as nickel and interstitial free steels that develop deformation microstructure similar to that of aluminum (*14*, *21*). Therefore, this strategy opens up a research area of both fundamental and applied importance.

References and Notes

1. Y. Wang, M. W. Chen, F. H. Zhou, E. Ma, *Nature* **419**, 912 (2002).
2. G. E. Fougere, J. R. Weertman, R. W. Siegel, S. Kim, *Scr. Metall. Mater.* **26**, 1879 (1992).
3. J. R. Weertman, P. G. Sanders, *Solid State Phenom.* **35–36**, 249 (1994).
4. J. R. Weertman, *Mater. Sci. Eng. A* **166**, 161 (1993).
5. Y. M. Wang *et al.*, *Scr. Mater.* **51**, 1023 (2004).
6. F. Ebrahimi, Q. Zhai, D. Kong, *Scr. Mater.* **39**, 315 (1998).
7. R. Z. Valiev, F. Chmelik, F. Bordeaux, G. Kapelski, B. Baudelet, *Scr. Metall. Mater.* **27**, 855 (1992).
8. J. Languillaume *et al.*, *Acta Metall. Mater.* **41**, 2953 (1993).
9. N. Kamikawa, thesis, Osaka University (2005).
10. J. R. Bowen, P. B. Prangnell, D. Juul Jensen, N. Hansen, *Mater. Sci. Eng. A* **387–389**, 235 (2004).
11. A. Hasnaoui, H. V. Swygenhoven, P. M. Derlet, *Acta Mater.* **50**, 3927 (2002).
12. N. Tsuji, Y. Saito, S. H. Lee, Y. Minamino, *Adv. Eng. Mater.* **5**, 338 (2003).
13. See supporting material on *Science* Online.
14. D. A. Hughes, N. Hansen, *Acta Mater.* **48**, 2985 (2000).
15. Q. Liu, X. Huang, D. J. Lloyd, N. Hansen, *Acta Mater.* **50**, 3789 (2002).
16. E. O. Hall, *Proc. Phys. Soc. London* **B64**, 747 (1951).
17. N. J. Petch, *J. Iron Steel Inst. London* **174**, 25 (1953).
18. J. R. Greer, C. O. Warren, W. D. Nix, *Acta Mater.* **53**, 1821 (2005).
19. J. Schiøtz, K. W. Jacobsen, *Science* **301**, 1357 (2003).
20. N. Tsuji *et al.*, *Mater. Sci. Eng. A* **350**, 108 (2003).
21. B. L. Li, A. Godfrey, Q. C. Meng, Q. Liu, N. Hansen, *Acta Mater.* **52**, 1069 (2004).
22. Supported by the Danish National Research Foundation through the Center for Fundamental Research: Metal Structures in Four Dimensions, within which this work was performed, and by the 21st Century COE Program (the Center of Excellence for Advanced Structural and Functional Materials Design) at Osaka University through MEXT Japan. We thank D. Juul Jensen, B. Ralph, and J. A. Wert for critical reading of the manuscript and helpful discussions; E. Johnson for help with HRTEM; and N. Kamikawa for preparing the samples used in this study.

Supporting Online Material

www.sciencemag.org/cgi/content/full/312/5771/249/DC1
Materials and Methods
Tables S1 and S2
References

23 December 2005; accepted 16 March 2006
10.1126/science.1124268

Diels-Alder in Aqueous Molecular Hosts: Unusual Regioselectivity and Efficient Catalysis

Michito Yoshizawa, Masazumi Tamura, Makoto Fujita*

Self-assembled, hollow molecular structures are appealing as synthetic hosts for mediating chemical reactions. However, product binding has inhibited catalytic turnover in such systems, and selectivity has rarely approached the levels observed in more structurally elaborate natural enzymes. We found that an aqueous organopalladium cage induces highly unusual regioselectivity in the Diels-Alder coupling of anthracene and phthalimide guests, promoting reaction at a terminal rather than central anthracene ring. Moreover, a similar bowl-shaped host attains efficient catalytic turnover in coupling the same substrates (although with the conventional regiochemistry), most likely because the product geometry inhibits the aromatic stacking interactions that attract the planar reagents to the host.

Effective synthetic homogeneous catalysts have generally been structurally simple small molecules, which act by binding to substrates at or near the reaction site. In contrast, enzymes are much larger and more complex and derive much of their selectivity by bonding substrates through multiple interactions in elaborate pockets, thereby forcing the substrates into orientations that favor specific reaction paths (*1*, *2*). In the past decade, chemists have made substantial progress in building molecular hosts that emulate these enzymatic pockets (*3*, *4*). Self-assembly of carefully constructed organic and/or metallic building blocks in solution produces hollow host structures that can bind small molecule guests (*5*, *6*). Among the many potential advantages of this strategy is the creation of hydrophobic reaction environments in aqueous solution, widening the scope of accessible reactivity in ecologically friendly media. However, these synthetic hosts have rarely conferred the orientational precision necessary to guide reactions along otherwise unfavored pathways. Moreover, catalytic turnover has been inhibited because the hosts bind products as effectively as reactants, if not more so. In earlier reports by Rebek (*7*, *8*), Sanders (*9*), and our

Department of Applied Chemistry, School of Engineering, University of Tokyo, and Core Research for Evolutional Science and Technology (CREST), Japan Science and Technology Agency (JST), 7-3-1 Hongo, Bunkyo-ku, Tokyo 113-8656, Japan.

*To whom correspondence should be addressed. E-mail: mfujita@appchem.t.u-tokyo.ac.jp

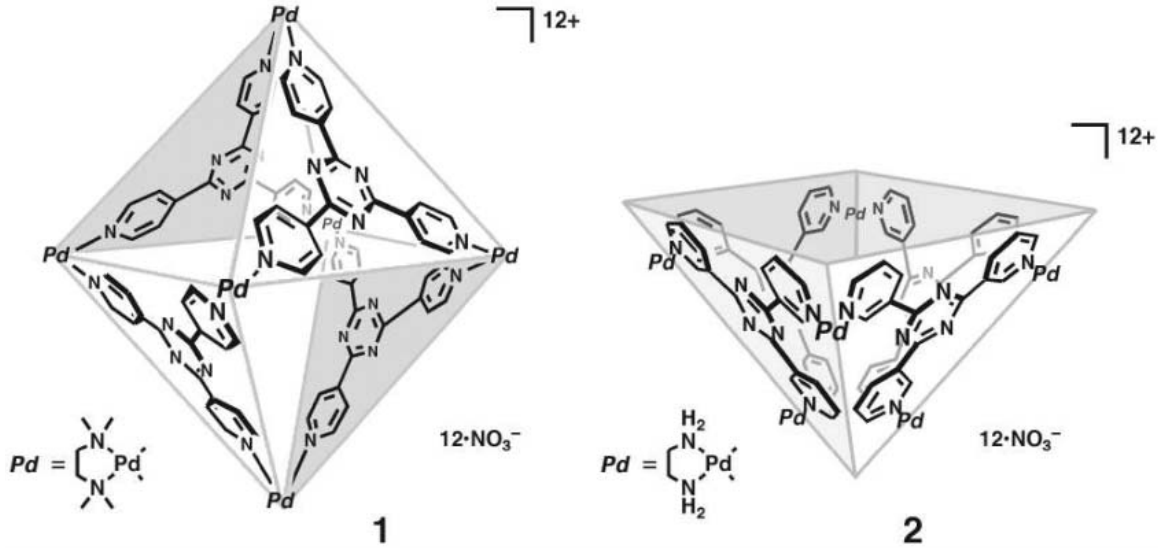

Fig. 1. Self-assembled coordination cages (**1** and **2**), which are prepared by simple mixing of an exo-tridentate organic ligand and an end-capped Pd(II) ion in a 4:6 ratio in water.

group (*10*), the Diels-Alder and related cycloadditions are significantly accelerated in synthetic pockets, but the product inhibition prevents the reactions from showing turnover and the stereochemical courses are not well controlled by the pockets. For catalytic reactions by self-assembled hosts, there have appeared only a few examples, including the Diels-Alder (*11*), epoxidation (*12*), and the aza-Cope rearrangement (*13*). Controlling reaction pathways by encapsulation has been discussed in the excited-state chemistry of aromatic guests (*14*) and also realized by a regioselective cycloaddition (*8*).

We investigated the host-mediated Diels-Alder coupling of anthracenes and phthalimides. The Diels-Alder reaction of anthracenes in the absence of hosts is extremely well studied and generally yields an adduct bridging the center ring (9,10-position) of the anthracene framework (*15*–*17*) as a consequence of the high localization of π-electron density at that site (*18*, *19*). We find that an appropriately designed cage structure can alter this well-established selectivity to favor adduct formation at a terminal ring (1,4-position). This unusual regioselectivity likely stems from topochemical control induced by the proximity of the 1,4-position of the anthracene to the dienophile in the cage. The 1,4-selective Diels-Alder of anthracenes has been previously reported only for a benzyne addition (*20*) and for the addition with 9,10-diarylanthracenes (*21*). We further find that the same reaction, through conventional regioselectivity, can be catalyzed with efficient turnover by a related, bowl-shaped host. As in enzymatic reactions (*2*, *22*), the product geometry, bent at the 9,10-position, precludes the aromatic stacking interactions that underlie the host's affinity for the reagents.

The coordination hosts we used here are octahedral cage **1** and square-pyramidal bowl **2** (Fig. 1) (*23*–*25*). Both of them assemble from cis end-capped Pd(II) ions and triazine-cored tridentate ligands in a surprisingly efficient manner (100°C, <5 min, quantitative yields). In aqueous solution, these structures provide an efficient hydrophobic pocket capable of binding a variety of neutral organic compounds. Cage **1** features a three-dimensionally enclosed cavity, which binds substrates in precisely fixed positions. Geometry-fixed encapsulation (*26*), iso-

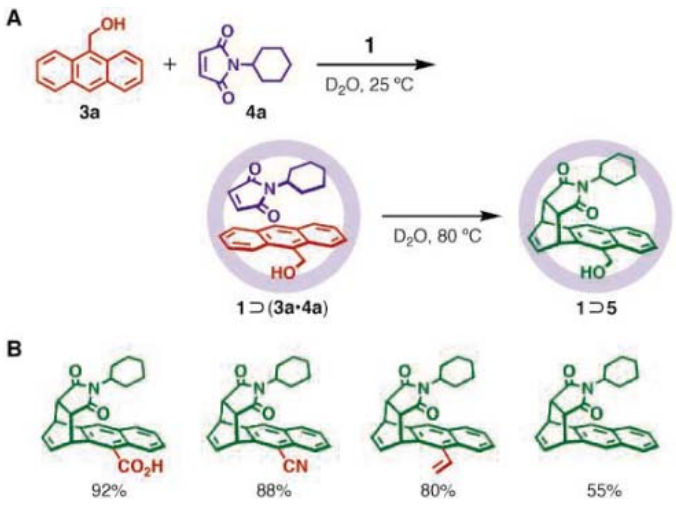

Fig. 2. (**A**) Pair-selective encapsulation of two types of reactants, 9-hydroxymethylanthrancene (**3a**) and *N*-cyclohexylphthalimide (**4a**), within cage **1** and the subsequent Diels-Alder reaction leading to syn isomer of 1,4-adduct **5** within the cavity of **1**. (**B**) Syn-1,4-regioselective Diels-Alder products within cage **1**. The structures of the adducts and the yields are shown.

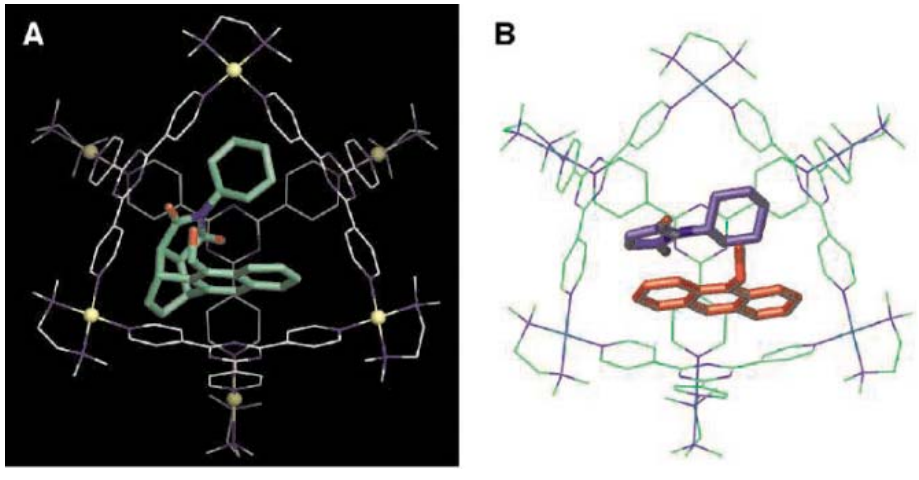

Fig. 3. (**A**) Crystal structure of **1** ⊃ **5** and (**B**) optimized structure of **1** ⊃ (**3a**•**4a**) by a force-field calculation.

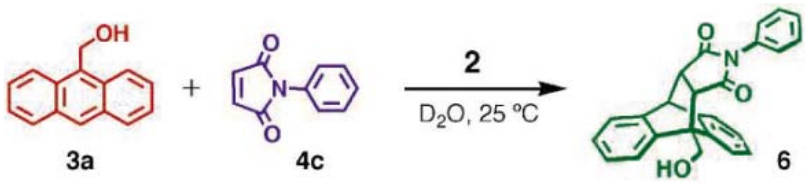

Fig. 4. Catalytic Diels-Alder reaction of 9-hydroxymethylanthracene (**3a**) and *N*-phenylphthalimide (**4c**) in the aqueous solution of bowl **2**, leading to 9,10-adduct **6**.

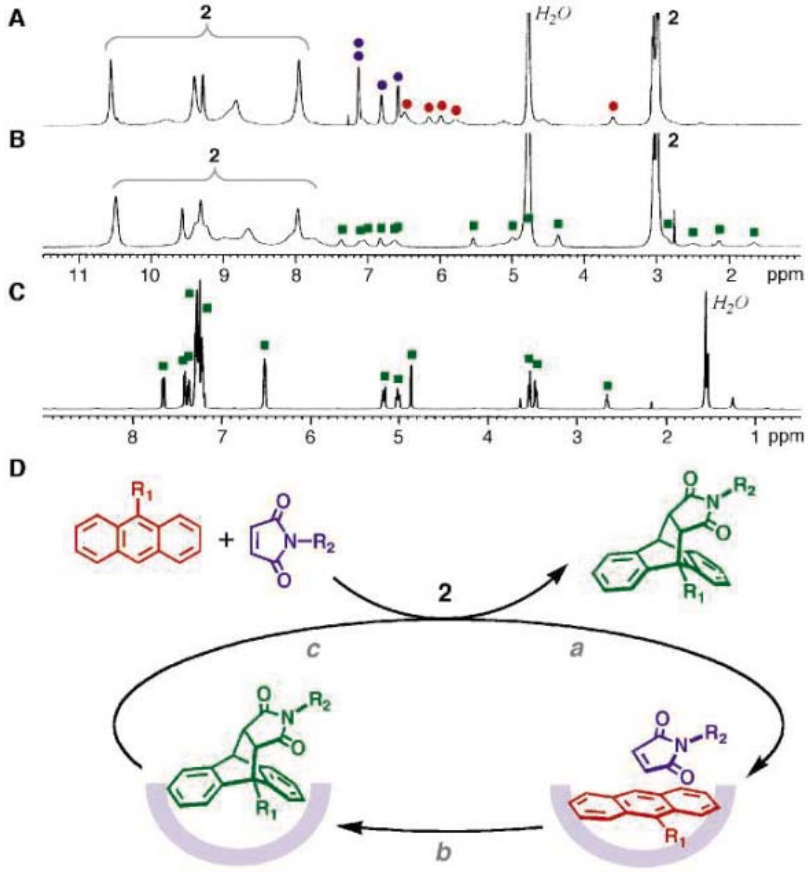

Fig. 5. The ^{1}H NMR spectra (500 MHz, room temperature) of the catalytic Diels-Alder reaction of 9-hydroxymethylanthrancene (**3a**) and *N*-phenylphthalimide (**4c**) in an aqueous solution of bowl **2**. (**A**) Before and (**B**) after the reaction at room temperature for 5 hours (red circles, **3a**; blue circles, **4c**; and green squares, **6**). (**C**) Diels-Alder product **6** after extraction with $CDCl_3$. (**D**) Schematic representation of the catalytic Diels-Alder reaction of anthracenes and phthalimide in the presence of bowl **2**. Autoinclusion of substrates into **2** (step a) and autoexclusion of the product from **2** (step c) underlie the efficient catalytic Diels-Alder reaction.

mer separation (*27*), pairwise selective inclusion of two guests (*28*), and stereocontrolled cyclic siloxane formation (*29*) have been reported. Bowl **2** has an open cavity that facilitates rapid binding and dissociation of substrates (*25*).

When 9-hydroxymethylanthrancene (**3a**) and *N*-cyclohexylphthalimide (**4a**) (6.0 mM) were suspended in an aqueous solution of cage **1** (5.0 mM) at room temperature, the inclusion complex **1** ⊃ (**3a**•**4a**) (this set notation denotes that **1** includes **3a** and **4a**) formed selectively within 5 min (Fig. 2A). A ^{1}H nuclear magnetic resonance (NMR) analysis confirmed the encapsulation, with the resonances of **3a** and **4a** shifted far upfield because of interaction with the cage (fig. S1a) (*30*). No signals indicating **1** ⊃ $(\mathbf{3a})_n$ or **1** ⊃ $(\mathbf{4a})_n$ ($n \leq 2$) were observed in the NMR spectrum. On heating the solution at 80°C for 5 hours, the signals derived from **3a** and **4a** disappeared and were replaced by resonances consistent with a Diels-Alder adduct, distributed between 6.8 and –2.1 parts per million (ppm) (fig. S1b). Sixteen signals in the 9.7- to 8.4-ppm range were observed for cage **1**, indicating the desymmetrization of the cage from T_d to C_3 symmetry (*26*). This symmetry agreed with the restricted motion of a noncentrosymmetric product along the C_3 axis, which is perpendicular to one of the triazine ligands (*30*). After insoluble solids were removed by filtration, the product was extracted into $CDCl_3$ and fully assigned as the syn isomer of 1,4-Diels-Alder adduct **5** (fig. S4). No other regio- or stereoisomers (1,9-adduct or anti-1,4-adduct) were detected. The yield of **5** was estimated to be >98% (based on **1**) from the ^{1}H NMR spectra (*30*). In contrast, in the absence of **1**, the reaction gave only the conventional 9,10-Diels-Alder adduct in 44% yield based on **3a**.

The unusual structure of the 1,4-Diels-Alder adduct was unambiguously determined by x-ray crystallographic analysis of **1** ⊃ **5** (Fig. 3A). A single crystal suitable for x-ray analysis was obtained by the slow evaporation of water from an aqueous solution of **1** ⊃ **5** over 5 days (*30*). The crystal structure displays the syn stereochemistry of 1,4-adduct **5**, which is tightly accommodated in the cavity of **1** via π-π stacking interactions (3.3 Å) between the naphthalene ring of **5** and a triazine ligand of **1**.

Because the Diels-Alder reaction has an early transition state (*15*), the unusual regio- and stereoselectivities can be explained by the fixed orientation of the guests before the reaction. The geometries of **3a** and **4a** in the **1** ⊃ (**3a**•**4a**) complex were modeled by force-field calculation (*31*). Randomly oriented **3a** and **4a** guests in several initial structures converged in all cases to a parallel orientation with the C=C bond of **4a** in close contact with the 1,4-position of **3a** (Fig. 3B). The center-to-center distance between the two reaction centers is only circa (ca.) 3.8 Å, which is comparable to the sum of van der Waals radii. Because of the steric restrictions induced by the cage, the C=C bond of **4a** hardly interacts with the 9,10-position of **3a** (ca. 4.7 Å). It is also interesting that the cavity of **1** directs exo-selective addition of **4a** to the 1,3-diene moiety of **3a**, yielding only exo-selective syn adduct **5**.

The 1,4-regioselective Diels-Alder reaction also proceeded with varied substrates. Carboxyl-, cyano-, and vinyl-substituted anthracenes coupled with phthalimide **4a** to give the corresponding 1,4-adducts in 92, 88, and 80% yields, respectively (Fig. 2B) (*30*). Unsubstituted anthracene also afforded only the 1,4-adduct in 55% yield. The moderate yield for this substrate is due not to reduced regio- or stereoselectivity but to the less efficient inclusion process before the reaction. The steric bulkiness of the *N*-substituent on the dienophile is crucial to the 1,4-selectivity. When sterically less demanding *N*-propylphthalimide (**4b**) was used, only the 9,10-adduct was formed.

We turned next to investigating Diels-Alder mediation by bowl-shaped host **2** and, strikingly, observed efficient catalytic turnover. Only 10 mole percent (mol %) of **2** sufficed to catalyze the Diels-Alder reaction of **3a** and *N*-phenylphthalimide (**4c**) (Fig. 4). When **3a** (10.0 μmol) and *N*-phenylphthalimide (**4c**, 10.0 μmol) were suspended in an aque-

ous solution of **2** (1.0 μmol in 1.0 ml) at room temperature for 5 hours (Fig. 5, A and B), the Diels-Alder adduct formed quantitatively (>99% based on **3a**), as evaluated by NMR analysis of the product (*32*). NMR analysis also indicated that the reaction took place at the normal 9,10-position of anthracene to give **6** (Fig. 5C). In the absence of bowl **2**, the reaction hardly proceeded (only 3% yield) under the same conditions. Surprisingly, even in the presence of 1 mol % of **2**, adduct **3a** was obtained in >99% yield after 1 day as estimated by the NMR spectrum in $CDCl_3$. Moreover, the metal component, $(en)Pd(NO_3)_2$ (where en is ethylenediamine) alone, did not catalyze the reaction (*30*). Therefore, the data support promotion of the reaction by the hydrophobic pocket of **2**.

Bowl **2** also efficiently catalyzed Diels-Alder coupling of a variety of anthracene and phthalimide derivatives (*30*). When **3a** and *N*-propyl- or *N*-benzylphthalimide were suspended in an aqueous solution of **2**, the corresponding Diels-Alder products were obtained in almost quantitative yields after 5 hours at room temperature. In addition, 9-methyl and 9-viynylanthracene reacted with **4c** in the presence of a catalytic amount of **2** (10 mol %).

Product inhibition has been a serious problem in previous examples of cavity-promoted Diels-Alder reactions with synthetic hosts (*7*–*11*). Because of the entropic disadvantage arising from the need to bind two reactant molecules, the encapsulated product has generally been a thermodynamic sink. Therefore, the reactions require near-stoichiometric quantities of host. It is noteworthy that, in contrast to previous examples, the present Diels-Alder reaction involves an exclusion step in the catalytic cycle. Before the reaction, anthracene can stack onto the triazine ligand of **2**, gaining considerable stabilization via aromatic-aromatic or charge-transfer interactions (Fig. 5D, step a). The reactant-like transition state is similarly stabilized. However, once the reaction is complete, the product framework is bent at the 9,10-position, cutting off the host-guest aromatic stacking interaction (Fig. 5D, step b). Accordingly, the encapsulated product is considerably destabilized and smoothly replaced by incoming reagents (Fig. 5D, step c → a). In this sense, the affinity of the host for reactive substrates and the disaffinity for product is markedly similar to enzymatic behavior.

References and Notes

1. L. Pauling, *Am. Sci.* **36**, 51 (1948).
2. W. P. Jencks, *Catalysis in Chemistry and Enzymology* (McGraw-Hill, New York, 1969).
3. D. J. Cram, J. M. Cram, *Container Molecules and Their Guests* (Royal Society of Chemistry, Cambridge, 1994).
4. J. W. Steed, J. L. Atwood, *Supramolecular Chemistry* (Wiley, Chichester, UK, 2000).
5. F. Hof, S. L. Craig, C. Nuckolls, J. Rebek Jr., *Angew. Chem. Int. Ed. Engl.* **41**, 1488 (2002).
6. D. M. Vriezema *et al.*, *Chem. Rev.* **105**, 1445 (2005).
7. J. Kang, J. Rebek Jr., *Nature* **385**, 50 (1997).
8. J. Chen, J. Rebek Jr., *Org. Lett.* **4**, 327 (2002).
9. M. Marty, Z. C.-Watson, L. J. Twyman, M. Nakash, J. K. M. Sanders, *Chem. Commun.* **1998**, 2265 (1998).
10. T. Kusukawa, T. Nakai, T. Okano, M. Fujita, *Chem. Lett.* **32**, 284 (2003).
11. J. Kang, J. Santamaría, G. Hilmersson, J. Rebek Jr., *J. Am. Chem. Soc.* **120**, 7389 (1998).
12. M. L. Merlau, M. P. Mejia, S. T. Nguyen, J. T. Hupp, *Angew. Chem. Int. Ed. Engl.* **40**, 4239 (2001).
13. D. Fiedler, R. G. Bergman, K. N. Raymond, *Angew. Chem. Int. Ed. Engl.* **43**, 6748 (2004).
14. L. S. Kaanumalle, C. L. D. Gibb, B. C. Gibb, V. Ramamurthy, *J. Am. Chem. Soc.* **127**, 3674 (2005).
15. F. Fringuelli, A. Taticchi, *The Diels-Alder Reaction: Selected Practical Methods* (Wiley, Chichester, UK, 2002).
16. R. Breslow, *Acc. Chem. Res.* **24**, 159 (1991).
17. F. Stuhlmann, A. Jäschke, *J. Am. Chem. Soc.* **124**, 3238 (2002).
18. M.-F. Cheng, W.-K. Li, *Chem. Phys. Lett.* **368**, 630 (2003).
19. Computational study [MP2(FULL)/6-31G(d) level] of the Diels-Alder reactions of anthracene and ethylene indicates that the reaction barrier to formation of the 1,4-adduct is much higher than that characterizing the 9,10-adduct (ΔE = 29.6 kJ/mol).
20. B. H. Klanderman, *J. Am. Chem. Soc.* **87**, 4649 (1965).
21. J. Rigaudy, P. Scribe, C. Breliere, *Tetrahedron* **37**, 2585 (1981).
22. T. Ose *et al.*, *Nature* **422**, 185 (2003).
23. M. Fujita *et al.*, *Nature* **378**, 469 (1995).
24. Coordination cages (**1′** and **2**) are now commercially available from Wako Pure Chemicals Industries Limited, Osaka, Japan (Pd-Nanocage and Pd-Nanobowl, respectively). Cage **1** is an analog of **1′** in which ethylenediamine on the Pd(II) ions is replaced by *N,N,N′,N′*-tetramethylethylenediamine.
25. S.-Y. Yu, T. Kusukawa, K. Biradha, M. Fujita, *J. Am. Chem. Soc.* **122**, 2665 (2000).
26. T. Kusukawa, M. Yoshizawa, M. Fujita, *Angew. Chem. Int. Ed. Engl.* **40**, 1879 (2001).
27. T. Kusukawa, M. Fujita, *J. Am. Chem. Soc.* **121**, 1397 (1999).
28. M. Yoshizawa, M. Tamura, M. Fujita, *J. Am. Chem. Soc.* **126**, 6846 (2004).
29. M. Yoshizawa, T. Kusukawa, S. Sakamoto, K. Yamaguchi, M. Fujita, *J. Am. Chem. Soc.* **123**, 10454 (2001).
30. See Materials and Methods available at *Science* Online. Metrical data for the crystal structure of **1** ⊃ **5** are available free of charge from the Cambridge Crystallographic Data Centre under reference CCDC-293777.
31. Force-field calculations were carried out with the use of the Cerius^2 3.5 software package (Molecular Simulation Incorporated, San Diego, CA, 1997).
32. Because no decomposition or side products were observed in the NMR spectra of the reactions catalyzed by **2** either during reaction in D_2O or after extraction into $CDCl_3$, the reported NMR yields have their basis in the product purity observed in the spectra of the $CDCl_3$ extract.

33. This work was financially supported by a Grant-in-Aid for Scientific Research (S), no. 14103014, from the Ministry of Education, Culture, Sports, Science, and Technology of Japan.

Supporting Online Material

www.sciencemag.org/cgi/content/full/312/5771/251/DC1
Materials and Methods
Figs. S1 to S18
Tables S1 and S2

17 January 2006; accepted 13 March 2006
10.1126/science.1124985

Double Perovskites as Anode Materials for Solid-Oxide Fuel Cells

Yun-Hui Huang, Ronald I. Dass, Zheng-Liang Xing, John B. Goodenough*

Extensive efforts to develop a solid-oxide fuel cell for transportation, the bottoming cycle of a power plant, and distributed generation of electric energy are motivated by a need for greater fuel efficiency and reduced air pollution. Barriers to the introduction of hydrogen as the fuel have stimulated interest in developing an anode material that can be used with natural gas under operating temperatures 650°C < *T* < 1000°C. Here we report identification of the double perovskites $Sr_2Mg_{1-x}Mn_xMoO_{6-\delta}$ that meet the requirements for long-term stability with tolerance to sulfur and show a superior single-cell performance in hydrogen and methane.

Development of an anode material for a solid-oxide fuel cell (SOFC) that operates on natural gas is widely recognized to be an important technical objective (*1*–*6*). The conventional NiO/electrolyte composite anode gives good performance with pure H_2 as fuel. The H_2 fuel reduces the NiO to elemental nickel, which leaves a porous oxide-ion electrolyte in which the walls of the pores are coated with Ni^0 particles that not only catalyze breaking of the H_2 bond but also provide electronic conduction from the reaction site to the current collector. However, with natural gas, nickel is fouled by carbon deposition (*7*) unless a large amount of steam is added to the fuel (*8*), and it has a low tolerance to sulfur due to the formation of NiS, which requires a high-grade desulfurization for the fuel (*9*).

Early attempts to identify an alternative anode material consisted of doping transition-metal ions into zirconia (*10*, *11*) or a rare-earth into ceria (*12*). Even where the doped ceria was fabricated as a porous structure with inactive copper on the pore surfaces to provide electronic conduction or with a $Y_xCe_{1-x}O_{2-0.5x}$ buffer layer to improve the electrode/electrolyte bonding, preliminary studies of the catalytic activity of the anode suggest that it remains too low (*13*). However, the ceria-based anode was reported to be effective in preventing carbon formation (*14*) and also to have good tolerance to sulfur (*15*).

Texas Materials Institute, ETC 9.102, The University of Texas at Austin, Austin, TX 78712, USA.

*To whom correspondence should be addressed. E-mail: jgoodenough@mail.utexas.edu

Two different approaches to the anode problem are presently under investigation. One involves identification of a mixed oxide-ion/electron conductor (MIEC) that is stable in the anodic atmosphere and more catalytically active for fuel oxidation than is doped ceria; the other introduces a catalytic layer on the fuel side of a conventional anode that acts as an internal reformer of the fuel to pure H_2 before it reaches the NiO/electrolyte composite. Using the former approach, Tao *et al*. (*3*) have reported that a $(La_{1-x}Sr_x)_{0.9}Cr_{0.5}Mn_{0.5}O_{3-\delta}$ (LSCM) perovskite is an MIEC that is catalytically active to CH_4 oxidation; however, it has a low electronic conductivity in the reducing anodic atmosphere and is unstable against 10% sulfur in the fuel (*16*). With the other approach, Zhan and Barnett (*6*) have introduced a Ru-doped CeO_2 layer between the fuel and a NiO/YSZ composite anode (YSZ, yttria-stabilized zirconia) to reform the CH_4 to H_2 and CO. This innovative approach has promise.

We have explored the former approach with an MIEC double-perovskite system $Sr_2Mg_{1-x}Mn_xMoO_{6-\delta}$ as an anode operating on H_2 or CH_4 as the fuel. Our strategy in the selection of this system was based on four observations:

1) The perovskite structure can support oxide-ion vacancies to give good oxide-ion conduction, as is illustrated by the electrolyte $La_{0.8}Sr_{0.2}Ga_{0.83}Mg_{0.17}O_{2.815}$ (LSGM).

2) A perovskite containing a mixed-valent cation from the 4d or 5d block can provide good electronic conduction even where these ions only occupy one subarray of the double-perovskite structure.

3) The ability of Mo(VI) and Mo(V) to form molybdyl ions allows a sixfold-coordinated Mo(VI) to accept an electron while losing an oxide ligand; this ability is the basis of the catalytic activity of the $(PMo_{12}O_{40})^{3-}$ Keggin ion to partially oxidize acrolein to acrylic acid (*17*). However, the use of the Mo(VI)/Mo(V) couple as the catalytic agent in a perovskite requires a double perovskite with an M(II) partner ion to balance the charge.

4) If the two octahedral-site cations of the double perovskite are each stable in less than sixfold oxygen coordination, the perovskite structure can remain stable on the partial removal of oxygen.

To demonstrate the need to use a partner cation like Mg(II) or Mn(II) that is not further reduced by the fuel and is stable in either fourfold or sixfold oxygen coordination, we prepared Sr_2CaMoO_6 and showed that it is not reduced in an anodic atmosphere. However, thermogravimetric analysis of $Sr_2MgMoO_{6-\delta}$ and $Sr_2MnMoO_{6-\delta}$ under the reducing atmosphere at an anode showed loss of oxygen with retention of the double-perovskite structure. Moreover, measurement of the conductivity of polycrystalline $Sr_2MgMoO_{6-\delta}$ and $Sr_2MnMoO_{6-\delta}$ in an atmosphere of H_2 and CH_4 gave an electronic conductivity at 800°C of $\sigma_e \approx 10$ S/cm. With increasing oxygen pressure pO_2, the conductivity decreases for both samples, indicative of an *n*-type conductivity as the dominant electronic mechanism. Single test cells were fabricated by an electrolyte-supported technique with 300-μm-thick LSGM as the electrolyte, $Sr_2Mg_{1-x}Mn_xMoO_{6-\delta}$ (SMMO) as the anode, and $SrCo_{0.8}Fe_{0.2}O_{3-\delta}$ (SCF) as the cathode. A thin buffer layer of $La_{0.4}Ce_{0.6}O_{2-\delta}$ (LDC) between the anode and the electrolyte was used to prevent interdiffusion of ionic species between SMMO and LSGM (*18*–*20*). Pt gauze with a small amount of Pt paste in separate dots was used as a current collector at both the anode and cathode sides for ensuring contact. Details of materials synthesis, characterization, and fuel-cell assembly are given in the Supporting Online Material (*21*).

Cell voltage and power density as a function of current density at different temperatures are shown in Fig. 1 for the single fuel cells with typical anodes of $Sr_2MgMoO_{6-\delta}$ and $Sr_2MnMoO_{6-\delta}$ in H_2, H_2 containing 5 parts per million (ppm) H_2S (H_2/H_2S), and CH_4. For $Sr_2MgMoO_{6-\delta}$, the maximum power density P_{max} reached 968 mW/cm² at 850°C, 838 mW/cm² at 800°C, and 642 mW/cm² at 750°C in H_2. For $Sr_2MnMoO_{6-\delta}$, the P_{max} values were lower: 658 mW/cm² at 800°C and 467 mW/cm² at 750°C. Anodes with unreduced Sr_2CaMoO_6 gave negligible power densities (<10 mW/cm² at 800°C). With dry CH_4 as the fuel, the P_{max} values were 438 mW/cm² for $Sr_2MgMoO_{6-\delta}$ and 118 mW/cm² for $Sr_2MnMoO_{6-\delta}$ at 800°C. Such a high P_{max} for $Sr_2MgMoO_{6-\delta}$ indicates that it is not necessary to add steam to the fuel for methane oxidation with this anode. With wet methane (97% CH_4–3% H_2O), P_{max} decreased to 338 mW/cm² at 800°C. Dry CH_4 can be converted by electrochemical oxidation on the $Sr_2MgMoO_{6-\delta}$ anode, provided that oxide ions are transferred through the electrolyte: $CH_4 + 4O^{2-} = CO_2 + 2H_2O + 8e^-$. In H_2/H_2S, P_{max} changed only slightly for $Sr_2MgMoO_{6-\delta}$, but it decreased considerably compared to that in pure H_2 for $Sr_2MnMoO_{6-\delta}$ (Fig. 1). For the series of $Sr_2Mg_{1-x}Mn_xMoO_{6-\delta}$ anodes, P_{max} decreased with increasing values of x for all of the fuel gases used. $Sr_2MgMoO_{6-\delta}$ always exhibited superior performance. At 800°C, P_{max} was still as high as 811 mW/cm² in 97% H_2–3% H_2O, 829 mW/cm² in H_2/H_2S, and 800 mW/cm² in 97% H_2/H_2S–3% H_2O.

To test the stability of the anodes, we initially operated the cell under a constant current

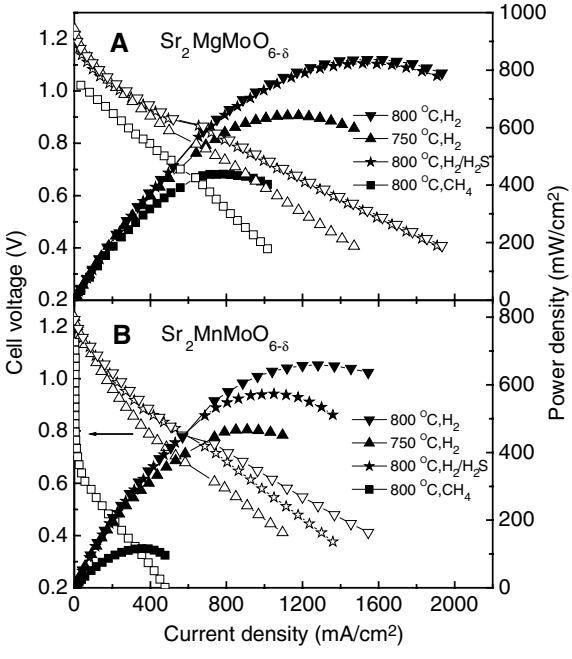

Fig. 1. Cell voltage and power density as a function of current density for the single fuel cells with anodes of (**A**) $Sr_2MgMoO_{6-\delta}$ and (**B**) $Sr_2MnMoO_{6-\delta}$ in H_2, H_2/H_2S, and CH_4 fuels. Cell voltages are represented by open symbols, and power densities by closed symbols.

Table 1. The cell performance at 800°C for several double perovskites, $Sr_2MMoO_{6-\delta}$: $Sr_2Mg_{1-x}Mn_xMoO_{6-\delta}$ and $Sr_2Mg_{0.9}Cr_{0.1}MoO_{6-\delta}$. $P_{max,1}$ is the maximum power density of the first cycle. Power loss is calculated as $\frac{P_{max,1} - P_{max,50}}{P_{max,1}} \times 100\%$, where $P_{max,50}$ is the maximum power density of the 50th cycle. Fade in P_{max} by H_2S is obtained by $\frac{P_{max}(H_2) - P_{max}(H_2/H_2S)}{P_{max}(H_2)} \times 100\%$. The data for LSCM are displayed for comparison.

	Mg	$Mg_{0.80}Mn_{0.20}$	$Mg_{0.50}Mn_{0.50}$	Mn	$Mg_{0.90}Cr_{0.10}$	LSCM
$P_{max,1}$ (mW/cm²), H_2	838	700	650	650	791	577
Power loss over 50 cycles (%), H_2	3.5	1.3	1.4	6.3	7.5	14.1
$P_{max,1}$ (mW/cm²), H_2/H_2S	829	659	595	568	607	395
Power loss over 50 cycles (%), H_2/H_2S	2.5	0.7	9.2	4.8	1.7	16.1
Fade in P_{max} by H_2S (%)	1.1	5.8	8.5	12.6	23.3	31.5

density near where the maximum power density was achieved; only about 0.1% loss in output was observed over 2 days. This minor loss is not large enough for evaluating these anodes in a short time. Instead, we ran the cells for repeated power cycles from open circuit voltage (OCV) to 0.4 V and back to OCV. Figure 2 provides a measure of P_{max} of the single cells at 800°C against cycle number for different anodes. First, we concentrate on the performance of $Sr_2MgMoO_{6-\delta}$. As shown in Fig. 2A, P_{max} dropped very slightly after 50 cycles. Whether in dry fuel or in wet fuel, it performed stably for 50 power cycles. The P_{max} curves versus cycle number in H_2 and H_2/H_2S essentially overlapped, indicative of an excellent tolerance to this amount of sulfur. To further test the stability in H_2/H_2S, we ran the cell in H_2 containing 50 ppm H_2S at a fixed current density of 920 mA/cm^2. After 200 hours, the power density dropped from the initial 595 mA/cm^2 to 566 mA/cm^2, showing only 4.8% fade (fig. S7) (*21*). Power cycling of the $Sr_2MgMoO_{6-\delta}$ anode in dry and wet CH_4 was tested after it cycled in H_2 and H_2/H_2S. P_{max} varied from 412 to 346 mW/cm^2 in dry CH_4, and from 338 to 304 mW/cm^2 in wet CH_4, which shows that CH_4 is oxidized without poisoning the anode in the absence of steam. The cycling stability in H_2 and H_2/H_2S for other anodes (Fig. 2, B and C) showed that P_{max} decreased a bit more rapidly with power cycling for $Sr_2MnMoO_{6-\delta}$. For the doped $Sr_2Mg_{1-x}Mn_xMoO_{6-\delta}$ anodes, the P_{max} values obtained were between those of $Sr_2MgMoO_{6-\delta}$ and $Sr_2MnMoO_{6-\delta}$, as anticipated; the performance was also more stable than that of $Sr_2MnMoO_{6-\delta}$. We compare the cell performances of the $Sr_2Mg_{1-x}Mn_xMoO_{6-\delta}$ anodes in Table 1. With increasing x, P_{max} decreases, power loss for 50 cycles increases, and the fade in P_{max} caused by H_2S also increases. We conclude that in the SMMO anode family, $Sr_2MgMoO_{6-\delta}$ gives an extremely stable performance in a reducing fuel and has an excellent tolerance to sulfur. We analyzed the structure of the anode film by x-ray diffraction after testing it in H_2, H_2/H_2S, and CH_4 for 2 days; we did not find any phase change or any impurity caused by sulfur. Energy dispersive spectrometric (EDS) analysis of the anode surface also confirmed the stability of the $Sr_2MgMoO_{6-\delta}$ phase, and no sulfur or carbon species were detected.

A cell with $(La_{0.75}Sr_{0.25})_{0.9}Cr_{0.5}Mn_{0.5}O_{3-\delta}$ (LSCM) as an anode was fabricated with the same technique used to fabricate the SMMO cells (LSGM as electrolyte, LDC as buffer layer, and SCF as cathode), and its performance was measured under strictly identical conditions. The data obtained at 800°C are shown in Fig. 2 and Table 1 for comparison. The P_{max} value in H_2/H_2S is less than 70% of that in pure H_2, indicative of a large suppression due to the influence of sulfur. Furthermore, after 50 cycles, the power loss was as high as 14% in H_2 and 16% in H_2/H_2S. The large degradation in performance caused by sulfur may be due to the instability of Cr^{3+} in the sulfur atmosphere. To confirm the influence of Cr^{3+} on the performance, we doped a small amount of Cr^{3+} into $Sr_2MgMoO_{6-\delta}$ and prepared $Sr_2Mg_{0.9}Cr_{0.1}MoO_{6-\delta}$ as the anode. The P_{max} value of $Sr_2Mg_{0.9}Cr_{0.1}MoO_{6-\delta}$ in H_2 is 791 mW/cm^2 (first cycle) (Fig. 2 and Table 1), which is comparable to that of $Sr_2MgMoO_{6-\delta}$. However, in H_2/H_2S, P_{max} is only 607 mW/cm^2 for the first cycle. Existence of 5 ppm H_2S in H_2 led to a 23.3% decrease in P_{max} for $Sr_2Mg_{0.9}Cr_{0.1}MoO_{6-\delta}$ and 31.5% fade for LSCM, much larger values than those for $Sr_2Mg_{1-x}Mn_xMoO_{6-\delta}$. We believe that $Sr_2MgMoO_{6-\delta}$ exhibits a very high tolerance to sulfur because Mg^{2+} is more resistant to sulfide formation compared with Cr^{3+} and even Mn^{2+} ions.

The anode overpotentials, η_a, of the single cells operating at 800°C are compared in Fig. 3. In H_2, η_a increases with x for the $Sr_2Mg_{1-x}Mn_xMoO_{6-\delta}$ series at the same current density. $Sr_2MgMoO_{6-\delta}$ shows the lowest η_a. In H_2/H_2S, the variation of η_a with x is similar to that in H_2, except for the sample containing Cr.

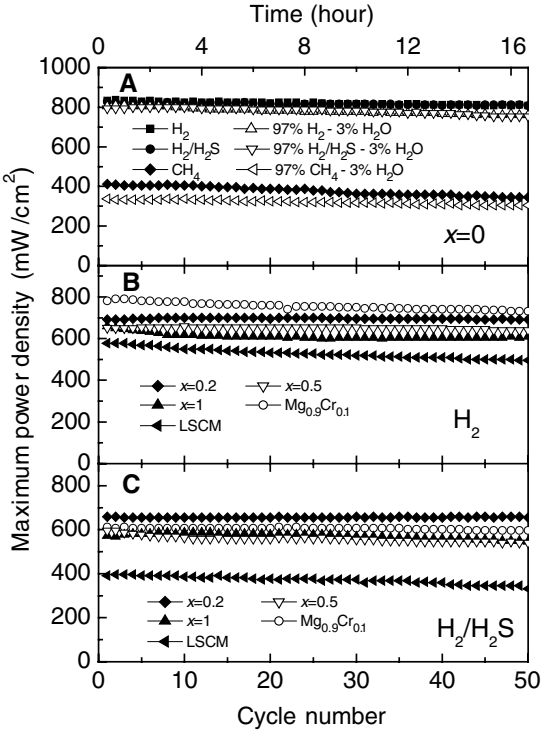

Fig. 2. The maximum power density at 800°C versus cycle number and testing time for the single fuel cells with various $Sr_2Mg_{1-x}Mn_xMoO_{6-\delta}$ anodes. (**A**) $Sr_2MgMoO_{6-\delta}$ (x = 0) obtained in dry and wet H_2, H_2/H_2S, and CH_4. (**B**) Other anodes in dry H_2. (**C**) Other anodes in dry H_2/H_2S. The data for $(La_{0.75}Sr_{0.25})_{0.9}Cr_{0.5}Mn_{0.5}O_{3-\delta}$ (LSCM) and $Sr_2Mg_{0.9}Cr_{0.1}MoO_{6-\delta}$ anodes are shown for comparison.

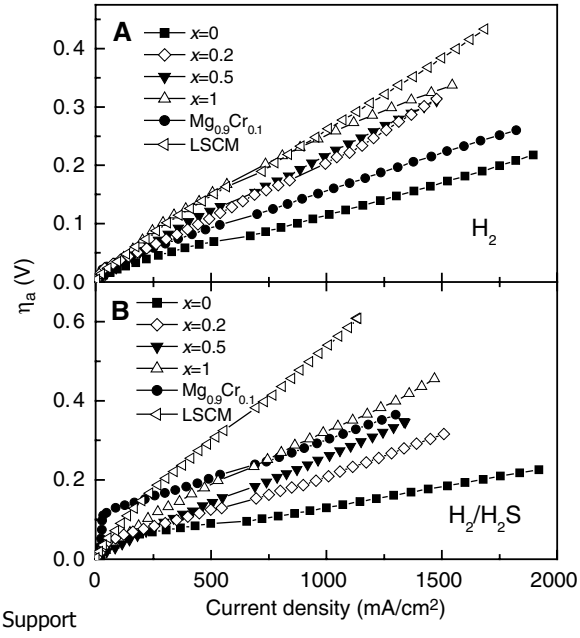

Fig. 3. Overpotential, η_a, of various $Sr_2MMoO_{6-\delta}$ anodes as a function of current density for the single fuel cells operating at 800°C in dry H_2 (**A**) and H_2/H_2S (**B**).

$Sr_2MgMoO_{6-\delta}$ exhibits a lower η_a compared to $Sr_2MnMoO_{6-\delta}$. The dependence of η_a on the current density agrees well with that of the power density in Fig. 2. In addition, in most of the cases we observed, η_a is lower than the corresponding cathode overpotential, η_c. Here, LSCM exhibits a large η_a in H_2 and especially in H_2/H_2S, which shows that SMMO gives a superior performance.

Because the LDC buffer layer is also an MIEC that is catalytically active for fuel oxidation, a cell with only the LDC layer as anode and with Pt mesh and Pt paste as current collector was tested. The values of P_{max} were 528 and only 27 mW/cm^2 in dry H_2 and CH_4, respectively, much lower than those of a cell with $Sr_2MgMoO_{6-\delta}$ as anode. Furthermore, EDS results for the $Sr_2MgMoO_{6-\delta}$/LDC/LSGM/SCF cell after operating in H_2, H_2/H_2S, and CH_4 for a total of 10 days showed no Pt in the LDC layer. This result demonstrates that the high performance of our cells with SMMO as anode was not dominated by the LDC layer. We further tried to use Au mesh and Au paste as the current collector. A drop in P_{max} occurred because of Au melting and a possible formation of Au-Mg alloy (*21*). In addition, because the $Sr_2MgMoO_{6-\delta}$ anode was poisoned by the existence of Au, the activity in CH_4 became very poor, which could not be improved by sputtering Pt on the anode surface. Instead, the observation reinforces the conclusion that SMMO plays an important catalytic role in oxidation of CH_4. We note that Pt paste is also catalytic for CH_4 oxidation. However, even without Pt paste, the $Sr_2MgMoO_{6-\delta}$ anode with buried Pt mesh as current collector still showed a P_{max} of 340 mW/cm^2 at 800°C in dry CH_4.

With a 300-μm-thick LSGM electrolyte and SCF as the cathode, the double-perovskite anodes that we investigated show a high power density and a stable performance on power cycling. Moreover, they exhibit an excellent tolerance to sulfur. $Sr_2MgMoO_{6-\delta}$ also shows a very high power density in dry methane. Our results are also applicable to YSZ as electrolyte. These preliminary results indicate that optimization of the chemistry and the morphology of these double perovskites can provide an anode material for a SOFC that operates on natural gas.

References and Notes

1. B. A. Boukamp, *Nat. Mater.* **2**, 294 (2003).
2. A. Atkinson *et al.*, *Nat. Mater.* **3**, 17 (2004).
3. S. W. Tao, J. T. S. Irvine, *Nat. Mater.* **2**, 320 (2003).
4. S. W. Tao, J. T. S. Irvine, *J. Electrochem. Soc.* **151**, A252 (2004).
5. E. P. Murray, T. Tsai, S. A. Barnett, *Nature* **400**, 649 (1999).
6. Z. L. Zhan, S. A. Barnett, *Science* **308**, 844 (2005).
7. B. C. H. Steele, I. Kelly, H. Middleton, R. Rudkin, *Solid State Ionics* **28-30**, 1547 (1988).
8. A. L. Lee, R. F. Zabransky, W. J. Huber, *Ind. Eng. Chem. Res.* **29**, 766 (1990).
9. Y. Matsuzaki, I. Yasuta, *Solid State Ionics* **132**, 261 (2000).
10. X. J. Huang, W. Weppner, *J. Chem. Soc. Faraday Trans.* **92**, 2173 (1996).
11. S. W. Tao, J. T. S. Irvine, *J. Solid State Chem.* **165**, 12 (2002).
12. O. A. Marina, C. Bagger, S. Primdahl, M. Mogensen, *Solid State Ionics* **123**, 199 (1999).
13. S. Park, J. M. Vohs, R. J. Gorte, *Nature* **404**, 265 (2000).
14. S. A. Barnett, *Handbook of Fuel Cell Technology* (Wiley, Hoboken, NJ, 2003), vol. 4, p. 98.
15. H. P. He, R. J. Gorte, J. M. Vohs, *Electrochem. Solid-State Lett.* **8**, A279 (2005).
16. S. Zha, P. Tsang, Z. Cheng, M. Liu, *J. Solid State Chem.* **178**, 1844 (2005).
17. J. B. Goodenough, *Solid State Ionics* **26**, 87 (1988).
18. K. Q. Huang, J. B. Goodenough, *J. Alloys Compds.* **303-304**, 454 (2000).
19. K. Q. Huang, J. H. Wan, J. B. Goodenough, *J. Electrochem. Soc.* **148**, A788 (2001).
20. J. H. Wan, J. Q. Yan, J. B. Goodenough, *J. Electrochem. Soc.* **152**, A1511 (2005).
21. Details of the materials synthesis, characterization, fuel cell assembly, and performance are available as supporting material on *Science* Online.

22. We thank J. C. Denyszyn for assistance with the Labview 7.1 software, R. Caudillo for EDS measurement, J. S. Zhou for useful discussion on overpotentials, and the Robert A. Welch Foundation (Houston, TX) for support of this work.

Supporting Online Material

www.sciencemag.org/cgi/content/full/312/5771/254/DC1
Materials and Methods
Figs. S1 to S19
Tables S1 to S3
References

6 February 2006; accepted 13 March 2006
10.1126/science.1125877

Catalytic Alkane Metathesis by Tandem Alkane Dehydrogenation–Olefin Metathesis

Alan S. Goldman,[1]* Amy H. Roy,[2] Zheng Huang,[2] Ritu Ahuja,[1] William Schinski,[3] Maurice Brookhart[2]*

With petroleum supplies dwindling, there is increasing interest in selective methods for transforming other carbon feedstocks into hydrocarbons suitable for transportation fuel. We report the development of highly productive, well-defined, tandem catalytic systems for the metathesis of *n*-alkanes. Each system comprises one molecular catalyst (a "pincer"-ligated iridium complex) that effects alkane dehydrogenation and olefin hydrogenation, plus a second catalyst (molecular or solid-phase) for olefin metathesis. The systems all show complete selectivity for linear (*n*-alkane) product. We report one example that achieves selectivity with respect to the distribution of product molecular weights, in which *n*-decane is the predominant high-molecular-weight product of the metathesis of two moles of *n*-hexane.

The interconversion of alkanes via alkane metathesis is a reaction with enormous potential applicability:

$$H_3C\text{-}(CH_2)_n\text{-}CH_3 + H_3C\text{-}(CH_2)_m\text{-}CH_3 \rightarrow H_3C\text{-}(CH_2)_{m+n-x}\text{-}CH_3 + H_3C\text{-}(CH_2)_x\text{-}CH_3 \quad (1)$$

Alkanes are the major constituents of petroleum. As oil reserves dwindle, the world will increasingly rely on the Fischer-Tropsch process (reductive oligomerization of CO and H_2) to produce liquid hydrocarbons—specifically *n*-alkanes—from the vast reserves of coal, natural gas, oil shale, and tar sands, or from biomass. The energy content of U.S. coal reserves alone, for example, is about 40 times that of U.S. petroleum reserves and is comparable to that of the entire world's petroleum reserves (*1*).

Unfortunately, neither natural sources nor Fischer-Tropsch production yield alkane mixtures with a tightly controlled molecular weight (MW) distribution, which is important for varied applications. For example, *n*-alkanes in the range of ~C_9 to C_{20} constitute the ideal fuel for a diesel engine (which runs ~30% more efficiently than a gasoline engine); the absence of aromatic impurities results in cleaner burning than that of conventional diesel fuel or even gasoline (*2*, *3*). *n*-Alkanes lower than ~C_9, however, suffer from high volatility and lower ignition quality (cetane number) (*4*). In addition to F-T product mixtures, low–carbon number, low-MW alkanes are also major constituents of a variety of refinery and petrochemical streams. In general, there is currently no practical method for the interconversion of alkanes to give products of higher MW; this challenge provides extremely large-scale potential applications of alkane metathesis (Eq. 1). Additionally, Eq. 1 might be applied to the formation of low-MW products from high-MW reactants (e.g., by reaction with ethane). Although hydrocracking is already a well-established process for this purpose, Eq. 1 might offer an advan-

[1]Department of Chemistry and Chemical Biology, Rutgers University, Piscataway, NJ 08854, USA. [2]Department of Chemistry, University of North Carolina at Chapel Hill, Chapel Hill, NC 27599, USA. [3]Chevron Research and Technology Co., 100 Chevron Way, Richmond, CA 94802, USA.

*To whom correspondence should be addressed. E-mail: agoldman@rutchem.rutgers.edu; brookhar@email.unc.edu

tage, for some applications, of higher selectivity and/or less severe conditions.

We report two systems in which the metathesis of linear alkanes is achieved efficiently and selectively at moderate temperatures via a tandem combination of two independent catalysts, one with activity for alkane dehydrogenation and the other for olefin metathesis. In particular, we exploit highly selective, soluble molecular catalysts developed for each of these reactions, as well as solid-phase olefin metathesis catalysts.

The basic tandem catalytic process is outlined in Fig. 1 for metathesis of an alkane of carbon number n (C_n) to give ethane and $C_{(2n-2)}$. A dehydrogenation catalyst, M, reacts with the alkane to give the corresponding C_n terminal alkene and MH_2. Olefin metathesis of the 1-alkene generates ethylene and an internal $C_{(2n-2)}$ alkene. The alkenes thus produced serve as hydrogen acceptors and generate the two new alkanes via reaction with MH_2, regenerating M and closing the catalytic cycle.

To date, two heterogeneous catalyst systems have been reported to effect the interconversion of alkanes. Burnett and Hughes showed that passage of butane over a mix of platinum on alumina (a dehydrogenation catalyst) and tungsten oxide on silica (an olefin metathesis catalyst) at high temperatures (399°C) results in formation of lower and higher MW alkanes, predominantly propane and pentane (24.7% and 15.9%, respectively, with 37.6% *n*-butane unreacted) (*5*, *6*). In addition to linear saturated hydrocarbons, small quantities of branched C_4 and C_5 alkanes, methane, and alkenes were also formed. Supported Ta and W hydride catalysts that function as alkane metathesis catalysts at much lower temperatures were reported by Basset (*7*–*9*), but product yields were low. For example, a turnover number (mol of propane transformed per mol of catalyst) of 60 and conversion of 6% was observed for metathesis of propane to give C_1 to C_6 alkanes with the use of a supported Ta hydride species (120 hours, 150°C) (*8*). More recent work showed that an alumina-supported tungsten hydride species gave somewhat increased turnover numbers (*8*). Basset has shown that these systems operate via the reaction of metal centers with alkanes to give metal-carbene complexes (via α-H elimination) as well as free olefins (via β-H elimination and β-alkyl transfer) (*10*). Such pathways, unlike the one outlined in Fig. 1, are consistent with the reported formation, from linear alkanes, of both branched and linear products, as well as catalytic methane production (*7*–*10*).

Our investigation was largely based on the use of Ir-based pincer complexes, first reported by Jensen and Kaska (*11*, *12*) and explored extensively in our own laboratories (*13*–*17*); specifically, complexes **1**, **2a**, and **2b** were used (Fig. 2). These systems exhibit high stability, but their dehydrogenation activity is inhibited by buildup of even moderate concentrations of alkene product. The dual catalytic system (Fig. 1) would require only a very low steady-state concentration of alkenes during catalysis; thus, inhibition of catalysis by product could be avoided. Numerous olefin metathesis catalysts are available (*18*–*20*); we examined the Schrock-type catalyst **3** (*21*, *22*) after determining that the widely used Grubbs-type catalysts (*19*) react with and deactivate the iridium-based dehydrogenation catalysts.

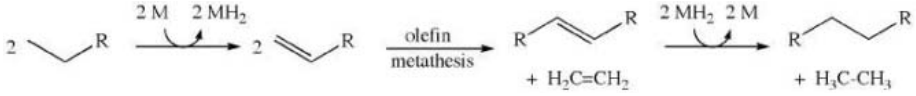

Fig. 1. Alkane metathesis via tandem transfer dehydrogenation–olefin metathesis illustrated with the formation and metathesis of two molecules of 1-alkene. M, active catalyst in the transfer dehydrogenation cycle [e.g., (pincer)Ir].

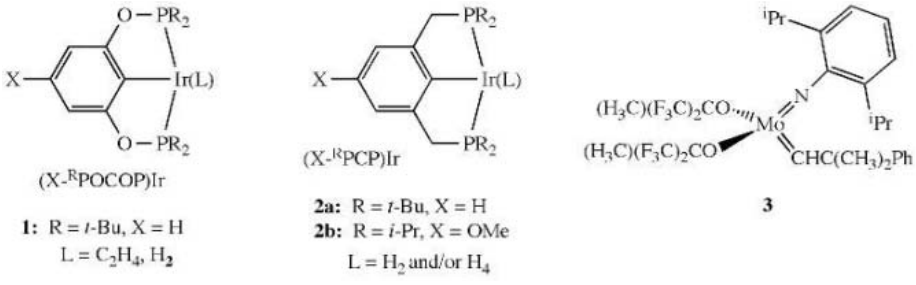

Fig. 2. Dehydrogenation catalysts **1** and **2** and Schrock-type metathesis catalyst **3**.

Initial experiments combining **3** with Ir-based dehydrogenation catalysts in solution proved successful. An *n*-hexane solution containing 10 mM dehydrogenation catalyst precursor **1**-C_2H_4 (0.14 mol % relative to hexane) and 16 mM Schrock catalyst **3** was heated at 125°C under argon in a sealed glass vessel for 24 hours. This process converted 135 equivalents (relative to Ir) of *n*-hexane to a range of C_2 to C_{15} *n*-alkanes. No branched or cyclic alkanes were detected. Products were monitored by gas chromatography (GC) using mesitylene as an internal standard. The product distribution was concentrated in the C_2 to C_5 and C_7 to C_{10} ranges (Table 1, entry 1). Heating for longer times resulted in few additional turnovers. However, upon addition of more olefin metathesis catalyst **3**, alkane metathesis was reinitiated, indicating that decomposition of **3** is responsible for the deactivation of the system under these conditions. Using **1**-H_2 and two equivalents of *t*-butylethylene (TBE) as a hydrogen acceptor, along with catalyst **3**, similar results were obtained (Table 1, entry 2). [The reaction of the dihydride catalyst precursor **1**-H_2 with one equivalent of TBE is presumed to generate the catalytically active species (^{tBu}POCOP)Ir (**1**). The use of two equivalents of TBE per mol of **1**-H_2 is expected to give results most comparable to those obtained with **1**-C_2H_4, because **1**-C_2H_4 constitutes the same catalytically active species plus 1 mol of olefin].

Controls were conducted, including experiments with (i) **1**-C_2H_4 and no metathesis catalyst; (ii) **2a**-H_2 and TBE, but with no metathesis catalyst; and (iii) metathesis catalyst **3**, but with no iridium-based catalyst. In none of these cases was any alkane metathesis observed after heating the *n*-hexane solutions for 24 hours at 125°C.

Pincer-ligated iridium complexes have been reported to dehydrogenate *n*-alkanes with high kinetic selectivity for the formation of the corresponding 1-alkene (*15*). Thus, the product distributions indicated in entries 1 and 2 in Table 1 presumably reflect a substantial degree of olefin isomerization before olefin metathesis under these conditions. For example, isomerization of 1-hexene to 2-hexene, followed by cross-metathesis between 2-hexene and 1-hexene, could give 1-pentene plus 2-heptene (Fig. 3) (*18*–*20*). Alternatively, or in addition, 5-decene (from the cross-metathesis of 2 mol of 1-hexene) could be isomerized to give 4-decene; metathesis with ethylene would then give 1-pentene and 1-heptene. The pincer-iridium complexes are well known to catalyze olefin isomerization (*15*). Thus, terminal dehydrogenation of *n*-hexane in tandem with olefin metathesis, when coupled with rapid olefin isomerization, can account for the C_3 to C_5 and C_7 to C_9 alkanes (Fig. 3).

Alkanes with carbon number greater than 10, produced from hexane, must derive from olefin metathesis of at least one alkene of $C_{n>6}$. The $C_{n>6}$ alkene may result from dehydrogenation of the corresponding *n*-alkane primary product, or it may be obtained directly via cross-metathesis of hexenes, before the resulting olefin (e.g., 5-decene) is hydrogenated.

Consistent with the hypothesis that 1-alkenes are the initial dehydrogenation products, under certain conditions *n*-decane is the major heavy ($C_{n>6}$) product of *n*-hexane metathesis (the non-degenerate cross-metathesis of 1-hexene can

Table 1. Representative examples of the metathesis of *n*-hexane (7.6 M) by **1** or **2** (10 mM) and **3** (16 mM): distribution of C_2 to C_{15} *n*-alkane products.

Entry	Ir catalyst	[TBE] (mM)	Temp. (°C)	Time	Product concentration (mM)													Total product (M)
					C_2	C_3	C_4	C_5	C_7	C_8	C_9	C_{10}	C_{11}	C_{12}	C_{13}	C_{14}	$C_{\geq 15}$	
1	**1**-C_2H_4	0	125	6 hours	123		105	183	131	73	70	47	10	4	2	1	0.3	0.75
				24 hours	233		191	319	234	133	122	81	22	9	5	2	1	1.35
				2 days	261		215	362	265	147	138	89	25	11	6	3	1	1.52
				4 days	264		218	372	276	154	146	95	26	12	6	3	1	1.57
Added additional **3** (8 mM)																		
				5 days	502		436	721	420	239	223	153	56	30	18	10	5	2.81
2	**1**-H_2	20	125	1 day	458		345	547	258	151	139	95	29	13	6	3	2	2.05
3	**2a**-H_2*	20	125	23 hours	(131)	176	127	306	155	37	49	232	18	4	4	10	2	1.25
Added additional **3** (6.4 mM)																		
				46 hours	(189)	255	193	399	208	61	81	343	31	9	9	22	7	1.81

*6.4 mM catalyst **3** added initially. Ethane concentrations for entry 3 are extrapolated as explained in the text. For entries 1 and 2, no separation of C_2 and C_3 peaks was obtained (values shown are not extrapolated).

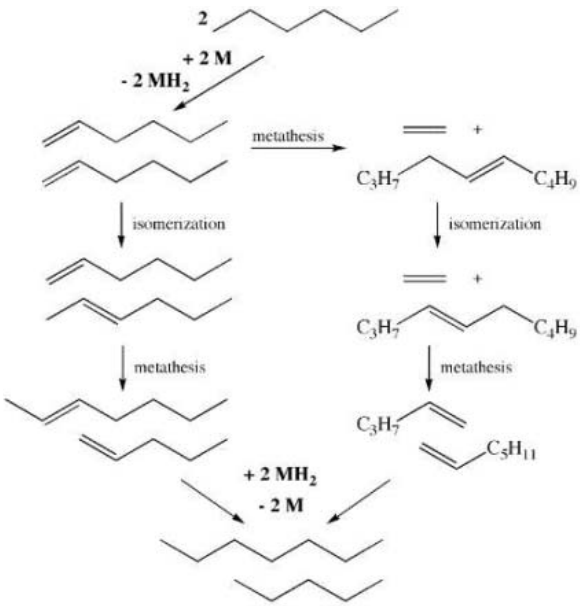

Fig. 3. Two possible pathways for the metathesis of *n*-hexane to give *n*-pentane and *n*-heptane, initiated by dehydrogenation at the *n*-hexane terminal position.

Table 2. Concentrations of C_2 to C_{38} *n*-alkane products resulting from the metathesis of *n*-hexane (4.36 M) and eicosane (*n*-$C_{20}H_{42}$; 1.09 M) by **1**-C_2H_4 (7.14 mM) and **3** (11.43 mM) at 125°C.

Time	Product concentration (M)						Total product
	C_{2-5}	C_{7-10}	C_{11-14}	C_{15-19}	C_{21-24}	C_{25-38}	
1 day	0.44	0.36	0.24	0.31	0.14	0.066	1.56
6 days	0.56	0.64	0.31	0.27	0.12	0.070	1.97

only yield ethene and 5-decene). Combining dehydrogenation catalyst **2a** and metathesis catalyst **3** (Table 1, entry 3) leads to this outcome. (The formation of *n*-tetradecane presumably results from the secondary metathesis reaction of *n*-decane with *n*-hexane.) Presumably, under the conditions of this reaction, diphosphine-ligated **2a** catalyzes isomerization more slowly (or more slowly relative to hydrogenation) than does the diphosphinite-ligated species **1**. This reaction was also monitored by ^{13}C nuclear magnetic resonance spectroscopy (NMR), a method that yields less precise results than GC but facilitates continuous monitoring in a sealed reaction vessel. The NMR results were generally consistent with those obtained by GC, and in particular they revealed that the ratio of the major *n*-alkane products did not considerably change with time.

Although it is difficult to precisely quantify ethane production under our conditions, the solution concentration for the first run in entry 3 was measured by GC as 128 mM. GC analysis of the gas phase indicated the presence of 1.7 μmol of ethane; if this quantity were also in solution, the total ethane concentration would have been 131 mM. (Likewise, a small amount of propane in the gas phase brings the effective concentration from 175 mM to 176 mM.) The average carbon number of all products was found to be ~6.0 (measured as 5.95), an indication that no significant loss of lighter alkanes had occurred (which would raise the observed value above 6.0). The "effective ethane concentration" of 131 mM is substantially lower than the concentration of *n*-decane observed (232 mM). This discrepancy between ethane and *n*-decane production is probably largely attributable to secondary metathesis of the ethene product with 2- or 3-hexenes (which would then contribute to the formation of propene, butene, and pentene). It is also worth noting in the context of this experiment that only trace quantities of methane were observed [0.5 mM effective concentration, probably formed via decomposition of the expected molybdenum methylidene intermediate (*18–20*)]. This result contrasts sharply with the Basset systems, in which methane is formed catalytically; this difference is in accord with the key role played by α-H elimination and β-alkyl elimination in the Basset systems (*7–10*). The catalytic cycle in the systems reported here does not involve either of these elimination steps.

In addition to the alkane disproportionation (self-metathesis) illustrated above, the catalyst system may be used for alkane comproportionation (cross-metathesis)—that is, the production of intermediate-MW alkanes from low-MW and high-MW reactants. Table 2 shows the result of treating a mixture of 4:1 (mol:mol) *n*-hexane and the C_{20} alkane, *n*-eicosane, with catalysts **1** and **3**.

Monitoring the reactions by NMR spectroscopy affords insight into the resting state(s) of the catalysts as well as the extent of alkane metathesis. ^{31}P and ^{1}H NMR spectroscopy indicates that some loss of catalyst **2a**-H_2 occurs during the reaction of *n*-hexane solution. However, a substantial concentration of **2a**-H_2 remains, even when the reaction is no longer progressing. The olefin metathesis catalyst is less

Table 3. Distribution of C_2 to C_{34} *n*-alkane products from the metathesis of *n*-decane (5.1 M) by Ir-based catalysts (9.0 to 9.5 mM) and Re_2O_7/Al_2O_3 (16 mM effective Re_2O_7 concentration) at 175°C.

Ir catalyst	[TBE] (mM)	Time	*n*-Alkane concentration (mM)																	Total product (M)
			C_2	C_3	C_4	C_5	C_6	C_7	C_8	C_9	C_{10}	C_{11}	C_{12}	C_{13}	C_{14}	C_{15}	C_{16}	C_{17}	C_{18}	[>C_{18}]	
1-C_2H_4 (9.5 mM)	0	3 hours	3.9	2.8	8.3	10	12	12	13	16	4980	15	11	9.3	7.2	6.0	4.6	2.1	1.3	1.9	0.14
		18 hours	5.4	9.7	39	43	43	48	55	64	4580	61	46	38	28	23	17	6.9	3.7	5.4	0.54
		7 days	26		101	117	118	115	140	163	3760	154	115	94	71	58	43	18	9.8	16.3	1.36
2a-H_2 (9.0 mM)	18	3 hours	16		61	86	98	122	142	152	3990	137	104	78	53	37	23	9.3	5.2	6.3	1.13
		11 days	39		207	299	327	382	427	446	1500	408	314	245	174	129	87	48	32	58	3.62
2b-H_4 (9.1 mM)	35	3 hours	15		81	117	134	146	172	181	3490	177	147	120	91	72	52	34	26	63	1.63
		18 hours	39		160	234	265	280	318	324	1870	317	271	226	176	145	110	76	61	194	3.20
		9 days	44		220	332	346	405	456	457	753	429	362	300	233	195	151	108	88	241	4.37

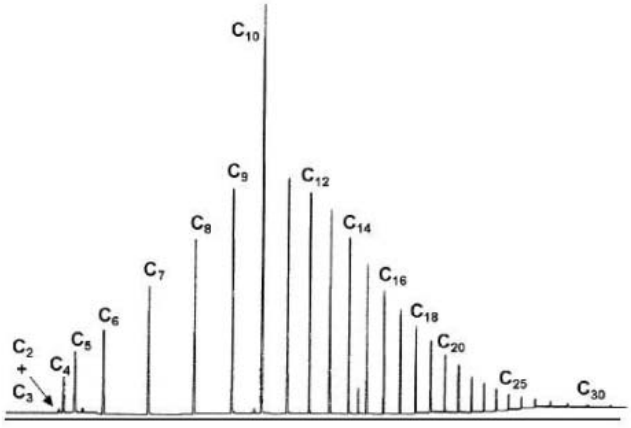

Fig. 4. GC trace of product mixture resulting from the metathesis of *n*-decane (solvent) by **2b**-H_4 and Re_2O_7/Al_2O_3 after 9 days at 175°C (see Table 3).

easily monitored because its resting state depends on the nature of the olefins present in solution; the loss of the 2-methyl-2-phenylpropylidene ligand and the expected formation of 2-methyl-2-phenylbutane (resulting from hydrogenation of 3-methyl-3-phenylbutene) are observed early in the course of the reaction. However, the appearance of free 2,6-diisopropylaniline is observed to approximately coincide with the decreased reaction rate; thus, decomposition of **3** appears to be an important factor limiting turnover numbers in this case. This conclusion is in accord with the experiments in which addition of **3** reinitiates catalytic activity.

In contrast to (^{tBu}PCP)Ir-based **2a**-H_2, the resting state of the (^{tBu}POCOP)Ir-based catalysts (**1**) is the Ir(I)(alkene) complex. For example, monitoring by ^{31}P NMR spectroscopy of *n*-hexane metathesis by **1**-C_2H_4 and **3** indicates that at early stages of the reaction (~150 min), **1**-C_2H_4 is the major Ir resting state, with **1**-(1-propene), **1**-(1-butene), **1**-(1-pentene), **1**-(1-hexene), and **1**-(internal-hexene) present in small concentrations. However, at later stages of the reaction (4 days), **1**-(1-hexene) is observed as the major iridium species in solution. The resting state of the Ir species appears to reflect the activity of the metathesis catalyst. Because the metathesis catalyst decays at the late stage of the reaction, ethylene is no longer produced, although it continues to be consumed as a hydrogen acceptor. As a result, the dehydrogenation of hexane results in the gradual conversion of **1**-C_2H_4 to **1**-(1-hexene).

Given the instability of the molybdenum alkylidene catalysts, we turned to investigation of the supported Re metathesis catalyst Re_2O_7/Al_2O_3, which exhibits greater stability at high temperatures (*23*). Reactions were conducted at 175°C with *n*-decane as the solvent/substrate (Table 3) (*24*). (Control experiments with Re_2O_7/Al_2O_3, with no iridium catalyst present, gave no alkane metathesis after 3 days at 175°C.) The (PCP)Ir catalysts (**2**) proved more effective than the (POCOP)Ir systems (**1**). In a typical experiment, an *n*-decane (2.5 ml, 12.8 mmol) solution of **2b**-H_4 (12.8 mg, 0.0227 mmol), TBE (10 μl, 0.078 mmol), and hexamethylbenzene (10 mg, internal standard) was heated over Re_2O_7/Al_2O_3 (535 mg, 3 wt % Re_2O_7) at 175°C under argon and monitored by GC. After 3 hours, C_2 to C_{28} alkanes were observed with total product concentration estimated at 1.6 M (corresponding to 180 mol of product per mol of Ir). Catalysis slowed, but after 9 days, product concentrations reached 4.4 M. Remarkably, at 9 days, the *n*-decane starting material was comparable in molar quantity to *n*-nonane and *n*-undecane products, with measured C_9:C_{10}:C_{11} molar ratios of 0.6:1:0.6 (Table 3 and Fig. 4).

Because decomposition of the olefin metathesis catalysts appears to limit conversions, we expect that more robust olefin metathesis catalysts will yield higher turnover numbers in future studies. We also expect that more active dehydrogenation catalysts will give more turnovers before decomposition of the metathesis catalyst, and that catalysts that are less prone to isomerize the olefin intermediates will yield greater selectivity for $C_{(2n-2)}$ products. The nature of the tandem system permits the detailed investigation of the component catalysts individually, and the development of more suitable catalysts for both dehydrogenation and olefin metathesis (*25*) is under way.

References and Notes

1. O. Levenspiel, *Ind. Eng. Chem. Res.* **44**, 5073 (2005).
2. M. E. Dry, *J. Chem. Technol. Biotechnol.* **77**, 43 (2001).
3. J. P. Szybist, S. R. Kirby, A. L. Boehman, *Energy Fuels* **19**, 1484 (2005).
4. M. J. Murphy, J. D. Taylor, R. L. McCormick, *Compendium of Experimental Cetane Number Data* (National Renewable Energy Laboratory, Golden, CO, 2004) (www.nrel.gov/vehiclesandfuels/pdfs/sr368051.pdf).
5. R. L. Burnett, T. R. Hughes, *J. Catal.* **31**, 55 (1973).
6. References to earlier related patent work are contained in (*5*).
7. J. M. Basset *et al.*, *J. Am. Chem. Soc.* **127**, 8604 (2005).
8. E. L. Roux *et al.*, *Angew. Chem. Int. Ed.* **44**, 6755 (2005).
9. V. Vidal, A. Theolier, J. Thivolle-Cazat, J.-M. Basset, *Science* **276**, 99 (1997).
10. C. Thieuleux *et al.*, *J. Mol. Catal. A* **213**, 47 (2004).
11. M. Gupta, C. Hagen, R. J. Flesher, W. C. Kaska, C. M. Jensen, *Chem. Commun.* **1996**, 2083 (1996).
12. M. Gupta, C. Hagen, W. C. Kaska, R. E. Cramer, C. M. Jensen, *J. Am. Chem. Soc.* **119**, 840 (1997).
13. I. Göttker-Schnetmann, P. White, M. Brookhart, *J. Am. Chem. Soc.* **126**, 1804 (2004).
14. I. Göttker-Schnetmann, M. Brookhart, *J. Am. Chem. Soc.* **126**, 9330 (2004).
15. F. Liu, E. B. Pak, B. Singh, C. M. Jensen, A. S. Goldman, *J. Am. Chem. Soc.* **121**, 4086 (1999).
16. W. Xu *et al.*, *Chem. Commun.* **1997**, 2273 (1997).
17. K. Zhu, P. D. Achord, X. Zhang, K. Krogh-Jespersen, A. S. Goldman, *J. Am. Chem. Soc.* **126**, 13044 (2004).
18. D. Astruc, *N. J. Chem.* **29**, 42 (2005).
19. R. H. Grubbs, *Tetrahedron* **60**, 7117 (2004).
20. R. R. Schrock, A. H. Hoveyda, *Angew. Chem. Int. Ed.* **42**, 4592 (2003).
21. R. R. Schrock, *Chem. Commun.* **2005**, 2773 (2005).
22. R. R. Schrock *et al.*, *J. Am. Chem. Soc.* **112**, 3875 (1990).
23. C. Pariya, K. N. Jayaprakash, A. Sarkar, *Coord. Chem. Rev.* **168**, 1 (1998).
24. The iridium-based dehydrogenation catalysts appear to be adsorbed on alumina. Accordingly, when alumina is treated with alkane solutions of the iridium complexes, the solutions turn colorless and the support acquires the red color of the catalyst. However, we have yet to

determine whether dehydrogenation is actually catalyzed by supported-phase iridium complexes, or whether it is effected by a low concentration of catalyst that may slowly leach into solution.
25. S. Scott *et al.*, in *Abstracts of Papers, 229th ACS National Meeting* (American Chemical Society, Washington, DC, 2005), abstract PETR-022.
26. This material is based on work supported by NSF under the auspices of the Center for the Activation and Transformation of Strong Bonds, grant CHE-0434568.

Supporting Online Material
www.sciencemag.org/cgi/content/full/312/5771/257/DC1
Materials and Methods
Figs. S1 and S2
References

13 December 2005; accepted 3 March 2006
10.1126/science.1123787

High Natural Aerosol Loading over Boreal Forests

P. Tunved,[1]* H.-C. Hansson,[1] V.-M. Kerminen,[2] J. Ström,[1] M. Dal Maso,[3] H. Lihavainen,[2] Y. Viisanen,[2] P. P. Aalto,[3] M. Komppula,[2] M. Kulmala[3]

Aerosols play a key role in the radiation balance of the atmosphere. Here, we present evidence that the European boreal region is a substantial source of both aerosol mass and aerosol number. The investigation supplies a straightforward relation between emissions of monoterpenes and gas-to-particle formation over regions substantially lacking in anthropogenic aerosol sources. Our results show that the forest provides an aerosol population of 1000 to 2000 particles of climatically active sizes per cubic centimeter during the late spring to early fall period. This has important implications for radiation budget estimates and relevancy for the evaluation of feedback loops believed to determine our future climate.

The boreal forest plays an important role in both climate regulation and carbon cycling (*1*–*3*). Boreal forests represent one-third of all forested land and cover 15 million square kilometers of land. The boreal region is characterized by large seasonal variations in temperature, and the flora is dominated by different pine and spruce species. Most boreal forests contain few large sources of anthropogenic pollution.

In the northern European boreal region, long-term studies of aerosol formation and transformation processes have been performed at several measurement sites. One of the major research aims of these studies, including those performed at the Finnish background station Hyytiälä (*4*–*7*), has been to investigate the role of particle formation. This is important because homogeneous or ion-induced nucleation can provide substantial numbers of aerosols in an environment otherwise deficient of primary sources contributing to the fine-particle mode. This has clear relevance for understanding radiation budgets. Similar issues have been addressed at other locations in northern Europe. Particle-formation events over the boreal forest are well-studied phenomena at stations located in Finnish Lapland [Pallas and Värriö (*8*–*10*)] and at the Scandinavian rim of the boreal region in Sweden [Aspvreten (*11*)]. The mechanisms responsible for the formation and growth of these particles are still uncertain. Although sulfuric acid is one of the most likely candidates thought to be responsible for the formation of the initial nanometer-sized particles, sulfur chemistry does not sustain enough sulfuric acid in the atmosphere to explain more than a small fraction of the observed particle-size growth rate. To explain the observed growth, which is up to a diameter of 50 to 100 nm, other compounds are required (*12*).

Organic constituents comprise a large fraction of the global aerosol burden (*13*, *14*) and there is growing evidence that naturally emitted terpenes contribute notably to gas-to-particle formation (*15*). In the boreal region of northern Europe, monoterpenes are abundant at concentrations ranging from some tens of parts per trillion up to parts per billion depending on season, boundary layer conditions, and temperature (*16*–*18*). When released into the atmosphere, monoterpenes undergo oxidation by ozone, hydroxyl radical, and nitrate radical to yield numerous compounds, the most interesting of which are oxygenated carbon compounds such as mono- and dicarboxylic acids (*19*). Similar compounds may contribute considerably, either directly or through polymerization in the particle phase (*20*), to the gas-to-particle conversion rate over forested areas.

Here, we present evidence of substantial contributions to the aerosol mass and abundance from natural emissions of aerosol precursor gases, most likely terpenes. The approach utilizes a statistical method including long-term observations of the submicrometer aerosol number-size distribution at three different stations in the Finnish boreal zone. The three locations selected for this purpose are the station for Measuring Forest Ecosystem-Atmosphere Relations (SMEAR I) located at Värriö [67°46′N, 29°35′E, 390 m above sea level (asl)], the Pallas-Sodankylä Global Atmospheric Watch (GAW) station located close to Pallas (68°01′N, 24°10′E, 303 m asl), and the SMEAR II station (Hyytiälä, 61°51′N, 24°17′E, 170 m asl). The database used includes 5 years (1999 to 2004) of aerosol number-size distribution data from the stations. The study considers only the period from April to September.

The current ambition is to investigate the characteristic changes of the aerosol population in air masses undergoing marine to continental transition over forested areas in northern Norway, Sweden, and Finland. Previous investigations (*11*, *21*) have shown that substantial sources affect the aerosol during this transition. However, these investigations only account for a

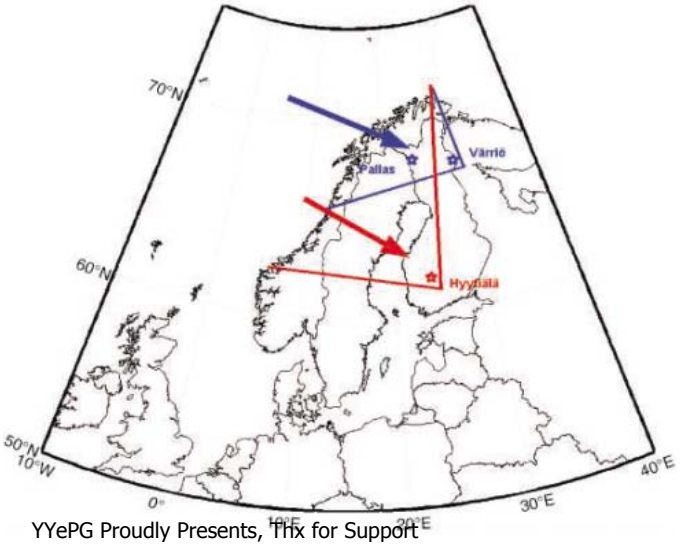

Fig. 1. The transport sectors of the trajectories used in the study. To qualify, each trajectory must spend 90% of the time in the sector. The selection of sectors assures minimum input from anthropogenic sources. The northerly stations share the same sector. Red, Hyytiälä; blue, Värriö and Pallas.

[1]Department of Applied Environmental Science (ITM), Air Pollution Laboratory, Frescativägen 54, SE-106 91, Stockholm, Sweden. [2]Finnish Meteorological Institute, Post Office Box 503 (Erik Palmenin Aukio 1), FI-00101 Helsinki, Finland. [3]Department of Physical Sciences, University of Helsinki, Gustav Hällströmin katu 2, FI-00014 Helsinki, Finland.

*To whom correspondence should be addressed. E-mail: peter.tunved@itm.su.se

limited number of cases. By combining previous findings with the current long-term study, we derive a mechanistic explanation of the seemingly rapid changes in aerosol properties during the marine-to-continental transition.

Trajectories were calculated [with the HYSPLIT4 model (*22*)] for each station with a resolution of 1 hour, throughout the measurement period. From this data set, we extracted trajectories that described transport during 90% of the time in an 80° sector west-north over land relative to each station (Fig. 1). In total, 3700 trajectories described transport to Värriö and Pallas stations, and 4400 trajectories described transport in the Hyytiälä sector. Furthermore, for each single trajectory, we calculated the time of transport over land and measured number-size distribution. Observations were averaged 1 hour around the time of arrival for each trajectory (*23*).

The approach is conceptual. Any change in source profile will result in either buildup or depletion of aerosol mass (assuming constant sink processes). The accumulation of mass is in turn closely related to the time the air parcel spent over the sources. Our results show that an equally simple model can be used to describe the marine-to-continental transition, which evidently involves a change in source profiles large enough to result in an apparent accumulation of mass (i.e., integrated effect of sources and sinks of particles smaller than 0.450 μm, assuming a density of ρ = 1500 kg m^{-3}). In Fig. 2A, the average binned mass increase per hourly increment in time spent over land is displayed for the northerly and southerly stations (in blue and red, respectively). The increase in mass is linear for both receptor stations. On average, the two northerly stations gain approximately 0.014 μg m^{-3} per hour over land with a correlation coefficient of r^2 = 0.83. The corresponding fit for the Hyytiälä data shows that the average mass increase is twice as high, 0.028 μg m^{-3} per hour (r^2 = 0.86).

An apparent mass increase could result from either primary or secondary aerosol sources. The average evolution of the aerosol size distribution and a clear relation between observed size distribution properties and the time spent over land is present at both the northerly stations (Fig. 2B) and at Hyytiälä (Fig. 2C). A continuous growth as time over land increases is evident. The average growth rate for the dominating nuclei/Aitken mode was calculated to be 0.69 nm per hour at the northerly stations and 0.5 nm per hour at the southerly station Hyytiälä (fig. S1). Based on the observed growth rate, we estimated that the vapor generation rate necessary to support this growth of particles less than 80 nm (*23*) was 6.3 × 10^3 molecules cm^{-3} s^{-1} at Pallas and Värriö and 10^4 molecules cm^{-3} s^{-1} at Hyytiälä. Compared with the overall mass increase, this result indicates that at least 26% (21% at Hyytiälä) of the condensed material has vapor pressure low enough to be partitioned in this size range.

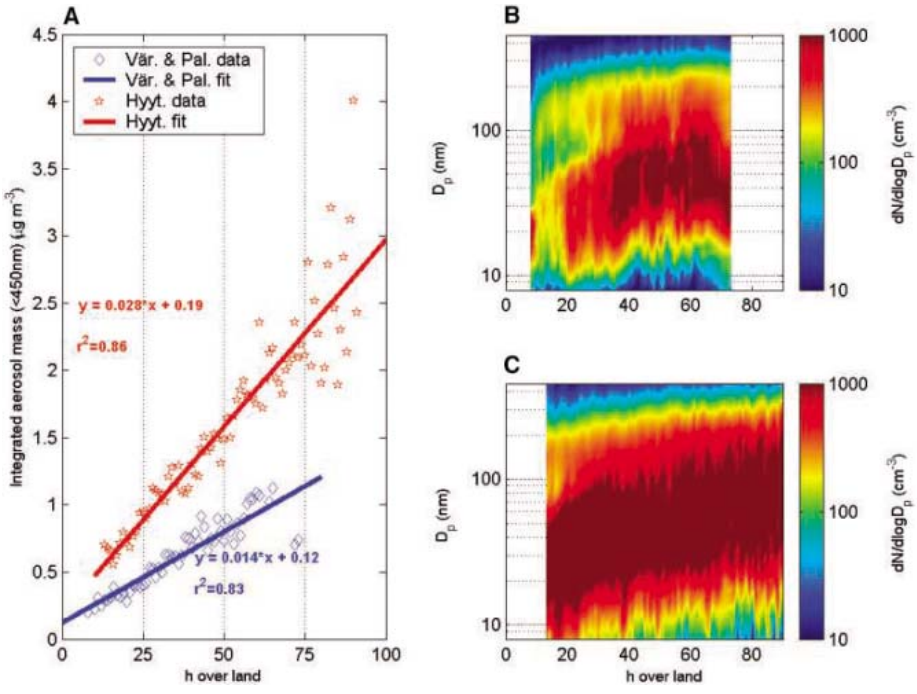

Fig. 2. (**A**) Average observed mass (particle diameter D_p < 0.45 μm, ρ = 1500 kg m^{-3}) versus time over land for Hyytiälä (red) and Värriö+Pallas (blue). Data are fitted linearly. The slope and intersect are displayed in the figure for each combination of stations. Only bins contributing more than 10 observational points were considered in the analysis. (**B**) Size distribution as $dN/d\log D_p$ (cm^{-3}) plotted against time over land for Värriö and Pallas. (**C**) Same as (B) but for Hyytiälä. h, hours.

An increase in mass dominated by primary emissions would not result in an apparent growth of the size distribution modes as we observed. This means that the sources of nucleating and/or condensing gases are much larger over land they are over the marine environment. Based on the selection of trajectories, this source is most likely the boreal forest. Because emission of monoterpenes along the transport path is the most promising explanation for substantial gas-to-particle formation over the boreal forest, we tried to estimate the emission of each trajectory. We adopted an approach for monoterpene emission calculations (*24*) that uses relevant values of emission potential (*25*) along with estimates of foliar biomass density for the northern parts of Scandinavia and Finland. Using this approach, we calculated emissions in the range of 0.5 to 15 μg m^{-3} for the transport region of Värriö and Pallas and emissions reaching 30 μg m^{-3} in the fetch area of the Hyytiälä station (*23*). We assume that the emissions are confined and well mixed in the lowermost 1000 m of the atmosphere.

The previous calculations were repeated with the use of the accumulated monoterpene emissions as the input variable. In Fig. 3A, the result is shown as mass (μg m^{-3}) versus estimated terpene emissions (μg m^{-3}). Recall that the emission equals the total amount that has been emitted during transport, and not the emission rate. When calculated mass was compared with time over land (Fig. 2A), the slope of the Hyytiälä data set was twice that of the northerly stations. However, the slope of the aerosol mass versus the total emitted monoterpenes (Fig. 3A) is almost identical for the northerly and the southerly stations. The curve is best described by a straight line. The slope at both stations is ~0.075 and correlation of r^2 = 0.79 and r^2 = 0.93 for the northerly and southerly stations, respectively. Given that monoterpenes show a high reactivity toward the major atmospheric oxidants (ozone, hydroxyl radical, and nitrate radical), the lifetime during the studied seasons (*16*) (April to September) will be short enough (at most a couple of hours) to allow us to assume that most terpenes have undergone primary oxidation steps before reaching the receptors. Because the slope roughly describes the aerosol mass gained per mass of the oxidized biogenic volatile organic carbon (BVOC), this is an indirect estimate of the aerosol mass yield resulting from oxidation of terpenes (*26*). Assuming a reasonably good representation of terpene emission, this apparent mass yield (apparent because we omit the possible effect of the sinks that are also present during transport) would correspond to ~7.5% [5 to 10% as fits of 25th and 75th percentiles (supporting online material text)]. Although the monoterpene emission estimates are crude, it is clear that latitude- and temperature-dependent emissions of similar compounds are sufficient to support the observed growth. The constant slope of the aerosol mass increase compared with the total terpene emissions indicates that an irreversible and continuous formation of secondary organic aerosol (SOA) from terpenes takes place during transport over forested areas.

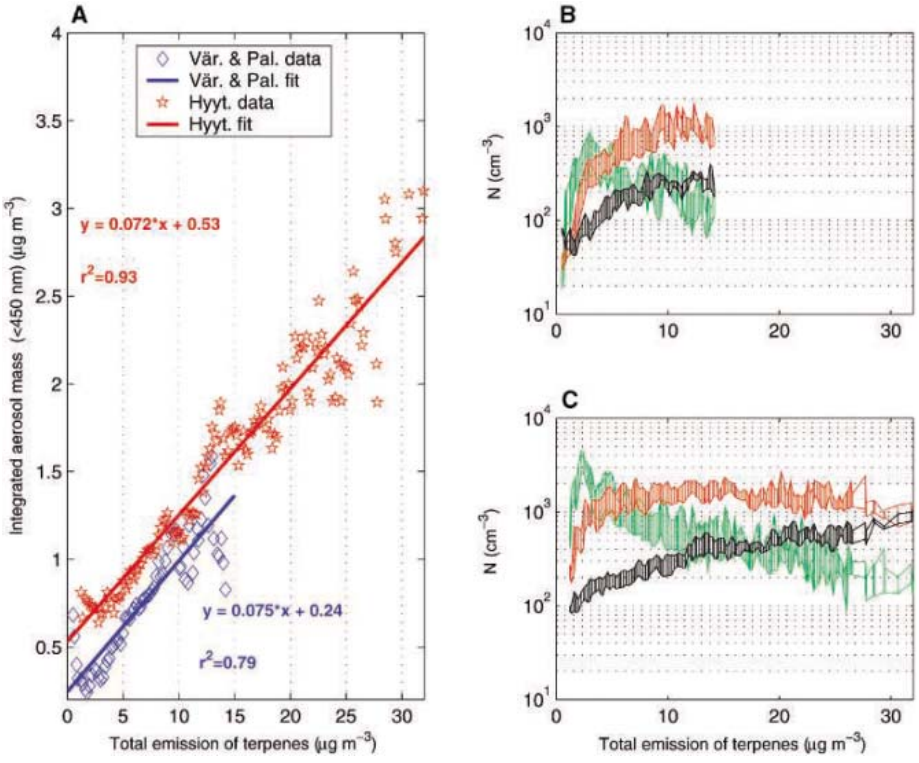

Fig. 3. (**A**) Average observed mass (D_p < 0.45μm, ρ = 1500 kg m^{-3}) versus binned total emissions of terpenes for Hyytiälä (red) and Värriö+Pallas (blue). Data are fitted linearly. The slope and intersect are displayed for each combination of stations. Only bins contributing more than 10 observational points were considered in the analysis. (**B**) 50th to 75th percentile ranges for observed and averaged number concentration (cm^{-3}) in the size range from 10 to 30 nm (green), 30 to 90 nm (red), and >90 nm (black) plotted against calculated total emission of terpenes, Värriö and Pallas. (**C**) Same as (B) but for Hyytiälä.

Figure 3, B and C, gives the evolution of the number concentration in different size ranges per 0.2 μg m^{-3} increment in emitted terpenes. The size ranges described are 10 to 30 nm (green), 30 to 90 nm (red), and 90 to 450 nm (black), shown as 50th to 75th percentile range of the mass in each bin. Both figures clearly show that the highest concentrations of very small particles are present when accumulated emissions are low. As emissions increase, more mass is added to the existing particles and they start to grow into the size range between 30 to 90 nm. Throughout the transport over land and the associated emissions, the accumulation mode concentration (>90 nm) increases almost linearly. This means that emissions of monoterpenes (most likely in combination with other trace gases such as H_2SO_4, H_2O, and NH_3) serve as an efficient way of contributing to an increased aerosol number concentration. The formation of particles remains high only as long as the balance between production and removal of condensable gases supports a high enough concentration of condensable gases for nucleation to occur. Because formation of particles adds to the overall sink of precursor gases, this balance becomes distorted, disfavoring further nucleation as condensable gases are preferentially partitioned on existing larger particles. The nucleation quenches itself. Nucleation thus serves as a regulatory mechanism for building up and maintaining high number concentrations over land. Only during the first stages of the transition does nucleation contribute to a substantial increase in number. This means that the forest at high latitudes can typically support 1000 to 2000 cm^{-3}, reflecting a steady-state aerosol population representative of the typical source strength in this region. This equilibrium in particle number is established rapidly (Fig. 3, B and C).

Our results clearly show that a substantial gas-to-particle formation of BVOC to SOA takes place over the boreal forest in northern Europe. These BVOCs are most likely emitted from the forest itself and, based on previous findings, are most likely constituted of terpenes. Based on modeled monoterpene emission, our analysis suggests an apparent mass yield in the range of 5 to 10%. The investigations further show that the boreal forest typically sustains 1000 to 2000 particles cm^{-3} in a climatic relevant size range (~40 to 100 nm). This notable level of particle number is established rapidly, making estimates of the natural aerosol loadings over the boreal forest comparably easy. Because we provided a similar mechanistic and quantitative behavior for two widely separate locations (more than 700 km apart), the derived relations suggest that similar mechanisms control the aerosol number and mass evolution over large areas in the boreal regions of the Northern Hemisphere.

The high natural aerosol loading in the boreal forest environment should be contrasted with other natural aerosol systems, such as the remote marine environment, in which substantially lower number densities of climate-active particles have been observed (*27*).

Recent findings (*28*) further support the role of aerosol production over the boreal forest in contributing to the cloud condensation nuclei (CCN) and cloud droplet populations in remote areas. These findings together with our study clearly establish that the forest is a major source of climate-relevant aerosol particles, most likely also capable of competing with the anthropogenic CCN loadings transported over forested areas.

References and Notes

1. P. Ciais *et al.*, *J. Geophys. Res.* **100**, 5051 (1995).
2. P. P. Tans, I. Y. Fung, T. Takahashi, *Science* **247**, 1431 (1990).
3. G. B. Bonan, D. Pollard, S. L. Thompson, *Nature* **359**, 716 (1992).
4. J. M. Mäkelä *et al.*, *Geophys. Res. Lett.* **24**, 1219 (1997).
5. J. M. Mäkelä *et al.*, *Boreal Environ. Res.* **5**, 299 (2000).
6. M. Kulmala, A. Toivonen, J. M. Mäkelä, A. Laaksonen, *Tellus B* **50**, 449 (1998).
7. M. Kulmala *et al.*, *Tellus B* **53**, 324 (2001).
8. M. Komppula *et al.*, *Boreal Environ. Res.* **8**, 395 (2003).
9. M. Kulmala *et al.*, *J. Aerosol. Sci.* **35**, 143 (2004).
10. H. Vehkamäki *et al.*, *Atmos. Chem. Phys* **4**, 2015 (2004).
11. P. Tunved *et al.*, *Atmos. Chem. Phys* **3**, 2183 (2003).
12. M. Boy *et al.*, *J. Geophys. Res.* **108**, 4667 (2003).
13. T. Novakov, J. E. Penner, *Nature* **365**, 823 (1993).
14. M. O. Andreae, P. J. Crutzen, *Science* **276**, 1052 (1997).
15. C. D. O'Dowd, P. Aalto, K. Hämeri, M. Kulmala, T. Hoffmann, *Nature* **416**, 497 (2002).
16. H. Hakola, *Atmos. Environ.* **37**, 1623 (2003).
17. R. Janson, K. Rosman, H. Karlsson, H.-C. Hansson, *Tellus B* **53**, 423 (2001).
18. J. Spanke, U. Rannik, R. Forkel, W. Nigge, T. Hoffmann, *Tellus B* **53**, 406 (2001).
19. I. G. Kavouras, N. Mihalopoulos, E. G. Stephanou, *Nature* **395**, 683 (1998).
20. M. Kalberer *et al.*, *Science* **303**, 1659 (2004).
21. P. Tunved *et al.*, *J. Geophys. Res.* **110**, D07201 10.1029/2004JD005085 (2005).
22. R. R. Draxler, G. D. Hess, "Description of the Hysplit_4 modelling system" (NOAA Tech Memorandum, ERL ARL-224, 1997).
23. Materials and methods are available as supporting material on *Science* Online.
24. A. Guenther, *Ecol. Appl.* **7**, 34 (1997).
25. V. Lindfors, J. Rinne, T. Laurila, "Biogenic VOC emissions and photochemistry in the boreal regions of Europe (BIPHOREP) scientific final report" (Commission of European Communities, Luxembourg, 1999), chap. 10.
26. J. R. Odum *et al.*, *Environ. Sci. Technol.* **30**, 2580 (1996).
27. J. Heintzenberg, D. C. Covert, R. Van Dingenen, *Tellus B* **52**, 1104 (2000).
28. V.-M. Kerminen, H. Lihavainen, M. Komppula, Y. Viisanen, M. Kulmala, *Geophys. Res. Lett.* **32**, 10.1029/2005GL023130 (2005).

29. We acknowledge the financial support from International and National Abatement Strategies for Transboundary Air Pollution (ASTA) and Nordic Center of Excellence, research unit on Biosphere-Aerosol-Cloud-Climate Interactions (BACCI).

Supporting Online Material

www.sciencemag.org/cgi/content/full/312/5771/261/DC1
Materials and Methods
SOM Text
Figs. S1 to S6
References

28 November 2005; accepted 17 March 2006
10.1126/science.1123052

A Bifurcating Pathway Directs Abscisic Acid Effects on Stomatal Closure and Opening in *Arabidopsis*

Girish Mishra,* Wenhua Zhang,* Fan Deng, Jian Zhao, Xuemin Wang†

Terrestrial plants lose water primarily through stomata, pores on the leaves. The hormone abscisic acid (ABA) decreases water loss by regulating opening and closing of stomata. Here, we show that phospholipase Dα1 (PLDα1) mediates the ABA effects on stomata through interaction with a protein phosphatase 2C (PP2C) and a heterotrimeric GTP-binding protein (G protein) in *Arabidopsis*. PLDα1-produced phosphatidic acid (PA) binds to the ABI1 PP2C to signal ABA-promoted stomatal closure, whereas PLDα1 and PA interact with the Gα subunit of heterotrimeric G protein to mediate ABA inhibition of stomatal opening. The results reveal a bifurcating signaling pathway that regulates plant water loss.

Abscisic acid (ABA) mediates plant response to environmental stresses (*1*–*4*). During drought, ABA levels in plants increase, and ABA promotes the closing of opened stomata and inhibits the opening of closed stomata. The resulting closure of stomata is crucial to reducing water loss and maintaining the plant's hydration status for survival. The ABA effects on stomatal closure and opening are genetically separable (*5*). Several signaling proteins have been implicated in mediating the ABA effects in signaling networks perhaps linked through G proteins, protein phosphatases, kinases, and phospholipases (*5*–*14*).

Phospholipase D (PLD) hydrolyzes membrane lipids to generate phosphatidic acid (PA), a lipid signaling mediator (*15*–*17*). *Arabidopsis* has 12 PLD genes that form a family of enzymes with heterogeneous regulatory, structural, and biological properties (*15*). We showed that in response to ABA treatments, PLDα1 produces PA that binds to the ABI1 PP2C (*14*). ABI1 is a negative regulator of ABA response (*4*, *8*, *18*), but its specific function in ABA-regulated stomatal closure and opening is not defined. It was proposed that PLD-derived PA in the plasma membrane interacted with ABI1 and removed its inhibition of ABA response (*14*). In addition, PLDα1 binds to GPA1, the Gα subunit of a heterotrimeric GTP-binding protein (G protein) (*19*). Knockout of *GPA1* impedes ABA inhibition of stomatal opening but not promotion of stomatal closure (*5*). These findings prompted us to determine the role of the PLDα1-PA interaction with ABI1 and GPA1 in stomatal movements.

To characterize the interaction between PA and ABI1, we purified ABI1 and the mutant protein $ABI1_{R73A}$ (in which Arg^{73} is replaced with Ala) expressed in *Escherichia coli* (fig. S1A). Analysis with isothermal titration calorimetry (ITC) indicates that PA interacts with ABI1 at 1:1 ratio with the dissociation constant at ~0.3 μM (Fig. 1A), a PA concentration attainable in *Arabidopsis* cells (*14*). The mutant protein $ABI1_{R73A}$ has lost its ability to bind PA (Fig. 1B), indicating that Arg^{73} in ABI1 is essential for PA-ABI1 interaction. Mutation $ABI1_{R73A}$ does not alter the phosphatase activity in the absence of PA, but renders enzyme insensitive to PA inhibition (fig. S1B).

To determine the functional significance of PA-ABI1 interaction, we introduced wild-type $ABI1_{WT}$ or the mutant $ABI1_{R73A}$ gene into a T-DNA insertional ABI1-null mutant (*abi1-ko*) *Arabidopsis* (Fig. 1, C and D). We reasoned that if the PA binding to ABI1 is critical to ABA response, *abi1-ko* plants expressing the $ABI1_{R73A}$ that cannot bind PA should disrupt ABA signaling. The expression of $ABI1_{WT}$ and $ABI1_{R73A}$ transgenes were under the control of the native

Department of Biology, University of Missouri, St. Louis, MO 63121, USA, and Donald Danforth Plant Science Center, St. Louis, MO 63132, USA.

*These authors contributed equally to this work.
†To whom correspondence should be addressed. E-mail: wangxue@umsl.edu

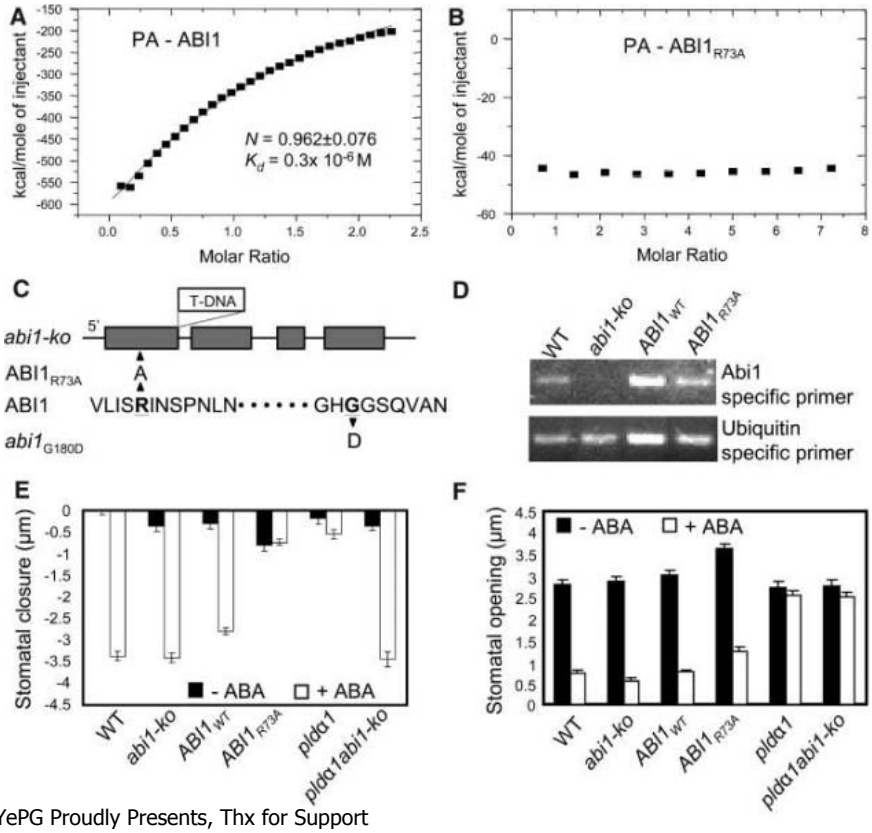

Fig. 1. PA and ABI1 interaction and its role in ABA effect on stomatal closure and opening. (**A** and **B**) Measurements of PA binding to *Arabidopsis* ABI1 and $ABI1_{R73A}$, respectively, by isothermal titration calorimetry. ABI1 and $ABI1_{R73A}$ proteins were purified from proteins expressed in *E. coli*. (**C**) Positions of T-DNA insertion in *abi1-ko* and sequence changes of $ABI1_{R73A}$ and the *abi1* mutant. Boxes denote exons of ABI1; underlined letters show mutated amino acid residues. Abbreviations for the amino acid residues are as follows: A, Ala; D, Asp; G, Gly; H, His; I, Ile; L, Leu; N, Asn; P, Pro; Q, Gln; R, Arg; S, Ser; and V, Val. (**D**) Reverse transcriptase–polymerase chain reaction analysis of *ABI1* or $ABI1_{R73A}$ expression in wild type (WT), *abi1-ko*, and *abi1-ko* carrying the $ABI1_{WT}$ or $ABI1_{R73A}$ transgene. (**E**) Effect of *ABI1* and *PLDα1* mutations on ABA promotion of stomatal closure. Stomata were induced open by 2.5-hours light treatment, then 50 μM ABA was added, and epidermal peels were incubated for another 2 hours under light. Aperture size is expressed as difference from that of open stomata from wild-type plants before ABA treatment. (**F**) Effect of mutations on ABA inhibition of stomatal opening. Stomata were closed after 2.5-hours treatment in dark and then incubated for 2 hours under light with or without 50 μM ABA. Values are means ± SD (n = 20). $ABI1_{WT}$ and $ABI1_{R73A}$ denote *abi1-ko* plants carrying the wild-type *ABI1* and mutant $ABI1_{R73A}$ transgene, respectively.

ABI1 promoter to mimic *ABI1*'s normal temporal and spatial expression. $ABI1_{WT}$ and *abi1-ko* plants showed a normal response to ABA, as did the wild type (Fig. 1, E and F). However, *abi1-ko* plants carrying the $ABI1_{R73A}$ transgene were insensitive to ABA, but for only part of the ABA signaling responses. $ABI1_{R73A}$ plants were insensitive to the promotion of stomatal closure (Fig. 1E), but retained normal sensitivity to the inhibition of stomatal opening (Fig. 1F). This altered response indicates that PA binding to ABI1 is required for ABA promotion of stomatal closure but not for ABA inhibition of stomatal opening.

We also generated *Arabidopsis* plants lacking both PLDα1 and ABI1 by crossing *pldα1* and *abi1-ko* mutants. The double mutations, *pldα1abi1-ko*, were confirmed by real-time polymerase chain reaction (PCR) and by immunoblotting with a PLDα1-specific antibody. The single mutant *pldα1* was insensitive to ABA for both promotion of stomatal closure and inhibition of stomatal opening (Fig. 1, E and F). The double mutant *pldα1abi1-ko* was insensitive to ABA for inhibition of stomatal opening, but was sensitive to ABA for promotion of stomatal closure (Fig. 1, E and F). The ABA responses of *pldα1abi1-ko* and $ABI1_{R73A}$ plants both indicate the bifurcation of the ABA signaling at this point: The PLDα1 and PA interaction with ABI1 promotes stomatal closure, but does not inhibit stomatal opening. The double mutant resembled *abi1-ko* in the stomatal-closure pathway because ABI1, which inhibits the ABA response, is downstream of PLDα1. The normal response of *pldα1abi1-ko* to ABA in closure suggests that an ABA-responsive pathway is operating when both PLDα1 and ABI1 are removed, but this pathway in normal guard cells is controlled by *PLDα1* through removal of the ABI1 inhibition of ABA response. This ABA-responsive pathway is not constitutive, which may explain why the *abi1-ko* mutant has no overt ABA phenotype in stomatal closure. In contrast, inhibition of the stomatal-opening pathway is not governed by ABI1, and thus for this pathway the double mutant behaved like the PLDα1 knockout.

To identify the component that interacts with PLDα1 to inhibit stomatal opening, we studied PLDα1 binding with GPA1. PLDα1 binds to GPA1 through a DRY (Asp-Arg-Tyr) motif that is usually found in animal G protein–coupled receptors (*19*). We used the yeast two-hybrid system to verify the interaction in cells; mutation at the DRY motif residue Lys^{564} decreases the ability of PLDα1 to bind to GPA1 (fig. S2A). ITC analysis showed that wild-type PLDα1 binds to GPA1 in equimolar ratio (N = 1.07 ± 0.075). The affinity of wild-type PLDα1 for GPA1 (dissociation constant K_d = 0.3 μM) is ~150 times that of $PLD\alpha1_{K564A}$ for GPA1 (K_d = 50 μM). The amount of $PLD\alpha1_{K564A}$ that coprecipitated with GPA1 was ~10% of that of wild-type PLDα1 (*19*). Thus, the mutant $PLD\alpha1_{K564A}$ diminishes but does not abolish the binding of PLDα1 to GPA1.

To determine the function of PLDα1-GPA1 interaction, we perturbed the interaction by introducing the mutant $PLD\alpha1_{K564A}$ (in which Lys^{564} is replaced with Ala) and wild-type $PLD\alpha1_{WT}$ genes into *PLDα1*-null *Arabidopsis* (fig. S2B). Expression of the transgenes was controlled by the *PLDα1* native promoter. Except for the decreased ability to bind GPA1, $PLD\alpha1_{K564A}$ is enzymatically as active as PLDα1 (*19*). Introducing $PLD\alpha1_{WT}$ should and did restore the normal ABA response (Fig. 2, A and B). By comparison, $PLD\alpha1_{K564A}$ plants were more sensitive than wild-type plants to ABA for inhibition of stomatal opening, responding to 5 μM ABA, a concentration that had no effect on wild-type plants (Fig. 2C). The increase in ABA sensitivity was reflected in the rate of water loss: $PLD\alpha1_{K564A}$ mutant plants lost less water than wild-type plants, whereas *pldα1* and *gpa1* plants lost more water from their leaves (Fig. 2D). On the other hand, $PLD\alpha1_{K564A}$ plants showed normal sensitivity to ABA for promotion of stomatal closure (Fig. 2A). Thus, blunting the PLDα1-GPA1 interaction renders plants hypersensitive to ABA in inhibiting stomatal opening, but it does not affect the ABA-induced closure of open stomata.

Arabidopsis plants with abrogation of both PLDα1 and GPA1 were generated by crossing *pldα1* and *gpa1*. The double-mutant *pldα1 gpa1* plants resembled the single-mutant *pldα1* plants in that both were insensitive to ABA effects on both pathways, inhibition of stomatal opening and promotion of stomatal closure (Fig. 2, A and B). When the PLD product PA was supplied to epidermal peels of the single and double mutants, PA promoted stomatal closure and inhibited opening in wild-type and *pldα1* plants (Fig. 2, E and F). However, for *gpa1* or *pldα1 gpa1* plants,

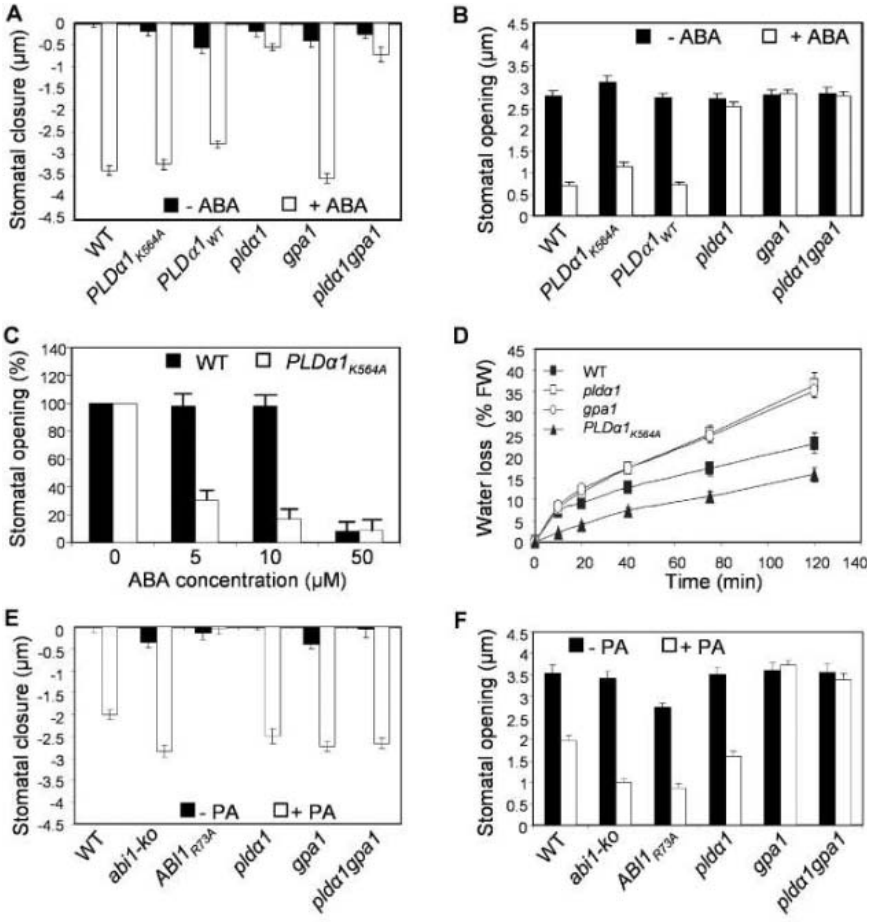

Fig. 2. Effects of PLDα1-GPA1 interaction and PA on ABA regulation of stomatal closure and opening. (**A**) ABA promotion of stomatal closure in *GPA1* and *PLDα1* mutants. Aperture size was measured after 2-hours treatment of open stomata with or without 50 μM ABA. (**B**) ABA inhibition of stomatal opening in *GPA1* and *PLDα1* mutants. Stomata were closed in the dark and then incubated for 2 hours under light with or without 50 μM ABA. (**C**) Response of PLD_{WT} and $PLD\alpha1_{K564A}$ plants to increasing ABA concentrations in inhibition of stomatal opening. (**D**) Water loss from detached *Arabidopsis* leaves as a function of time. Values are means ± SD (n = 20). FW, fresh weight. (**E**) PA promotion of stomatal closure. Stomata were induced open by 2.5-hours light treatment and then transferred to a solution with or without 50 μM dioleoyl-PA and incubated for another 2 hours under light. (**F**) PA inhibition of stomatal opening. Stomata were closed after 2.5-hours treatment in the dark and then incubated for 2 hours under light with or without 50 μM dioleoyl-PA. Values are means ± SD (n = 15).

PA promoted only stomatal closure, but had no effect on inhibiting opening (Fig. 2, E and F). By contrast, for $ABI1_{R73A}$ plants that are unable to bind PA, PA did not promote stomatal closure, but inhibited stomatal opening (Fig. 2, E and F). These results indicate that PLDα1 and PA act upstream of GPA1 and ABI1 in the pathway regulating stomatal responses to ABA signals.

We propose that stomatal responses to ABA are regulated by a bifurcating pathway that includes PLDα1, PA, ABI1, and GPA1 (Fig. 3). To promote closure of open stomata, PLDα1 regulates ABI1 with the use of its lipid product PA. PA binds to ABI1, and this interaction is necessary to remove the ABI1 inhibition of the ABA promotion of stomatal closure. PA regulates ABI1 function by inhibiting its phosphatase activity and by sequestering it to the plasma membrane. The membrane tethering by PA decreases ABI1's translocation from the cytosol to the nucleus and promotes ABA signaling (*14*).

To inhibit opening of closed stomata, PLDα1 modulates the GPA1 function through multiple interactions (Fig. 3). Biochemical data suggest that PLDα1 activates the intrinsic guanosine triphosphatase activity that converts active $Gα\text{-}_{GTP}$ to inactive $Gα\text{-}_{GDP}$ (*19*). In turn, $Gα\text{-}_{GDP}$ binds to PLDα1 and decreases its activity (*19*, *20*). Thus, in $PLDα1_{K564A}$ plants, the ABA signal transduction is sensitized because both the GPA1 and PLDα1 functions are less inhibited by the subdued interaction between $PLDα1_{K564A}$ and GPA1. In contrast, the ABA responses of the *pldα1* and *gpa1* single mutants indicate that both PLDα1 and GPA1 are positive regulators in ABA inhibition of stomatal opening. The positive role of GPA1 may result from the exchange of GTP with GDP; the binding of GTP to GPA1 ($Gα\text{-}_{GTP}$) dissociates Gα from PLDα1, thus removing the inhibition of PLDα1 activity (*19*). PA resulting from PLDα1 activity promotes inhibition of stomatal opening (Fig. 3). Thus, the PLDα1-GPA1 interaction regulates mutually the activity of both proteins. However, the activation of PLDα1 acts upstream of GPA1 because *pldα1* plants display a broader alteration in ABA sensitivity than do *gpa1* plants, and because PA inhibits stomatal opening in *pldα1*, but not in *gpa1 or pldα1gpa1* plants. One potential target of PA is a sphingosine kinase that acts upstream of GPA1 (*7*). ABA activates both PLDα1 and sphingosine kinase (*7*, *14*), and PA has been implicated in binding sphingosine kinase in animal cells (*21*).

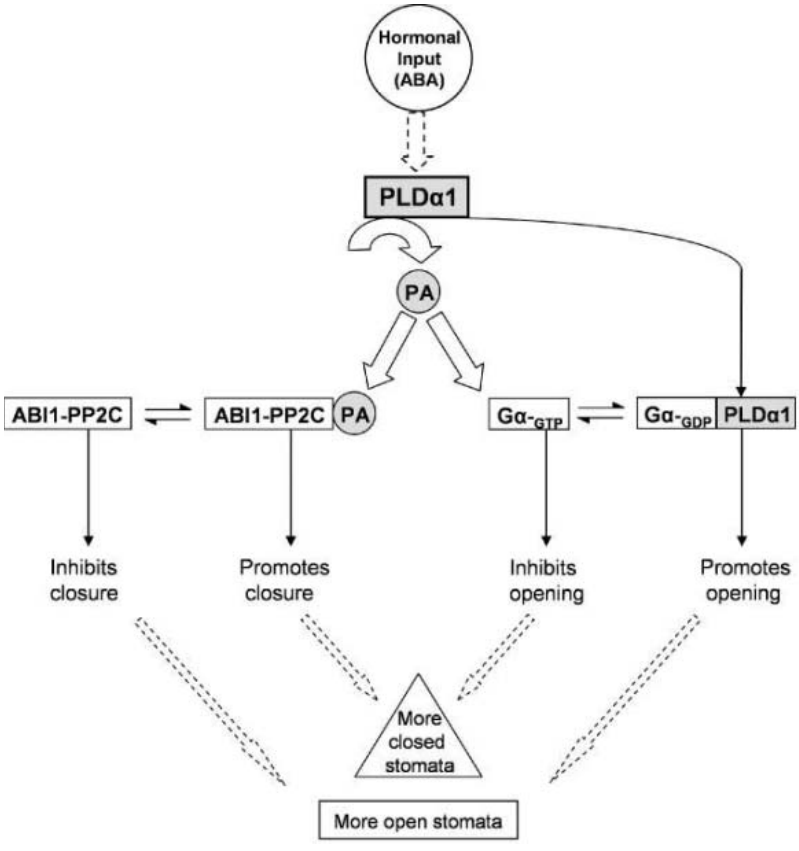

Fig. 3. A bifurcating model for interaction among PLDα1, PA, ABI1, and GPA1 (Gα) in mediating ABA effects on stomatal closure and opening. PLDα1-produced PA binds to ABI1, and this binding removes ABI1 inhibition of ABA promotion of stomatal closure. On ABA inhibition of stomatal opening, PLDα1-produced PA acts upstream of GTP-bound Gα ($Gα\text{-}_{GTP}$) to inhibit stomatal opening, whereas GDP-bound Gα ($Gα\text{-}_{GDP}$) binds to PLDα1 to suppress PLD activity. This model is not comprehensive and concerns only components studied here.

Thus, we conclude that the PLDα1 signaling pathway in guard cells bifurcates at ABI1 and GPA1 to mediate the ABA effects on stomatal closure and opening. Such interaction between PLDα1 and Gα would be unusual for animal cells, in which heterotromeric G proteins typically regulate the function of phospholipases (*22*). However, plants and animals diverge greatly in the PLD and G protein families; *Arabidopsis* has 10 more PLD genes than do humans, but only one canonical Gα (*22*, *23*), and thus their signaling pathways may be organized differently. ABA can act as an intracellular signal (*24*), and activation of membrane-associated PLDα1 may be one initial step that directs the ABA response in guard cells. Although *Arabidopsis* has multiple PLD and PP2C genes, the clear phenotypes from the various mutants in this study indicate that the interaction between PLDα1-PA and ABI1 is specific. The PA binding region in ABI1 is located at its N terminus, which is highly variable among PP2Cs. Our insights into the pathways regulating stomatal function may be used to produce plants with enhanced water-usage efficiency and drought tolerance.

References and Notes

1. L. M. Fan, Z. Zhao, S. M. Assmann, *Curr. Opin. Plant Biol.* **7**, 537 (2004).
2. A. M. Hetherington, C. Brownlee, *Annu. Rev. Plant Biol.* **55**, 401 (2004).
3. R. Desikan *et al.*, *J. Exp. Bot.* **55**, 205 (2004).
4. J. I. Schroeder, G. J. Allen, V. Hugouvieux, J. M. Kwak, D. Waner, *Annu. Rev. Plant Physiol. Plant Mol. Biol.* **52**, 627 (2001).
5. X. Q. Wang, H. Ullah, A. M. Jones, S. M. Assmann, *Science* **292**, 2070 (2001).
6. C. K. Ng, K. Carr, M. R. McAinsh, B. Powell, A. M. Hetherington, *Nature* **410**, 596 (2001).
7. S. Coursol *et al.*, *Nature* **423**, 651 (2003).
8. F. Gosti *et al.*, *Plant Cell* **11**, 1897 (1999).
9. J. P. Sanchez, P. Duque, N. H. Chua, *Plant J.* **38**, 381 (2004).
10. S. Pandey, S. M. Assmann, *Plant Cell* **16**, 1616 (2004).
11. N. Leonhardt *et al.*, *Plant Cell* **16**, 596 (2004).
12. L. Hunt *et al.*, *Plant J.* **34**, 47 (2003).
13. T. Jacob, S. Ritchie, S. M. Assmann, S. Gilroy, *Proc. Natl. Acad. Sci. U.S.A.* **96**, 12192 (1999).
14. W. Zhang, C. Qin, J. Zhao, X. Wang, *Proc. Natl. Acad. Sci. U.S.A.* **101**, 9508 (2004).
15. X. Wang, *Plant Physiol.* **139**, 566 (2005).
16. C. Testerink, T. Munnik, *Trends Plant Sci.* **10**, 368 (2005).
17. M. McDermott, M. J. Wakelam, A. J. Morris, *Biochem. Cell Biol.* **82**, 225 (2004).
18. J. Sheen, *Proc. Natl. Acad. Sci. U.S.A.* **95**, 975 (1998).
19. J. Zhao, X. Wang, *J. Biol. Chem.* **279**, 1794 (2004).
20. W. Lein, G. Saalbach, *Biochim. Biophys. Acta* **1530**, 172 (2001).
21. C. Delon *et al.*, *J. Biol. Chem.* **279**, 44763 (2004).
22. S. M. Assmann, *Science* **310**, 71 (2005).
23. X. Wang, *Curr. Opin. Plant Biol.* **7**, 329 (2004).
24. V. Levchenko, K. R. Konrad, P. Dietrich, M. R. Roelfsema, R. Hedrich, *Proc. Natl. Acad. Sci. U.S.A.* **102**, 4203 (2005).

25. We thank D. Schachtman for critical comments on the manuscript and M. Zolkiewski for help in ITC experiments. This work was supported by grants from the National Science Foundation (IBN-0454866) and U.S. Department of Agriculture (2005-35818-15253).

Supporting Online Material

www.sciencemag.org/cgi/content/full/312/5771/264/DC1
Materials and Methods
Figs. S1 and S2
References

13 December 2005; accepted 24 February 2006
10.1126/science.1123769

Selection on Gamete Recognition Proteins Depends on Sex, Density, and Genotype Frequency

Don R. Levitan* and David L. Ferrell*

Gamete recognition proteins can evolve at astonishing rates and lie at the heart of reproductive isolation and speciation in diverse taxa. However, the source of selection driving this evolution remains unknown. We report on how the sperm bindin genotype influences reproductive success under natural conditions. An interaction between genotype frequency and spawning density determines how sperm bindin genotype influences reproductive success. Common genotypes are selected under sperm-limited conditions, whereas rare genotypes are selected under conditions of intense sperm competition and sexual conflict. Variation in the evolutionary rates of bindin may reflect historic differences in sperm availability.

Gamete recognition proteins determine whether sperm and eggs are compatible at fertilization and often evolve at an exceptionally rapid pace. This is manifested as positive selection, an excess of nonsynonymous nucleotide substitutions, and can be associated with divergent proteins across species, polymorphic proteins within species, or both (*1*). Theory suggests that sexual selection might drive the rapid divergence in these proteins across species and that sexual conflict over the rate of fertilization might result in selection for polymorphic genotypes within species (*1*–*7*). Within species, high sperm concentration may select for eggs with rare alleles that slightly mismatch with sperm, thereby reducing gamete affinities and preventing egg death by polyspermy. The conflict is that sperm compete to be the first sperm to fertilize an egg and "chase" the evolution of these rare alleles. Despite the popularity of these ideas, (i) alternate hypotheses exist for why these proteins evolve quickly, (ii) it is unclear why rates of evolution in these proteins vary across species and, most important, (iii) no data examine how these proteins influence reproductive success in nature (*1*). Measuring the success of different genotypes under natural conditions is the only way to determine how selection influences the evolution of these proteins. We show how sperm bindin genotypes influence sea urchin reproductive success in the sea.

Our expectation is that under sperm-limited conditions, binding rates between eggs and sperm should be selected to be fast (high affinity) for both males and females (*8*). Under sperm-saturating conditions, sexual conflict over fusion rates might result in selection for slow binding rates (low affinity) in females but high binding rates in males. Polyspermy is costly to both sexes, but it never pays to be the second sperm to reach an egg. Thus, males are selected to have fast binding rates, assuming multiple males are competing for fertilizations. Consequently, we investigated the effect of spawning density and bindin genotype frequency on reproductive success and specifically the interaction between frequency and density.

First, we explored the pattern of genotype frequency and reproductive success. Then, because laboratory experiments suggest that matched genotypes have an increased chance of fertilization (*4*), we examined how the degree of matching between male and female genotypes influences reproductive success. Experiments were conducted in the ocean in natural populations of the sea urchin *Strongylocentrotus franciscanus*. Independent groups of sea urchins were induced to spawn at 35 population densities along the outer west coast of British Columbia (*9*). Reproductive success was determined by capturing eggs from each spawning female in the water column, measuring the fraction of eggs developing, and freezing the produced larvae for parentage analysis (*8*). For each spawning event, adult locations were mapped and water movement was recorded (*8*). Female reproductive success first increased and then decreased with male spawning density because of sperm limitation and polyspermy, respectively (Fig. 1) (*8*). Multiple paternity was rampant within females, setting the conditions for sexual conflict (*9*). The 127 adults that spawned in nine of these events (range 8 to 29 adults) were sequenced for a 273–base pair variable portion of the bindin locus (*8*); four events were under sperm-limited conditions at low density, and five events were under sperm-saturated and polyspermic conditions at high density (Fig. 1).

The bindin locus was polymorphic, and genotype frequencies did not differ from Hardy-Weinberg expectations. There was 1 common allele (0.58), 2 alleles at moderate frequency (0.15, 0.14), and 12 rare alleles. The sequences of 3 of the most common alleles and 2 of the rare alleles were identical to and not detectably different in frequency from alleles obtained from 134 individuals spread from Baja, Mexico, to Alaska, USA (*10*). This geographically broader sample, our population and the combined data, showed no evidence of positive selection in this variable domain of bindin (*8*). Because we sequenced only a subset of the bindin gene, we assumed that all substitutions, both synonymous and nonsynonymous, could be used as a genetic marker for unique phenotypes. Possible recombination with linked substitutions outside the sequenced region makes this a conservative test for detecting effects of density and frequency.

Despite the large variation in distance to the nearest mate (0.07 to 11.25 m) and average water flow (0.002 to 0.077 m/s) that largely determine reproductive success (*11*, *12*), there was a significant relation between bindin genotype frequency and male reproductive success. The overall variation explained by a male's bindin genotype frequency was small, but the average effect was large (Fig. 2A) (table S1). Males with common genotypes had an average of four times the reproductive success of males with rare genotypes. This runs counter to the expectation of rapid or even neutral evolution of diverse genotypes. Strong selection against rare genotypes, combined with common genotypes being widespread geographically, should constrain evolutionary diversification. What maintains variation in the face of this selection?

Females exhibited the opposite pattern; females with those same common genotypes had

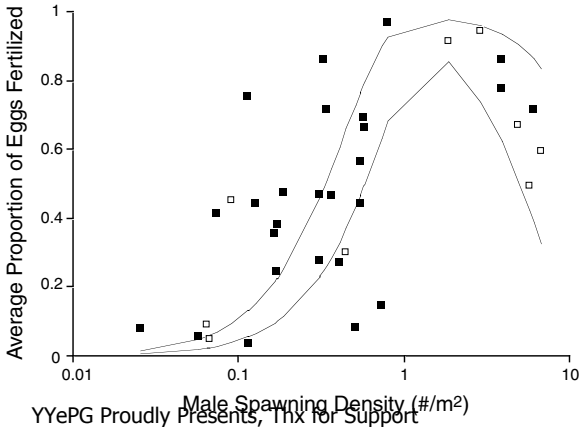

Fig. 1. Average female success and male density. Solid lines indicate the 95% confidence intervals from a fertilization kinetics model fit to these data. Reduced fertilization at low densities is caused by sperm limitation and at high densities by polyspermy. The four spawning events at low density (< 1 m²) and five at high density (> 1 m²) examined in the present study are highlighted as open symbols.

Department of Biological Science, Florida State University, Tallahassee, Florida 32306–1100, USA.

*E-mail: levitan@bio.fsu.edu (D.R.L.); ferrell@bio.fsu.edu (D.L.F.)

half the reproductive success of females with rare genotypes (Fig. 2B and table S2). As a result of the divergent patterns of male and female success, there was no pooled effect of genotype frequency on reproductive success ($P > 0.5$).

We examined how genotype frequency influenced reproductive success across densities, but because frequencies vary among small discrete spawning events, we measured the reproductive success of an individual as a function of how common his or her genotype was among potential mates for each spawning event. A positive relationship indicates that individuals matching genotypes with a high proportion of mates will have increased success. A negative relationship indicates the reciprocal. For each event, this slope was plotted as a function of male spawning density (*8*). There was a significant frequency by density interaction for both sexes (Fig. 3). At low density, individuals that shared their genotype with a high frequency of mates had high reproductive success, whereas at high density the reciprocal was evident. This suggests that the direction and intensity of frequency-dependent selection depends on density. In addition, the relationship passes through zero (no frequency dependence) at the approximate spawning density where the transition from sperm limitation to polyspermy and sexual conflict occurs.

The significance of female bindin genotype (Fig. 2B and Fig. 3) suggests that patterns of matching between male and female genotypes might explain pairwise reproductive success. We examined pairwise reproductive success as a function of spawning density, bindin genotype matching, male and female genotype frequency, mate distance, number of competing males, and water flow ($N = 514$ matings). As predicted (*9*, *11*, *12*), increases in mate distance, competitors, and water flow often decreased reproductive success. Rising out of the variance of these demographic and environmental effects was a complex pattern of interactions between male genotype frequency, genotype matching, and spawning density (tables S3 to S5) (*8*). As noted above, males with common genotypes had higher overall levels of reproductive success compared to males with rare genotypes. However, the effect of female genotype frequency was not significant; female success was a function of genotype matching with the male. The critical result was a significant density by matching interaction. At low density, nonmatched mates had the lowest reproductive success, whereas at high density, fully matched mates had the lowest reproductive success (Fig. 4A). The most common male genotype (AA) had poor reproductive success with non-A females at low density but had the highest reproductive success with these females at high density (Fig. 4B). Rare males did better at high density compared to low density with either matched or unmatched mates, because they were closer to females but not likely to cause polyspermy (rare matches are not likely close neighbors). Rare females are successful because they have high success with partial matches at all densities (Fig. 4A) and do particularly well with common, but unmatched, AA males at high density (Fig. 4B).

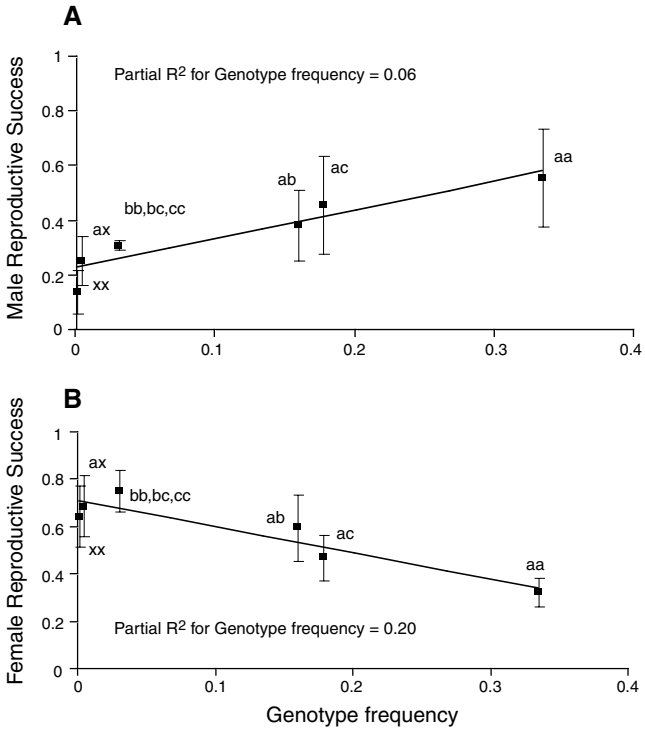

Fig. 2. Bindin genotype frequency (standard error) and total reproductive success. Allele x refers to the pool of rare alleles, and xx refers to any combination of rare genotypes not specifically listed. (**A**) Common genotypes have higher success in males, and (**B**) rare genotypes have higher success in females.

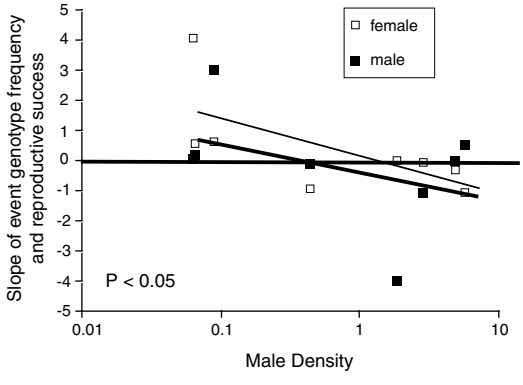

Fig. 3. Relationship between frequency-dependent reproductive success and male spawning density. Positive values indicate an advantage to commonly matching mates, negative values an advantage to rarely matching mates.

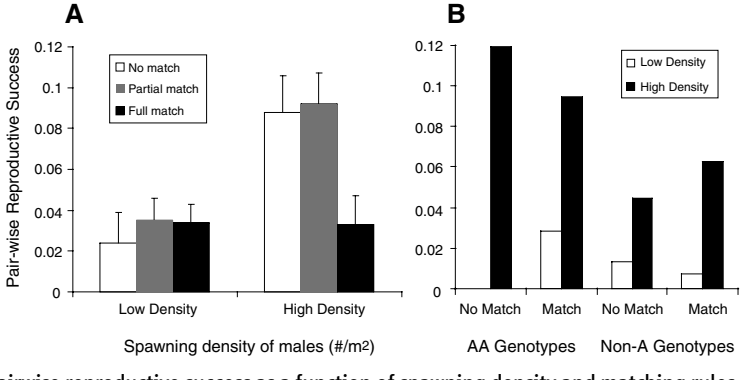

Fig. 4. Pairwise reproductive success as a function of spawning density and matching rules. (**A**) There was a significant interaction between density and matching rules and a significant effect of matching within each density. (**B**) Pairwise reproductive success of AA males and non-A males with females that match at some allele or no alleles at high and low densities.

There are at least three possible mechanisms for the association of female success with their bindin genotype [also noted in (*4*)]. First, although bindin transcription has yet to be detected in eggs or ovaries (*13*), bindin might be pleiotropic and expressed in females. Second, models (*14*, *15*) indicate that female preferences and male traits can become associated by linkage disequilibrium through assortative mating. Third, there may be a tight physical linkage between sperm bindin and a female receptor locus. A female receptor locus has been found in this species (*16*), but it has not been mapped. There may be a cascade of different recognition proteins involved in fertilization (*17*), and linkage disequilibrium at any of these loci might result in this association.

Regardless of the mechanisms that explain why the female bindin genotype influences fitness, these results provide an explanation for the maintenance of rare bindin alleles and the prevention of selective sweeps from common alleles. Rare females are favored because, as the degree of sperm competition increases, matings between unmatched genotypes become increasingly successful. Although common males do best with unmatched females at high density, they also outcompete rare males for the matched eggs that survive at these high sperm concentrations. These results are consistent with sexual conflict driving diversifying selection. Some mutations might simply result in inefficient binding, which would reduce polyspermy. Other mutations might match a complementary rare allele in the other sex. These novel matched proteins would increase in frequency under sperm competitive conditions, because matches are rare and less likely to cause polyspermy (e.g., non-A males in Fig. 4B). As their frequency increased, these alleles would be less advantageous under sperm-competitive conditions but increasingly advantageous under sperm-limited conditions (e.g., AA males in Fig. 4B). The initial process of mutation to an egg that slows binding might facilitate the second by allowing the persistence of rare alleles until the emergence of a complementary mutation. These processes set the stage for not only diversifying selection but also divergent selection, because different, but matched, loci are potentially selected allopatrically or even sympatrically, as males chase the evolution of different female receptors (*6*, *7*).

The interaction between spawning density and genotype frequency provides insight into why different species evolve at different rates. About half the echinoid species sequenced for bindin, including *S. franciscanus*, do not exhibit positive selection (*4*). However, as shown here, bindin genotypes are not selectively neutral and have a dramatic influence on reproductive success. While mate distance and water flow explain the majority of the variation in reproductive success, bindin has a large average effect, particularly given the dozens to hundreds of spawning events an individual may experience (*18*). The genetic signature of bindin in this species does not differ from neutral expectations because of counteracting, density-dependent selective forces in this species that experiences a wide range of spawning densities (*9*, *12*). Species found at either end of the continuum of sperm availability are more likely to show a consistent pattern of selection.

Data on bindin evolution from two congeners suggest stronger evidence of positive selection in *S. purpuratus* compared with *S. droebachiensis* (*8*, *19*). The species with the strongest evidence lives at higher densities than *S. franciscanus*, and the species without supporting evidence lives at lower densities along the Pacific Coast. These species also show patterns of gamete traits that match expectations of sperm limitation and competition across this gradient of sperm availability (*12*, *20*, *21*). Interestingly, *S. droebachiensis* has higher bindin allelic diversity in the Atlantic (*19*), where populations are often at higher densities (*9*). This is consistent with increasing sperm competition resulting in selection for polymorphic genotypes. Similarly, in the genus *Echinometra*, the highest level of positive selection was noted in the species most likely to experience high levels of sperm competition (*22*). Overall, these results demonstrate the powerful force of density-dependent selection on gametes and show how the interaction of density- and frequency-dependent selection can lead to a spectrum of evolutionary rates in recognition proteins.

References and Notes

1. W. J. Swanson, V. D. Vacquier, *Annu. Rev. Ecol. Syst.* **33**, 161 (2002).
2. L. Rowe, G. Arnqvist, A. Sih, J. Krupa, *Trends Ecol. Evol.* **9**, 289 (1994).
3. B. Holland, W. R. Rice, *Evolution Int. J. Org. Evolution* **52**, 1 (1998).
4. S. R. Palumbi, *Proc. Natl. Acad. Sci. U.S.A.* **96**, 12632 (1999).
5. S. Gavrilets, *Nature* **403**, 886 (2000).
6. S. Gavrilets, D. Waxman, *Proc. Natl. Acad. Sci. U.S.A.* **99**, 10533 (2002).
7. R. Haygood, *Evolution Int. J. Org. Evolution* **58**, 1414 (2004).
8. Materials, methods, and discussion of results are available as supporting material on *Science* Online.
9. D. R. Levitan, *Am. Nat.* **164**, 298 (2004).
10. P. Debenham, M. A. Brzezinski, K. R. Foltz, *J. Mol. Evol.* **51**, 481 (2000).
11. J. T. Pennington, *Biol. Bull.* **169**, 417 (1985).
12. D. R. Levitan, *Ecology* **83**, 464 (2002).
13. B. Gao, L. E. Klein, R. J. Britten, E. H. Davidson, *Proc. Natl. Acad. Sci. U.S.A.* **83**, 8634 (1986).
14. R. J. H. Payne, D. C. Krakauer, *Evolution Int. J. Org. Evolution* **51**, 1 (1997).
15. M. Doebeli, *J. Evol. Biol.* **18**, 1587 (2005).
16. N. Kamei, C. G. Glabe, *Genes Dev.* **17**, 2502 (2003).
17. S. A. Mah, W. J. Swanson, V. D. Vacquier, *Mol. Biol. Evol.* **22**, 533 (2005).
18. T. A. Ebert, J. R. Southon, *Fish. Bull.* **101**, 915 (2003).
19. C. H. Biermann, *Mol. Biol. Evol.* **15**, 1761 (1998).
20. D. R. Levitan, *Am. Nat.* **141**, 517 (1993).
21. D. R. Levitan, *Evolution Int. J. Org. Evolution* **52**, 1043 (1998).
22. M. A. McCartney, H. A. Lessios, *Mol. Biol. Evol.* **21**, 732 (2004).

23. We thank M. DeRoos, N. Fogarty, E. Franke, D. Houle, D. Johnson, C. Hayes, N. Jue, K. Lotterhos, M. McCartney, K. McGhee, M. McNeilly, A. Plata-Stapper, T. Sheridan, M. Sierra, C. Swanson, C. terHorst, the NSF, and the Bamfield Marine Sciences Centre.

Supporting Online Material

www.sciencemag.org/cgi/content/full/312/5771/267/DC1
Materials and Methods
SOM Text
Tables S1 to S5
References

3 November 2005; accepted 15 March 2006
10.1126/science.1122183

CTCF Mediates Interchromosomal Colocalization Between *Igf2/H19* and *Wsb1/Nf1*

Jian Qun Ling,[1] Tao Li,[1] Ji Fan Hu,[1] Thanh H. Vu,[1] Hui Ling Chen,[1] Xin Wen Qiu,[1] Athena M. Cherry,[2] Andrew R. Hoffman[1]*

Gene transcription may be regulated by remote enhancer or insulator regions through chromosome looping. Using a modification of chromosome conformation capture (3C) and fluorescence in situ hybridization, we found that one allele of the insulin-like growth factor 2 (*Igf2*)/*H19* imprinting control region (ICR) on chromosome 7 colocalized with one allele of *Wsb1/Nf1* on chromosome 11. Omission of CCCTC-binding factor (CTCF) or deletion of the maternal ICR abrogated this association and altered *Wsb1/Nf1* gene expression. These findings demonstrate that CTCF mediates an interchromosomal association, perhaps by directing distant DNA segments to a common transcription factory, and the data provide a model for long-range allele-specific associations between gene regions on different chromosomes that suggest a framework for DNA recombination and RNA trans-splicing.

Igf2 and *H19* are coordinately regulated adjacent imprinted genes located ~80 kb apart on mouse chromosome 7 (*1*). An ICR located between the genes contains four binding regions for CTCF (*2*–*5*), a zinc finger–binding protein that binds to a variety

of DNA sequences and serves as an insulator and regulator of gene transcription (*6*–*8*). Using 3C (*9*), Reik and colleagues demonstrated that on the paternal chromosome, differentially methylated region DMR2 loops out to interact with the methylated ICR, pushing the *Igf2* promoter into contact with the *H19* enhancer, which results in *Igf2* transcription. On the maternal chromosome, DMR1 interacts with the unmethylated ICR, partitioning the *Igf2* promoter into a silent loop, inhibiting *Igf2*, and promoting *H19* transcription (*1*). To determine whether the ICR has other long-range associations, we developed an associated chromosome trap (ACT) assay to identify previously unknown, remote interacting sequences (fig. S1).

We identified three bands corresponding to unique DNA sequences that appear to interact with the ICR (Fig. 1A). One sequence was identified as *Igf2* DMR1 on chromosome 7 (*10*–*12*). A DNA fragment, termed IAS1 (ICR-associated site), corresponded to an intergenic sequence on chromosome 11, located between the *Wsb1* and *Nf1* genes (Fig. 1B; fig. S2), and DNA fragment IAS2 was localized to a gene-poor region on chromosome 6 (Fig. 1B).

A chromatin immunoprecipitation (ChIP) assay using a CTCF-specific antibody identified two regions in the ICR, corresponding to CTCF binding sites numbers 1 and 3 (Fig. 2A; figs. S2 and S3), as well as a region around IAS1, but no interaction with IAS2 was found. CTCF binds to the maternal ICR allele only, which leads to looping and interactions with DMR1. The interaction of CTCF with IAS1 was restricted to the paternal chromosome (Fig. 2B; figs. S2B, S4, and S5).

These allele-specific interactions suggest colocalization or a close juxtapositioning of ICR on chromosome 7 with IAS1 on chromosome 11. In order to demonstrate this physical colocalization, we used fluorescence in situ hybridization (FISH) with bacterial artificial chromosome (BAC) probes for each locus. According to a strict definition of colocalization, one and only one pair of alleles colocalized in each of three cell lines in 30 to 42% of all cells examined (Fig. 3; fig. S6), thereby demonstrating the close association between these two chromosomes.

When the 3.8-kb maternal ICR was deleted (*13*), no interchromosomal interaction was detected, but when the paternal ICR was deleted, the colocalization of these interchromosomal regions was preserved (Fig. 3), which confirmed the allele-specific requirement for the CTCF-binding maternal allele. *Igf2* was biallelically expressed in the cells in which the maternal, but not the paternal, ICR was deleted, and *H19* was biallelically expressed in both ICR-deleted cell lines. *Nf1* and *Wsb1* mRNA abundance was slightly higher in the maternally deleted ICR cells compared with the paternally deleted ICR cells (figs. S7 and S8).

Finally, the role of CTCF in promulgating this interchromosomal interaction was examined by knocking-down endogenous CTCF levels. In cells expressing very low levels of CTCF (Fig. 4), FISH analysis revealed absence of colocalization between IAS1 and the ICR (Fig. 3), and the expression of *Nf1* and *Wsb1* from the paternal allele was reduced by ~50%, while the expression of these genes from the maternal allele was unchanged (Fig. 4; fig. S9). Loss of *Igf2*, but not *H19*, imprinting was detected in the BMshRNA4-4 cell line (fig. S10).

We developed the ACT assay to identify distant DNA regions that are in propinquity or interact with a defined target DNA region, and ACT predicted the colocalization of *Igf2/H19* ICR with *Wsb1/Nf1*. Using FISH, we showed that one *Igf2/H19* ICR allele on chromosome 7 was frequently in close association with one allele of *Wsb1/Nf1* IAS1 on chromosome 11. We hypothesize that the maternal allele on chromosome 7 interacts with the paternal allele of chromosome 11, because only these parental alleles bind CTCF, and the interaction disappears when CTCF levels are diminished or when the maternal ICR is deleted. Moreover, when CTCF abundance is reduced by short hairpin–mediated RNA interference (shRNA)-induced knockdown, there is both loss of imprinting of *Igf2* and decreased expression of *Wsb1* and *Nf1*.

The existence of long-range interactions between regions of a chromosome separated by ~80 kb led to the discovery of intrachromosomal loops that juxtapose downstream enhancers to promoter regions to increase gene transcription (*1*, *10*–*12*). Intrachromosomal looping has been described for the *Hgb* locus and for the *Dlx5/Dlx6* imprinted dyad, as well as *Igf2/H19* (*14*–*18*). Associations between chromosomes were recently described by Spilianakis *et al*. (*19*), who demonstrated a regulatory interaction between the interferon-γ promoter region on chromosome 10 and regions of the T helper cell T_H2 cytokine locus on chromosome 11. They suggested that interchromosomal associations might also be seen in other systems where gene expression is monoallelic.

In intermitotic cells, much of the chromatin is decondensed into a three-dimensional chromosomal territory within a highly organized nuclear architecture (*20*). There is

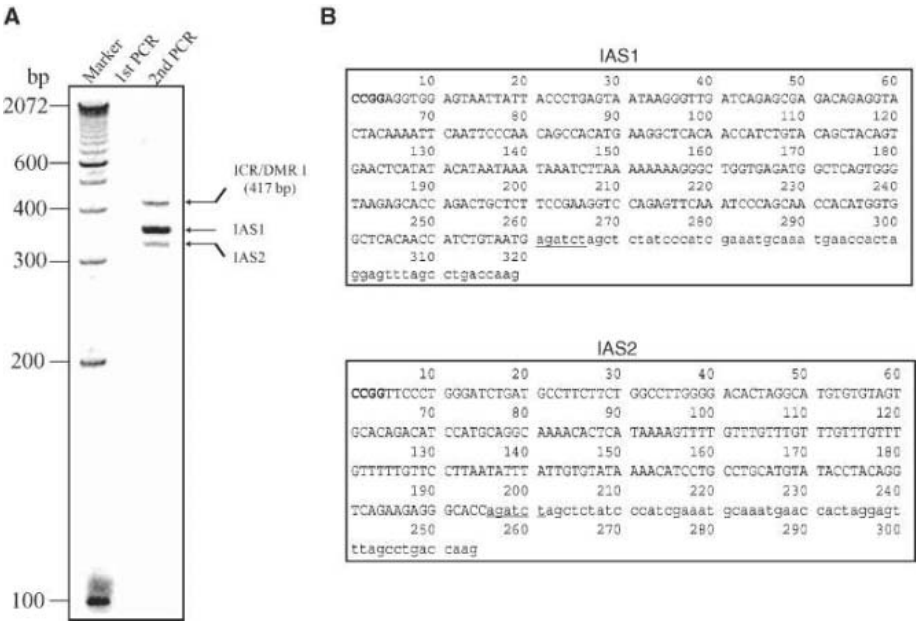

Fig. 1. Associated chromosome trap (ACT) assay searching for DNA segments interacting with *Igf2/H19* ICR in mouse bone marrow fibroblast cell line, BMM3-4. (**A**). Nested polymerase chain reaction (PCR) products were run on 5% polyacrylamide electrophoresis gels and analyzed with a PhosphoImager. Three bands appear on the gel after the nested PCR reaction; one is an amplified fragment between ICR and DMR1; the other two bands are IAS1 and IAS2. (**B**) IAS1 and IAS2 sequences (linker sequence not included). Upper case letters, DNA fragment between Bgl II (agatct) and Msp I (CCGG) sites ligated with ICR; lower case, ICR partial sequence.

[1]Medical Service, Department of Veterans Affairs, Palo Alto Health Care System, and Department of Medicine, Stanford University, Palo Alto, CA 94304, USA. [2]Departments of Pathology and Pediatrics, Stanford University, Stanford, CA 94305, USA.

*To whom correspondence should be addressed. E-mail: arhoffman@stanford.edu

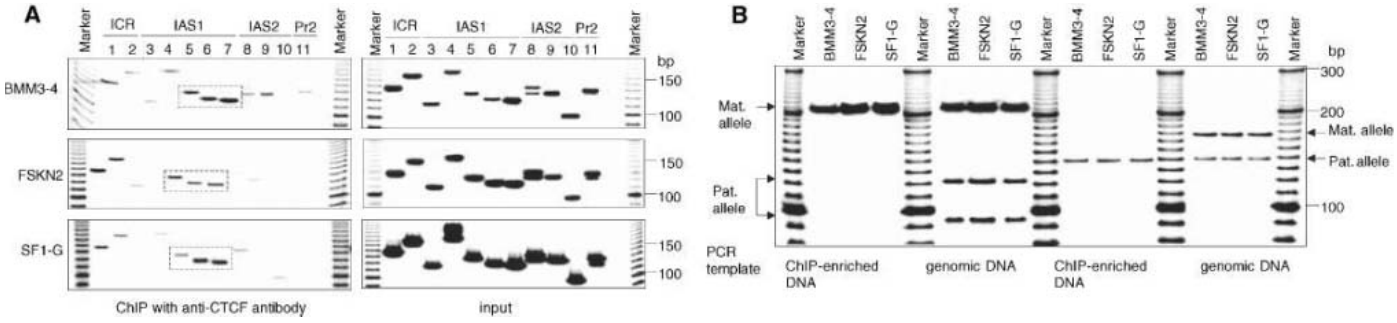

Fig. 2. ChIP assay with mouse CTCF-specific antibody in BMM3-4, FSKN2, and SF1-G cells. (**A**) ChIP PCR results. Boxes in broken lines represent IAS1 regions identified by CTCF-specific antibody in ChIP. ICR of *Igf2/H19*; IAS1 on chromosome 11; IAS2 on chromosome 6; marker, 100–base pair DNA marker; one primer pair, 2930/2941 (see table S1 for primer sequences) encompassing *Igf2* promoter 2 region (Pr2) was used in ChIP PCR as a negative control. (**B**) Allele-specific binding of ICR (left) and IAS1 (right) with CTCF. PCR products were subjected to digestion by allele-specific restriction enzymes BsmA I for ICR and Mse I for IAS1. Only maternal ICR and paternal IAS1 showed specific binding. Genomic DNA served as a control.

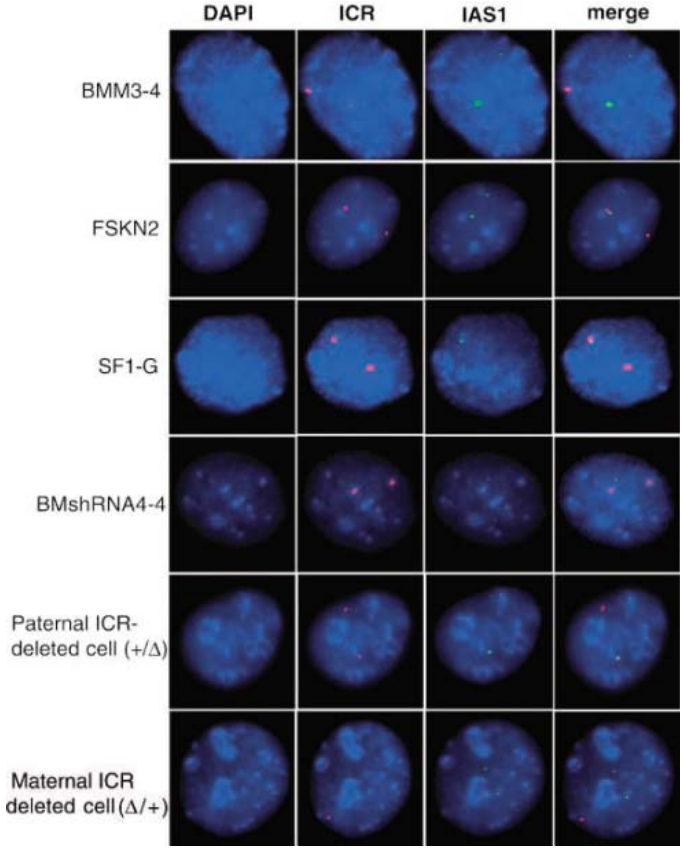

Fig. 3. FISH results in BMM3-4, FSKN2, SF1-G, BMshRNA4-4, and ICR-deleted cells. *H19*-BAC1 probe is labeled by Spectrum Red deoxyuridine triphosphate (dUTP); RP23-256H2 probe is labeled by Spectrum Green dUTP. Fifty random nuclei from each cell line were counted on each of three slides for each cell line to determine the colocalization percentage of the two alleles. Colocalization is defined as overlapping or touching of the two signals; any separation of the signals (i.e., any intervening pixels) is defined as nonoverlapping. The degree of colocalization (average of three slides) of the two loci is BMM3-4 cells (15 out of 50; 30%), FSKN2 cells (16 out of 50; 32%), SF1-G cells (21 out of 50; 42%), BMshRNA4-4 cells (0 out of 50; 0%), paternal ICR-deleted (+/Δ) cells (8 out of 50; 16%), and maternal ICR-deleted (Δ/+) cells (0 out of 50; 0%).

evidence that each chromosome occupies a distinct territory, and three-dimensional maps have been proposed that delineate precise neighborhoods for each chromosome. Repressed genes may be localized to loops that are positioned within silent compartments inside or outside of the chromosome territory. Actively transcribed genes may reside on loops that extend from the chromosomal territory into interchromatin compartments, where they may share transcriptional machinery with other nearby genes or, potentially, with active genes that are located on nearby chromosomes.

Although it is likely that these two genes on chromosomes 7 and 11 physically interact with and regulate each other's expression with CTCF as a necessary intermediary, it is also possible that these DNA regions are present on loops that occupy the same transcription factory and that they are in close juxtaposition, but do not directly interfere with or enhance each others' transcriptional activity (*21*–*23*). Transcription factories, in which numerous preassembled transcription complexes are concentrated are presumed to exist in the nucleus. As there are fewer factories than transcribed genes in each cell, several genes probably share common factories (*21*, *24*). Transcriptionally active genes are recruited into these factories and then may leave when transcription ceases. Osborne *et al*. (*21*) have recently demonstrated that genes over 40 megabases (Mb) of mouse chromosome 7 can interact in cis in these factories, and they postulate that chromatin loops from nearby chromosomes could also occupy the same transcription factory. In our experiments, the absence of CTCF abrogated the association of the interchromosomal regions and decreased *Nf1* and *Wsb1* mRNA abundance, suggesting that the chromosome 11 loop may only be recruited to the factory when bound to CTCF. The absence of the maternal ICR on chromosome 7 also abolished the conformational propinquity of these two chromosomal loops, suggesting that the mutated maternal allele of *Igf2/H19* may no longer be present in the factory. The two regions may also interact in a more direct way, perhaps by binding to dimerized CTCF (*25*) or to another common factor and stabilizing each others' presence in the factory; in the absence of this factor or the ability to bind this factor, the presence of one or both chromosome loops within the factory may be compromised.

The decrease of paternal *Nf1* and *Wsb1* expression in the cells in which CTCF was knocked down indicates that the colocalization and/or the lack of CTCF regulates paternal expression of these genes. In cells in which the maternal ICR has been deleted, expression of *Nf1* and *Wsb1* are increased. It is possible that the amount of CTCF at the transcription factory is limiting, and maternal chromosome 7 ICR and paternal IAS1 on chromosome 11 actively compete for CTCF. In the absence of the maternal ICR, there

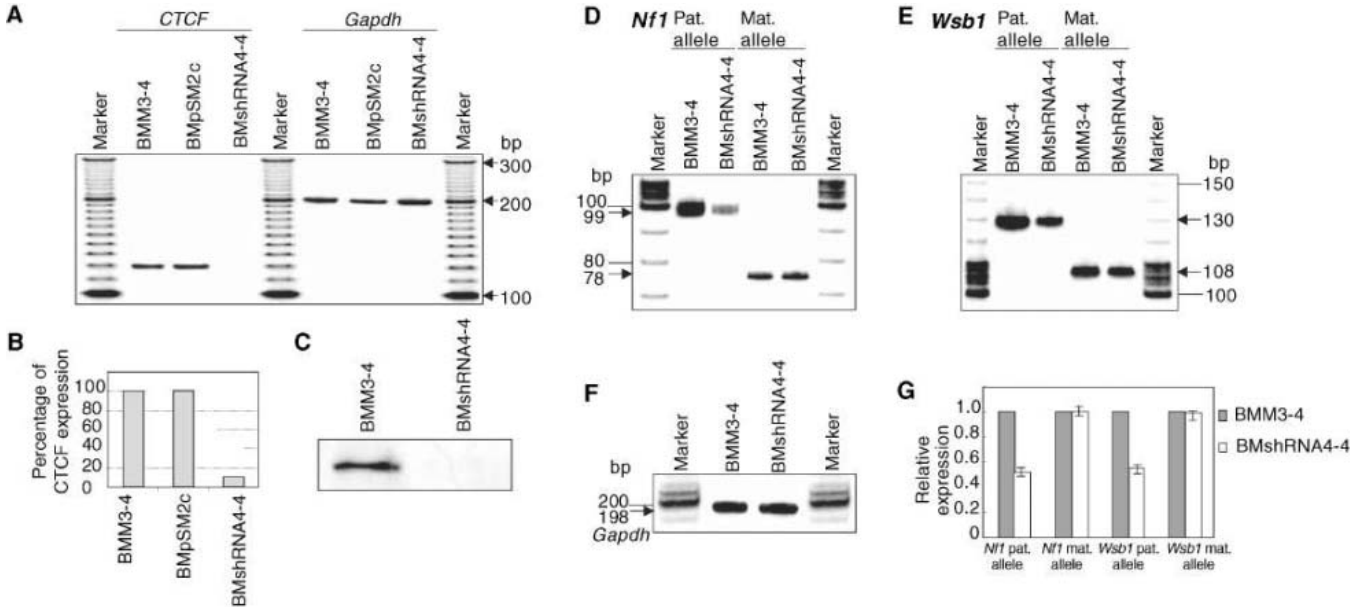

Fig. 4. Decreased expression of *Nf1* and *Wsb1* paternal alleles in CTCF knocked-down BMshRNA4-4 cells. (**A**) CTCF expression by PCR analysis in BMM3-4, BMpSM2c, and BMshRNA4-4 cell lines. BMM3-4 has no vector; BMpSM2c cells: BMM3-4 cells in which an empty pSM2c vector is transferred to serve as a control; BMshRNA4-4 cells: BMM3-4 cells in which a pSMshRNA4-4 vector that expressed CTCF shRNA is transferred to knockdown CTCF expression. (**B**) Quantitative PCR results show mouse CTCF mRNA abundance was inhibited by 89% in BMshRNA4-4 cells. (**C**) Western blot analysis of BMM3-4 and BMshRNA4-4 using mouse CTCF monoclonal antibody. No CTCF protein could be detected in BMshRNA4-4 cells. (**D** and **E**) Allele-specific PCR of *Nf1* and *Wsb1* in BMM3-4 and BMshRNA4-4 cells. (**F**) *Gapdh* expression by PCR (as a control). (**G**) Allele-specific quantitative PCR. Abundance of *Nf1* and *Wsb1* in BMM3-4 and BMshRNA4-4 cells ($n = 6$).

might be more CTCF available to IAS1, which would lead to increased gene transcription. Because there is strict parental allele specificity for CTCF binding (paternal chromosome 11 and maternal chromosome 7), it is tempting to implicate this interchromosome association in the imprinting process. There was loss of *Igf2* imprinting in cell lines in which CTCF was knocked down and in which the maternal ICR was deleted (figs. S8 and S10).

Our data suggest that CTCF acts as an organizer of higher-order chromatin structure, directing DNA segments into transcription factories and/or facilitating interactions with other DNA segments. In this way, CTCF may enable epistasis in addition to its other important roles of regulating transcription and serving an insulator function. Absence of CTCF resulted in the disassociation of the *Wsb1/Nf1* locus from the *Igf2/H19* locus, which altered gene expression.

The association between the *Igf2/H19* locus on chromosome 7 and the *Wsb1/Nf1* locus on chromosome 11 provides an ideal model to study the relation between spatial genome organization and gene expression. The ACT assay can discover new interchromosomal associations or confirm the existence of previously suspected ones. The close association of different chromosomes could provide a model to elucidate RNA trans-splicing leading to interchromosomal mRNA fusion (*26*, *27*). Interchromosomal associations, such as those discovered in T_H cells (*19*), demonstrate the complexity and sophistication of remote regulation of gene expression and indicate the need to study gene expression in the context of whole-nucleus architecture. By so doing, we can enhance our understanding of gene regulation and interchromosomal DNA recombination in normal physiology and diseases caused by translocation and transposition (*28*, *29*).

References and Notes

1. A. Murrell, S. Heeson, W. Reik, *Nat. Genet.* **36**, 889 (2004).
2. A. C. Bell, G. Felsenfeld, *Nature* **405**, 482 (2000).
3. A. T. Hark *et al.*, *Nature* **405**, 486 (2000).
4. C. Kanduri *et al.*, *Curr. Biol.* **10**, 853 (2000).
5. P. Szabo, S. H. Tang, A. Rentsendorj, G. P. Pfeifer, J. R. Mann, *Curr. Biol.* **10**, 607 (2000).
6. A. C. Bell, A. G. West, G. Felsenfeld, *Cell* **98**, 387 (1999).
7. G. N. Filippova *et al.*, *Mol. Cell. Biol.* **16**, 2802 (1996).
8. P. E. Szabo, S. H. Tang, F. J. Silva, W. M. Tsark, J. R. Mann, *Mol. Cell. Biol.* **24**, 4791 (2004).
9. J. Dekker, K. Rippe, M. Dekker, N. Kleckner, *Science* **295**, 1306 (2002).
10. S. Lopes *et al.*, *Hum. Mol. Genet.* **12**, 295 (2003).
11. H. Sasaki, K. Ishihara, R. Kato, *J. Biochem. (Tokyo)* **127**, 711 (2000).
12. M. Weber *et al.*, *Mol. Cell. Biol.* **23**, 8953 (2003).
13. J. L. Thorvaldsen, M. R. Mann, O. Nwoko, K. L. Duran, M. S. Bartolomei, *Mol. Cell. Biol.* **22**, 2450 (2002).
14. J. D. Engel, K. Tanimoto, *Cell* **100**, 499 (2000).
15. S. Horike, S. Cai, M. Miyano, J. F. Cheng, T. Kohwi-Shigematsu, *Nat. Genet.* **37**, 31 (2005).
16. A. Kim, A. Dean, *Proc. Natl. Acad. Sci. U.S.A.* **101**, 7028 (2004).
17. T. Ragoczy, A. Telling, T. Sawado, M. Groudine, S. T. Kosak, *Chromosome Res.* **11**, 513 (2003).
18. C. R. Vakoc *et al.*, *Mol. Cell* **17**, 453 (2005).
19. C. G. Spilianakis, M. D. Lalioti, T. Town, G. R. Lee, R. A. Flavell, *Nature* **435**, 637 (2005).
20. T. Cremer, C. Cremer, *Nat. Rev. Genet.* **2**, 292 (2001).
21. C. S. Osborne *et al.*, *Nat. Genet.* **36**, 1065 (2004).
22. P. J. Verschure, I. van Der Kraan, E. M. Manders, R. van Driel, *J. Cell Biol.* **147**, 13 (1999).
23. S. K. Zaidi *et al.*, *EMBO Rep.* **6**, 128 (2005).
24. M. A. Grande, I. van der Kraan, L. de Jong, R. van Driel, *J. Cell Sci.* **110**, 1781 (1997).
25. V. Pant *et al.*, *Mol. Cell. Biol.* **24**, 3497 (2004).
26. M. Puttaraju, S. F. Jamison, S. G. Mansfield, M. A. Garcia-Blanco, L. G. Mitchell, *Nat. Biotechnol.* **17**, 246 (1999).
27. L. Yang *et al.*, *J. Biol. Chem.* **279**, 46253 (2004).
28. V. S. Lestou *et al.*, *Cancer Genet. Cytogenet.* **138**, 153 (2002).
29. J. Walter, M. Paulsen, *Hum. Mol. Genet.* **12**, R215 (2003).

30. This work was supported by NIH grants DK036054, DK065283, and HD047013; the March of Dimes; and the Research Service of the Department of Veterans Affairs. We thank J. E. Wrede for advice and assistance in performing the FISH analyses. We are indebted to M. Bartolomei, R. Feil, W. Reik, W. Dean, and A. Wagschal for providing us with cell lines, and to K. Pfeifer and U. Franke for BAC clones.

Supporting Online Material

www.sciencemag.org/cgi/content/full/312/5771/269/DC1
Materials and Methods
Figs. S1 to S10
Tables S1 and S2
References

29 November 2005; accepted 9 February 2006
10.1126/science.1123191

Conformational Switches Modulate Protein Interactions in Peptide Antibiotic Synthetases

Alexander Koglin,[1] Mohammad R. Mofid,[2]* Frank Löhr,[1] Birgit Schäfer,[1] Vladimir V. Rogov,[1,3] Marc-Michael Blum,[1] Tanja Mittag,[1]† Mohamed A. Marahiel,[2] Frank Bernhard,[1] Volker Dötsch[1]‡

Protein dynamics plays an important role in protein function. Many functionally important motions occur on the microsecond and low millisecond time scale and can be characterized by nuclear magnetic resonance relaxation experiments. We describe the different states of a peptidyl carrier protein (PCP) that play a crucial role in its function as a peptide shuttle in the nonribosomal peptide synthetases of the tyrocidine A system. Both apo-PCP (without the bound 4′-phosphopantetheine cofactor) and holo-PCP exist in two different stable conformations. We show that one of the apo conformations and one of the holo conformations are identical, whereas the two remaining conformations are only detectable by nuclear magnetic resonance spectroscopy in either the apo or holo form. We further demonstrate that this conformational diversity is an essential prerequisite for the directed movement of the 4′-PP cofactor and its interaction with externally acting proteins such as thioesterases and 4′-PP transferase.

A vast number of small and structurally diverse bioactive peptides with broad therapeutic potential is produced by the modular megaenzyme super family of nonribosomal peptide synthetases (NRPSs) (*1*–*4*). These complex peptides are synthesized by multiple-step mechanisms that require amino acyl adenylation of the building blocks followed by thioesterification on distinctive cysteamine thiol groups of intrinsic 4′-phosphopantetheine (4′-PP) cofactors (*1*, *4*). The cofactors are attached to the side chain of conserved serine residues of small internal peptidyl carrier proteins (PCPs) (*5*). PCPs shuttle intermediates between individual NRPS modules during the assembly line peptide synthesis. The N termini of the PCP domains are fused to acyl-adenylate–forming domains (A-domains) of the NRPS modules. These A-domains are responsible for the selection and activation of the specific amino acid constituents of the final peptide products. Peptide-bond–forming condensing domains (C-domains) are attached to the C termini of the PCPs (*1*). The transfer of peptide intermediates between A- and C-domains by PCPs therefore requires large movements of the 4′-PP cofactor that have been described by a "swinging arm" model (*6*). However, the mobility has not been characterized at a molecular level.

Detailed analysis of [^{15}N, 1H]-TROSY (transverse relaxation optimized spectroscopy) spectra of the apo-PCP domain of the third module of tyrocidine A synthetase (TycC3-PCP) indicated that several backbone resonances show two distinct chemical shifts, suggesting the existence of two different and slowly exchanging conformations. These residues are mainly clustered in two regions (fig. S1), one comprising the N terminus of helix αII and the adjacent loop (H44 to A53), including the active site residue S45, and the second one spanning residue R57 to T73, including most residues between helices αII and αIV.

Upon conversion to the holo form by modification with the 4′-PP cofactor, the pattern of peak doubling of the TycC3-PCP domain changes (figs. S1 and S2), suggesting that the holo form also exists in two conformations, of which at least one is different from the conformations found for the apo form (fig. S3). Detailed comparison of all four structures indicated that one conformation of the holo state and one conformation of the apo state are—with the exception of the attachment of the cofactor—virtually identical. In contrast, the two remaining states (the A state for the apo form and the H state for the holo form) are distinct from each other and from the structurally identical common state (A/H form). A-state PCP generally shows the most flexible and extended three-dimensional (3D) structure having very large loop regions (Fig. 1). Helix αIII does not exist; instead, the amino acid sequence forms a large loop (loop III). Helix αI (V15 to A20) is shorter as compared with the A/H state and is reduced to only 1.5 turns. The helices αII (M49 to A53) and αIV (A76 to Y80) are reduced to only two α-helical turns, and helix αII shows a kink at position Q54. Loop III thus becomes stretched and embedded in the core of the protein between helices αII and αIV. Interestingly, a 2-ns molecular dynamics simulation (*7*, *8*) suggests that this fixation of loop III allows the formation of an H-bond between the carbonyl of S45 and the side chain of R47. The equivalent simulation of the A/H-state PCP showed that this H-bond is eliminated in favor of a new one between S45-OH and the side chain of H44. The active site residue S45, therefore, seems to play a crucial role for the observed conformational diversity of apo-TycC3-PCP. Accordingly, mutating the active site serine to alanine is sufficient to abolish any structural heterogeneity in apo-TycC3-PCP, and the protein represents a completely "frozen" A state (fig. S1).

The orientation of the helices in the A/H state is similar to the orientation in the A state of apo-TycC3-PCP (Fig. 1). However, the helices in the A/H state are longer and more stable. Helix αI is extended from A14 to V26, helix αII from K47 to Q54, and helix αIV from I74 to Y80. The loop III now forms a very short one-turn helix αIII (L65 to A70) that is located outside of the globular protein core. This relocation of the loop III area is one of the most striking differences compared with the A state.

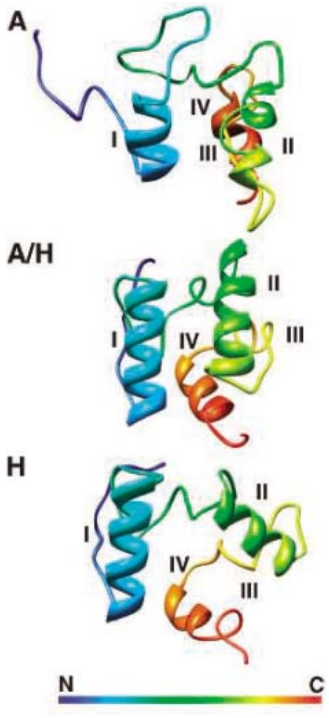

Fig. 1. Ribbon diagrams of the average NMR solution structures of the TycC3-PCP conformers in the A, A/H, and H states.

[1]Institute of Biophysical Chemistry, Centre for Biomolecular Magnetic Resonance (BMRZ), J.W. Goethe University of Frankfurt, Marie-Curie-Strasse, D-60439 Frankfurt/Main, Germany. [2]Fachbereich Chemie-Biochemie, Philipps University of Marburg, Hans-Meerwein-Strasse D-35032 Marburg, Germany. [3]Institute of Protein Research, Puschino, Russia.

*Present address: Institute of Organic Chemistry, University of Munich, Munich, Germany.

†Present address: Structural Biology and Biochemistry, Hospital for Sick Children, 555 University Avenue, Toronto, Ontario M5G 1X8, Canada.

‡To whom correspondence should be addressed. E-mail: vdoetsch@em.uni-frankfurt.de

The major difference between the holo-TycC3-PCP–specific H state and the A/H state is that the single-turn helix αIII unravels and becomes extended. As a consequence, the orientation of helix αIV is moved parallel to helix αI by approximately 3 Å (Fig. 1). The transition of loop III induces a relocation of helix αII and the region connecting helices αI and αII containing the active site residue S45 with the attached 4′-PP cofactor.

Analysis of the different conformations suggests that the transition between the H and A/H states of holo-TycC3-PCP results in a large movement of the 4′-PP cofactor. To define these potential different states of the cofactor, we identified the chemical shifts of its two amide protons and nitrogens, NBR and NBQ. The NBQ amide proximal to the thiol-group was detected as a well-resolved double peak, whereas the distal amide NBR showed a single very broad signal. The observed double-peak formation indicates that the 4′-PP cofactor adopts two clearly distinct positions in holo-TycC3-PCP. In agreement with this model, a 3D ^{15}N-edited NOESY (three-dimensional ^{15}N-edited nuclear Overhauser effect spectroscopy) spectrum of completely ^{15}N-labeled holo-TycC3-PCP, including the cofactor, revealed distinct NOE pattern for the two signals of the NBQ amide exhibiting either NOEs to the amino acids L68, F69, and probably also L65, or to V26 and probably E24 (fig. S3). Modeling of holo-TycC3-PCP combined with the analysis of these NOE patterns revealed that in the A/H state the cofactor is located close to the N terminus of the PCP, whereas in the H state it is located in the vicinity of the C-terminal end (Fig. 2). This result indicates a large movement of the 4′-PP cofactor by ~100°, resulting in an ~16 Å relocation of the thiol group.

To investigate the importance of these different conformations for the biological function of the PCP domain, we analyzed its interaction by NMR titration assays (*9*) with two cognate binding partners, the 4′-PP transferase Sfp (*10*–*12*) that is responsible for loading the cofactor onto PCPs and the type II thioesterase enzyme (*13*) that is responsible for the regeneration of misprimed PCP domains. ^{15}N-labeled TycC3-PCP was stepwise titrated with the unlabeled proteins up to a final ratio of 1:2 (Fig. 3). As expected, the 4′-PP transferase Sfp does not interact with holo-TycC3-PCP. A titration with apo-TycC3-PCP in the presence of CoA/Mg^{2+} immediately resulted in conversion into holo-TycC3-PCP, and thus no interaction could be monitored. The titration of apo-TycC3-PCP in the absence of CoA/Mg^{2+} revealed a weak interaction primarily, with few residues surrounding the active site residue S45. To prevent the rapid conversion to holo-PCP by Sfp in the presence of CoA, we analyzed the interaction with the active site mutant TycC3-PCP_{S45A} (*14*). Again only a weak interaction was monitored in the absence of CoA. In contrast, a strong interaction with Sfp is visible in the presence of CoA/Mg^{2+}. The interaction site includes residues 30 to 55 of helix αII and the 4′-PP recognition site within the loop between helix αI and αII. Only the A-state conformer is detectable with the mutant TycC3-PCP_{S45A}, showing that Sfp specifically recognizes the A state. Guided by these titration experiments as well as mutational analysis of the Sfp–PCP interaction (*15*), we built a model of the complex (*16*, *17*), starting with the crystal structure of Sfp (*11*) and our NMR structure of the A state of TycC3-PCP (Fig. 4). A-state PCP fits perfectly on top of CoA, which is located in a large groove in the surface of Sfp where the essential Mg^{2+} ion coordinates the pyrophosphate of CoA. The interface of the complex is composed of helix αII, including the loop to helix αI of A-state PCP and parts of helices αH2 and αH6, the β strands B4 and B6, and the loop region between αH6 and αH7 of Sfp (*12*). The reactive hydroxyl group of S45 in A-state PCP is brought into very close contact with the pyrophosphate group of CoA, putatively enabling an efficient hydrolysis and 4′-PP transfer. This model also explains the selective interaction of the A state with Sfp. The reduction of helix αII to two turns extends the loop between helices αI and αII containing the active site residue S45, and thus makes this region more accessible for an interaction with Sfp than the more compact H and A/H conformers. Another major difference between the A and the A/H state is the conformation of the helix/loop III region. Modeling of the A/H-state PCP in complex with Sfp and CoA suggests that the formation of helix αIII in the A/H state leads to a steric hindrance of this interaction. This steric clash is removed by the unfolding of helix αIII and its embedding between helices αII and αIV.

In contrast to Sfp, only a weak interaction is observable between the thioesterase SrfTEII and apo-TycC3-PCP. Based on the number and magnitude of the observed chemical shifts, the interaction is considerably enhanced with holo-TycC3-PCP and involves mainly the active site motif and the complete loop III region. Even bigger chemical shift differences are observed with the misprimed acetyl-holo-TycC3-PCP derivative, indicating that the acetyl moiety plays a major role in the recognition mechanism. For this titration, we used the active site mutant $SrfTEII_{S86A}$ containing a defective catalytic triad (*15*) to prevent the rapid hydrolysis of the acetyl residue. The interaction of $SrfTEII_{S86A}$ with

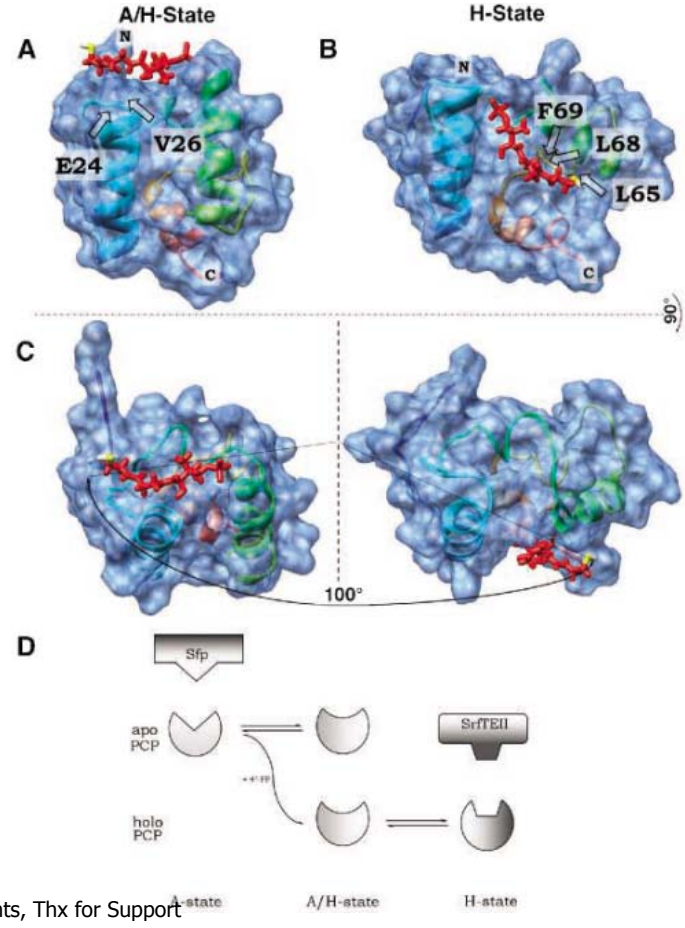

Fig. 2. Directed repositioning of the 4′-PP cofactor on the surface of holo-TycC3-PCP. (**A**) A/H state of holo-TycC3-PCP with the 4′-PP cofactor located close to residue V26 in the vicinity of the N-terminal end. (**B**) H state of holo-TycC3-PCP showing the 4′-PP cofactor located in the vicinity of residue F69 and L68. (**C**) Rotation of the proteins shown in (A) and (B) by 90° and comparison of the two different locations of the 4′-PP cofactor. The degree of movement of the 4′-PP arm is indicated, and identified residues with contacts to the 4′-PP cofactor are shown. (**D**) Proposed model of the dual two-state equilibrium.

holo-TycC3-PCP was identical to that of wild-type SrfTEII with holo-TycC3-PCP, suggesting that the point mutation did not affect the complex formation. Specific H-state selection by SrfTEII is evident from (i) almost no interaction with apo-TycC3-PCP that also forms the A/H state, (ii) gradually reduced A/H-state–specific signals in TROSY-HSQC spectra with increased SrfTEII concentrations, and (iii) line-shape analysis (*18*) of double peaks from selected residues that clearly demonstrate the shift of the preformed conformer equilibrium toward the H state upon titration with SrfTEII (fig. S4). Key recognition elements for the interaction of the H state with the SrfTEII are the loop III region, the loop containing the active site S45, and the N-terminal part of helix II. In the H state, these key recognition elements form a contiguous interaction surface, whereas in the A/H state the affected amino acid residues are distributed over a larger area and disrupted by regions not involved in complex formation (fig. S6). Again, the conformational exchange of the helix/loop III region plays a major role in creating this contiguous interaction surface. Although this region forms a short helix in the A/H state that is removed from the center of the protein, in the H state it forms a loop that is located in close proximity to the N terminus of helix αII and to the active site loop.

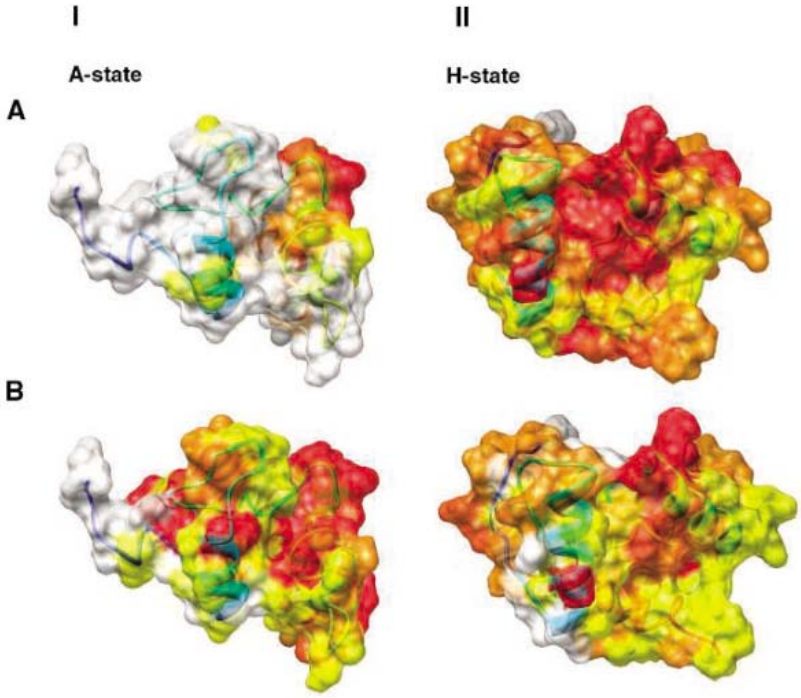

Fig. 3. Specific interaction of TycC3-PCP conformers with binding partners. Interaction surfaces of the A state of apo-PCP are shown on the left (I), and interaction surfaces of the H-state holo-PCP are shown on the right (II). Residues that show chemical-shift differences in titration experiments are colored, with red representing the largest chemical-shift differences. (**IA**) interaction between A-state apo-PCP_{S45A} with Sfp; (**IB**) interaction of apo-PCP_{S45A} with Sfp activated with CoA and Mg^{2+}; (**IIA**) interaction of H-state acetyl-holo-PCP with $SrfTEII_{S86A}$; (**IIB**) interaction of H-state holo-PCP with $SrfTEII_{S86A}$.

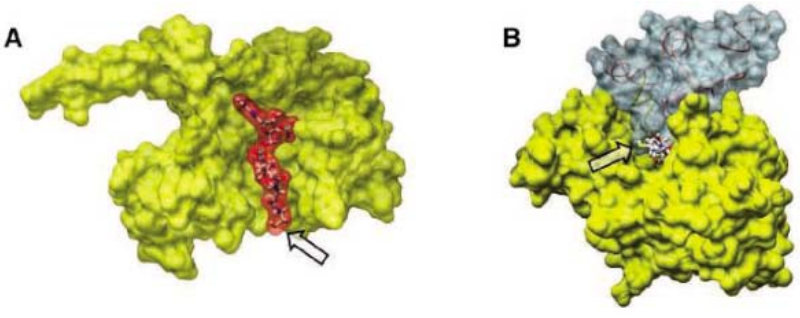

Fig. 4. Model of the A-state TycC3-PCP/Sfp complex. The Sfp protein is shown in yellow, TycC3-PCP in blue, and CoA in red. The arrow indicates the position of the reactive thiol group of CoA. (**A**) Proposed position of CoA in Sfp based on the electron density of the adenyl phosphorus in the Sfp crystal structure (*11*) and calculations with the program auto-Dock 3 (*27*). (**B**) Space-filling model of the Sfp/A-state TycC3-PCP complex.

The two conformational equilibria of the apo- and the holo form that overlap in the A/H state as a common conformer constitute a new type of regulation of a protein's function by extending the "pre-existing equilibrium" hypothesis (*19*, *20*). In our "double two-state equilibrium" model, the A and the H states represent the active conformations that are specifically recognized by the interaction partners Sfp and SrfTEII, respectively (Fig. 3). Binding of the 4′-PP cofactor transforms the A-state equilibrium into the H-state equilibrium, altering, in particular, the conformation of the helix/loop III region that is not directly linked to the cofactor attachment site. The conformational change of this region is essential for the recognition by SrfTEII. This mechanism could therefore be interpreted as an allosteric regulation (*20*), although the 4′-PP cofactor itself might additionally play a role in the recognition by SrfTEII. The TycC3-PCP double two-state equilibrium, therefore, combines the pre-existing equilibrium model that describes the equilibria within the individual apo and holo forms with the "allosteric regulation" model that explains the switch between the forms.

The studies described in this paper have focused on binding partners that interact in trans with the PCP domain. Holo-PCP also interacts with adjacent enzymatic domains of the NRPS systems that are involved in peptide product formation, such as the amino acid adenylation and condensation domains. For the interaction with these in cis-interacting components, the location of the 4′-PP cofactor on the PCP surface is important. The assembly-line mechanism proposed for the function of the NRPS systems requires the directed movement of this cofactor to transport the substrate between the A- and C-domains. Our results indicate that the 4′-PP cofactor is indeed located in two distinct positions, in proximity either to the N-terminal end of holo-TycC3-PCP in the A/H state or to the C-terminal end in the H state. It is tempting to speculate that the structural rearrangements in the two holo-TycC3-PCP forms modulate specific interactions with the A- and C-domains. In contrast to the integrated PCP domains, type II ACPs in prokaryotic and eukaryotic cells are isolated small acidic proteins (*21*, *22*). NMR investigations of an acyl carrier protein (ACP) from Mycobacterium *tuberculosis* did not reveal a defined position of the 4′-PP cofactor (*21*), although internal dynamics has been discussed for other ACP domains (*23*, *24*). A non-ordered solvent exposed state of the cofactor is, however, reasonable for the efficient loading with acyl intermediates by enzymes

of the fatty acid synthetase complex that act in trans.

Very recently, the crystal structures of the mammalian and fungal fatty acid synthetases were published that contain cis-acting ACP domains (*25*, *26*). In both crystal structures, the ACP domains are not visible, most likely due to their inherent dynamics. These structures, however, also show that, in addition to the conformational flexibility (*23*) the entire ACP domain has to move to bridge the distance between the individual active sites. In contrast to the fatty acid synthase (FAS) system, where one ACP domain has to shuttle the substrates between multiple and distantly located catalytic centers, the PCP domains of NRPS systems transfer the substrate between an A-domain and the two neighboring C-domains, thus potentially making the intradomain dynamics sufficient for substrate shuttling. For a detailed understanding of the molecular mechanism of the FAS, polyketide synthase, and NRPS systems, the characterization of the intradomain and interdomain dynamics of the PCP and ACP domains will be crucial.

References and Notes

1. C. T. Walsh, *Science* **303**, 1805 (2004).
2. S. A. Sieber, M. A. Marahiel, *Chem. Rev.* **105**, 715 (2005).
3. T. Stachelhaus, A. Hüser, M. A. Marahiel, *Chem. Biol.* **3**, 913 (1996).
4. H. D. Mootz, D. Schwarzer, M. A. Marahiel, *ChemBioChem* **3**, 490 (2002).
5. T. Stein, *J. Biol. Chem.* **271**, 15428 (1996).
6. T. Weber, R. Baumgartner, C. Renner, M. A. Marahiel, T. A. Holak, *Structure* **8**, 407 (2000).
7. W. F. van Gunsteren, P. H. Hünenberger, A. E. Mark, P. E. Smith, I. G. Tironi, *Comput. Phys. Commun.* **91**, 305 (1995).
8. H. J. C. Berendsen, D. van der Spoel, R. van Drunen, *Comput. Phys. Commun.* **91**, 43 (1995).
9. E. R. P. Zuiderweg, *Biochemistry* **41**, 1 (2002).
10. R. H. Lambalot *et al.*, *Chem. Biol.* **3**, 923 (1996).
11. K. Reuter, M. R. Mofid, M. A. Marahiel, R. Ficner, *EMBO J.* **18**, 6823 (1999).
12. M. R. Mofid, R. Finking, M. A. Marahiel, *J. Biol. Chem.* **277**, 17023 (2002).
13. D. Schwarzer, H. D. Mootz, U. Linne, M. A. Marahiel, *Proc. Natl. Acad. Sci U.S.A* **99**, 14083–14088 (2002).
14. R. Finking, M. R. Mofid, M. A. Marahiel, *Biochemistry* **43**, 8946 (2004).
15. M. R. Mofid, R. Finking, L. O. Essen, M. A. Marahiel, *Biochemistry* **43**, 4128 (2004).
16. A. T. Brünger *et al.*, *Acta Crystallogr.* **54**, 905 (1998).
17. C. Dominguez, R. Boelens, A. M. J. J. Bonvin, *J. Am. Chem. Soc.* **125**, 1731 (2003).
18. T. Mittag, B. Schaffhausen, U. L. Günther, *Biochemistry* **42**, 11128 (2003).
19. C. S. Goh, D. Milburn, M. Gerstein, *Curr. Opin. Struct. Biol.* **14**, 104 (2004).
20. D. Kern, E. R. P. Zuiderweg, *Curr. Opin. Struct. Biol.* **13**, 748 (2003).
21. H. C. Wong, G. Liu, Y. M. Zhang, C. O. Rock, J. Zheng, *J. Biol. Chem.* **277**, 15874 (2002).
22. M. A. C. Reed *et al.*, *Org. Biomol. Chem.* **1**, 463 (2003).
23. Y. Kim, J. H. Prestegard, *Biochemistry* **28**, 8792 (1989).
24. M. Andrec, R. B. Hill, J. H. Prestegard, *Protein Sci.* **4**, 983 (1995).
25. T. Maier, S. Jenni, N. Ban, *Science* **311**, 1258 (2006).
26. S. Jenni, M. Leibundgut, T. Maier, N. Ban, *Science* **311**, 1263 (2006).
27. G. M. Morris, D. S. Goodsell, R. Huey, A. J. Olson, *J. Comput. Aided Mol. Des.* **10**, 293 (1996).

28. This work was supported by the Centre for Biomolecular Magnetic Resonance Frankfurt (BMRZ) and DFG grants BE 19-11 and MA 811/19-1. Coordinates of the A state (2GDY), the A/H state (2GDW), the H state (2GDX), and the complex of the cofactor CoA with Sfp (2GE0) and of the complex of Sfp with CoA, Mg^{2+} and the A state of the apo-PCP (2GE1) have been deposited in the Protein Data Bank.

Supporting Online Material

www.sciencemag.org/cgi/content/full/312/5771/273/DC1
Materials and Methods
Figs. S1 to S6
Table S1

22 November 2005; accepted 20 March 2006
10.1126/science.1122928

Conservation of *RET* Regulatory Function from Human to Zebrafish Without Sequence Similarity

Shannon Fisher,[1,2]*† Elizabeth A. Grice,[1]* Ryan M. Vinton,[1] Seneca L. Bessling,[1] Andrew S. McCallion[1,3]†

Evolutionary sequence conservation is an accepted criterion to identify noncoding regulatory sequences. We have used a transposon-based transgenic assay in zebrafish to evaluate noncoding sequences at the zebrafish *ret* locus, conserved among teleosts, and at the human *RET* locus, conserved among mammals. Most teleost sequences directed *ret*-specific reporter gene expression, with many displaying overlapping regulatory control. The majority of human *RET* noncoding sequences also directed *ret*-specific expression in zebrafish. Thus, vast amounts of functional sequence information may exist that would not be detected by sequence similarity approaches.

A current hypothesis is that sequences conserved over greater evolutionary distances are more likely to be functional than those conserved over lesser distances (*1*). Many recent publications have focused attention on the regulatory potential of "ultra-conserved" noncoding sequences, conserved across great evolutionary distances, e.g., human to fugu (*2–9*) [≥300 million years, or average 74% protein identity (*10*)]. These are frequently enhancers associated with developmental genes, consistent with strong selective pressure to preserve critical mechanisms. Analyses of identified sequences have generally fallen into two categories: analyses confined to mammals, with functional verification done in mice, or analyses including mammalian and teleost sequences, focusing on highly conserved sequences alignable at the extremes. However, simply because an expression pattern is preserved through evolution, it does not necessarily follow that the cis-regulatory elements controlling that expression in one species will function in a second.

We have explicitly tested two hypotheses: First, using selective pressure as a guide across moderate evolutionary distances, we can identify the majority of enhancers controlling expression at a particular locus by functional testing in a comprehensive, unbiased manner, and second, regulatory function of noncoding sequences will be conserved over evolutionary distances beyond the limit of overt sequence conservation.

We have focused on the regulatory control of the gene encoding the RET receptor tyrosine kinase. *RET* is expressed in neural crest, urogenital precursors, adrenal medulla, and thyroid during embryogenesis, and in specific central and peripheral neurons and endocrine cells during development and postnatally (*11*). Although *RET* expression is highly conserved across evolution (*12–15*), only the exons encoding the tyrosine kinase domain are overtly conserved [≥70%, ≥100 base pairs (bp)] from humans to zebrafish (*16–18*). We first compared the genomic sequence of a ~200–kilobase (kb) segment encompassing the zebrafish *ret* gene with the orthologous interval in fugu (Fig. 1), using AVID/VISTA (*19*, *20*). We generated 10 ZCS (zebrafish conserved sequence) amplicons, corresponding to 14 discrete noncoding sequences (table S1).

We also used these criteria to identify conserved noncoding human sequences, comparing a ~200-kb segment encompassing human *RET* with the orthologous genomic intervals in 12 nonhuman vertebrates (*16*). We selected sequences shared among human and at least three nonprimate mammals (*21*). In total 13 HCS (human conserved sequence) amplicons, encompassing 28 discrete conserved sequences (table S2) were generated for analysis.

[1]McKusick–Nathans Institute of Genetic Medicine, [2]Department of Cell Biology, [3]Department of Comparative Medicine, Johns Hopkins University School of Medicine, Baltimore, MD 21205, USA

*These authors contributed equally to this work.
†To whom correspondence should be addressed. E-mail: sfisher@jhmi.edu (S.F.); amccalli@jhmi.edu (A.S.M.)

Although zebrafish transgenesis has been used to evaluate the regulatory potential of conserved noncoding sequences (*2*, *7*, *22*), its efficacy is compromised by mosaicism in injected (G_0) embryos. We developed a reporter vector based on the Tol2 transposon; reporter expression in G_0 embryos, driven from the ubiquitous *ef1a* promoter, was extensive and was dependent on transposase RNA (*23*).

All but one ZCS amplicon drove reporter expression consistent with endogenous *ret* expression (Table 1). As in the mouse, zebrafish *ret* is expressed in sensory neurons of the cranial ganglia, motor neurons in the ventral hindbrain, cells of the hypothalamus and pituitary primordia, sensory and motor neurons in the spinal cord, and primary sensory neurons in the olfactory pit (*13*, *14*). We discovered elements driving expression consistent with all of these cell populations (Table 1), including small groups of cells, e.g., olfactory neurons (Fig. 2A) and lateral line placode ganglion (Fig. 3, A and B). Although *ret* is also expressed in amacrine and horizontal cell layers of the retina, we did not detect expression in the retina of G_0 embryos with any of the tested elements.

We found significant redundancy in the control of *ret* expression in the pronephric duct (Table 1; Fig. 2, C and D). Five elements drove expression in the intermediate mesoderm or pronephric duct; one was responsible for transient early expression (Fig. 2C), one for expression in the distal duct after 3 days (Fig. 2D), and three apparently redundantly control expression in the intervening period. Although three amplicons lie within a 5-kb region upstream of *ret*, they function independently in our assay. Similarly all but two ZCS amplicons drove expression in one or more cell populations of the central nervous system (Table 1), wherein *ret* is also dynamically expressed.

Surprisingly, 11 out of 13 HCS amplicons drove expression in cell populations consistent with zebrafish *ret* (Table 1). These included cells not present in mammals, such as the afferent neurons of the lateral line ganglia. We also observed multiple sequences driving expression in the excretory system, despite its developmental and anatomical differences between fish and mammals (Fig. 2G). Two sequences contained within a genomic interval deleted from the rodent lineage also functioned in zebrafish, in one case driving expression in the pituitary (Figs. 2E, 3E). Several pairs of elements drove similar expression patterns, despite lack of detectable sequence conservation (Table 1). To rule out the possibility that nonconserved sequences could fortuitously display enhancer activity, we analyzed expression from vectors containing nonconserved zebrafish (n = 5) or human (n = 3) genomic DNA, from the *RET* intervals (tables S1 and S2). None of these nonconserved sequences provided reproducible patterns of expression.

Through analysis of G_0 expression, we identified enhancers active in small cell populations such as the cranial ganglia and olfactory neurons (Fig. 2), suggesting that

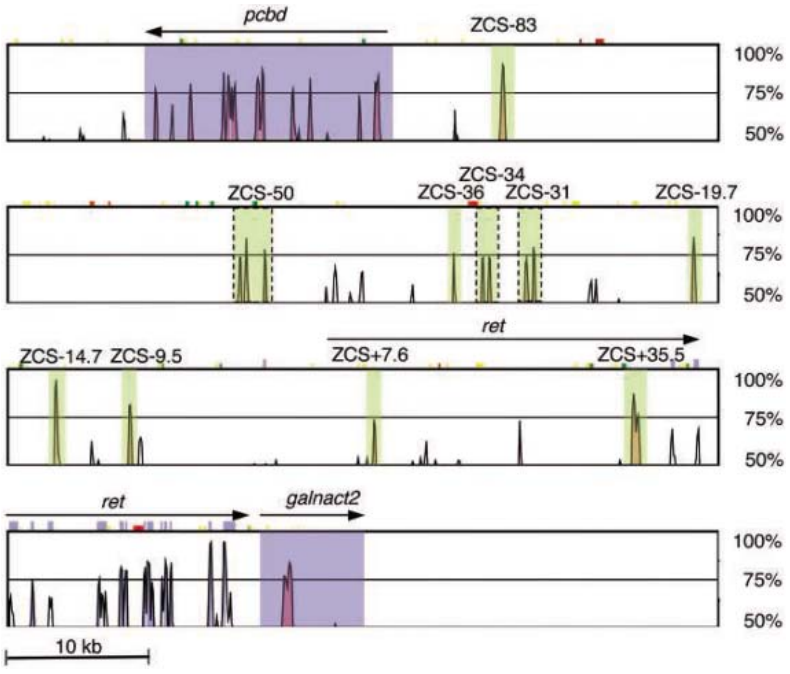

Fig. 1. Comparative sequence analysis of teleost *ret* loci reveals putatively functional noncoding sequences. VISTA plot displaying the alignment of the zebrafish *ret* locus with the orthologous fugu region. Red peaks represent conserved noncoding sequences; shaded green boxes represent ZCS amplicons. Boxes bordered by dashed lines denote amplicons containing two or more conserved sequences. *ret* exons are denoted by blue peaks. Red peaks boxed and shaded in blue denote 5′ and 3′ flanking genes *pcbd* and *galnact2*, respectively.

Table 1. Noncoding sequences from zebrafish *ret* or human *RET* direct expression consistent with endogenous *ret*. The elements are described by their species of origin and distance in kilobases from the translation start site, and (i.e., ZCS-50, HCS+16). Abbreviations: CG, cranial ganglia; SC, spinal cord; PND, pronephric duct; IM, intermediate mesoderm; NTC, notochord; OLF, olfactory pit/placode; +, present.

Constructs	Brain	SC	CG	ENS	NTC	OLF	Retina	Heart	IM/PND	Fin bud
ZCS-83	+	+	+			+				
ZCS-50	+	+	+		+			+		+
ZCS-36	+								+*	
ZCS-34	+								+	
ZCS-31	+								+	
ZCS-19.7	+	+	+	+			+		+	
ZCS-14.7	+	+								
ZCS-9.5	+	+	+							
ZCS+7.6									+	
ZCS+35.5		+	+	+				+		
HCS-32	+	+	+					+		+
HCS-30									+	
HCS-23					+					
HCS-12		+							+*	
HCS-8.7									+	
HCS-7.4										
HCS-5.2	+					+			+	
HCS+9.7				+					+	
HCS+16	+									
HCS+19	+	+								

*Expression before 24 hours.

mosaicism is not a significant limitation. We have passed a subset of transgenes through the germline (Fig. 3, A to C and E to G), to directly compare expression in G_0 and G_1 embryos. Expression of each transgene was largely consistent with that observed in G_0 phases (Fig. 3, A and B), although in some cases we observed additional expression, particularly in small groups of cells and at later time points [retina (Fig. 3G)]. We also evaluated many G_1 embryos using in situ hybridization (ISH) to detect *gfp* transcripts, which confirmed that green fluorescent protein (GFP) signal was present in *ret* positive cells (Fig. 3, C and D).

While still functioning as tissue-specific enhancers in zebrafish, some HCSs directed expression differing in timing or location from that of the endogenous *ret* gene. For example, HCS-32 drives GFP expression in dorsal spinal cord neurons, apparent between embryonic day 2 and 3. ISH analyses of G_1 transgenic embryos revealed expression at earlier stages in the posterior neural plate, where *ret* is not normally expressed. Additionally, two elements, HCS-23 and ZCS-50, directed expression strongly to the notochord, again not a site of endogenous *ret* expression. One possible reason for these discrepancies is that we are assaying elements out of context. Also, physical proximity does not mean that these elements normally regulate *ret* expression. In the case of HCSs, individual transcription factor–binding sites (TFBSs) may have evolved sufficiently to display different functions (i.e., binding related proteins, binding with different affinity), reflected in altered regulatory activity of the element as a whole.

HCS function in zebrafish may arise from sequence elements ≤100 bp that are conserved but fail to meet our original criteria for identification. Consequently, we repeated our sequence analysis with AVID/VISTA, reducing the window size to 30 bp. We also analyzed the *RET* orthologous intervals using the anchored alignment algorithms MultiLAGAN and Shuffle-LAGAN (*24*), the latter designed to detect alignable sequences in the presence of inversions and rearrangements. We also attempted to align each *RET* HCS independently, in both orientations, with the zebrafish *ret* interval (*25*). All analyses failed to detect sequences alignable between human and zebrafish *RET* intervals. We further searched the entire zebrafish genome (*26*) for homologies to the examined HCSs. Sixty-five sequences within these HCSs of ≥20 nucleotides in length demonstrated ≥70% identity with nonorthologous, intergenic zebrafish sequences, within 100 kb of a known or predicted gene; 41 out of 65 contain conserved TFBS motifs (table S3). However, we also aligned the nonconserved HCSs with the zebrafish genome and found alignments containing TFBSs at a similar frequency, which suggested that such analyses are not predictive of regulatory function. We posit that the responsible functional components in the conserved elements are single or multiple TFBSs (4 to 20 bp), beyond the ability of our current in silico tools to reliably detect. Our data suggest that restricting in vivo functional analyses to sequences conserved over great evolutionary distances (e.g., human to teleost) detects only a small fraction of functional information in the genome.

We have developed an efficient method to evaluate putative enhancer elements, allowing rapid assessment of in vivo function in a vertebrate embryo. This method is suitable for rapid screening of putative enhancers on a large scale, even where the orthologous zebrafish sequence is not available. Our approach represents a significant advance over previous methods because of the decreased mosaicism and improved germline transmission achieved with Tol2 vectors. The transparent external development of zebrafish facilitates dynamic analysis of reporter activity throughout embryogenesis, allowing detection of biological activity throughout development. This has allowed us to survey without bias all conserved sequences at a single, complex locus.

Our data strongly suggest that functional information is conserved in vertebrate sequences at levels below the radar of large-scale genomic sequence alignment, consistent with prior anecdotal observations (*27*, *28*). Two alternative models could be invoked to

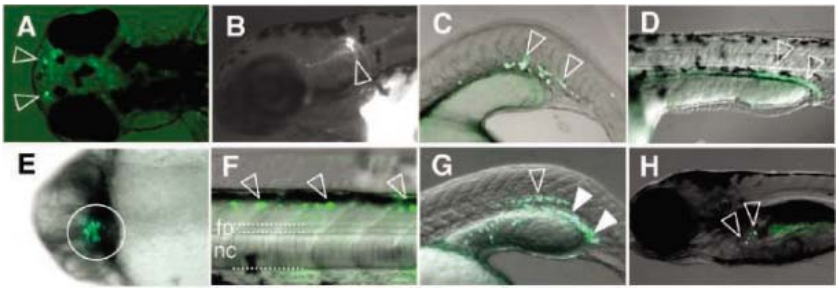

Fig. 2. Conserved noncoding sequences at the zebrafish and human *ret* loci drive reporter expression in zebrafish embryos consistent with the endogenous gene. Shown are GFP expression patterns in representative G_0 embryos. (**A** to **D**) Zebrafish elements drive expression in (A) bilateral olfactory pits (arrowheads; ZCS-83); (B) hindbrain neuron consistent with nVII facial motor neuron (arrowhead; ZCS-19.7); (C) pronephric duct before 24 hours (arrowhead; ZCS-34); and (D) pronephric duct at 3 days (arrowheads; ZCS-7.6). Human elements drive expression in (**E**), pituitary (encircled, HCS+16); (**F**) dorsal spinal cord neurons (arrowheads, HCS-32; fp, floor plate; nc, notochord); (**G**) pronephric duct (solid white arrowheads) and enteric neurons (open arrowhead; HCS+9.7); and (**H**) enteric neurons (open arrowheads, HCS+9.7).

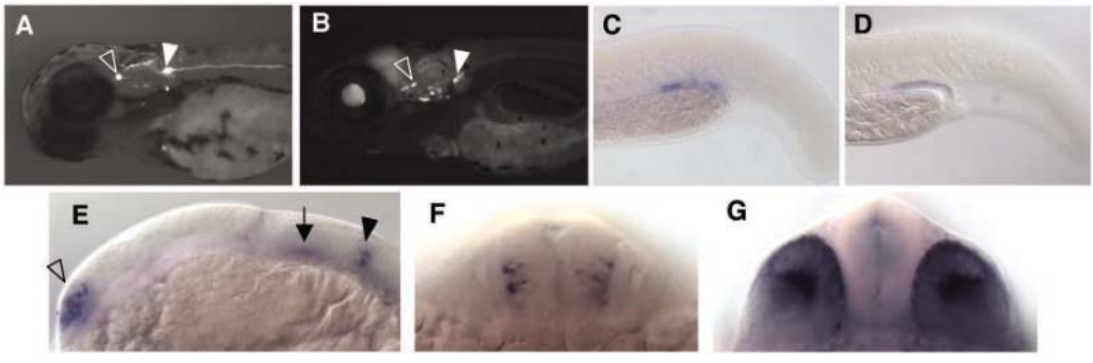

Fig. 3. Mosaic G_0 expression accurately reflects expression in G_1 fish. (**A**) ZCS-35.5 G_0 embryos display GFP in cells of the anterior (open arrowhead) and posterior (solid white arrowhead) lateral line placode ganglia. (**B**) ZCS-35.5 G_1 embryos display GFP in the anterior (open arrowhead) and posterior (solid white arrowhead) lateral line placode ganglia, as in (A). (**C**) GFP detected by in situ hybridization (ISH) in the distal pronephric duct of ZCS+7.6 G_1 embryo at 24 hours, consistent with ret expression at the same stage (**D**). (**E** and **F**) GFP detected by ISH in the pituitary (open arrowhead), trigeminal nuclei (arrow), and migrating nVII facial motor neurons [arrowhead in (E) and (F)] of a HCS+16 G_1 embryo. (**G**) GFP detected by ISH in the retina of G_1 ZCS-19.7 embryo.

explain our data. First, overall similar expression of the *RET* genes could be achieved through assemblage of analogously acting, although not orthologous, enhancers. A second, more parsimonious, explanation is that orthologous enhancer elements control expression of both *RET* genes, but have evolved beyond recognition through small changes in TFBSs, rearrangement of sites within enhancers, or multiple coevolved changes. Examination of enhancer evolution in *Drosophila* species reveals examples of these types of sequence changes, confounding traditional sequence alignment approaches while preserving enhancer function across species (*29*–*31*). Comparison of human and mouse enhancer sequences suggests that similar widespread turnover of TFBSs is observed in vertebrate evolution (*28*), although there is no corresponding functional data to confirm that such changes occur while preserving the function of the enhancers. Our data cannot distinguish between these two models; however, it must be the case that largely the same set of transcription factors regulate expression of either gene, and the binding of these is conserved from mammalian to teleost enhancer elements, which allows the HCSs to function in zebrafish. These data may now significantly alter the manner in which the biological relevance of vertebrate noncoding sequences is evaluated.

References and Notes

1. D. Boffelli, M. A. Nobrega, E. M. Rubin, *Nat. Rev. Genet.* **5**, 456 (2004).
2. A. Woolfe *et al.*, *PLoS Biol.* **3**, e7 (2005).
3. M. A. Nobrega, I. Ovcharenko, V. Afzal, E. M. Rubin, *Science* **302**, 413 (2003).
4. S. Bagheri-Fam, C. Ferraz, J. Demaille, G. Scherer, D. Pfeifer, *Genomics* **78**, 73 (2001).
5. N. Baroukh *et al.*, *Mamm. Genome* **16**, 91 (2005).
6. F. Poulin *et al.*, *Genomics* **85**, 774 (2005).
7. E. de la Calle-Mustienes *et al.*, *Genome Res.* **15**, 1061 (2005).
8. A. Sandelin *et al.*, *BMC Genomics* **5**, 99 (2004).
9. G. Bejerano *et al.*, *Science* **304**, 1321 (2004).
10. V. Veeramachaneni, W. Makalowski, *Nucleic Acids Res.* **33**, D442 (2005).
11. A. S. McCallion, A. Chakravarti, in *Inborn Errors of Development*, C. Epstein, R. Erikson, A. Wynshaw-Boris, Eds. (Oxford Univ. Press, Oxford, 2004).
12. M. Hahn, J. Bishop, *Proc. Natl. Acad. Sci. U.S.A.* **98**, 1053 (2001).
13. C. V. Marcos-Gutierrez, S. W. Wilson, N. Holder, V. Pachnis, *Oncogene* **14**, 879 (1997).
14. B. W. Bisgrove, D. W. Raible, V. Walter, J. S. Eisen, D. J. Grunwald, *J. Neurobiol.* **33**, 749 (1997).
15. V. Pachnis, B. Mankoo, F. Costantini, *Development* **119**, 1005 (1993).
16. E. S. Emison *et al.*, *Nature* **434**, 857 (2005).
17. A. S. McCallion *et al.*, *Cold Spring Harb. Symp. Quant. Biol.* **68**, 373 (2003).
18. C. S. Kashuk *et al.*, *Proc. Natl. Acad. Sci. U.S.A.* **102**, 8949 (2005).
19. K. A. Frazer, L. Pachter, A. Poliakov, E. M. Rubin, I. Dubchak, *Nucleic Acids Res.* **32**, W273 (2004).
20. Materials and methods are available as supporting material on *Science* Online.
21. E. A. Grice, E. S. Rochelle, E. D. Green, A. Chakravarti, A. S. McCallion, *Hum. Mol. Genet.* **14**, 3837 (2005).
22. S. Ellingsen *et al.*, *Development* **132**, 3799 (2005).
23. S. Fisher, E. A. Grice, R. M. Vinton, S. L. Bessling, A. S. MacCallion, unpublished observations.
24. See http://lagan.stanford.edu/lagan_web/index.shtml.
25. See http://genome.ucsc.edu/cgi-bin/hgBlat.
26. DanRer2 (www.sanger.ac.uk/Projects/D_rerio/), accessed June 2004.
27. B. Gottgens *et al.*, *Nat. Biotechnol.* **18**, 181 (2000).
28. L. A. Pennacchio *et al.*, *Science* **294**, 169 (2001).
29. B. P. Berman *et al.*, *Genome Biol.* **5**, R61 (2004).
30. M. Z. Ludwig, C. Bergman, N. H. Patel, M. Kreitman, *Nature* **403**, 564 (2000).
31. M. Z. Ludwig *et al.*, *PLoS Biol.* **3**, e93 (2005).
32. E. T. Dermitzakis, A. G. Clark, *Mol. Biol. Evol.* **19**, 1114 (2002).

33. The authors thank K. Kawakami for his generous gift of the pT2XIG vector. This study was supported by a Basil O'Conner award from the March of Dimes (A.S.M.) and grant AR048101 from the NIH (S.F.). Zebrafish sequence data (DanRer2) were produced by the *Danio rerio* Sequencing Group at the Sanger Institute and can be obtained by ftp transfer (ftp://ftp.ensembl.org/pub/assembly/zebrafish/Zv4release).

Supporting Online Material

www.sciencemag.org/cgi/content/full/1124070/DC1
Materials and Methods
Tables S1 to S3
References

19 December 2005; accepted 8 March 2006
Published online 23 March 2006;
10.1126/science.1124070
Include this information when citing this paper.

A Common Genetic Variant Is Associated with Adult and Childhood Obesity

Alan Herbert,[1*] Norman P. Gerry,[1] Matthew B. McQueen,[2] Iris M. Heid,[3,4] Arne Pfeufer,[5,6] Thomas Illig,[3,4] H.-Erich Wichmann,[3,4,7] Thomas Meitinger,[5,6] David Hunter,[2,8,9] Frank B. Hu,[2,8,9] Graham Colditz,[8,9] Anke Hinney,[10] Johannes Hebebrand,[10] Kerstin Koberwitz,[6,10] Xiaofeng Zhu,[11] Richard Cooper,[11] Kristin Ardlie,[12] Helen Lyon,[13,14,15] Joel N. Hirschhorn,[13,14,15] Nan M. Laird,[16] Marc E. Lenburg,[1] Christoph Lange,[9,13] Michael F. Christman[1*]

Obesity is a heritable trait and a risk factor for many common diseases such as type 2 diabetes, heart disease, and hypertension. We used a dense whole-genome scan of DNA samples from the Framingham Heart Study participants to identify a common genetic variant near the *INSIG2* gene associated with obesity. We have replicated the finding in four separate samples composed of individuals of Western European ancestry, African Americans, and children. The obesity-predisposing genotype is present in 10% of individuals. Our study suggests that common genetic polymorphisms are important determinants of obesity.

Obesity is associated with an increased risk of type 2 diabetes mellitus, heart disease, metabolic syndrome, hypertension, stroke, and some forms of cancer (*1*). It is commonly assessed by calculating an individual's body mass index (BMI) [weight/(height)^2 in kg/m^2] as a surrogate measurement. Individuals with a BMI $\geq$ 25 kg/m^2 are classified as overweight, and those with a BMI $\geq$ 30 kg/m^2 are considered obese. Having a BMI over 25 kg/m^2 increases the risk of death (*2*). Presently, 65% of Americans are overweight and 30% are obese (*3*). Genetic factors contribute significantly to the etiology of obesity (*4*, *5*), with estimates of the heritability of BMI ranging from 30 to 70% (*6*–*9*).

To identify common genetic variants associated with elevated BMI, we have studied individuals from the National Heart, Lung, and Blood Institute (NHLBI) Framingham Heart Study (FHS) (*10*). The participants were enrolled from the community without being selected for a particular trait or disease and were followed over 24 years (table S1). In this population, heritability estimates for BMI range between 37 and 54% (*11*, *12*).

Using families from this sample, we performed a genome-wide association analysis, using a testing strategy for quantitative traits in

[1]Department of Genetics and Genomics, Boston University Medical School, E613, 715 Albany Street, Boston, MA 02118, USA. [2]Department of Epidemiology, Harvard School of Public Health, 677 Huntington Avenue, Boston, MA 02115, USA. [3]Institute of Epidemiology, [4]KORA Group, [5]Institute of Human Genetics, Forschungszentrum für Umwelt und Gesundheit, D-85764 Neuherberg, Germany. [6]Institute of Human Genetics, Technical University Munich, D-81671 Munich, Germany. [7]Institute for Medical Informatics, Biometry and Epidemiology, Ludwig Maximilians University, Munich, Germany. [8]Nurses Health Study, [9]Channing Laboratory, Department of Medicine, Brigham and Women's Hospital and Harvard Medical School, 181 Longwood Avenue, Boston, MA 02115, USA. [10]Department of Child and Adolescent Psychiatry of the University of Duisburg-Essen, D-45147 Essen, Germany. [11]Department of Preventive Medicine and Epidemiology, Loyola University Medical Center, Maywood, IL 60153, USA. [12]Genomics Collaborative, SeraCare Life Sciences, Cambridge, MA, USA. [13]Program in Genomics and Divisions of Genetics and Endocrinology, Children's Hospital, Boston, MA 02115, USA. [14]Department of Genetics, Harvard Medical School, Boston, MA 02115, USA. [15]Broad Institute of Harvard and MIT, Cambridge, MA 02139, USA. [16]Department of Biostatistics, Harvard School of Public Health, 655 Huntington Avenue, Boston, MA 02115, USA.

*To whom correspondence should be addressed. E-mail: aherbert@bu.edu (A.H.); mfc@bu.edu (M.F.C.)

family-based designs (*13*, *14*). To bypass the multiple comparisons, we used a two-stage testing strategy implemented in the software package PBAT (*15*, *16*). In the screening step, parental genotypes are used to select single-nucleotide polymorphisms (SNPs) and genetic models that best predict offspring phenotypes. Formally, the screening step estimates the power to detect an association in the second step (Fig. 1 and fig. S1). The second step uses a family-based association test (FBAT) (*17*) to test the selected SNPs for association with BMI levels using measured offspring genotypes. The FBAT is a generalization of the transmission disequilibrium test (*18*) and assesses whether the over- or undertransmission of an allele is correlated with offspring phenotypes. Because the allele that is transmitted from the parent to the offspring is selected stochastically, the test step is statistically independent of the screening step, which conditions only on parental genotypes (*19*, *20*). Thus, the power estimates from the screening step do not bias the significance level of any subsequently computed FBAT statistic in the test step (*13*, *14*, *19*, *20*). Hence, the FBAT results need to be adjusted only for the number of comparisons performed during the test step. A SNP that reaches significance after adjustment for the number of tests performed in the test step is considered significant at a genome-wide level (*13*). Following the guidelines of Van Steen *et al*. (*13*), we tested the 10 SNPs with the highest power estimates in the screening step for association, using the FBAT (*21*, *22*).

We genotyped 116,204 SNPs in 694 participants from the FHS offspring cohort (*20*). After exclusions, 86,604 SNPs were tested for association with BMI. We used FBAT-PC, which incorporates BMI data across multiple exams and increases our power to detect a genetic effect (*14*). Of the top 10 SNPs tested under a recessive model [which we determined during the screening procedure had greatest power (Table 1)], only SNP rs7566605 reached overall significance (unadjusted FBAT-PC P value, 0.0026). Other genetic models that did not capture the underlying biology of the SNP were less robust. In such cases, rs7566605 was not ranked in the top 10 for power. The frequency of the rs7566605 C allele is 0.37, and the SNP is in Hardy-Weinberg equilibrium (Table 2). We found no association with BMI for Affymetrix SNPs close to rs7566605 (Fig. 2A and Table 2), This result was expected because none of these SNPs are good proxies for rs7566605 at a r^2 threshold of 0.8 (Fig. 2B) (*23*).

Another analysis based on a larger sample of 923 FHS individuals, including those already tested, indicated that the SNP is a significant predictor of BMI. For all exams, rs7566605 CC homozygotes are about 1 BMI unit heavier than individuals with GC or GG genotypes ($P < 0.0001$), regardless of sex or age (Fig. 3). CC homozygotes were also more likely to be obese than non-obese [for example, at exam 5, odds ratio (OR) = 1.33, 95% confidence interval (CI) (1.20 to 1.48)].

Many reported associations with common gene polymorphisms have not been replicated, presumably because of factors such as population stratification, inadequate statistical power, and genotyping errors (*24*). Therefore, we sought to confirm the association between BMI and rs7566605 in five additional unrelated samples of varying ethnicity and age.

We examined the association of rs7566605 with obesity in 3996 participants of the KORA S4 cohort, a population of Western European

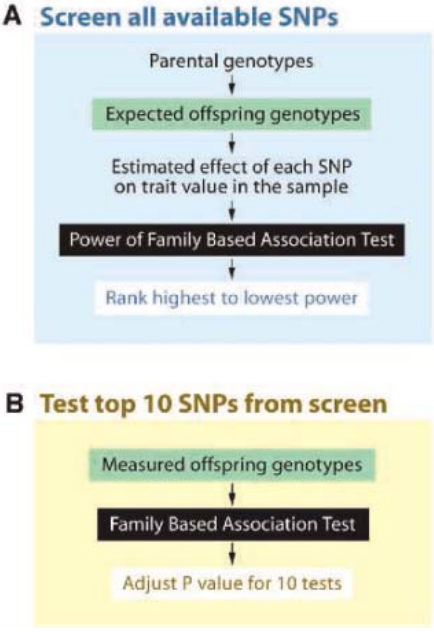

Fig. 1. Family-based design for the whole-genome SNP scan. The same data set was used to both screen and test SNP-phenotype associations (*13*). (**A**) In the screening step, the difference in offspring trait values due to a particular SNP allele is estimated based on the expected offspring genotypes, computed assuming Mendelian transmission of the parental genotypes. This information, along with the minor allele frequency, is used to compute the power of the FBAT to detect an association. (**B**) In the test step, the top 10–ranked SNPs are evaluated and the FBAT statistic is adjusted for 10 tests. SNPs that are significant after adjustment are also significant genome-wide. The screening and test steps use statistically independent components of the data; hence, the P values computed at the test step are not biased by the screening step (*20*).

Table 1. Screening and testing of SNPs for association with BMI. Genome-wide SNPs (86,604) were screened using parental genotypes to find those likely to affect offspring BMI. The top 10 SNPs from the screening step (ranked by power from most likely to least likely) are shown. These SNPs were tested using offspring genotypes for association with BMI using the FBAT. The rs7566605 SNP is highlighted in bold.

Ranking from screen	SNP	Chromosome	Frequency	Informative families	*P* value FBAT
1	rs3897510	20p12.3	0.36	30	0.2934
2	rs722385	2q32.1	0.16	15	0.1520
3	rs3852352	8p12	0.33	34	0.7970
4	**rs7566605**	**2q14.1**	**0.37**	**39**	**0.0026**
5	rs4141822	13q33.3	0.29	27	0.0526
6	rs7149994	14q21.1	0.35	31	0.0695
7	rs1909459	14q21.1	0.39	38	0.2231
8	rs10520154	15q15.1	0.36	38	0.9256
9	rs440383	15q15.1	0.36	38	0.8860
10	rs9296117	6p24.1	0.40	44	0.3652

Table 2. SNPs genotyped in the region of *INSIG2* along with their minor allele frequency (MAF). Results for the FBAT are given for a recessive model without covariate adjustment. SNPs were also tested for Hardy-Weinberg equilibrium (HWE). The coordinates for *INSIG2a* are 118,562,280 to 118,583,824 and for *INSIG2b* are 118,570,224 to 118,582,624. The rs7566605 SNP is highlighted in bold.

	FBAT (*P* value)	Physical position	Distance from rs7566605	HWE (*P* value)	MAF
rs1385923	0.33562	118550089	2166	0.107	0.057
rs10490626	0.07777	118552071	184	0.118	0.087
rs7566605	**0.00258**	**118552255**	**0**	**0.197**	**0.373**
rs10490625	0.34606	118575786	23531	0.251	0.063
rs10490624	0.20954	118578722	26467	0.02	0.082

ancestry in a town near Munich, Germany (table S2) (*25*). Genetic determinants of BMI have been studied in this cohort using candidate gene–based approaches (*26*). The mean BMI of rs7566605 CC homozygotes under a recessive model was 0.60 kg/m^2 higher than for GC and GG genotypes combined (P = 0.008). The CC genotype was also significantly more frequent in obese individuals [BMI ≥ 30 kg/m^2, OR = 1.32, 95% CI (1.05 to 1.66), P = 0.0167] than in non-obese individuals, again with a recessive model. These results confirmed the association that we found in the original genome scan of the FHS sample.

We also tested for an association in a case-control study consisting of self-described white or Caucasian subjects from Poland and the United States (1775 cases and 926 controls, table S3). Cases were drawn from the 90th to 97th percentile of the BMI distribution and controls were drawn from the 5th to 12th percentile, with distributions determined for each combination of gender, country of origin, and age by decade. The results for rs7566605 showed no evidence of heterogeneity between the Polish and U.S. subsamples, so we performed a combined analysis using a Mantel-Haenzsel procedure, as described (*27*). The CC genotype showed a significant association of the SNP with obesity under a recessive model [OR = 1.37, 95% CI (1.05 to 1.78), P = 0.02], with an odds ratio similar to that estimated from the KORA data.

The SNP was also genotyped in the Nurses Health Study cohort, using the 2726 control DNAs from two nested case-control studies examining diabetes (*28*) and breast cancer cases (*29*) (table S4). The participants are, by self-report, >95% Caucasian. No significant association or trend was observed between rs7566605 and BMI levels. There are fewer individuals with a high BMI in this sample as compared to the KORA and FHS samples (*20*). The lack of replication thus may reflect a different BMI distribution in the Nurses Health Study or differences in environment and lifestyle.

The rs7566605 SNP was also typed in 368 Western European parent-child trios in which either a child or adolescent offspring was obese (mean BMI percentile 98.4 ± 1.93) (*30*) (table S5). Analysis using the transmission disequilibrium test (*18*) revealed an overtransmission of the C allele to the obese offspring (P = 0.0017), indicating that rs7566605 is associated with BMI from an early age.

The finding was also replicated in two samples from a self-reported African American population from Maywood, Illinois (table S6). The samples consisted of 866 individuals from a family-based sample consisting of nuclear families and sibships and 402 unrelated individuals (186 chosen from the top and bottom quartiles of the BMI distribution, plus the parents from the family-based sample, whose

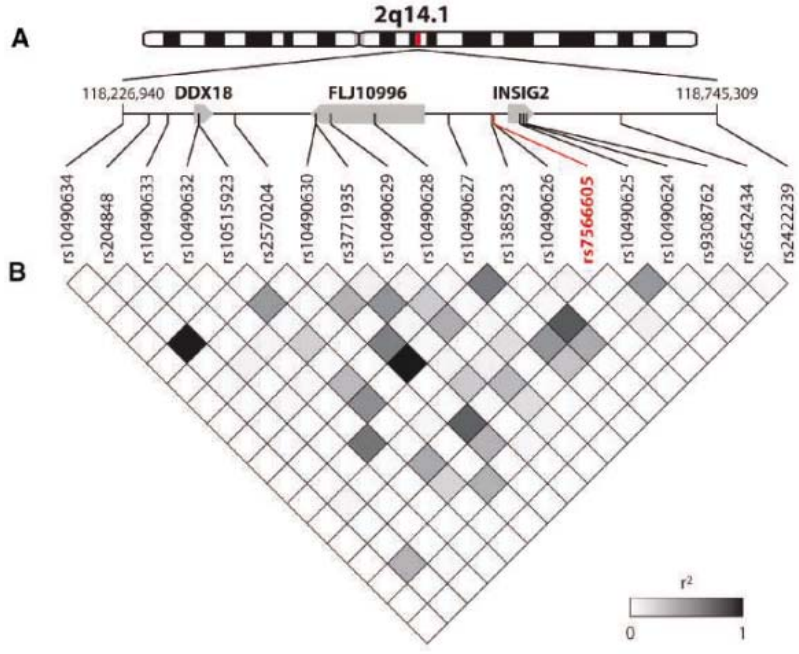

Fig. 2. SNPs present on the Affymetrix 100K chip near 2q14.1 Mapping of 100K SNPs in the chromosomal region from 2q14.1 to 2q14.2 is shown. (**A**) Known genes in the region of association. (**B**) A plot showing the pairwise r^2 values indicating the correlation between the SNP genotypes in our sample over this region prepared in Haploview (*23*). The rs7566605 SNP is shown in red. Black squares, $r^2 = 1$; white squares, $r^2 = 0$; squares in shades of gray, $0 < r^2 < 1$ (the intensity of the gray is proportional to r^2) (for example, r^2 between rs7566605 and rs3771935 equals 0.286).

Table 3. Summary of study results and meta-analysis. All values given are for a recessive model. NHS, Nurses Health Study; TDT, transmission disequilibrium test; PBAT, tools for FBATs.

Study	Design	Total genotyped	Obese	Non-obese	Test	Total number of families		P value
FHS	Family	694			PBAT	288		0.0030
Maywood	Family	866	361	505	PBAT dichotomous	342		0.0090
Maywood	Family	866			PBAT quantitative	342		0.0700
Essen children/adolescents	Trios	1104	368	–	TDT	368		0.0020
						Adjustments		
KORA	Cohort	3996			Linear regression	Sex, age		0.0080
NHS	Cohort	2726			Linear regression	Age		–
			Obese	*Non-obese*	*Test*	*OR*	*95% CI*	
KORA	Cohort	3996	935	3061	Logistic regression	1.32	1.06–1.65	0.0167
NHS	Cohort	2726	503	2223	Chi-squared test	0.81	0.58–1.13	–
American/Polish Caucasian	Case-control	2761	1835	926	Chi-squared test	1.40	1.08–1.78	0.0200
Maywood	Case-control	398	216	182	Fischer's exact test	2.36	–	0.0400
Pooled OR (all)		9881	3445	6426	2-tailed Mantel-Haenszel	1.22	1.05–1.42	0.0080

phenotypic information is not used in the family-based analysis). The samples were dichotomized into obese (BMI ≥ 30 kg/m^2) and lean (BMI < 30 kg/m^2) individuals. The CC genotype was associated with obesity under recessive models in both the family-based (P = 0.009) and unrelated samples (OR = 2.36, P = 0.04 by Fisher's exact test), adding further confirmation to our finding.

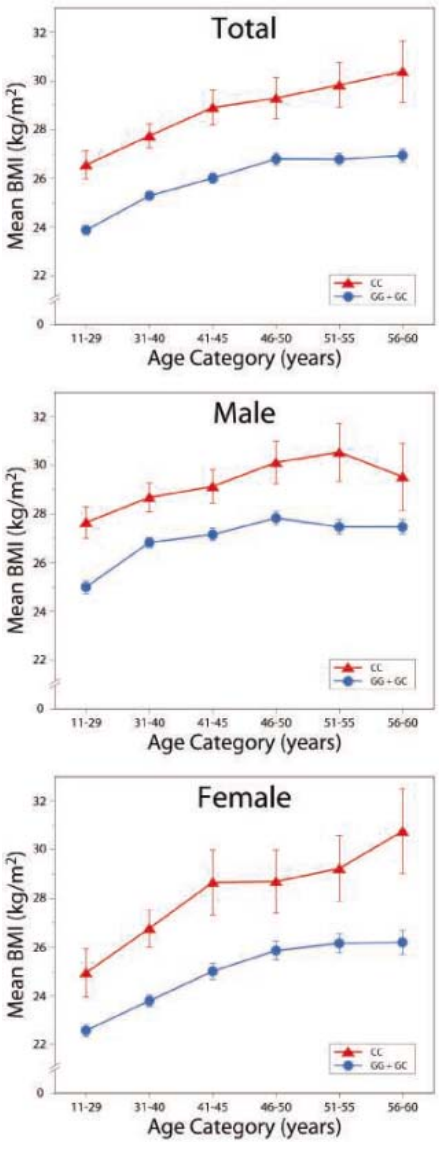

Fig. 3. BMI as a function of age, sex, and rs7566605 genotype. Unadjusted mean values for BMI comparing individuals homozygous for the minor allele (CC) with those that are either heterozygous or homozygous for the major allele (CG or GG) are shown. Data are for 923 related offspring and combine all the measurements from the first five offspring exams. Panels are for the pooled sample and for sex-specific analysis. Data are shown as mean ± SEM for each age category. Data from individuals over age 60 are omitted because few of those individuals have the CC genotype.

The rs7566605 CC genotype was associated with obesity in three different family-based samples and three studies of unrelated individuals. A meta-analysis of all the case-control samples showed that the CC genotype was significantly associated with obesity under a recessive model, with an OR of 1.22 [95% CI (1.05 to 1.42), P = 0.008; Table 3].

The result from both Western Europeans and African Americans suggests that the risk allele predates human migration out of Africa. By comparing chromosomes of individuals with different ancestry from the HapMap project (*31*) in a 750–kilobase (kb) region near *INSIG2* (*insulin-induced gene 2*), it is apparent that rs7566605 is present on a single haplotype in the European samples (haplotype 2) and on two haplotypes in the Yoruba samples (haplotypes 2 and 8) (Fig. 4; the rs7566605 C allele is shown in red). All of these haplotypes extend to include the intergenic region near *INSIG2* and the nearby *FLJ10996* gene. We also typed the rs11684454 SNP on European haplotype 2, located within an intron of *FLJ10996*. It too was associated with BMI in KORA samples (P = 0.0093) and in Western European parent-child trio samples (P = 0.0015), confirming that the associated region in Europeans extends at least 70 kb. Nonsynonymous SNPs (rs2229616 and rs17512204) in *FLJ10996* were not associated with BMI in Western European parent-child trio samples. We are not aware of any nonsynonymous SNPs in *INSIG2*. The region harboring the causal variant (Fig. 4) may be narrowed by detailed analysis of African haplotypes 2 and 8, because they are only similar close to rs7566605.

rs7566605 is 10 kb upstream of the transcription start site of *INSIG2*. *INSIG2* is an attractive candidate gene for the quantitative trait locus affecting BMI because its protein product inhibits the synthesis of fatty acid and cholesterol (*32*). For example, in the ZDF (*fa/fa*) rat model, overexpression of *insig2* in the liver reduces plasma triglyceride levels (*33*). A model in which altered *insig2* activity leads to obesity by elevating plasma triglyceride levels with subsequent storage in adipose tissue is certainly plausible. Indeed, the *INSIG2* region has been implicated as a factor in obesity by linkage studies in mice (*34*) and humans (*35*).

By studying a population not selected for a particular phenotype (the FHS Cohort), we hoped to identify common genetic variants affecting BMI levels. The high frequency of the rs7566605 C allele suggests that it is ancient and is consistent with the hypothesis that such alleles have become deleterious only in modern times (*36*). Although these variants are likely to carry low relative risk, their impact on health is substantial because of their prevalence in the population.

We expect that other common variants affecting BMI were not detected in our screen because of either lack of power in the screening step or insufficient coverage of the genome at the density provided by the Affymetrix 100K SNP chip. Taken together, the findings in four of the five samples from different populations using two different study designs confirm a consistent association between the rs7566605 polymorphism and obesity.

References and Notes

1. *NIH Publication No. 98-4083* (National Institutes of Health, Bethesda, MD, 1998).
2. J. E. Manson *et al.*, *N. Engl. J. Med.* **333**, 677 (1995).
3. A. A. Hedley *et al.*, *JAMA* **291**, 2847 (2004).
4. J. M. Friedman, *Nat. Med.* **10**, 563 (2004).
5. H. N. Lyon, J. N. Hirschhorn, *Am. J. Clin. Nutr.* **82**, 215S (2005).
6. C. G. Bell, A. J. Walley, P. Froguel, *Nat. Rev. Genet.* **6**, 221 (2005).
7. I. S. Farooqi, S. O'Rahilly, *Int. J. Obes.* **29**, 1149 (2005).
8. J. Hebebrand, S. Friedel, N. Schauble, F. Geller, A. Hinney, *Obes. Rev.* **4**, 139 (2003).
9. K. Schousboe *et al.*, *Twin Res.* **6**, 409 (2003).
10. W. B. Kannel, *J. Atheroscler. Thromb.* **6**, 60 (2000).
11. The lower estimate is that for narrow-sense heritability that estimates the proportion of phenotypic variance due to additive genetic factors, whereas the upper estimate is for broad-sense heritability, where all genetic factors, such as recessive and dominant alleles, are considered.
12. L. D. Atwood *et al.*, *Am. J. Hum. Genet.* **71**, 1044 (2002).
13. K. Van Steen *et al.*, *Nat. Genet.* **37**, 683 (2005).
14. C. Lange, D. DeMeo, E. K. Silverman, S. T. Weiss, N. M. Laird, *Am. J. Hum. Genet.* **74**, 367 (2004).
15. C. Lange, D. DeMeo, E. K. Silverman, S. T. Weiss, N. M. Laird, *Am. J. Hum. Genet.* **73**, 801 (2003).
16. C. Lange *et al.*, *Hum. Hered.* **56**, 10 (2003).
17. N. M. Laird, S. Horvath, X. Xu, *Genet. Epidemiol.* **19** (suppl. 1), S36 (2000).
18. R. S. Spielman, R. E. McGinnis, W. J. Ewens, *Am. J. Hum. Genet.* **52**, 506 (1993).
19. C. Lange, E. K. Silverman, X. Xu, S. T. Weiss, N. M. Laird, *Biostatistics* **4**, 195 (2003).
20. Supporting material is available on *Science* Online.
21. S. Horvath, X. Xu, N. M. Laird, *Eur. J. Hum. Genet.* **9**, 301 (2001).
22. C. Lange, D. L. DeMeo, N. M. Laird, *Am. J. Hum. Genet.* **71**, 1330 (2002).
23. J. C. Barrett, B. Fry, J. Maller, M. J. Daly, *Bioinformatics* **21**, 263 (2005).
24. J. N. Hirschhorn, K. Lohmueller, E. Byrne, K. Hirschhorn, *Genet. Med.* **4**, 45 (2002).
25. H. E. Wichmann, C. Gieger, T. Illig, *Das Gesundheitwesen* **Special Issue 1**, S26 (2005).
26. I. M. Heid *et al.*, *J. Med. Genet.* **42**, e21 (2005).
27. K. E. Lohmueller, C. L. Pearce, M. Pike, E. S. Lander, J. N. Hirschhorn, *Nat. Genet.* **33**, 177 (2003).
28. F. B. Hu *et al.*, *Diabetes* **53**, 209 (2004).
29. V. W. Setiawan, S. E. Hankinson, G. A. Colditz, D. J. Hunter, I. De Vivo, *Cancer Epidemiol. Biomarkers Prev.* **13**, 213 (2004).
30. A. Hinney *et al.*, *J. Clin. Endocrinol. Metab.* **88**, 4258 (2003).
31. The International HapMap Consortium, *Nature* **426**, 789 (2003).
32. D. Yabe, M. S. Brown, J. L. Goldstein, *Proc. Natl. Acad. Sci. U.S.A.* **99**, 12753 (2002).
33. K. Takaishi, L. Duplomb, M. Y. Wang, J. Li, R. H. Unger, *Proc. Natl. Acad. Sci. U.S.A.* **101**, 7106 (2004).
34. J. M. Cheverud *et al.*, *Diabetes* **53**, 3328 (2004).
35. H. W. Deng *et al.*, *Am. J. Hum. Genet.* **70**, 1138 (2002).
36. D. E. Reich, E. S. Lander, *Trends Genet.* **17**, 502 (2001).

37. The authors thank the participants of the FHS for their contribution and the NHLBI-FHS investigators for providing DNA samples and phenotypic data for our

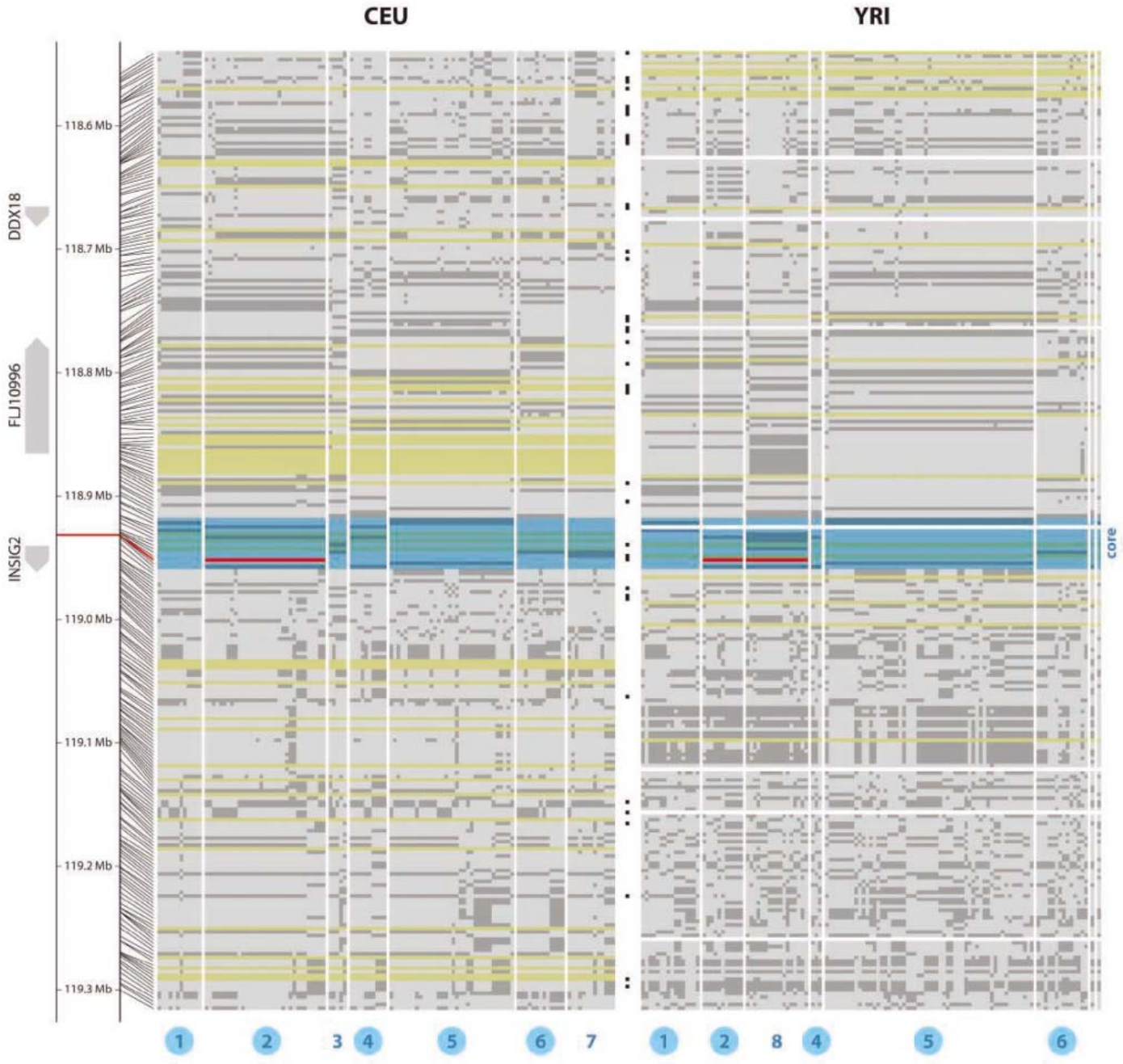

Fig. 4. Linkage disequilibrium around rs7566605 Alignment of the phased HapMap genotypes (release 16c.1) for 120 chromosomes from Utah residents of Northern and Western European ancestry (CEU) and 120 chromosomes from Yoruba in Ibadan, Nigeria (YRI) over a 750-kb region surrounding rs7566605. A core haplotype block containing rs7566605 was identified using Haploview (*23*) and was used to organize the chromosomes from left to right. The region containing this core haplotype block is highlighted in blue, and each haplotype with a frequency greater than 1% is designated with a number at the bottom. Haplotypes shared between the CEU and YRI samples are circled. The SNP rs7566605 minor allele is present on one major haplotype in Utah residents (haplotype 2) and on two in Yoruba samples (haplotypes 2 and 8). Minor alleles are represented with dark grey boxes and major alleles with light gray boxes, with the exception of the rs7566605 minor allele (shown in red). SNPs not found to be polymorphic in one of the samples are shaded yellow. SNPs present on the Affymetrix Mapping 100K set are indicated in black between the CEU and YRI panels.

analysis. This work was supported by a Leadership Award from the Whitaker Foundation (A.H. and M.F.C.); grants from the American Diabetes Association to A.H. and an ADA Smith Family Pinnacle Program Project to J.N.H.; and partially by the following NIH grants: R01GM046877 (M.F.C.), K23DK067288 (H.L), R01HL54485 and R01HL074166 (R.C. and X.Z.), P30DK46200 (principal investigator B. Corkey), and R01MH59532, U01HL65899, and R01HL66289 (N.M.L. and C. L.). A.P., I.H., T.I., T.M., H.-E.W., A. Hi., J. He., and K.K. were supported by the German Ministry of Education and Research (BMBF, grant 031U212C) through the National Genome Research Network (NGFN, grants 01GR0411, N2NV-S31T10, PGE-S04T13, PGE-S15T04, NHK-S19T19, and NHK-S38T01) and Bioinformatics for the Analysis of Mammalian Genomes (BFAM) and by DFG WI621/12-1. The Nurses Health Study is funded by National Cancer Institute grant CA87969 and thanks C. Guo for data analysis. We thank D. Pellman, N. Levin, and J. Kirkland for comments on the manuscript.

Supporting Online Material

www.sciencemag.org/cgi/content/full/312/5771/279/DC1
Materials and Methods
Fig. S1
Tables S1 to S6
References

10 January 2006; accepted 14 March 2006
10.1126/science.1124779

Evidence for a Functional Second Thymus in Mice

Grzegorz Terszowski,[1]* Susanna M. Müller,[1]* Conrad C. Bleul,[3] Carmen Blum,[1] Reinhold Schirmbeck,[2] Jörg Reimann,[2] Louis Du Pasquier,[4] Takashi Amagai,[5] Thomas Boehm,[3] Hans-Reimer Rodewald[1]†

The thymus organ supports the development of T cells and is located in the thorax. Here, we report the existence of a second thymus in the mouse neck, which develops after birth and grows to the size of a small lymph node. The cervical thymus had a typical medulla-cortex structure, was found to support T cell development, and could correct T cell deficiency in athymic nude mice upon transplantation. The identification of a regular second thymus in the mouse may provide evolutionary links to thymus organogenesis in other vertebrates and suggests a need to reconsider the effect of thoracic thymectomy on de novo T cell production.

The thymus is a primary lymphoid organ supporting the development of self-tolerant T cells, which are the mainstay of the cellular immune system [reviewed in (*1*–*3*)]. In the mouse, thymus anlagen arise as bilateral structures from the third pharyngeal pouch in the embryonic foregut [reviewed in (*4*–*6*)] and are colonized by hematopoietic progenitors in midgestation around embryonic day 11.5 (E11.5) (*7*). The thymus lobes descend ventrally and caudally to their final destination in the upper chest in proximity to the heart. Despite in-depth information about the distinct capacity of thymus tissue to foster T cell development, important questions remain about the onset and duration of thymus function, the putative capacity of nonthymus sites such as skin, gut, or liver to function as sites of T cell development, and the immunological consequences of surgical removal of the thoracic thymus.

In the course of our experiments, we observed several structures with lymphoid characteristics, located superficially or concealed below cervical muscle strings in the ventral necks of mice. Because these lymphoid-like organs could not be unambiguously identified as lymph nodes (LNs), their in situ positions were documented for further analyses (Fig. 1, A and K) (*8*). We recognized that some of these cervical lymphoid organs displayed hallmarks of thymus structure, including a medulla-cortex architecture (Fig. 1B) marked by cytokeratin expression (Fig. 1D), $CD4^+CD8^+$ double-positive (DP) (Fig. 1, C and E), and $CD4^+CD8^-$ and $CD4^-CD8^+$ single-positive (SP) thymocytes with low and high levels of T cell receptor (TCR)/CD3 expression, respectively (Fig. 1, C, E, and F). Thoracic thymus tissue is shown for comparison in Fig. 1, G to J. In contrast, cervical LN (Fig. 1, K and L) harbored only mature T cells (Fig. 1, M, O, and P), and lacked cytokeratin$^+$ epithelium (Fig. 1N). In agreement with ongoing thymopoiesis, *Rag*1, *Rag*2, *TdT*, and *pTα* genes (*2*) were expressed in cervical thymuses but not in cervical LNs (fig. S1). Cervical thymus stroma harbored normal numbers of regularly distributed dendritic cells and endothelial cells (fig. S2), and expression of the transcriptional regulators *Foxn1* and *Aire* also indicated the existence of a typical thymus microenvironment (fig. S3).

Although thymus structure and thymocyte phenotypes were very similar in a comparison of neck and chest organs, they were not identical. Cervical thymus lobes harbored $\approx 1.6 \times 10^5$ thymocytes compared with $\approx 10^8$ thymocytes in the thoracic thymus (fig. S4), and thoracic thymuses were multilobulated, whereas cervical thymuses appeared as single lobes (Fig. 1 and fig. S4). The proportion of mature thymocytes in cervical thymuses was also higher than in their thoracic counterpart [fig. S4 and supporting online material (SOM) text 1].

Foxn1 is a transcription factor essential for thymic epithelial differentiation and hence thymopoiesis (*9*). To facilitate the rapid identification of cervical thymuses, we created a reporter mouse strain (Foxn1::Egfp), in which an enhanced green fluorescent protein (Egfp) transgene is driven by *Foxn1* regulatory sequences. Direct visualization of the position of cervical and thoracic thymuses was possible by virtue of thymus tissue–specific in situ fluorescence (Fig. 1Q). Consistent with the localization of additional thymuses (Fig. 1, A and R) and their *Foxn1* expression, we observed two small Egfp$^+$ organs in the neck (Fig. 1Q). In normal BALB/c mice, we detected cervical thymuses in 19 out of 21 analyzed animals (90%) with one, two, and three ectopic thymuses in 11 out of 19, 7 out of 19, and 1 out of 19 mice, respectively. In the C57BL/6 strain ($n = 21$ mice), the incidence of cervical thymuses was reduced by about 50% compared with BALB/c mice, suggesting a strain-dependent penetrance of the phenotype. Cervical thymuses were also detected in the FVB mouse strain (*10*). A topographical analysis of cervical thymuses in 10 BALB/c mice (here, incidence = 100%) indicated that half of the mice had two organs and the other half presented with a single cervical thymus (Fig. 1R). Hence, the anatomical position and the number of cervical thymuses showed a degree of variability.

Next, we determined whether cervical thymuses could be colonized by T cell progenitors and support their T cell development. In a first set of experiments, cervical thymuses from adult BALB/c [major histocompatibility complex (MHC, termed H-2 in the mouse) haplotype = H-2^d] mice were grafted under the kidney capsules of adult C57BL/6 nude (H-2^b) mice and analyzed after 6 weeks (Fig. 2, A to C). Cortical and medullary zones were clearly marked by the presence of DP and SP thymocytes (Fig. 2C). MHC marker expression demonstrated hematopoietic colonization from host progenitors. In contrast to fetal thymus grafts that can expand to near thorax thymus size under the kidney capsule, and consistent with the constant size of adult tissues, cervical thymus grafts retained their original size (Fig. 2, SOM text 2, and fig. S5).

A crucial function of the thymus is the generation of self–MHC-restricted, immunologically self-tolerant T cells (*11*). To examine whether this was also supported in the cervical thymus, negative and positive thymocyte selection were compared in cervical and thoracic thymuses. An endogenous superantigen (mammary tumor virus 6) deletes autoreactive TCR V$\beta 3^+$ thymocytes in BALB/c but not in C57BL/6 mice (*12*). This deletion occurred in thoracic and cervical thymuses (fig. S4E). Positive selection of MHC class II–restricted DO.11.10 TCR-transgenic (*13*) $CD4^+$ thymocytes expressing the transgenic TCR α and β chains occurred in both thorax and neck thymuses (fig. S4, G and H). The results indicate that the processes of positive selection and clonal deletion of T cells occurred normally in the cervical thymus (SOM text 3).

In a second series of transplantation experiments aimed at measuring T cell export from the grafts, BALB/c nude mice (H-2 K^{d+} H-2 L^{d+}) (Fig. 2F) were transplanted with cervical thymuses from BALB/c congenic dm2 mice lacking H-2 L^d (H-2 K^{d+} H-2 L^{d-}) (Fig. 2E). H-2 L^d expression was analyzed to track peripheral blood T cells to the thymus graft (H-2 L^{d-}) or nude bone marrow (H-2 L^{d+}) origin. Euthymic BALB/c (Fig. 2D) and dm2 (Fig. 2E) mice had between 30 and 65% $CD3^+$ T cells per total leukocytes in their blood (Fig. 2H), with CD4 to CD8 ratios of about 4 to 1 (Fig. 2, D and E). In contrast, BALB/c nude mice had only about 10 to 15% $CD3^+$ T cells

[1]Department of Immunology, [2]Department for Internal Medicine I, University of Ulm, D-89081 Ulm, Germany. [3]Max-Planck-Institute of Immunobiology, Stuebeweg 51, D-79108 Freiburg, Germany. [4]Institute of Zoology and Evolutionary Biology, University of Basel, CH4051 Basel, Switzerland. [5]Department of Immunology and Microbiology, Meiji University of Oriental Medicine, Hiyoshi-cho, Funai-gun, Kyoto 629-0392, Japan.

*These authors contributed equally to this work.
†To whom correspondence should be addressed. E-mail: hans-reimer.rodewald@uni-ulm.de

in their blood (Fig. 2H), and these were mostly CD8$^+$ (Fig. 2F). Eight weeks after grafting, 7 out of 7 mice showed significant percentages (mean = 5%, range = 1.4 to 12.7%) of thymus-derived (H-2 K^{d+} H-2 L^{d-}) cells in their blood. These cells were exclusively CD3$^+$ T cells, predominantly CD4$^+$ but also CD8$^+$ (Fig. 2G, blue). In addition, overall numbers of T cells increased after grafting of the cervical thymus (Fig. 2H). Cervical thymus grafts were able to produce T cells bearing diverse TCRs, as shown by comparing Vβ usage among LN T cells from untransplanted BALB/c and BALB/c nude with BALB/c nude mice that had been grafted with a cervical thymus. Analysis for L^d expression revealed that cervical thymus grafts promoted diverse Vβ usage of thymus graft-derived as well as host-derived T cells (Fig. 2I).

To test for the thymus's capacity to provide immune-competent peripheral T cells, BALB/c nude mice were grafted with a cervical thymus, and 6 weeks later immunized with recombinant hepatitis B surface antigen particles (HBsAg), a T-dependent B cell antigen. Three weeks after immunization, sera of grafted and control mice were analyzed for the anti-HBsAg immunoglobulin G1 (IgG1) titers to assess the capacity of T cells to provide B cell help and to instruct Ig class switching. Nongrafted BALB/c nude mice failed to respond. In contrast, 4 out of 6 mice transplanted with a cervical thymus mounted a substantial IgG1 response against HBsAg (Fig. 2J). Hence, the cervical thymus could transfer T cell immune competence to mice lacking an endogenous thymus.

In a search for possible origins of the cervical thymus, a potential cervical thymus anlage was detected lateral to the parathyroid gland in the neck of newborn mice. This epithelial structure displayed morphological hallmarks of thymus epithelium cells (TECs), such as expression of keratin 5 (K5), K18, MHC class II, and Foxn1 (Fig. 3). The parathyroid gland, located adjacent to the thymus anlage, lacked expression of K5 and MHC class II but expressed K18. At high resolution, the neonatal cervical thymus anlage showed immature morphological characteristics similar to embryonic orthotopic thymuses (*3*). At E12.5 and E13.5, immature TECs begin to express MHC class II and coexpress K5 and K18 in the orthotopic thymus. However, a medulla-cortex structure, marked by K5 and K18 expression, was not apparent until E14.5 (fig. S6) (*14*, *15*). In the neonatal cervical thymus, TECs also coexpressed K5 and K18, and no clear demarcation of cortex and medulla was apparent (fig. S6), highly reminiscent of the E12.5 to E13.5 embryonic thymus. By contrast, the thoracic thymus of newborn mice showed a much more advanced TEC maturation (Fig. 3). Failure to detect evidence for TCR rearrangement in the E18.5 neck (fig. S7 and SOM text 4) supports the late onset of cervical thymopoiesis. Although at this stage we cannot directly demonstrate a developmental relationship, our

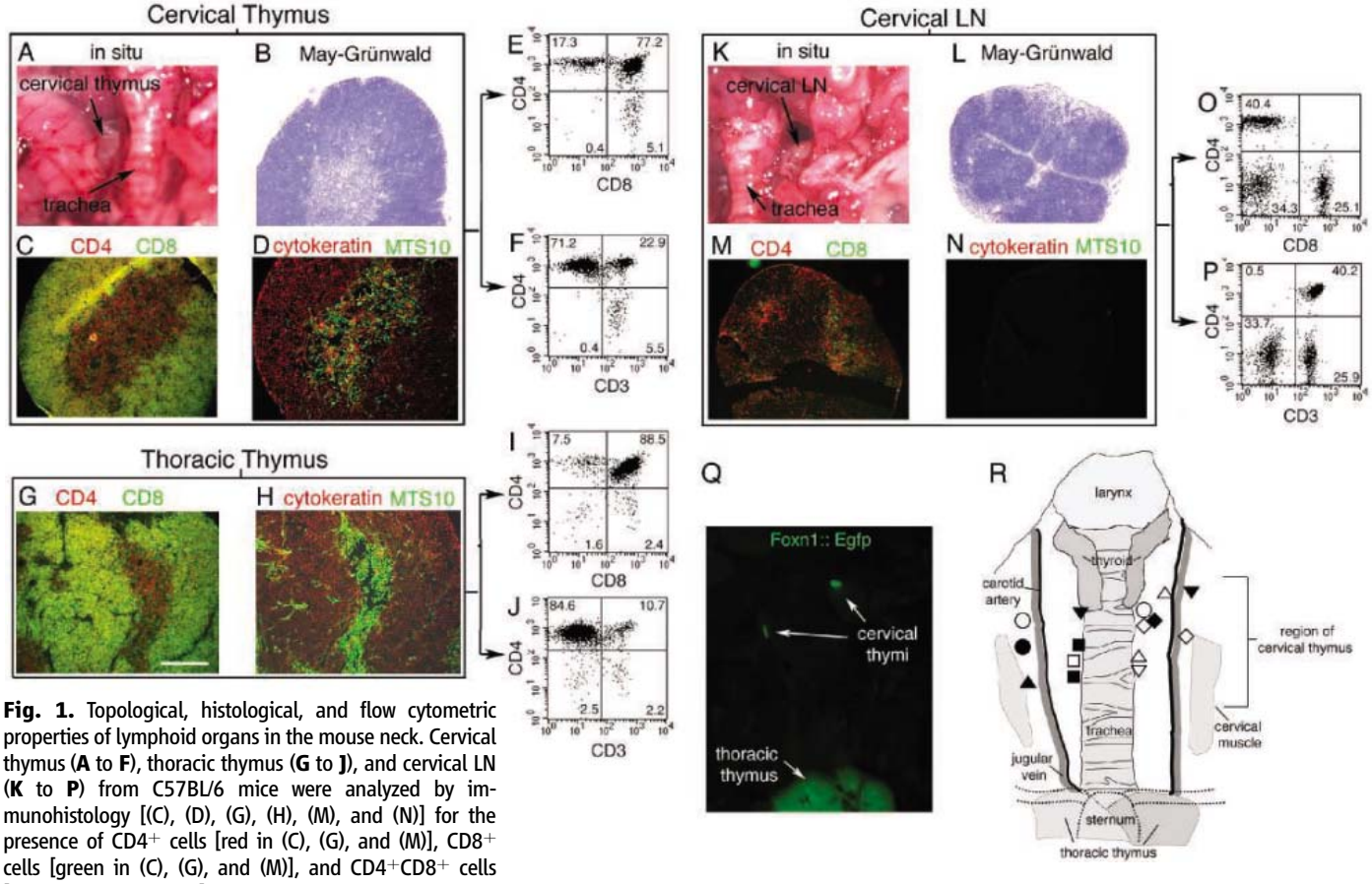

Fig. 1. Topological, histological, and flow cytometric properties of lymphoid organs in the mouse neck. Cervical thymus (**A** to **F**), thoracic thymus (**G** to **J**), and cervical LN (**K** to **P**) from C57BL/6 mice were analyzed by immunohistology [(C), (D), (G), (H), (M), and (N)] for the presence of CD4$^+$ cells [red in (C), (G), and (M)], CD8$^+$ cells [green in (C), (G), and (M)], and CD4$^+$CD8$^+$ cells [yellow in (C) and (G)], or for expression of cytokeratin and the medullary epithelial marker MTS10 [(D), (H), (N)]. In situ location [(A) and (K)] and May-Grünwald-Giemsa–stained morphology [(B) and (L)] are shown for cervical thymus and LN. Flow cytometry for expression of CD4 versus CD8 [(E), (I), and (O)] and CD3 versus CD4 [(F), (J), and (P)]. Scale bar in (G), 300 μm; applies to (B) to (D), (G), (H), and (L) to (N). The widths of panels (A) and (K) correspond to 12 mm. (**Q**) Thymus-specific in situ fluorescence of two cervical thymuses (upper part) and the thoracic thymus (lower part) by *Foxn1*-Egfp reporter expression. The width of panel (Q) corresponds to 10 mm. (**R**) Topology of cervical thymuses in BALB/c mice. The position of 15 cervical thymus lobes identified in 10 BALB/c mice was plotted onto an anatomical drawing of the neck. Each symbol represents the position of cervical thymus lobes in an individual mouse. Symbols used twice indicate two cervical thymuses in that mouse. Of 10 mice, 5 had one cervical thymus lobe. Of these, three lobes were on the right (solid circle, open square, and solid triangle) and two were on the left side (solid diamond and open upside-down triangle). The other five mice had two thymus lobes in each neck. Of these five mice, two had two left lobes (open triangles and open diamonds), one had two right lobes (solid squares), and two had one lobe on each side (open circles and solid upside-down triangles).

data do support the possibility that the second thymus arises postnatally from the anlage found in the neonatal neck in proximity to the parathyroid. It also exhibits a delay in maturation by at least 1 week compared with the thoracic thymus.

Based on the criteria we used in our experiments, the cervical thymus appears to faithfully support thymocyte selection and export T cells bearing diverse TCRs into peripheral lymphoid organs, where they have the potential to assist in T cell–dependent antibody responses. Based on these criteria, at least, the cervical thymus appears fully functional in supporting T cell development. BALB/c and C57BL/6 strains are highly relevant as immunological models, but further inbred and also outbred strains should be comprehensively analyzed in future work. Our results raise phylogenetic, ontogenetic, and immunological questions. Although cervical thymus tissue has been observed in several other species, including humans, it is important to consider whether thymus tissue in the neck is detected during early development or later in life. During embryogenesis, cervical thymus tissue is often the result of an extension of descending thoracical thymus reaching into the neck. Accordingly, in human fetuses, classical literature has reported the cervical thymus to be quite frequent (*16*) [reviewed in (*17*)]. However, in humans, the presence of cervical thymus is considered rare after birth and has been associated with pathological conditions (*17*–*21*). In these cases, it has been assumed that the thymus fails in its descent to the final mediastinal location, giving rise to remnants or accessory nodules anywhere along the neck. In contrast, because the cervical thymus occurred regularly in adult mice, we propose that it does not arise as an accidental abnormality. Although a histological section of mouse neck resembling thymic tissue was observed about 40 years ago (*22*), it was not known at the time whether this tissue was functional thymus. Further phylogenetic and ontogenetic aspects are discussed in SOM text 5.

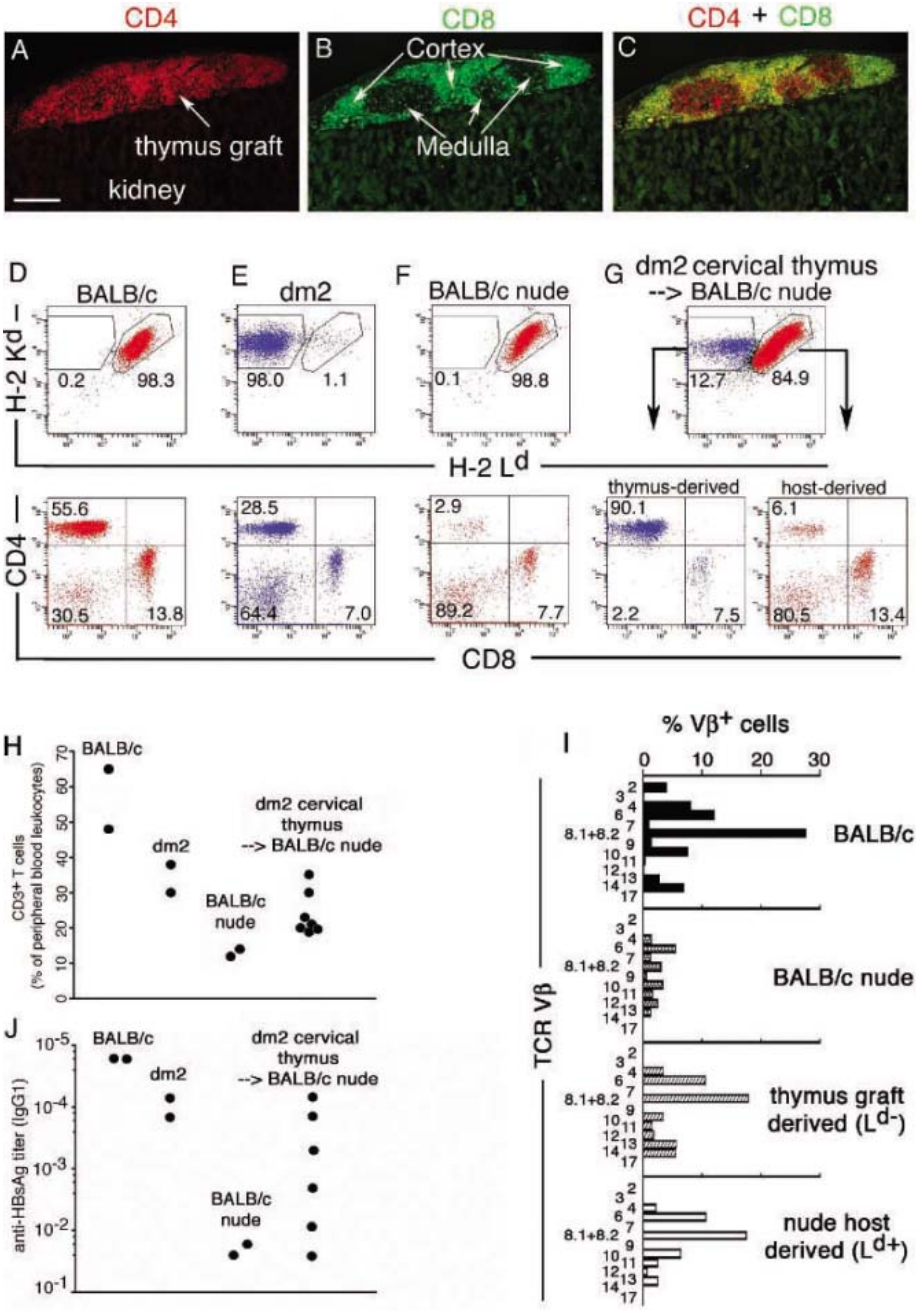

Fig. 2. Function of cervical thymus grafts in athymic nude mice. Tissue sections from a cervical thymus graft located under the host kidney capsule were analyzed for expression of CD4 (**A**) and CD8 (**B**). The overlay (**C**) indicates the presence of immature DP thymocytes (yellow) in the cortex and mature SP cells in the medulla. These short-lived thymocytes expressed mostly host-MHC class I. Scale bar in (A), 200 μm; applies to all panels. (**D** to **G**) Peripheral blood leukocytes from BALB/c mice (D), BALB/c congenic dm2 mice (E), BALB/c nude mice (F), and BALB/c nude mice grafted with cervical thymus from dm2 donors (G) were analyzed for MHC class I (H-2 K^d and H-2 L^d) expression [(D) to (G), upper panels]. Lymphoid blood cells were analyzed for CD4 and CD8 expression [(D) to (G), lower panels]. (**H**) Percentages of $CD3^+$ among peripheral blood leukocytes (defined as total MHC class I^+ cells) are shown. (**I**) $CD3^+$ LN T cells were analyzed for expression of the indicated Vβ genes by flow cytometry. (**J**) Immunization with a T-dependent antigen (HBsAg). Three weeks after immunization, mouse sera were tested for the presence of IgG1 antibodies against HBsAg.

In some regards, it is surprising that the functional cervical thymus has not been detected before in the mouse, which is a much-studied immunological organism. We originally detected cervical thymuses in normal mice that were used as controls for tetraparental chimeric mice (*23*), constructed from embryonic stem cells deficient in *Tbx1* [a gene defective in DiGeorge Syndrome (*24*, *25*)] (*26*) together with nude mouse blastocysts, where we searched for defects in thymus development. As part of the protocol in these studies, all lymphoid tissues in the neck were systematically analyzed, allowing us to define the cervical thymus, whereas it has previously escaped detection.

The thoracic thymus descends from its origin in the third pouch into the chest, with the cervical thymus probably taking a lateral route. We still do not have a complete picture of the mechanism regulating thymus descent and positioning; further experiments and comparisons of neck and chest thymic tissue will be necessary to address the remaining questions about the timing and origin of the cervical thymus.

From the immunological point of view, a regular second thymus in mice raises important questions about previous studies that have used thymectomized mice. Thoracic thymectomy has been a major experimental tool to study the T

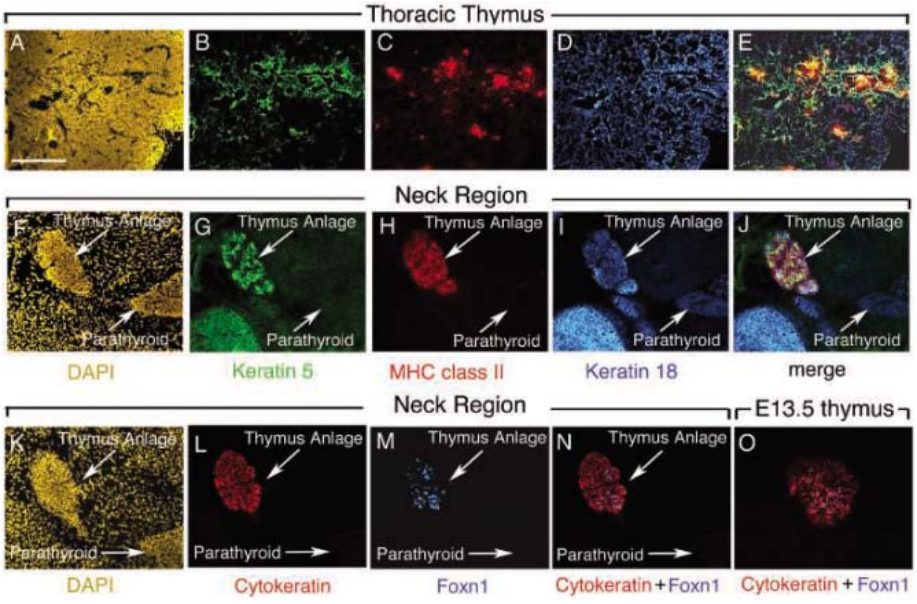

Fig. 3. A candidate anlage for the second thymus in newborn mice. Thoracic thymus (**A** to **E**) and transversal sections of the neck region (**F** to **N**) from newborn BALB/c mice, and from embryonic day 13.5 (E13.5) (**O**) were analyzed by immunofluorescence for expression of K5 [(B) and (G)], MHC class II [(C) and (H)], K18 [(D) and (I)], cytokeratin (L), and Foxn1 (M). Overlays for K5, MHC class II, and K18 shown in (E) and (J), and for cytokeratin and Foxn1 in (N) and (O). Nuclear staining with 4′,6′-diamidino-2-phenylindole (DAPI) reveals tissue structure [(A), (F), and (K)]. Scale bar in (A), 160 μm; applies to all panels.

cell system in the absence of de novo production of naive T cells (*27*). In cases of residual adaptive immunity after neonatal thymectomy, it has been assumed that the thymectomy has either been surgically incomplete or that immunologically competent cells left the thymus before birth. There are, indeed, paradoxical results in the wake of experiments involving thoracic thymectomy. For example, postthymic, naive-phenotype peripheral T cells are considered nondividing cells until activated by antigen. Proliferation-dependent in vivo labeling suggested, however, that this T cell population proliferates, albeit at a reduced rate, even in mice after thoracic thymectomy (*28*). In these, and in other cases, a cervical thymus in mice may provide an alternative source of ongoing thymopoiesis, and the ability of the cervical thymuses to transfer immune competence to nude mice lacking an endogenous thymus supports this view. In addition to the notion that a second thymus in mice may have confounded experiments based on thoracic thymectomies, our results provide a different perspective for the ongoing debate about the physiological relevance of extrathymic T cell development (*29*, *30*).

References and Notes

1. C. Benoist, D. Mathis, in *Fundamental Immunology*, W. Paul, Ed. (Lippincott-Raven, Philadelphia, 1999), p. 367–409.
2. H. von Boehmer, *Adv. Immunol.* **84**, 201 (2004).
3. G. Anderson *et al.*, *Immunol. Rev.* **209**, 10 (2006).
4. L. J. Picker, M. H. Siegelman, in *Fundamental Immunology*, W. Paul, Ed. (Lippincott-Raven, Philadelphia, 1999), p. 486–494.
5. N. R. Manley, *Semin. Immunol.* **12**, 421 (2000).
6. T. Boehm, C. C. Bleul, M. Schorpp, *Immunol. Rev.* **195**, 15 (2003).
7. M. Itoi, H. Kawamoto, Y. Katsura, T. Amagai, *Int. Immunol.* **13**, 1203 (2001).
8. Materials and methods are available as supporting material on *Science* Online.
9. M. Nehls *et al.*, *Science* **272**, 886 (1996).
10. T. Boehm, H.-R. Rodewald, unpublished data.
11. H. Von Boehmer *et al.*, *Immunol. Rev.* **191**, 62 (2003).
12. A. M. Pullen, P. Marrack, J. W. Kappler, *Nature* **335**, 796 (1988).
13. K. M. Murphy, A. B. Heimberger, D. Y. Loh, *Science* **250**, 1720 (1990).
14. D. B. Klug *et al.*, *Proc. Natl. Acad. Sci. U.S.A.* **95**, 11822 (1998).
15. J. Gill, M. Malin, G. A. Hollander, R. Boyd, *Nat. Immunol.* **3**, 635 (2002).
16. E. H. Norris, *Contrib. Embryol.* **166**, 191 (1938).
17. B. von Gaudecker, in *Humanembryologie*, K. V. Hinrichsen, Ed. (Springer-Verlag, Berlin, 1990), vol. 183, p. 340–353.
18. D. A. Loney, N. M. Bauman, *Int. J. Pediatr. Otorhinolaryngol.* **43**, 77 (1998).
19. S. L. Wu, D. Gupta, J. Connelly, *Arch. Pathol. Lab. Med.* **125**, 842 (2001).
20. A. S. Cornu, M. Moerman, K. Bonte, H. Vermeersch, *Acta Otorhinolaryngol. Belg.* **55**, 295 (2001).
21. I. Pai *et al.*, *Int. J. Pediatr. Otorhinolaryngol.* **69**, 573 (2005).
22. L. W. Law, T. B. Dunn, N. Trainin, R. H. Levy, in *Wistar Institute Symposium Monograph No. 2*, V. Defendi, D. Metcalf, Eds. (The Wistar Institute Press, Philadelphia, PA, 1964), pp. 105–120.
23. S. M. Muller *et al.*, *Proc. Natl. Acad. Sci. U.S.A.* **102**, 10587 (2005).
24. L. A. Jerome, V. E. Papaioannou, *Nat. Genet.* **27**, 286 (2001).
25. E. A. Lindsay *et al.*, *Nature* **410**, 97 (2001).
26. V. Papaioannou, H.-R. Rodewald, unpublished data.
27. J. F. A. P. Miller, *Lancet* **2**, 748 (1961).
28. D. F. Tough, J. Sprent, *J. Exp. Med.* **179**, 1127 (1994).
29. B. Rocha, *Science* **308**, 1553a (2005).
30. G. Eberl, D. R. Littman, *Science* **308**, 1553b (2005).

31. We thank A. Farr for sharing results before publication, H. J. Fehling for comments, H. Acha-Orbea and K. D. Fischer for advice, A. Haas-Assenbaum and C. Costa for technical help, M. Itoi and N. Tsukamoto for support, and R. Boyd for generously providing antibody MTS24. Supported by grants DFG MU1607/1-1 (S.M.M.), SFB592, SFB620, and EU FP6503410 (C.B. and T.B.), MEXT-Japan14570288 and MEXT-Japan14780529 (T.A.), funds raised by I. Rodewald (donations by Marlies Möller and R. Walker), and by SFB 497-B5 (H.R.R.).

Supporting Online Material

www.sciencemag.org/cgi/content/full/1123497/DC1
Materials and Methods
SOM Text
Figs. S1 to S7
References

6 December 2005; accepted 20 February 2006
Published online 2 March 2006;
10.1126/science.1123497
Include this information when citing this paper.

TIRF Objective

A new 150×, 1.45 numerical aperture (NA) oil objective offers excellent light transmission for total internal reflectance fluorescence (TIRF) research microscopy over an unprecedented range of the spectrum from the ultraviolet (UV) to the infrared (IR). The high-NA Olympus U Apochromat 150× TIRF objective enables easy TIRF observation using a standard coverglass and standard immersion oil. The objective offers both high UV transmission down to 330 nm and a very high numerical aperture, making it possible to perform TIRF microscopy and UV applications such as uncaging and photo-activation with just one lens. In addition, the objective offers IR transmission well beyond 1000 nm, making it suited for IR fluorescence imaging and IR laser applications, and opening up the potential for live-cell microscopy and future applications in the growing IR microscopy field.

Olympus For information 800-455-8236 www.olympusamerica.com

Real-Time PCR System

The Mastercycler ep realplex is a real-time thermal cycler for the latest in quantitative, real-time polymerase chain reaction (PCR) applications. The realplex combines the advanced thermal cycling technology of the Mastercycler ep gradient thermocyclers with intuitive, multipurpose software and an expertise in optical systems. A modular design allows the user to choose from two 96-well options—a fast aluminum gradient block or the high-speed gradient S. Two optical modules permit the use of nearly all fluorescent dyes used in real-time PCR.

Eppendorf For information 800-645-3050 www.eppendorf.com

Thermostable DNA Ligase

High-fidelity gene synthesis is greatly facilitated by performing ligations with Ampligase Thermostable DNA Ligase. This unique enzyme catalyzes the NAD-dependent ligation of adjacent 3′-hydroxylated and 5′-phosphorylated termini in duplex DNA at much higher temperatures than conventional DNA ligases. Its half-life is 48 hours at 65° C and greater than one hour at 95° C. This thermostability permits the high hybridization stringency and ligation specificity that are critical for successful gene construction.

Epicentre Biotechnologies For information 800-284-8474 www.EpiBio.com

Peptide and Protein Analysis

New chips are available for increased sensitivity and throughput in peptide and protein analysis through matrix-assisted laser desorption ionization-mass spectrometry (MALDI-MS). Functionalized hydrophobic surfaces on Mass-Spec-Focus Chips enable large sample volumes to be loaded, concentrated, and processed in situ, minimizing sample loss and maximizing signals. Mass-Spec-Turbo Chips contain up to 1600 pre-spotted matrix spots, enabling high-throughput analysis of liquid chromatography fractions and two-dimensional polyacrylamide gel electrophoresis gels in biomarker identification. For phosphorylation mapping, Mass-Spec-Focus IMAC Chips offer on-chip purification and concentration of phosphopeptides. Mass-Spec-Focus Desalting Chips provide efficient on-chip clean-up and concentration of peptide samples, such as from tryptic digests. The highly homogenous matrix spots on Mass-Spec-Turbo Chips are easily loaded using automatic sample spotters or microfraction collectors. Direct application of sample onto matrix spots streamlines the MALDI-MS process by reducing handling and minimizes the chance of sample loss.

Qiagen For information 800-426-8157 www.qiagen.com

High Yield In Vitro Transcription

The AmpliScribe T7-Flash Transcription Kit produces a high yield of RNA from an in vitro transcription reaction in a short reaction time. The standard 30-min AmpliScribe T7-Flash reaction produces 160 to 180 μg (8 to 9 mg/ml) of RNA from 1 mg of DNA template, more RNA than some transcription kits produce in 2 hours. High yields of full-length transcripts are readily obtained from both long and short DNA templates.

Epicentre Biotechnologies For information 800-284-8474 www.EpiBio.com

Point-of-Use Ultrapure Water

The Simplicity system produces ultrapure water on demand from pretreated water (distilled, deionized, or reverse osmosis). Designed for scientists who require less than five liters of ultrapure water per day, the system is suitable for the production of mobile phases for chromatography, preparation of samples and standard solutions for spectrophotometry, spectrosocpy, and other analytical techniques; and buffer preparations for biochemical experiments. The Simplicity system's Type I water provides an economical alternative for laboratories currently using bottled water. Because the system's water is produced at the point-of-use, the water quality is not subject to contamination from containers or degradation from airborne contaminants. For sensitive applications such as high-performance liquid chromatography and gas chromatography, the system's built-in, dual-wavelength ultraviolet lamp reduces organic contaminants to less than 5 ppb. A range of final polishers is available to provide bacteria-free, pyrogen-free, or nuclease-free water.

Millipore For information 800-MILLIPORE www.millipore.com

Newly offered instrumentation, apparatus, and laboratory materials of interest to researchers in all disciplines in academic, industrial, and government organizations are featured in this space. Emphasis is given to purpose, chief characteristics, and availability of products and materials. Endorsement by *Science* or AAAS of any products or materials mentioned is not implied. Additional information may be obtained from the manufacturer or supplier by visiting www.science.labvelocity.com on the Web, where you can request that the information be sent to you by e-mail, fax, mail, or telephone.

TaKaRa

GENE EXPRESSION

Single Protein Production System

SPP System™

Takara Bio Introduces:

Takara Bio, in collaboration with Dr. Masayori Inouye, introduces the SPP System™ (Single Protein Production System). This *E. coli*-based system exploits the unique properties of MazF, a bacterial ssRNA and ACA-specific endoribuclease. Expression of this endoribonuclease along with an engineered ACA-less target protein results in high-level target gene synthesis and dramatically reduced background. In addition, *csp*A-based cold-temperature expression increases protein solubility and stability, and easily aggregated proteins can be expressed.

SPP System™ offers:

- **Exceptional Signal to Noise Ratios:** Degradation of cellular mRNAs leads to virtual absence of background protein synthesis.
- **Expression of Difficult Proteins:** Easily aggregated proteins can be successfully expressed.
- **Increased Protein Stability and Solubility:** Cold-temperature expression suppresses protease activity and increases protein solubility.
- **Excellent for Labeling Applications (i.e. NMR):** High-level (up to 90%) target gene expression simplifies structural analysis of proteins.

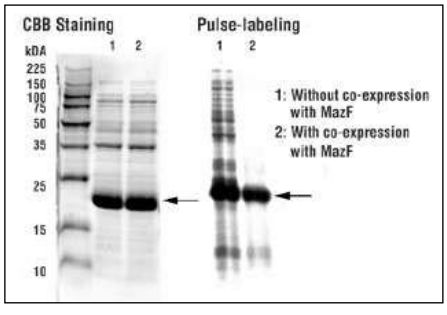

Synthesis of *csp*A-Promoter Expressed envAB with and without MazF. *E. coli* BL21 cells co-expressing MazF and pCold™ I (SP-4) envZB showed good envZB expression and extremely low background synthesis of host proteins, with M9 glucose medium.

Ref: Suzuki, M.; *et. al. Molecular Cell,* 2005, 18, 253-261.

TAKARA BIO INC.
The Biotechnology Company™

Otsu, Shiga, Japan
Phone: +81 77-543-7247
Fax: +81 77-543-9254

USA: Takara Mirus Bio Inc. Phone: 888-251-6618 • www.takaramirusbio.com
Europe: Takara Bio Europe S.A.S. Phone: +33 1 3904 6880 • www.takarabioeurope.com
Korea: Takara Korea Biomedical Inc. Phone: +82 31 739 3300 • www.takara-bio.kr.com
China: Takara Biotechnology (Dalian) Co., Ltd. Phone: +86 411 8764 1681 • www.takara.co.cn

For more information and a list of Takara distributors worldwide, please visit our website today!

www.takara-bio.com

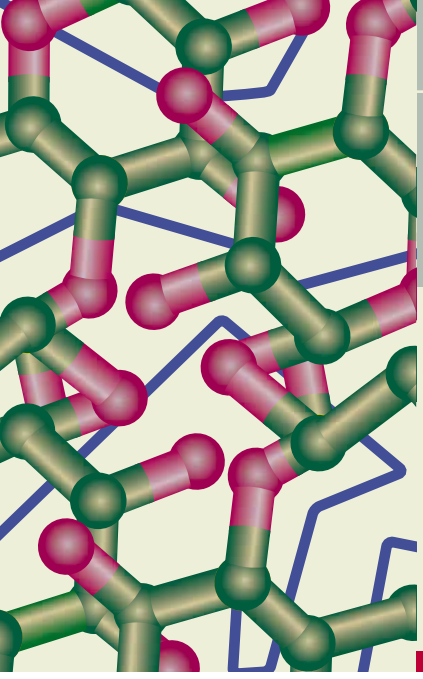

Life Science Technologies

Proteomics:
INTERACTING INSTRUMENTS

To study a proteome, scientists often examine interactions between proteins. Doing that more efficiently and completely, however, depends on using a variety of instruments, making them work as a team. For example, the data from mass spectroscopy need the right informatics tools to mine the results. These interacting tools will reveal more about protein function and how pathways really work. **by Mike May and Gary Heebner**

As scientists delve more deeply into proteomics, they focus more on studying the natural characteristics and interactions of proteins. Ikunoshin Kato, president and chief executive officer at **Takara Bio**, says the most significant challenge for proteomics today is "an efficient protein expression system, which can produce large amounts of correctly folded recombinant protein. This is critical for structural and functional studies." He adds, "The protein's purity is also important, especially for structural analysis." Proteins of interest can be screened against thousands of compounds for biological activity or function to explore their properties.

Protein scientists turn to a number of tools and techniques to analyze protein-protein interactions. Methods like chromatography and 2-D gel electrophoresis help researchers separate and purify mixtures of proteins. Techniques like two-hybrid systems, surface plasmon resonance (SPR), and mass spectrometry (MS) help uncover interactions between proteins, thereby leading to a better understanding of how cells function. Methods like nuclear magnetic resonance (NMR) shed light on the 3-D structure of proteins and can also be used to study protein folding and dynamics. In the end, proteomics could reveal much more about how proteins work, as well as helping biomedical scientists take advantage of proteins as tools.

Express Yourself

A variety of systems—ranging from bacteria to cell-free systems—can express recombinant proteins. Different systems provide various benefits and challenges. For example, *Escherichia coli* provides rapid expression but may not produce a functional protein due to issues surrounding posttranscriptional modification. Proteins from eukaryotic organisms, on the other hand, are more likely to be functional, because they conserve the processes of transcription, translation, and posttranscriptional modifications. In comparison to cell-based systems, cell-free protein expression systems offer several advantages: easy introduction of labels into proteins, the possibility to express toxic or apoptotic proteins, and compatibility with studies that require coexpression of proteins. Protein expression systems are offered by companies like **ATCC**, **Invitrogen**, **Promega**, **Qiagen**, and Takara Bio.

Takara Bio's Single Protein Production (SPP) System, for example, expresses proteins in bacteria. Kato says that this system was developed in collaboration with Masayori Inouye, professor in the Department of Biochemistry at the University of Medicine and Dentistry of New Jersey. Kato calls this "a novel system for generating large amounts of soluble and pure protein for structural analysis studies." He adds, "The SPP System utilizes the *E. coli* toxin protein, MazF, and cold shock technology." The MazF protein—called an mRNA interferase—cleaves single stranded RNA at adenosine-cytosine-adenosine (ACA) sequences. In this system, the transcript of interest, which should not contain any ACA sequences, and MazF are co-expressed in *E. coli*. The MazF cleaves most everything but the transcript of interest. "The result is a high level—up to 90 percent of the newly synthesized protein—of target protein expression with relatively low cellular protein background," says Kato.

In an *E. coli* system, however, some proteins do not fold properly. To enhance the proportion of correctly folded proteins, scientists at Takara Bio again collaborated with Inouye on the pCold DNA Vectors. Kato calls these "a series of unique protein expression vectors for generating large amounts of soluble and pure protein in *E. coli.* The pCold Vectors provide increased in vivo protein yield, purity, and solubility of expressed recombinant proteins at lowered incubation temperature." He adds, "They can be used in conjunction with Takara's Chaperone Plasmid Set to further increase the amount of correctly folded protein."

For expression in mammalian cells, **New England Biolabs** offers its RheoSwitch Mammalian Inducible Expression System. "The key to this system is that it is precisely inducible," says Chris Taron, head of gene expression research at New England Biolabs. "This system relies on a specific interaction between an engi-

continued ›

IN THIS ISSUE:

- Protein expression
- Affinity chromatography
- Protein arrays
- Mass spectrometry
- Surface plasmon resonance
- Nuclear magnetic resonance
- Bioinformatics

Inclusion of companies in this article does not indicate endorsement by either AAAS or *Science*, nor is it meant to imply that their products or services are superior to those of other companies.

neered nuclear receptor and a synthetic inducer called RSL1, which triggers a chain of events that lead to protein expression." Taron adds that using a nonnative receptor and synthetic inducer leads to little cross-talk with native cellular receptors. "The induction is proportional to the amount of RSL1 that you add," says Taron. "You can fine tune the level of expression like a rheostat, or like turning up or down the volume knob on a radio."

Taron notes, however, that all questions about protein expression cannot be answered in the same system. So New England Biolabs offers other systems, such as the *K. lactis* Expression Kit, which is a yeast-based expression system. Taron says, "*K. lactis* was developed in the food industry in the 1980s as a means of producing proteins at industrial scale." The same system can now produce high levels of proteins for research.

To keep track of which proteins are being expressed, scientists often use luciferase as a reporter. Another recent product from New England Biolabs—the *Gaussia* Luciferase Assay Kit—provides a new reporter. Taron says, "*Gaussia* luciferase behaves fantastically in secretory systems and is more sensitive than other available luciferases."

Purifying Proteins

As Kato mentioned, the purity of a protein impacts results. Various methods are used to enrich or purify a protein of interest. One of the most powerful of these methods is affinity chromatography, also called affinity purification, where the protein of interest is purified based on its specific binding properties to an immobilized ligand. This process can be performed with products from several companies, including **EMD Biosciences**, **GE Healthcare**, **Pierce**, and Qiagen.

Brian Johnson, market segment manager at Pierce says, "Affinity purification can provide 10,000-fold purification in a single step. It takes advantage of a highly specific interaction between a protein and a binding partner, such as an antibody." This process can be used in many ways, including purifying a specific protein or class of proteins, such as glycoproteins or cell surface proteins.

Pierce also makes the Pinpoint Cell Surface Protein Isolation Kit. Johnson says, "This kit labels cell surface proteins with biotin that has a cleavable spacer arm. It allows you to pull out proteins labeled with biotin and specifically elute the labeled cell surface proteins."

Jutta Drees, protein product manager at Qiagen, says, "The addition of a His tag is the most commonly used method for affinity purification of recombinant proteins. Since their launch, Qiagen's Ni-NTA matrices have set the standard for highly selective purification of His-tagged proteins." She adds, "Our most recent addition to the Ni-NTA range is the easy-to-use Ni-NTA Fast Start Kit, which purifies up to 10 milligrams of protein in as little as 90 minutes." For purification of nonrecombinant proteins, Qiagen has developed Qproteome affinity-based kits for isolating phosphoproteins, glycoproteins, and plasma membrane proteins.

Getting the best result from proteomic studies, though, depends on sample handling, according to Eric Fung, vice president of medical and clinical affairs at **Ciphergen Biosystems**. Fung says, "We seek a balance between running enough samples to keep the statisticians happy and doing extensive fractionation since the more you fractionate, the more information you can get. But doing this on lots of samples in high throughput is very challenging." To pull out the desired proteins, Fung says that scientists can use Ciphergen's ProteinChip Arrays. These provide a variety of surface chemistries that allow researchers to optimize protein capture and analysis. The surface chemistries of the arrays include a series of classic chromatographic chemistries and specialized affinity capture surfaces. Fung says, "The different chromatographic surfaces generate an additional degree of fractionation."

These arrays are often used for comparative protein profiling. For example, Fung says that a scientist can take samples from patients with a disease and compare the proteins to patients without the disease. "These arrays can also be used for protein identification or to look at protein-protein interactions or different types of protein modification," says Fung.

Cataloging the Characteristics

Once a protein is captured, scientists characterize it. "Characterization is a broad term," says Dave Hicks, senior director of proteomics at **Applied Biosystems**. "In general, it means having a full understanding of a protein, including its full amino acid sequence, the splice edits, and the identification of all posttranslational modifications."

Protein scientists can characterize proteins with a wide range of approaches, like two-hybrid systems, MS, NMR, and SPR. Each of these offers a somewhat different view into protein-protein interactions. The two-hybrid method, for instance, can identify protein-protein interactions, protein cascades, and mutations that affect protein-protein binding. Two-hybrid systems are available from companies like **Clontech** (a Takara Bio Company), Invitrogen, and **Stratagene**.

Various forms of MS also characterize proteins. For example, 2-D gel profiles can be further analyzed using MS and matrix-assisted laser desorption ionization-time of flight (MALDI-TOF) techniques. Several companies manufacture these instruments including Applied Biosystems, **Bruker Daltonics**, and **Thermo Electron**.

Hicks says that one of Applied Biosystem's most popular MS systems for proteomics is the 4800 MALDI TOF/TOF Analyzer. "This is often used in protein expression analysis, with and without tagging chemistries," he says. Hicks adds that the QSTAR Elite Hybrid LC/MS/MS System is often used for protein identification and characterization studies. For studies of phosphorylation and other posttranslational modifications, Hicks says that scientists might use the 4000 Q TRAP LC/MS/MS System. He says, "This system can be used in protein quantitation studies, looking at expres-

continued ›

Protein interaction analysis

from discovery to quality control

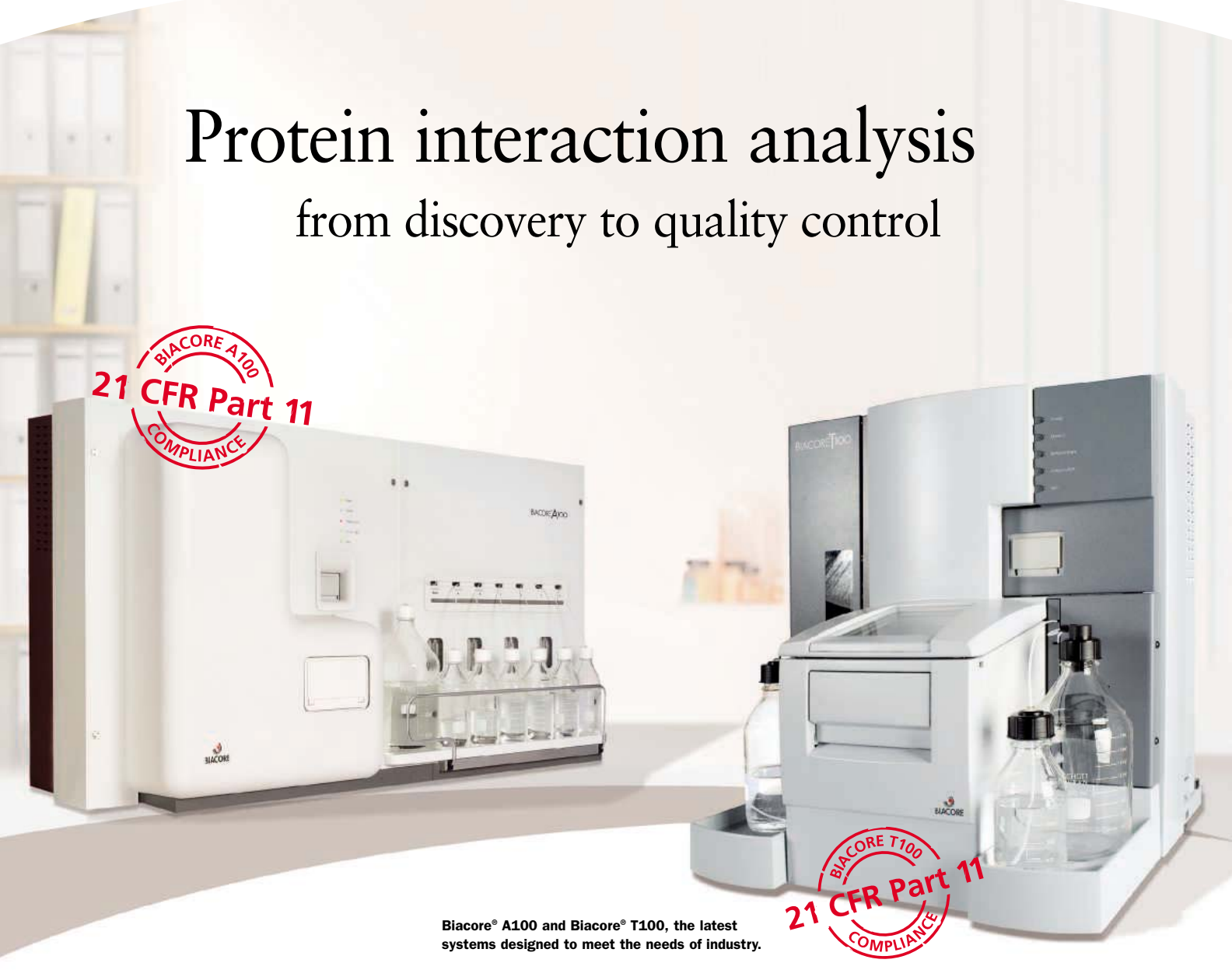

Biacore® A100 and Biacore® T100, the latest systems designed to meet the needs of industry.

The name Biacore is synonymous with the high quality, information-rich protein interaction analysis needed throughout drug discovery and development, biotherapeutic development, manufacturing and QC.

Biacore systems are used in the world's leading pharmaceutical and biotechnology companies.

Unique insights into protein interactions ensure confident decision-making at every stage, resulting in greater productivity, reduced development costs, improved safety and efficacy, as well as shortened timelines.

For screening, selection, characterization and quality control in:

- **Development of biotherapeutics**
- **LMW drug discovery and development**
- **Preclinical and clinical immunogenicity studies**
- **In-process control and release testing**

Define · Decide

BIACORE

www.biacore.com

YYePG Proudly Presents, Thx for Support

Life Science Technologies: PROTEOMICS

sion and quantity across multiple samples, or even studying multiple proteins in multiple samples, all at high throughput."

To increase sensitivity and facilitate analysis of low-abundance proteins in MALDI analysis, Anke Cassing, associate protein business director at Qiagen, says, "We looked at how to put the maximum amount of sample on the MALDI target. By providing on-target processing—for example, purification of phosphopeptides, sample desalting, and concentration—Mass·Spec·Focus Chips eliminate sample losses due to 'offline' processing. Users can pipette large sample volumes directly onto the chip, enabling analysis of dilute samples without the need for a concentration step using a pipette tip device." Mass·Spec·Focus Chips are available for Applied Biosystems, Bruker Daltonics, **Waters**, **Shimadzu**, and Thermo Electron instruments. For high-throughput MALDI analyses using ABI 4700, QSTAR, and Voyager instruments, Qiagen has developed Mass·Spec·Turbo Chips, which are high-density, ready-to-use MALDI targets that carry up to 1,600 matrix spots.

Binding the Biologics

Today's proteomics goes beyond the structure and identity of proteins. Stefan Löfås, vice president and chief scientific officer at **Biacore**, says, "We see an increasing interest to learn more about protein function, especially through binding and interactions. This is really determining how proteins talk with each other."

Some scientists follow protein interactions using SPR detection, which can monitor proteins as they interact with various targets: proteins, carbohydrates, lipid bilayer vesicles, nucleic acids, and even whole cells. Moreover, the information appears in real time, thereby giving the affinity and kinetics of the binding event. The events are detected as molecules in solution interact with a partner attached to a gold surface. This interaction causes a change in refractive index that causes a change in the SPR signal.

In the past year, Biacore introduced several new systems based on SPR detection. For example, the Biacore T100 is what Löfås calls "our new flagship system." He says, "It compiles all of the knowledge and experience we have gained into the most modern and versatile system for research through quality control, including various proteomics applications." He adds, "For in-depth analyses, this instrument can even smoothly extract the thermodynamic parameters driving an interaction."

For higher productivity, scientists can use the Biacore A100. Löfås says, "In comparison to Biacore T100, this generates the same type of data with the same level of quality and sensitivity, but, with parallel processing and multiplex analysis capability. Biacore A100 can monitor up to thousands of protein interactions per day." For those working with large numbers of samples who want to rapidly select interactions of interest for in-depth study, Löfås recommends the Flexchip, which offers an array format that "can profile up to 400 interactions at the same time."

Other companies also use SPR on arrays. Timothy G. Burland, president and chief executive officer at **GWC Technologies**, says, "Our SPRimagerRII instrument is an SPR system with an array format so you can take a picture of the array." Burland notes several examples of using this SPR instrument. For instance, his company has collaborated with **Neoclone** to show "that you obtain the same affinity values for antibody-antigen interactions whether you make antibody arrays using purified antibody or the corresponding ascites fluid. In other words, you don't need to purify the ascites fluid to use antibodies as probes on our arrays." He also notes that scientists in the laboratory of Lloyd Smith at the University of Wisconsin used the SPRimagerRII to show the presence of specific cell receptors on baby hamster kidney cells. Likewise, Robert M. Corn, at the University of California, Irvine, used SPR imaging arrays to characterize transcription factors and antibodies.

To help scientists create other proteomic applications, GWC Technologies produced its SpotReadyT16 and SpotReadyT25, which have 16 and 25 gold spots, respectively, for attaching probes. Burland says, "Some people only need about a dozen probes per array to study protein function. With SpotReady arrays, you use a pipette to spot half a microliter or less per probe." He adds, "This is quick and does not require a robot for spotting."

Structural Specifics

"NMR has been used for some time to study protein structure," says Steve Smallcombe, manager of applications laboratories at **Varian**. NMR places a molecule in a strong magnetic field, irradiates the molecules with radio frequency waves, and then detects changes in the spin of atoms. "NMR is very nice," says Smallcombe, "because you see signals from all of the atoms in a protein." Also, NMR can reveal time dependent phenomena. Judit Losonczi, product marketing manager at Varian, says, "NMR can provide an understanding of protein dynamics, folding, and kinetics." NMR systems are offered by companies like **Bruker BioSpin**, **Jeol**, and Varian.

"A downside to NMR has been that it is less sensitive than MS," says Smallcombe, "but we increased NMR's sensitivity with a cryogenic probe—essentially an antenna in the instrument's magnet—that is cooled down to 25 Kelvin. This technology provides improved sensitivity." He adds that Varian's Salt Tolerant Cold Probe can be used in physiological conditions.

Smallcombe adds that most NMR in the past used proteins in solution. However, proteins in membranes cannot be studied continued ›

FUJIFILM
I&I – Imaging & Information

Life Science

HIGHLY VERSATILE BIO-IMAGING SYSTEM

FLA-7000

473nm 532nm 635nm 650nm 670nm

A multi-functional, high-performance, compact system with enhanced modularity to meet your life science needs

RADIOISOTOPE

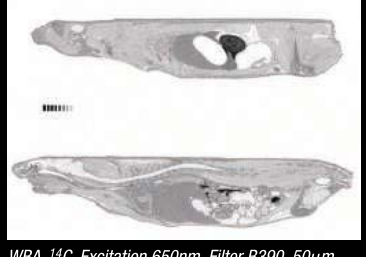

WBA, ^{14}C, Excitation 650nm, Filter B390, 50µm
Data courtesy of Institute of Whole Body Metabolism

A radioisotope-labeled sample image can be acquired with high throughput and high sensitivity using Fujifilm's unique proprietary technology: integrated Imaging Plate technology and high-speed detection technology (Light Collecting Guide).

FLUORESCENCE

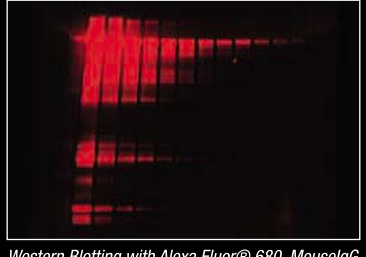

Western Blotting with Alexa Fluor® 680, MouseIgG, Excitation 670nm, Filter R710, 50µm

A maximum of four lasers are optionally available for use with the following: LD473nm, SHG532nm, LD635nm, LD650nm and LD670nm.
This enables the system to be upgraded to cover a broader range of fluorescent dyes including near-IR.

DIGITIZING

Silver-stained BSA, SDS-PAGE, Excitation 473nm, Filter Y520, 50µm

Able to take digitized (Gel Documentation) images of silver-stained gel or CBB-stained gel.

http://lifescience.fujifilm.com

Fuji Photo Film Co., Ltd. 26-30, Nishiazabu 2-Chome, Minato-ku, TOKYO 106-8620, JAPAN, Tel: +81-3-3406-2201, Fax: +81-3-3406-2158 • E-mail: sginfo@fujifilm.co.jp
Fujifilm Medical Systems U.S.A., Inc. 419 West Avenue, Stamford, CT 06902, U.S.A, Tel: +1-203-324-2000 ext.6112 (1-800-431-1850 ext.6112 in the U.S.), Fax: +1-203-351-4713 • E-mail: SSG@fujimed.com
Fuji Photo Film (Europe) GmbH Heesenstr. 31, 40549 Dusseldorf, Germany, Tel: +49-211-5089-174, Fax: +49-211-5089-139 • E-mail: lifescience@fujifilmeurope.de
Fuji Photo Film (U.K.) Ltd., Unit 12 St Martins way, St Martins Business Centre, Bedford, MK42 OLF, UK, Tel: +44-1234-245901, Fax: +44-1234-245903 • E-mail:lifesciences@fuji.co.uk
Fuji Photo Film (China) Investment Co., Ltd. 31st floor, Hong Kong New World Tower, No. 300 Huai Hai Zhong Road, Shanghai, P.R China, Tel: +86-21-3302-4655 ext.363, Fax: +86-21-6384-3322 • E-mail: wgxiang@fujifilm.com.cn

this way," says Smallcombe. Nonetheless, Varian's new Bio-MAS probe allows for studies of membrane bound proteins in a solid state.

Building Better Bioinformatics

"The current situation in proteomics reminds me of the struggle with microarrays for gene expression about seven or eight years ago," says Lee Weng, director of applied research at **Rosetta Biosoftware**. "At that time, the focus was on perfecting the instrument, getting the resulting numbers right." Now, with more confidence in the results from proteomic instruments, Weng says that scientists can focus on extracting information. "We need to get the useful information," Weng says, "so that we can do something with it." Some companies—including Applied Biosystems, **Beckman Coulter**, **Bio-Rad Laboratories**, **Caliper Life Sciencess** and **Syngene**—develop core instruments for proteomic research along with integrated software systems. Other companies—including **Accelrys**, **Elsevier MDL**, and Rosetta Biosoftware—offer software suites for proteomics research.

Weng says that, last year, Rosetta Biosoftware introduced its Elucidator Protein Expression Data Analysis system. This system can capture large volumes of data from various MS instruments and then manages and analyzes the results. "The Elucidator does data preparation and manages data in very large-scale, label-free quantification studies," says Weng. "Sometimes, hundreds of samples are analyzed all together, and each can have several gigabytes of information."

This system can be used in a wide range of proteomics research. For instance, Weng says, "Output from this system can be a list of biomarker candidates that scientists can go after and map to pathways to understand disease. We can also see what protein has been affected by a drug or compare protein expression in normal versus diseased samples."

Defining the Details

"It's easy to find the stable interactions," says Johnson of Pierce, "but harder to get the weak and transient ones." Still, understanding the finer points of proteomics might resolve many questions in both basic and applied biological research. "The problem is nailing down the details," says Johnson. As proteomics scientists hammer out the specifics, the applications of this field will continue to grow.

Mike May (mikemay@mindspring.com) is a publishing consultant for science and technology based in Minnesota. Gary Heebner (gheebner@cell-associates.com) is a marketing consultant with Cell Associates in St. Louis, Missouri, U.S.A.

Hatching a big idea?

Present your research or a groundbreaking topic by proposing a symposium for the 2007 AAAS Annual Meeting in San Francisco.

The 2007 AAAS Annual Meeting, 15–19 February 2007 in San Francisco, CA, attracts a diverse audience from all scientific disciplines and from the industrial, academic, non-profit, and policy communities. The meeting is also attended by more than 1,000 press registrants, including most of the world's major news outlets.

To accommodate the tremendous variety of subjects proposed for the Annual Meeting, and due to time and space constraints, 90-minute symposia are strongly encouraged.

The Program Committee is particularly interested in sessions that highlight the interdisciplinary strengths of AAAS, or that address one of the identified themes for the 2007 Annual Meeting. Successful proposals are characterized by interesting topics that are thoughtfully developed and include capable and articulate presenters who are representative of the diversity of science and society.

All proposals will be peer-reviewed. The deadline for proposal submission is Monday, 1 May 2006. Decisions will be announced in July. Remember, the early bird gets the worm—submit a proposal today!

For more information on submitting a proposal, visit:

www.aaasmeeting.org

AAAS
ADVANCING SCIENCE, SERVING SOCIETY

YYePG Proudly Presents, Thx for Support

ScienceCareers.org

Classified Advertising

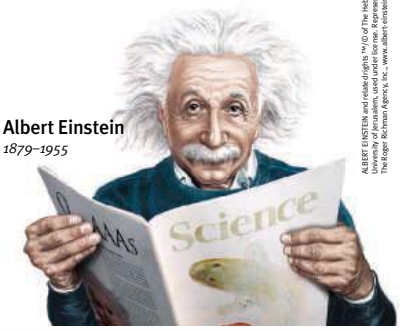

Albert Einstein
1879–1955

For full advertising details, go to **www.sciencecareers.org** and click on **How to Advertise,** or call one of our representatives.

United States & Canada

E-mail: advertise@sciencecareers.org
Fax: 202-289-6742

JILL DOWNING
(CT, DE, DC, FL, GA, MD, ME, MA, NH, NJ, NY, NC, PA, RI, SC, VT, VA)
Phone: 631-580-2445

KRISTINE VON ZEDLITZ
(AK, AZ, CA, CO, HI, ID, IA, KS, MT, NE, NV, NM, ND, OR, SD, TX, UT, WA, WY)
Phone: 415-956-2531

KATHLEEN CLARK
Employment: AR, IL, LA, MN, MO, OK, WI, Canada; Graduate Programs; Meetings & Announcements (U.S., Canada, Caribbean, Central and South America)
Phone: 510-271-8349

EMNET TESFAYE
(Display Ads: AL, IN, KY, MI, MS, OH, TN, WV; Line Ads)
Phone: 202-326-6740

GABRIELLE BOGUSLAWSKI
(U.S. Recruitment Advertising Sales Director)
Phone: 718-491-1607

Europe & International

E-mail: ads@science-int.co.uk
Fax: +44 (0) 1223-326-532

TRACY HOLMES
Phone: +44 (0) 1223-326-525

HELEN MORONEY
Phone: +44 (0) 1223-326-528

CHRISTINA HARRISON
Phone: +44 (0) 1223-326-510

SVITLANA BARNES
Phone: +44 (0) 1223-326-527

JASON HANNAFORD
Phone: +81 (0) 52-789-1860

To subscribe to *Science*:
In U.S./Canada call 202-326-6417 or 1-800-731-4939
In the rest of the world call +44 (0) 1223-326-515

Science makes every effort to screen its ads for offensive and/or discriminatory language in accordance with U.S. and non-U.S. law. Since we are an international journal, you may see ads from non-U.S. countries that request applications from specific demographic groups. Since U.S. law does not apply to other countries we try to accommodate recruiting practices of other countries. However, we encourage our readers to alert us to any ads that they feel are discriminatory or offensive.

POSITIONS OPEN

ASSISTANT PROFESSOR / NEUROBIOLOGY

The Department of Biology at the University of Victoria invites applications for a tenure-track Assistant Professor position in neurobiology to begin January 1, 2007. We are particularly interested in applicants who follow a strong multidisciplinary research theme.

The candidate must have a Ph.D., appropriate postdoctoral training and a proven research record in the field of neurobiology. The successful applicant will be expected to develop an independent, innovative, and externally funded research program and participate in teaching at both the undergraduate and graduate levels. The Department of Biology encompasses a broad range of teaching and research interests. We are searching for an individual that complements the broad range of the Department's interests. Potential applicants should visit the Departmental **website: http://web.uvic.ca/biology/.**

Applications should be sent to: **Dr. William Hintz, Chair, Department of Biology, University of Victoria, P.O. Box 3020, STN CSC, Victoria, B.C. V8W 3N5, Canada; fax: 250-721-7120; e-mail: biochair@uvic.ca.** The closing date for the position is August 31, 2006. Curriculum vitae and research and teaching statements should be included as well as contact information (names, addresses, fax, e-mail) for four referees.

All qualified applicants are encouraged to apply: however, in accordance with Canadian Immigration requirements, Canadians and permanent residents will be given priority.

The University of Victoria is an equity employer and encourages applications from women, persons with disabilities, visible minorities, Aboriginal Peoples, people of all sexual orientations and genders, and others who may contribute to the further diversification of the University.

ASSISTANT/ASSOCIATE/FULL PROFESSORS
Primate Cognitive Neuroscience
Carolina Primate Center
Medical University of South Carolina, Charleston

The Department of Neurosciences at the Medical University of South Carolina (MUSC) seeks applications for several Tenure-Track Faculty positions in primate cognitive neuroscience. Candidates will partake in the development of a new Carolina Primate Center located in Yemassee (60 to 90 minutes from Charleston). Applicants must have a strong academic record of independent research with a Ph.D. or M.D. degree and expertise in neurophysiology or other cognitive neuroscience approach in behaving monkeys. Newly constructed laboratory space and attractive startup packages and benefits are available. Rank commensurate with experience.

Applicants must apply online at **website: http://www.musc.edu/hrm/careers/faculty.htm.** Position requisition number is 041704. Applicants should also submit online a cover letter expressing their interest and qualifications, curriculum vitae, and names of three references addressed to: **Gary Aston Jones, Ph.D., Director, Carolina Primate Center, Department of Neurosciences, Medical University of South Carolina, 173 Ashley Avenue, BSB 403, Charleston SC 29425.** *MUSC is an Equal Employment Opportunity/Affirmative Action Employer.*

A **POSTDOCTORAL POSITION** is available in the laboratory of **Dr. Aziz Sancar** in the Department of Biochemistry and Biophysics at the University of North Carolina at Chapel Hill to study the interface between human nucleotide excision repair and the DNA damage checkpoints. Applicants with a strong working background in biochemistry and molecular biology are encouraged to apply. Please contact Dr. Sancar directly to apply, or for more information:

Dr. Aziz Sancar
University of North Carolina at Chapel Hill
Department of Biochemistry and Biophysics
CB 7260
Chapel Hill, NC 27499-7260
E-mail: aziz_sancar@med.unc.edu

POSITIONS OPEN

ASSISTANT PROFESSOR
Terrestrial Ecology

The Department of Biological Sciences, University of Rhode Island (URI), invites applications for a tenure-track position in terrestrial ecology, with a specialization in plant-animal interactions, available August 2006. Ph.D. in biological sciences or related field by August 2006 required. Postdoctoral research and teaching experience preferred. Teaching duties will include undergraduate and graduate courses in ecology and area of specialization. Candidates must demonstrate through education, publications, letters of recommendation and/or experience, strong potential for excellence in teaching, mentoring undergraduate and graduate students, and developing a high quality, nationally recognized and externally-funded research program in terrestrial ecology, with an emphasis on plant-animal interactions. Visit our **website: http://www.uri.edu/human_resources** for additional information. Qualified applicants should send (no e-mails or faxes, please) a letter of application, current curriculum vitae, three letters of reference, statement of teaching experience and philosophy, a summary of research interests and future plans, and copies of up to three published papers postmarked by May 5, 2006, to: **Dr. Frank H. Heppner, Search Chair (Req SM011375), University of Rhode Island, P.O. Box G, Kingston, RI 02881.** *URI is an Affirmative Action/Equal Employment Opportunity employer and values diversity and also is an NSF ADVANCE institutional transformation university, working to advance the careers of women faculty, especially in the science and engineering disciplines.*

BIOLOGY. The Biology Department at Whitman College invites applications for a one-year position as **ASSISTANT PROFESSOR** of biology beginning August 2006. Possibility of renewal. Ph.D. required. Duties include one section of the Department's required introductory biological principles course (with laboratory), supervision of undergraduate research/thesis preparation, and two courses suitable for students in the college's Biology and Biochemistry, Biophysics and Molecular Biology (BBMB) major programs. We seek applicants familiar with the molecular, cell biological, and/or physiological material covered in the biological principles course, and who have research interests complementary to others in the Department. (Information on this course, the Biology and BBMB programs, and current faculty is available at **website: http://www.whitman.edu/biology.**) Applicants should send as hardcopy or e-mail attachments: application letter, curriculum vitae, statements of research and teaching interests, college and graduate transcripts (unofficial okay), and three letters of recommendation, to: **Dr. Daniel M. Vernon, Biology One-Year Search, Biology Department, Whitman College, Hall of Science, 345 Boyer Avenue, Walla Walla, WA, 99362. E-mail: vernondm@whitman.edu.** Deadline: April 18, 2006. Whitman College is a top-tier undergraduate institution located in historic Walla Walla, near the Blue Mountains in eastern Washington state. *No applicant will be discriminated against on the basis of race, national or ethnic origin, age, gender, sexual orientation, marital status, religion, or disability.*

POSTDOCTORAL RESEARCH ASSOCIATE
in molecular endocrinology and metabolism for studies regarding the role of FoxO transcription factors in the regulation of gene expression and metabolism. Studies focus on identification of novel targets and mechanisms mediating effects of FoxO proteins on cell signaling and metabolic pathways in liver and muscle using cell culture and transgenic/knockout models. Ph.D. and appropriate experience in molecular biological, cell signaling, metabolic analysis desired. For full consideration, send curriculum vitae and three letters of recommendation by May 15, 2006, to: **Dr. Terry Unterman, Endocrine Section (M/C 640), Department of Medicine, University of Illinois at Chicago College of Medicine, 1819 West Polk Street, Chicago, IL 60612-7333; e-mail: unterman@uic.edu.** *Equal Opportunity Employer.*

Positions @ NIH

The National Institutes of Health

National Institutes of Health
Office of the Director

Chief NIH Ethics Officer

The Office of the Director, National Institutes of Health (NIH) in Bethesda, Maryland, is seeking a Chief NIH Ethics Officer (CNEO), who will also serve as Director for the NIH Ethics Office. If you are an exceptional candidate with a M.D. and/or Ph.D. and have the vision and skills to oversee and provide strategic direction to NIH activities relating to ethics policy, oversight, and operations for scientific administration, we encourage your application.

To achieve its mission of advancing biomedical and behavioral research to improve the health of the public, the NIH must have the trust of the public that the decisions and activities of the agency and its employees are unbiased. The creation of the new position of CNEO is part of a comprehensive effort to strengthen the program of ethics oversight for NIH employees. As CNEO, you will be responsible for the executive leadership, strategic direction, and oversight of the scientific, clinical, and administrative activities of NIH staff as they relate to ethics policies. This includes: assuring compliance with Federal, departmental, and agency ethics laws, regulations, and policies that apply to the official-duty activities, outside activities, and financial holdings of NIH's 18,000+ employees; overseeing a rigorous program of quality control and risk management including assessing the effectiveness activities of conflict of interest operations the NIH Ethics Office and the application of delegated authority; conducting a comprehensive ethics training program; and developing/maintaining an effective enterprise information technology system. Additional functions include serving as the NIH spokesperson and principal advisor to the Director and Deputy Director, NIH on relevant NIH ethics policy and programs. In addition, you will serve as the NIH Agency Research Integrity Liaison Officer (ARILO) and will be responsible for all matters related to NIH's intramural and extramural research integrity programs to include oversight and coordination of NIH activities related to research misconduct and the promotion of research integrity of NIH intramural and extramural research programs. Understanding the value of scientific expertise for leadership of ethics at NIH, you will have the flexibility to devote up to 25% of your time to conduct or oversee research in an NIH intramural research laboratory or in an appropriate NIH extramural scientific programmatic role.

Salary is commensurate with experience; a full package of benefits is available, including retirement, health, life, long term care insurance, Thrift Savings Plan participation, etc.

Applications for this position will be reviewed by a Search Committee chaired by Dr. Duane Alexander, Director, National Institute of Child Health and Human Development. Applicants may send a Curriculum Vitae to **Teresa Leary, 31 Center Drive - MSC 2207, Room 4B-41, Bethesda, MD 20892-2207 or visit http://www.jobs.nih.gov and apply to Announcement OD-06-109779 (for Ph.Ds) or OD-06-109626 (for M.Ds)**. If you need additional information, please contact **Ms. Teresa Leary at learyte@od.nih.gov or (301) 496-1443**. Applications must be received by close of business **May 19, 2006**.

Staff Clinician - Endocrinology

The National Center for Complementary and Alternative Medicine (NCCAM) seeks outstanding candidates for a Staff Clinician position in Endocrinology in its Laboratory of Clinical Investigation (LCI) on the National Institutes of Health campus in Bethesda, Maryland. Applicants must possess an M.D. or D.O. degree, be licensed to practice medicine within the United States, have substantial clinical and research training in endocrinology, and be American Board of Internal Medicine (ABIM) eligible or certified in endocrinology and metabolism.

The successful candidate will be expected to contribute to existing clinical protocols in the Endocrine Section, LCI, and to conceptualize, write, and conduct new patient-oriented research studies designed to assess the potential efficacy, safety, and mechanisms of action of selected, complementary and alternative (CAM) modalities. A specific research interest and experience in the areas of neuroendocrinology, aging and/or stress biology, and a strong publication record in phase I, II and/or III clinical trials, are required.

The LCI, NCCAM provides state-of-the-art research facilities in the intramural program at NIH in addition to a collegial and nurturing working environment. The extensive clinical research facilities of the NIH Clinical Center will be made available to the successful applicant. Salary and benefits will be commensurate with experience. Applications from women and minorities are encouraged.

Please email your CV, bibliography, the names of three references, and a one page cover letter stating your scientific interests and experience to:

nccam jobs@mail.nih.gov
Subject Line: Staff Clinician-Endo Search

Candidates needing reasonable accommodation may fax application materials to **301-402-4741.**

THIS ANNOUNCEMENT WILL REMAIN OPEN UNTIL FILLED

MRI Scientist Position
National Institute of Neurological Disorders and Stroke

With nation-wide responsibility for improving the health and well being of all Americans, the Department of Health and Human Services oversees the biomedical research programs of the National Institutes of Health.

The NIH MRI Research Facility (NMRF) in the National Institute of Neurological Disorders and Stroke is seeking an MRI scientist to support the human brain imaging studies conducted by the NIH investigators. NMRF offers state-of–the-art MRI facilities for users throughout the NIH. The NMRF is a part of the NIH In Vivo NMR Center which houses active research programs in brain and cardiac MRI. Four 3T MRI (GE) scanners and a 7T MRI (GE) scanner are available in the NMR Center for human brain research. The successful candidate will have a Ph.D. in a relevant field and interest in application of MRI to study brain function and disorders. Experience in MRI pulse sequence design and programming is required. Knowledge and interest in image processing or MRI hardware is desirable. In addition to collaborative research, the candidate will have the opportunity to initiate new projects that will impact ongoing research. Salary is very competitive and commensurate with education and experience.

Please send a CV and three letters of reference to **Dr. Lalith Talagala, NIH MRI Research Facility, National Institutes of Health, 10 Center Drive, Room B1D69, Bethesda, MD 20892-1060, Email: talagala@nih.gov.**

WWW.NIH.GOV

Department of Health and Human Services
National Institutes of Health
Office of the Director

Deputy Director of NIH for Portfolio Analysis and Strategic Initiatives
and
Director, Office of Portfolio Analysis and Strategic Initiatives

The Office of the Director, National Institutes of Health (NIH) in Bethesda, Maryland, is seeking a Director for the new Office of Portfolio Analysis and Strategic Initiatives (OPASI). If you are an exceptional candidate with an M.D. and/or Ph.D. and the vision and ability to integrate science across multiple disciplines, we encourage your application.

As the OPASI Director, you will serve as a Deputy Director of the NIH and directly report to the NIH Director. As a prominent senior leader reporting directly to the Director of NIH, you will be responsible for executive leadership and coordination of the overall NIH research portfolio analysis and strategic initiatives that fall within the OPASI's scope. The OPASI's primary objective is to develop: a transparent process of planning and priority-setting characterized by a defined scope of review with broad input from the scientific community and the public; valid and reliable information resources and tools, including uniform disease coding and accurate, current and comprehensive information on burden of disease; an institutionalized process of regularly scheduled evaluations based on current best practices; the ability to weigh scientific opportunity against public health urgency; a method of assessing outcomes to enhance accountability; and a system for identifying areas of scientific and health improvement opportunities and supporting regular trans-NIH scientific planning and initiatives. You will serve as the principal advisor to the NIH Director on issues involving OPASI's planning, analysis, and policy formulation and implementation activities, including efforts to strengthen trans-NIH strategic planning and funding, and improve data quality and develop analytical techniques for assessing the NIH research portfolio.

This position requires that the OPASI Director exercise leadership, initiative, and creativity in establishing and maintaining relationships with key Federal and non-Federal officials, nationally and internationally recognized scientific leaders and officials of academic, research, and other institutes and organizations, and professional and advocacy groups.

Salary is commensurate with experience; a full package of benefits (including retirement, health, life, long term care insurance, Thrift Savings Plan participation, etc.) is available.

Applications for this position will be reviewed by a Search Committee chaired by Dr. Jeremy Berg, National Institute of General Medical Sciences and Dr. Elizabeth Nabel, Director, National Heart, Lung and Blood Institute.

Interested applicants should send a Curriculum Vitae to **Ms. Teresa Leary, 31 Center Drive – MSC 2207, Room 4B-41, Bethesda, MD 20892-2207 OR visit: http://www.jobs.nih.gov and apply to Announcement OD-06-109905 (for Ph.Ds) or OD-06-109915 (for M.Ds).** If you need additional information, please contact **Ms. Teresa Leary at learyte@od.nih.gov or by calling 301-496-1443.**

Applications must be received by close of business May 19, 2006

STONY BROOK POSTDOCTORAL POSITIONS

The Research Foundation of Stony Brook University/SUNY anticipates the following postdoctoral positions being available between May 2006 and Fall 2006.

- **ANATOMICAL SCIENCES**
  Paleontology, Archaeology, or Geology of Africa. John Fleagle, #HS-R-3131-06-03-S
- **APPLIED MATH AND STATISTICS**
  Computational Biology: Multiscale studies of protein-protein interactions. David Green, #WC-R-3092-06-03-S
  Development of quantitative studies of gene expression in the Drosophila *blastoderm.* John Reinitz, #WC-R-3091-06-03-S
- **BIOCHEMISTRY AND CELL BIOLOGY**
  Endocannabinoid metabolism. Dale Deutsch, #WC-R-3093-06-03-S
  Role of MESD in folding LRP receptors and mouse development. Bernadette Holdener, #WC-R-3094-06-03-S
  Biosynthesis and catabolism of glycoproteins. William J. Lennarz, #WC-R-3095-06-03-S
- **CHEMISTRY**
  Polymer synthesis, colloids, fibers, modified fullerenes, and membranes. Ben Chu, #WC-R-3098-06-03-S
  Flow-induced polymer crystallization, spinning processes, nanoparticles, biodegradable polymers, and nanocomposites. Benjamin Hsiao, #WC-R-3097-06-03-S
  Relativistic Heavy Ion reaction studies. Roy Lacey, #WC-R-3099-06-03-S
- **ENVIRONMENTAL MOLECULAR**
  Sequestration of contaminants by natural/engineered materials. (two positions) Richard J. Reeder, #WC-R-2962-06-04-F
- **MEDICINE**
  Study the role of complement receptor in inflammation. Berhane Ghebrehiwet, #HS-R-3146-06-03-S
  Molecular studies of Heart Development and Disease. Hal Skopicki, #HS-R-3129-06-03-S
- **NEUROBIOLOGY AND BEHAVIOR**
  Molecular interventions to strengthen synaptic connections in injured spinal cord. Victor Arvanian, #WC-R-3056-06-02-S
  Synaptic transmission and ion channel function in retinal neurons. Gary Matthews, #WC-R-3055-06-02-S
  Mechanisms regulating glutamatergic synaptic transmission in the brain. Lonnie Wolmuth, #WC-R-3057-06-02-S
- **NEUROSURGERY AND RADIOLOGY**
  MRI flow imaging in animals and humans. Mark Wagshul, #HS-R-3100-06-03-S
- **PHARMACOLOGY**
  Conduct study on molecular carcinogenesis and toxicogenomics. Arthur Grollman, #HS-R-3118-06-03-S
  Molecular cellular pharmacology; molecular toxicology; structural biology; cell biology; animal pharmacology. Jeffrey E. Pessin, #HS-R-3106-06-03-S
  WNT signaling in Development and Disease. Ken-ichi Takemura, #HS-R-3118-06-03-S
- **PSYCHIATRY**
  Neural circuitry relating biological rhythms, visuomotor function, and sleep . Lawrence P. Morin, #HS-R-3102-06-03-S
- **PSYCHOLOGY**
  Operant analysis of self-control and social cooperation. Howard Rachlin, #WC-R-3103-06-03-S
- **PULMONARY/CRITICAL CARE**
  Molecular biology, pulmonary hypertension, airway inflammation, genetics, nanotechnology, signal transduction. Sami I. Said, #HS-R-3104-06-03-S
- **RADIOLOGY**
  Medical informatics virtual colonoscopy project. Jerome Liang, #HS-R-3105-06-03-S

To apply online and for information, see *www.postdocs.stonybrook.edu* or mail résumés to: Murray Lamond, Office of the President, Stony Brook University, Stony Brook, NY 11794-0701.

Equal Opportunity/Affirmative Action Employer.

Scripps Institution of Oceanography Faculty Position in Marine Organismal Environmental Physiology

The Scripps Institution of Oceanography of the University of California at San Diego invites applications at the Assistant, Associate, or Full Professor level (tenure track or tenured) in the area of environmental physiology of marine animals with emphasis on whole organism or organ-system function. Applicants must hold a Ph.D. degree or equivalent and will be expected to teach, supervise graduate research, conduct an active research program, and participate in administrative functions at SIO and UCSD. Assistant-level applicants will be expected to show evidence of their potential by a publication record appropriate for their experience. More senior applicants must show evidence of a strong research record in their specialty. The level will depend on the experience of the successful applicant. Salary will be based on the University of California pay scale.

The closing date for applications is **May 15, 2006**, with interviews to begin immediately after the search is closed. Applicants should send a letter including descriptions of their teaching experience, research interests, a list of publications, and the names of at least five potential referees to: **Chair, SIO Graduate Department, 0208, Scripps Institution of Oceanography, University of California at San Diego, 9500 Gilman Drive, La Jolla, CA 92093-0208, USA.**

UCSD is an Equal Opportunity Employer with a strong institutional commitment to excellence through diversity.

HUMAN GENETICS
FACULTY POSITION

The Dept of Molecular Genetics at the Albert Einstein College of Medicine of Yeshiva University is seeking a tenure-track Asst Professor. Applicants should demonstrate novel and innovative approaches in genetics/genomics research. Programs with a focus on translational studies of common human diseases are of particular interest.

The Molecular Genetics Dept has strengths in developmental biology using diverse model organisms. Additional interests include transcriptional regulation, cancer genetics, HIV replication, segmental aneuploidies, movement disorders, chromatin remodeling, human genome retroviruses and epigenomics. Siuated within the Department are Human Genetics cores providing FISH, aCGH, microarray, SNP genotyping ans lymphoblastoid cell transformation.

Candidates are expected to have a PHD or MD degree, postdoctoral experience and a strong publication record. Exceptional candidates at a more senior rank will be considered.

Applicants should send a CV as well as a brief research plan of up to 4 pages in the form of a single PDF file to: **gradus@aecom.yu.edu.** Letters from three or more references should be sent to the same address or to: **Search Committee, Dept of Molecular Genetics, Albert Einstein College of Medicine, Jack and Pearl Resnick Campus, 1300 Morris Park Avenue, Bronx, NY** 10461 EOE

ALBERT EINSTEIN COLLEGE OF MEDICINE
Advancing science, building careers

Research Opportunities

Virginia Bioinformatics Institute

Associate and Full Professorships in Bioinformatics

The Virginia Bioinformatics Institute (VBI) at Virginia Tech has built an internationally recognized scientific program with significant extramural funding. Areas of strength among the 16 research groups at VBI include infectious diseases, ranging from the molecular to the population scale, systems biology approaches to study stress response in several organisms, modeling and simulation of biological networks, functional genomics, metabolomics, proteomics and bioinformatics/computational biology. Candidates are expected to have an established research program and a track record of extensive extramural research funding.

About VBI. Established in 2000 by the Commonwealth of Virginia, the Institute is a part of Virginia Tech (VT) and has its own 130,000 sq ft research facility with state-of-the-art core laboratory and computational facilities. VBI strongly emphasizes synergistic interactions among faculty and is organized around the concept of team science. VBI places strong emphasis on systems biology and bioinformatics rather than organizing research according to academic disciplines. Instead, research areas represented at VBI organize themselves around the specific needs of individual research projects. Extensive national and international collaborations complement the expertise of the faculty, including strong interactions with several biomedical research centers. Faculty entrepreneurial activities are strongly encouraged and the university provides support for the establishment of commercial ventures.

State-of-the-art facilities. VBI is currently establishing a facility in the Washington, DC area, as part of Virginia Tech's expansion into that region. Faculty members whose programs will not require laboratory facilities will have the option of basing their primary research operation there. Faculty whose research programs require laboratory facilities will necessarily be primarily located at VBI's on-campus facility in Blacksburg, where state-of-the-art laboratory facilities are available. The new faculty may also have the option of joint affiliations with other departments at Virginia Tech and two prominent medical schools on the East Coast. Reference posting 042478.

Along with a strong research environment, the Institute actively participates in "Genetics, Bioinformatics, and Computational Biology" (GBCB), an interdepartmental Ph.D. program, widely recognized for its strengths in computational and experimental sciences, which attracts outstanding students with an interdisciplinary research focus.

Research Opportunities at VBI:

- Associate and Full Professorships in Bioinformatics, posting 042478
- AIDS Therapy Modeler Postdoctoral Associate, posting 042829
- Bacterial Genome Annotator Postdoctoral Associate, posting 042721
- Bioinformatics Scientists, postings 060012 and 060043
- Computational Biologist Postdoctoral Associate, posting 042479
- Computer Support Specialist, posting 043222
- Functional Genomicist Postdoctoral Associate, posting 060336
- IT Production Lead, posting 043200
- Metabolomics Specialist Postdoctoral Associate, posting 041979
- Metabolomics Specialist, posting 060044
- Microfluidics and Mass Spectrometry Specialist Postdoctoral Associate, posting 043287
- Molecular Biologist, posting 060045
- Nucleotide Metabolism Modeler Postdoctoral Associate, posting 060105
- Proteomics Specialist, posting 042940
- Software Engineer or Senior Software Engineer, posting 060286
- Software Quality Engineer Lead, posting 043285
- Systems Administrator, posting 043168

For more Information:

To apply, visit www.jobs.vt.edu and search by posting number.
To learn more about VBI and our research, please visit us at www.vbi.vt.edu

To learn more about the Interdisciplinary PhD program in Genetics, Bioinformatics, and Computational Biology (GBCB), visit http://www.grads.vt.edu/academics/programs/gbcb/index.html

VBI

VirginiaTech
Invent the Future

D. E. Shaw Research, LLC

Structural Biology Opportunities

Extraordinarily gifted structural biologists are sought to join a rapidly growing New York–based research group that is pursuing an ambitious, long-term strategy aimed at fundamentally transforming the process of drug discovery.

Candidates should have world-class credentials in structural or computational biology, and must have unusually strong research skills. Relevant areas of experience might include structural bioinformatics, computational studies of biomolecular interactions, X-ray crystallography, and NMR spectroscopy—but specific knowledge of any of these areas is less critical than exceptional intellectual ability and a demonstrated track record of achievement. Current areas of interest within the group include the application of simulation methods to both fundamental and practical problems in molecular biophysics, such as dynamics and allostery. Systems of interest range from ultrafast-folding proteins to functionally significant biomolecules such as protein kinases and membrane transporters.

This research effort is being financed by the D. E. Shaw group, an investment and technology development firm with approximately $19 billion in aggregate capital. The project was initiated by the firm's founder, Dr. David E. Shaw, and operates under his direct scientific leadership.

We are eager to add both senior- and junior-level members to our world-class team, and are prepared to offer above-market compensation to candidates of truly exceptional ability.

Please send your curriculum vitae (including list of publications, thesis topic, and advisor, if applicable) to *sciencemag-bio@career.deshawresearch.com*.

D. E. Shaw Research, LLC does not discriminate in employment matters on the basis of race, color, religion, gender, national origin, age, military service eligibility, veteran status, sexual orientation, marital status, disability, or any other protected class.

D E Shaw & Co

MERCK RESEARCH LABORATORIES

Our work is someone's hope. Join us.

Sr. Research Immunologist

Enhancing and preserving the quality of life. This is the commitment that **Merck & Co., Inc**. stands on and it's what has distinguished us as the world's leading research-driven health products company. Recently ranked by Fortune among "America's Most Admired Companies," we discover, develop and manufacture a wide range of innovative products.

Merck develops breakthrough medicines and treatments that offer a new lease on life. At Merck, improving patient health isn't just what we do. It's who we are, sharing a passion for life that brings out the best in a diverse workforce of 60,000 people. That's why Merck enjoys over $32 billion in annual sales as one of America's largest pharmaceutical companies.

The Department of Immunology within Merck Research Laboratories is seeking a highly motivated and innovative scientist with a strong track record of success in Immunology, Inflammation, and/or Experimental Hematology to conduct basic research in support of drug discovery initiatives. The research will be aimed at the development of novel therapeutic agents for the treatment of diseases impacted by dysregulation of the immune system. The position involves participation in and leadership of cross-functional teams seeking to validate novel biological targets and to identify new chemical and biologic entities suitable for clinical testing. The position also involves the initiation and coordination of external research collaborations with thought leaders in the field.

Qualifications include a Ph.D. and /or M.D. with a background in Cellular/Molecular Biology and experience in Immunology, Inflammation or Hematology. A minimum of 2 years of additional postdoctoral research experience is required. The successful candidate will have strong research achievements and a solid publication record. Experience with in vivo models of disease is advantageous. Prerequisites also include excellent interpersonal and presentation skills and an ability to work in a highly collaborative team setting.

We offer a competitive salary, an outstanding benefits package and a professional work environment with a high growth company. To apply, please visit **www.merck.com/careers** and reference **BIO0001067**. We are an Equal Opportunity Employer, M/F/D/V.

Where patients come first MERCK

DIRECTOR
Chemical Sciences, Geosciences and Biosciences Division

The US. Department of Energy, Office of Science, Office of Basic Energy Sciences is seeking candidates for the position of the Director, Chemical Sciences, Geosciences and Biosciences Division. This position is a Senior Executive Service position located in Germantown, Maryland. The incumbent of this position provides leadership and direction in establishing vision, strategic plans, goals, and objectives for the research activities in the area of responsibility; plans, develops, and implements vital, productive, forefront research programs conducted in DOE laboratories, universities, and other public and private institutions; assures adequate financing for the activities, sets priorities for activities, and apportions available funding among them; manages the budget in accordance with prescribed practices set forth by the Office of Science and the DOE; reviews and makes final approvals on staff recommendations concerning research agreements and individual proposals for research projects; implements rigorous merit evaluation for all new and ongoing activities in accordance with the federal requirements for the grant program and published guidelines for DOE laboratory programs and facilities; assists in the formulation and management of new programs and policies; coordinates research activities with those of other Federal agencies; represents the Division, the Office, and DOE on professional societies, committees, task forces, etc.; supervises a staff of professional, scientific and administrative employees.

For more detailed information on this position, go to the website: **http://jobsearch.usajobs.opm.gov/**. Go to Search Jobs and in the Key Word Search box type **06PH-ES-22-001**.

For information on how to apply for this position, please follow the instructions as stated in the following website: **http://jobsonline.doe.gov**. **NOTE: Applications must be submitted online**.

POSTDOCTORAL POSITIONS

A postdoctoral position is available in mouse genetics to study the neuropathology of tuberous sclerosis complex (TSC), an autosomal dominant disorder responsible for seizures, developmental delay and autism. Mutations in the TSC2 gene, encoding tuberin, are one cause of TSC. While recent work has placed the *TSC2* gene in the mTOR pathway, the role of *TSC2* in normal brain development, as well as the molecular perturbations that occur in TSC are not well understood. We have generated a conditional disruption of the *TSC2* in the mouse to aid in the understanding of the normal brain function of *TSC2* as well as TSC pathogenesis. We are currently using several Cre driver mice to investigate disruption of *Tsc2* in specific neuronal populations. Current work will focus on characterizing mice with brain specific *Tsc2* disruptions. Long term goals will be to better understand the genetic networks important for TSC pathogenesis, normal brain development, and to shed light on complex genetic disorders such as autism. The position is suited to individuals who have experience in mouse genetics, neuroscience, and microarray analysis.

Applications, including a curriculum vitae, three letters of reference, and a brief summary of accomplishments and future research directions should be sent by regular mail or e-mail to: **Michael J. Gambello, M.D., Ph.D., Department of Pediatrics, Division of Medical Genetics, 6431 Fannin, MSB 3.144, Houston, TX 77030. E-mail: Michael.J.Gambello@uth.tmc.edu.**

A postdoctoral position is available immediately at The University of Texas Medical School at Houston in the Department of Pediatrics. Several ongoing projects relating to lung development, biology and immunology with emphasis on pulmonary surfactant proteins and airway epithelial cells provide various venues of investigations; (1) the identification and characterization of mRNA-binding proteins that regulate the stability of surfactant protein mRNA and (2) the characterization of both lung biology and the regulation of surfactant proteins in response to environmental insults such as viruses and pollutants. These positions require knowledge of molecular and techniques in RNA analysis, knowledge of analytical techniques used in protein purification and characterization, or knowledge of analytical techniques used in investigating proteolytic pathways. Applicants should also have prior experience in molecular biology and cell culture techniques.

Please send curriculum vitae, letter of interest, names and contact information of three references to: **Joseph Alcorn, Ph.D., Department of Pediatrics, 6431 Fannin, MSB 3.222, Houston, TX 77030. E-mail: Joseph.L.Alcorn@uth.tmc.edu.**

A postdoctoral position is available in human genetics to study tuberous sclerosis complex (TSC). TSC is a single gene disorder of benign tumors that can affect any organ system. The most serious medical consequences involve the brain with affected individuals potentially having any of the following symptoms: seizures, mental retardation, autism and a variety of psychiatric disorders. Mutations in either of two genes, TSC1 and TSC2, can result in the disease. The project will involve searching for modifier genes affecting the phenotype. The TSC1 and TSC2 genes form a complex within the cell that is important in down-regulating small G-protein RHEB in the mTOR cell signaling pathway. The TSC1/TSC2 complex is also known to affect functioning in the Wnt/βcatenin pathway and the functioning of several small G-proteins (Rho, RAC, RAP1A, RAB5). We have a large cohort of affected individuals and their family members with identified TSC1 or TSC2 mutations. By utilizing this resource, we would like to identify other genes that affect the phenotypic expression. The long-term goal is to identify pharmacologic targets for treatment strategies.

Applications, including a curriculum vitae, three letters of reference, and a brief summary of accomplishments and future research directions should be sent by regular mail or e-mail to: **Hope Northrup, M.D., Department of Pediatrics, Division of Medical Genetics, 6431 Fannin, MSB 3.144, Houston, TX 77030. E-mail: Hope.Northrup@uth.tmc.edu.**

A postdoctoral position is available to study the mechanisms by which mutations in cartilage oligomeric matrix protein (COMP) genes affects transport and processing of extracellular matrix proteins. We have human and murine reagents ready for these studies. Candidates should possess a Ph.D. degree in molecular biology, cell and or cartilage biology or a related field. Experience in transgenic and knockout mice is desirable. The University of Texas Medical School at Houston is situated in the Texas Medical Center, the largest medical center in the world composed of 35 medical and research facilities including The University of Texas M. D. Anderson Cancer Center, The University of Texas School of Public Health at Houston, and Harris County Hospital District. Facilities within the university include state-of-the-art genomics, proteomics, histopathology and mouse cores and vivarium.

Applicants should send a letter of application that includes a summary of career aspirations, curriculum vitae and names and addresses of three references to: **Dr. Jacqueline T. Hecht, The University of Texas Medical School at Houston, Department of Pediatrics, P.O. Box 20706, Houston, TX 77225. E-mail: Jacqueline.T.Hecht@uth.tmc.edu.**

The Division of Medical Genetics in the Department of Pediatrics at UT Health Science Center at Houston is an interactive and collegial research environment with state-of-the-art facilities including transgenic/knockout technology and core facilities for microarray and gene expression analysis. We are located in the Texas Medical Center, a rich environment for a multitude of research collaborations.

Women and minority candidates are encouraged to apply. The University of Texas Health Science Center at Houston is an EO/AA employer. M/F/D/V. This is a security sensitive position and thereby subject to Texas Education Code §51.215. A background check will be required for the final candidate.

THE UNIVERSITY *of* TEXAS
HEALTH SCIENCE CENTER AT HOUSTON

Colipa, the Brussels based European trade association of the cosmetic industry represents 23 national associations and 21 international companies. It covers a wide range of regulatory issues impacting the cosmetic industry.

THE EUROPEAN COSMETIC TOILETRY AND PERFUMERY ASSOCIATION
COLIPA

Colipa has immediate openings for:

1. Project Manager Alternative Methods to Animal Testing

Temporary assignment -
Reference 2006/02/PMAMAT

The role of Project Manager involves effective management of a portfolio of R&D projects in the field of alternative methods to animal testing. The successful Project Manager will contribute to a wider recognition of the industry sector's efforts in the development of alternative methods.
A three years' - renewable - contract is offered.

Main Responsibilities:

- To co-ordinate and pro-actively manage the R&D programme together with the association management and membership;
- To ensure delivery of the agreed programme according to the milestones and timelines agreed with members and research partners;
- To develop an overall administrative framework for the R&D programme and implement effective management processes/tools for initiating, monitoring and reporting on progress of the research projects, including contractual negotiations with research collaborators and the planning, monitoring and reporting of the annual research budget;
- To organise meetings, including the preparation of documents, production of minutes, monitoring progress with actions, and general support for industry working groups;
- To effectively liaise with relevant regulatory bodies (e.g. European Commission, OECD), scientific circles and other industry sectors.

Required Qualifications and Skills

- Degree in a biology/toxicology related discipline;
- Excellent knowledge of English, good command of a second major European language is a plus;
- A team player, having at least five years experience with research project management;
- Excellent communication skills (oral and in writing);
- Attention to detail; a "hands on" mentality; creativity and problem solving skills.

2. Issue Manager Science and Research

Permanent position -
Reference 2006/03/IMSR

As a member of the Directorate Science and Research, the successful Issue Manager contributes to an effective management of scientific and regulatory issues, relevant for the cosmetics industry.

Main responsibilities:

- To contribute to the development of issue related strategies and objectives;
- To implement work plans and strategies;
- To effectively prepare and implement projects;
- To build and maintain a successful network with stakeholders (notably European institutions), scientific circles and other industry sectors;
- To represent the association to external audiences in the area of responsibility;
- To support project teams and task forces in the association;
- To identify pertinent trends in the area of science and research, relevant for the industry and act as adviser to membership.

Required Qualifications and Skills

- Relevant University Degree in a scientific discipline (chemistry, biology, toxicology);
- 2-3 years working experience in a company or industry association;
- Knowledge of the cosmetics industry desirable;
- Excellent knowledge of English, good command of a second major European language is a plus;
- Team player, excellent communication skills;
- Attention to detail, "hands on" mentality, creativity and problem solving skills.

Only candidates fulfilling these requirements should apply – clearly specifying the reference of the position applied for - by sending an introductory letter in English and a full c.v., which will be treated in the strictest confidence, to:

Mrs Danièle VRANKEN-MARTEAUX, Director, Finance & Administration, COLIPA, Avenue Herrmann-Debroux, 15a, B-1160 Brussels (Auderghem), Belgium
Email: dmarteaux@colipa.be

DEADLINE FOR APPLICATIONS: 30 April 2006
Telephone enquiries cannot be answered.

Vice-Chair for Research
In Reproductive Science and Medicine
Department of Reproductive Medicine
University of California, San Diego

The University of California, San Diego, Department of Reproductive Medicine, is seeking a leading PhD and/or PhD/MD investigator in Reproductive Biology/Medicine to become the Vice-Chair for Research. The responsibilities and duties of the Vice-Chair for Research will augment one of the open positions currently under recruitment and posted at **http://academicaffairs.ucsd.edu/offices/adeo/recruitment/**.

The Department of Reproductive Medicine is presently engaged in a major expansion of its renowned reproductive research programs, with plans to recruit up to six basic/translational scientists. Ample recruitment packages have been assigned by the Dean, UCSD School of Medicine, for this effort and excellent research space is available. The department is particularly interested in scientists with interests in developmental biology, placentation, ovarian biology or cancer, neuroendocrinology of reproduction, and germ cell - stem cell research.

The Vice Chair for research will lead and coordinate these recruitment efforts, assist existing programs in expanding their funding base and develop new research programs relevant to reproductive biology. He or she will also be expected to serve in a broader leadership role in the scientific enterprise within the department and the School of Medicine. Applicants should have senior academic experience in obtaining extramural support as an independent investigator and have a currently funded established research program in the reproductive sciences. Proven teaching skills in Reproductive Physiology/Medicine, outstanding scholarly achievements, a deep commitment to academic excellence, strong leadership and administrative skills, and a vision for basic science and translational research in an academic setting are expected. The candidate should be committed to furthering interdisciplinary research, both within the department and in the larger institutional setting.

Applicants are encouraged to directly contact **Thomas R. Moore (trmoore@ucsd.edu), MD, Professor and Chair, Department of Reproductive Medicine**, or submit a letter of interest, curriculum vitae, separate statements of research and teaching interests, a statement of administrative philosophy, and a list of five references to: **Ms. Jackie McElveny (jmcelveny@ucsd.edu), The University of California, San Diego, Department of Reproductive Medicine, 9500 Gilman Drive, La Jolla, CA 92093-8433**. Review of applications will continue until the position is filled.

The University of California, San Diego, is one of the ten campuses in the University of California, the largest higher education system in the world. It is located in the heartland of La Jolla surrounded by the Salk/Scripps/Burnham Institutes and 500-plus biotechnology companies.

The University of California, San Diego is an Equal Opportunity/Affirmative Action Employer with a strong institutional commitment to the achievement of diversity among its faculty and staff.

BROOKHAVEN
NATIONAL LABORATORY

Director

Brookhaven Science Associates LLC (BSA) announces the search for Director of the Brookhaven National Laboratory (BNL). The BSA Board comprises representatives from the partners Stony Brook University and Battelle Memorial Institute as well as from the six collaborating universities that are core participants in the missions of the Lab: Columbia, Cornell, Harvard, MIT, Princeton, and Yale.

Founded in 1947, Brookhaven National Laboratory is located on Long Island in Upton, New York, and is one of five multipurpose laboratories operated by the Office of Science of the U.S. Department of Energy. The Laboratory's primary mission is scientific research in fields frequently requiring the design, construction and operation of complex facilities for external users as well as for its own scientists. BNL scientific programs are organized in five directorates: Basic Energy Sciences, Energy/Environment/National Security, High-Energy and Nuclear Physics, Life Sciences, and Light Sources. Major facilities include the Relativistic Heavy Ion Collider (RHIC), the National Synchrotron Light Source (NSLS), and the Center for Functional Nanomaterials (CFN). The Laboratory has over 2,600 employees, an annual budget of approximately $500 million, and more than 4,500 scientific users of its facilities per year.

The Director of Brookhaven National Lab also serves as President of BSA. The new director must have strong scientific credentials, experience in developing and operating a complex scientific organization, and demonstrated success in engaging all the stakeholders associated with the functioning of such an organization.

Nominations and expressions of interest should be submitted, in total confidence, to:

Shelly Weiss Storbeck, Managing Director
A.T. Kearney Education Practice
333 John Carlyle Street,
Alexandria, VA 22314
Telephone: 703-739-4613
Fax: 703-518-1733
E-mail may be addressed to BNL@es.atkearney.com

For best consideration, please submit applications or nominations no later than **May 15, 2006**. Electronic submissions are particularly encouraged.

Further information about BNL can be found on the website: **www.bnl.gov**.

Recruitment of the President of the Cyprus Institute (CyI)

The objective of the CyI project is the establishment in Cyprus of a novel non-profit research and educational institution, with a scientific and technological orientation, the highest standards of excellence and an emphasis on international partnerships with world-class universities and research organizations. The Cyprus Institute was launched in January 2005, with the support of the government of Cyprus and the Cyprus Development Bank, and is being developed at the initiative of the Cyprus Research and Educational Foundation (CREF), governed by a Board of Trustees -chaired by Prof. Edouard Brézin, president of the French Science Academy- and advised by an international council -chaired by Prof. Jose Mariano Gago, Minister of Science and Technology of the government of Portugal. Its development is planned in three successive phases: the progressive implementation of several cross-disciplinary research centres, followed by the establishment of a Graduate College, and later on of an Undergraduate College. The first research centre will deal with Energy, Environment and Water; it has been planned under the leadership of Prof. Ernest Moniz, Professor at the Massachusetts Institute of Technology and former Undersecretary for Energy of the US government. The President of CyI will be instrumental in realizing this centre and in developing the ensuing research centres. The Institute is intended to serve as an important research and educational resource for the Eastern Mediterranean, Middle East, and North Africa and to serve as a gateway between the EU and the region for addressing areas of mutual interest on the basis of science, technology and analysis. Further information can be found at ***www.cyprusinstitute.ac.cy***

Position Description:
The incumbent will be the President of the Cyprus Institute, he/she will be responsible for the conduct of all affairs of the Institute, in collaboration with the Board of Trustees of CREF. He/she will work in Cyprus, and will be offered a 5-year appointment, renewable upon mutual agreement, with a very attractive salary and benefits package, commensurate to his/her high degree of responsibility and qualification.

Responsibilities:
The incumbent will be directly responsible for developing strategies and actions, as appropriate to the Institute's missions and objectives.
He/she will be responsible for:

- keeping the Board informed of all relevant affairs, and for executing all decisions of the Board.
- developing organisational structures for the appropriate functioning of CyI, as well as coordinating such structures and their activities.
- raising financial and other resources for the needs of CyI.
- recommending the recruitment of future employees, and generally supervising the human resources of CyI.

He/she will have authority and responsibility for all members of CyI, and represent the Institute in high-level external contacts.

Profile:
The incumbent should be an outstanding individual of international calibre, with a minimum of 5 years' experience in research management. He/she must have a strong vision of the role of research and education and of the importance of science and technology capacity building in Europe in the 21st century. Previous responsibility for institution building and/or managing complex projects from development to implementation would be a strong advantage. Proficiency in spoken and written English is indispensable, while knowledge of the Greek language would be an advantage but is not a requirement. The incumbent must have excellent interpersonal skills, with strong capacities for managing human resources, and for generating and maintaining contacts in the academic, business, political and governmental circles, as well as obtaining support from them for the Institute.

Please reply before 15/05/2006 to Dr. Michalis Yangou – CREF, PO Box: 22745, CY 1523 Nicosia, Cyprus.
Tel: +357 22 761101 Telefax: +357 22 447800 email: sec.cref@cytanet.com.cy

---

The Medical College of Georgia Vascular Biology Center is recruiting two **pulmonary vascular biologists at the Assistant, Associate or Full Professor levels**, tenure-track. The successful candidates will have an earned Ph.D., M.D. or M.D./Ph.D. degree. They will join an active group of extramurally funded vascular biologists (currently about $8 million annually, see: **http://www.mcg.edu/centers/VBC/index.html)** in recently renovated laboratories utilizing state-of-the-art equipment. They will have the opportunity to participate in the two institutional pre- and post-doctoral training programs in Integrative Cardiovascular Biology. Ample opportunities for collaborative basic and clinical research are available and encouraged. The candidates are expected to have and further develop an active, extramurally-funded research program in aspects of pulmonary vascular disease. Highly competitive salary and start-up package, commensurate with prior experience, will be provided.

Applications should include detailed CV, statement of career goals and names of three references and be e-mailed to: **John D. Catravas, Ph.D. (jcatrava@mcg.edu)**.

The Medical College of Georgia is an AA/EOE. Applications from women and under-represented minorities are particularly encouraged.

Fred Patterson Endowed Chair:
Translational Genomics for Crop Improvement
Associate/Full Professor (Tenure track, academic year appointment)
Purdue University (Posting 001597-2006)
Position available September 2006

To further strengthen a comprehensive plant genetics/genomics/crop improvement program, Purdue Agronomy Department seeks to fill a tenure track endowed chair position with a mid-career scientist in translational genomics of crops. The Fred Patterson Endowed Chair provides recurring funds to the successful candidate for the development of a strong crop research program in translational genomics. The successful candidate is expected to provide leadership and interact with a dynamic group of scientists engaged in plant genomics research and crop improvement. Research foci could encompass, but are not limited to, genetics of seed biochemistry/metabolism/development, biofuels, biotic and abiotic stress tolerance, or developing creative molecular/quantitative approaches for the exploitation of genomics and genomic data in germplasm enhancement and improvement of economically important crops. The incumbent must have a proven track record of grantsmanship and scholarly publication, experience in interdisciplinary research, and ability to interact with a diverse group of researchers and clientele groups. Although experience in the genetic improvement of crop plants is desired, persons who have established excellent research programs in the genetics or genomics of other plant systems but with a desire and plan to develop a successful interdisciplinary program in crop improvement will also be considered. The successful candidate will be expected to teach and mentor undergraduate and graduate students, as well as participate in outreach activities.

Applicant must hold a PhD in plant genetics, genomics, plant breeding, or related field. A record of excellence in research, mentoring of graduate students, and engagement in outreach activities is required. Interest and/or experience in the international dimensions of the discipline is desirable. The candidate must be committed to expanding and fostering diversity. Salary is commensurate with experience. Compensations include an excellent fringe benefit package with TIAA-CREF retirement program, as well as medical, life and disability insurance and sabbatical leave program.

Qualified persons are requested to send a letter of application including a statement of research goals and teaching philosophy, curriculum vitae, and representative examples of their scholarly work to: **Dr. Craig Beyrouty, Head, Department of Agronomy; 915 W. State St., Purdue University, West Lafayette, IN 47907-2054; Phone: 765-494-4774**. Application review will begin **June 1, 2006** and continue until a successful candidate is identified. For more information, contact Search Chair, **Gebisa Ejeta (gejeta@purdue.edu)** or **Craig Beyrouty (beyrouty@purdue.edu)**, Department Head.

Purdue University is an Affirmative Action/Equal Access/Equal Opportunity Employer. Women and individuals in under-represented groups are encouraged to apply.

ANNOUNCEMENTS

Harold M. Weintraub Graduate Student Awards – 2006

The Fred Hutchinson Cancer Research Center congratulates the following recipients of the 2006 Harold M. Weintraub Graduate Student Award in recognition of outstanding achievement during Graduate Studies in the Biological Sciences.

Melissa W. Adkins	University of Colorado Health Sciences Center
David M. Altman	Stanford University
Brenda L. Bloodgood	Harvard University
Curtis R. Chong	Johns Hopkins University School of Medicine
Sophie Dumont	University of California, Berkeley
Liang Feng	Princeton University
Ryan C. Heller	Cornell University
Takaki Komiyama	Stanford University
Yoontae Lee	Seoul National University
Anna V. Molofsky	University of Michigan
Ying Peng	Brandeis University
Ryan T. Phan	Columbia University
Benjamin A. Pinsky	Fred Hutchinson Cancer Research Center
Daniel R. Rhodes	University of Michigan
Sarah E. Siegrist	University of Oregon
Tomomi Tsubouchi	Yale University

The recipients will participate in a Symposium this spring honoring Hal Weintraub and his commitment to innovative science. More information on this award can be found at:

http://www.fhcrc.org/science/basic/weintraub

POSITIONS OPEN

CORE LABORATORY MANAGER

The Institute of Human Virology (IHV), University of Maryland Biotechnology Institute, invites applications for a Core Laboratory Manager at its MicroQuant Core facility. The successful applicant will manage and perform routine core activities and services to IHV investigators. Qualifications: Advanced degree in biological sciences, molecular biology or immunology; or B.S. with significant experience with cores. Capability to manage infrastructure and logistics; to interact effectively and efficiently with a variety of investigators; and to manage the financial aspects of the core. Experience to include cell stock preparation, HIV virus stock preparation and characterization, cell culture-based assays, ELISAs and other immunochemical assays, routine protein purification, quantitative PCR and maintenance of common use equipment. Experience in core services and core facility management, and in developing novel purification techniques and immunoassays preferred. Please send resume and three references referencing Position 300278 to: **Debi Delker, Institute of Human Virology, UMBI, 725 West Lombard Street, Baltimore, MD 21201,** or **e-mail: delker@umbi.umd.edu.** *The University of Maryland Biotechnology Institute is an Equal Opportunity/Affirmative Action Employer. Women, minorities, veterans, and candidates with disabilities are encouraged to apply.*

NEURAL CIRCUITS
University of Pittsburgh

The Department of Neurobiology, University of Pittsburgh School of Medicine, in conjunction with the Center for the Neural Basis of Cognition and the new Systems Neuroscience Institute, invites applications for a **TENURE-TRACK POSITION** at all ranks. The position is designed to complement current Departmental strengths in the analysis of neural circuits mediating sensory/motor and related functions in higher vertebrates. Preference will be given to candidates investigating neural circuit function in in vivo rodent systems using cellular physiological approaches in combination with anatomical and/or computational methods. The position requires a Ph.D. or M.D. with at least two years of postdoctoral experience. Competitive salary support and startup funds will be made available. Applicants should submit curriculum vitae, a statement of present and future research goals, representative recent publications, and names and addresses of three references to: **Dr. Daniel Simons, Chair, Neural Circuits Search, Department of Neurobiology, University of Pittsburgh School of Medicine, E1440 Biomedical Science Tower, Pittsburgh, PA 15261.** The application deadline is July 1, 2006. *The University of Pittsburgh is an Affirmative Action, Equal Opportunity employer.*

Pending final budgetary approval, Drake University invites applications for a full-time, nine-month, nontenure-track position as **VISITING ASSISTANT PROFESSOR** of microbiology/virology, beginning fall semester 2006. Teaching responsibilities include microbiology for pharmacy students, virology, and two specialty courses, one preferably with a broad interest in environmental health issues. Qualifications include a Ph.D., with postdoctoral experience desirable. A commitment to inquiry-based teaching in an interdisciplinary setting is expected, along with research that can engage undergraduates. Please send curriculum vitae, e-mail addresses of references, philosophical statement on teaching and research, publication sample, and transcripts, to:

Dr. Richard Wacha
Chair, Department of Biology
Drake University
2507 University Avenue
Des Moines, IA 50311

Review of applications begins May 1, 2006, and continues until filled. **E-mail: richard.wacha@drake.edu. Website: http://www.drake.edu.** *Drake University is an Equal Opportunity Employer and actively seeks applicants who reflect the diversity of the nation.*

POSITIONS OPEN

University of Nebraska Medical Center

CANCER BIOLOGY AND IMMUNOLOGY

The Department of Pathology and Microbiology at the University of Nebraska Medical Center (UNMC) invites applications from experienced **RESEARCHERS** with a research program in cancer biology and molecular genetics with a special emphasis on lymphoma and leukemia or in areas of immunology relevant to lymphoid malignancy. Individuals with peer-reviewed funding and a strong track record of research will be given preference.

UNMC provides a vibrant and interactive community of researchers with a wide range of interests and particular strengths in cancer biology and transplantation research. There are state-of-the-art core facilities. The successful faculty candidate will be provided a modern laboratory in the newly-established Center of Research in Leukemia and Lymphoma and a generous startup package. Clinical and research faculties in the Center have a long track record of strong collaborative research.

Send curriculum vitae, statement of research interests and the names of at least three references to: **Samuel Cohen, M.D., Ph.D., Chair, Department of Pathology and Microbiology, University of Nebraska Medical Center, 983135 Nebraska Medical Center, Omaha, NE 68198-3135.**

University of Nebraska Medical Center is an Equal Opportunity/Affirmative Action Employer. Minorities and women are encouraged to apply.

NONTENURE RESEARCH ASSISTANT PROFESSOR/ RESEARCH ASSOCIATE/ SENIOR POSTDOCTORAL FELLOW POSITION
Department of Environmental and Occupational Health
Graduate School of Public Health
University of Pittsburgh

Several positions are available in the laboratory of **Dr. Valerian E. Kagan** (Center for Free Radical and Antioxidant Biochemistry, Department of Environmental and Occupational Health, University of Pittsburgh). Candidates with interests in research on: (1) mass spectrometry/oxidative lipidomics/metabolomics, (2) mass-spectrometry and oxidative neurolipidomics, (3) lipid signaling in apoptosis and phagocytosis (from nematodes to humans), (4) effects of nano-particles on cells in vitro and in vivo are invited to apply. Participation in ongoing collaborations with laboratories in Sweden and the United Kingdom is possible. Candidates should have Ph.D. with background in analytical biochemistry/chemistry, molecular/cell biology, redox biochemistry/biophysics or related fields. Experience with mass spectrometry of lipids and other small molecules, analytical chemistry/biochemistry as well as live cell (fluorescence) microscopy, immunoblotting, immunocytochemistry, DNA transfection are desirable. Interested applicants should send curriculum vitae and names of three references to: **Dr. Valerian E. Kagan, e-mail: vkagan@eoh.pitt.edu.** *University of Pittsburgh is an Equal Opportunity, Affirmative Action Employer.*

ENVIRONMENTAL MODELER for Cincinnati, Ohio. Will develop quantitative structure activity relationship (QSAR) models to predict toxicities for cancer and noncancer health endpoints; identify and develop algorithms to calculate parameters that contribute to each endpoint including quantum chemical and Kier and Hall type parameters. Competitive wages, requires Ph.D. in environmental science, statistics, chemistry or equivalent with one year of experience, programming experience. Send resume to: **Pegasus Technical Services, e-mail: asis@pegasustechserv.com.**

POSITIONS OPEN

FACULTY POSITION IN INFECTIOUS DISEASE
Georgia State University

The Molecular Basis of Disease Area of Focus (MBD) at Georgia State University invites applications for an anticipated senior level, Tenure-Track Faculty position in the area of infectious disease. The MBD is an interdisciplinary program that includes faculty and students in several departments. Applications are sought from individuals with research interests that complement those of the current faculty in the MBD. The successful applicant will have a primary appointment in the Department of Biology. The successful applicant should have an established, externally funded research program, to collaborate with other MBD faculty, to direct independent graduate student research, and instruct appropriate upper level undergraduate and graduate courses. The Department has excellent research facilities. For more information, consult the Department's **website: http://biology.gsu.edu.** Review of applications will commence as soon as possible and will continue until the position is filled; the position is available for a start date of August 2006. Applications including curriculum vitae, reprints, statement of research interests and plans, and three letters of recommendation should be sent to: **Chair of Molecular Basis of Disease Search Committee, Attn: Ms. Tara Alexander, Department of Biology, P.O. Box 4010, Georgia State University, Atlanta, GA 30302-4010.** *Georgia State University, a Research University of the University System of Georgia, is an Equal Opportunity Employer.*

A **POSTDOCTORAL POSITION** in microbial pathogenesis is available to investigate virulence mechanisms of Haemophilus ducreyi, the etiologic agent of chancroid. Emphasis will be placed on the elucidation of the genetic regulatory mechanism(s) by which H. ducreyi controls the differential expression of the LspA1 and LspA2 proteins; these exoproteins are major virulence determinants. Position requires a Ph.D. in microbiology, biochemistry, genetics, or a related biological science and experience with recombinant DNA techniques. Position includes salary, fringe benefits, and the opportunity to work in a dynamic research environment. Position available immediately. Send curriculum vitae and the names and telephone numbers of three references to:

Dr. Eric J. Hansen
Department of Microbiology
The University of Texas Southwestern Medical Center at Dallas
5323 Harry Hines Boulevard
Dallas, TX 75390-9048
Fax: 214-648-5905
E-mail: eric.hansen@utsouthwestern.edu

UT Southwestern is an Equal Opportunity/Affirmative Action Employer.

FACULTY POSITION
Environmental and Evolutionary Biology
University of Louisiana, Lafayette

The Department of Biology at the University of Louisiana (UL) at Lafayette invites applications for a tenure-track position at the **ASSISTANT** or **ASSOCIATE** level. The candidate must have a Ph.D. in a biological science and a strong track record of funding for research and support of graduate students. Substantial postdoctoral experience is preferred. This tenure-track position will support our doctoral program in Environmental and Evolutionary Biology; the specific area of research is open. Candidates should send curriculum vitae and statements of research and teaching, and arrange to have three letters of recommendation sent to: **Biology Search Committee, Department of Biology, University of Louisiana at Lafayette, P.O. Box 42451, Lafayette, LA 70504.** Review of applications will begin immediately and continue until a suitable candidate is identified. Inquiries regarding this position may be sent to: **Joe Neigel, Chair, Biology Search Committee, e-mail: jneigel@louisiana.edu.**

UL Lafayette is an Equal Employment Opportunity/Affirmative Action employer.

Federal Ministry of Education and Research

bccn

"Bernstein Award" 2006

Young Scientists Research Award in Computational Neuroscience

The German Federal Ministry of Education and Research (BMBF) has established the "National Network for Computational Neuroscience" with four high-performing "Bernstein Centers for Computational Neuroscience" as the major structural elements.

The "Bernstein Award" is equipped with up to 1.250 Mio € in the form of a grant over a period of five years. It will be awarded to a highly qualified young researcher, considering the candidates' verifiable research profile in the field of computational neuroscience and the scientific concept for a future young research group. Young researchers can apply for their own position and group. The group funded by the "Bernstein Award" will become an integral part of the National Network for Computational Neuroscience. Future announcements of the "Bernstein Award" are in the scope of the Ministry's planning.

The grant is provided for a scientific project of a young research group headed by a postdoc regardless of nationality. The project will be conducted at a German university or research institution – within or outside the Bernstein Centers. It is a prerequisite for funding that the university or research institution concerned employs the young researcher during the funding period and supports him/her with the basic equipment in terms of laboratory space and other infrastructure. A statement made to that effect by the receiving institution must be included with the project outline to be submitted.

Deadline for applications is June 30th, 2006.

For more detailed information about the "Bernstein Award" including application conditions please visit

www.bernstein-centers.de

POSITIONS OPEN

DIRECTOR, OFFICE OF SCIENCE AND TECHNOLOGY
National Oceanic and Atmospheric Administration
National Marine Fisheries Service

The Department of Commerce, National Oceanic and Atmospheric Administration's National Marine Fisheries Service is advertising to fill the vacant Director, Office of Science and Technology position in the Agency's headquarters office in Silver Spring, Maryland. This is a senior executive position with a salary range of $109,808 to $162,000. The Director, Office of Science and Technology provides national oversight and coordination for the planning, development, and execution of a multi-disciplinary program of research, fisheries landing data, long-term science and technology strategy. The incumbent monitors national and international trends in science and technology, ensures a sound scientific basis for Agency science programs in resource conservation and management decisions. Additional primary responsibilities may be reviewed in the vacancy announcement. The announcement number is NOAA#06-13. NJH and may be accessed via **website: http://www.USAJOBS.opm.gov.** Please contact: **Gloria Thompson, Office of the Assistant Administrator for Fisheries,** at **telephone: 301-713-2239** if you require additional information.

POSTDOCTORAL FELLOWSHIPS
Immunology

NIH-funded Postdoctoral Fellow positions are available in the Department of Microbiology and Immunology at Drexel University College of Medicine, Philadelphia, Pennsylvania, United States. Projects include the investigation of defects of virus-specific CD8+ T cells in Human Immunodeficiency virus (HIV)-infected humans and SIV-infected nonhuman primates. Other projects available examine the role of dendritic cells and costimulation in virus-specific CD8+ T cell responses using influenza virus- and HSV-infected mice. Experience in immunological assays and flow cytometry will be a plus. For further information please contact: **Peter D. Katsikis, M.D., Ph.D., Department of Microbiology and Immunology, Drexel University College of Medicine, e-mail: peter.katsikis@drexelmed.edu.**

POSTDOCTORAL POSITION immediately available to develop novel therapeutic modalities for the treatment of Graft-versus-Host Disease (GVHD) in the context of allogeneic hematopoietic stem cell transplantation by targeting inflammatory signaling pathways. Requirements: M.D. or Ph.D. degree in immunology, cell biology, or molecular biology. Strong background in murine models, molecular biologic methodologies, and flow cytometry is highly desirable. Curriculum vitae with names, telephone numbers, and e-mail addresses of three references should be sent to: **Markus Y. Mapara, M.D., Ph.D., Division of Hematology-Oncology, University of Pittsburgh Cancer Institute. E-mail: maparamy@upmc.edu. Telephone: 412-623-1112.**

The Department of Ecology and Evolutionary Biology at Tulane University has up to three **VISITING ASSISTANT PROFESSOR** positions for 2006-2007 **(see website: http://www.tulane.edu/~ebio/).** Applications should include a statement of teaching philosophy, list of courses one could teach, curriculum vitae, and three letters of reference addressing one's teaching experience and capabilities. Send applications via **e-mail: jbattis@tulane.edu** or by mail to: **Visiting Assistant Professor Search, Department of Ecology and Evolutionary Biology, Tulane University, New Orleans, LA 70118.** *Tulane University is an Affirmative Action/Equal Employment Opportunity Employer.*

POSITIONS OPEN

MAYO CLINIC

The Mayo Clinic Section of Scientific Publications seeks a full-time **MANUSCRIPT EDITOR.** The Section has offices at Rochester, Minnesota, Jacksonville, Florida, and Scottsdale, Arizona, and is one of the largest academic departments of biomedical editing in the United States. This position supplements the current seven biomedical editors and 20 editorial assistants and proofreaders. Candidates should have significant experience in editing peer-reviewed manuscripts, book chapters, and NIH grants. A relevant Ph.D. degree or substantial academic editing experience is required. Candidates will be expected to furnish examples of their work so that the edited manuscript can be compared with the unedited copy. Successful applicants will hold a faculty position at Mayo Clinic College of Medicine (level commensurate with experience). Excellent salary and benefits.

Send curriculum vitae to:

Rosemary Perry
Administrative Assistant
Scientific Publications
Plummer Building, S-10
200 First Street SW
Rochester, MN 55905
E-mail: perry.rosemary@mayo.edu

Mayo Foundation is an Affirmative Action and Equal Opportunity Employer and Educator.

STAFF FELLOWSHIP OPPORTUNITY
Immunity to Influenza Virus Infection

A Staff Fellowship or Visiting Scientist position is available in the Center for Biologics Evaluation and Research, FDA, on the main NIH campus, to study control of influenza virus infection by vaccination. Experimental vaccines under study use highly conserved viral features shared by different strains and even different subtypes of influenza A. They induce broad cross-protection in animals against challenge infection with divergent subtypes. Qualifications: Ph.D. in immunology, molecular biology, virology, or related fields; excellence, productivity, and long-term interest in laboratory research. Willingness to learn and perform animal procedures. Previous post-doctoral experience expected but not required. *Proof of U.S. citizenship or permanent residency required.* Salary is dependent on qualifications and number of years of postdoctoral experience.

In addition to research, the Staff Fellow will have opportunities to learn and perform regulatory review work in the Division of Cellular and Gene Therapies. For more information about the regulatory oversight by this Division, please see **website: http://www.fda.gov/cber/gene.htm.**

To apply, send curriculum vitae and names and contact details for three references to:

Suzanne Epstein, Ph.D.
FDA/CBER/OCTGT/DCGT
HFM-730
1401 Rockville Pike
Rockville, MD 20852
E-mail: suzanne.epstein@fda.hhs.gov
Fax: 301- 827-0450

Equal Opportunity Employer.

UNIVERSITY OF PENNSYLVANIA
School of Medicine

POSTDOCTORAL POSITION in signal transduction to examine the role of prolyl hydroxylases in the regulation of Hypoxia Inducible Factor (see **Yu et al.,** *PNAS* **98:** 9630, 2001; **Percy et al.,** *PNAS* **103:** 654, 2006). Experience in molecular biology required, and with mouse models preferred. Send curriculum vitae and names of three references to: **Dr. Frank Lee, Department of Pathology and Lab Medicine, University of Pennsylvania School of Medicine, 605 Stellar Chance Labs, Philadelphia, PA 19104. E-mail: franklee@mail.med.upenn.edu.** *Affirmative Action/Equal Opportunity Employer.*

POSITIONS OPEN

TENURE-TRACK FACULTY position in skeletal biology is available in the Schulich School of Medicine and Dentistry at the University of Western Ontario (London, Canada). The successful candidate will join an outstanding research group with state-of-the-art infrastructure for molecular, cellular, and in vivo approaches. Applications will be accepted until the position is filled. For more details, go to **website: http://www.cihrskeletal.ca.**

ScienceCareers.org
We know science AAAS

Find out about jobs before you get your issue. Sign up for customized e-mail notification of jobs at **website: http://www.sciencecareers.org** by clicking on Job Alerts. You can also post your resume (open or confidentially) and check how many employers have viewed your resume at your own convenience.

MARKETPLACE

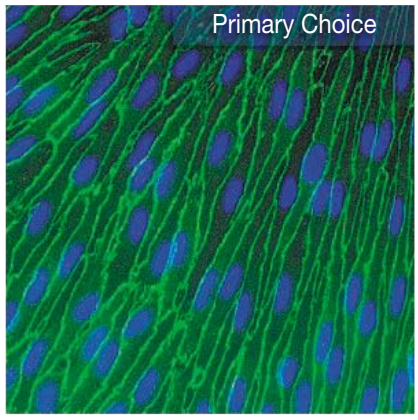

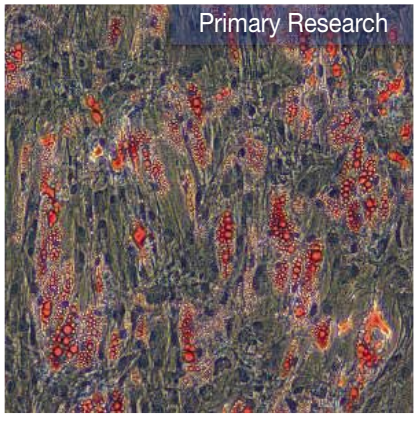

Primary Cells for Pioneering Research

Clonetics® Primary Cell and Media Systems

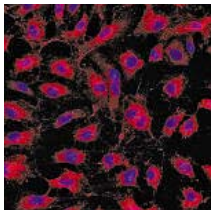

Our Clonetics Primary Cell and Media Systems are optimized and guaranteed for maximum performance. These primary cell systems are convenient, easy to use and provide physiologically relevant tools to accelerate your work. Select from a variety of optimized cell and media systems to suit your research needs including:

- Human Smooth Muscle Cells and Media
- Human & Animal Microvascular Endothelial Cells and Media
- Human Mammary Epithelial Cells and Media
- Human & Animal Vascular Endothelial Cells and Media
- Human Bronchial Epithelial Cells and Media

Poietics™ Progenitor Cells and Media

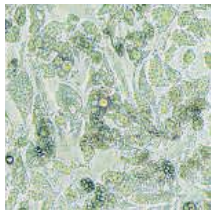

We offer a variety of products centered around adipose research and its applications in obesity, type II diabetes, cardiovascular disease, and other related disorders. Our products are tested and guaranteed to the highest level of industry standards. Our adipose product offering includes:

- Cryopreserved subcutaneous preadipocytes isolated from abdominal fat.
- Cryopreserved visceral preadipocytes isolated from fat surrounding kidney or bladder.
- Matched sets of subcutaneous and visceral preadipocytes from the same donor.
- NEW • Preadipocyte Growth Medium-2 (PGM-2) BulletKit® for the best proliferation and differentiation of these cells on the market.
- AdipoRed™ Assay Reagent for a simple, quantitative measure of lipid accumulation.

Cambrex, the source for Clonetics® and Poietics™ Cell Systems, BioWhittaker™ Classical Media, SeaPlaque® and NuSieve® Agarose, and PAGEr® *Precast Gels.*

For more information contact us at:
www.cambrex.com
U.S. **800-638-8174** | Europe **32 (0) 87 32 16 11**

Cambrex Bio Science Walkersville, Inc.
8830 Biggs Ford Road | Walkersville, MD 21793

YYePG Proudly Presents, Thx for Support

CAMBREX

Innovation. Experience. Performance.